# Study of the properties of modified cyclic butylene terephthalate and its composites

Memoria presentada por:

**Tobias Abt**

para optar al grado de

Doctor en Ingeniería Industrial

Director:

**Dr. Miguel Sánchez-Soto**

Profesor Titular de la Universidad

**Departament de Ciència del Materials i Enginyeria Metal·lúrgica**

**Abril 2014**

"*Without natural polymers, there is no life,*

*without synthetic polymers, no standard of living*"

**– Hans Uwe Schenck**

## Acknowledgement

*Fur meine Eltern,*

*die mir eine akademische Ausbildung ermöglichten,*

*und für Sonia,*

*die mich durch ihre Liebe unterstützte.*

# Summary

The thesis at hand deals with the modification of cyclic butylene terephthalate (CBT) with the aim to improve its final properties. CBT polymerizes in an entropically-driven ring-opening polymerization into polymerized CBT (pCBT), which is typically brittle. To increase the toughness of pCBT, a series of chemical and physical modifications of CBT with toughening agents and nano-reinforcements have been investigated. The role of the used processing routes on the properties of unmodified pCBT has been studied and in all cases a brittle pCBT has been obtained. However, it was found that a small amount of tetrahydrofuran can toughen pCBT. Nevertheless, this toughening mechanism was found to be only temporarily.

Reactive chain extension using low molecular weight, bi- or polyfunctional chain extenders such as epoxy resins or isocyanates was particularly effective and showed a remarkable toughening effect on pCBT. The epoxy- and isocyanate-modified pCBT polymers exhibited increased failure strain in tensile tests while modulus and strength were not significantly affected; contrary to other common toughening methods such as blending with other polymers, plasticization or copolymerization with soft segments.

Nanocomposites of toughened CBT and nano-reinforcements such as organo-montmorillonite, graphene and polyhedral oligomeric silsesquioxanes (POSS) were prepared and thoroughly analysed. The organoclay nanocomposites showed an intercalated-flocculated structure with high stiffness and strength together with a semi-ductile deformation behaviour. The organoclay was further modified by tethering the chain extender to the clay surfactant which resulted in an intercalated organoclay. This chain extender-grafted organoclay reacted then with pCBT and therefore could be exfoliated and randomly dispersed in the pCBT matrix during polymerization. A similar strategy was followed in the synthesis of pCBT/graphene nanocomposites. However, graphene exfoliation could not be achieved due to the strong $\pi$–$\pi$ interactions between the graphene sheets. Binary blends containing a polyisocyanate- grafted graphene showed an improved stiffness and strength due to enhanced compatibility. pCBT/POSS nanocomposites showed a good potential for nano-modification. However, the challenge was to find a compatible POSS type which did not affect the ring-opening polymerization of CBT.

Moreover, toughened carbon fibre fabric-reinforced pCBT composites have been prepared applying the developed toughening methods. Interlaminar shear strength,

flexural strength and failure strain of the chemically modified composites increased up to 60% with respect to unmodified pCBT composites.

This thesis has been prepared in the Centre Català del Plàstic (CCP) and the Department of Materials Science of the Polytechnic University of Catalonia (UPC) in Terrassa, Spain. A part of the experimental work has been accomplished in the Department of Mechanics and Industrial Production, Mondragon Unibertsitatea (Mondragón, Spain) and in the Department of Polymer Engineering of Budapest University of Technology and Economics (Budapest, Hungary).

## Resumen

La presente tesis trata de la modificación del butilén tereftalato cíclico (CBT) con el propósito de mejorar alguna de sus propiedades finales y expandir sus aplicaciones. En presencia de un catalizador y temperatura, el CBT reacciona y a través de un proceso de apertura de anillo, polimeriza dando lugar al pCBT. Sin embargo, el polímero resultante es intrínsecamente frágil. En este trabajo se han estudiado diversas modificaciones tanto físicas como químicas (procesado, extensores de cadena, nanopartículas) con el objetivo de incrementar la tenacidad del pCBT. En primer término se estudió el efecto que la ruta específica de procesado tiene sobre las propiedades y si bien en todos los casos se obtuvo un material frágil, se ha descubierto también que una pequeña cantidad de tetrahidrofurano puede hacer el pCBT más tenaz aunque sea de manera temporal.

El uso de extensores de cadena polifuncionales de bajo peso molecular, como resinas epoxídicas o isocianatos ha resultado ser particularmente efectivo. Así en el pCBT modificado con dichos agentes se obtuvieron notables incrementos de tenacidad sin significativa afectación de otras propiedades como el módulo de Young o la tensión de fluencia, como normalmente ocurre en procesos como la plastificación o la copolimerización.

Por otra parte se han preparado y analizado diversos nanocompuestos con CBT modificado añadiendo diferentes nanopartículas como montmorillonita, grafeno o polyhedral oligomeric silsesquioxanes (POSS). Los nanocompuestos formados con arcilla exhibieron unas estructuras intermedias entre intercaladas y floculadas, con alta

resistencia y rigidez en tracción y deformación a rotura de tipo semi-dúctil. El posterior injerto de un extensor de cadena en la superficie de la arcilla modificada permitió la reacción con el pCBT durante la polimerización, alcanzándose en este caso estructuras con arcilla exfoliada y dispersada a lo largo de la matriz. La aplicación de esta estrategia con el grafeno no dio lugar a su exfoliación debido a las fuertes interacciones existentes entre sus láminas. El uso de partículas POSS tiene un gran potencial para la modificación del pCBT, sin embargo el reto es encontrar una nanopartícula de este tipo que no interfiera con la polimerización de anillo del CBT.

Finalmente las estrategias de incremento de tenacidad descritas se han aplicado en la fabricación de compuestos de pCBT reforzados con fibras de carbono. En este caso la resistencia a cizalla interlaminar, a flexión y la deformación a rotura se incrementaron hasta casi un 60% con respecto a los compuestos no modificados.

Esta Tesis se ha realizado en el Centre Català del Plàstic (CCP) y en el Departamento de Ciencia de Materiales e Ingeniería Metalúrgica de la Universidad Politécnica de Catalunya (UPC). Asimismo, una parte del trabajo experimental se ha llevado a cabo en el Departamento de Mecánica y Producción Industrial de la Universidad de Mondragón y también en el Department of Polymer Engineering of Budapest University of Technology and Economics (Budapest, Hungría).

## Declaration

I declare to have developed the results presented in this thesis by myself, and with the help of no other than the cited references and resources. This work has not been presented to any inspecting authority in the same or a similar form before.

Tobias Abt

Terrassa / Spain, April 2014

# Contents

**List of figures**

## List of tables

## Nomenclature

### Abbreviations

| | |
|---|---|
| a.u. | Arbitrary unit |
| BOX | Bis-oxazoline |
| BPA | Bisphenol A |
| CBC | Carbonylbiscaprolactam |
| CBT | Cyclic butylene terephthalate (tradename, Cyclics Inc.) |
| CDP | Cyclo-depolymerization |
| CEC | Cation exchange capacity |
| CF | Carbon fibre |
| CFRP | Carbon fibre reinforced polymer |
| $CHCl_3$ | Chloroform |
| Cl30B | Cloisite 30B (tradename, Southern Clay Products Inc.) |
| CM | Compression moulding |

| | |
|---|---|
| CNT | Carbon nanotube |
| $CO_2$ | Carbon dioxide |
| c-pCBT | Macrocyclic polymerized CBT |
| DABCO | 1,4-diazabicyclo[2,2,2]octane |
| DMF | N,N-dimethylformamide |
| DMTA | Dynamic mechanical thermal analysis |
| DSC | Differential scanning calorimetry |
| ED-ROP | Entropically driven ring-opening polymerization |
| EDX | Energy-dispersive X-ray spectroscopy |
| EP | Epoxy resin |
| EVA | Poly(ethylene-*co*-vinyl acetate) |
| FBG | Fibre Bragg grating |
| FRP | Fibre reinforced polymer |
| FT-IR | Fourier-transform infrared spectroscopy |
| FWHM | Full width at half maximum intensity |
| G | Graphene |
| GC-MS | Gas chromatography-mass spectrometry |
| GO | Graphite oxide |
| GPC | Gel permeation chromatography |
| HDI | Hexamethylene diisocyanate |
| HFIP | 1,1,1,3,3,3-hexafluoroisopropanol |
| HNBR | Hydrogenated nitrile rubber |
| HPLC | High pressure liquid chromatography |
| ILSS | Short beam interlaminar shear strength |
| IM | Injection moulding |
| ISP | *In situ* polymerization |
| LCM | Liquid composite moulding |
| MB | Melt blending |
| MDI | 4,4"-methylenebis(phenyl isocyanate) |
| MDSC | Modulated DSC |
| MMA | Methylmethacrylate monomers |
| MW | Molecular weight |
| MWCNT | Multiwalled carbon nanotubes |

| | |
|---|---|
| NCO | Isocyanate |
| NMR | Nuclear magnetic resonance spectroscopy |
| o-DCB | Ortho-dichloro-benzene |
| OM | Optical microscopy |
| o-MMT | Organo-montmorillonite |
| PBN | Poly(butylene naphthalate) |
| PBT | Poly(butylene terephthalate) |
| PC | Polycarbonate |
| PCL | Polycaprolactone |
| pCBT | Polymerized cyclic butylene terephthalate |
| PEEK | Poly(ether ether ketone |
| PEK | Poly(ether ketone) |
| PEN | Poly(ethylene naphthalate) |
| PES | Poly(ether sulfone) |
| PET | Poly(ethylene terephthalate) |
| PLM | Polarized light microscopy |
| PLS | Polymer/layered silicate nanocomposite |
| PMDI | Polymeric methylenebis(phenyl isocyanate) |
| PMDI-$g$-Cl30B | PMDI-modified Cloisite 30B |
| PMDI-$g$-G | PMDI-modified graphene |
| PMMA | Poly(methyl methacrylate) |
| PolyTHF | Polytetrahydrofuran |
| POSS | Polyhedral oligomeric silsesquioxane (tradename, HybridPlastics) |
| PPS | Polyphenylenesulfide |
| PTFE | Poly(tetrafluoroethene) |
| PTT | Poly(trimethylene terephthalate) |
| RFI | Resin film infusion |
| RIM | Reaction injection moulding |
| RIP | Reactive injection pultrusion |
| ROMP | Ring-opening metathesis polymerization |
| ROP | Ring-opening polymerization |
| RP | Reprocessed |

| | |
|---|---|
| RRIM | Reinforced reaction injection moulding |
| RTM | Resin transfer moulding |
| S.A. | Sociedad anónima, *span.* for incorporation (Inc.) |
| SALS | Small-angle light scattering |
| SAXS | Small-angle X-ray scattering |
| SB | Solvent blending |
| SEM | Scanning electron microscopy |
| SINC | Solvent-induced crystallization |
| SRIM | Structural reaction injection moulding |
| SWCNT | Single-walled carbon nanotube |
| TEM | Transmission electron microscopy |
| TFA | Trifluoroacetic acid |
| TGA | Thermogravimetric analysis |
| THF | Tetrahydrofuran |
| TPC | Thermoplastic composite |
| TPE | Thermoplastic elastomer |
| TP-RTM | Thermoplastic resin transfer moulding |
| TPU | Thermoplastic polyurethanes |
| TRGO | Thermally reduced graphite oxide |
| VARI | Vacuum-assisted resin infusion |
| VARTM | Vacuum-assisted resin transfer moulding |
| VI | Vacuum infusion |
| VOC | Volatile organic compound |
| WAXS | Wide-angle X-ray scattering |
| XRD | X-ray diffraction |

## Symbols

| | | |
|---|---|---|
| $\alpha$ | Degree of conversion | [-] |
| $\Delta F$ | Force difference | [N] |
| $\Delta L_0$ | Gauge length increase | [mm] |
| $\Delta p$ | Pressure gradient | [Pa], [MPa] |

| | | |
|---|---|---|
| $\Delta H_m$ | Melting enthalpy | [J/g] |
| $\Delta H^0_m$ | Fully crystalline melting enthalpy | [J/g] |
| $\Delta s$ | Deflection difference | [mm] |
| $\Delta T$ | Temperature difference | [°C], [K] |
| $\varepsilon$ | Strain | [%], [-] |
| $\varepsilon_b$ | Strain at break | [%], [-] |
| $\varepsilon_f{}', \varepsilon_f{}''$ | Flexural strain | [%], [-] |
| $\eta$ | Viscosity | [Pa·s] |
| $2\theta$ | Bragg angle | [°] |
| $\lambda$ | Wavelength | [Å] |
| $\rho$ | Density | [g/cm$^3$], [kg/m$^3$] |
| $\rho_c$ | Theoretical composite density | [g/cm$^3$], [kg/m$^3$] |
| $\rho_f$ | Fibre density | [g/cm$^3$], [kg/m$^3$] |
| $\rho_{IL}$ | Immersion liquid density | [g/cm$^3$], [kg/m$^3$] |
| $\rho_{mc}$ | Measured composite density | [g/cm$^3$], [kg/m$^3$] |
| $\rho_r$ | Resin density | [g/cm$^3$], [kg/m$^3$] |
| $\sigma$ | Strength | [MPa] |
| $\sigma_1, \sigma_2$ | Flexural stress | [MPa] |
| $\sigma_f$ | Flexural strength | [MPa] |
| $\varphi$ | Porosity | [-] |
| $X_C$ | Degree of crystallinity | [%], [-] |
| $X_t$ | Relative crystallinity | [-] |
| $A$ | Cross-section area | [mm$^2$], [m$^2$] |
| $a_{tU}$ | Unnoched tensile-impact strength | [kJ/m$^2$] |
| $D_{hkl}$ | Apparent crystallite size | [Å], [nm] |
| $d_{hkl}$ | Interlaminar distance | [Å], [nm] |
| $E$ | Young´s modulus | [GPa] |
| $E^*$ | Complex dynamic modulus | [GPa] |
| $E'$ | Storage modulus | [GPa] |
| $E''$ | Loss modulus | [GPa] |
| $E_0$ | Nominal impact energy | [J] |
| $E_{abs}$ | Absorbed energy | [J] |

| | | |
|---|---|---|
| $E_C$ | Corrected tensile-impact energy | [J] |
| $E_{crit}$ | Critical energy | [J] |
| $E_f$ | Flexural modulus of elasticity | [MPa] |
| $E_M$ | Maximum energy | [J] |
| $E_{max}$ | Maximum tensile-impact energy | [J] |
| $E_q$ | Toss energy | [J] |
| $E_s$ | Absorbed tensile-impact energy | [J] |
| $EEW$ | Epoxy equivalent weight | [g/eq] |
| $F, F', F''$ | Force | [F] |
| $F_d$ | Delamination threshold force | [N] |
| $F_M$ | max. contact force during impact | [N] |
| $F_{max}$ | Failure or maximum load | [N] |
| $f$ | Frequency | $[s^{-1}]$, [Hz] |
| $I$ | Electric current | [A] |
| $L$ | Span length | [mm] |
| $L_0$ | Gauge length of the specimen | [mm] |
| $l$ | Flow distance | [m] |
| $l, b, h$ | Dimensions | [mm], [$\mu$m] |
| $l_M$ | Deflection at peak force | [mm] |
| $K$ | Scherrer shape factor | [-] |
| $K$ | One-dimensional permeability | [m$^2$] |
| $k$ | Avrami rate constant | [-] |
| $M_n$ | Number average molecular weight | [g/mol] |
| $M_w$ | Mass average molecular weight | [g/mol] |
| $m$ | Mass | [g], [kg] |
| $m_{S,A}$ | Apparent specimen mass in air | [g] |
| $m_{S,IL}$ | Apparent specimen mass in liquid | [g] |
| $n$ | Avrami exponent | [-] |
| $p$ | Pressure | [bar], [MPa] |
| $P$ | Degree of polymerization | [-] |
| $PDI$ | Polydispersity index | [-] |
| $Q$ | Volumetric flow rate | [m$^3$/s] |
| $Q/A$ | Flow rate | [m/s] |

| | | |
|---|---|---|
| $R_m$ | Tensile strength | [MPa] |
| $RT$ | Room temperature | [°C], [K] |
| $s$ | Beam mid-point deflection at break | [mm] |
| $s'$, $s''$ | Beam mid-point deflections | [mm] |
| $t$ | Time | [s], [min], [h], [d] |
| $t_c$ | Total contact time | [ms] |
| $t_{imp}$ | Impregnation time | [s] |
| $tan\ \delta$ | Dynamical loss factor | [-] |
| $T$ | Temperature | [°C], [K] |
| $T_0$ | Reference temperature | [°C], [K] |
| $T_c$ | Crystallization temperature | [°C], [K] |
| $T_g$ | Glass transition temperature | [°C], [K] |
| $T_m$ | Melting temperature | [°C], [K] |
| $T_P$ | Polymerization temperature | [°C], [K] |
| $U$ | Voltage | [V] |
| $V$ | Volume | [mm$^3$], [m$^3$] |
| $V$ | Void content | [wt.%] |
| $V_f$ | Fibre volume fraction | [-] |
| $v_0$ | Impact velocity | [m/s] |
| $w_f$ | Fibre weight fraction | [-] |
| $w_r$ | Resin weight fraction | [-] |

# Chapter 1: Introduction

## 1.1 Prologue

Nowadays it has been widely acknowledged that carbon dioxide is the main greenhouse gas and plays a major role in global warming. According to the European Commission[1], road transport is responsible for about one fifth of the EU's total emissions of $CO_2$. The latter increased by nearly 23% between 1990 and 2010, mainly because of light-duty vehicles (*i.e.* cars and vans) which contributed around 15% of $CO_2$ emission. Thus transport is the only major sector in the EU where greenhouse gas emissions are still rising.

As a countermeasure, the European Union legislation decided a mandatory emission reduction for new cars sold on the European market in 2009 (EC 443/2009). This regulation reduces the average $CO_2$ emissions for new passenger cars to 130 grams of $CO_2$ per kilometre (g/km) by 2015 and 95 g/km by 2020. The 2015 and 2020 targets represent reductions of 18% and 40%, respectively, with respect to the 2007 average of 158.7 g/km.

These emission reductions may be achieved through improving powertrain efficiency as well as through weight reduction. A common strategy for the latter is replacing metal parts in vehicles by fibre reinforced polymer (FRPs) composites. This strategy is also pursued in aeronautics, for instance Airbus aircrafts[2] have seen a step-by-step introduction of composite materials that started with the A310 in 1982. Nowadays, 53% of the A350 XWB's airframe is made up of carbon fibre reinforced polymer (CFRP) including Airbus' first carbon fibre fuselage.

This shows that FRP's are gaining importance as structural materials because of their better strength-to-weight and stiffness-to-weight ratios as compared to steel or aluminium. FRPs consist of a polymer matrix which may be a thermoset or thermoplastic polymer and a variety of reinforcements such as glass, carbon, aramid or natural fibres. On one hand, thermosets are commonly employed for composite production due to their straightforward processing. On the other hand, thermoplastics show some advantages

---

[1] Data from www.ec.europa.eu
[2] Data from www.airbus.com

over thermosets, namely a higher toughness, faster manufacturing without releasing harmful volatiles as well as the possibility of welding, postforming and recycling. However, the main disadvantage in the production of thermoplastic composites (TPCs) is the need for high processing temperatures and pressures due to the high melt viscosity of the thermoplastic matrix which often results in products with poor fibre impregnation and high void content. Impregnation can be improved on one hand by reducing the flow lengths of the thermoplastic matrix by intimate mingling of the reinforcement and the matrix prior to composite production. Nevertheless, this results in more expensive semi-finished products. On the other hand, fibre wet-out can be improved using reactive processing of TPCs. The fibre reinforcement is impregnated with low viscosity mono- or oligomeric precursors. The latter are then *in situ* polymerized after impregnation. Moreover, the low viscosity of the precursors allows for processing routes which are traditionally used in thermoset processing, such as vacuum infusion or resin transfer moulding.

Recently, cyclic oligomers of the engineering thermoplastic poly(butylene terephthalate) have become commercially available. These cyclic butylene terephthalate oligomers (CBT®) exhibit a water-like melt viscosity and are capable of rapid polymerization into polymerized CBT (referred to as pCBT) in the presence of a catalyst. The growing interest in CBT is depicted in figure 1.1. Despite this considerable body of work on CBT and pCBT, there still remain problems with the final properties of pCBT which are associated with the processing-structure-properties relation. A literature review on cyclic butylene terephthalate and its composites is presented in chapter 2. Based on the state-of-the-art, problems are identified and possible solutions are proposed.
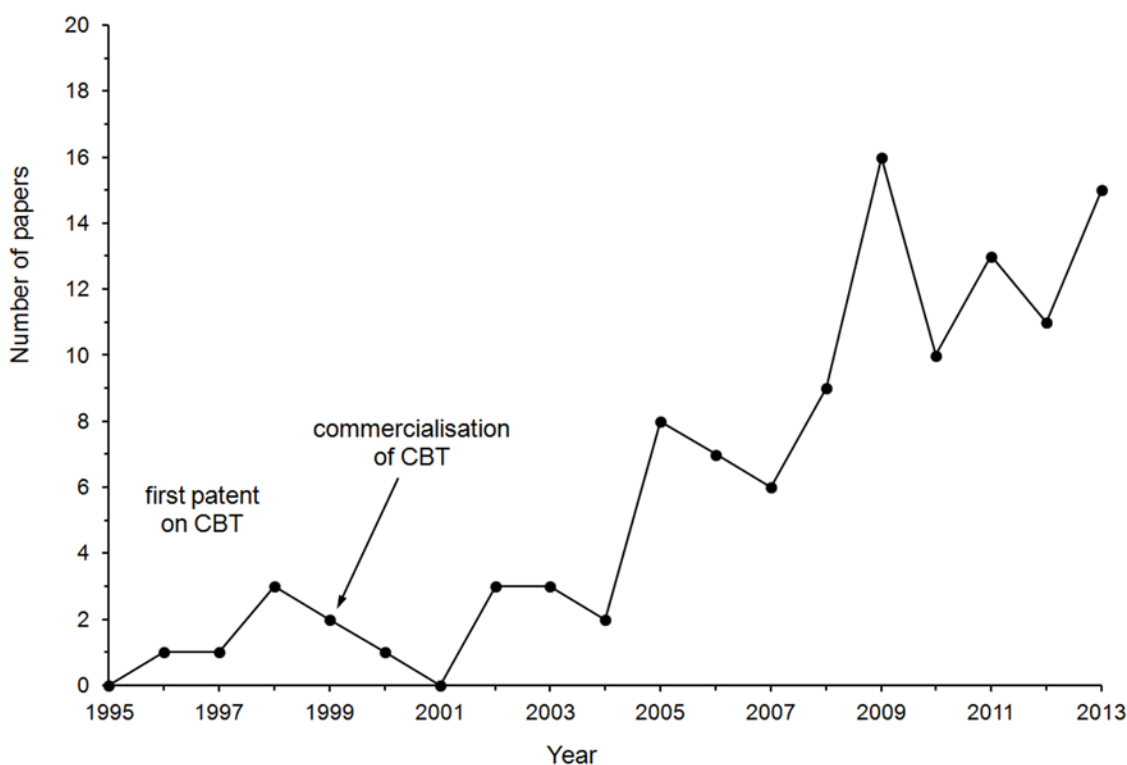
Fig. 1.1: Number of scientific articles and conference papers dealing with cyclic butylene terephthalate oligomers as a function of time; data from scopus.com.

## 1.2    Objectives

The intention of this research is to investigate possibilities to improve the properties of polymerized cyclic butylene terephthalate, most importantly the inherent brittleness. It was pointed out in the literature review that chemical modification such as reactive chain extension is an effective method to improve toughness without significantly altering other relevant properties. Moreover, this method might be also useful for improving the properties of pCBT nanocomposites. Potential synergetic effects between CBT and nano-reinforcements such as chemical interactions are usually ignored. The reactive nature of CBT oligomers, together with chemical modifiers, may be employed for chemical grafting of the nano-reinforcements with the pCBT. Therefore, the experimental work is divided into four parts:

i.)     Investigation of the processing-structure-properties relationships in polymerized cyclic butylene terephthalate obtained by compression moulding, melt blending and solvent blending.

ii.)    Improvement of the pCBT toughness by exploring toughening methods such as reactive chain extension using bi- and polyfunctional compounds.

iii.)   Preparation and characterization of pCBT nanocomposites using various types of nano-reinforcements in combination with toughening agents.

iiii.)  Preparation and characterization of fibre reinforced pCBT composites applying the most effective toughening methods.

# Chapter 2: State-of-the-art

In this chapter a comprehensive literature review is presented, starting with an overview of fibre reinforced thermoplastic composites and the different types of cyclic oligomers of engineering thermoplastics useful for TPC manufacture. Then the state-of-the-art regarding cyclic butylene terephthalate and its (nano-)composites with emphasis on the relationship between the synthesis, processing, structure and properties is presented. On this basis, problems related with the final properties of polymerized cyclic butylene terephthalate are addressed, namely the inherent brittleness of pCBT. Publications related to the toughening of pCBT are critically reviewed. Moreover, commonly used toughening methods for conventional thermoplastic polyesters are analysed for their toughening performance and applicability to pCBT.

## 2.1 Thermoplastic composites

Thermoplastic composites exhibit some important advantages over their thermoset counterparts. This is due to the fact that thermoplastics typically outperform thermosets in toughness and impact strength and this also applies to TPCs. Moreover, TPCs can be produced in a shorter time compared to thermosets because no curing step is needed. Additionally, thermoplastic composites offer the possibility to be welded, postformed and recycled due to their thermoplastic nature [1]. The possibility of recycling is an increasingly important argument for TPCs in many markets, especially in the automotive sector. A TPC part can be grinded into fine particles at the end of its life cycle. The grinded material (together with virgin polymer) can then be injection moulded into new short fibre reinforced parts which then also can be recycled at the end of their life.

The main disadvantage of thermoplastics over thermosets is their high melt viscosity which complicates a proper fibre impregnation. The latter is crucial for stress transfer between fibres and matrix as well as for a low void content of the composite. The viscosity of thermoplastics during melt processing is orders of magnitude higher than that of thermosets, namely $10^3$ to $10^6$ Pa·s for thermoplastics versus 1 Pa·s or lower for thermosets [2].

### 2.1.1 Reinforcement impregnation

In composite production, a maximum matrix viscosity of 1 Pa·s is generally accepted for good fibre impregnation [3-4]. The latter occurs on two different length scales; macro flow between fibre bundles which is mainly driven by a hydrodynamic pressure gradient and micro flow within the fibre bundles which is governed by capillary pressure [5]. The mathematical description of macro flow in a porous medium is given by Darcy's law [5-7]. Fibre impregnation, assuming fluid incompressibility and constant reinforcement volume fraction, can be described as follows.

$$\frac{Q}{A} = -\frac{K}{\eta} \cdot \frac{\Delta P}{l} \tag{2.1}$$

where the quantity $Q/A$ is the flow rate, also called Darcy velocity $u$ (m/s), $Q$ is the volumetric flow rate (m$^3$/s), $A$ is the cross-section area through which the flow occurs (m$^2$), $K$ is the one-dimensional permeability of the fibre reinforcement (m$^2$), $\eta$ is the viscosity of the resin (Pa·s), $\Delta P$ is the pressure gradient (Pa) and $l$ is the flow distance (m). For unidirectional flow in $z$ direction (*i.e.* normal to the fibre axis), Equation 2.1 can be written as

$$\frac{Q}{A} = \varphi \cdot \frac{dl}{dt} = (1 - V_f) \cdot \frac{dl}{dt} \tag{2.2}$$

where the quantity (1-$V_f$) is the porosity $\varphi$ of the reinforcement (-), $V_f$ is the fibre volume fraction (-), $l$ is the flow distance in $z$ direction (m) and $t$ is the impregnation time (s). Assuming constant permeability and viscosity, integration of Equation 2.2 yields the necessary time for complete fibre impregnation $t_{imp}$

$$t_{imp} = \frac{\varphi \eta l^2}{2K\Delta P} \qquad\qquad (2.3)$$

It can be seen from Equation 2.3 that the time for complete fibre impregnation is a function of the resin viscosity and flow distance. Consequently, a low resin viscosity and/or a low flow distance are desirable in order to minimize cycle time and hence production costs. Other parameters such as reinforcement porosity or permeability are inherent properties of the used materials, whereas the pressure gradient can only be varied in a limited range because excessive pressure can lead to a distortion of the fibre alignment.

### 2.1.2  Impregnation strategies

Direct fibre impregnation with thermoplastics having high viscosity can be achieved in a reasonably short time by [1, 8]

i)    decreasing the flow distance of the highly viscous thermoplastic
ii)   decreasing the viscosity of the matrix.

The different processing routes following these two strategies are depicted in figure 2.1.
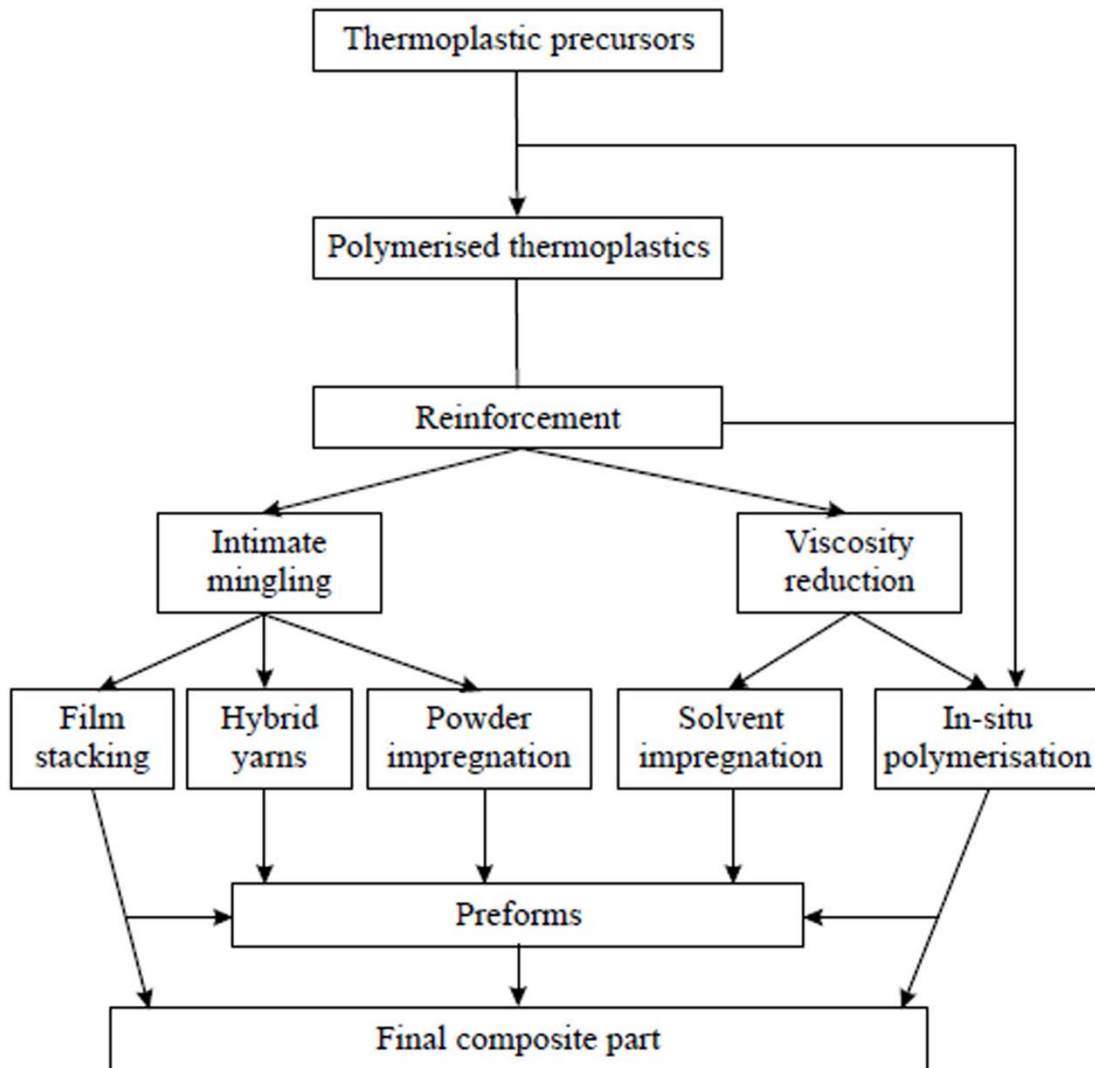
Fig. 2.1: Processing routes for continuous fibre reinforced thermoplastic composites; adapted from [9].

**Decreasing the flow distance**

Different concepts have been developed for the first strategy such as partial or full consolidation of stacked films (so-called prepregs), commingling and co-weaving of reinforcing and polymer fibres (so-called hybrid yarns), and powder coating as illustrated in figure 2.2.

In *film stacking*, polymer films are introduced between reinforcement layers which may have the form of a tow, mat or fabric. This assembly is pulled through a series of heated rollers in order to melt the matrix and reduce its viscosity sufficiently for impregnation, which occurs through the composite thickness. The void content is governed by the pressure-temperature history of the semi-finished sheets. However, melt impregnation is difficult or impractical for certain polymers due to their limited ability to withstand the high temperatures required for viscosity reduction and hence thermal degradation (*i.e.* molecular weight reduction) may occur. Moreover, complex shapes are difficult to produce due to the low drapability of the stacks.
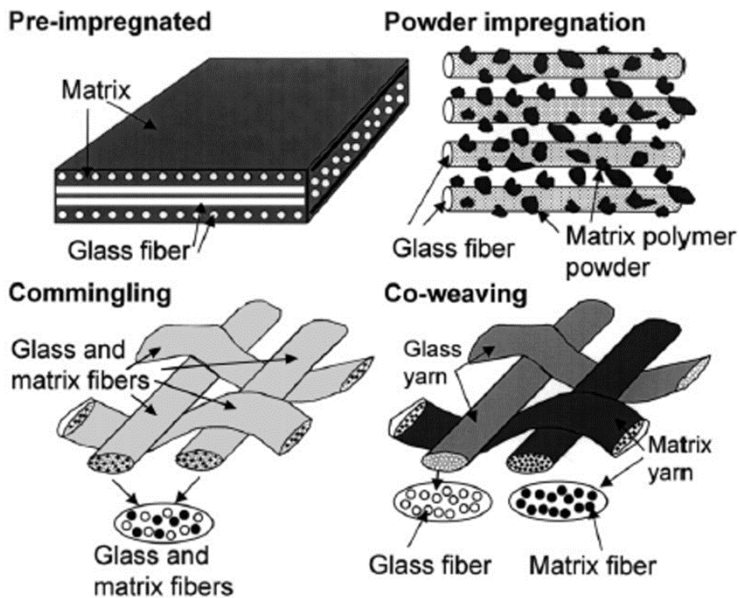


Fig. 2.2: Different methods for decreasing the flow distance during thermoplastic composite production; adapted from [8].

TPC production from *hybrid yarns* has been reviewed by Svensson *et al.* [10]. *Commingling* and *co-weaving* are well-established textile processes for achieving intimately blended hybrid yarns and fabrics of reinforcing and polymer fibres and hence minimized flow distances. The latter allows for substantially lower pressure during impregnation and consolidation as compared to conventional melt impregnation. These hybrid yarns can be used in further textile processing (*e.g.* weaving and braiding) due to their flexibility and stability. Another advantage is that the resulting fabrics can be readily

handled and formed at room temperature. Furthermore, fibre fraction can be closely controlled *via* the amount and size of the yarns, whereas the composite quality is controlled by the intimacy of the blend and the uniformity of the hybrid yarn. However, these intermediate products have additional costs due to the necessity of more than one processing step and the commingled textiles frequently exhibit fibre waviness and need to be de-bulked.

*Powder coating* involves the deposition and distribution of polymer powder onto a textile in which blending occurs on an intra-bundle level. The former can be achieved by wetting the reinforcement with a polymer suspension, aqueous slurry or direct powder deposition using an electrostatic coating method. The adherence of the solid particles is mainly governed by electrostatic forces. In all cases the yarns are spread prior to coating in order to reduce the flow distances. The individual yarns are then passed through an oven to sinter the powder on the fibre surface. The polymer particles form bridges between the fibres and fibre contents of 30 to 65% are typically obtained. The semi-impregnated tow is then fully impregnated by applying heat and pressure during the final consolidation stage. These intermediate products have also higher costs due to the additional step of cryogenic grinding to obtain the polymer powder.

A further improvement in impregnation is the *tow spreading technology* [11-12]. This method aims on reducing the weight per unit area of the reinforcement by thinning a conventional 12k carbon fibre tow (*i.e.* comprising 12,000 filaments). The tow width is increased from 5 mm to around 25 mm, resulting in a decrease in weight per unit area of approximately 500%. The un-spread CF tow is threaded though a spreading system that is provided with an air duct and a vacuum. The tow sags downward towards the air flow direction by the help of the vacuum, thus losing its tension. Back-and-forth vibrating spreaders equipped with hot air (200 °C) open and spread the tow uniformly. Sheets of unidirectional and/or woven fabric can be produced using this technology. El-Dessouky *et al.* [11] used a thermoplastic film of polyphenylene sulphide (PPS) to stabilise and impregnate the spread tow fabric. They obtained a partially consolidated prepreg which was then fully consolidated. A second laminate was produced from a conventional woven prepreg of 3k CF/PPS for comparison. The spread tow laminate exhibited better fibre packing, lower level of crimp, lower void content and improved mechanical properties as

compared to the conventional laminate. The authors could show that plain weave fabrics produced with these spread tows exhibited lower crimp angles than conventional fabric of satin weave. The spread tows are in closer proximity but maintain an adequate interfibre spacing for effective fibre impregnation. The low crimp angle of the spread tow fabric reduced the void content and resin-rich areas in the TPC, resulting in better mechanical properties of the composite.

## Decreasing the matrix viscosity

The viscosity of the polymer can be decreased in two different ways. The first method is solvent impregnation and the second one is *in situ* polymerization (ISP).

*Solvent impregnation* is an alternative to melt impregnation for generally amorphous thermoplastics. A low viscosity solution with around 10 wt.% of polymer is prepared and used for textile impregnation. Nevertheless, not all polymers are soluble at room temperature or even sufficiently solvent resistant. Harmful volatiles are produced during solvent impregnation and residual solvent in the final composite is frequently encountered.

*In situ polymerization* is substantially different from the above described processing routes because not thermoplastic polymers but their monomeric or oligomeric precursors are used to impregnate the reinforcement. The remarkably low melt viscosity of these precursors allows a good impregnation of fibre reinforcements prior to *in situ* polymerization. Hence, processes which are typically restricted to thermoset processing such as vacuum infusion, resin transfer moulding and the like may be used to produce TPCs. The major advantage of *in situ* polymerization is the possibility to directly produce the final part without the need of intermediate steps. Cyclic oligomers and their ring-opening polymerization potentially useful for the production of thermoplastic composites have been commercialized recently and will be reviewed in the subsequent sections.

### 2.1.3  Preform consolidation

The consolidation has been described by Campbell *et al.* [2]. Different processes can be used for the consolidation of partly or fully impregnated thermoplastic preforms, for instance compression moulding, pultrusion or filament winding. The consolidation determines the final void content of the composite part and thus its mechanical properties. During this process the preform is heated in order to melt the polymer, then consolidated and compacted and finally the part is solidified during cooling, as illustrated schematically in figure 2.3.
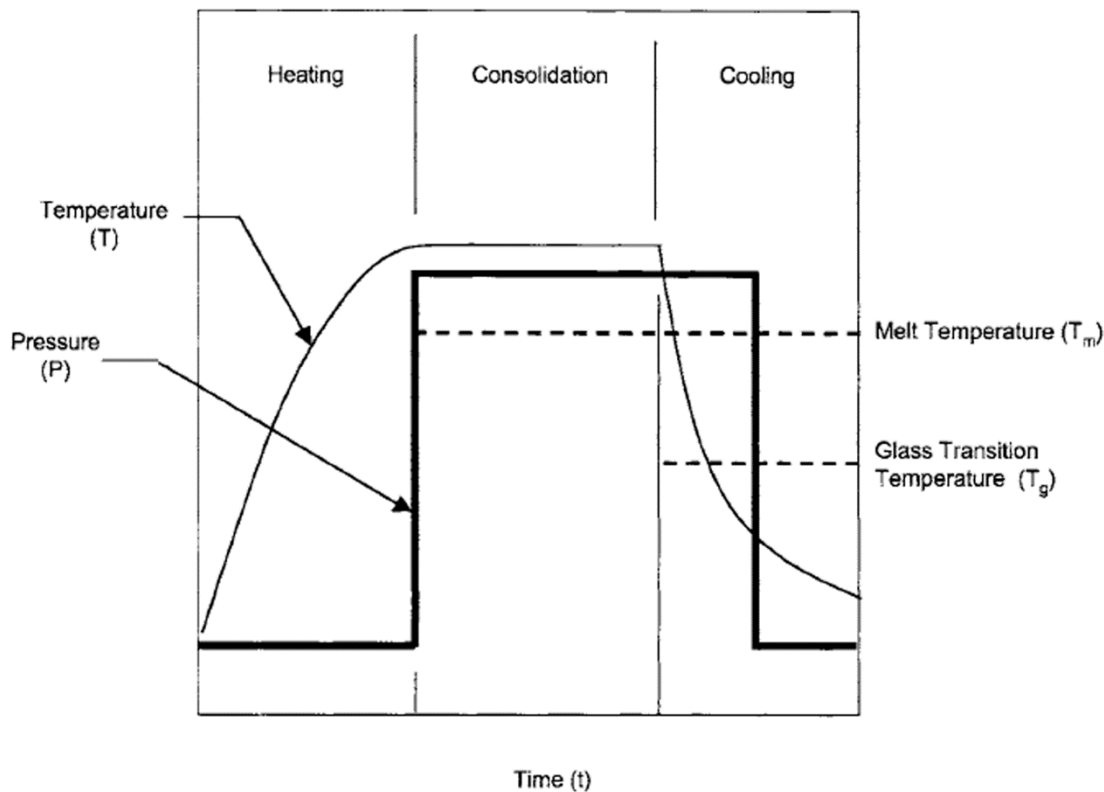


Fig. 2.3: Typical thermoplastic composite process cycle; adapted from [2].

Similar to thermoset composite production, the main processing variables are time, temperature and pressure. The preforms are heated with convection ovens, infrared heaters, hot plate presses or autoclaves. Consolidation times are usually longer for amorphous materials since they do not melt and generally maintain higher viscosities at

the processing temperature. However, shorter consolidation times can be achieved if higher pressures are employed.

The necessary time for consolidation mainly depends on the product form used. For instance, hot melt impregnated tape can be successfully consolidated in a few seconds to minutes, while woven powder coated or comingled prepregs require longer times for consolidation because the resin needs to flow and impregnate the fibres. Film stacking requires even longer consolidation times (up to 1 h) because the highly viscous resin has even longer distances to flow. In case of a semi-crystalline matrix, the final cooling step strongly determines the degree of crystallinity and hence the strength, stiffness and chemical resistance of the polymer matrix [1]. During cooling the pressure is maintained until the temperature falls well below the glass transition ($T_g$) of the matrix in order to inhibit the nucleation of voids and to maintain the desired part dimensions. Moreover, pressure during cooling puts the layers in intimate contact and helps to further impregnate the fibre bed.

It should be noted that the properties of solvent impregnated prepregs, powder coated, comingled and film stacked laminates are inferior to those made from hot melt impregnated prepregs due to the superior fibre-matrix interface formed during the hot melt impregnation process.

## 2.2   Reactive processing of TPCs

The reactive processing of TPCs is targeted on direct impregnation of fibre reinforcements without the need for intermediate processing steps. A number of requirements have been defined for achieving direct fibre impregnation with a liquid matrix [1, 4, 9, 13].

i)     The viscosity of the liquid matrix during impregnation is very low, *i.e.* $\eta \leq 1$ Pa·s.

ii)    After impregnation, the matrix can be physically or chemically solidified in a reasonably short time.

iii)   The polymerization reaction should not produce any by-products.

iv)    The matrix should exhibit good physical properties after solidification in order to obtain composite parts with good mechanical properties.

v)      Polymerization and crystallization should not produce large exotherms since they may create hot spots and hence result in through-the-thickness property variations.

The first and second requirement can be met by employing low viscous polymer precursors, *i.e.* monomers and oligomers. However, the types of polymerization are consequently narrowed down to addition-type polymerizations of mono- and bifunctional species, and condensation-type polymerizations where a small by-product is formed are excluded due to the third requirement. Vinyl polymerization and ring-opening polymerization are the most common types of addition polymerization useful for TPC production [1]. An overview of reactive polymer systems is presented in the next section.

### 2.2.1  Reactive polymer systems

Van Rijswijk and Bersee have reviewed the reactive processing of reactive polymer systems for TPC production [1].

**Vinyl polymerization**

Vinyl monomers are small molecules which contain C=C double bonds. These double bonds are broken into single bonds during polymerization, resulting in two free electrons. The free electrons act as reactive chain end and are used to join monomer units to form a macromolecular chain which only contains single bonds between atoms. Examples for free radical vinyl polymerization are the reaction of di-isocyanates and di-alcohols, forming thermoplastic polyurethanes (TPU), as illustrated in figure 2.4, and also methylmethacrylate monomers (MMA) combined with peroxide initiators which polymerize into polymethylmethacrylate (PMMA).
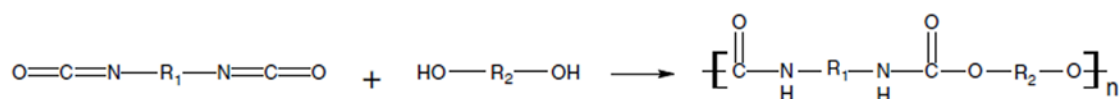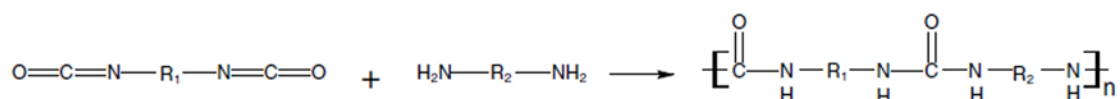
Fig. 2.4: Free radical vinyl polymerization of polyurethanes (a) and polyureas (b), adapted from [1].

**Ring-opening polymerization**

Ring-opening polymerization (ROP) is a polymerization mechanism in which cyclic molecules are opened into linear monomers or oligomers and subsequently bonded into high molecular weight polymers without generating by-products. Cyclic oligomers of polymers have been known for many years. They are formed in small amounts in many polymers during the condensation polymerization, typically less than 2 wt.% along with the high molecular weight linear chains [14-16]. The formation of these cyclic oligomers is due to statistical reasons; they are formed either under kinetic conditions or in their equilibrium concentration from melt polymerization [17].

In the 1930s Carothers and co-workers were the first who prepared aliphatic cyclic oligomeric esters and carbonates by distillative depolymerization of linear polyesters [18-19]. Since then, many cyclic oligomers of different polymers have been extracted and characterized by several researchers. Until recently, these oligomers have not been exploited commercially due to the fact that their synthesis could not afford high yields and high purities. Thus, early works on cyclic oligomers were only of academic interest. Moreover, most of these oligomers have high melting points, sometimes even higher than their polymeric counterparts, which limits melt processing of cyclic oligomers [14, 17, 20].

**Polyamide**

Polyamides can be synthesized either by polycondensation or by ROP. The polycondensation of diamime and diacid yields polyamide and water as a by-product and thus is not suitable for processing routes which use closed moulds. The oldest reactive processing of thermoplastics through ring-opening polymerization is the anionic polymerization of lactams. The ROP of $\varepsilon$-caprolactam into PA-6 was discovered in the early 1940s and has been commercially exploited by various companies since that time. Recently, the anionic ROP of laurolactam into PA-12 gained interest [4-5, 13, 21-22]. Both polymerizations are shown in figure 2.5. High molecular weight polyamide-6 is obtained by anionic ROP of $\varepsilon$-caprolactam at 130–170 °C, *i.e.* below the melting temperature of PA-6 (225–235 °C [23]), in the presence of an activator and a catalyst and conversions up to 99.3% can be obtained in 3–60 min, depending on the type and amount of added activator and catalyst.

Similarly, polyamide-12 is anionically polymerized from o-laurolactam but the polymerization has to be performed above the final polymer melting point of PA-12 (170–180 °C [23]) in order to increase the polymerization rate and to avoid premature crystallization. The ROP of both caprolactam and laurolactam yields a copolymer with tailored mechanical and thermal properties, depending on the monomer ratios. Due to the anionic nature of the ROP, the exothermal polymerization can be easily terminated by proton donors, *e.g.* water coming from ambient humidity. As a consequence, monomer storage and processing have to be performed in an environment absolutely free from moisture and oxygen.
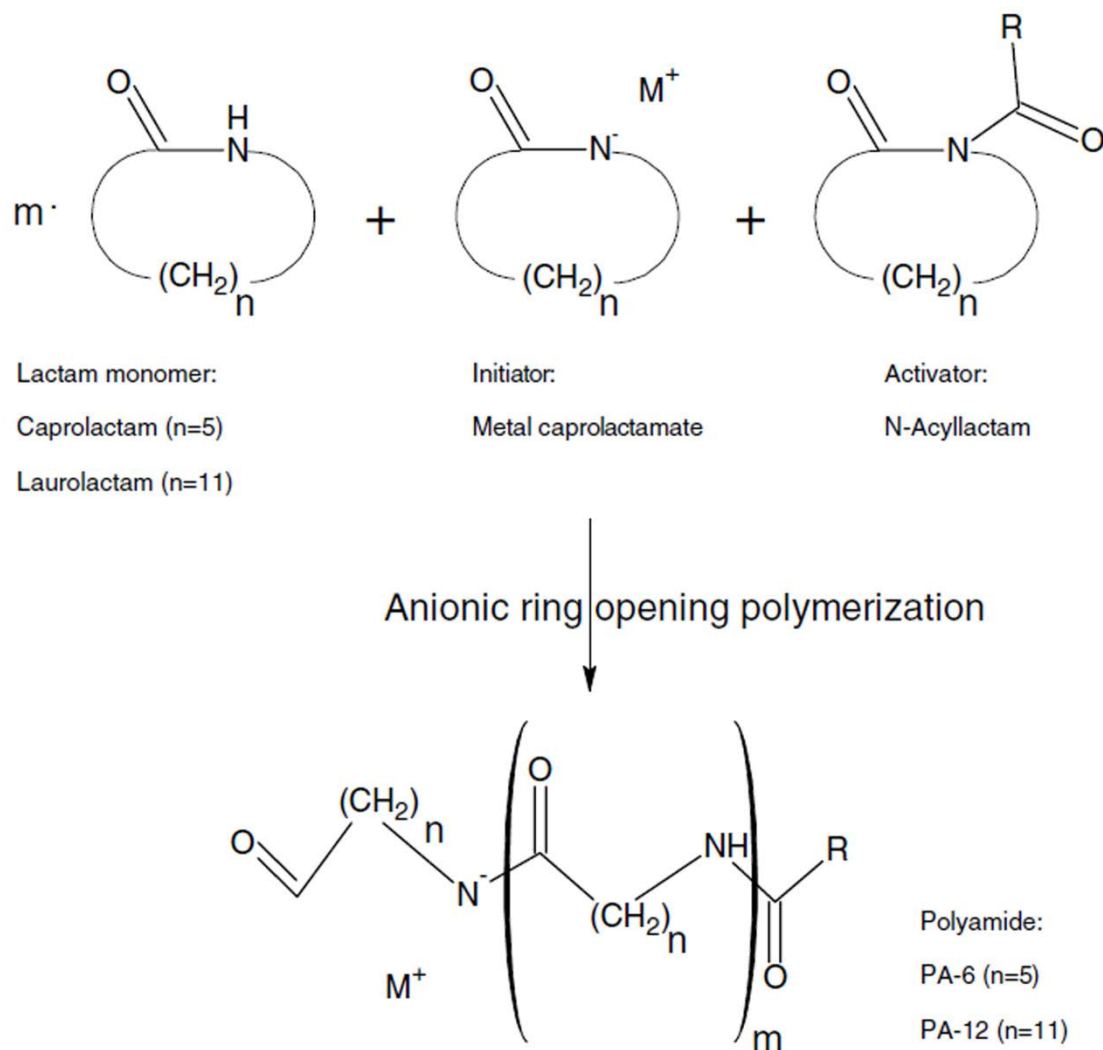
Fig. 2.5: Anionic ring-opening polymerization of polyamides, adapted from [1].

**Polyesters**

Cyclic oligomers of polymers obtained by condensation polymerization have been known for quite some time. They are found in commercial grades of polyester and polycarbonate at levels of 0.25–2% and are formed either under kinetic or in their equilibrium concentration from melt polymerization reactions. Spanagel and Carothers showed in the 1930s that aliphatic cyclic oligomeric esters and carbonates could be prepared by distillative depolymerization [19]. East and Girshab [24] extracted cyclic oligomers from poly(1,4-butylene terephthalate) and quantitatively determined them by high pressure liquid chromatography (HPLC). Most of the early work was only of academic interest and

was not commercialised due to the fact that syntheses were inefficient and purification of products was always necessary [14, 17, 20]. The systematic synthesis and subsequent ring-opening metathesis polymerization (ROMP) of macrocyclic polyesters were first developed by D.J. Brunelle and his research group in the late 1980s at the General Electric Corporation, USA. They initially explored macrocyclic polycarbonates (PC) but also developed the reactive processing of poly(ethylene terephthalate) (PET) and poly(butylene terephthalate) (PBT) [14]. The PBT technology passed on in 1999 to the Cyclics Corporation, USA, and is currently being marketed under the tradename Cyclics[®] [25]. More details about cyclic PBT, *i.e.* CBT[®] is provided in section 2.3 since this material was used in this work. Cyclic PET can be obtained by *cyclo-depolymerization* (CDP) of linear PET. The PET oligomers have an initial melt viscosity of 30 mPa·s and polymerize in presence of a catalyst through ROMP at 225 °C in 3–15 min, illustrated in figure 2.6.
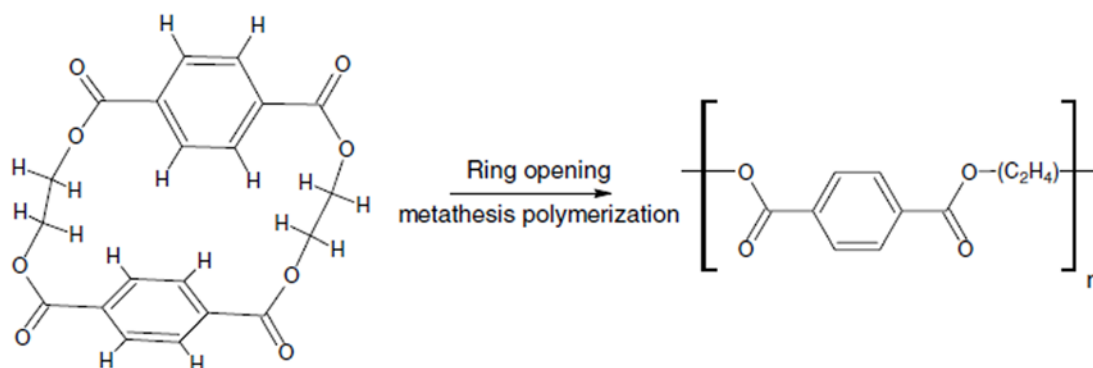


Fig. 2.6: Ring-opening metathesis polymerization of PET, adapted from [1].

**Polycarbonate**

Macrocyclic Bisphenol A with a melting range of 200–210 °C can be polymerized at 240–280 °C into PC through ROMP using anionic activators, as shown in figure 2.7. The initial viscosity of the oligomer melt is 1 Pa·s at 250 °C and the polymerization is completed within 2–5 min, resulting in high molecular weight PC ($M_w$ = 300 kg/mol) with conversions of over 99%. The reaction is entropy driven, in other words no exothermic heat is generated during the polymerization.
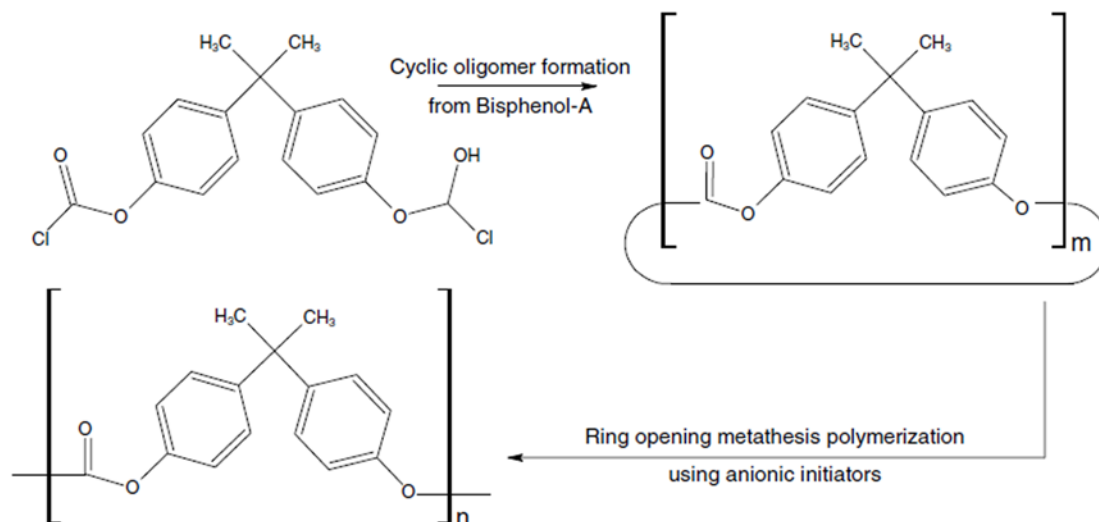
Fig. 2.7: Ring-opening metathesis polymerization of polycarbonates, adapted from [1].

**Reactive polymer systems of high-performance plastics**

Thermoplastic polymers are divided into engineering thermoplastics and high temperature thermoplastics based on the maximum service temperature of the polymers, which in turn depends on their glass transition temperature. This is the temperature at which the amorphous portion of the polymer changes from a glassy to a rubbery phase on heating. Thermoset polymers may not usefully carry mechanic loads above $T_g$, but semi-crystalline thermoplastic polymers may carry load above $T_g$, as only the amorphous phase of the polymer has become rubbery. The crystalline portion of the polymer remains solid until the melting temperature, $T_m$.

Several attempts were made to develop similar technologies for the reactive processing of high-performance plastics, mainly polyarylethers. However, complications arose which were directly related to the inherent properties of high-performance plastics. The extreme stiff polymer backbone combined with outstanding chemical resistance and thermal properties is not easily converted into cyclic oligomers of only a single or a few monomer units. Instead, a much larger number of monomers is required to form so-called macrocyclic precursors of the more rigid high-performance plastics. The higher molecular

weight of these cyclic precursors causes several problems. The cyclic precursors can only be synthesized in high-dilution or pseudo-high-dilution conditions and therefore requires large amount of solvent and leads to relatively low yields. High conversions can only be achieved at high temperatures exceeding the melting point of all oligomers and by keeping the viscosity low enough to induce sufficient chain mobility. However, at too high temperatures (300–400 °C) side reactions like cross-linking occur, which strongly reduce the polymer properties. These problems have been addressed recently by the use of monomer units containing *meta* and *ortho* rather than *para* linkages in order to produce macrocyclics with a lower molecular weight at the cost of  a slight reduction of thermal stability of their equivalent polymer in order to reduce the required polymerization temperature.

**Polyetheretherketone (PEEK)**

Macrocyclics from 4,4-difluorobenzophenone and hydroquinone were synthesized in pseudo-high-dilution conditions at a yield of 60%. They were then polymerized at 350 °C in 5 min using caesium fluoride as initiator, as depicted in figure 2.8.
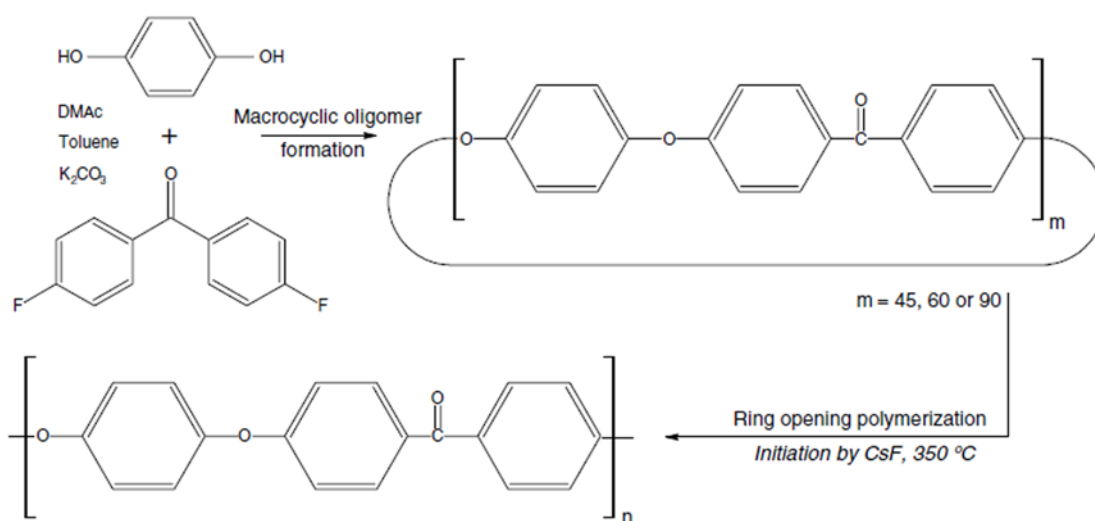


Fig. 2.8: Ring-opening polymerization of macrocyclic PEEK, adapted from [1].

**Polyetherketone (PEK)**

Macrocyclic oligomers of polyetherketones (PEK) were produced at a yield of 54% and were subsequently polymerized at 280 °C for 1 h, reaching a conversion of 93.5%. Work conducted at McGill University, Canada, demonstrated that macrocyclic PEK has a melt viscosity of 80 mPa·s at 330 °C and could be polymerized at 340 °C in 30 min after addition of a nucleophilic initiator.

**Polyethersulfone (PES)**

The ROP of macrocyclic polyethersulphone oligomers was conducted at 300 °C for 2 h, as illustrated in figure 2.9.
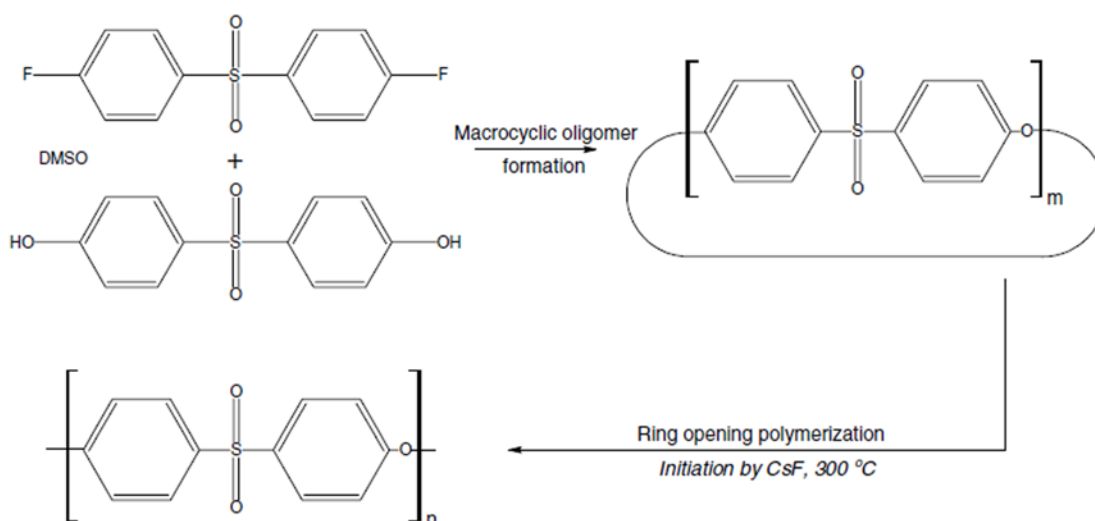


Fig. 2.9: Ring-opening polymerization of macrocyclic PES, adapted from [1].

**Polyphenylenesulfide (PPS)**

The free radical ring-opening polymerization of macrocyclic PPS atmosphere is shown in figure 2.10. When the melt polymerization was done in inert atmosphere at 300 °C, a highly crystalline, high molecular weight PPS was obtained.
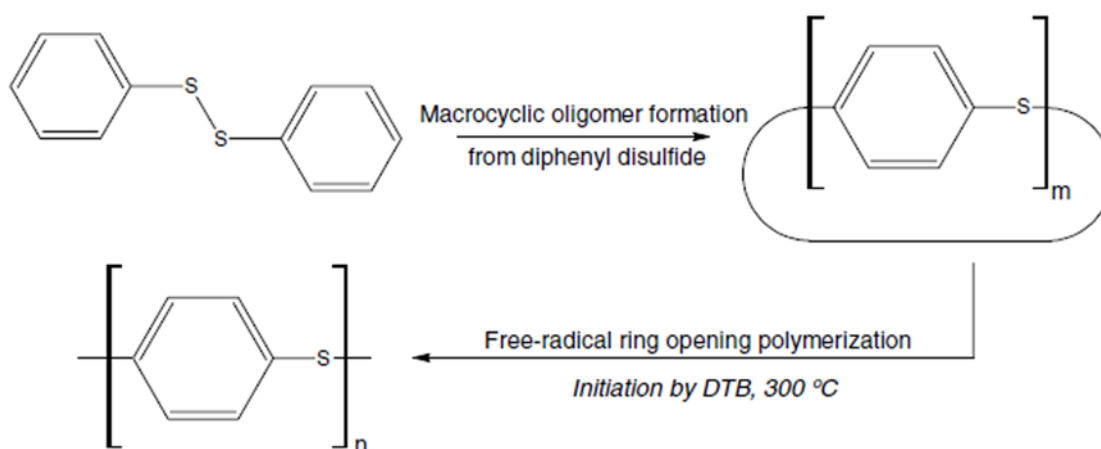
Fig. 2.10: Reactive processing route of PPS, adapted from [1].

**Polyethylenenaphthalate (PEN) and polybutylenenaphthalate (PBN)**

A mixture of macrocyclic PEN oligomers with a melting point of 250–285 °C was prepared in a 57% yield. The ROP was conducted in the presence of a peroxide initiator at 300 °C in 25 min. PBN macrcocylic precursors containing oligomers of various sizes and a melting range of 150–220 °C were prepared at a 75% yield. ROP was subsequently conducted in the presence of a tinoxide catalyst at 275 °C and was completed in 15 min. The linear low molecular weight impurities in the cyclic oligomer mixture strongly affected the final polymer properties. The reactive processing routes of both polymers are shown in figure 2.11.
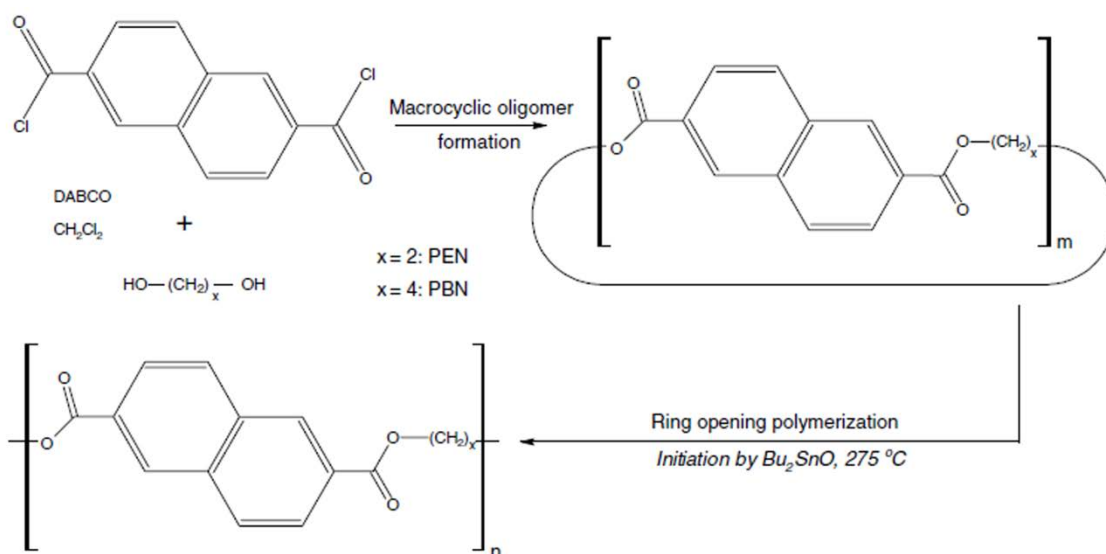
Fig. 2.11: Ring-opening polymerization of macrocyclic PEN and PBN, adapted from [1].

**Melt viscosities and processing temperatures of thermoplastic precursors**

The melt viscosities and processing temperatures of various monomeric and oligomeric thermoplastic precursors as well as for thermoset resins are illustrated in figure 2.12. The melt viscosity of the cyclic precursors is orders of magnitude smaller than the one of their corresponding linear polymer; it is even below the ones of thermoset resins. Moreover, it can be seen that the processing temperatures for engineering plastics are significantly reduced, whereas for high-performance plastics this temperature reduction is relatively small due to the high melting point of the oligomeric precursors. It is noteworthy that pure, discrete cyclic oligomers have very high melting points. Another problem is that some of the small present in the cyclic oligomer families of some high performance polymers and very poor solubilities in the molten larger cyclic oligomers. As a consequence it can be very difficult for them to become incorporated fully into the final linear polymer. In the next section potential processing routes for TPC manufacture with the aforementioned reactive polymer systems are presented.
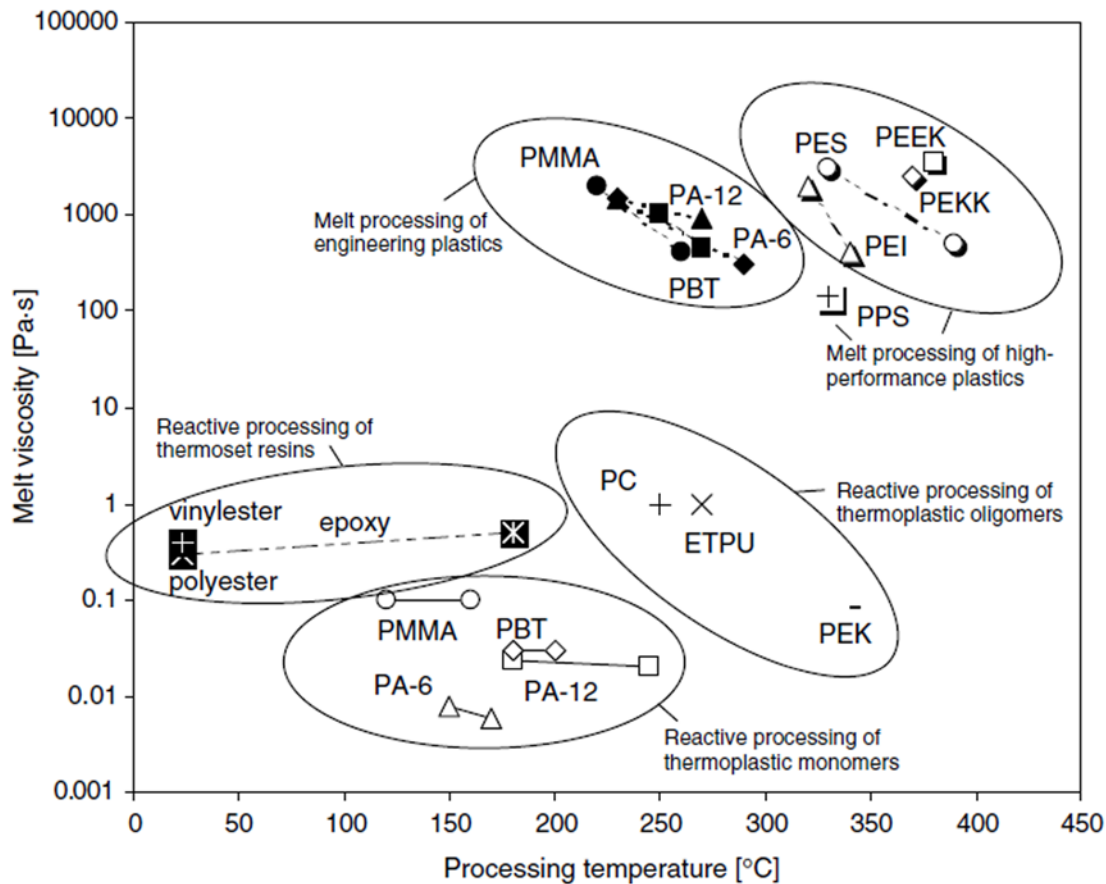
Fig. 2.12: Melt viscosities and processing temperatures of various matrix materials for both reactive and melt processing, adapted from [1].

### 2.2.2 Reactive processing routes

A variety of reactive processing routes can be used for TPC manufacture; most of them belong to the group of liquid composite moulding (LCM). The reactive processing of unreinforced polymer parts or short fibre reinforced composite parts can be achieved by casting, rotational moulding, reaction injection moulding (RIM) and reinforced reaction injection moulding (RRIM) as well as reactive injection pultrusion (RIP) of continuous fibre reinforced profiles. The review of these processes is beyond the scope of this literature review but the interested reader is referred to [1] and the references therein.

Liquid composite moulding has been exclusively used for thermoset matrix composite production due to the required low viscosity below 1 Pa·s, as pointed out in section 2.2. Structural reaction injection moulding, vacuum infusion, resin film infusion and

thermoplastic resin transfer moulding shall be considered here and are schematically illustrated in figure 2.13 [1].

*Structural reaction injection moulding* (SRIM) developed from traditional RIM. Low viscous monomers are injected at 8–10 bar into a mould which carries a dry fibre preform (*c.f.* figure 2.13 a). The polymerization is initiated by mixing the two components prior to injection and the final composite part can be demoulded after polymerization. One of the main advantages of this process is a short cycle time, whereas disadvantages are high tooling costs and limited part size due to limited clamping force of the mould.
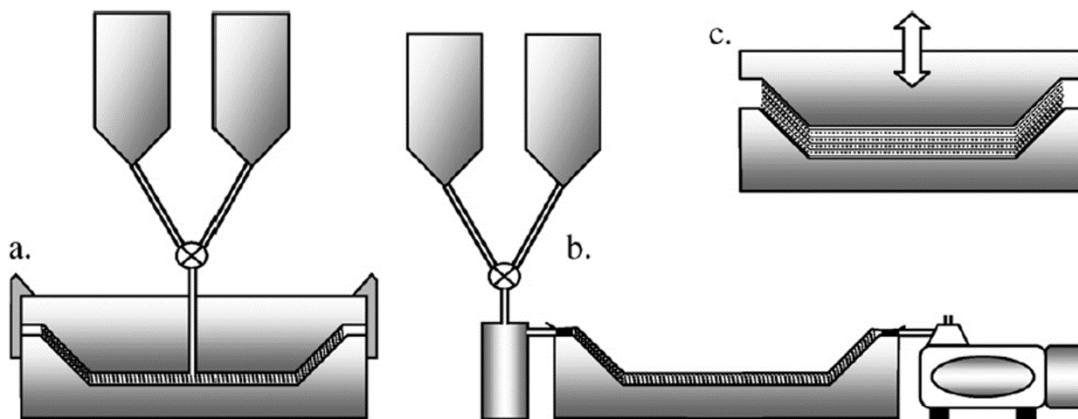


Fig. 2.13: Schematic representation of (a) structural reaction injection moulding, (b) vacuum infusion and (c) resin film infusion, adapted from [1].

*Vacuum infusion* (VI), also known as *Vacuum-assisted resin infusion* (VARI) is a process quite similar to SRIM. The main difference is that the textile reinforcement is infused with resin by applying vacuum at the mould outlet and not by overpressure (*c.f.* figure 2.13 b). Moreover, due to the considerably lower pressure a flexible mould half can be used, resulting in lower tooling costs. However, the flexible mould half leads to a poor surface quality on one side of the product and can often be used only once. The maximum achievable part size is only limited by the pot-life of the reactive system.

*Resin film infusion* (RFI) is similar to prepreg production for thermoset composites. Alternating layers of fibre textiles and sheets of an unreacted reactive mixture are stacked in a mould by hand lay-up (*c.f.* figure 2.13 c). Then heat and pressure are applied and the sheets melt and impregnate the reinforcement after which polymerization initiates. Premature solid-state polymerization or deactivation of the unreacted sheets or prepregs during storage or handling should be avoided. A significant volume reduction of the lay-up takes place during melting and impregnation and often multiple debulking steps are necessary to compress the lay-up. The main advantages of RFI are the easy preparation of the lay-up and the fast impregnation whereas debulking is considered to be the main disadvantage.

*Thermoplastic resin transfer moulding* (TP-RTM) is derived from conventional thermoset resin transfer moulding (RTM). This process has received increasing interest lately due to the advent of a patented liquid system with unlimited shelf life which contains both activator and catalyst for the anionic polymerization of lactams [4-5, 13, 21, 26-28] as well as the newly developed cyclic oligoesters [25, 29]. During the TP-RTM process, a low-viscous reactive resin is injected at relatively low pressure (0.1–1 MPa) into a closed mould which carries a dry reinforcement. The mould needs to be heated during impregnation and polymerization but may be also equipped with a cooling system for fast matrix crystallization. Reinforcement impregnation can be improved by applying vacuum at the mould outlets, known as vacuum-assisted RTM (VARTM). Large and complex parts can be produced with TP-RTM [9, 22]. The process is schematically illustrated in figure 2.14.
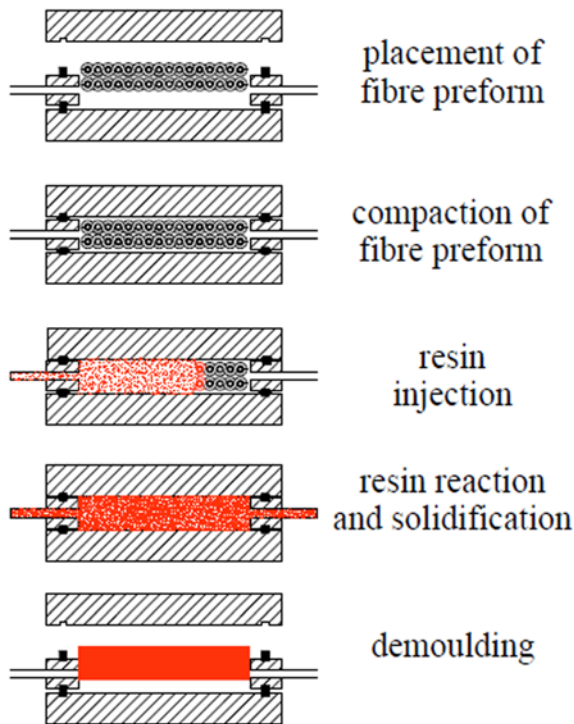
Fig. 2.14: Schematic representation of thermoplastic resin transfer moulding, adapted from [9].

It is important to recognize that there are significant differences between the reactive processing of thermoplastic and thermoset composites [1]. On one hand, the polymerization rate increases with increasing temperature for both thermoplastic and thermoset resins. On the other hand, the crystallization rate of semi-crystalline matrices is adversely affected by temperature. The processing temperature has to be chosen carefully in order to achieve a balanced polymerization and crystallization. Premature crystallization will occur when the temperature is too low, which means that the reactive chain ends and monomer can get trapped inside crystals before they can polymerize. A too high temperature on the other hand reduces the final degree of crystallinity which in turn reduces the strength, stiffness and chemical resistance of the matrix. As pointed out in section 2.2.1, cyclic oligomers have a remarkably low melt viscosity, around an order of magnitude lower than the one of common thermoset resins. Consequently, significant capillary forces occur during reinforcement impregnation and may form voids. Another difference is that most thermoset resins are liquid at room temperature while most

thermoplastic precursors are still solid. Therefore heated processing equipment is necessary to avoid a cooling down of the unreacted mixture.

## 2.3 Cyclic butylene terephthalate

This section gives an overview over current cyclic butylene terephthalate technology, *i.e.* CBT synthesis, ring-opening polymerization and properties of the resulting polymerized CBT (referred to as pCBT to distinguish from conventional PBT obtained by polycondensation reaction). The processing-structure-properties relationship of pCBT obtained by different processing routes is critically reviewed. CBT modifications such as blending or copolymerization with other mono- or polymers, pCBT micro- and nanocomposites with different types of reinforcement as well as continuous fibre reinforced pCBT composites are summarised.

### 2.3.1 Extraction of cyclic oligomers from polyesters

As already mentioned in section 2.2.1, conventional polyesters contain small amounts of cyclic oligomers. The latter can create problems during fibre processing such as spinning and dyeing [16, 30]. Moreover, they can significantly affect the properties of the polymer by acting as a plasticiser [31]. Cyclic oligomers usually can be extracted from the polymer by the Soxhlet extraction method using solvents such as chloroform, dioxane, dichloromethane or xylene. They can also be removed with dissolution methods. The polyester is dissolved in a solvent, such as phenol and tetrachloroethane mixture, dimethyl formamide, or 1,1,1,3,3,3-hexafluoro-2-propanol. The solution is cooled down, and then a nonsolvent is added (dioxane or chloroform), which precipitates the polymer. The solution is filtered off and evaporated to obtain dry oligomers. Cyclic oligomer removal is currently not practiced in industry [16].

During this procedure, solvent-induced crystallization (SINC) of the oligomers can occur [32-37]. Slow cooling of an oligomer-containing solution can create multiple prisms

at a single-crystal nucleation site, such as the star-like crystal habits illustrated in figure 2.15.



Fig. 2.15: Scanning electron microscopy showing the particle morphology of cyclic PET oligomer crystals produced by solvent-induced crystallization in hexadecane, adapted from [32].

### 2.3.2  Synthesis

The synthesis and possible applications of cyclic oligomers have been reviewed by several researchers [15-16, 31, 38-40]. As mentioned earlier, cyclic oligomers of condensation polymers have long been known. Condensation polymerization is a step growth mechanism which involves *intermolecular* reactions between monomer, oligomer or polymer end groups. Nevertheless, for statistical reasons *intramolecular* reactions between the end groups of the same molecule occasionally occur if the polycondensation is carried out at high concentrations, leading to cyclic oligomers. Unfortunately, conventional bulk

condensation polymerization yields only small amounts of cyclic oligomers. Direct synthesis of cyclic oligomers as major product can be achieved using conditions of high dilution, *i.e.* low concentrations of oligomers and polymer. These conditions favour intramolecular reactions over intermolecular reactions. It is a reaction at high dilution of diol and diacid, or diacid and diester, or diester only in the presence of a highly unhindered amine such as 1,4-diazabicyclo[2,2,2]octane (DABCO) [16]. The reaction is shown in figure 2.16. Since the condition of high dilution needs a large amount of solvent, this synthesis route is not very practical. It is more practical to obtain large amounts of cyclic oligomers by pseudo-high dilution, polymer-supported synthesis or cyclo-depolymerization rather than the real high dilution condition.
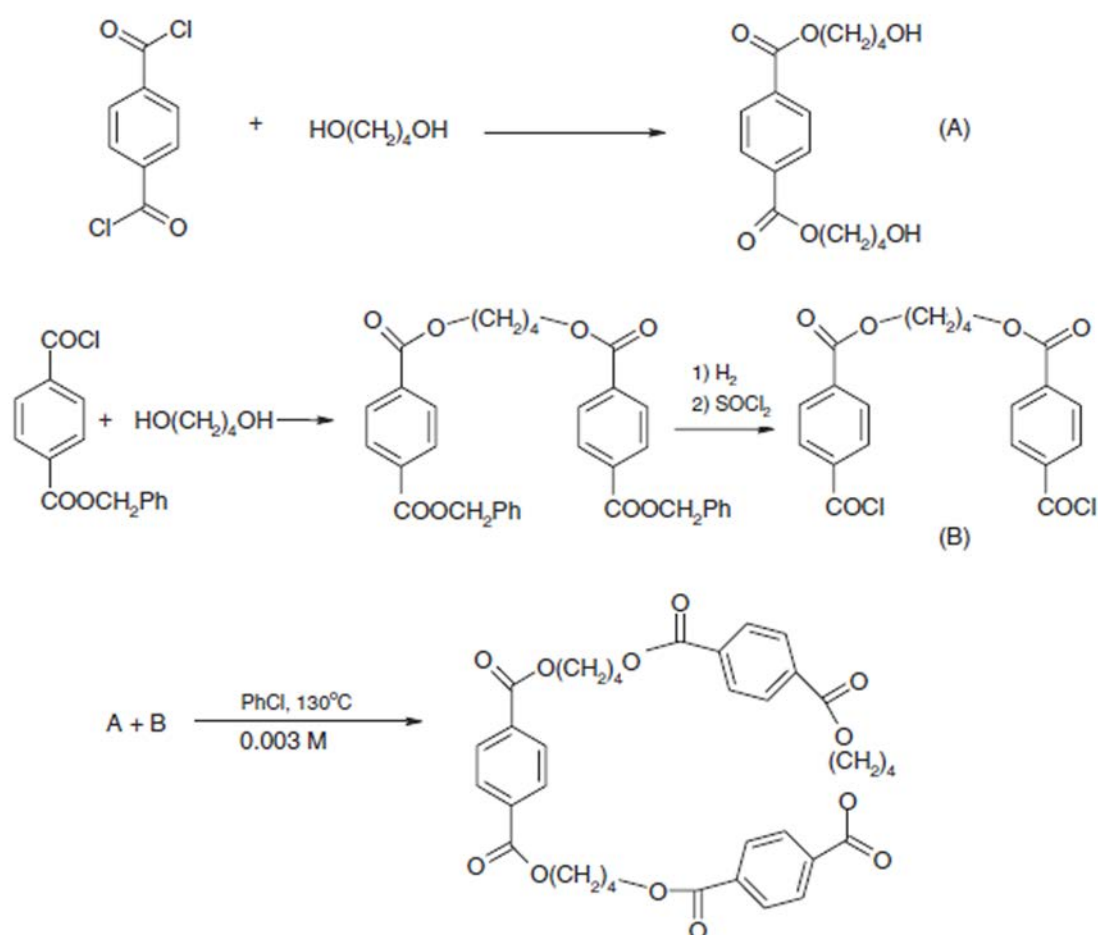


Fig. 2.16: Preparation of CBT oligomers by the classical high dilution method, adapted from [41].

**Pseudo-high dilution**

The use of high dilution conditions is the classical strategy for the synthesis cyclic oligomers. If the cyclic products are formed irreversibly, it is only necessary for the reactants themselves to be present at high dilution. Therefore solutions with a relatively high concentration of cyclic oligomers can be prepared. Moreover, large amounts of solvent are not necessary. Such syntheses are said to use pseudo-high dilution conditions and are more practical than simple high dilution conditions. The pseudo-high dilution route is illustrated in figure 2.17 and has been used to synthesize a wide variety of cyclic oligomers. For instance, cyclic polyamide 11, cyclic alkylene phthalates, cyclic polyetherketones, cyclic polyetheretherketones, cyclic polyethersulphones and cyclic polyetherketonesulphones have been reported [15-16].
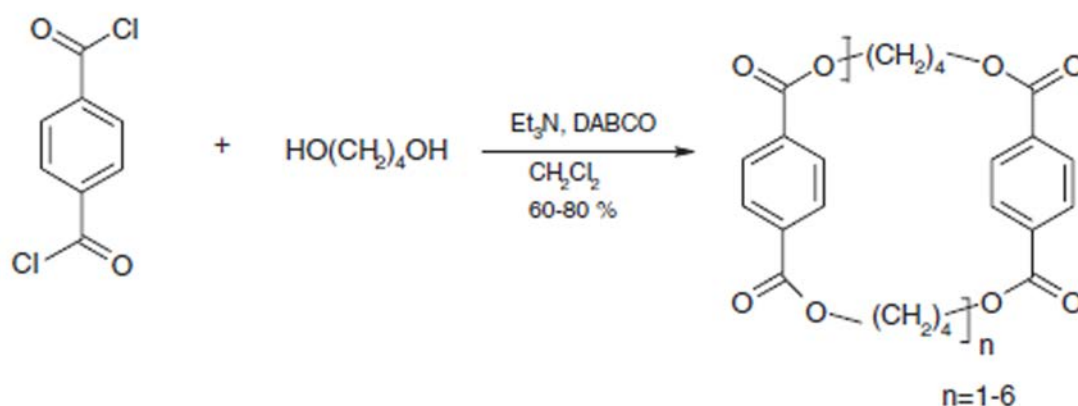


Fig. 2.17: Preparation of CBT oligomers by the pseudo-high dilution method, adapted from [41].

**Polymer supported synthesis**

The various syntheses in dilution conditions discussed above tend to produce some linear products together with the cyclic oligomers. The mixtures can be separated on the basis of solubility differences but this is not always the case. Polymer-supported syntheses start with A-B type monomers and achieve separations by covalent bonding of one of the types of end groups to crosslinked polymer beads. The monomers are linked with one type of

end group only to the polymer beads. Then chain growth and cyclization take place. If linear oligomers are produced in these reactions, then an end group of the linears remains bonded to the insoluble polymer beads. On the other hand, if cyclic oligomers are produced, the latter are released into solution. At the end of the reaction the polymer beads are simply filtered off and the cyclics are recovered by evaporation of the solvent. Nylon 6, nylon 11, ester and ester-amide cyclics could be produced with this synthesis route. Nevertheless, this method is only suitable for small-sale synthesis [16, 40, 42].

**Cyclo-depolymerization**

The cyclo-depolymerization (CDP), also known as ring-closing depolymerization, has been reviewed very recently by Hodge [43]. CDP uses linear polyesters to form cyclic oligomers and thus it is a suitable technique for the recycling of polyesters. An overview of the reported cyclics from different polymers is beyond the scope of this literature review, therefore the interested reader is referred to following references and the references therein [16-17, 30-32, 38-47].

The cyclic formation mechanism *via* CDP is basically a transesterification mechanism and is simply the reverse of an entropically driven ring-opening polymerization [30], which will be discussed later. Depolymerization is typically carried out by refluxing the starting polymer in a dilute solution for several hours in the presence of organotin or titanate catalysts. The ester bonds from the polymer are repeatedly broken and then recombined in an equilibration process. The remaining polymer is then removed from the solution by precipitation [16].

The mechanism for formation of CBT *via* cyclo-depolymerization of PBT is shown in figure 2.18. Brunelle *et al.* [17] used commercial PBT for CDP by dissolving the polymer in dry ortho-dichloro-benzene (o-DCB) at reflux and then adding the equilibration catalyst. Metal alkoxides such as tetraalkyl titanates or dibutyl tin alkoxides have proven to be the most effective catalysts for cyclo-depolymerization of PBT.
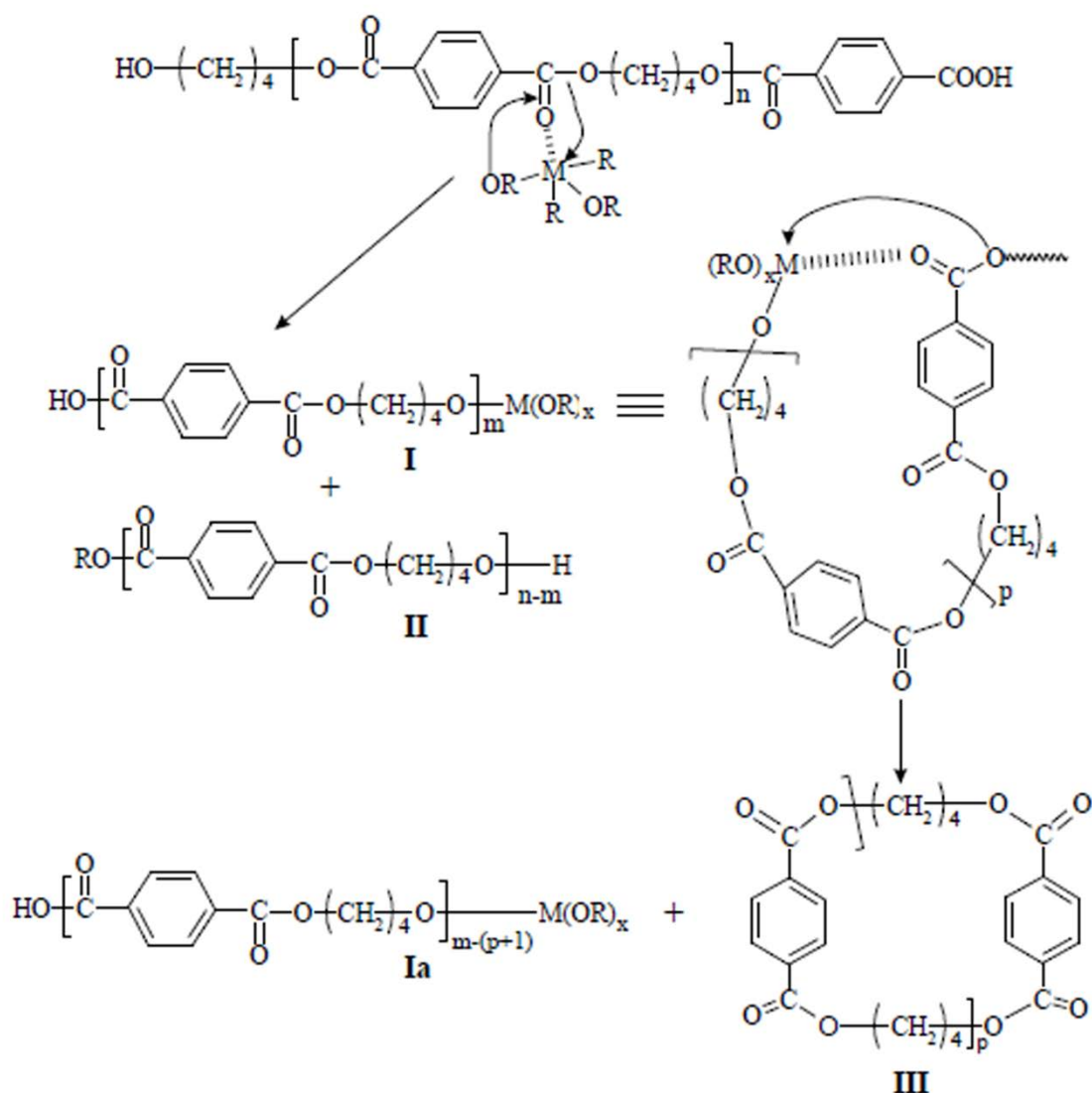
Fig. 2.18: Mechanism for metal alkoxide catalysed formation of cyclics *via* cyclo-depolymerization of PBT, adapted from [17].

The mechanism is as follows [17]. The metal alkoxides activate a carbonyl group of the PBT chain *via* complexation and then transfer an alkoxide ligand. As a consequence, the linear PBT interacts with the metal alkoxide catalyst and transfers an alkoxide onto the polymer chain, forming a species such as **I** and releasing a linear alkoxide which is terminated with the transferred ligand (**II**). The original polymer chain length ($n$) will be decreased by $m$ units in this reaction. The metal terminated polymer **I** can then react either by chain-chain transfer (polymerization reaction), or by a back-biting reaction to form cyclic oligomers. The degree of cyclization versus polymerization can only be controlled by the

concentration of species **I** in the solution. Dilute solutions favour *intra-* rather than *inter*molecular reactions. Cyclization to cyclics with degree of polymerization *p+1* releases another linear polymer chain terminated with a metal (**Ia**) which is shorter in length by *p+1* units and which can continue to react to form cyclics. Eventually, equilibrium is reached and the linear chains (**I**, **Ia**, **II**) react degenerately at the same rate as they form cyclics. A mixture of cyclic oligomers is being formed during this reaction. An attempt to correlate the experimental ring-size distribution to theory has been presented by Hubbard *et al.* [48].

Cyclics Corporation produces the CBT oligomers as a mixture of dimer, trimer and larger cyclic oligomers *via* depolymerization of commercial PBT [25, 29] and various patents are filed for this process (see for instance [49-50]).

### 2.3.3  Structure

The structure of CBT oligomers is displayed in figure 2.19. CBT is a mixture of oligomers having two to seven repeat units, *i.e.* ranging from cyclic dimer to cyclic heptamer [41]. An oligomer mixture has the advantage of melting point reduction, since pure, discrete cyclic have relatively high melting points. CBT softens at 140 °C and is completely molten at 160–190 °C, whereas the pure cyclic dimer melts at 196 °C [14] the pure cyclic tetramer melts at 248 °C [24]. This results in an initial melt viscosity of 0.02 Pa·s at 190 °C [3], whereas the dynamic viscosity of conventional PBT at 250 °C was reported to be around 1000 Pa·s [51].



n = 1-6
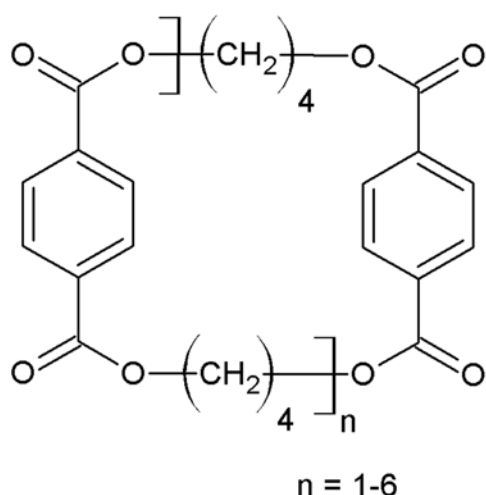
Fig. 2.19: Chemical structure of CBT oligomers, after [41].

### 2.3.4 Ring-opening polymerization

As mentioned earlier, ring-opening polymerizations (ROPs) are essentially the reverse of cyclo-depolymerizations. Both ROP and CDP are equilibration processes where the ester linkages are repeatedly broken and re-formed. Contrary to CDP however, reactions between oligomers are favoured over cyclizations in ROP because the equilibration is carried out at high oligomer concentrations.

Ring-opening polymerization exhibits some advantages over conventional step polymerization, namely higher molecular weights (up to 300 kg/mol) can be more readily achieved. Contrary to that, conventional step-growth polymerization typically yields molecular weights of 40–60 kg/mol [16]. Since in ring-opening polymerizations the broken bonds are simply re-formed, no exotherms or volatile organic compounds (VOCs) are released. The final molecular weight of the polymer solely depends on the molar ratio of cyclic oligoesters to linear end groups. Examples for the latter are a linear catalyst, humidity or remaining linear oligomers present the system [14, 42]. The molecular weight can rise quickly to a high value and since ROP is an equilibration process, the molecular weight dispersity is expected to be 2.0.

Despite the numerous advantages, ED-ROPs have also drawbacks. For instance, with proceeding polymerization the molecular weight and the viscosity rise too which in turn can seriously slow down the polymerization. This means that generally the polymerization temperature should at least exceed $T_m$ of the final polymer. In the case of certain high performance polymers the high polymerization temperatures can lead to undesired side reactions. Another problem is that some small cyclics present in the cyclic oligomer families of some high performance polymers have very high melting points and very poor solubilities in the molten larger cyclic oligomers. Consequently, the small cyclics might not become fully incorporated into the final linear polymer.

The ring-opening polymerization mechanism of CBT is displayed in figure 2.20. Although many types of compounds were reported to initiate the ROP of cyclic oligoesters, certain tin and titanium initiators were found to be most effective [41]. The role of the different available catalyst systems for the ROP of CBT will be discussed more in detail in the following section. The ring-opening polymerization mechanism has been explained by various researchers [41, 52-53] and is analogous to conventional ROP with initiation and propagation steps. The catalyst is thought to operate by Lewis acid activation of a CBT

ester group *via* complexation and then transferring an alkoxide ligand. This results in an active species which has a functional group originating from the initiator as end group. Propagation proceeds by coordination of another cyclic oligomer to the active species, followed by insertion of the cyclic into the metal-oxygen bond by rearrangement of the electrons. The process is repeated and more cyclics are successively added to the propagating linear polymer chain. The propagation reactions continue until all cyclics are depleted and the ring-chain equilibration becomes degenerate. In this case, the initiator becomes built into the polymer, which is not terminated unless quenched [17, 41, 52].

**Initiation:**
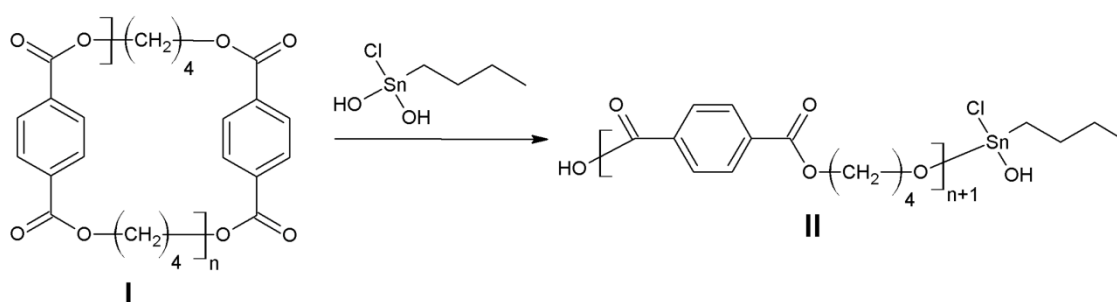


**Propagation:**
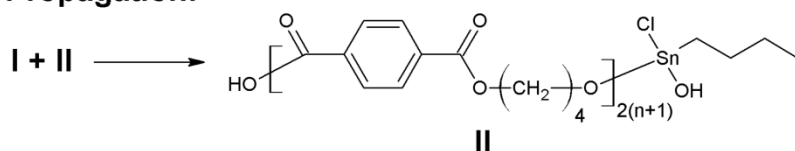


Fig. 2.20: Initiation and propagation steps during the ring-opening polymerization of CBT using a tin-based catalyst, after [41].

Cyclic oligomers exhibit almost no ring strain due to their large size. Consequently, the polymerization is almost thermoneutral which leads to complete equilibration of ester groups. In other words, initiation, propagation, and chain transfer have nearly the same rates [17]. Since the number of bonds in the final linear polymer is essentially the same as in the starting oligomers and since the oligomers are not significantly strained, there is little or no change in enthalpy related to the equilibration. The conversion from cyclics to polymer is therefore mainly driven by the change in entropy. This means that the cyclic oligomers have only limited translational entropy as well as limited available conformations

('conformational strain') owing to their cyclic nature. However, there is a significant increase in conformational entropy (although there is only a modest change in translational entropy) when the rings open [30]. Three factors control the final degree of conversion from cyclics to polymer during ROP [41]:

i)      purity of the monomers

ii)     complete mixing of the initiator and oligomers before ROP causes the viscosity to increase to the point where mixing is inefficient

iii)    polymerization at a high enough rate that polymerization is essentially complete before crystallization occurs.

### 2.3.5  Catalyst systems

Tripathy and associates [54] studied the effects of different catalysts and polymerization temperatures on the ROP of CBT. They melt blended CBT oligomers and catalyst at 160 °C and conducted the ROP at 185–205 °C. The used catalysts were cyclic stannoxane (**I**), butyltin chloride dihydroxide (**II**), and tetrakis-(2-ethylhexyl) titanate (**III**); their chemical structures are shown in figure 2.21.
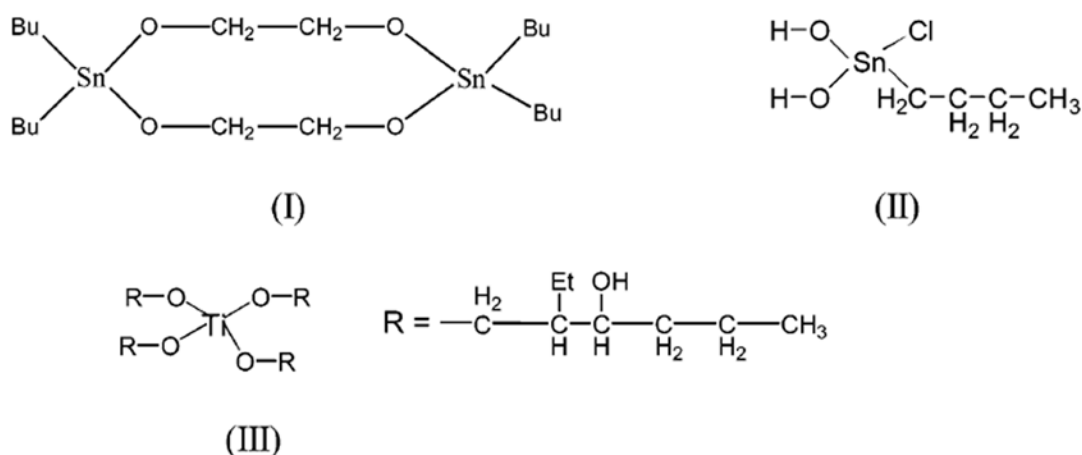


Fig. 2.21: CBT catalyst systems stannoxane (I), butyltin chloride dihydroxide (II) and tetrakis-(2-ethylhexyl) titanate (III), adapted from [54].

The authors analyzed the extent of polymerization by monitoring the change in light transmittance intensity at several temperatures of polymerization, ranging from 185 to 205 °C *via* time-resolved small-angle light scattering. Since the ROP was conducted below the pCBT melting temperature, it was assumed that crystallization followed polymerization (in the chosen polymerization temperature). The crystallization resulted in the loss of light intensity due to scattering from heterogeneous clusters of pCBT polymer crystals. They reported that cyclic stannoxane was the fastest catalyst and completed the *in situ* polymerization within 2–3 min at polymerization temperatures of 165 °C and above. On the other hand, about 15 min of induction time was reported for butyltin chloride dihydroxide and tetrakis-(2-ethylhexyl) titanate which is desired for RTM processes. Furthermore, the authors used gel permeation chromatography (GPC) to find the conditions for the highest possible conversion and highest molecular weight; results are shown in table 2.1.

Initiator (**III**) gave the highest molecular weight among all used initiators, and the molecular weight remained the same irrespective of polymerization temperature. The pCBT samples obtained using catalysts (**II**) and (**I**) have the lowest and the intermediate molecular weights, respectively (*c.f.* table 2.1). When cyclic stannoxane (**I**) was used as initiator, no decrease in molecular weight was observed with increasing catalyst level because no end groups were introduced [41]. The ROP of CBT initiated with cyclic stannoxane is a ring-expansion mechanism which results in a macrocyclic pCBT, as shown in figure 2.22. Macrocyclic pCBT is referred to c-pCBT in order to distinguish it from linear pCBT.
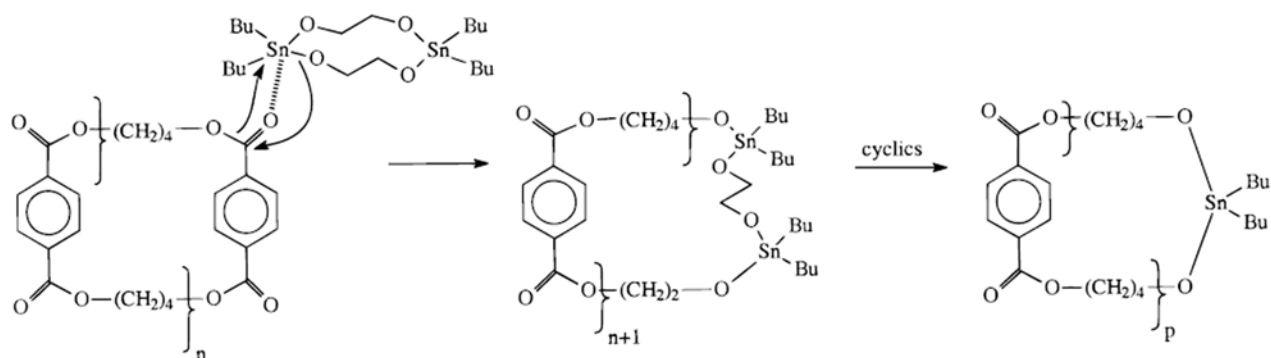


Fig. 2.22: Incorporation of cyclic stannoxane initiator into CBT and ring-expansion mechanism of macrocyclic c-pCBT, adapted from [41].

Table 2.1: Molecular weights and polydispersities of pCBT polymerized at different temperatures and with different catalysts, after [54].

| catalytic system | $T_p$ (°C) | conversion (%) | $M_n$ [kg/mol] | PDI ($M_w/M_n$) |
|---|---|---|---|---|
| stannoxane (**I**) | 175 | 83 | 45.0 | 2.7 |
| | 180 | 84 | 41.6 | 2.9 |
| | 185 | 84 | 41.0 | 2.9 |
| | 190 | 92 | 41.8 | 2.7 |
| | 195 | 94 | 42.2 | 2.8 |
| butyltin chloride dihydroxide (**II**) | 185 | 65 | 31.6 | 2.6 |
| | 190 | 77 | 34.8 | 2.6 |
| | 195 | 93 | 46.6 | 2.6 |
| | 200 | 94 | 46.2 | 2.6 |
| | 205 | 97 | 50.1 | 2.6 |
| tetrakis-(2-ethylhexyl) titanate (**III**) | 185 | 84 | 54.8 | 2.5 |
| | 190 | 87 | 55.1 | 2.4 |
| | 195 | 94 | 57.7 | 2.5 |
| | 200 | 95 | 54.7 | 2.5 |
| | 205 | 92 | 52.0 | 2.6 |

It is noteworthy that the catalyst system used throughout the thesis at hand was butyltin chloride dihydroxide (**II**). Although the above results demonstrate that this initiator results in a relatively low molecular weight, yet the commercially available one-component CBT160® resin contains 0.45 wt.% butyl tin chloride dihydroxide as catalyst [55]. The two-component CBT100® resin is provided with the same catalyst in form of Fascat® 4105 [56].

### 2.3.6  Conditioning

The final molecular weight of the pCBT depends on the amount of linear end groups (*i.e.* humidity) present during polymerization, as already mentioned in section 2.3.4. For this reason, a consequent drying of the CBT prior to processing is crucial. Steeg [57] studied in cooperation with Cyclics Europe GmbH the conditioning of CBT granules and powder. They dried the CBT in a circulating air oven at 80 and 100 °C and measured then the CBT water content over drying time *via* Karl-Fischer-titration (*c.f.* figure 2.23 a). It was stated that a CBT water content of <200 and <125 ppm results in a molecular weight of >100 and >150 kg/mol of the final pCBT, respectively. The lower limit of 125 ppm was reached after 1.5 h drying time at 100 °C. When vacuum was added, then this limit was already reached after 30 min. On the other hand, it took 5 h to reach a water content of 200 ppm at a drying temperature of 80 °C. Moreover, it was pointed out that excessive drying times (>36 h) leads to decreasing molecular weight and degree of conversion, probably due to catalyst inhibition.
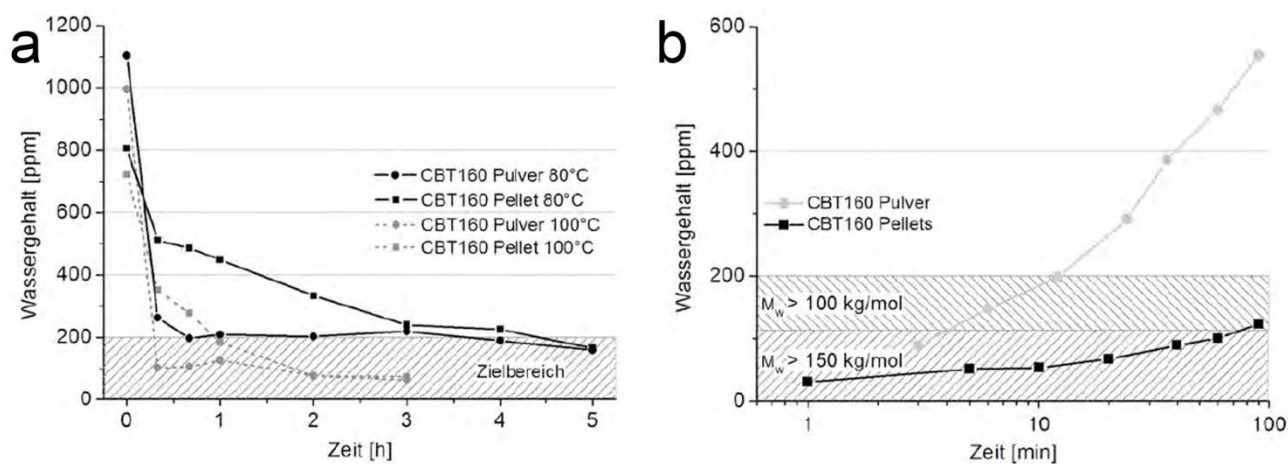


Fig. 2.23: Conditioning of CBT160 powder (●) and pellets (■) at 80 and 100 °C. CBT water content over drying time (a) and water uptake of dry CBT in ambient atmosphere at 60% relative humidity over time, adapted from [57].

In a further step, the water absorption of CBT was measured. First, CBT was dried in the circulating air oven at 100 °C for 5 h. Then the dried CBT was conditioned in ambient

atmosphere with a relative humidity of 60% and the water uptake was measured again using Karl-Fischer-titration. The results are shown in figure 2.23 b; hatched areas indicate the two humidity limits with corresponding achievable molecular weights, as mentioned above. Since powder particles exhibit a much higher surface-to-volume ratio as compared to pellets, the former adsorb humidity much faster. From a processing point of view, CBT powder exceeds the lower humidity limit of 125 ppm already after 4 min, whereas CBT pellets can be processed without the risk of catalyst inhibition even after being exposed to high humidity for 2 h.

### 2.3.7  Polymerization kinetics

The polymerization kinetics of CBT mainly depends on the type and amount of catalyst as well as on the processing temperature and has been studied by various techniques. Hakmé *et al.* [58] investigated the *in situ* monitoring of the ROP of CBT by dielectric sensing under isothermal conditions at different processing temperatures. Small electrical sensors were therefore introduced in the processing tool. The conductivity signal reflected the local viscosity of the molten CBT and decreased when the polymerization progressed or when the fraction of the amorphous phase decreased during crystallization. Therefore the change in conductivity depended on the increase of molecular weight but was also influenced by pCBT crystallization during or after polymerization. Dielectric sensing investigations were compared to GPC and differential scanning calorimetry (DSC) analysis and were found to agree well. The electrical conductivities as measured by dielectric sensing are illustrated in figure 2.24.
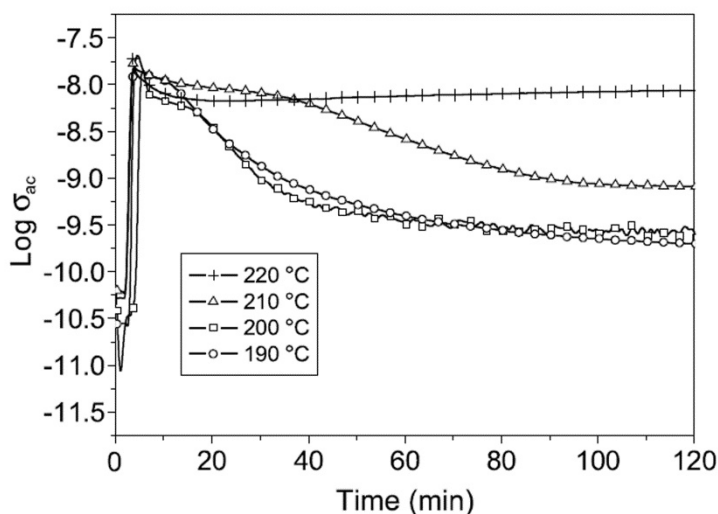
Fig. 2.24: *In situ* monitoring of the electrical conductivity by dielectric sensing at 10 Hz for several polymerization temperatures, adapted from [58].

They reported that simultaneous polymerization and crystallization occurs below 200 °C, whereas polymerization is followed by crystallization above 200 °C, and only polymerization occurs above 220 °C. Therefore it can be assumed that the processing conditions affect the crystal morphology. The influence of the morphology on the final properties of pCBT will be discussed later. At 220 °C only polymerization occurred, hence the small conductivity decrease was only related to the viscosity increase during the molecular weight build-up. At 210 °C the same small decrease related to the polymerization was observed, followed by another conductivity decrease related to the crystallization of the pCBT. Unfortunately, dielectric sensing could not distinguish between the polymerization and crystallization when they occurred simultaneously at temperatures below 210 °C. Therefore, this technique is suitable only to some extend to measure the polymerization kinetics of CBT.

GPC is a more direct technique which measures the amount of unreacted oligomers as well as the amount of pCBT polymer; therefore the degree of conversion $\alpha$ can be determined. Steeg and co-workers [51] determined the polymerization kinetics of CBT from over 200 single GPC measurements performed under isothermal conditions; results are depicted in figure 2.25.
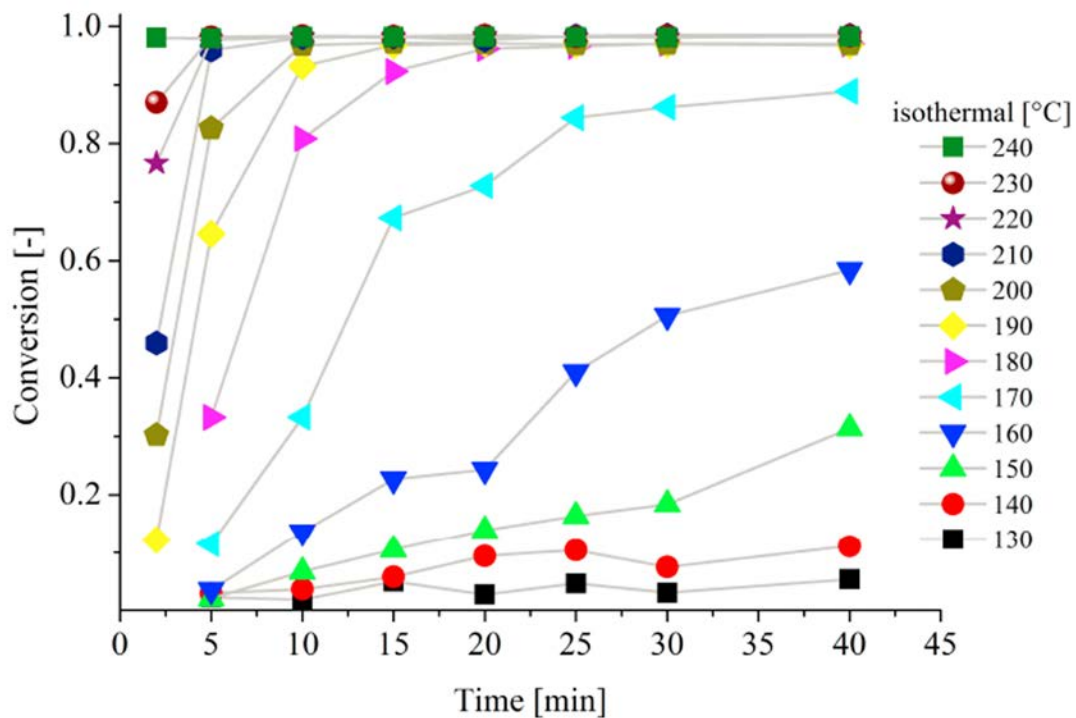
Fig. 2.25: Conversion data for isothermal polymerization of CBT based on GPC data, adapted from [51].

## Modeling of the polymerization kinetics of CBT

The polymerization kinetics can be also assessed by rheological measurements. Chen *et al.* [52] used a rheometer as a chemical reactor to monitor the ROP of CBT initiated by butylchlorotin dihydroxide. The authors found that both the complex viscosity and the modulus variation could be efficiently used to determine the degree of polymerization. Figure 2.26 illustrates the variation of the complex viscosity of CBT polymerized at different temperatures and also the modelled polymerization kinetics deduced from the rheological measurements.
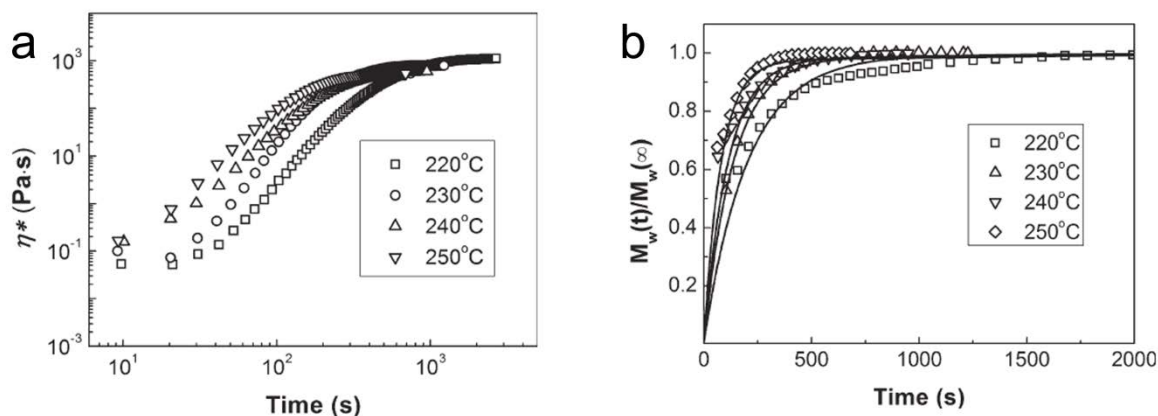
Fig. 2.26: Variation of complex viscosity of CBT with time (a) and variations of the relative molecular weight $M_w (t)/M_w (\propto)$ with time at different temperatures, adapted from [52].

They concluded from the viscosity measurements that it takes about 35, 16, 14, and 9 min to reach the plateau at 220, 230, 240, and 250 °C, respectively (*c.f.* figure 2.26 a). The complex viscosity, elastic and viscous modulus during the polymerization served to build up a method to determine the molecular weight and polymer concentration variation versus the reaction time. Additionally, they developed polymerization kinetics equations in order to simulate the polymerization process (*c.f.* figure 2.26 b). These equations could fit the molecular weight variation calculated by viscoelastic functions at arbitrary temperature. By fitting the molecular weight variation with kinetics equations, polymerization rate constants were determined at various temperatures. The authors reported that the molecular weight increased faster with increasing temperature due to the high polymerization rate and it took a shorter time to reach constant values. As the temperature increased, it took approximately 30, 13, 12, and 7 min for $M_w (t)/M_w (\propto)$ to reach steady values, respectively. This suggested that the weight average molecular weight did not change after that time. The trend is consistent with the results evaluated from the time evolution of complex viscosity in figure 2.26 a. Nevertheless, the polymerization time based on molecular weight in figure 2.26 b is systematically shorter as compared to the one from viscosity measurements.

Steeg *et al.* [51] measured conversion and viscosity of CBT using GPC and rheometer. The authors derived and optimized an Arrhenius-based conversion model from GPC results in order to predict the conversion of CBT under isothermal conditions. They

extended and validated the model up to an analytical conversion model for non-isothermal conditions. Furthermore, they successfully linked the conversion data with the dynamic viscosity. The results were validated and optimized by means of isothermal rheological measurements and a model, shown in figure 2.27, was generated that predicts conversion and dynamic viscosity for every thermal condition.
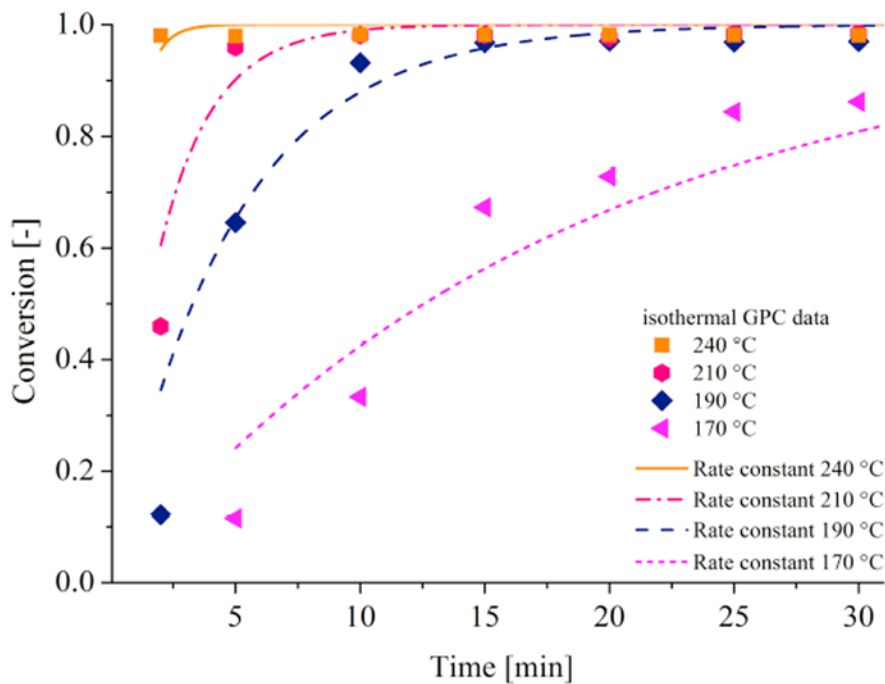


Fig. 2.27: Polymerization kinetics modelled with first order ordinary differential equation model from isothermal GPC data, adapted from [51].

### 2.3.8  Processing window

The processing window can be defined as the time for the molten CBT to reach a viscosity of 1 Pa·s, as pointed out in section 2.2. Therefore, the processing window is mainly governed by the polymerization kinetics. Mohd Ishak and co-workers [3] used rheological measurements to determine the melt viscosity increase with time and used the rheological data as an indirect tool to estimate the impregnation and apparent polymerization times; depicted in figure 2.28.
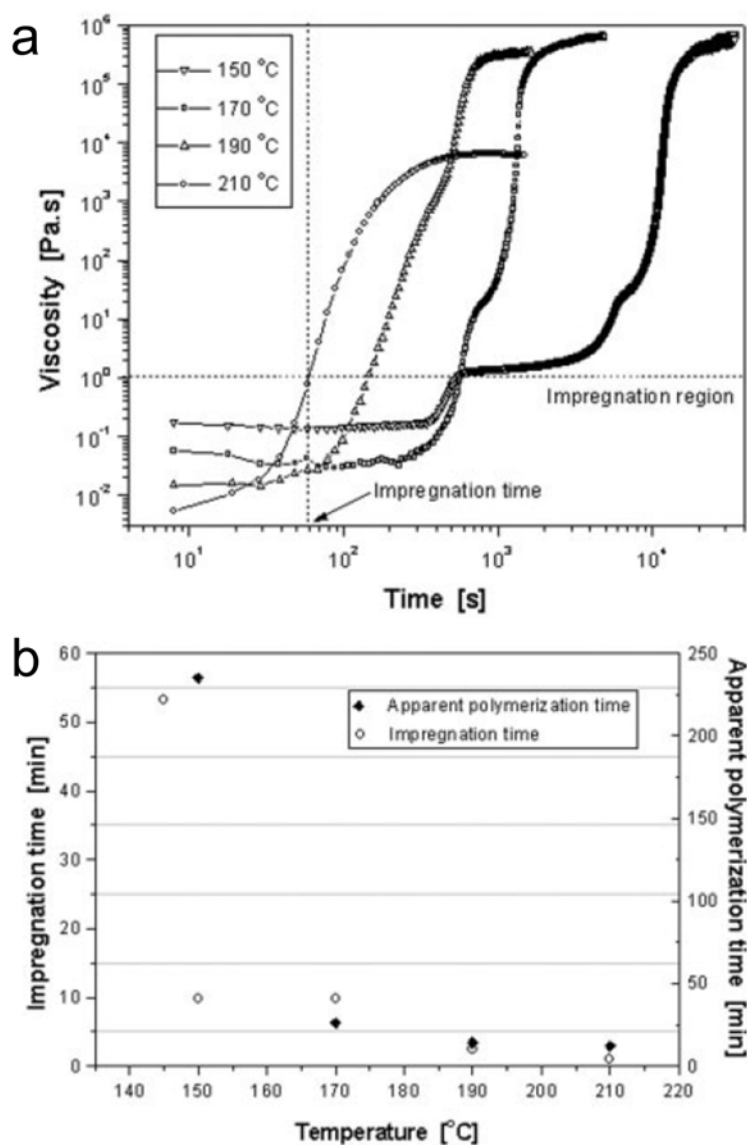
Fig. 2.28: Effect of testing temperatures on the variation of melt viscosity with time (a) and impregnation time and apparent polymerization time as a function of temperature (b), adapted from [3].

A phase angle of almost zero indicated the total transformation of the polymerized CBT into a solid phase *via* crystallization and a tangent could be drawn to the phase angle curve. An apparent polymerization time could then be obtained from the intersection of the tangent to the curve; whereas the impregnation time was simply the time when viscosity reached 1 Pa·s. A drastic reduction was found in the apparent polymerization time when the testing temperature increased from 150 to 170 °C. They assumed a rapid ring-opening polymerization at high temperatures due to the short apparent polymerization times for

temperatures 170°C and above. At a temperature of 210 °C, the viscosity limit of 1 Pa·s was already reached after around 1 min, whereas the same viscosity was reached after almost 1 h at a low temperature of 145 °C.

### 2.3.9 Crystallization

One of the main advantages of CBT over other reactive systems is that there are generally two processing routes, namely polymerization *below* or *above* the melting temperature of pCBT (≈225°C). In the latter case the ROP of CBT takes place in the molten state. Hence polymerization and crystallization are separate processes and the processing is non-isothermal. If the ROP is conducted below the $T_m$ of pCBT, namely below 200 °C as stated in [58], then crystallization during polymerization is possible and processing can be performed isothermally.

**Crystallization during polymerization**

According to Wunderlich [59-60], crystallization during polymerization can be either simultaneous or successive.
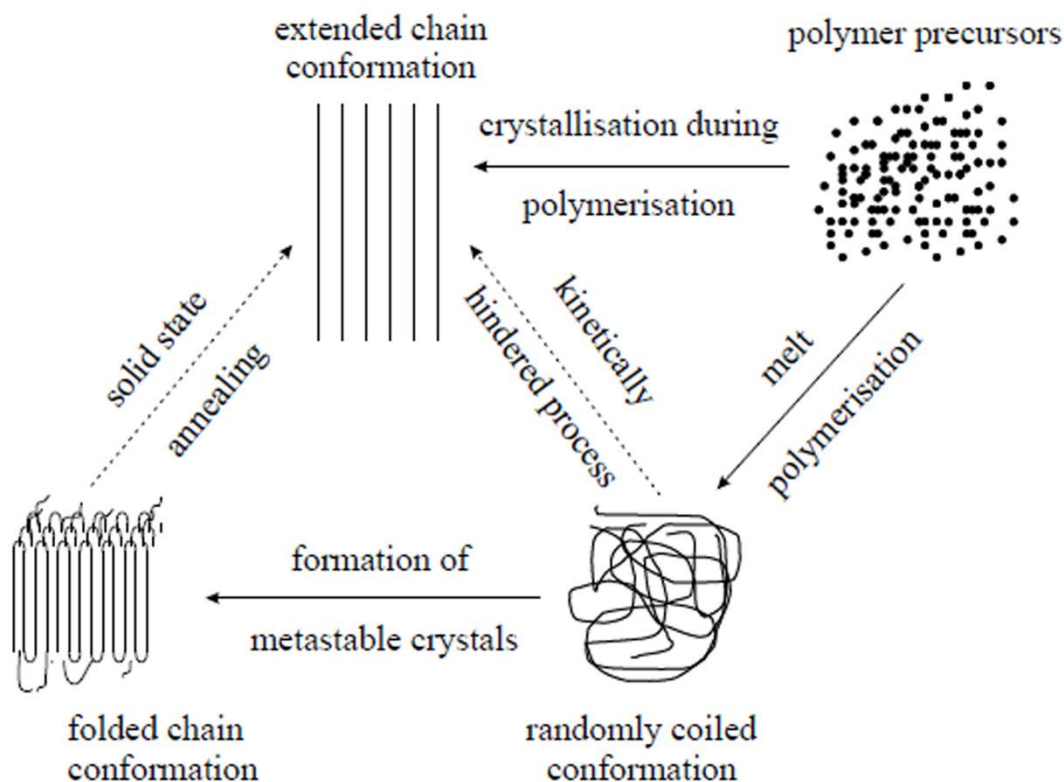
Fig. 2.29: Possible chain conformations in polymers, adapted from [60].

In the first case both processes are truly simultaneous, *i.e.* a mobile oligomer is added to the growing pCBT crystal and both covalent bonds (due to the ROP) and secondary bonds (due to crystallization) are set at the same time. In the second case, polymerisation is followed successively by crystallisation *before* polymerisation is completed. The described scenarios result in different morphologies. While separate polymerization and crystallization usually produces folded chain lamellar crystals, crystallization during polymerization can produce fibrillar extended chain crystals, as schematically shown in figure 2.29.

Zhang and co-workers [61] described simultaneous polymerization and crystallization more in detail. Molten CBT undergoes ring-opening and chain propagation which results in living chain ends due to the built-in initiator, as schematically shown in figure 2.30 and discussed in section 2.3.4. Subsequently, the propagated chains crystallize preferentially but the living chain end connected with the metal atom of the catalyst cannot be accommodated in the crystal lattice of pCBT because their lattice parameters are

incompatible [9, 60]. The dangling living ends remain hanging off the surfaces of the crystal nuclei, which the authors termed as "living crystal seeds". Recently ring-opened oligomers (which are still amorphous) do not need to move long distance towards to the fronts of crystal growth and can directly fold on the surface of these living crystal seeds according to the intramolecular crystal nucleation model.
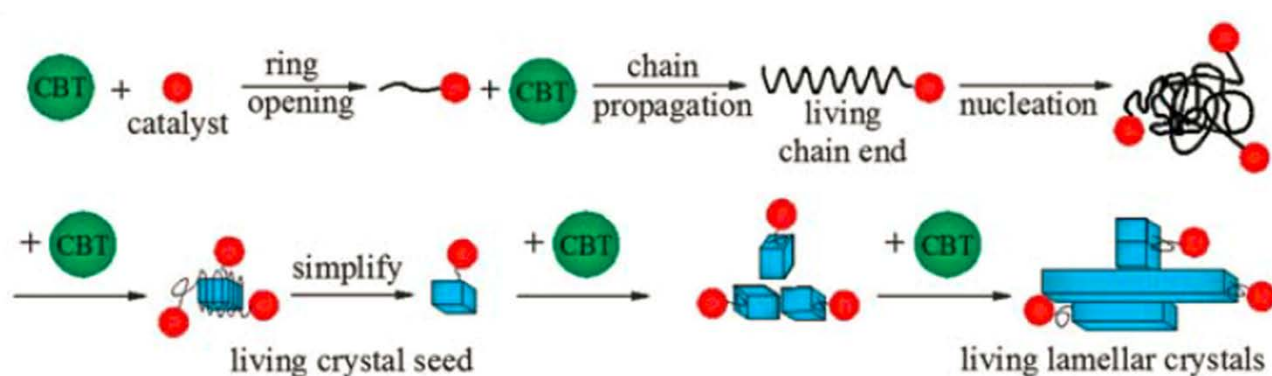


Fig. 2.30: Schematic representation of the evolution of living lamellar pCBT crystals, adapted from [61].

Harsch and co-workers [62] studied the polymerization and crystallization of CBT by fibre Bragg grating (FBG) and normal force measurements under isothermal conditions at 170 and 190 °C, respectively. Unfortunately, FBG and normal force measurements were only capable of sensing the crystallization-induced shrinkage but not the polymerization. The authors suggested that the polymerization of CBT does not produce any strain and force signals which was considered as a sign of the entropy-driven polymerization. The results from FBG and normal force measurements suggested that crystallization of pCBT is of stochastic nature and occurs in two steps; *i.e.* primary and secondary crystallization. They concluded that the polymerization is highly advanced or even completed before the crystallization starts. The primary crystallization rate is higher than the secondary one and was found to be higher at higher temperature. The activation energy of the primary crystallization was found between 80 and 150 kJ/mol by adopting an Arrhenius equation. This activation energy, estimated for the crystallization of in situ polymerized CBT, is far below that of measured for pCBT crystallizing from the melt. The pCBT polymerized at a temperature of 190 °C had somewhat higher crystallinity and larger crystallite sizes than

the pCBT polymerized at T = 170 °C, as determined by wide-angle X-ray scattering (WAXS) and DSC analysis.

**Crystallization kinetics**

Lehmann and Karger-Kocsis [63] studied the crystallization kinetics of *in situ* polymerized CBT and conventional PBT by DSC both under isothermal and non-isothermal conditions. The used materials were PBT B6550 and PBT B4520, two commercial PBT resins as well as two CBT resins, CBT-XB3-CA4 and CBT160. They have a slightly different composition, namely CBT160 contains more tetramer than CBT-XB3-CA4. The crystallization was analysed by adopting Avrami, Ozawa and Kissinger methods for the isothermal and non-isothermal crystallizations, respectively.

Crystallisation kinetics under isothermal conditions for various modes of nucleation and growth can be approximated by an Avrami equation [64-65]:

$$X_t = -\exp(-kt^n) \tag{2.4}$$

where $X_t$ is the relative crystallinity at different crystallization times $t$, $n$ is the Avrami exponent and depends on the mechanism of nucleation and the form of crystal growth. The Avrami rate constant $k$ is the crystallization rate constant related to nucleation and growth parameters; and it depends on the shape (*e.g.* sphere-, disc- or rod shaped [66]) of the growing crystallites. Equation 2.4 can be linearised which yields

$$\log(-\ln(1 - X_t)) = n\log t + \log k \tag{2.5}.$$

The plot of $\log(-\ln(1 - X_t))$ against $\log t$ is referred to as the Avrami plot and is depicted in figure 2.31.
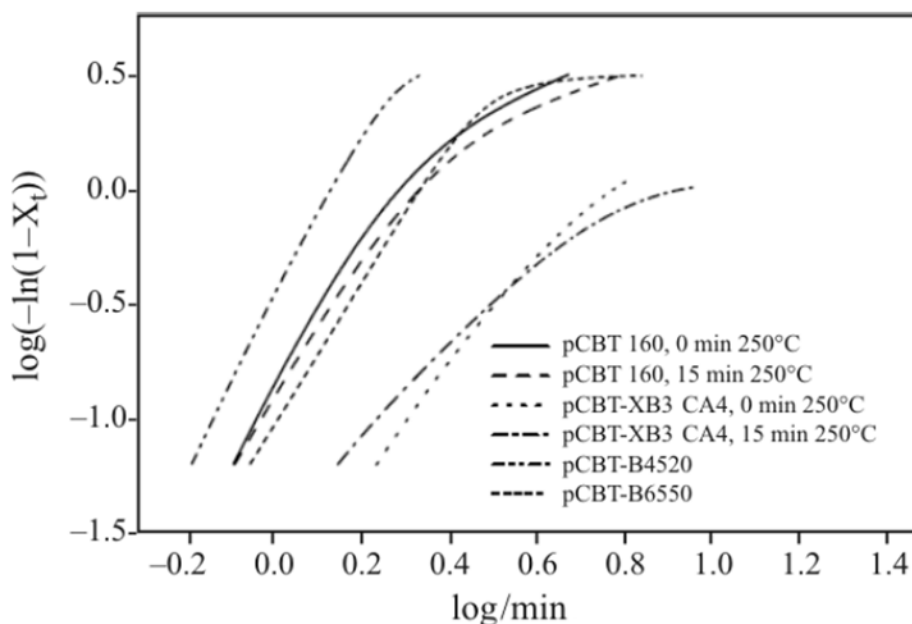
Fig. 2.31: Avrami plot of CBT160, CBT XB3-CA4, PBT B4520 and PBT B6550 as obtained at 195 °C, adapted from [63].

From this plot, the Avrami constants $n$ and $k$ can be obtained as the slope of the straight line and the intersection with the y-axis, respectively [63]. For polymerized CBT160, which is also used in the work at hand, an Avrami exponent of $n{\approx}3$ was found which corresponds to spherical crystal growth. Polymerized CBT XB3-CA4 exhibited an Avrami exponent of $n{\approx}2$, indicating two dimensional plate-like crystal growth. The crystallisation half time $t_{0.5}$ is the time in which a polymer undergoes half of the crystallization with respect to a crystallinity that it would exhibit after indefinite time at a given temperature. The crystallisation half times of polymerized CBT160 were in the range of 0.5–1.5 min for isothermal crystallization at 190–195 °C, respectively, and increased with crystallization temperature. Slightly longer crystallisation half times were found for polymerized CBT XB3-CA4. The authors assumed that the molecular weight of pCBT XB3-CA4 was higher than that of pCBT160. This was deduced to the fact that the crystallisation half times increase with increasing crystallisation temperature stronger for pCBT XB3-CA4 than for the pCBT160.

Similarly, Wu *et al.* [67] used DSC analysis to study the isothermal crystallization kinetics of pCBT polymerized at 230 °C and crystallized at 190–215 °C. They analysed the crystallization kinetics and regime using the Avrami theory and the Hoffman and Lauritzen

theory. The Avrami exponent ranged from 2.46 to 2.82, which was related to combined heterogeneous nucleation with a change in the spherulitic morphology. For an Avrami exponent *n* above 2.73, three-dimensional spherulitic morphology growth incorporated with boundary crystals was found at lower crystallization temperatures. The Avrami exponent decreased to 2.46 for crystallization temperatures greater than 200 °C, which corresponded to the disappearance of the boundary line and the irregular growth of the highly disordered spherulites was lost. The equilibrium melting temperature and glass transition temperature of pCBT were reported to be 257.8 °C and 41.1 °C, respectively.

## 2.4    Polymerized cyclic butylene terephthalate

In this section, the relationship between the synthesis, processing, structure and final properties of polymerized cyclic butylene terephthalate, pCBT, is reviewed. So far, continuous fibre reinforced composites made from CBT and glass fibres [77, 80, 83, 95, 111, 192], basalt fibres [97], and carbon fibres [88, 193-195] have been reported.

### 2.4.1  Morphology

The morphology of thermoplastics significantly influences their physical properties. This is also reflected in the matrix-governed properties of TPCs, such as transverse and shear properties, fracture toughness or fibre-matrix interface [68]. For PBT, two different morphologies have been identified both on the unit cell level and on the spherulitic level.

On the unit cell level, two triclinic polymorphs are known to exist (*c.f.* figure 2.32). The $\alpha$-crystal with *gauche-trans-gauche* conformation of the butylene moiety is the stable form under standard conditions, whereas the $\beta$ form with all-*trans* conformation develops only under stretching of unoriented crystals [69-73] or during crystallization at pressures above 2000 bar [74]. This $\alpha$ to $\beta$ crystal transition is completely reversible when the stress is removed [69, 71, 73, 75].
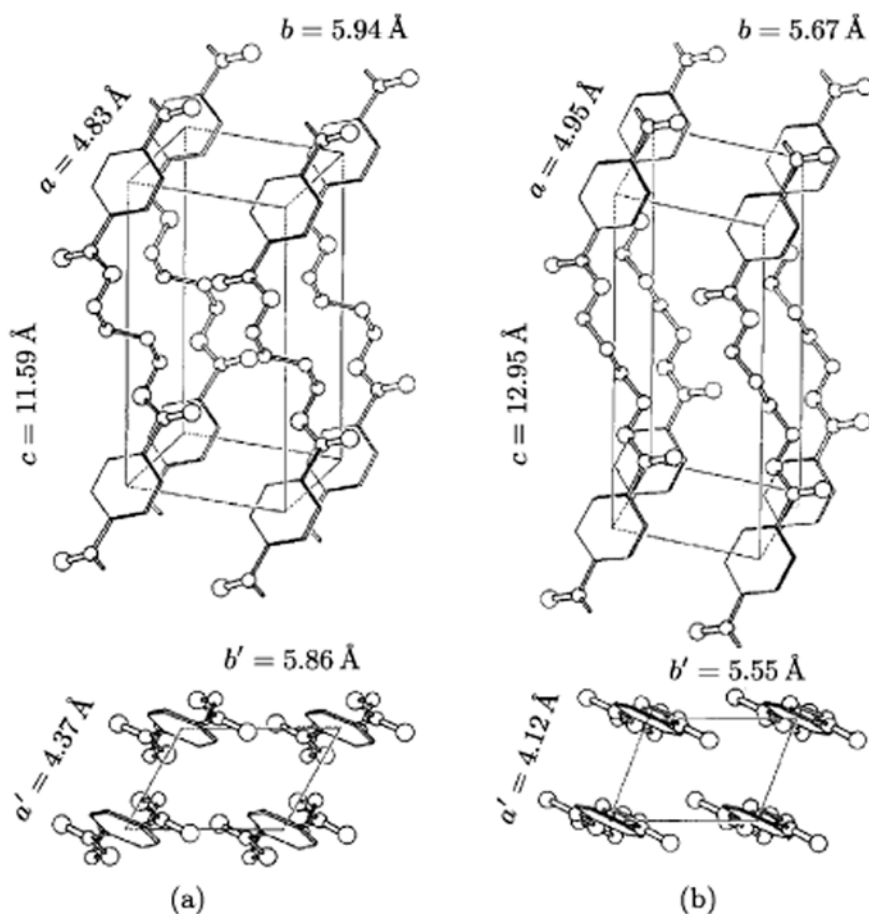
Fig. 2.32: Elementary cells of PBT: (a) $\alpha$-form and (b) $\beta$-form, adapted from [73].

On the spherulitic level, two types of spherulites can be distinguished in PBT. Stein and Misra [76] studied the morphology of PBT crystallized from the melt at various temperatures using small-angle light scattering (SALS), polarized light microscopy (PLM) and WAXS analysis. The two types of spherulites depend on the crystallization conditions. The usual type has its maltese cross parallel to the polarizers in PLM analysis and is formed at high temperatures or slow cooling rates, which results in increased spherulite size and crystallinity with increasing crystallization temperature. In contrast, the unusual type has its maltese cross parallel to the polarizers in polarizing microscopy and is formed at high temperatures or slow cooling rates.

Analogously, Wu *et al.* [67] studied the isothermal crystallization morphology of pCBT polymerized at 230 °C using PLM. The PLM morphologies of pCBT corresponding to the crystallization temperature range of 190–215 °C are illustrated in figure 2.33. Four

typical morphologic features of pCBT were reported; usual negative spherulite, unusual spherulite coexisting with boundary crystals, mixed birefringence spherulite coexisting with boundary crystals, and highly disordered spherulitic crystallites, corresponding to the crystallization temperature spectrum.
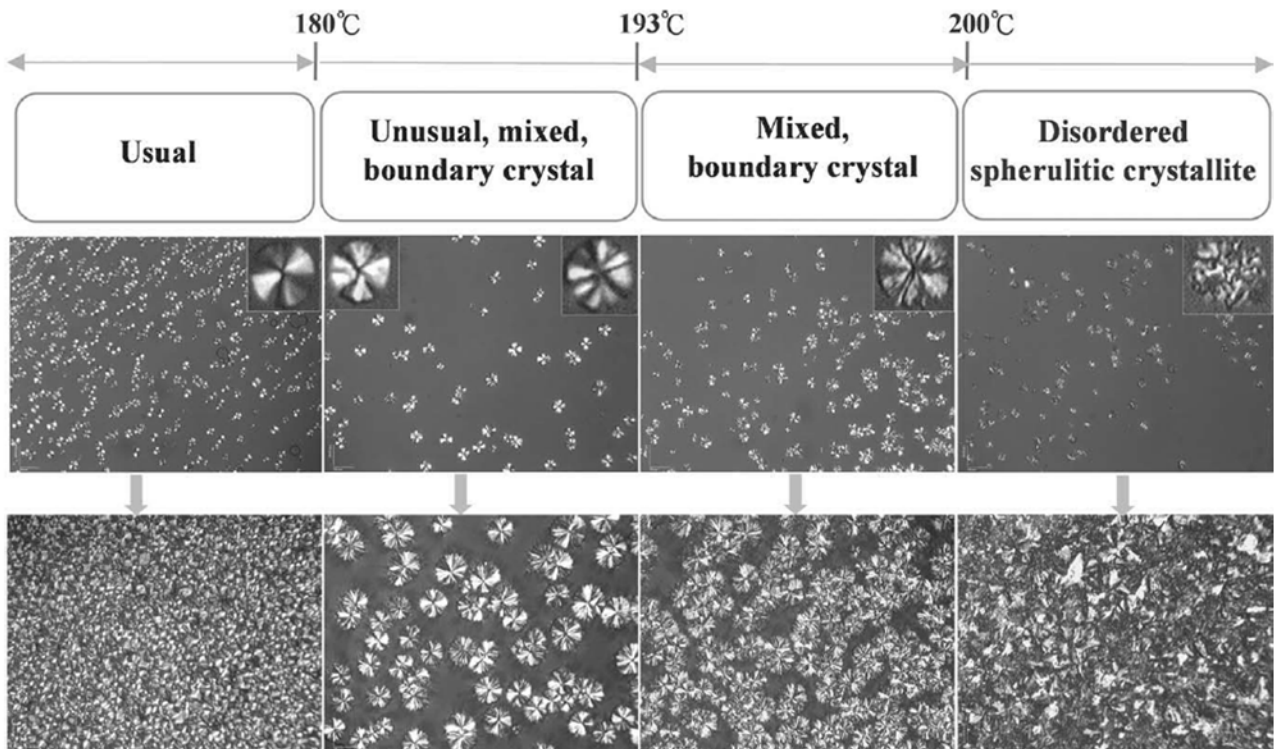


Fig. 2.33: PLM morphologies of pCBT corresponding to the crystallization temperature range of 190–215 °C, adapted from [67].

Parton *et al.* [77] examined the morphologies of PBT, pCBT isothermally processed at 190 °C and reprocessed pCBT (referred to as RP-pCBT); their respective morphologies obtained by transmission electron microscopy (TEM) are shown in figure 2.34.
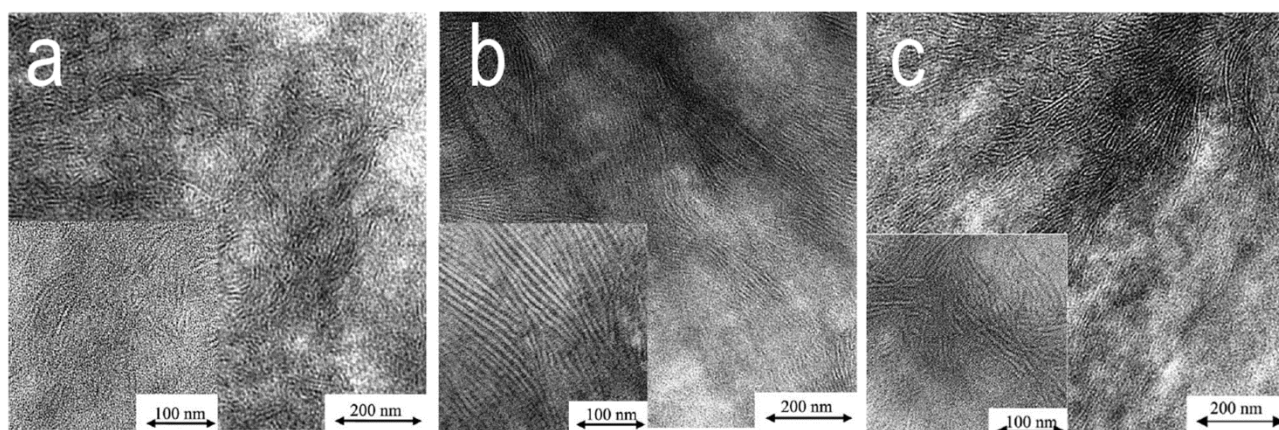
Fig. 2.34: TEM micrographs of PBT (a), pCBT (b) and reprocessed RP-pCBT (c), adapted from [77].

It is apparent that pCBT samples exhibited a microstructure with well defined, thicker and nicely oriented lamellae as compared to PBT. The transition from crystalline to amorphous regions is more pronounced and sharp in the pCBT samples, which might indicate a reduction of tie molecules. Miller [78] stated that the tie molecule density is influenced by simultaneous polymerization and crystallization. Parton *et al.* [9, 77] assumed that the transesterification catalyst of pCBT which remains in the polymer might also influence the amount of tie molecules. The catalyst molecules cannot be included into the polymer crystal, but probably concentrate at the surface of the growing crystals. Such a local transesterification enhancement may drastically decrease the amount of tie molecules owing to the mechanical tensions arising from packing density differences at the crystal boundaries.

### 2.4.2 Thermal properties of pCBT

The thermal properties of CBT and pCBT have been studied by various researchers using DSC analysis, see for instance [3, 9, 52-53, 67, 77, 79-82]. Mohd Ishak and co-workers [80] compared the thermal properties of injection moulded PBT (denoted as IM-PBT), CBT as well as pCBT isothermally polymerized at 190 °C during compression moulding (referred to as ISP-PBT); the corresponding thermograms are depicted in figure 2.35.
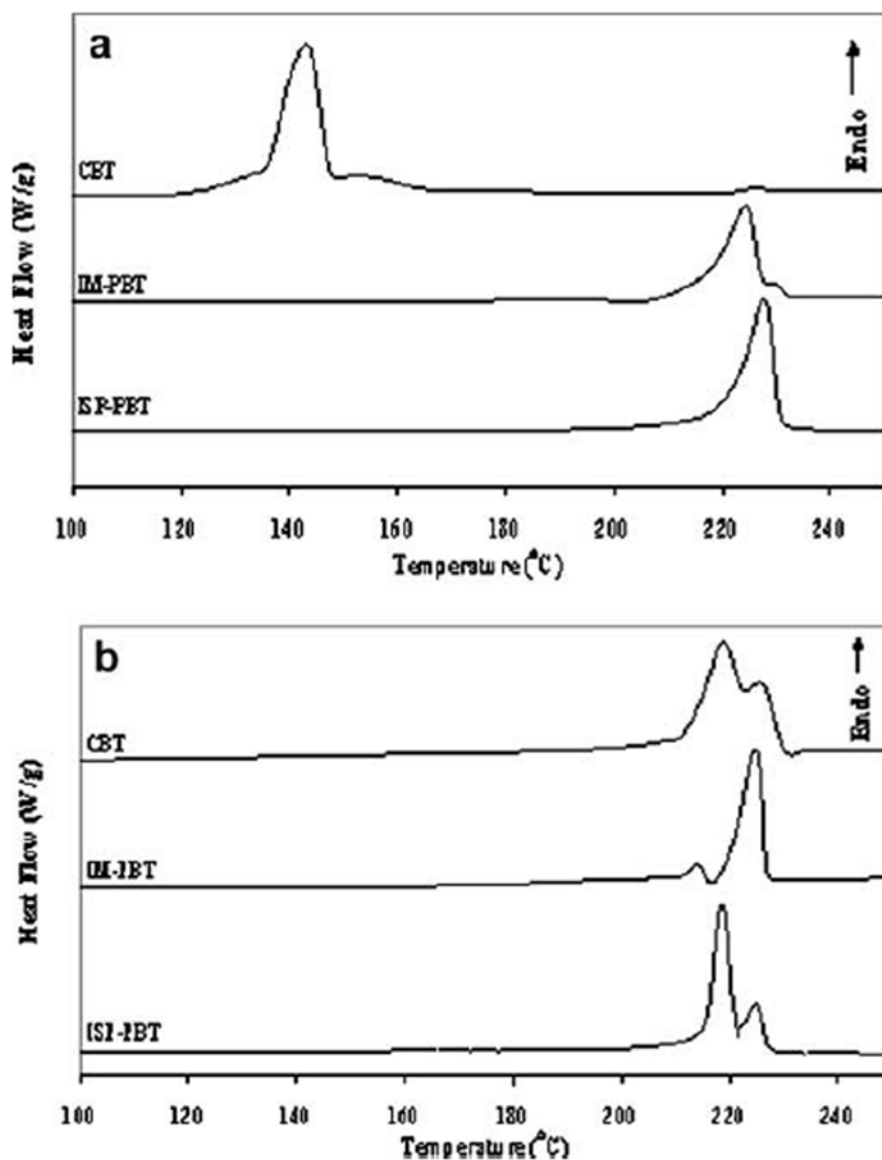
Fig. 2.35: DSC thermograms of CBT, injection moulded PBT (denoted as IM-PBT) and isothermally polymerized pCBT (denoted as ISP-PBT). First heating scan (a), second heating scan (b). Heating and cooling rates: 5 °C/min;  adapted from [80].

The samples were subjected to DSC heating and cooling rates of 5 °C/min in the temperature range of 0–250 °C. As can be seen from figure 2.35 a, CBT oligomers exhibited a broad melting range from about 120–170 °C together with a melting peak at 142 °C, as confirmed by other researchers [82-83]. The broad melting range has been ascribed to the different melting temperatures of the oligomers present in the CBT [41]. The ROP of CBT occurred during the first heating scan and a small pCBT melting peak

was observed at 226 °C. However, the related melting enthalpy was insignificant. It was assumed that the reason for the absence of crystallization (and subsequent melting) during the first heating is of kinetic origin. CBT undergoes crystallization during polymerization in the temperature range of 170–210 °C, as discussed in section 2.3.8. However, no evidence of any exothermic process linked with the polymerization or crystallization was detected. In contrast, ISP-PBT and IM-PBT exhibited a broad endotherm with a single melting peak at 228 and 224 °C and a heat of fusion of 71 and 50 J/g during first heating, respectively. The relatively higher melting temperature and enthalpy of ISP-PBT is due to the different crystalline structure of the resulting PBT. More specifically, isothermal polymerization of CBT below $T_m$ of pCBT leads to the formation of big, perfect crystals having a higher lamellar thickness, as was also pointed out by Parton [9].

Mohd Ishak *et al.* reported in an earlier publication [3] that the heating rates play an important role in the exothermic process during the first heating of CBT. They found that at a much lower heating rate of 0.5 C/min, the DSC thermogram showed a prominent exothermic peak at 195 °C which corresponded to the crystallization of pCBT. It was concluded that high DSC heating rates hinder the crystallization of pCBT and consequently its melting peak is missing. Regarding the first heating of ISP-PBT and IM-PBT, both samples showed a distinct polymer melting peak although ISP-PBT exhibited a higher melting enthalpy. This indicated that complete polymerization and crystallization of ISP-PBT have taken place during compression moulding.

Figure 2.35 b shows the DSC second heating scans of CBT (polymerized during the first heating scan), ISP-PBT and IM-PBT. A broad endotherm with two melting peaks was observed for all samples. The double melting behaviour was ascribed to the melting of small and defective crystals, followed by their immediate recrystallization into more stable structures and their subsequent melting. This was confirmed in a further work [81], where the authors used modulated DSC (MDSC) to study the polymerization of CBT as a function of the end temperature (200 and 260 °C) and holding time (5, 15 and 30 min). They used a heating rate of 5 °C/min with a modulation of ± 0.531 °C/min and a frequency of 40 s. The onset of double melting of pCBT was strongly affected by the polymerization route, *i.e.* ROP below or above the melting temperature of pCBT. During cooling, the glass transition was observed at 40 °C. Moreover, the authors could show that the polymerization of CBT is non athermic. The heat of polymerization derived from the non-

reversing DSC trace was found to be around 22 J/g, but was overlapped with the endothermic melting of CBT at 140 °C. Therefore, the apparently athermic ROP is the result of polymerization-related exothermic and melting-related endothermic effects.

### 2.4.3  Physical properties of pCBT

The morphology and hence the final properties of pCBT are strongly influenced by the processing route. Various researchers prepared unreinforced pCBT; an excerpt of the physical properties is presented in table 2.2.

Parton and associates [77] studied the influence of the processing conditions of a TP-RTM process on the properties of pCBT. One sample was isothermally processed at 190 °C (*i.e.* simultaneous polymerization and crystallization) whereas another sample was polymerized at 230 °C  and then crystallized at 190 °C. The two samples were compared to injection moulded PBT. The authors reported that pCBT was brittle in contrast to conventional PBT, irrespective of the processing route. PBT did not break in flexural tests but showed a yield point, whereas pCBT broke in a brittle manner. Simultaneous polymerization and crystallization of CBT at 190 °C yielded an even more brittle and weaker pCBT. Both pCBT190 and pCBT230 exhibited a higher modulus than PBT due to the markedly higher degree of crystallinity relative to PBT. Molecular weight and residual oligomer content were quite similar in all three samples. Both PBT and pCBT were reprocessed using injection moulding in order to decrease the degree of crystallinity, which in turn typically increases the toughness. As can be seen from table 2.2, the crystal fraction of RP-pCBT decreased to a similar level as PBT. Consequently, failure strain increased but at the same time the strength decreased. The latter might be attributed to the pronounced molecular weight reduction of RP-pCBT due to the reprocessing step. This reduction was also observed for PBT but to a much lesser extent. Reprocessing cannot be considered as a toughening method since it involves an extra processing step and the advantage of a one-step process would be lost.

Baets [84] also used a TP-RTM process for the isothermal polymerization of CBT at 190 °C and obtained similar results, *i.e.* a brittle pCBT.

Balogh [85] employed compression moulding (CM) for the *in situ* polymerization of CBT at 240 °C with subsequent non-isothermal melt crystallization. Due to the latter, one might expect a less crystalline but tougher pCBT. While the pCBT crystal fraction was indeed lower than the ones obtained from TP-RTM, the pCBT was equally brittle. This is in contrast to the results in [77], where it was stated that crystallization of the melt (*i.e.* reprocessing of pCBT) yields a relatively tougher pCBT.

Table 2.2: Physical properties of PBT, pCBT and macrocyclic c-pCBT.

| Reference | Sample | Processing | $T_{ROP}$ [°C] | $T_{cool}$ [°C] | Testing | $E$ [GPa] | $\sigma$ [MPa] | $\varepsilon$ [%] | $X_{c,\,DSC}$ [%] | $M_n$ [kg/mol] | $M_w$ [kg/mol] | $\alpha$ [%] |
|---|---|---|---|---|---|---|---|---|---|---|---|---|
| [76] | PBT | IM | 250 | non-iso | flexural | 2.2 ± 0.1 | 73 ± 11 | *3.3 ± 0.3 | 35 | 33.8 ± 0. | 69.3 | 99 |
| [76] | RP-PBT | IM | 250 | non-iso | tensile | 2.5 ± 0.2 | 50 ± 1 | 16–225 | 34 | 32.3 | 66.3 | 99 |
| [76] | pCBT190 | TP-RTM | 190 | 190-iso | flexural | 3.2 ± 0.1 | 54 ±5 | 1.6 ± 0.2 | 47 | 29.3 | 61.4 | 98 |
| [76] | pCBT230 | TP-RTM | 230 | 190-iso | flexural | 3.1 ± 0.2 | 73 ± 14 | 2.3 ± 0.7 | 42 | 35 | 73.3 | 99 |
| [76] | RP-pCBT | IM | n/a | n/a | tensile | 2.3 ± 0.2 | 46 ± 7 | 3–70 | 35 | 20.5 | 40.6 | 98 |
| [78] | pCBT | TP-RTM | 190 | 190-iso | flexural | 3.5 ± 0.1 | 61 ± 3 | 1.9 ± 0.1 | 44 | 36 | 78 | 99 |
| [79] | pCBT | CM | 240 | non-iso | tensile | 2.1 ± 0.3 | 57 ± 13 | 3.2 ± 1.1 | 33 | n/a | 67.6 | 99 |
| [77] | c-pCBT | CM | 190 | 190-iso | tensile | 3.0 | 46 | 2 | 50 | ~100 | ~300 | n/a |

*strain at yield; no break.

Miller *et al.* [78] used cyclic stannoxane as initiator of the ROP and obtained a macrocyclic c-pCBT. The crystal fraction and the molecular weight of c-pCBT were considerably higher than the ones of its linear counterparts. The higher molecular weight is due to the absence of linear end groups (coming from the initiator) during the ROP. Similarly, c-pCBT had a higher modulus as compared to PBT. Nevertheless, the macrocyclic c-pCBT exhibited an exceptionally low strength and failure strain.

**Influence of morphology**

Ludwig and Eyerer [86] discussed the influence of the processing conditions on morphology and deformation behaviour of PBT. Injection moulded samples were crystallized at mould temperatures of 60 and 118 °C and using sample thicknesses of 3 and 5 mm, respectively. The low mould temperature led to unusual spherulites, whereas the higher one resulted in usual or mixed type spherulites. Tensile tests showed an increase in yield stress from 50 $N/mm^2$ for the usual type and 55 $N/mm^2$ for the usual type spherulite while strain at yield was equal for both types. Slowly cooled PBT exhibited a relatively higher microhardness (148 $N/mm^2$ versus 138 $N/mm^2$).

Zhang and co-workers [87] studied the effect of the mould temperature during injection moulding of PBT on the mechanical properties. They found that tensile modulus and strength increased from 2.5 to 2.7 GPa and 54 to 58 MPa, respectively, when the mould temperature was increased from 20 to 120 °C. At the same time, failure strain decreased from 198 to 32%.

Yu *et al.* [88] studied the effect of different crystalline morphologies on the mechanical properties of carbon fibre reinforced pCBT composites. They prepared stacked films of CBT powder and reinforcement, which were then polymerized during compression moulding at 230 °C. After 30 min, the composites were quenched to crystallization temperatures of 185, 195 and 210 °C, respectively. The three samples had molecular weights, degrees of conversion and crystal fractions quite similar to the ones of linear pCBTs (*c.f.* table 2.2) and the morphology was analogous to the one of unreinforced pCBT. The mechanical properties of the pCBT composites were strongly affected by their crystalline morphologies and degree of crystallinity. The sample crystallized at 185°C

exhibited a relatively low crystal fraction, which resulted in a spherulitic superstructure with large spherulite/transcrystalline boundary regions. As a consequence, cracks tended to initiate and propagate along these weak spherulite/ transcrystalline boundaries, leading to low mechanical properties. The composite sample crystallized at 210 °C showed highly disordered spherulitic crystallites without spherulite/transcrystalline boundary lines or boundary crystals, which resulted in somewhat better mechanical properties.

It can be recocnised from table 2.2 that unmodified CBT yields an essentially brittle pCBT, irrespective of processing route, polymerization and crystallization temperature, molecular structure (*i.e.* linear versus macrocyclic pCBT), molecular weight, degree of conversion, degree of crystallinity or spherulitic morphology. Possible reasons for this brittleness will be discussed in the following section.

### 2.4.4  Brittleness mechanisms of pCBT

There a number of reasons for brittle behaviour of semi-crystalline thermoplastics [9, 41, 61, 78, 89-90], namely

- matrix defects such as voids and impurities, acting as stress concentrators
- very large spherulites, also acting as stress concentrators
- high degree of crystallinity
- low amount of intercrystalline tie molecules
- low molecular weight

While impurities are less likely to occur in the case of a proper processing of CBT, voids may form in thick-walled parts during a pressure-less crystallization due to volumetric shrinkage. The pCBT brittleness has been ascribed to the formation of large spherulites together with a high degree of crystallinity and crystal perfection, which typically leads to a reduction of intercrystalline tie molecules [9, 41, 77-78]. The brittleness was more severe for simultaneous polymerization and crystallization below the melting temperature of pCBT. Besides the above mentioned reasons for brittleness, some researchers have

focused on the residual CBT oligomers after polymerization. Wu and Huang [53] found some residual CBT crystals when the polymerization was performed at 190 °C in a hot stage. Xu and co-workers [91-92] showed that unpolymerized CBT was present in the form of large, well-developed oligomer crystals in a CBT/rubber matrix blend. It is also clear from literature that polymerization below $T_m$ might not be high enough to melt all cyclics present in CBT [40, 42]. Zhang *et al.* [61] confirmed this assumption while they studied the effects of these residual CBT crystals on the mechanical properties of pCBT. They demonstrated that CBT oligomer crystals with high melting points could not completely melt at 190 °C and appeared as well-developed crystals from nano- to micro-scale in the pCBT matrix, highlighted with ellipses in figure 2.36.
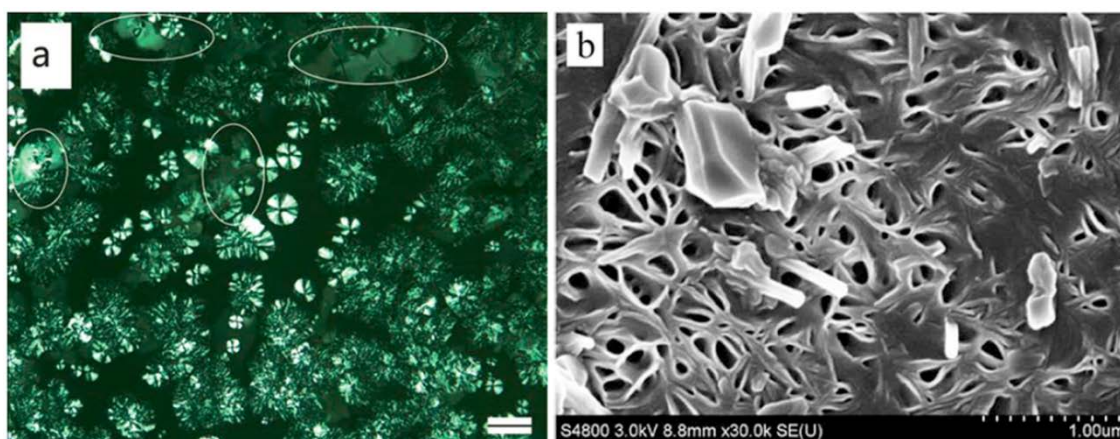


Fig. 2.36: Remaining cyclic oligomer crystals after polymerization at 190 °C for 30 min; PLM image (a) and SEM image (b), adapted from [61].

These crystals served as a self-compatible nucleating agent which reduced the induction time of crystallization during polymerization. Moreover, the crystals acted as stress concentration points and led to the brittleness of pCBT, as schematically shown in figure 2.37. The authors speculated that a high degree of crystallization and a perfect crystal structure together with a low density of intercrystalline tie molecules of pCBT is favoured by their so-called living lamellar crystal initiation mechanism, which was discussed in section 2.3.8. Furthermore they stated that the low viscosity of molten CBT may be favourable for entanglement reduction. Besides, polymerization at low temperatures may cause a decrease in the polymerization rate, leading to a low molecular weight [1, 42].
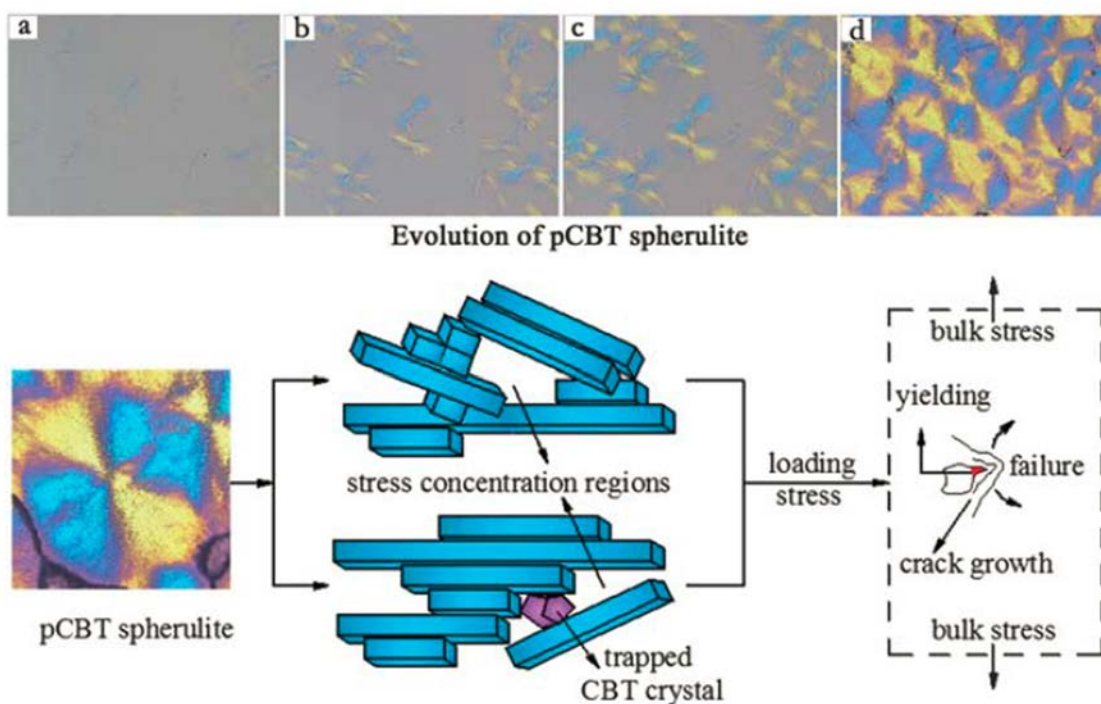
Fig. 2.37: Brittleness mechanism of remaining cyclic oligomer crystals in pCBT, adapted from [61].

One might expect that a polymerization temperature above $T_m$ with subsequent non-isothermal melt crystallization increases the toughness but it was shown by various researchers [9, 84-85] that the obtained pCBT is not significantly tougher (*c.f.* table 2.2). Since the ROP was conducted above $T_m$, it can be assumed that all CBT oligomer crystals were in the molten state. Therefore, remaining oligomer crystals cannot be the reason for brittleness of pCBT obtained by a non-isothermal processing route. A possible explanation might be a low molecular weight due to humidity which on one hand inhibits the catalyst [14, 17, 58] and on the other hand can cause hydrolysis [93].

It is known that if the molecular weight is below some critical value or if the polymer contains a large amount of a very low-molecular-weight fraction mixed in with a high-molecular-weight fraction, the polymer will be extremely brittle and will have a lower-than-normal strength. At higher loads or elongations the weak low-molecular-weight materials may break at considerably lower elongations than the high-molecular-weight polymers [94]. Although a high molecular weight is obtained when the ROP is conducted under inert atmosphere or in closed moulds in TP-RTM processing, the resulting pCBT is still brittle [1,

77, 95]. Therefore, ongoing research is focussed on the toughening of pCBT and will be reviewed in the next section.

### 2.4.5  Toughening of pCBT

Vincent [96] described the tough-brittle transition in thermoplastics and stated that the chances of brittle failure can be reduced by:

- reducing the crystallinity
- adding rubbery polymers
- adding plasticizer
- increasing the molecular weight

Decreasing the degree of crystallinity and thus introducing more tie molecules between crystals can be achieved by changing the processing conditions, namely by applying a fast cooling after polymerization. Baets and co-workers [97] compared slow cooling to quench cooling in a non-isothermal production process of basalt fibre-reinforced pCBT composites. They found that failure strain increased from 1.8% for slowly cooled composites to 2.6% for quench cooled samples. Nevertheless, quench cooling may not always be practical or applicable.

So far, adding rubbery polymers, plasticization or systematically increasing the molecular weight of pCBT has not been reported, although the latter possibility has been considered in patent literature [49, 98-99]. However, a hydrogenated nitrile rubber (HNBR) was modified with CBT and the HNBR/CBT hybrids exhibited improved mechanical and triblogical properties compared to pristine HNBR [91-92, 100].

Additional strategies to reduce the brittleness of thermoplastics are copolymerization with soft segments, chemical modification as well as physical modification with nano-particles and will be discussed in detail in the following sections.

## 2.4.6 Copolymerization

It is well known that the incorporation of even small amounts (10%) of flexible polytetrahydrofuran (polyTHF) blocks in polyester macromolecules result in a decrease in mechanical strength and in an increase in elongation at break [101]. The copolymer of PBT and polyTHF is known as copoly(butylene terephthalate-*b*-tetrahydrofuran) (coPBT-PTHF) and belongs to the relatively new material class of thermoplastic elastomers (TPEs). This multi block copolymer is also known as copoly(butylene terephthalate)-poly(tetramethylene ether glycol) (coPBT-PTMG) or copoly(butylene terephthalate)-poly(tetramethyelene oxide) (coPBT-PTMO). More specifically, coPBT-PTHF is a poly(ester-*b*-ether) block copolymer with alternating hard sequences of crystallisable polyester and soft segments of amorphous polyether [101-107], as illustrated in figure 2.38. The properties of the TPEs mainly depend on type and amount of hard segments. The latter act as reversible physical crosslinks, contrary to covalent sulphur bonds in vulcanized rubbers.
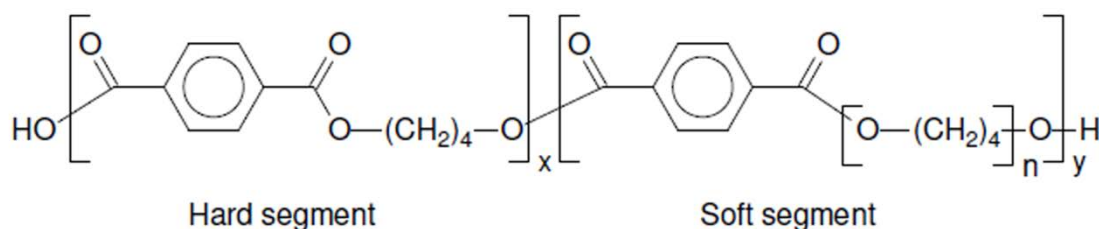


Fig. 2.38: Chemical structure of copoly(butylene terephthalate-b-tetrahydrofuran), adapted from [102]

Polyether ester elastomers are produced by melt polymerization *via* ester interchange of a long-chain glycol and a short-chain glycol with the methyl ester of a dicarboxylic acid in presence of a butyl titanate catalyst. High molecular weights can be attained by evaporation of the excess short-chain glycol or alternatively by chain extension with di-or polyepoxides, polycarbodiimides, isocyanates, diphenyl terephthalate [107], bis-oxazolines (BOX) or carbonylbiscaprolactam (CBC) [103, 108]. Maier and associates [103, 108] prepared segmented coPBT-PTHF block copolymers by reacting PBT with dihydroxy-

functionalized polyTHF oligomers in presence of a transesterification catalyst. The addition of diols (*i.e.* dihydroxy-functionalized polyTHF oligomers) to PBT leads to a disruption of OH-COOH stoichiometry of PBT, resulting in a strong decrease in molecular weight of PBT. This transesterification yields low molecular weight difunctional OH-terminated PBT-polyTHF oligomers which were then further reacted with CBC in a chain extension reaction, yielding segmented coPBT-PTHF block copolymers.

Polyether ester elastomers exhibit outstanding elasticity, tear strength, solvent resistance, low-temperature flexibility and strength at elevated temperatures. Due to these properties they were commercialized under the trademark Hytrel® by DuPont in 1972 [103, 107].

Analogous to copolymerization of conventional PBT, several researchers have copolymerized CBT with poly(ethylene-co-vinyl acetate) (EVA) [109], poly(vinyl butyral) [110], $\varepsilon$-caprolactone [82], polycaprolactone [53, 111], hydroxyl terminated tetrabromobisphenol A (TBBPA) [112], bisphenol A diglycidyl ether (BPADGE) [112], hydroxylated polydimethylsiloxane (Carbinol PDMS) [112] and styrene maleimide (SMI) [113]. Nevertheless, only some reports on the mechanical properties of these pCBT copolyesters are available and are summarized in table 2.3.

Conventional PBT does not break in flexural tests but exhibits a yield point [77]. In tensile tests, PBT typically shows a failure strain of >50% [23]. It is apparent from the failure strain in table 2.3 that in the case of CBT copolymerized with polytetrahydrofuran or polycaprolactone, a toughness similar to the one of conventional PBT could not be achieved. Copolymerization with $\varepsilon$-caprolactone or EVA resulted in ductile materials which exhibited a yield point, necking, strain hardening and very high failure strains. On the other hand, stiffness and strength drastically decreased. This decrement of mechanical properties together with $T_g$ and $T_m$ reduction are the major disadvantages of copolymerization with soft segments as a toughening method.

Table 2.3: Physical properties of pCBT copolymers.

| Ref. | Modifier | Modifier content [wt.%] | Testing | $E$ [GPa] | $\sigma$ [MPa] | $\varepsilon$ [%] |
|---|---|---|---|---|---|---|
| [84] | polytetrahydrofuran | 10 | flexural | 2.1 ± 0.1 | 27 ± 4 | 1.3 ± 0.4 |
| [109] | EVA | 75 | tensile | 0.004 | 4 | 1030 |
| [82] | $\varepsilon$-caprolactone | 20 | tensile | 0.06 | 9 | 368 |
| [82] | $\varepsilon$-caprolactone | 30 | tensile | 0.17 | 13 | 704 |
| [82] | $\varepsilon$-caprolactone | 40 | tensile | 0.05 | 5 | 397 |
| [82] | $\varepsilon$-caprolactone | 50 | tensile | 0.02 | 2 | 690 |
| [82] | $\varepsilon$-caprolactone | 70 | tensile | 0.0004 | 0.8 | 820 |
| [84] | polycaprolactone | 7 | flexural | 2.7 ± 0.1 | 95 ± 7 | 5 ± 0.8 |
| [85] | polycaprolactone | 7.5 | tensile | 1.25 | 27 | 6 |

## 2.4.7  Chemical modification

Chemical modification is commonly used to improve certain properties of thermoplastics but has not been employed for the toughening of pCBT so far. It exploits the reactions of polymer functional groups with low molecular weight bi- or polyfunctional compounds [114-119]. Polyesters are especially accessible to chemical modification because they bear reactive functional groups in their main chain and chain ends, such as hydroxyls and carboxyls as in the case of *e.g.* PET and PBT. The chemical modification of polyesters comprises four main techniques [118, 120]:

- controlled degradation to decrease the molecular weight or to produce monomers/oligomers
- capping of carboxylic end groups
- compatibilization of  partially miscible polymer blends
- chain extension/branching to increase the molecular weight by coupling of two or more polymer chains

Carbodiimide



Isocyanate



Epoxide



Oxazoline



Fig. 2.39: Reactions of carboxylic groups with various electrophilic groups, adapted from [118].

Reactive chain extension of polyesters with low molecular weight bi- or polyfunctional compounds is a suitable technique to improve the toughness, impact strength and hydrolytic stability [118]. The reactive agents, so-called chain extenders, are preferably bifunctional and should react easily through an addition reaction without generating any by-products [115-116]. Inata and Matsumura [121-126] studied a variety of electrophilic chain extenders for polyesters. Among the different studied compounds, epoxides, isocyanates, oxazolines, carbodimides and carbonylbiscaprolactam [103] were found to be particularly effective. Figure 2.39 depicts some of the chain extension reactions of these electrophilic compounds with carboxylic end groups.

Although epoxies and isocyanates were mentioned as potential toughening agents for pCBT in the open patent literature [49, 98-99], there has been no publication on this subject. The physical modification of pCBT with nano-reinforcements will be discussed in the subsequent sections.

## 2.5    pCBT nanocomposites

Polymer nanocomposites, in which the reinforcement has at least one dimension in the nanometre range, have received increasing interest in the last few years. It is well recognised that the behaviour of composites largely depends on interfacial interactions. This means that the smaller the size of the reinforcement, the greater the contribution of interfacial interactions to the composite properties. Thus, a major challenge in the development of high performance nanocomposites is the control of nano-reinforcement dispersion. The mechanical, thermal and physical properties are greatly enhanced by the incorporation of nano-particles of different sizes and aspect ratios. Moreover, the incorporation of nano-particles in thermoplastic matrices can increase the toughness [95, 127-128]. These improvements can already be obtained with very low nano-reinforcement contents, usually less than 5 wt.%. Nevertheless, property improvements are typically only observed when the nano-particles are randomly and homogeneously dispersed on a nanoscale level in the polymer matrix. Thus, nanocomposites exhibit unique properties not shared by their micro- and macro-composite counterparts [129-131].

Three types of nanocomposites can be distinguished, depending on how many dimensions of the dispersed particles are in the nanometre range [129].

- two-dimensional (2D) nano-particles (*i.e.* having one dimension in the nano-scale) such as layered silicates [131] or graphene nano-platelets [132-133]
- one-dimensional (1D) nano-particles such as carbon nanofibres [134], carbon nanotubes [135] or cellulose whiskers [129]
- zero-dimensional (0D) nano-particles such as fullerenes or polyhedral oligomeric silsesquioxane (POSS) molecules [136-138]

Examples for 0D, 1D and 2D-type nano-reinforcements are schematically depicted in figure 2.40.
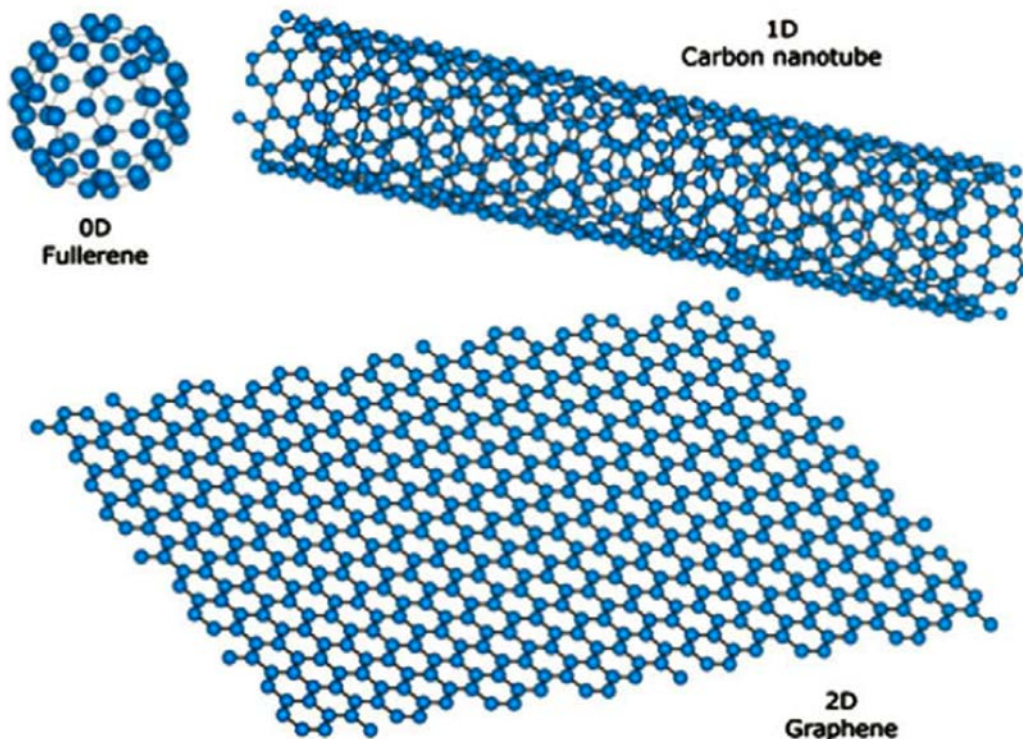


Fig. 2.40: Low-dimensional carbon allotropes: fullerene (0D), carbon nanotube (1D) and graphene (2D), adapted from [139].

CBT has been extensively used in nanocomposites due to the low melt viscosity prior to ROP which is advantageous for a good dispersion of the nano-reinforcement.

## 2.5.1  Nanocomposites with layered silicates

Layered silicates for the preparation of polymer/layered silicate nanocomposites (PLS) belong to the general family of 2:1 layered or phyllosilicates [131]. Montmorillonite, hectorite and saponite are the most commonly used layered silicates. Their crystal structure consists of layers made up of two tetrahedrally coordinated silicon atoms fused to an edge-shared octahedral sheet of either aluminium or magnesium hydroxide. The layers have a thickness of around 1 nm and lateral dimensions from 30 nm to several microns or larger, depending on the layered silicate.

Layered silicates are typically rendered organophilic in order to increase the compatibility between the hydrophobic polymer and hydrophilic silicate. This is achieved by ion-exchange reactions with cationic surfactants including primary, secondary, tertiary, and quaternary alkylammonium or alkylphosphonium cations. These ion-exchanged organic surfactants increase the interlayer spacing and lower the surface energy of the inorganic layered silicates which improves intercalation. Three methods for the preparation of PLS are reported [129, 131]:

- melt intercalation: silicate delamination *via* shear flow and dispersion in the molten polymer
- *in situ* intercalative polymerization: swelling of the layered silicate with the liquid monomer/oligomer and subsequent polymerization
- exfoliation adsorption: exfoliation of the silicate layers in a suitable solvent, adsorbing the polymer onto the delaminated sheets and then solvent evaporation

Many researchers studied PBT/organoclay nanocomposites obtained by traditional melt intercalation or *in situ* polymerization of PBT monomers [140-144]. An increasing amount of reports on pCBT/organoclay nanocomposites can also be found [79, 145-153]. The low viscosity of molten or dissolved oligomers is utilized to obtain a CBT-intercalated

organoclay. Subsequent ring-opening polymerization causes then an increase in interlayer distance along with the disintegration of the layered clay structure. On one hand, only few reports on complete clay exfoliation of the final nanocomposites are available [145, 153]. On the other hand, intercalated or flocculated-intercalated structures are more commonly observed [147-148, 150-152]. Although the organoclay was successfully intercalated with CBT oligomers or even completely exfoliated before ROP, the silicate layers tended to reorganize due to the low viscosity of the molten CBT during ROP. Thus the exfoliated structure was lost and a flocculated-intercalated structure was obtained after polymerization [148, 151-152].

Tripathy and co-workers [151] prepared pCBT/organoclay nanocomposites (using Cloisite$^®$ 20A) with a clay content of 2, 4 and 6 wt.%. CBT oligomers and organoclay were solvent blended for 20 h and then *in situ* polymerized. The thermal stability of these nanocomposites was found to increase by 8–10 °C in nitrogen atmosphere.

Karger-Kocsis *et al.* [79] studied pCBT/organoclay nanocomposites (using Cloisite$^®$ 30B) with a clay content of 5 wt.% by modulated DSC analysis. They found that the organoclay hinders the cold crystallization of pCBT during the first heating scan. Similarly, Lanciano *et al.* [148] studied pCBT/organoclay nanocomposites (using Dellite$^®$ HPS and Dellite$^®$ 43 B) and suggested that the presence of the montmorillonite shifts the ring-opening polymerization of CBT towards higher temperatures.

### 2.5.2  Nanocomposites with graphene

Graphene (referred to as G) is a one-atom-thick layer of sp$^2$-bonded carbon atoms densely arranged in a two-dimensional honeycomb crystal lattice and recently has received enormous attention due to its outstanding mechanical, thermal and electrical properties [132, 154-155]. Graphene can be obtained from graphite intercalation compounds using the Hummers method [156]. This method involves the oxidation of naturally occurring graphite using a water-free mixture of concentrated sulfuric acid, sodium nitrate and potassium permanganate and yields graphite oxide (commonly referred to as GO) with a C:O ratio of approximately 2:1. GO is highly oxygenated and bears epoxide, diol, ketone, hydroxyl and carboxyl functional groups on the basal plane and additional carbonyl and

carboxyl groups located at the edges of the GO sheets. These functional groups render GO platelets highly hydrophilic, allowing them to readily swell and disperse in water [132, 154-155] but direct exfoliation into non-aqueous solvents or hydrophobic polymer matrices is difficult [157]. Exfoliated and reduced GO is then obtained by solution-based chemical reduction of GO [155, 158] or most commonly by thermal shocking [132]. The latter yields thermally reduced graphite oxide (TRGO) which retains some of the oxygenated functional groups originally present on the GO platelets [132].

Similar to other 2D-type reinforcements such as layered silicates, proper exfoliation and homogeneous dispersion of single graphene sheets in the polymer matrix is crucial for property improvements [132, 155, 159]. However, G exfoliation remains a major challenge due to the strong $\pi$–$\pi$ stacking of the $\pi$ orbitals of graphene [154-155]. Since the high melt viscosity of most thermoplastics complicates exfoliation, G is therefore commonly intercalated/exfoliated by solvents and/or monomers prior to melt blending with thermoplastics [132, 154-155, 157, 159-161]. The low melt viscosity of CBT may be favourable for G exfoliation. However, only few pCBT/G nanocomposites have been reported.

Fabbri and associates [161] prepared pCBT/G nanocomposites by solvent blending CBT oligomers and 0.5–1 wt.% of graphene nano-platelets. Then the solvent was extracted and the dried compound was polymerized during melt blending. On one hand good graphene dispersion was observed, while on the other hand the pCBT molecular weight strongly decreased with increasing G content. Due to this low molecular weight the nanocomposites were too brittle for standard specimen preparation and nano-indentation was performed instead. It was found that the elastic modulus and indentation hardness increased for G contents lower than 0.75 wt.%. Moreover, thermal stability in oxygen was improved by up to 20 °C and all prepared samples were electrically conductive.

Balogh *et al.* [162] used melt blending to prepare pCBT/G nanocomposites with G contents of 1–5 wt.%. While poor G dispersion was obtained, it was found that G had a reinforcing effect on pCBT. DMTA storage modulus at room temperature increased by 39–89% and the heat conductivity was also markedly enhanced. Moreover, G was found to act as nucleating agent.

Chen *et al.* [160] prepared pCBT nanocomposites with thermally reduced graphite oxide (TRGO) by solvent blending, vacuum drying and then polymerization at 200 °C. The rate and degree of CBT polymerization decreased with TRGO content, which was ascribed

to the reaction between carboxyl groups of growing pCBT chains and hydroxyl/epoxy groups situated on the surface of TRGO. The pCBT grafted onto TRGO was confirmed by various characterization techniques and the grafting content was found to be up to 53%.

It is apparent that graphene may be difficult to exfoliate and disperse homogeneously in the pCBT matrix. More importantly, it seems that G interferes with the ROP of CBT because the final pCBT molecular weight was rather low and the reported pCBT/G nanocomposites were brittle. On the other hand, it is clear from literature that chemical functionalization of graphene is of crucial importance in the synthesis of polymer-graphene nanocomposites with good dispersion [132, 154-155, 157, 159]. The oxygen-containing functional groups of TRGO can be used to enhance the compatibility of the latter with various polymer matrices *via* chemical functionalization [132, 154] for instance with isocyanate compounds, as illustrated in figure 2.41. In this chemical functionalization, organic isocyanates react with the hydroxyl (left oval) and carboxyl groups (right oval) of graphene oxide to form carbamate and amide functionalities, respectively.
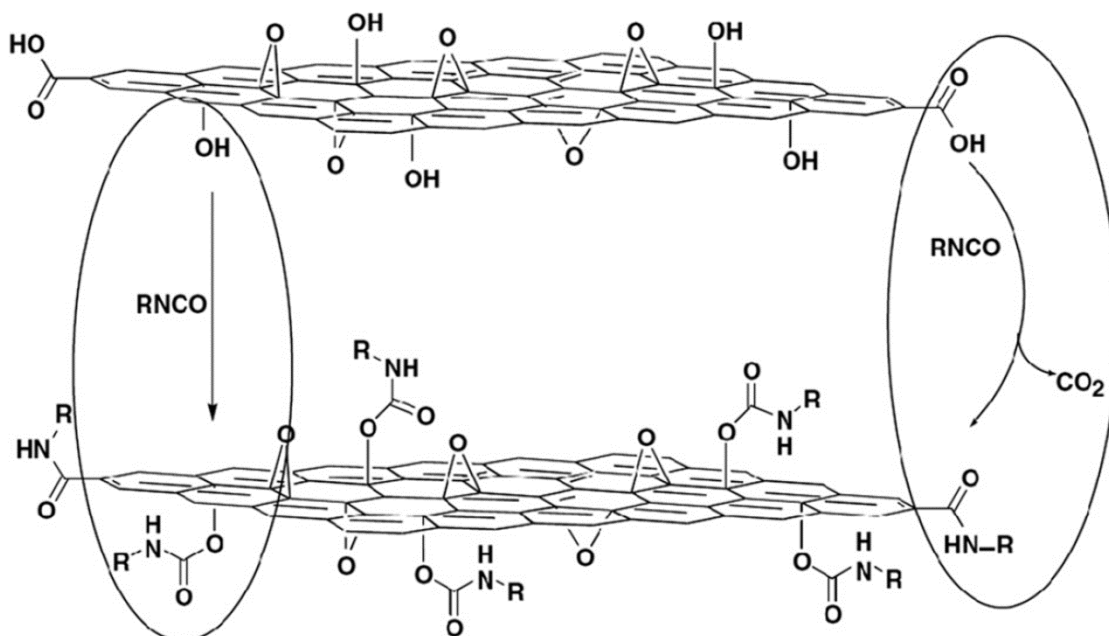


Fig. 2.41: Chemical functionalization of graphene oxide, adapted from [157].

The functionalization reduces the hydrophilic character of GO and effectively prevents restacking of the exfoliated graphene sheets due to reduced $\pi$–$\pi$ interactions. Moreover, it can be employed for covalent bonding of the polymer chains [157, 159]. This has not been reported for pCBT/graphene nanocomposites so far.

### 2.5.3  Nanocomposites with carbon nanotubes

Carbon nanotubes (CNT) are relatively new materials that can be thought as graphene sheets rolled into a cylindrical shape [139]. They exist either as single-walled (SWCNT) or multiwalled (MWCNT) carbon nanotubes and have gained considerable interest due to their remarkable physical, mechanical and electronic properties as well as a thermal conductivity higher than diamond [163]. Particularly, their exceptional mechanical properties combined with their low density make CNTs a promising nano-reinforcement and many polymer/CNT nanocomposites including PBT/CNT have been prepared [163-164]. However, only few pCBT/CNT nanocomposites have been reported in the literature.

Wu and co-workers [165] synthesized a cyclic initiator from dibutyl tin(IV) oxide and hydroxyl-functionalized multiwalled carbon nanotubes. This initiator was then used to initiate the ROP of CBT, resulting in pCBT/MWCNT nanocomposites. It was reported that pCBT was grafted onto the MWCNTs during ROP which enhanced the interfacial adhesion between the MWCNTs and the pCBT and thus improved the compatibility. The MWCNTs were found to be homogeneously dispersed in the matrix when the content was lower than 0.75 wt %, while higher MWCNT contents resulted in agglomeration. The MWCNTs acted as nucleation agent and significantly increased the crystallization rate of pCBT due to heterogeneous nucleation. The degree of crystallinity markedly increased with the addition of MWCNTs and the nanocomposites showed a nearly two-fold crystal fraction as compared to that of pCBT. The thermal stability of pCBT was found to be somewhat improved by the addition of MWCNT. However, residual carboxyl groups of the MWCNTs facilitated the thermal degradation of the pCBT matrix.

Romhány *et al.* [166] prepared pCBT/MWCNT nanocomposites by solid-phase high-energy ball milling of CBT with MWCNT with subsequent *in situ* polymerization. They reported that the MWCNTs did not significantly affect the crystallinity of the isothermally

produced pCBT but acted as nucleation agents during crystallization. The pCBT/MWCNT nanocomposites apparently exhibited an optimum MWCNT content because flexural modulus, strength, and impact strength went through a maximum as a function of the MWCNT content. Optimum properties were found in the MWCNT range of 0.25–0.5 wt.%.

Baets and associates [95, 127] used rotational mixing to disperse small amounts of MWCNTs (up to 0.1 wt.%) in CBT in an attempt to increase the toughness of the final pCBT. The addition of MWCNTs to pCBT resulted in an increase in stiffness, strength and energy to failure. However, the failure strain was found to decrease.

More recently, Noh *et al.* [167] studied the role of different surface treatments of MWCNTs on the electrical conductivity of pCBT/MWCNT nanocomposites. The authors used simple powder mixing of the components with subsequent ROP at 250 °C during compression moulding. The surface treatments included acid, hydrogen peroxide and heat treatments. The different functionalities of the MWCNTs (induced by the different surface treatments) altered the dispersion state of the incorporated MWCNTs in the MWCNT/pCBT nanocomposites, and the dispersion state was found to be the dominant physical factor that determined the electrical percolation behaviour of the nanocomposites.

### 2.5.4  Nanocomposites with POSS

Polyhedral oligomeric silsesquioxane, commonly referred to as POSS, is a new class of 0D-type nano-reinforcement and has attracted a great deal of attention in recent years. The term silsesquioxane refers to molecules, whose chemical structure follows the basic composition of $R_nSi_nO_{1.5n}$ [138]. The R-group, also called the vertex group, may be hydrogen, alkyl, alkylene, aryl arylene, amine, glycidyl among others. These organic vertex groups are responsible for the functionality, solubility, polarity and reactivity of the POSS molecules and can be easily tailored. The interactions and/or reactions of these organic functional groups with a polymer may result in the nanometric dispersion of POSS into the matrix [136-138]. The molecular architecture of POSS can be divided into caged structures and non-caged structures as shown in figure 2.42 a and b, respectively. Non-caged structures can be further classified into random, ladder and partial-cage structures.
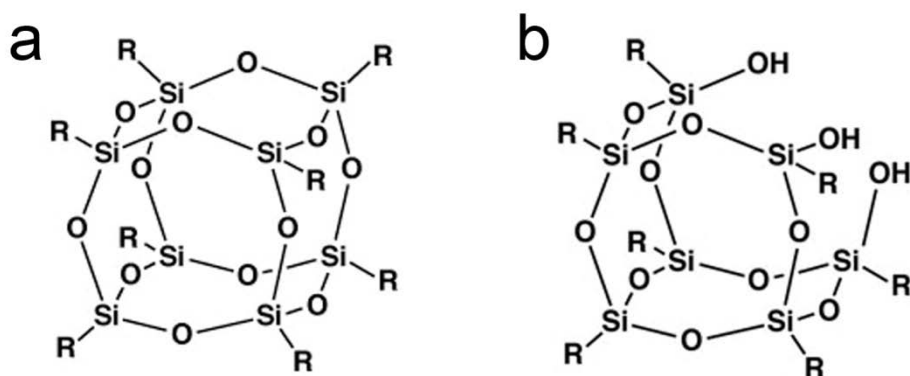
Fig. 2.42: Chemical structures of POSS; cage structure (a) and partial cage structure (b), after [138].

Polymer/POSS nanocomposites have been prepared using traditional melt blending routes [168-169], reactive blending [170] as well as copolymerization or grafting [171-173] *via* reactive R-groups of POSS. POSS has been successfully incorporated in various commodity [170, 174], engineering [168, 175] and high-performance [176-177] thermoplastic polymers. The incorporation of POSS can lead to dramatic improvements of several properties such as increases in use temperature, oxidation resistance, as well as reductions in flammability and viscosity during processing [136-137, 178].

Many polyester/POSS nanocomposites have been prepared using PET [179-184], polycarbonate [168-169, 185] or PBT [186-187] as matrix. Similar to other types of nano-reinforcements, synergetic reinforcing effects of POSS were only observed when good compatibility existed. Otherwise aggregation occurred which led to a decrease in mechanical properties.

Only few reports on pCBT/POSS nanocomposites are available. Wan *et al.* [152] used aminopropylisooctyl POSS as a surfactant for sodium montmorillonite and incorporated then CBT catalyst into the POSS-modified clay. This POSS-clay-catalyst complex was used as initiator of the ROP of CBT and clay exfoliation even at 10 wt.% of clay loading was achieved. This pCBT/POSS/clay nanocomposite was further used as a masterbatch for conventional PBT. While an increase in stiffness and strength was found for the PBT nanocomposites, no information on the mechanical properties of the pCBT nanocomposites was given.

Similarly, McLauchlin *et al.* [150] prepared a masterbatch of pCBT and POSS-modified clay which was subsequently melt blended with PBT to give nanocomposites containing 3 wt.% of clay. On one hand, an intercalated/exfoliated morphology with the related increase in stiffness and strength were observed for the PBT nanocomposite. On the other hand, the CBT catalyst present in the masterbatch caused a depolymerization of the PBT.

Wu *et al.* [188] reacted trisilanolisooctyl POSS with the butyltin trichloride initiator of CBT. This POSS-Sn initiator was used to prepare pCBT/POSS nanocomposites with up to 20 wt.% of POSS content. Glass transition temperature and crystallization temperature slightly increased with POSS loading and thermal stability of the nanocomposites improved by up to 11 °C. However, molecular weight decreased due to the increasing amounts of catalyst bonded to the POSS.

## 2.6   Conclusion

Cyclic butylene terephthalate oligomers are a promising alternative for thermoset matrices for fibre reinforced composites and also for conventional thermoplastic matrices in nanocomposites due to their remarkably low melt viscosity prior to polymerization. This unique property of CBT allows for facile impregnation of both fibrous and nano-reinforcements. Since the ring-opening polymerization is conducted *in situ*, CBT can be readily used as building blocks for copolymerization as well as for chemical modification. Moreover, isothermal processing of CBT with simultaneous polymerization and crystallization is possible.

However, pCBT is considerably more brittle as compared to conventional PBT and the toughening of pCBT has become of great interest since brittleness is an undesired property for structural materials. Despite the great attention paid to the toughening of pCBT, the reasons for the brittleness remain uncertain and a pCBT having similar toughness as PBT have not been achieved yet.

## 2.7    References

1.    van Rijswijk, K and Bersee, HEN. Reactive processing of textile fiber-reinforced thermoplastic composites – An overview. Composites Part A: Applied Science and Manufacturing **38**(3), 666-681 (2007).

2.    Campbell, FC. Chapter 10 - Thermoplastic composites: An unfulfilled promise. In: Campbell FC, editor. Manufacturing Processes for Advanced Composites. Amsterdam: Elsevier Science, 2003. pp. 357-397.

3.    Mohd Ishak, ZA, Gatos, KG, and Karger-Kocsis, J. On the in-situ polymerization of cyclic butylene terephthalate oligomers: DSC and rheological studies. Polymer Engineering & Science **46**(6), 743-750 (2006).

4.    Ó Máirtín, P, McDonnell, P, Connor, MT, Eder, R, and Ó Brádaigh, CM. Process investigation of a liquid PA-12/carbon fibre moulding system. Composites Part A: Applied Science and Manufacturing **32**(7), 915-923 (2001).

5.    Zingraff, L, Michaud, V, Bourban, PE, and Månson, JAE. Resin transfer moulding of anionically polymerised polyamide 12. Composites Part A: Applied Science and Manufacturing **36**(12), 1675-1686 (2005).

6.    Miller, AH, Dodds, N, Hale, JM, and Gibson, AG. High speed pultrusion of thermoplastic matrix composites. Composites Part A: Applied Science and Manufacturing **29**(7), 773-782 (1998).

7.    Steggall-Murphy, C, Simacek, P, Advani, SG, Yarlagadda, S, and Walsh, S. A model for thermoplastic melt impregnation of fiber bundles during consolidation of powder-impregnated continuous fiber composites. Composites Part A: Applied Science and Manufacturing **41**(1), 93-100 (2010).

8.    Wakeman, MD and Rudd, CD. 2.27 - Compression Molding of Thermoplastic Composites. In: Kelly A and Zweben C, editors. Comprehensive Composite Materials. Oxford: Pergamon, 2000. pp. 915-963.

9.    Parton, H. Characterization of the in-situ polymerization production process for continuous fibre reinforced thermoplastics. PhD thesis. Department of Metallurgy and Materials Engineering. Katholieke Universiteit Leuven: Leuven, Belgium, 2006

10.   Svensson, N, Shishoo, R, and Gilchrist, M. Manufacturing of Thermoplastic Composites from Commingled Yarns-A Review. Journal of Thermoplastic Composite Materials **11**(1), 22-56 (1998).

11. El-Dessouky, HM and Lawrence, CA. Ultra-lightweight carbon fibre/thermoplastic composite material using spread tow technology. Composites Part B: Engineering **50**(0), 91-97 (2013).

12. Sihn, S, Kim, RY, Kawabe, K, and Tsai, SW. Experimental studies of thin-ply laminated composites. Composites Science and Technology **67**(6), 996-1008 (2007).

13. Luisier, A, Bourban, PE, and Månson, JAE. Time–temperature–transformation diagram for reactive processing of polyamide 12. Journal of Applied Polymer Science **81**(4), 963-972 (2001).

14. Brunelle, DJ. Cyclic oligomer chemistry. Journal of Polymer Science Part A: Polymer Chemistry **46**(4), 1151-1164 (2008).

15. Hall, AJ and Hodge, P. Recent research on the synthesis and applications of cyclic oligomers. Reactive and Functional Polymers **41**(1-3), 133-139 (1999).

16. Pang, K, Kotek, R, and Tonelli, A. Review of conventional and novel polymerization processes for polyesters. Progress in Polymer Science **31**(11), 1009-1037 (2006).

17. Brunelle, D. Cyclic Oligomers of Polycarbonates and Polyesters. In: Semlyen JA, editor. Cyclic Polymers: Springer Netherlands, 2002. pp. 185-228.

18. Hill, JW and Carothers, WH. Cyclic and Polymeric Formals1. Journal of the American Chemical Society **57**(5), 925-928 (1935).

19. Spanagel, EW and Carothers, WH. Macrocyclic Esters. Journal of the American Chemical Society **57**(5), 929-934 (1935).

20. Brunelle, DJ. Macrocyclic Oligomers of Engineering Thermoplastics. In: Editors-in-Chief:  KHJB, Robert WC, Merton CF, Bernard I, Edward JK, Subhash M, and Patrick V, editors. Encyclopedia of Materials: Science and Technology (Second Edition). Oxford: Elsevier, 2001. pp. 4712-4720.

21. Luisier, A, Bourban, PE, and Månson, JAE. Reaction injection pultrusion of PA12 composites: process and modelling. Composites Part A: Applied Science and Manufacturing **34**(7), 583-595 (2003).

22. Wakeman, MD, Zingraff, L, Bourban, PE, Månson, JAE, and Blanchard, P. Stamp forming of carbon fibre/PA12 composites – A comparison of a reactive impregnation process and a commingled yarn system. Composites Science and Technology **66**(1), 19-35 (2006).

23. Ehrenstein, GW. Polymeric Materials: Carl Hanser Verlag GmbH & Co. KG, 2001.

24. East, GC and Girshab, AM. Cyclic oligomers in poly(1,4-butylene terephthalate). Polymer **23**(3), 323-324 (1982).

25. Tullo, A. BEST OF BOTH WORLDS. Chemical & Engineering News Archive **80**(44), 22 (2002).

26. Luisier, A, Bourban, PE, and Månson, JAE. Initiation mechanisms of an anionic ring-opening polymerization of lactam-12. Journal of Polymer Science Part A: Polymer Chemistry **40**(20), 3406-3415 (2002).

27. Luisier, A, Bourban, P-E, and Månson, J-A. In-situ polymerisation of polyamide 12 for thermoplastic composites. In: Proceedings of 12th international conference on composite materials (ICCM-12). Paris, France, 1999.

28. Schmid, E and Eder, R. Flüssiges System zur Durchführung der anionischen Lactampolymerisation. Ger. Pat. DE 19602684 C1. 1997.

29. Rösch, M. PBT Oligomers: Always in Good Form. Kunststoffe international **2005**(1), 91-93 (2005).

30. Hodge, P. Some applications of reactions which interconvert monomers, polymers and/or macrocycles. Reactive and Functional Polymers **48**(1–3), 15-23 (2001).

31. Kamau, SD, Hodge, P, and Helliwell, M. Cyclo-depolymerization of poly(propylene terephthalate): Some ring-opening polymerizations of the cyclic oligomers produced. Polymers for Advanced Technologies **14**(7), 492-501 (2003).

32. Burch, RR, Lustig, SR, and Spinu, M. Synthesis of Cyclic Oligoesters and Their Rapid Polymerization to High Molecular Weight†. Macromolecules **33**(14), 5053-5064 (2000).

33. Lee, WH, Ouyang, H, Shih, MC, and Wu, MH. Kinetics of solvent-induced crystallization of poly(ethylene terephthalate) at the final stage. Journal of Polymer Research-Taiwan **10**(2), 133-137 (2003).

34. Ouyang, H, Lee, W-H, Ouyang, W, Shiue, S-T, and Wu, T-M. Solvent-Induced Crystallization in Poly(ethylene terephthalate) during Mass Transport: Mechanism and Boundary Condition. Macromolecules **37**(20), 7719-7723 (2004).

35. Perovic, A and Murti, DK. The effect of coatings on the surface precipitation of oilgomeric crystals in poly(ethylene terephthalate) films. Journal of Applied Polymer Science **29**(12), 4321-4327 (1984).

36. Perovic, A and Sundararajan, PR. Crystallization of cyclic olicomers in commercial poly(ethyleneterephthalate) films. Polymer Bulletin **6**(5-6), 277-283 (1982).

37. Zhang, JL. Alkaline-solution-induced crystallization in poly(butylene terephthalate). Journal of Polymer Science Part B-Polymer Physics **42**(10), 1938-1948 (2004).

38. Bryant, JJL and Semlyen, JA. Cyclic polyesters: 7. Preparation and characterization of cyclic oligomers from solution ring-chain reactions of poly(butylene terephthalate). Polymer **38**(17), 4531-4537 (1997).

39. Hodge, P. Entropically Driven Ring-Opening Polymerization of Strainless Organic Macrocycles. Chemical Reviews, (2014).

40. Hodge, P and Colquhoun, HM. Recent work on entropically-driven ring-opening polymerizations: some potential applications. Polymers for Advanced Technologies **16**(2-3), 84-94 (2005).

41. Brunelle, DJ, Bradt, JE, Serth-Guzzo, J, Takekoshi, T, Evans, TL, Pearce, EJ, and Wilson, PR. Semicrystalline Polymers via Ring-Opening Polymerization: Preparation and Polymerization of Alkylene Phthalate Cyclic Oligomers. Macromolecules **31**(15), 4782-4790 (1998).

42. Hall, AJ and Hodge, P. Recent research on the synthesis and applications of cyclic oligomers. Reactive and Functional Polymers **41**(1–3), 133-139 (1999).

43. Hodge, P. Cyclodepolymerization as a method for the synthesis of macrocyclic oligomers. Reactive and Functional Polymers (http://dx.doi.org/10.1016/j.reactfunctpolym.2013.12.008), (2014).

44. Bryant, JJL and Semlyen, JA. Cyclic polyesters: 6. Preparation and characterization of two series of cyclic oligomers from solution ring-chain reactions of poly(ethylene terephthalate). Polymer **38**(10), 2475-2482 (1997).

45. González-Vidal, N, Martínez de Ilarduya, A, Herrera, V, and Muñoz-Guerra, S. Poly(hexamethylene terephthalate-co-caprolactone) Copolyesters Obtained by Ring-Opening Polymerization. Macromolecules **41**(12), 4136-4146 (2008).

46. González-Vidal, N, Martínez de Ilarduya, A, and Muñoz-Guerra, S. Poly(hexamethylene terephthalate-co-caprolactone) copolymers: Influence of cycle size on ring-opening polymerization. European Polymer Journal **46**(4), 792-803 (2010).

47. Hall, AJ, Hodge, P, McGrail, CS, and Rickerby, J. Synthesis of a series of cyclic oligo(alkylidene isophthalate)s by cyclo-depolymerisation. Polymer **41**(4), 1239-1249 (2000).

48.     Hubbard, PA, Brittain, WJ, Mattice, WL, and Brunelle, DJ. Ring-Size Distribution in the Depolymerization of Poly(butylene Terephthalate). Macromolecules **31**(5), 1518-1522 (1998).

49.     Brunelle, DJ. Method for polymerizing macrocyclic polyester oligomers. U.S. Patent 5,498,651. (1996).

50.     Brunelle, DJ and Takekoshi, T. Process for preparing macrocyclic polyester oligomers. Google Patents, 1995.

51.     Steeg, M, Mitschang, P, Chakraborty, P, and Hartmann, T. Modeling the viscosity and conversion of in-situ polymerizing PBT using empirical data. In: Proceedings of 17th international conference on composite materials (ICCM-17). Edinburgh, UK, 2009.

52.     Chen, H, Yu, W, and Zhou, C. Entropically-driven ring-opening polymerization of cyclic butylene terephthalate: Rheology and kinetics. Polymer Engineering & Science **52**(1), 91-101 (2012).

53.     Wu, C-M and Huang, C-W. Melting and crystallization behavior of copolymer from cyclic butylene terephthalate and polycaprolactone. Polymer Engineering & Science **51**(5), 1004-1013 (2011).

54.     Tripathy, AR, Elmoumni, A, Winter, HH, and MacKnight, WJ. Effects of catalyst and polymerization temperature on the in-situ polymerization of cyclic poly(butylene terephthalate) oligomers for composite applications. Macromolecules **38**(3), 709-715 (2005).

55.     Cyclics. CBT®160. Datasheet, available online: www.cyclics.com. [Accessed Sep. 28, 2009].

56.     Arkema. Fascat®4105. Datasheet, available online: www.arkemainc.us. [Accessed Sep. 28, 2009].

57.     Steeg, M. Prozesstechnologie für Cyclic Butylene Terephthalate im Faser-Kunststoff-Verbund. PhD thesis. Fachbereich Maschinenbau und Verfahrenstechnik. Technische Universität Kaiserslautern: Kaiserslautern, Germany, 2009

58.     Hakmé, C, Stevenson, I, Maazouz, A, Cassagnau, P, Boiteux, G, and Seytre, G. In situ monitoring of cyclic butylene terephtalate polymerization by dielectric sensing. Journal of Non-Crystalline Solids **353**(47–51), 4362-4365 (2007).

59.   Wunderlich, B. Crystallization during Polymerization. Angewandte Chemie International Edition in English **7**(12), 912-919 (1968).

60.   Wunderlich, B. Crystallization during polymerization. Fortschritte der Hochpolymeren-Forschung, vol. 5/4: Springer Berlin Heidelberg, 1968. pp. 568-619.

61.   Zhang, J, Wang, Z, Wang, B, Gou, Q, Zhang, J, Zhou, J, Li, Y, Chen, P, and Gu, Q. Living lamellar crystal initiating polymerization and brittleness mechanism investigations based on crystallization during the ring-opening of cyclic butylene terephthalate oligomers. Polymer Chemistry **4**(5), 1648-1656 (2013).

62.   Harsch, M, Karger-Kocsis, J, and Apostolov, AA. Crystallization-induced shrinkage, crystalline, and thermomechanical properties of in situ polymerized cyclic butylene terephthalate. Journal of Applied Polymer Science **108**(3), 1455-1461 (2008).

63.   Lehmann, B and Karger-Kocsis, J. Isothermal and non-isothermal crystallisation kinetics of pCBT and PBT. Journal of Thermal Analysis and Calorimetry **95**(1), 221-227 (2009).

64.   Avrami, M. Kinetics of Phase Change. I General Theory. The Journal of Chemical Physics **7**(12), 1103-1112 (1939).

65.   Avrami, M. Kinetics of Phase Change. II Transformation-Time Relations for Random Distribution of Nuclei. The Journal of Chemical Physics **8**(2), 212-224 (1940).

66.   Dangseeyun, N, Srimoaon, P, Supaphol, P, and Nithitanakul, M. Isothermal melt-crystallization and melting behavior for three linear aromatic polyesters. Thermochimica Acta **409**(1), 63-77 (2004).

67.   Wu, C-M and Jiang, C-W. Crystallization and morphology of polymerized cyclic butylene terephthalate. Journal of Polymer Science Part B: Polymer Physics **48**(11), 1127-1134 (2010).

68.   Hull, D. Matrix-dominated properties of polymer matrix composite materials. Materials Science and Engineering: A **184**(2), 173-183 (1994).

69.   Chen, X, Xu, J, Lu, H, and Yang, Y. Isothermal crystallization kinetics of poly(butylene terephthalate)/attapulgite nanocomposites. Journal of Polymer Science Part B: Polymer Physics **44**(15), 2112-2121 (2006).

70.   Radusch, HJ. Poly(Butylene Terephthalate). Handbook of Thermoplastic Polyesters: Wiley-VCH Verlag GmbH & Co. KGaA, 2005. pp. 389-419.

71. Shi, XQ, Aimi, K, Ito, H, Ando, S, and Kikutani, T. Characterization on mixed-crystal structure of poly(butylene terephthalate/succinate/adipate) biodegradable copolymer fibers. Polymer **46**(3), 751-760 (2005).

72. Yasuniwa, M, Tsubakihara, S, Ohoshita, K, and Tokudome, SI. X-ray studies on the double melting behavior of poly(butylene terephthalate). Journal of Polymer Science Part B: Polymer Physics **39**(17), 2005-2015 (2001).

73. Yokouchi, M, Sakakibara, Y, Chatani, Y, Tadokoro, H, Tanaka, T, and Yoda, K. Structures of Two Crystalline Forms of Poly(butylene terephthalate) and Reversible Transition between Them by Mechanical Deformation. Macromolecules **9**(2), 266-273 (1976).

74. Moneke, M. Die Kristallisation von verstärkten Thermoplasten während der schnellen Abkühlung und unter Druck. PhD thesis. TU Darmstadt: Darmstadt, 2001

75. Geil, PH. Crystal Structure, Morphology, and Orientation of Polyesters: Section 2.2. Handbook of Thermoplastic Polyesters: Wiley-VCH Verlag GmbH & Co. KGaA, 2005. pp. 154-167.

76. Stein, RS and Misra, A. Morphological studies on polybutylene terephthalate. Journal of Polymer Science: Polymer Physics Edition **18**(2), 327-342 (1980).

77. Parton, H, Baets, J, Lipnik, P, Goderis, B, Devaux, J, and Verpoest, I. Properties of poly(butylene terephthatlate) polymerized from cyclic oligomers and its composites. Polymer **46**(23), 9871-9880 (2005).

78. Miller, S. Macrocyclic polymers from cyclic oligomers of poly(butylene terephthalate). PhD thesis. University of Massachusetts Amherst: Amherst, USA, 1998

79. Karger-Kocsis, J, Shang, PP, Mohd Ishak, ZA, and Rösch, M. Melting and crystallization of in-situ polymerized cyclic butylene terephthalates with and without organoclay: A modulated DSC study. eXPRESS Polymer Letters **1**(2), 60-68 (2007).

80. Mohd Ishak, ZA, Leong, YW, Steeg, M, and Karger-Kocsis, J. Mechanical properties of woven glass fabric reinforced in situ polymerized poly(butylene terephthalate) composites. Composites Science and Technology **67**(3–4), 390-398 (2007).

81. Mohd Ishak, ZA, Shang, PP, and Karger-Kocsis, J. A modulated dsc study on the in situ polymerization of cyclic butylene terephthalate oligomers. Journal of Thermal Analysis and Calorimetry **84**(3), 637-641 (2006).

82. Tripathy, AR, MacKnight, WJ, and Kukureka, SN. In-Situ Copolymerization of Cyclic Poly(butylene terephthalate) Oligomers and ε-Caprolactone. Macromolecules **37**(18), 6793-6800 (2004).

83. Parton, H and Verpoest, I. In situ polymerization of thermoplastic composites based on cyclic oligomers. Polymer Composites **26**(1), 60-65 (2005).

84. Baets, J. Toughening of in-situ polymerized cyclic butyleneterephthalate for use in continuous fiber reinforced thermoplastic composites. PhD thesis. Department of Metallurgy and Materials Engineering. Katholieke Universiteit Leuven: Leuven, Belgium, 2008

85. Balogh, G. Development of cyclic butylene terephthalate matrix composites. PhD thesis. Department of Polymer Engineering. Budapest University of Technology and Economics: Budapest, Hungary, 2012

86. Ludwig, HJ and Eyerer, P. Influence of the processing conditions on morphology and deformation behavior of poly(butylene terephthalate) (PBT). Polymer Engineering & Science **28**(3), 143-146 (1988).

87. Zhang, J. Study of poly(trimethylene terephthalate) as an engineering thermoplastics material. Journal of Applied Polymer Science **91**(3), 1657-1666 (2004).

88. Yu, T, Wu, CM, Chang, CY, Wang, CY, and Rwei, SP. Effects of crystalline morphologies on the mechanical properties of carbon fiber reinforcing polymerized cyclic butylene terephthalate composites. eXPRESS Polymer Letters **6**(4), 318-328 (2012).

89. Mandelkern, L. The Relation between Structure and Properties of Crystalline Polymers. Polymer Journal **17**(1), 337-350 (1985).

90. Mandelkern, L. The structure of crystalline polymers. Accounts of Chemical Research **23**(11), 380-386 (1990).

91. Xu, D and Karger-Kocsis, J. Rolling and sliding wear properties of hybrid systems composed of uncured/cured HNBR and partly polymerized cyclic butylene terephthalate (CBT). Tribology International **43**(1-2), 289-298.

92. Xu, D, Karger-Kocsis, J, and Apostolov, AA. Hybrids from HNBR and in situ polymerizable cyclic butylene terephthalate (CBT): Structure and rolling wear properties. European Polymer Journal **45**(4), 1270-1281 (2009).

93. Bikiaris, DN and Karayannidis, GP. Effect of carboxylic end groups on thermooxidative stability of PET and PBT. Polymer Degradation and Stability **63**(2), 213-218 (1999).

94. Nielsen, LE and Landel, RF. Mechanical Properties of Polymers and Composites., 2nd ed. ed. New York: Marcel Dekker, 1994.

95. Baets, J, Godara, A, Devaux, J, and Verpoest, I. Toughening of polymerized cyclic butylene terephthalate with carbon nanotubes for use in composites. Composites Part A: Applied Science and Manufacturing **39**(11), 1756-1761 (2008).

96. Vincent, PI. The tough-brittle transition in thermoplastics. Polymer **1**(0), 425-444 (1960).

97. Baets, J, Devaux, J, and Verpoest, I. Toughening of basalt fiber-reinforced composites with a cyclic butylene terephthalate matrix by a nonisothermal production method. Advances in Polymer Technology **29**(2), 70-79 (2010).

98. Dion, RP, Bank, DH, Beebe, MC, Walia, P, LeBaron, C, Oelberg, JD, Barger, MA, Paquette, MS, and Read, MD. Polymerized macrocyclic oligomer nanocomposite compositions. U.S. Patent Application US 2005/0059768 A1. (2005).

99. Takekoshi, T, Phelps, PD, Wang, Y, and Winckler, SJ. Methods for polymerizing macrocyclic polyester oligomers using catalyst promoters. U.S. Patent Application Publication US 2006/0115666 A1. (2006).

100. Karger-Kocsis, J, Felhos, D, Bárány, T, and Czigány, T. Hybrids of HNBR and in situ polymerizable cyclic butylene terephthalate (CBT) oligomers: Properties and dry sliding behavior. eXPRESS Polymer Letters **2**(7), 520-527 (2008).

101. Mozheiko, YM. Properties of Block Copolymers of Poly(Butylene Terephthalate) and Polyoxytetramethylene Glycol. Fibre Chemistry **34**(4), 254-259 (2002).

102. Devroede, J. Study of the THF formation during the TPA-based synthesis of PBT. PhD thesis. Dutch Polymer Institute. Technische Universiteit Eindhoven: Eindhoven, Netherlands, 2007

103. Maier, S. Carbonylbiscaprolactam (CBC): Isocyanat-freier Zugang zu blockierten Isocyanaten, Blockcopolymeren und reaktiven Dispersionen. PhD thesis. Institut für

Makromolekulare Chemie Albert-Ludwigs-Universität Freiburg im Breisgau: Freiburg im Breisgau, Germany, 2003

104. Maréchal, E. Creation and Development of Thermoplastic Elastomers, and Their Position among Organic Materials. Handbook of Condensation Thermoplastic Elastomers: Wiley-VCH Verlag GmbH & Co. KGaA, 2006. pp. 1-31.

105. Nagai, Y, Ogawa, T, Nishimoto, Y, and Ohishi, F. Analysis of weathering of a thermoplastic polyester elastomer II. Factors affecting weathering of a polyether–polyester elastomer. Polymer Degradation and Stability **65**(2), 217-224 (1999).

106. Nagai, Y, Ogawa, T, Yu Zhen, L, Nishimoto, Y, and Ohishi, F. Analysis of weathering of thermoplastic polyester elastomers—I. Polyether-polyester elastomers. Polymer Degradation and Stability **56**(1), 115-121 (1997).

107. Quirk, RP, Holden, G, and Kricheldorf, HR. Thermoplastic Elastomers: Hanser, 2004.

108. Maier, S, Loontjens, T, Scholtens, B, and Mülhaupt, R. Isocyanate-Free Route to Caprolactam-Blocked Oligomeric Isocyanates via Carbonylbiscaprolactam- (CBC-) Mediated End Group Conversion. Macromolecules **36**(13), 4727-4734 (2003).

109. Bahloul, W, Bounor-Legare, V, Fenouillot, F, and Cassagnau, P. EVA/PBT nanostructured blends synthesized by in situ polymerization of cyclic cBT (cyclic butylene terephthalate) in molten EVA. Polymer **50**(12), 2527-2534 (2009).

110. Tripathy, AR, Chen, WJ, Kukureka, SN, and MacKnight, WJ. Novel poly(butylene terephthalate)/poly(vinyl butyral) blends prepared by in situ polymerization of cyclic poly(butylene terephthalate) oligomers. Polymer **44**(6), 1835-1842 (2003).

111. Baets, J, Dutoit, M, Devaux, J, and Verpoest, I. Toughening of glass fiber reinforced composites with a cyclic butylene terephthalate matrix by addition of polycaprolactone. Composites Part A: Applied Science and Manufacturing **39**(1), 13-18 (2008).

112. Tripathy, AR, Farris, RJ, and MacKnight, WJ. Novel fire resistant matrixes for composites from cyclic poly(butylene terephthalate) oligomers. Polymer Engineering & Science **47**(10), 1536-1543 (2007).

113. Samsudin, SA, Kukureka, SN, and Jenkins, MJ. Miscibility in cyclic poly(butylene terephthalate) and styrene maleimide blends prepared by solid-dispersion and in situ polymerization of cyclic butylene terephthalate oligomers within styrene maleimide. Journal of Applied Polymer Science **126**(S2), E290-E297 (2012).

114. Aróstegui, A and Nazábal, J. Compatibilization of a poly(butylene terephthalate)/poly(ethylene octene) copolymer blends with different amounts of an epoxy resin. Journal of Applied Polymer Science **91**(1), 260-269 (2004).

115. Bikiaris, DN and Karayannidis, GP. Chain extension of polyesters PET and PBT with two new diimidodiepoxides. II. Journal of Polymer Science Part A: Polymer Chemistry **34**(7), 1337-1342 (1996).

116. Guo, B and Chan, C-M. Chain extension of poly(butylene terephthalate) by reactive extrusion. Journal of Applied Polymer Science **71**(11), 1827-1834 (1999).

117. Tang, X, Guo, W, Yin, G, Li, B, and Wu, C. Reactive extrusion of recycled poly(ethylene terephthalate) with polycarbonate by addition of chain extender. Journal of Applied Polymer Science **104**(4), 2602-2607 (2007).

118. Xanthos, M. Reactive Modification/Compatibilization of Polyesters. Handbook of Thermoplastic Polyesters: Wiley-VCH Verlag GmbH & Co. KGaA, 2005. pp. 815-833.

119. Xanthos, M, Young, MW, Karayanndis, GP, and Bikiaris, DN. Reactive modification of polyethylene terephthalate with polyepoxides. Polymer Engineering & Science **41**(4), 643-655 (2001).

120. Dhavalikar, RR. Reactive melt modification of polyethylene terephthalate. PhD thesis. Department of Chemical Engineering. New Jersey Institute of Technology: Newark, NJ, USA, 2003

121. Inata, H and Matsumura, S. Chain extenders for polyesters. I. Addition-type chain extenders reactive with carboxyl end groups of polyesters. Journal of Applied Polymer Science **30**(8), 3325-3337 (1985).

122. Inata, H and Matsumura, S. Chain extenders for polyester. II. Reactivities of carboxyl-addition-type chain extenders; bis cyclic-imino-ethers. Journal of Applied Polymer Science **32**(5), 5193-5202 (1986).

123. Inata, H and Matsumura, S. Chain extenders for polyesters. III. Addition-type nitrogen-containing chain extenders reactive with hydroxyl end groups of polyesters. Journal of Applied Polymer Science **32**(4), 4581-4594 (1986).

124. Inata, H and Matsumura, S. Chain extenders for polyesters. IV. Properties of the polyesters chain-extended by 2,2′-bis(2-oxazoline). Journal of Applied Polymer Science **33**(8), 3069-3079 (1987).

125. Inata, H and Matsumura, S. Chain extenders for polyesters. V. Reactivities of hydroxyl-addition-type chain extender; 2,2′-bis(4h-3,1-benzoxazin-4-one). Journal of Applied Polymer Science **34**(7), 2609-2617 (1987).

126. Inata, H and Matsumura, S. Chain extenders for polyesters. VI. Properties of the polyesters chain-extended by 2,2′-bis(4H-3,1-benzoxazin-4-one). Journal of Applied Polymer Science **34**(8), 2769-2776 (1987).

127. Baets, J, Godara, A, Devaux, J, and Verpoest, I. Toughening of isothermally polymerized cyclic butylene terephthalate for use in composites. Polymer Degradation and Stability **95**(3), 346-352 (2010).

128. Broza, G, Kwiatkowska, M, Rosłaniec, Z, and Schulte, K. Processing and assessment of poly(butylene terephthalate) nanocomposites reinforced with oxidized single wall carbon nanotubes. Polymer **46**(16), 5860-5867 (2005).

129. Alexandre, M and Dubois, P. Polymer-layered silicate nanocomposites: preparation, properties and uses of a new class of materials. Materials Science and Engineering: R: Reports **28**(1–2), 1-63 (2000).

130. Kiliaris, P and Papaspyrides, CD. Polymer/layered silicate (clay) nanocomposites: An overview of flame retardancy. Progress in Polymer Science **35**(7), 902-958 (2010).

131. Sinha Ray, S and Okamoto, M. Polymer/layered silicate nanocomposites: a review from preparation to processing. Progress in Polymer Science **28**(11), 1539-1641 (2003).

132. Potts, JR, Dreyer, DR, Bielawski, CW, and Ruoff, RS. Graphene-based polymer nanocomposites. Polymer **52**(1), 5-25 (2011).

133. Singh, V, Joung, D, Zhai, L, Das, S, Khondaker, SI, and Seal, S. Graphene based materials: Past, present and future. Progress in Materials Science **56**(8), 1178-1271 (2011).

134. Sandler, JKW and Shaffer, MSP. Carbon Nanotube/Nanofibre Polymer Composites. Processing and Properties of Nanocomposites. pp. 1-59.

135. Coleman, JN, Khan, U, and Gun'ko, YK. Mechanical Reinforcement of Polymers Using Carbon Nanotubes. Advanced Materials **18**(6), 689-706 (2006).

136. Joshi, M and Butola, BS. Polymeric Nanocomposites—Polyhedral Oligomeric Silsesquioxanes (POSS) as Hybrid Nanofiller. Journal of Macromolecular Science, Part C **44**(4), 389-410 (2004).

137. Kuo, S-W and Chang, F-C. POSS related polymer nanocomposites. Progress in Polymer Science **36**(12), 1649-1696 (2011).

138. Wu, J and Mather, PT. POSS Polymers: Physical Properties and Biomaterials Applications. Polymer Reviews **49**(1), 25-63 (2009).

139. Soldano, C, Mahmood, A, and Dujardin, E. Production, properties and potential of graphene. Carbon **48**(8), 2127-2150 (2010).

140. Berti, C, Fiorini, M, and Sisti, L. Synthesis of poly(butylene terephtahlate) nanocomposites using anionic clays. European Polymer Journal **45**(1), 70-78 (2009).

141. Chang, Y-W, Kim, S, and Kyung, Y. Poly(butylene terephthalate)–clay nanocomposites prepared by melt intercalation: morphology and thermomechanical properties. Polymer International **54**(2), 348-353 (2005).

142. Hwang, S-s, Liu, S-p, Hsu, PP, Yeh, J-m, Chang, K-c, and Lai, Y-z. Effect of organoclay on the mechanical/thermal properties of microcellular injection molded PBT–clay nanocomposites. International Communications in Heat and Mass Transfer **37**(8), 1036-1043 (2010).

143. Li, X, Kang, T, Cho, W-J, Lee, J-K, and Ha, C-S. Preparation and Characterization of Poly(butyleneterephthalate)/Organoclay Nanocomposites. Macromolecular Rapid Communications **22**(16), 1306-1312 (2001).

144. Xiao, J, Hu, Y, Wang, Z, Tang, Y, Chen, Z, and Fan, W. Preparation and characterization of poly(butylene terephthalate) nanocomposites from thermally stable organic-modified montmorillonite. European Polymer Journal **41**(5), 1030-1035 (2005).

145. Berti, C, Binassi, E, Colonna, M, Fiorini, M, Zuccheri, T, Karanam, S, and J. Brunelle, D. Improved dispersion of clay platelets in poly(butylene terephthalate) nanocomposite by ring-opening polymerization of cyclic oligomers: Effect of the processing conditions and comparison with nanocomposites obtained by melt intercalation. Journal of Applied Polymer Science **114**(5), 3211-3217 (2009).

146. Dion, RP, Bank, DH, Beebe, MC, Walia, P, LeBaron, C, Oelberg, JD, Barger, MA, Paquette, MS, and Read, MD. Polymerized macrocyclic oligomer nanocomposite compositions. U.S. Patent Application US 2005/0059768 A1. 2005.

147. Hong, Y, Yoon, H, and Lim, S. Preparation of PBT/clay nanocomposites using supercritical process. International Journal of Precision Engineering and Manufacturing **10**(3), 115-118 (2009).

148. Lanciano, G, Greco, A, Maffezzoli, A, and Mascia, L. Effects of thermal history in the ring opening polymerization of CBT and its mixtures with montmorillonite on the crystallization of the resulting poly(butylene terephthalate). Thermochimica Acta **493**(1-2), 61-67 (2009).

149. Lee, S-S, Ma, YT, Rhee, H-W, and Kim, J. Exfoliation of layered silicate facilitated by ring-opening reaction of cyclic oligomers in PET–clay nanocomposites. Polymer **46**(7), 2201-2210 (2005).

150. McLauchlin, A, Bao, X, and Zhao, F. Organoclay polybutylene terephthalate nanocomposites using dual surfactant modified montmorillonite prepared by the masterbatch method. Applied Clay Science **53**(4), 749-753 (2011).

151. Tripathy, AR, Burgaz, E, Kukureka, SN, and MacKnight, WJ. Poly(butylene terephthalate) nanocomposites prepared by in-situ polymerization. Macromolecules **36**(23), 3 (2003).

152. Wan, C, Zhao, F, Bao, X, Kandasubramanian, B, and Duggan, M. Surface Characteristics of Polyhedral Oligomeric Silsesquioxane Modified Clay and Its Application in Polymerization of Macrocyclic Polyester Oligomers. The Journal of Physical Chemistry B **112**(38), 11915-11922 (2008).

153. Wu, FM and Yang, GS. Poly(butylene terephthalate)/organoclay nanocomposites prepared by in-situ bulk polymerization with cyclic poly(butylene terephthalate). Materials Letters **63**(20), 1686-1688 (2009).

154. Kuila, T, Bose, S, Mishra, AK, Khanra, P, Kim, NH, and Lee, JH. Chemical functionalization of graphene and its applications. Progress in Materials Science **57**(7), 1061-1105 (2012).

155. Kuilla, T, Bhadra, S, Yao, D, Kim, NH, Bose, S, and Lee, JH. Recent advances in graphene based polymer composites. Progress in Polymer Science **35**(11), 1350-1375 (2010).

156. Hummers, WS and Offeman, RE. Preparation of Graphitic Oxide. Journal of the American Chemical Society **80**(6), 1339-1339 (1958).

157. Stankovich, S, Piner, RD, Nguyen, ST, and Ruoff, RS. Synthesis and exfoliation of isocyanate-treated graphene oxide nanoplatelets. Carbon **44**(15), 3342-3347 (2006).

158. Stankovich, S, Dikin, DA, Piner, RD, Kohlhaas, KA, Kleinhammes, A, Jia, Y, Wu, Y, Nguyen, ST, and Ruoff, RS. Synthesis of graphene-based nanosheets via chemical reduction of exfoliated graphite oxide. Carbon **45**(7), 1558-1565 (2007).

159. Stankovich, S, Dikin, DA, Dommett, GHB, Kohlhaas, KM, Zimney, EJ, Stach, EA, Piner, RD, Nguyen, ST, and Ruoff, RS. Graphene-based composite materials. Nature **442**(7100), 282-286 (2006).

160. Chen, H, Huang, C, Yu, W, and Zhou, C. Effect of thermally reduced graphite oxide (TrGO) on the polymerization kinetics of poly(butylene terephthalate) (pCBT)/TrGO nanocomposites prepared by in situ ring-opening polymerization of cyclic butylene terephthalate. Polymer **54**(6), 1603-1611 (2013).

161. Fabbri, P, Bassoli, E, Bon, SB, and Valentini, L. Preparation and characterization of poly (butylene terephthalate)/graphene composites by in-situ polymerization of cyclic butylene terephthalate. Polymer **53**(4), 897-902 (2012).

162. Balogh, G, Hajba, S, Karger-Kocsis, J, and Czigány, T. Preparation and characterization of in situ polymerized cyclic butylene terephthalate/graphene nanocomposites. Journal of Materials Science **48**(6), 2530-2535 (2013).

163. Thostenson, ET, Ren, Z, and Chou, T-W. Advances in the science and technology of carbon nanotubes and their composites: a review. Composites Science and Technology **61**(13), 1899-1912 (2001).

164. Wu, D, Wu, L, Yu, G, Xu, B, and Zhang, M. Crystallization and thermal behavior of multiwalled carbon nanotube/poly(butylenes terephthalate) composites. Polymer Engineering & Science **48**(6), 1057-1067 (2008).

165. Wu, F and Yang, G. Poly(butylene terephthalate)-functionalized MWNTs by in situ ring-opening polymerization of cyclic butylene terephthalate oligomers. Polymers for Advanced Technologies **22**(10), 1466-1470 (2011).

166. Romhány, G, Vígh, J, Thomann, R, Karger-Kocsis, J, and Sajó, IE. pCBT/MWCNT Nanocomposites Prepared by In situ Polymerization of CBT After Solid-Phase High-Energy Ball Milling of CBT with MWCNT. Macromolecular Materials and Engineering **296**(6), 544-550 (2011).

167. Noh, YJ, Pak, SY, Hwang, SH, Hwang, JY, Kim, SY, and Youn, JR. Enhanced dispersion for electrical percolation behavior of multi-walled carbon nanotubes in polymer nanocomposites using simple powder mixing and in situ polymerization with surface treatment of the fillers. Composites Science and Technology **89**(0), 29-37 (2013).

168. Sánchez-Soto, M, Schiraldi, DA, and Illescas, S. Study of the morphology and properties of melt-mixed polycarbonate–POSS nanocomposites. European Polymer Journal **45**(2), 341-352 (2009).

169. Zhao, Y and Schiraldi, DA. Thermal and mechanical properties of polyhedral oligomeric silsesquioxane (POSS)/polycarbonate composites. Polymer **46**(25), 11640-11647 (2005).

170. Fina, A, Tabuani, D, Peijs, T, and Camino, G. POSS grafting on PPgMA by one-step reactive blending. Polymer **50**(1), 218-226 (2009).

171. Misra, R, Alidedeoglu, AH, Jarrett, WL, and Morgan, SE. Molecular miscibility and chain dynamics in POSS/polystyrene blends: Control of POSS preferential dispersion states. Polymer **50**(13), 2906-2918 (2009).

172. Romo–Uribe, A, Mather, PT, Haddad, TS, and Lichtenhan, JD. Viscoelastic and morphological behavior of hybrid styryl-based polyhedral oligomeric silsesquioxane (POSS) copolymers. Journal of Polymer Science Part B: Polymer Physics **36**(11), 1857-1872 (1998).

173. Zhang, W, Fu, BX, Seo, Y, Schrag, E, Hsiao, B, Mather, PT, Yang, N-L, Xu, D, Ade, H, Rafailovich, M, and Sokolov, J. Effect of Methyl Methacrylate/Polyhedral Oligomeric Silsesquioxane Random Copolymers in Compatibilization of Polystyrene and Poly(methyl methacrylate) Blends. Macromolecules **35**(21), 8029-8038 (2002).

174. Chen, J-H, Yao, B-X, Su, W-B, and Yang, Y-B. Isothermal crystallization behavior of isotactic polypropylene blended with small loading of polyhedral oligomeric silsesquioxane. Polymer **48**(6), 1756-1769 (2007).

175. Huang, K-W, Tsai, L-W, and Kuo, S-W. Influence of octakis-functionalized polyhedral oligomeric silsesquioxanes on the physical properties of their polymer nanocomposites. Polymer **50**(20), 4876-4887 (2009).

176. Verker, R, Grossman, E, Gouzman, I, and Eliaz, N. TriSilanolPhenyl POSS–polyimide nanocomposites: Structure–properties relationship. Composites Science and Technology **69**(13), 2178-2184 (2009).

177. Zeng, K, Liu, Y, and Zheng, S. Poly(ethylene imine) hybrids containing polyhedral oligomeric silsesquioxanes: Preparation, structure and properties. European Polymer Journal **44**(12), 3946-3956 (2008).

178. Zheng, L, Farris, RJ, and Coughlin, EB. Novel Polyolefin Nanocomposites: Synthesis and Characterizations of Metallocene-Catalyzed Polyolefin Polyhedral Oligomeric Silsesquioxane Copolymers. Macromolecules **34**(23), 8034-8039 (2001).

179. Ciolacu, FCL, Choudhury, NR, Dutta, N, and Kosior, E. Molecular Level Stabilization of Poly(ethylene terephthalate) with Nanostructured Open Cage Trisilanolisobutyl-POSS. Macromolecules **40**(2), 265-272 (2006).

180. Kim, JK, Yoon, KH, Bang, DS, Park, Y-B, Kim, H-U, and Bang, Y-H. Morphology and rheological behaviors of poly(ethylene terephthalate) nanocomposites containing polyhedral oligomeric silsesquioxanes. Journal of Applied Polymer Science **107**(1), 272-279 (2008).

181. Sirin, H, Turan, D, Ozkoc, G, and Gurdag, S. POSS reinforced PET based composite fibers: "Effect of POSS type and loading level". Composites Part B: Engineering **53**(0), 395-403 (2013).

182. Vannier, A, Duquesne, S, Bourbigot, S, Castrovinci, A, Camino, G, and Delobel, R. The use of POSS as synergist in intumescent recycled poly(ethylene terephthalate). Polymer Degradation and Stability **93**(4), 818-826 (2008).

183. Yoon, KH, Polk, MB, Park, JH, Min, BG, and Schiraldi, DA. Properties of poly(ethylene terephthalate) containing epoxy-functionalized polyhedral oligomeric silsesquioxane. Polymer International **54**(1), 47-53 (2005).

184. Zeng, J, Kumar, S, Iyer, S, Schiraldi, DA, and Gonzalez, RI. Reinforcement of Poly(ethylene terephthalate) Fibers with Polyhedral Oligomeric Silsesquioxanes (POSS). High Performance Polymers **17**(3), 403-424 (2005).

185. Hao, N, Böhning, M, Goering, H, and Schönhals, A. Nanocomposites of Polyhedral Oligomeric Phenethylsilsesquioxanes and Poly(bisphenol A carbonate) as Investigated by Dielectric Spectroscopy. Macromolecules **40**(8), 2955-2964 (2007).

186. Cozza, ES, Ma, Q, Monticelli, O, and Cebe, P. Nanostructured nanofibers based on PBT and POSS: Effect of POSS on the alignment and macromolecular orientation of the nanofibers. European Polymer Journal **49**(1), 33-40 (2013).

187.  Zhou, Z, Yin, N, Zhang, Y, and Zhang, Y. Properties of poly(butylene terephthalate) chain-extended by epoxycyclohexyl polyhedral oligomeric silsesquioxane. Journal of Applied Polymer Science **107**(2), 825-830 (2008).

188.  Wu, F, Xie, T, and Yang, G. Characterization of PBT/POSS nanocomposites prepared by in situ polymerization of cyclic poly(butylene terephthalate) initiated by functionalized POSS. Journal of Polymer Science Part B: Polymer Physics **48**(16), 1853-1859 (2010).

# Chapter 3: Materials

## 3.1    Cyclic butylene terephthalate

Cyclic butylene terephthalate oligomers were used throughout this work. The oligomers were supplied by Cyclics Europe GmbH, Schwarzheide, Germany. These oligomers exhibit two to seven repeat units per macrocycle which results in a melting range of 120–160 °C [1-2]. Two different grades of CBT were used: CBT[®]100 and CBT[®]160.

### 3.1.1  CBT100[®]

CBT100 are uncatalysed  oligomers which have to be mixed with the catalyst butyl tin chloride dihydroxide (grade: Fascat[®] 4105 [3], Arkema, Inc., Philadelphia, PA, USA) prior to ROP [4]. The resin was in granule form and was ground into a fine powder using mortar and pestle; vacuum dried for 8 h at 80 °C and stored in a desiccator over silica gel until further use.

### 3.1.2  CBT160[®]

CBT160 is a one-component resin and contains 0.45 wt.% butyl tin chloride dihydroxide as catalyst [5]. It is a mixture of low molecular weight oligomers (around dimer 40 wt.%, trimer 35 wt.%, tetramer 15 wt%, and pentamer and higher 10 wt.%) with two to seven butyl groups [6]. This resin was also provided in granule form and was ground into a fine powder using mortar and pestle; vacuum dried for 8 h at 80 °C and kept in a desiccator over silica gel until further use.

Only few samples were produced with the two-component CBT100; the material of choice was mostly the one-component CBT160. This was due to the ease of processing of a one-component system compared to a two-component resin. CBT100 requires an

additional processing step of mixing the molten oligomers with the catalyst whereas CBT160 can be processed directly.

## 3.2    Polytetrahydrofuran

Polytetrahydrofuran (polyTHF) was supplied by Sigma-Aldrich (St. Louis, MO, USA) and was used as received. The OH-terminated polyTHF had a molecular weight of 1000 g/mol according to the producer [7]; its chemical structure is shown in figure 3.1.
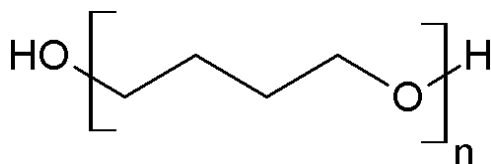


Fig. 3.1: Chemical structure of polyTHF [7].

## 3.3    Solvents

### 3.3.1  Tetrahydrofuran

Analytical grade tetrahydrofuran (referred to as THF; $C_4H_8O$; MW = 72.1 g/mol; purity = 99.5%; water content = 0.05%) was purchased from Panreac Química S.A. (Barcelona, Spain) and was used as received. The THF was stabilized with ~300 ppm of butylated hydroxytoluene to prevent the formation of explosive peroxides during storage.

### 3.3.2  Hexafluoroisopropanol

1,1,1,3,3,3-hexafluoroisopropanol (denoted as HFIP; $C_3H_2F_6O$; MW = 168.0 g/mol; purity ≥ 99%) was supplied by Fluka Analytical (St. Louis, MO, USA). The HFIP was of analytical

grade and was stabilized with 6.8 g/L sodium fluoroacetate to prevent polyelectrolyte effect.

### 3.3.3 Ethanol

Analytical grade absolute dry ethanol ($C_2H_6O$; MW = 46.1 g/mol; purity = 99.8%; water content = 0.02%) was purchased from Panreac Química S.A. (Barcelona, Spain) and was used as received.

### 3.3.4 Acetone

Analytical grade dry acetone ($C_3H_6O$; MW = 58.1 g/mol; purity = 99%; water content = 0.01%) was purchased from Panreac Química S.A. (Barcelona, Spain) and was used as received.

### 3.3.5 Dimethylformamide

Analytical grade N,N-dimethylformamide (referred to as DMF; $C_3H_7NO$; MW = 73.1 g/mol; purity = 99%; water content = 0.3%) was purchased from Panreac Química S.A. (Barcelona, Spain) and was used as received.

## 3.4 Toughening agents

### 3.4.1 Epoxy resins

Four types of epoxy resins (referred to as EP) were used as toughening agents; ranging from low molecular weight, liquid resin to intermediate and high molecular weight, solid epoxy resin.

A liquid, low molecular weight epoxy resin (Eporai® 450/A) was purchased from IQRaisa S.L., Valencia, Spain and was used as received. The epoxy resin was a low-viscous, bifunctional type based on Bisphenol A (BPA) and was characterized by an epoxy equivalent weight (EEW) of 148–155 g/eq according to the manufacturer [8].

A solid, medium molecular weight epoxy resin based on BPA (Araldite® GT 7071, Jubail Chemical Industries Co. (JANA), Saudi Arabia) was used as received. The epoxy resin was a bifunctional type and had an epoxy equivalent weight of 500–525 g/eq (ASTM D-1652) and a $T_g$ of 42 °C according to the material data sheet [9].

A solid, medium molecular weight epoxy resin based on BPA (Araldite® GT 7004, Jubail Chemical Industries Co. (JANA), Saudi Arabia) was used as received. The bifunctional epoxy resin had an EEW of 714–752 g/eq (ASTM D-1652) and a $T_g$ of 57 °C according to the manufacturer [10].

A solid, high molecular weight epoxy resin based on BPA (Araldite® GT 6097, Jubail Chemical Industries Co. (JANA), Saudi Arabia) was used as received. The bifunctional epoxy resin had an EEW of 1695–1885 g/eq (ASTM D-1652) and a $T_g$ of 73 °C according to the material data sheet [11].

The chemical structures of low molecular weight epoxy resin and medium- and high molecular weight epoxy resins are depicted in Figure 3.2a and b, respectively.
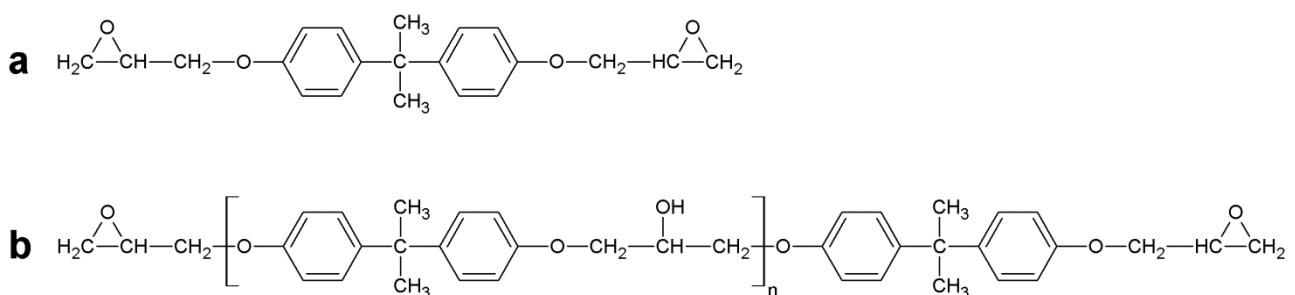


Fig. 3.2: Chemical structures of Eporai® 450/A (a), Araldite® GT 7071, Araldite® GT 7004 and Araldite® GT 6097 (b) [8-11].

### 3.4.2 Isocyanates

Three different types of isocyanates were used as toughening agents; their chemical structures are depicted in Figure 3.3. Hexamethylene diisocyanate (referred to as HDI) had a molecular weight of 168.2 g/mol and was a liquid aliphatic diisocyanate according to the material data sheet [12]. 4,4"-methylenebis(phenyl isocyanate) (referred to as MDI) had a molecular weight of 250.3 g/mol and was a solid aromatic diisocyanate according to [13]. Both types were analytical grades from Sigma-Aldrich (St. Louis, MO, USA) and were used as received. A polymeric methylene diphenyl diisocyanate (referred to as PMDI) was purchased from BASF Poliuretanos Iberia S.A., Rubí, Spain and was used as received. The PMDI was a brown, viscous liquid of grade IsoPMDI 92410. According to the material data sheet [14] the PMDI was based on 4,4"-methylenebis(phenyl isocyanate) and contained oligomers with an average functionality of ~2.7 and a NCO content of 31.8%.
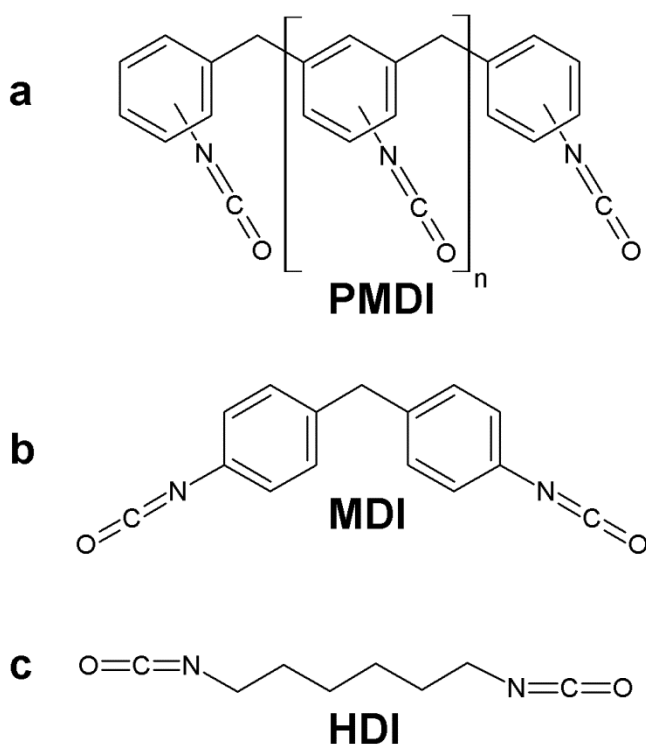


Fig. 3.3: Chemical structures of polymeric isocyanate (a), aromatic 4,4"-methylenebis(phenyl isocyanate) (b) and aliphatic hexamethylene diisocyanate (c) [12-14].

### 3.4.3  Benzoxazine

N-phenyl bisphenol A based 1,3-benzoxazine (Araldite MT 35600 CH, Huntsman Advanced Materials, Basel, Switzerland) was used for chemical modification of pCBT. According to the producer [15], this type of benzoxazine (referred to as BOX) was characterized by a density of 1.18 g/cm$^3$, a melting range of 55–65 °C, a melt viscosity range of 80–180 mPa·s at 125 °C, a glass transition temperature in the range of 170–190 °C and was used as received. Its chemical structure is shown in figure 3.4.
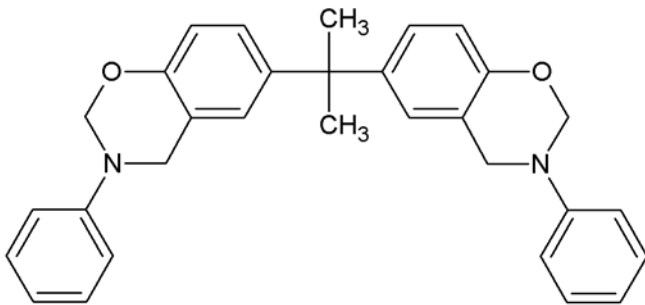


Fig. 3.4: Chemical structure of N-Phenyl Bisphenol A Benzoxazine [15].

### 3.5    Nano-sized reinforcements

### 3.5.1  POSS

Octamethyl POSS$^®$ (referred to as OM-POSS), Isooctyl POSS$^®$ (I-POSS), Trisilanolphenyl POSS$^®$ (T-POSS), Triglycidylisobutyl POSS$^®$ (TG-POSS) and Glycidyl POSS$^®$ (G-POSS) were supplied by Hybrid Plastics, Inc. (Hattiesburg, MS, USA) and used as received. Figure 3.5 shows the chemical structures; physical properties of the used POSS grades are collected in table 3.1.
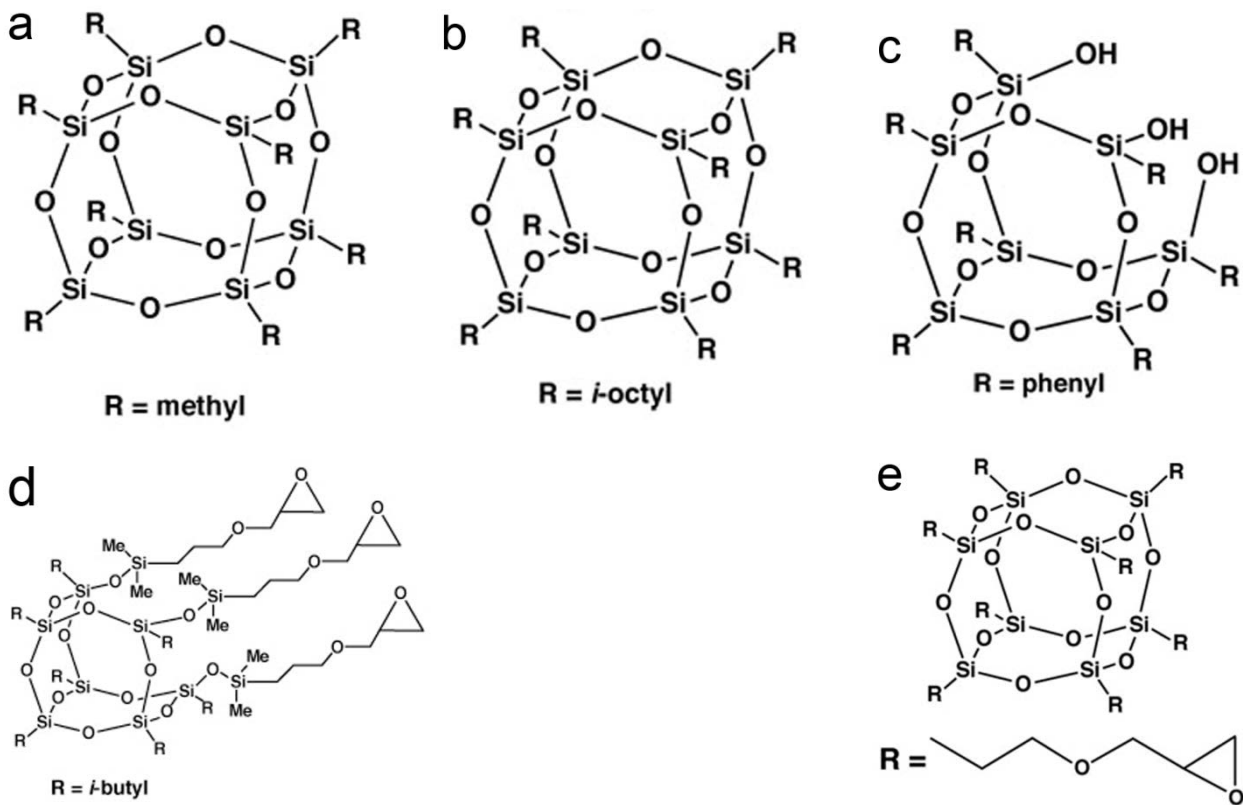
Fig. 3.5: Chemical structures of (a) OM-POSS, (b) I-POSS, (c) T-POSS, (d) TG-POSS and (e) G-POSS [16].

Table 3.1: Physical properties of the used POSS grades [16].

| Compound name | Grade | Molecular weight [g/mol] | Appearance |
| --- | --- | --- | --- |
| Octamethyl POSS | MS0830 | 537.0 | crystalline solid |
| Isooctyl POSS | MS0805 | 1322.5 | viscous liquid |
| Trisilanolphenyl POSS | SO1458 | 931.3 | crystalline solid |
| Triglycidylisobutyl POSS | EP0423 | 1308.3 | viscous liquid |
| Glycidyl POSS | EP0409 | 1337.9 | viscous liquid |

### 3.5.2 Organoclay

A natural montmorillonite modified with a quaternary ammonium salt, namely Cloisite[®] 30B (Southern Clay Products, Inc., Gonzales, TX, USA) was vacuum dried over silica gel at 80 °C for 12 h and stored in a desiccator over silica gel until further use. The chemical structure of the organic modifier is illustrated in figure 3.6. According to the producer [17], the organoclay was characterized by a density of 1.98 g/cm$^3$, a moisture content of <3% and a typical dry particle size $d_{50}$ of <10 μm . The interlaminar distance $d_{001}$ was 1.85 nm.

$$\begin{array}{c} CH_2{-}CH_2{-}OH \\ | \\ H_3C{-}\overset{+}{N}{-}T \\ | \\ CH_2{-}CH_2{-}OH \end{array}$$
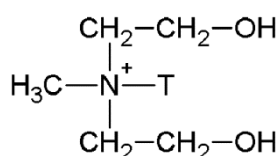
Fig. 3.6: Chemical structure of methyl, tallow, bis-2-hydroxyethyl, quaternary ammonium where T is tallow (~65% C18; ~30% C16; ~5% C14) [17].

### 3.5.3 Graphene

A commercial graphene (xGnP graphene nano-platelets grade h, XG Sciences, East Lansing, MI, USA) was used in this work. Physical properties of the graphene nano-platelets are collected in table 3.2. According to the technical data sheet [18], the bulk graphene powder had a bulk density of 0.03–0.1 g/cm$^3$, an average layer thickness of 15 nm and a specific surface area of 50–80 m$^2$/g. The nano-platelets had naturally occurring functional groups like ethers, carboxyls, or hydroxyls that can react with atmospheric humidity to form acids or other compounds. The oxygen content was <1% and the residual acid content was <0.5 wt.%.

The as-received graphene nano-platelets were further analysed using WAXS; the diffraction pattern is depicted in figure 3.7. It exhibits reflections at $2\theta = 26.4°$ and 12.4°; the former is the (002) basal reflection of graphite with a corresponding $d$ spacing of 0.34 nm. The reflection at $2\theta = 12.4°$ is the (002) reflection of graphite oxide which is shifted to a lower angle due to the intercalation of water molecules and generation of oxygen-

containing functional groups in the interlayer spacing ($d$ spacing = 0.71 nm) of the graphene nano-platelets [19-20]. This suggests that the used graphene type had mostly an exfoliated structure, but also showed crystalline features typical for both graphite and graphite oxide.

Table 3.2: Physical properties of the used graphene nano-platelets [18].

| Property | Typical value parallel to surface | Typical value perpendicular to surface | Unit |
|---|---|---|---|
| Density | 2.2 | 2.2 | g/cm$^3$ |
| Carbon Content | >99.5 | >99.5 | % |
| Thermal Conductivity | 3000 | 6 | W/m·K |
| Thermal Expansion (CTE) | 4 -6 x 10$^{-6}$ | 0.5 – 1.0 x 10$^{-6}$ | m/m°C |
| Tensile Modulus | 1000 | n/a | GPa |
| Tensile Strength | 5 | n/a | GPa |
| Electrical Conductivity | 10$^7$ | 10$^2$ | S/m |

n/a: not available
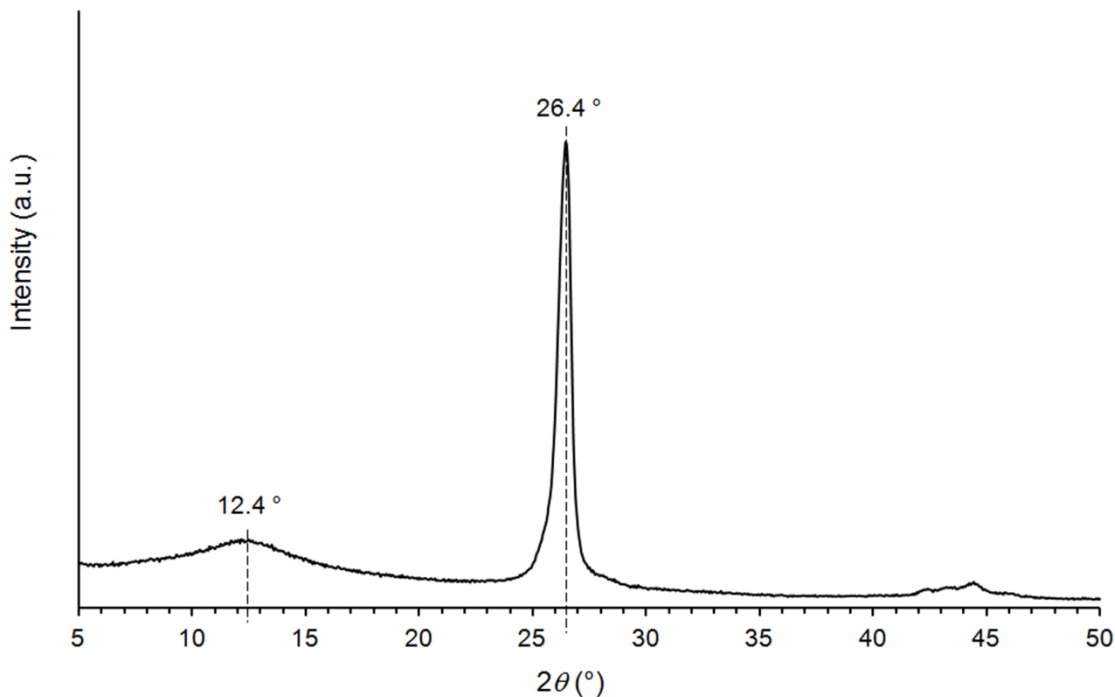


Fig. 3.7: WAXS diffraction pattern of as-received graphene nano-platelets.

## 3.6   Continuous fibre reinforcements

The reinforcement used in unmodified and modified pCBT composites was a high strength carbon fibre fabric with balanced plain weave architecture, referred to as CF. It consisted of two sets of interlacing threads, commonly referred to as warp and weft, and was bi-directional [0/90]. It was characterised by a surface weight of 193 g/m$^2$ and was supplied by Jordi Sagrisà, S.L., Barcelona, Spain with the reference TAFE 3K [21]. Ten or twenty plies of carbon fibre reinforcement with a size of 10x10 cm$^2$ were used in each laminate panel.

## 3.7   References

1.   Mohd Ishak, ZA, Gatos, KG, and Karger-Kocsis, J. On the in-situ polymerization of cyclic butylene terephthalate oligomers: DSC and rheological studies. Polymer Engineering & Science **46**(6), 743-750 (2006).

2.   Parton, H. Characterization of the in-situ polymerization production process for continuous fibre reinforced thermoplastics. PhD thesis. Department of Metallurgy and Materials Engineering. Katholieke Universiteit Leuven: Leuven, Belgium, 2006

3.   Arkema. Fascat®4105. Datasheet, available online: www.arkemainc.us. [Accessed Sep. 28, 2009].

4.   Cyclics. CBT®100. Datasheet, available online: www.cyclics.com. [Accessed Sep. 28, 2009].

5.   Cyclics. CBT®160. Datasheet, available online: www.cyclics.com. [Accessed Sep. 28, 2009].

6.   Chen, H, Yu, W, and Zhou, C. Entropically-driven ring-opening polymerization of cyclic butylene terephthalate: Rheology and kinetics. Polymer Engineering & Science **52**(1), 91-101 (2012).

7.   Sigma-Aldrich. Poly(tetrahydrofuran). Datasheet, available online: www.sigmaaldrich.com. [Accessed Jan. 12, 2011].

8.   IQRaisa. Eporai® 450/A. Datasheet, available online: www.iqraisa.com. [Accessed Mar. 10, 2012].

9.  Jubail Chemical Industries. Araldite® GT 7071. Datasheet, available online: www.jana-ksa.net. [Accessed Mar. 10, 2012].

10. Jubail Chemical Industries. Araldite® GT 7004. Datasheet, available online: www.jana-ksa.net. [Accessed Mar. 10, 2012].

11. Jubail Chemical Industries. Araldite® GT 6097. Datasheet, available online: www.jana-ksa.net. [Accessed Mar. 10, 2012].

12. Sigma-Aldrich. Hexamethylene diisocyanate. Datasheet, available online: www.sigmaaldrich.com. [Accessed Feb. 5, 2013].

13. Sigma-Aldrich. 4,4′-Methylenebis(phenyl isocyanate). Datasheet, available online: www.sigmaaldrich.com. [Accessed Feb. 5, 2013].

14. BASF. IsoPMDI 92410. Datasheet, available online: www.basf.com. [Accessed Feb. 5, 2013].

15. Huntsman Advanced Materials. Araldite MT 35600 CH. Datasheet, available online: www.huntsman.com. [Accessed Jun. 7, 2011].

16. Hybrid Plastics, Inc. POSS R&D chemicals. Datasheet, available online: www.hybridplastics.com. [Accessed Oct. 22, 2009].

17. Rockwood Additives. Cloisite® 30B. Datasheet, available online: www.rockwoodadditives.com. [Accessed Sep. 17, 2012].

18. XG Sciences. xGnP® Graphene Nanoplatelets - Grade H. Datasheet, available online: www.xgsciences.com. [Accessed Jun. 16, 2011].

19. Bian, J, Lin, HL, He, FX, Wang, L, Wei, XW, Chang, IT, and Sancaktar, E. Processing and assessment of high-performance poly(butylene terephthalate) nanocomposites reinforced with microwave exfoliated graphite oxide nanosheets. European Polymer Journal **49**(6), 1406-1423 (2013).

20. Kuila, T, Bose, S, Mishra, AK, Khanra, P, Kim, NH, and Lee, JH. Chemical functionalization of graphene and its applications. Progress in Materials Science **57**(7), 1061-1105 (2012).

21. Jordi Sagrisà. Tejido de carbono TAFE 3K. Datasheet, available online: www.jordisagrista.com. [Accessed May. 11, 2013].

# Chapter 4: Sample preparation & experimental techniques

## 4.1    Compression moulding (CM)

An IQAP LAP PL-15 hot plate press equipped with temperature- and pressure-controlled plates (IQAP Masterbatch group SL, Barcelona, Spain), depicted in figure 4.1, and was used for compression moulding. The mould setup was as follows: Two steel plates were covered with a thin polytetrafluoroethylene (PTFE) fabric (thickness: 0.2 mm) which served as release agent. A 'picture-frame' with inner dimensions of 120 × 120 mm$^2$ and a nominal thickness of 0.5 mm was used as mould cavity. The frame was placed between the two PTFE-covered steel plates, as illustrated in figure 4.2.



Fig. 4.1: IQAP LAP PL-15 hot plate press equipped with temperature- and pressure-controlled plates

In a typical compression moulding operation the preheated mould was filled with around 12 g of oligomers or polymer, placed in the hot part of the press and moulded for a predetermined time under a certain pressure. Then the mould was placed in the cold part (equipped with a cooling water circuit) of the press and was quickly cooled to room temperature, either pressure-less or under a certain pressure. The cooling rate was previously determined to be approximately -50 °C/min. After the cooling step the mould was opened and the polymer sheet was removed from the picture frame and used for further analysis.
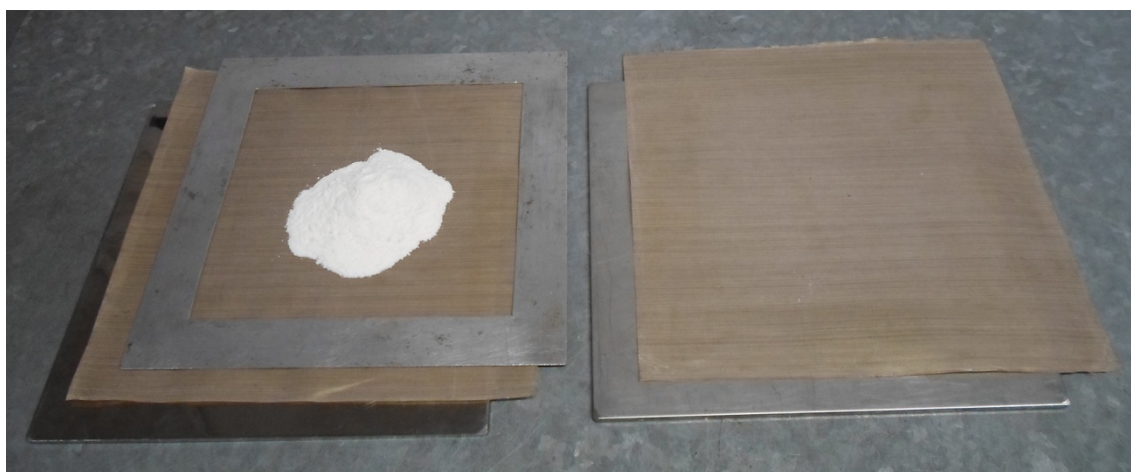


Fig. 4.2: Compression moulding setup

## 4.2 Melt blending (MB)

The *in-situ* ring-opening polymerization of unmodified and modified CBT was conducted in a lab-scale batch mixer (Brabender Plasti-Corder W50EHT, Brabender GmbH & Co. KG, Duisburg, Germany), equipped with a torque measuring system. WinMix Brabender Mixer Program version 3.2.31 was used for torque data acquisition. This setup allowed a maximum operating temperature of 500 °C and a maximum operating torque of 200 Nm. The mixing chamber had a volume of 55 cm$^3$ and was equipped with two counter-rotating mixing rotors (roller blade type "W") and a nitrogen inlet, as shown in fig. 4.3. The rotor speed ratio was 2:3 (driven to non-driven rotor). According to the manufacturer, this results

in a high torque resolution, especially when testing low viscosity polymers. The special shape of the rotors as well as the tight clearance between rotors and mixing chamber provide an intensive high shear mixing. Temperature conditioning in the mixing chamber was achieved by electrical heating elements and compressed air cooling. The mixing chamber temperature was controlled by three thermocouples and the bulk temperature of the processed material was measured by a separate thermocouple.

Melt blending is an excellent process for CBT which does not only allow continuous mixing during ROP, but also gives useful information about the torque evolution with time.
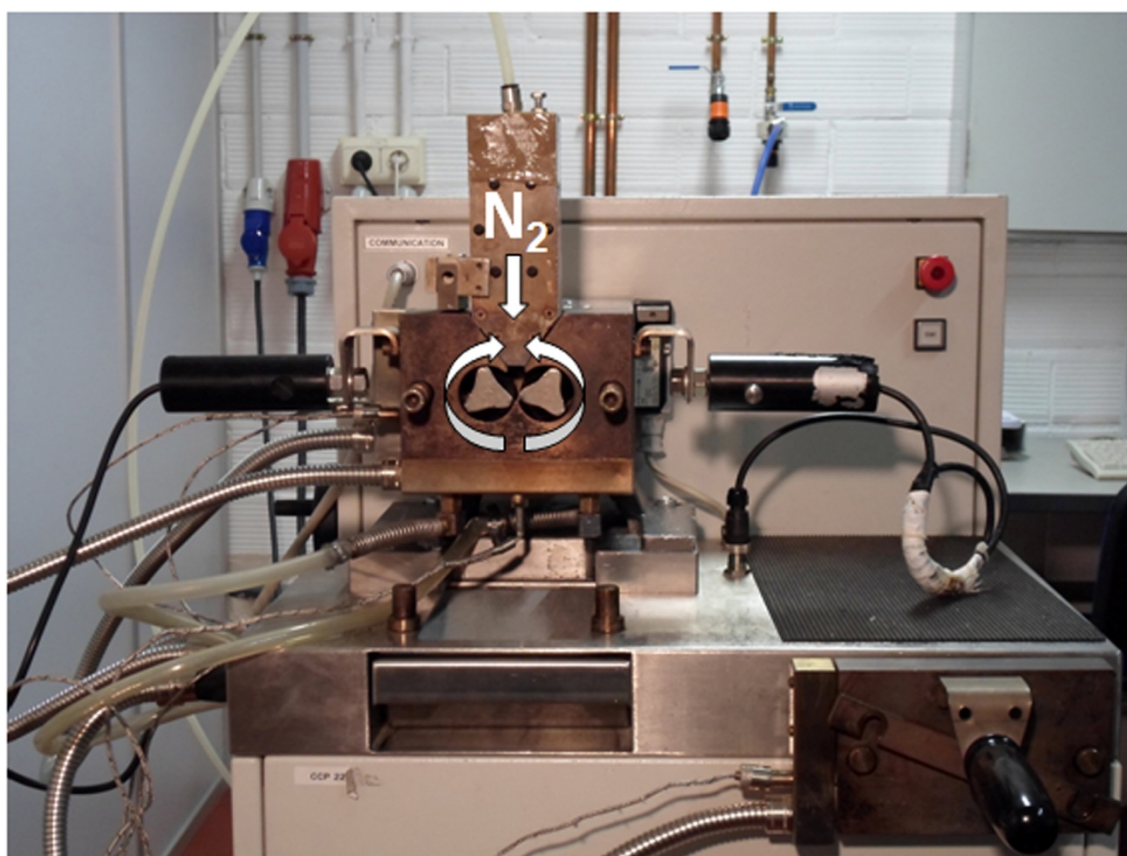


Fig. 4.3: Melt blending setup

A typical procedure was as follows: First, the batch mixer was preheated to the desired temperature and the desired rotor speed was set. Then the mixing chamber was purged with $N_2$ for 5 min to minimize thermo-oxidative and hydrolytic degradation. The torque measurement system was internally calibrated and set to zero. After calibration a

predetermined amount of pre-dried oligomers or polymer was introduced into the mixing chamber and the nitrogen blanket was established again. At the end of the experiment, the batch mixer was stopped; the polymer was collected and allowed to cool to room temperature. The collected polymer was ground into granules using a cutting mill (Pulverisette 15, Fritsch GmbH, Idar-Oberstein, Germany), vacuum dried for 8 h at 80 °C and subsequently compression moulded in an IQAP LAP PL-15 hot plate press at a temperature of 250 °C and a pressure of 4 MPa for 5 min.

## 4.3    Solvent blending (SB)

Solvent blending was used to homogeneously disperse toughening agents and/or nanofillers in CBT prior to ROP. In a typical procedure a 150 ml beaker equipped with a magnetic stirrer was charged with 50 ml THF and 20 g of previously dried one-component CBT powder together with the toughening agent and/or nanofiller. Stirring was performed at room temperature and at a stirring speed of 300 $min^{-1}$ for 1 h. Stirring speed was adjusted to the value at which a vortex begins to form, which appeared to be the optimal condition for homogeneous mixing. Then the blend was vacuum dried at 80 C for 8 h, ground into a fine powder using mortar and pestle and subsequently vacuum dried at 80 C for at least 3 days to completely remove the THF.

## 4.4    Chemical modification of nanofillers

Graphene and different types of organo-montmorillonite were chemically modified with isocyanates to improve its compatibility with pCBT. The characterization and blending with CBT of these modified nanofillers is described in detail in chapters 13 and 14.

In a typical procedure a 500 ml flat bottom flask was equipped with a 5 cm magnetic stir bar, a nitrogen inlet and a Liebig condenser. This setup was placed on a hot plate stirrer. The flask was charged with 200 ml THF and heated up to the boiling point. Five to ten grams of nanofiller and the corresponding amount of isocyanate (in excess) were added to the boiling THF under constant stirring at 300 $min^{-1}$ and a stream of nitrogen. These

conditions were maintained for 8–12 h. After the experiment the solution with the modified nanofiller was allowed to cool to room temperature and was filtered. The filtrate was washed thoroughly with fresh THF in order to remove unreacted isocyanate. The filtration and washing procedure was repeated tree times and finally the filtrate was vacuum dried at 60 °C for 24 h and stored in a desiccator over silica gel until further use.

## 4.5    Continuous fibre reinforced composite production

A simple powder prepreg method was used to manufacture unmodified and modified pCBT/carbon fibre composites *via* compression moulding; the CBT/CF composite lay-up and a pCBT-CF composite are exemplarily shown in figure 4.4 and in figure 4.5, respectively.

The composite lay-up was as follows. Previously dried CBT powder (1.5 g) was evenly spread on a CF fabric (size: 10x10 cm$^2$; weight: ~2 g). In this manner, two types of powder prepreg consisting of 10 or 20 layers of [0/90] CF fabric and 9 or 19 layers of CBT powder, respectively, were prepared and compression moulded between two PTFE-covered steel plates, as illustrated in the insert in figure 4.4.
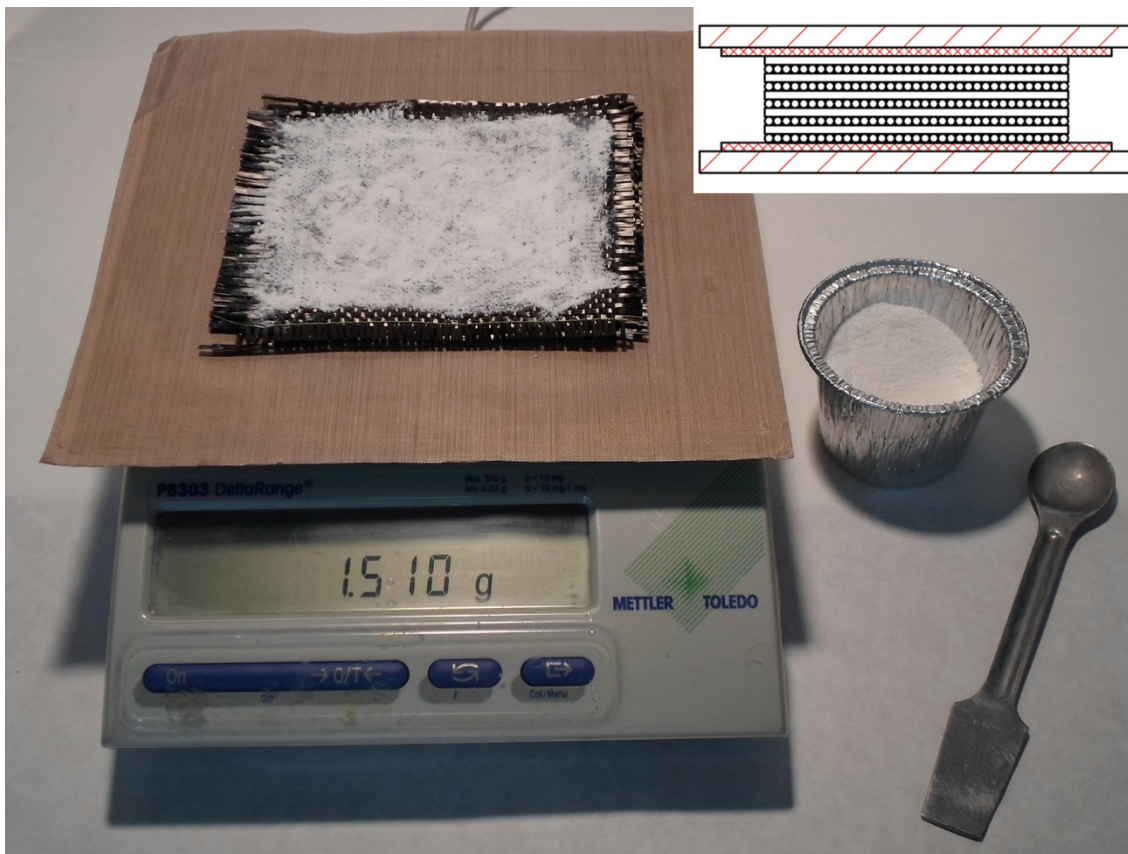
Fig. 4.4: CBT/CF composite lay-up

The powder prepregs were dried under vacuum at 80 °C for 4 h. After drying, a powder prepreg was placed between two PTFE-covered steel plates and introduced in the preheated hot plate press. A pressure of 0.5 MPa was applied for 10 s in order to compact the powder prepreg and to facilitate melting. Then the pressure was released, *i.e.* the moving hot plate remained in its position without applying pressure, and the powder prepreg was *in situ* polymerized for a predetermined time. During the last two minutes of the polymerization step a pressure of 4 MPa was applied in order to compact the composite. Then the composite sheet was cooled at ca. -50 °C/min to room temperature in the cold part of the press under a pressure of 4 MPa.
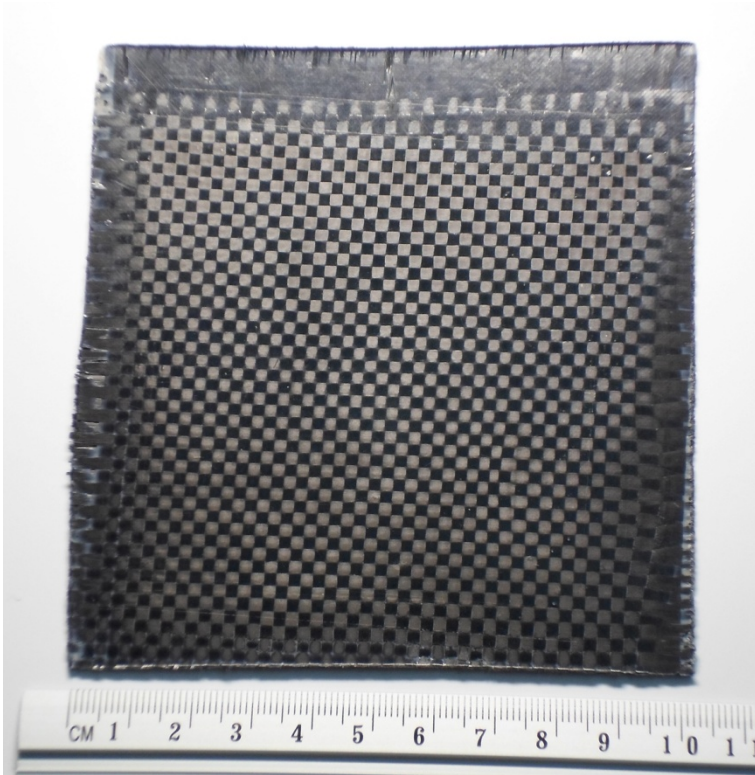
Fig. 4.5: pCBT-CF composite

$[0/90]_{10}$ composites had a nominal thickness of 1.5 mm and were used for short beam interlaminar shear strength determination as well as for flexural tests. These samples were obtained by water jet cutting the composite sheets as illustrated in figure 4.6. $[0/90]_{20}$ composites had a nominal thickness of 3 mm and were used for puncture impact properties determination.
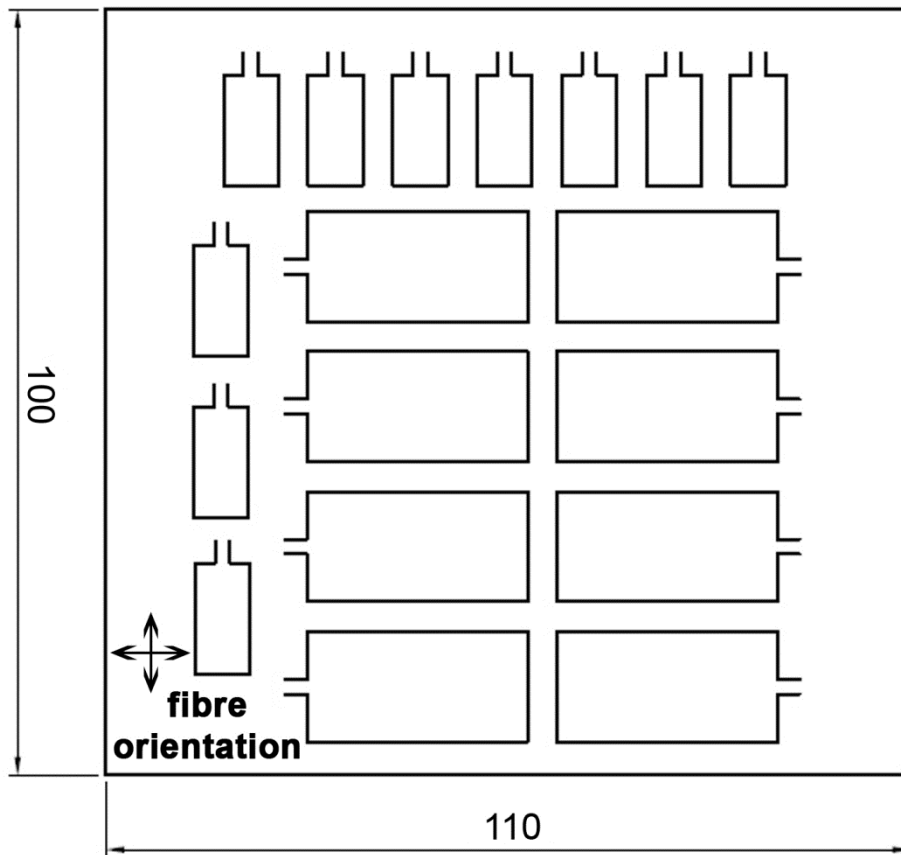
Fig. 4.6: Water jet cutting plan for short beam interlaminar shear strength and flexural specimens.

# Chapter 5: Characterization techniques

## 5.1 Thermal analysis

### 5.1.1 Torque *versus* time measurements

The viscosity evolution of the ring-opening polymerization of CBT, chain extension reactions or melt blending processes were monitored by torque/temperature *versus* time measurements in the Brabender batch mixer. Unless otherwise stated, 40 g of pre-dried oligomers or polymer were polymerized for a predetermined time at 230 °C mixing chamber temperature, 60 min$^{-1}$ screw speed and under a nitrogen blanket.

The measured torque depends on one hand on the molten polymer, *i.e.* its molecular weight and chain architecture. On the other hand, torque also depends on the processing parameters, *i.e.* the amount of molten polymer in the mixing chamber, mixing chamber temperature, mixing roller speed and mixing roller blade geometry.

Torque variations can be seen as viscosity variations of the molten polymer. Since the processing parameters are kept constant during melt blending, a torque variation can be attributed to changes in the polymer, *i.e.* changes in molecular weight and/or chain architecture. For instance, the ring-opening polymerization of CBT yields linear pCBT chains and branching normally does not occur. Thermal or hydrolytic degradation of PBT also yields linear chains, whereas thermo-oxidative degradation can lead to crosslinking [1-3]. So if neat CBT is polymerized within a temperature range where thermo-oxidative degradation can be neglected, and torque variations are observed, they can be solely attributed to changes in molecular weight since chain architecture is assumed to be strictly linear during melt blending.

Contrary to this, if CBT is processed together with a polyfunctional compound and chain extension reactions take place in the melt, branching and eventually crosslinking may occur. Therefore the chain architecture is changed which leads to a change in torque. In this case a torque variation is due to changes in both molecular weight and chain architecture and therefore care must be taken in the interpretation of torque curves.

### 5.1.2 Differential Scanning Calorimetry (DSC)

Differential scanning calorimetry was performed on a PerkinElmer Pyris 1 device (PerkinElmer, Waltham, MA, USA) in conjunction with a 2P intracooler. Pyris Thermal Analysis System software version 3.70 was used for data analysis. The temperature and enthalpy calibration of the equipment was performed using indium and lead. DSC was carried out under dry nitrogen atmosphere to prevent hydrolytic and oxidative degradation. Unless otherwise stated, all samples were subjected to the following protocol. The sample weight was 8 – 12 mg and standard aluminium DSC crucibles were used. Samples were heated from 30 °C to 250 °C at a heating rate of 10 °C/min. Since the reported equilibrium melting temperature of PBT was reported as 245 °C [4], all DSC samples were isothermally hold at 250 °C for 3 min to destroy all nuclei. After the isothermal step the samples were cooled from 250 °C to 30 °C at a cooling rate of -10 °C/min. Second heating and cooling scans were performed equally. Melting and crystallization parameters were obtained from heating and cooling scans, respectively. The crystallization temperature ($T_c$) was taken as the maximum of the exothermic peak from the first cooling scan and the melting temperature ($T_m$) was considered to be the maximum of the endothermic peak from the second heating scan. Crystallization and melting enthalpies were determined by integrating the corresponding areas underneath the peaks. The degree of crystallinity ($X_C$) was calculated from the melting enthalpy of the second heating scan according to

$$X_C = \frac{\Delta H_m}{\Delta H_m^0 (1 - W_f)} \cdot 100\%$$

(5.1)

where $\Delta H_m$ is the measured melting enthalpy, $\Delta H_m^0$ is the melting enthalpy for a fully perfect crystalline PBT and $W_f$ is the weight fraction of the used reinforcement (if any). The melting enthalpy of alpha form, fully perfect crystalline PBT is found in literature to be 142 J/g [5]. It is noteworthy to mention that all DSC thermograms in the subsequent chapters are shifted on the y-axis for better visibility.

### 5.1.3  Dynamic Mechanical Thermal Analysis (DMTA)

DMTA was used to study the dynamic mechanical properties of unmodified and modified pCBT and the respective fibre reinforced composites. A Q800 TA Instruments DMA (TA Instruments, New Castle, DE, USA) was used in tensile mode at a frequency of 1 Hz and a strain of 0.05% for samples without fibre reinforcement. The temperature range was set from 30 °C to 220 °C at a heating rate of 2 °C/min. Samples were prepared from compression moulded pCBT films and had dimensions of *ca.* 27x5x0.5 mm$^3$. Carbon fibre reinforced pCBT composites were tested in single cantilever bending mode at a frequency of 1 Hz and a strain of 0.01%. Temperature range was set from 30 °C to 210 °C at a heating rate of 2 °C/min. Samples were obtained by water jet cutting the composite sheets and had dimensions of *ca.* 20x15x1.5 mm$^3$. The span length was set to 17 mm for all experiments. The viscoelastic properties were evaluated, namely the complex dynamic modulus *E\**, the storage modulus *E'*, the loss modulus *E''* and the dynamical loss factor *tan δ*, which is defined as follows.

$$\tan \delta = \frac{E''}{E'}$$

(5.2)

### 5.1.4  Thermogravimetric Analysis (TGA)

TGA was performed in air and dry nitrogen, respectively, with a flow rate of 30 mL/min using a TA Instruments Q600 device (TA Instruments, New Castle, DE, USA). Weight loss was analysed by heating the samples from room temperature to 600 °C at a heating rate of 10 °C/min. The weight of the samples was 10 mg and aluminium oxide pans were used.

## 5.2    Morphological analysis

### 5.2.1   X-ray diffraction (XRD)

The crystalline structure as well as degree of nanofiller exfoliation of the different pCBT samples was determined by small and wide angle X-ray scattering, commonly referred to as SAXS and WAXS. Diffraction data was collected on a Bruker D4 Endeavor (Bruker, Billerica, MA, USA) using Ni-filtered Cu $K_\alpha$ radiation ($\lambda$ = 1.54 Å, V = 40 kV; I = 40 mA). SAXS scattering patterns were recorded in the diffraction angle ($2\theta$) range of 1.5° < $2\theta$ < 10° at a scanning rate of 8 s/step using steps of 0.02°. WAXS scattering patterns were recorded in the diffraction angle ($2\theta$) range of 5° < $2\theta$ < 40° at a scanning rate of 6 s/step using steps of 0.02°. Interplanar spacing ($d_{hkl}$) between crystallographic planes was calculated according to Bragg´s law [6]:

$$n \cdot \lambda = 2 \cdot d_{hkl} \cdot \sin \theta \qquad (5.3)$$

where $n$ is the order of diffraction (usually $n$ =1), $\lambda$ is the wavelength of the X-ray radiation and $d_{hkl}$ is the spacing between planes of given Miller indices $h$, $k$ and $l$.

The apparent crystallite size $D_{hkl}$ in direction perpendicular to the planes (001), (0$\overline{1}$ 1) and (010) was calculated from the full width at half maximum intensity (FWHM) of the corresponding diffraction peaks using the Scherrer equation [7], which relates the width of the diffraction peak to the crystallite size:

$$D_{hkl} = \frac{K \cdot \lambda}{\beta_{hkl} \cdot \cos \theta} \qquad (5.4)$$

where $D_{hkl}$ is the apparent crystallite size, $K$ is the Scherrer shape factor, $\lambda$ is the X-ray wavelength, $\beta_{hkl}$ is the FWHM (in radians) of the $hkl$ diffraction peak, and $\theta$ is half the Bragg angle. $K$ depends on the definition of the 'breadth' of the diffraction peak under study, $i.e.$ FWHM, integral-breadth, variance-slope or variance-intercept. Moreover, $K$ also depends on the crystallite shape and the crystallite-size distribution and usually takes

values from 0.62 to 2.08. Regarding the Scherrer shape factor for the half-width, a value of 0.90 may be taken as a first approximation for spherical crystals with cubic symmetry [8]. Nevertheless, the value unity was used in this work, as proposed elsewhere [9].

### 5.2.2  Scanning Electron Microscopy (SEM)

The morphology of unmodified and modified pCBT was analysed by SEM. Tensile test specimens of type 1BA according to ISO 527-2 were submerged in liquid nitrogen and equilibrated for 15 min. The specimens were quickly extracted and cryo-fractured by bending. The fracture surfaces were then sputter coated with a thin Au/Pd layer using a Bal-Tec SCD005 Sputter Coater (Bal-Tec, Liechtenstein). SEM analysis was performed on a Jeol JSM-5610 scanning electron microscope (Jeol, Tokyo, Japan) using an acceleration voltage of 10 kV.

### 5.2.3  Energy-dispersive X-ray spectroscopy (SEM-EDX)

Additionally to scanning electron microscopy, some pCBT nanocomposite samples containing POSS nanoparticles were analysed by energy-dispersive X-ray spectroscopy element mapping (SEM-EDX) in order to identify the presence of POSS in the bulk. These samples were sputtered with carbon because of the interference between palladium and silicon signals. The combination of SEM and EDX analysis allowed determining the dispersion degree of the POSS within the pCBT matrix. In the case of EDX, the study was focused on the determination of Si signal as it is specific and characteristic of the POSS presence.

### 5.2.4  Transmission Electron Microscopy (TEM)

TEM analysis was performed on a Jeol JEM2011 transmission electron microscope (Jeol, Tokyo, Japan) using an acceleration voltage of 200 kV. Thin (60–100 nm) specimens were prepared at room temperature using an ultramicrotome (Leica EM UC6, Leica Microsystems GmbH, Wetzlar, Germany).

### 5.2.5  Optical Microscopy (OM)

The morphology of unmodified and modified fibre reinforced pCBT composites was analysed using optical microscopy (Leica MEF4, Leica Microsystems GmbH, Wetzlar, Germany). Prior to analysis, samples were mounted in epoxy resin and sections normal to the thickness of the samples were polished using fine sandpaper.

## 5.3  Structural analysis

### 5.3.1  Gas chromatography-mass spectrometry (GC-MS)

Gas chromatography-mass spectrometry was carried out using a Shimadzu QP 2010 (Shimadzu, Kyoto, Japan) with head space technique for the injection of samples. About 1 mL of sample was heated to 80 °C for 40 min in a 30 mL vial sealed with a PTFE septum and 1 mL of air was injected into the GC-MS system. The GC oven was held at 40 °C for 10 min, then heated to 150 °C at 4 °C/min and finally held at 150 °C for 10 min. Injection was performed at 200 °C using helium as carrier gas at a flow rate of 22.1 mL/min. The column (TRB-624) had a length of 30 m and an inner diameter of 0.25 mm with a film thickness of 0.25 µm. The column flow was set to 0.95 mL/min. Identification of the compounds was performed using Nist 147, Nist 27 and Wiley 229 as reference libraries.

### 5.3.2  Gel content

The insoluble content of epoxy-modified pCBT samples was determined by dissolving around 50 mg of sample in 5 mL of a mixture of CHCl$_3$/TFA (9/1) at ambient temperature with agitation for 30 min. The solution was subsequently centrifuged and the soluble part was removed. The insoluble fraction was washed with 5 mL of the same solvent mixture two additional times and finally with CHCl$_3$. It was then dried in an oven at 80° C for 12 h and weighted. The gel content was calculated by insoluble fraction weight over sample weight expressed in percent.

### 5.3.3  Gel permeation chromatography (GPC)

Gel permeation chromatography was performed at room temperature using an Agilent Technologies 1200 Series modular system (Agilent Technologies, Santa Clara, CA, USA) comprising an Agilent 1200 refractive index detector operated at a temperature of 35 °C. A linear Styragel HR5E column (Waters, Milford, MA, USA) with a separation range from 10$^3$ to 5 × 10$^6$ g/mol was employed. HFIP (*c.f.* section 3.3.2) was used as solvent at a flow rate of 0.5 mL/min. The pressure of the column was 6 MPa and the amount of sample was 1 mg of polymer. The insoluble content of the samples was removed by filtration before analysis. Low-dispersion poly(methyl methacrylate) samples (Fluka, Buchs, Switzerland) were used as internal standards. The degree of conversion $\alpha$ (%) from CBT oligomers to pCBT was determined using

$$\alpha = 1 - \frac{A_{oligomer}}{A_{total}}$$
(5.5)

where $A_{oligomer}$ is the area under the oligomer peak of the GPC trace and $A_{total}$ the total area under the GPC trace.

### 5.3.4  Fourier Transform-Infrared Spectroscopy (FT-IR)

Infrared spectra were recorded on a Nicolet 6700 FT-IR/Attenuated Total Reflection spectrometer (Thermo Fisher Scientific, Waltham, MA, USA) using OMNIC software version 7.3 Service Pack 1. Spectra were obtained in the wavenumber interval between 4000 and 400 $cm^{-1}$ at a scan number of 32 scans and a resolution of 4 $cm^{-1}$.

### 5.3.5  Nuclear magnetic resonance spectroscopy (NMR)

The structural characterization of the modified pCBT samples was performed using ^{1}H NMR spectroscopy. Spectra were collected on a Bruker AMX-300 spectrometer (Bruker, Billerica, MA, USA) operated at a frequency of 300.1 MHz and at a temperature of 90 °C. Sample concentrations were 1% (w/v) and a 1,1,2,2-tetrachloroethane-$d_2$ solvent was used. A total of 640 scans with 32,000 data points were recorded with a relaxation delay of 2 s.

### 5.4  Mechanical analysis

### 5.4.1  Tensile test

The tensile properties were determined on a Galdabini Sun 2500 universal testing machine (Galdabini, Cardano al Campo, Italy), equipped with a 5 kN load cell according to ISO 527 [10]. Tensile tests were performed at room temperature (*i.e.* 23 ± 2 °C) and a crosshead speed of 10 mm/min was used. Strain was measured using a video extensometer (Mintron OS-65D, Mintron, Taipei, Taiwan) in conjunction with Messphysik software (Messphysik Materials Testing GmbH, Fürstenfeld, Austria). Type 1BA specimens according to ISO 527-2 were punched from compression moulded pCBT films. The tensile modulus $E$, tensile strength $R_m$ and strain at break $\varepsilon_b$ were calculated using the following expressions

$$E = \frac{\sigma_2 - \sigma_1}{\varepsilon_2 - \varepsilon_1} \cdot 10^3 \qquad (5.6)$$

where $E$ is the tensile modulus of elasticity, in MPa, $\sigma_1$ is the stress measured at a deformation $\varepsilon_1 = 0.0005$ and $\sigma_2$ is the stress measured at a deformation $\varepsilon_2 = 0.0025$.

$$R_m = \frac{F_{max}}{A} \qquad (5.7)$$

where $R_m$ is the tensile strength, in MPa, $F_{max}$ is the failure or maximum load, in N, and $A$ is the initial cross-section of the specimen, in mm$^2$.

$$\varepsilon_b = \frac{\Delta L_0}{L_0} \cdot 100\% \qquad (5.8)$$

where $\varepsilon_b$ is the strain at break, in %, $L_0$ is the gauge length of the specimen, in mm, and $\Delta L_0$ is the increase in the specimen length between the gauge marks, in mm. A minimum of five specimens were tested for each reported value. The toughness in terms of strain energy, in MJ/m$^3$, was determined by integrating the area under the stress-strain curve from the origin until rupture.

### 5.4.2   Instrumented tensile impact testing

The impact properties could not be determined using impact tests according to ISO 179 (Charpy impact) or ISO 180 (Izod impact) because the compression moulded samples were too thin (~0.5 mm) and too flexible to be tested using these methods. Tensile tests at high strain rate (impact) were performed instead and the tensile-impact strength of unnoched specimens, $a_{tU}$ according to ISO 8256 method A was determined [11]. A minimum of 10 unnotched specimens of type 1BA according to ISO 527-2 were tested at room temperature (*i.e.* 23 ± 2 °C) using a Ceast Resil Impactor Junior (Ceast, Pianezza,

Italy). Impact data was stored at a sampling rate of 625 kHz using a DAS 16000 data acquisition system and analysed using the software DAS8WIN from CEAST. The pendulum had a nominal impact energy of 1.18 J and an impact speed of 1.47 m/s. A striker with a reduced mass of 1.096 kg and a length of 0.374 m was used in conjunction with an aluminium crosshead with a mass of 33.0 g. A constant clamping length of 42 mm was used. The tensile-impact strength of unnoched specimens, $a_{tU}$, was calculated using

$$a_{tU} = \frac{E_C}{x \cdot h} \cdot 10^3 \qquad (5.9)$$

where $x$ is the width, in mm, of the narrow, parallel-sided section of the specimen, $h$ is the specimen thickness, in mm, and $E_C$ is the corrected tensile-impact energy, in J, calculated as follows

$$E_C = E_s - E_q \qquad (5.10)$$

where $E_s$ is the impact energy, in J, absorbed during the impact, as measured by the instrument and $E_q$ is the toss energy, in J, due to the plastic deformation and the kinetic energy of the crosshead, calculated using

$$E_q = \frac{E_{\max} \cdot \mu \cdot (3 + \mu)}{2 \cdot (1 + \mu)} \approx \frac{3}{2} \cdot E_{\max} \cdot \mu \qquad (5.11)$$

where $E_q$ is the energy correction, in J, due to the plastic deformation and the kinetic energy of the crosshead, $E_{max}$ is the maximum impact energy, in J, of the pendulum and m is the mass of the crosshead divided by the reduced mass of the striker.

### 5.4.3  Flexural test

The flexural properties of pCBT-CF composites were determined on a Galdabini Sun 2500 universal testing machine (Galdabini, Cardano al Campo, Italy), equipped with a 5 kN load

cell according to ISO 14125 method A [12]. The tests were performed at room temperature (*i.e.* 23 ± 2 °C) and a crosshead speed of 1 mm/min. The specimens had dimensions of *l*=30 mm, *b*=15 mm, *h*=1.5 mm and the span *L* was 24 mm. Flexural modulus, flexural strength and the flexural strain at failure were calculated using the following expressions

$$E_f = \frac{L^3}{4 \cdot b \cdot h^3} \cdot \left( \frac{\Delta F}{\Delta s} \right) \tag{5.12}$$

where $E_f$ is the flexural modulus of elasticity, in MPa, $\Delta s$ is the difference in deflection between $s''$ and $s'$ and $\Delta F$ is the difference in load $F''$ and $F'$ at $s''$ and $s'$, respectively. $L$ is the span, in mm, $b$ is the specimen width, in mm, and $h$ is the specimen thickness, in mm. The deflections $s'$ and $s''$, which correspond to the given values of flexural strain $\varepsilon_f' = 0.0005$ and strain $\varepsilon_f'' = 0.0025$, were determined as follows

$$s' = \frac{\varepsilon_f' \cdot L^2}{6 \cdot h} \tag{5.13}$$

$$s'' = \frac{\varepsilon_f'' \cdot L^2}{6 \cdot h} \tag{5.14}$$

where $s'$ and $s''$ are the beam mid-point deflections, in mm, and $\varepsilon_f'$ and $\varepsilon_f''$ are the flexural strains, whose values are given above.

The flexural strength was determined using the following expression

$$\sigma_f = \frac{3 \cdot F \cdot L}{2 \cdot b \cdot h^2} \tag{5.15}$$

where $\sigma_f$ is the flexural strength, in MPa, $F$ is the maximum load, in N, $L$ is the span, in mm, $b$ is the specimen width, in mm, and $h$ is the specimen thickness, in mm. The flexural strain at failure was calculated as follows

$$\varepsilon_b = \frac{6 \cdot s \cdot h}{L^2} \cdot 100\% \tag{5.16}$$

where $\varepsilon_b$ is the flexural strain at failure, in %, $s$ is the beam mid-point deflection at break, in mm, $h$ is the specimen thickness, in mm, and $L$ is the span, in mm. A minimum of five tests were performed for each reported value.

### 5.4.4 Short beam interlaminar shear strength (ILSS)

Short beam interlaminar shear strengths of the pCBT-CF composites were determined at room temperature (*i.e.* 23 ± 2 °C) and a crosshead speed of 1 mm/min on a Galdabini Sun 2500 universal testing machine (Galdabini, Cardano al Campo, Italy), equipped with a 5 kN load cell according to ISO 14130 [13]. The specimens had dimensions of $l$=15 mm, $b$=7.5 mm and a thickness of $h$=1.5 mm. The nominal span $L$ was 7.5 mm but actually depended on sample thickness. A minimum of five tests were performed for each reported value. Apparent interlaminar shear strength, *ILSS*, was calculated using

$$ILSS = \frac{3}{4} \cdot \frac{F_{\max}}{b \cdot h} \tag{5.17}$$

where $F_{max}$ is the failure or maximum load, in N, $b$ is the specimen width, in mm and $h$ is the specimen thickness, in mm. The average values of *ILSS* were derived from a minimum of five tests for each composite.

### 5.4.5 Instrumented impact testing

Drop weight impact properties of the pCBT-CF composites were determined at room temperature (*i.e.* 23 ± 2 °C) according to ISO 6603-2 [14]. A Ceast Fractovis Plus (Ceast,

Pianezza, Italy) instrumented drop weight impact testing machine was used to perform the tests. The impact testing machine consisted of a drop tower, an impactor equipped with a variable weight arrangement and a 20 kN strain gauge load cell. Contact force–real time history was stored at a sampling rate of 333 kHz using a DAS 4000 data acquisition system. Based on Newton's second law and assuming that the impactor is perfectly rigid [15-17], energy, velocity and deflection were numerically deduced from the force–time data using the software DAS4WIN from CEAST. The hemispherical striker tip had a diameter of 20 mm and was lubricated prior to impact tests. $[0/90]_{20}$ composite specimens with a thickness of $h$=3.0 ± 0.1 mm were placed simply supported on an annular ring with inner and outer diameter of 40 mm and 60 mm, respectively, and impacted at a predetermined impact energy. The nominal impact energy ($E_0$) ranged from 0.5 to 20 J; impact velocity ($v_0$) ranged from 0.5 to 3.3 m/s.

## 5.5    Physical analysis

### 5.5.1   Density determination

The density of the pCBT-CF composites was determined according to ISO 1183 method A [18]. Distilled water at a temperature of 23 ± 2 °C was used as the immersion liquid and the density was calculated from

$$\rho_S = \frac{m_{S,A} \cdot \rho_{IL}}{m_{S,A} - m_{S,IL}}$$

(5.18)

where $m_{S,A}$ is the apparent mass, in grams, of the specimen in air, $m_{S,IL}$ is the apparent mass, in g, of the specimen in the immersion liquid and $\rho_{IL}$ is the density of the immersion liquid (in this case distilled water) at 23 °C, in $kg/m^3$.

### 5.5.2  Fibre content

The fibre weight contents of the pCBT-CF composites were determined by direct calcination in nitrogen atmosphere in order to prevent oxidation of the carbon fibres. Fibre weight contents were measured in a TA Instruments Q600 device (TA Instruments, New Castle, DE, USA) using dry nitrogen with a flow rate of 30 mL/min. Samples with a weight of 20–30 mg were heated in aluminium oxide pans from room temperature to 900 °C at a heating rate of 10 °C/min. The residual weight at 900 °C was considered to be the fibre weight content, which was then converted into fibre volume fraction using the following expression:

$$V_f = \frac{\dfrac{W_f}{\rho_f}}{\left( \dfrac{W_f}{\rho_f} + \dfrac{(1 - W_f)}{\rho_{pCBT}} \right)} \tag{5.19}$$

where $V_f$ is the fibre volume fraction (-), $W_f$ is the fibre weight fraction (-), $\rho_f$ is the fibre density expressed in g/cm$^3$ and $\rho_{pCBT}$ is the density of the matrix expressed in g/cm$^3$.

### 5.5.3  Void content

The void content of pCBT-CF composites was calculated according to ISO 7822 method A [19]. First, the densities of unmodified and modified pCBT resins, carbon fibre reinforcement and pCBT-CF composites were measured as described in section 5.5.1. Then, the fibre contents of the pCBT-CF composites were determined as described in section 5.5.2. The theoretical densities of the pCBT-CF composites can be calculated from

$$\rho_C = \frac{100}{\left( \dfrac{w_r}{\rho_r} + \dfrac{w_f}{\rho_f} \right)} \tag{5.20}$$

where $\rho_c$ is the theoretical composite density expressed in g/cm$^3$, $w_r$ is the resin in the composite expressed in wt.%, $\rho_r$ is the density of the resin expressed in g/cm$^3$, $w_f$ is the reinforcement in the composite expressed in wt.% and $\rho_f$ is the density of the reinforcement expressed in g/cm$^3$.

The theoretical composite density is then compared to the measured composite density; the difference in densities indicates the void content, which can be calculated using the expression:

$$V = \frac{(\rho_c - \rho_{mc})}{\rho_c} \cdot 100\% \tag{5.21}$$

where $V$ is the void content expressed in wt.%, $\rho_c$ is the theoretical composite density and $\rho_{mc}$ is the measured composite density; both expressed in g/cm$^3$.

## 5.6    References

1.    Levchik, SV and Weil, ED. A review on thermal decomposition and combustion of thermoplastic polyesters. Polymers for Advanced Technologies **15**(12), 691-700 (2004).

2.    Pilati, F, Manaresi, P, Fortunato, B, Munari, A, and Passalacqua, V. Formation of poly(butylene terephthalate): Secondary reactions studied by model molecules. Polymer **22**(11), 1566-1570 (1981).

3.    van Bennekom, ACM, Willemsen, PAAT, and Gaymans, RJ. Amide-modified poly(butylene terephthalate): thermal stability. Polymer **37**(24), 5447-5459 (1996).

4.    Cheng, SZD, Pan, R, and Wunderlich, B. Thermal analysis of poly(butylene terephthalate) for heat capacity, rigid-amorphous content, and transition behavior. Die Makromolekulare Chemie **189**(10), 2443-2458 (1988).

5.    Yeh, JT and Runt, J. Multiple melting in annealed poly(butlene terephthalate). Journal of Polymer Science Part B: Polymer Physics **27**(7), 1543-1550 (1989).

6.    Bragg, WL. The diffraction of short electromagnetic waves by a crystal. Proceedings of the Cambridge Philosophical Society **17**, 43-57 (1913).

7.    Scherrer, P. Bestimmung der Größe und der inneren Struktur von Kolloidteilchen mittels Röntgenstrahlen. Nachrichten von der Gesellschaft der Wissenschaften zu Göttingen, Mathematisch-Physikalische Klasse **26**, 98-100 (1918).

8.    Langford, JI and Wilson, AJC. Scherrer after sixty years: A survey and some new results in the determination of crystallite size. Journal of Applied Crystallography **11**(2), 102-113 (1978).

9.    Jian, Z and Hejing, W. The physical meanings of 5 basic parameters for an X-ray diffraction peak and their application. Chinese Journal of Geochemistry **22**(1), 38-44 (2003).

10.   ISO 527: Plastics – Determination of tensile properties. International Organization for Standardization, 2001.

11.   ISO 8256: Plastics – Determination of tensile-impact strength. International Organization for Standardization, 2004.

12.   ISO 14125: Plastics – Determination of flexural properties. International Organization for Standardization, 1998.

13.   ISO 14130: Plastics – Determination of apparent interlaminar shear strength by short-beam method. International Organization for Standardization, 1997.

14.   ISO 6603-2: Plastics – Determination of puncture impact behaviour of rigid plastics. International Organization for Standardization, 2002.

15.   Agirregomezkorta, A, Martínez, AB, Sánchez-Soto, M, Aretxaga, G, Sarrionandia, M, and Aurrekoetxea, J. Impact behaviour of carbon fibre reinforced epoxy and non-isothermal cyclic butylene terephthalate composites manufactured by vacuum infusion. Composites Part B: Engineering **43**(5), 2249-2256 (2012).

16.   Atas, C and Sayman, O. An overall view on impact response of woven fabric composite plates. Composite Structures **82**(3), 336-345 (2008).

17. Cartié, DDR and Irving, PE. Effect of resin and fibre properties on impact and compression after impact performance of CFRP. Composites Part A: Applied Science and Manufacturing **33**(4), 483-493 (2002).

18. ISO 1183: Plastics – Methods for determining the density of non-cellular plastics. International Organization for Standardization, 2004.

19. ISO 7822: Plastics – Determination of void content. International Organization for Standardization, 2000.

# Chapter 6: Results and discussion

# Characterization of CBT and pCBT

## 6.1 Introduction

It is of paramount importance to know the processing-structure-properties relationships in polymerized cyclic butylene terephthalate in order to understand the influence of the different processing routes and the thermal history on the final properties of pCBT. In this chapter the used processing techniques and subsequent characterization of unmodified pCBT are described. The properties of the different pCBT samples are compared to the ones of a commercial PBT. Three different processing routes were investigated in this research:

1. *In-situ* polymerization during compression moulding (*hot press*).
2. *In-situ* polymerization during melt blending followed by compression moulding (*Brabender Plasti-Corder + hot press*).
3. Solvent blending with subsequent *in-situ* polymerization during compression moulding (*hot press*).

The first processing route was used for simple physical blends of CBT powder and solid powders or liquids. The blends were obtained using a mortar and pestle, dried and *in-situ* polymerized in the hot plate press.

The second processing technique was used for blending and/or reacting CBT with various modifiers in the melt state with simultaneous *in-situ* polymerization in a batch mixer. Torque *versus* time was measured to study the evolution of the polymerization. This processing route requires subsequent grinding, drying and reprocessing of the obtained materials in a hot plate press in order to obtain films useful for testing.

The third processing route was used for blending CBT with chain extenders and nanofillers in the solution/dispersion state. After solvent blending the blends were vacuum dried, ground using mortar and pestle and *in-situ* polymerized in the hot plate press.

Unmodified pCBT samples were prepared by compression moulding, (referred to as pCBT-CM), melt blending (referred to as pCBT-MB) and solvent blending (henceforth denoted as pCBT-SB). The abbreviations *CM*, *MB* and *SB* will be used throughout this thesis and generally refer to compression moulded, melt blended and solvent blended samples, respectively. PBT was prepared by compression moulding and was denoted as PBT-CM. All samples were processed above the melting temperatures of pCBT and PBT, *i.e.* ~225 °C, except the sample pCBT-CM190°C. This sample represents the preferred industrial processing route: Isothermal polymerization at 190 °C for 30 min without cooling prior to demoulding.

Besides the study of these three processing routes, an additional investigation on the influence of the thermal history on the final properties of pCBT was performed. This investigation focussed on one hand on CBT *in-situ* polymerized directly in the DSC apparatus during the first heating scan and melt crystallized under various cooling rates and on the other hand on three pCBT-CM samples which were polymerized during compression moulding. One sample was crystallized in the cold part of the hot plate press at a cooling rate of -50 °C/min (*i.e.* conventional pCBT-CM as described above). Another sample was crystallized at 205 °C for 120 min and then slowly cooled to room temperature (referred to as pCBT-CM205°C). The third sample was quenched in liquid nitrogen from the melt state (referred to as pCBT-CM-Q).

The above described samples were characterized using various techniques and the results are compared to each other in order to see the influence of the processing route and the thermal history on the properties of unmodified pCBT. The obtained results are compared to the ones from the literature and also to the properties of conventional PBT. Sample designations and processing parameters are listed in table 6.1.

Table 6.1: Overview over produced PBT and pCBT samples.

| Sample | Processing | Temperature [°C] | Time [min] |
|---|---|---|---|
| pCBT-CM | CM | 250 | 20 |
| pCBT-MB | MB + CM | 230 - 250 | 15 + 5 |
| pCBT-SB | SB | 250 | 20 |
| PBT-CM | CM | 250 | 5 |
| pCBT-CM190°C | CM | 190 | 30 |
| pCBT-CM205°C | CM | 250 - 205 | 5 + 120 |
| pCBT-CM-Q* | CM | 250 | 20 |

CM: compression moulding; MB: melt blending; SB: solvent blending. *Quenched in liquid nitrogen from the melt state

## 6.2    Experimental section

### 6.2.1  Materials

One-component cyclic butylene terephthalate oligomers (CBT160®) were used throughout this chapter.

### 6.2.2  Sample preparation

**pCBT-CM, pCBT-CM205°C, pCBT-CM-Q**

Approximately 12 g of previously dried CBT powder was *in-situ* polymerized in the hot plate press at 250 °C for 20 min in ambient atmosphere and conventionally cooled in the cold stage of the press at a cooling rate of -50 °C/min (*c.f.* section 4.1). This sample was referred to as pCBT-CM and served as reference sample. Similarly, another sample (referred to as pCBT-CM205°C) was polymerized at 250 °C for 5 min. Then the temperature was slowly reduced to 205 °C at a cooling rate of -2 °C/min, isothermally

held for 120 min and finally the heating system of the press was switched off, allowing the sample to slowly cool to room temperature inside the press. Yet another sample (~1 g CBT) was polymerized between two thin household aluminium films at 250 °C for 20 min. The sample, together with the aluminium films was then submerged in liquid nitrogen for 30 min. This sample was referred to as pCBT-CM-Q and was used for DSC analysis without further treatment.

## pCBT-CM190°C

Similar to the above described compression moulded samples, one sample was isothermally polymerized and crystallized at 190 °C for 30 min. This sample was directly demoulded from the hot mould without prior cooling and was referred to as pCBT-CM190°C.

## PBT-CM

A commercial PBT was compression moulded at 250 °C for 5 min and cooled in the cold stage of the press. This sample was referred to as PBT-CM.

## pCBT-MB

Around 40 g of CBT powder was *in-situ* polymerized during melt blending at 230 °C for 20 min in nitrogen atmosphere. These processing parameters were considered as an optimum as will be explained later in section 6.4.2. The pCBT was collected, ground into granules, vacuum dried and then compression moulded at 250 °C for 5 min into a film. This sample was referred to as pCBT-MB.

**pCBT-SB**

Previously dried CBT powder (20 g)was dispersed in 50 ml THF at room temperature and at 300 rpm for 1 h, using a glass beaker and a magnetic stirrer. The CBT/THF dispersion was vacuum dried at 80 °C for 8 h, ground into a fine powder using mortar and pestle and then vacuum dried at 80 °C for 3 days to completely remove the THF. Once dried, the material was *in-situ* polymerized in the hot plate press at 250 °C for 20 min in ambient atmosphere and conventionally cooled in the cold stage of the press. This sample was referred to as pCBT-SB.

## 6.3    Characterization

The CBT, pCBT and PBT samples were characterized using torque versus time measurements, differential scanning calorimetry, X-ray diffraction, scanning electron microscopy and dynamic mechanical thermal analysis. The mechanical properties of the samples were determined by tensile tests and by instrumented tensile-impact tests. All characterization methods are described in detail in chapter 5.

## 6.4    Results and Discussion

The influence of temperature and atmosphere on the ring-opening polymerization of CBT was studied by torque *versus* time measurements in the batch mixer. The measured torque signal is an indicator for the viscosity evolution. An increase in melt viscosity can be seen as a molecular weight built-up of the polymerizing CBT. The maximum observed torque value during polymerization was considered as the end of the ROP. Longer polymerization times led to a decreasing torque which was attributed to thermo-mechanical degradation and hydrolysis for samples processed without the protecting atmosphere. The time corresponding to the observed maximum torque was hence considered as the optimum polymerization time for the given polymerization conditions (*i.e.* temperature, screw speed, atmosphere).

### 6.4.1  Torque *versus* time measurements of pCBT and PBT

A preliminary experiment with compression moulded pCBT (*i.e.* milled pCBT-CM) and a commercial PBT was carried out in order to determine the intrinsic torque levels of the two fully polymerized materials in the molten state. Torque *versus* time measurements were performed with 40 g dried granules at 230 °C mixing chamber temperature and 60 min$^{-1}$ screw speed in ambient atmosphere, the torque signals are shown in figure 6.1.

It can be seen that both materials generated a considerable initial torque peak after introducing the granules in the mixing chamber. The higher initial torque peak of PBT is probably caused by the bigger PBT granules which may have generated higher frictional forces in the mixing chamber before melting compared to the smaller pCBT flakes.

The torque signals of both materials rapidly decreased and levelled out after complete melting. The torque value of molten pCBT stabilized at 1 Nm after 1 min whereas the one of PBT levelled out at 10 Nm after 2 min. Both torque curves marginally decreased after stabilization due to thermo-mechanical and hydrolytic degradation.

This indicates on the one hand a low molecular weight of pCBT-CM compared to that of commercial PBT and on the other hand an intrinsic torque level of 10 Nm for high molecular weight PBT. It can be concluded from this preliminary experiment that a torque level of 10 Nm or higher is desirable for pCBT *in situ* polymerized in the batch mixer. The reason for this is that a higher molecular weight (as indicated by a higher torque level) leads to a decreased crystallinity with more intercrystalline tie molecules and more entanglements which in turn improve the polymer toughness [1-2].
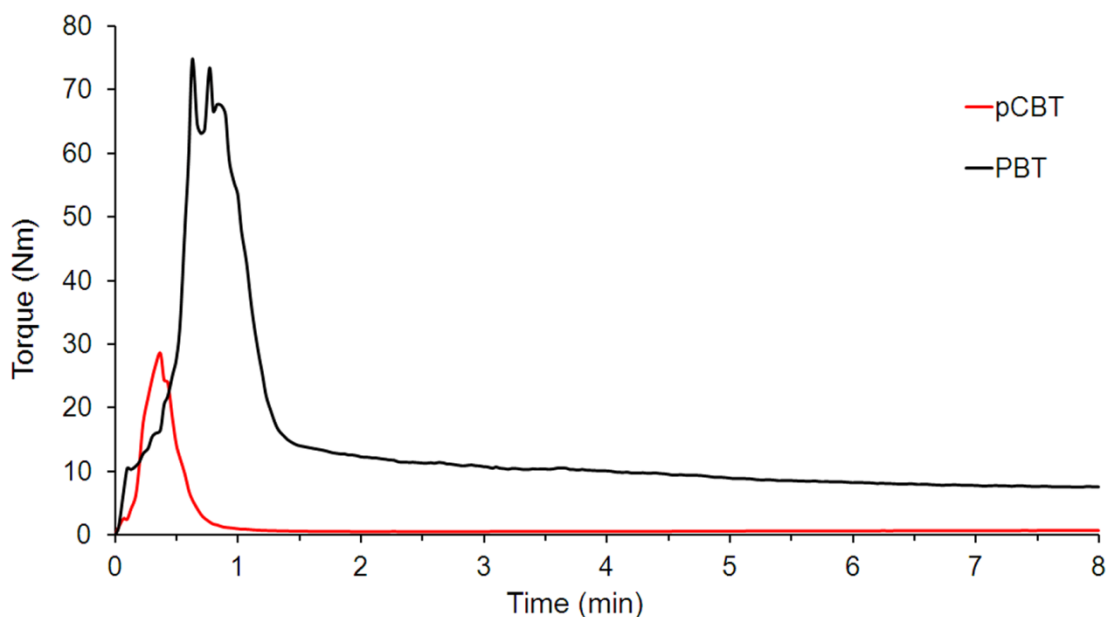
Fig. 6.1: Torque signals of pCBT and PBT melt processed at 230 °C and 60 min$^{-1}$ screw speed in ambient atmosphere.

### 6.4.2  Torque *versus* time measurements of CBT

Dried CBT was *in situ* polymerized in the batch mixer at two different temperatures, 230 and 250 °C, with and without nitrogen blanket. The torque curves are depicted in figure 6.2 and the maximum torque values with the corresponding times to reach maximum torque are reported in table 6.2.

The melt viscosity of the molten CBT was below the detection limit of the measuring system after introduction and melting of the CBT powder in the batch mixer. The torque signal was first detected after a few minutes which was considered as the onset of the ROP. Faster polymerization kinetics at higher temperatures were expected but no clear tendency regarding the onset time of the torque signal is apparent; the onset times fall in between 1.5 to 4.8 min for the four different polymerization conditions. When comparing the two samples polymerized in ambient atmosphere, torque onset time decreased about 220% when the temperature was increased by 20 °C. In case of the samples polymerized under $N_2$ an opposite tendency can be seen, the sample polymerized at 230 °C showed only half of the onset time compared to the one polymerized at 250 °C (*c.f.* table 6.1).
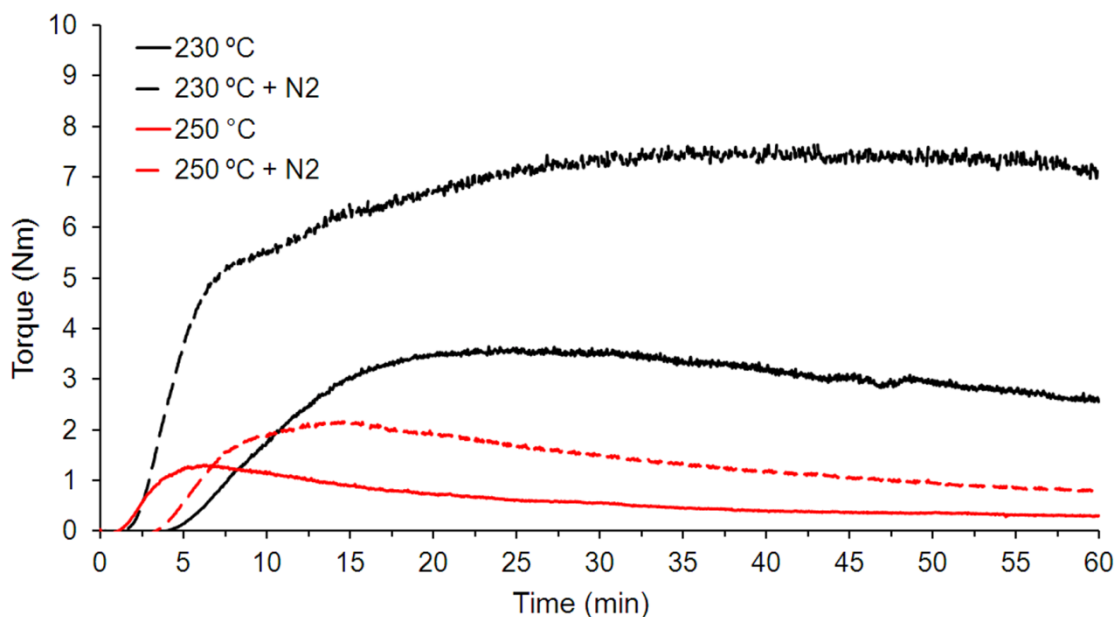
Fig. 6.2: Influence of temperature and atmosphere on the polymerization of CBT.

The maximum torque value and the corresponding time were considered to be the most important set of parameters in these experiments since a higher torque level of a molten polymer subjected to shear stress is attributed to a higher molecular weight [3-5]. It is well known that a higher melt temperature leads to a viscosity reduction of the molten polymer. Consequently, measured torque values are only comparable for equal temperatures. Torque values for both studied temperatures doubled when the polymerization was conducted under a nitrogen blanket. This was attributed to less influence of ambient humidity because it is known to inhibit the polymerization catalyst [6] and to cause hydrolysis [7] of pCBT.

Table 6.2: Torque onset times, maximum torque values and corresponding times during ROP of CBT in the batch mixer at 230 and 250 °C, with and without nitrogen blanket

| Sample designation | Time$_{torque\ onset}$* [min] | Torque max. [Nm] | Time$_{torque\ max}$** [min] |
|---|---|---|---|
| CBT-230 °C | 4.8 | 3.7 | 23.4 |
| CBT-230 °C + N2 | 1.9 | 7.7 | 40.8 |
| CBT-250 °C | 1.5 | 1.3 | 6.3 |
| CBT-250 °C + N2 | 3.8 | 2.2 | 13.6 |

* Time corresponding to onset of torque signal

** Time to reach maximum torque

The highest overall torque of 7.7 Nm was found for the polymerization condition 230 °C and nitrogen blanket. In respect to the maximum torque level of PBT (~10 Nm, *c.f.* section 6.4.1), it was assumed that the final molecular weight of this particular pCBT sample was lower than the one of PBT. The time to reach this torque was over 40 min but after 15 min almost 90% of the maximum torque was reached, further polymerization time resulted in a marginal torque improvement. A similar tendency can be observed for the sample polymerized at the same temperature but without nitrogen blanket. Moreover, it is apparent that all other samples reached their maximum torque in considerably less time and showed a decreasing torque due to melt degradation in the range around 40 min. Hence, for a temperature of 230 °C a polymerization time of 40 min was not considered as an optimum time. An optimum polymerization time of 20 min was established instead.

At the end of the experiment, degradation was evident after melt blending in the batch mixer during one hour as can be seen in figure 6.3. Samples polymerized at 250 °C had much lower viscosity and readily flowed out of the mixing chamber when the pCBT was collected after the experiment, as can be assumed from the greyish/brownish fibre-like material (*c.f.* figs. 6.3c and d). Once solidified, these samples were very brittle. The samples polymerized at 230 °C had an apparently higher viscosity as indicated by the much bulkier materials (*c.f.* figs. 6.3a and b) and confirmed by the corresponding torque curves (*c.f.* fig. 6.2). Moreover, these samples appeared less greyish/brownish compared to the ones polymerized at 250 °C. CBT polymerized at 230 °C and under nitrogen

atmosphere showed the highest torque level and apparently yielded a whiter and somewhat less brittle pCBT compared to the other three polymerization conditions.
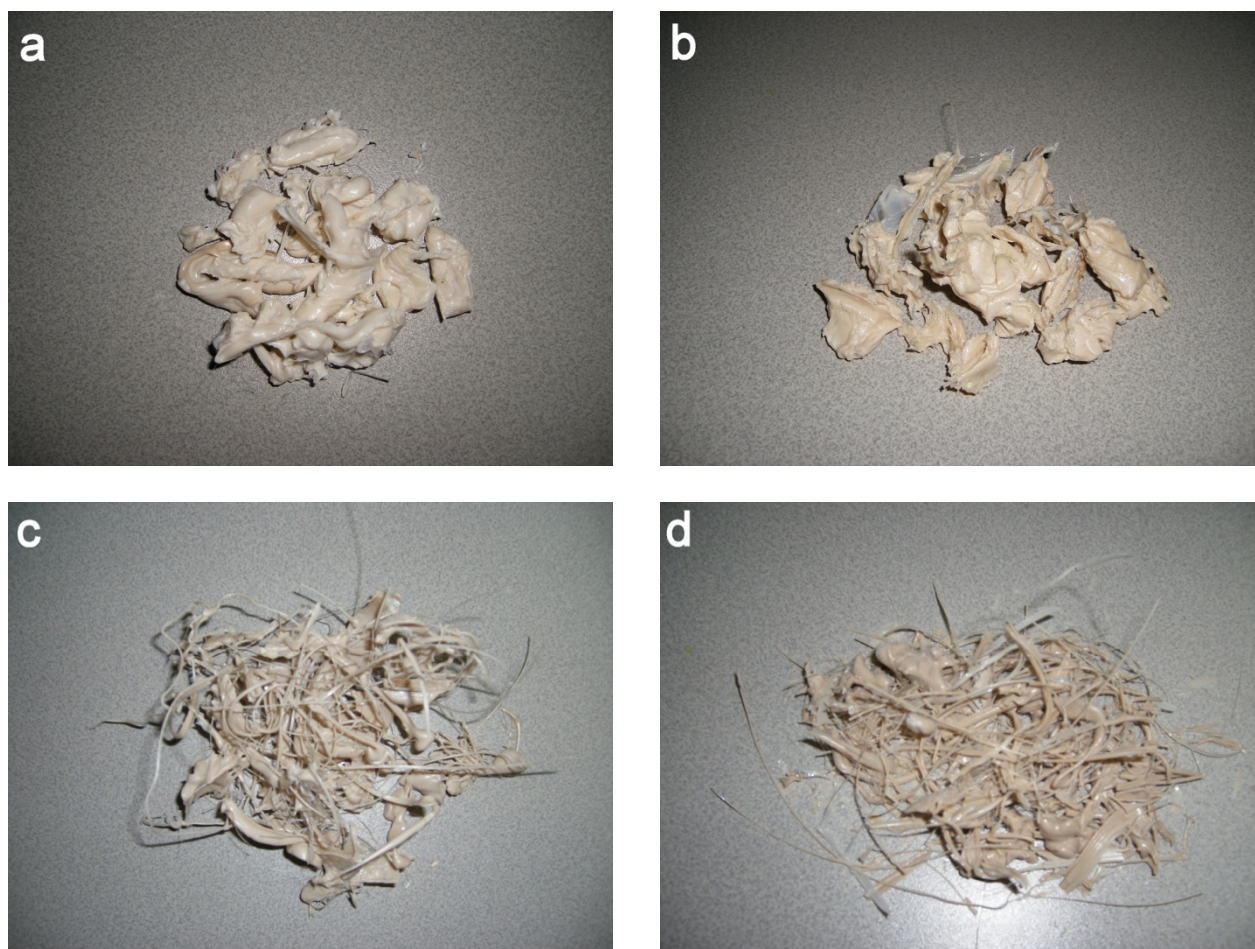


Fig. 6.3: As-collected pCBT samples polymerized in the batch mixer at 230 °C with (a) and without nitrogen blanket (b). pCBT samples polymerized at 250 °C with (c) and without nitrogen blanket (d)

To conclude, melt blending in the batch mixer at a mixing chamber temperature of 230 °C and a polymerization time of 20 min under nitrogen atmosphere was established as an optimum polymerization condition of unmodified CBT.

### 6.4.3  DSC analysis of CBT

The influence of the processing route on the thermal properties of pCBT, namely the melting temperature and melt enthalpy, multiple melting peak behaviour, crystallization temperature and degree of crystallinity, was studied by DSC. In a first approach, neat CBT was *in-situ* polymerized in a DSC crucible during the first heating run, then crystallized using various cooling rates and finally subjected to a second heating scan in order to assess the thermal properties. Then the samples processed by the aforementioned processing routes were analysed and the results are discussed in this chapter.

**DSC thermogram**

The thermogram of predried CBT *in situ* polymerized during the first heating scan at a heating and cooling rate of 5 °C·min$^{-1}$ is exemplarily shown in figure 6.4.
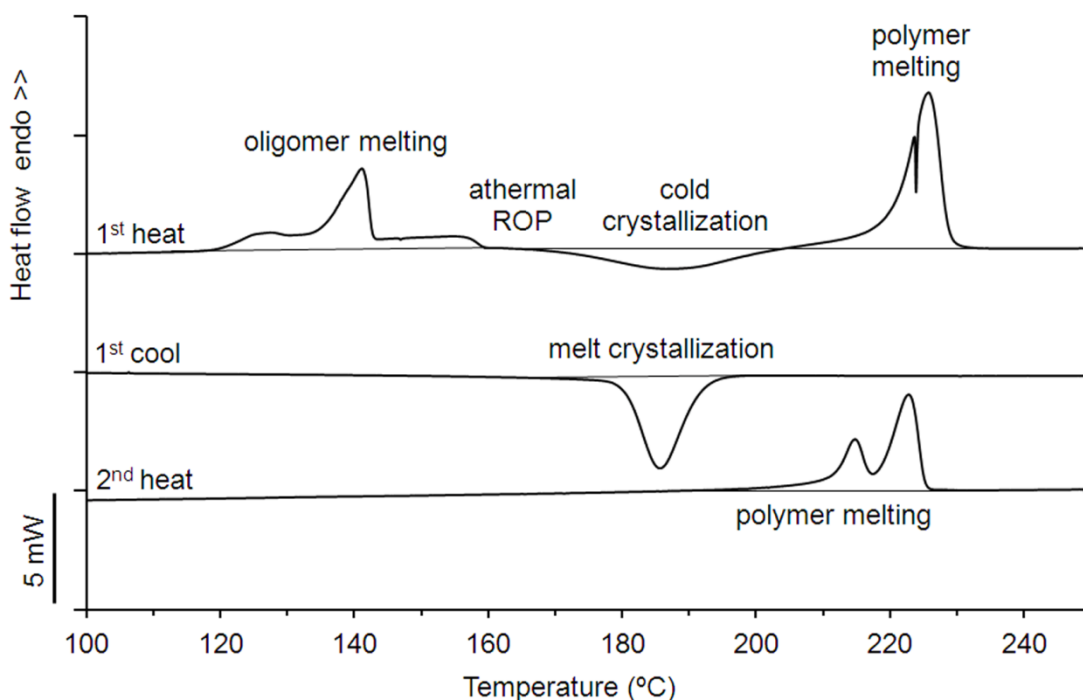


Fig. 6.4: DSC thermogram of one-component CBT, heating and cooling rate: 5 °C·min$^{-1}$

The CBT oligomers melt in a broad melting range of 120–160 °C, exhibiting a melt enthalpy of 46 J/g and a main melting peak at 140 °C. The oligomer melting is subsequently followed by the ring-opening polymerization. Since the cyclic oligomers are nearly strain-free, the ring-opening polymerization is essentially athermal [8] and therefore cannot be studied by conventional DSC. If the ROP starts below the melting temperature of the final polymer, cold crystallization may occur. The latter can be observed in the temperature range of 165–205 °C as a broad exothermic peak with a crystallization enthalpy of -23 J/g and a peak temperature at 187 °C. Cold crystallization is followed by polymer melting at 226 °C with a melt enthalpy of 60 J/g, *i.e.* a degree of crystallinity of 42% was reached during cold crystallization. Moreover, double melting behaviour becomes evident, although the two peaks are merged together.

Upon cooling from the melt, pCBT crystallizes in the range of 200–170 °C (peak at 186 °C), liberating a heat of crystallization of -40 J/g. In the second heating scan only polymer melting is observed; the absence of oligomer melting around 140 °C during second heating indicates a complete conversion from CBT oligomers to pCBT polymer. A well-defined double melting peak is seen with a low-temperature peak at 215 °C and a high-temperature peak at 223 °C and a total melt enthalpy of 40 J/g which translates to a degree of crystallinity of 28%. Under these experimental conditions the degree of crystallinity formed during cold crystallization is 1.5 times higher than the one formed during crystallization from the melt.

## Kinetic study: cold crystallization and polymer melting

It was stated in literature that cold crystallization and hence polymer melting may be kinetically hindered when high heating rates or reinforcements such as organo-clays are used [9-10]. To further investigate this effect, CBT was subjected to different heating rates; the first heating scans are depicted in figure 6.5.

It can be noticed that the oligomer melting is not affected by the heating rate. But a clear influence of the latter on the cold crystallization and subsequent polymer melting is observed. When CBT is heated at a low rate (*i.e.* 1 °C/min), cold crystallization is observed between 155 and 185 °C with an appreciable amount of heat of crystallization. When the heating rate is increased to 5 and 10 °C/min, the temperature range of the cold

crystallization is shifted towards higher temperatures; namely by 15 and 20 °C, respectively.

It is noteworthy to mention that the peak height and intensity apparently increased with increasing heating rate. This is ascribed to a known kinetic effect inherent in DSC analysis. High heating rates lead to an increase in peak intensity but at the same time also to less peak resolution [11]. Nevertheless, the measured enthalpy data is provided in figure 6.5.
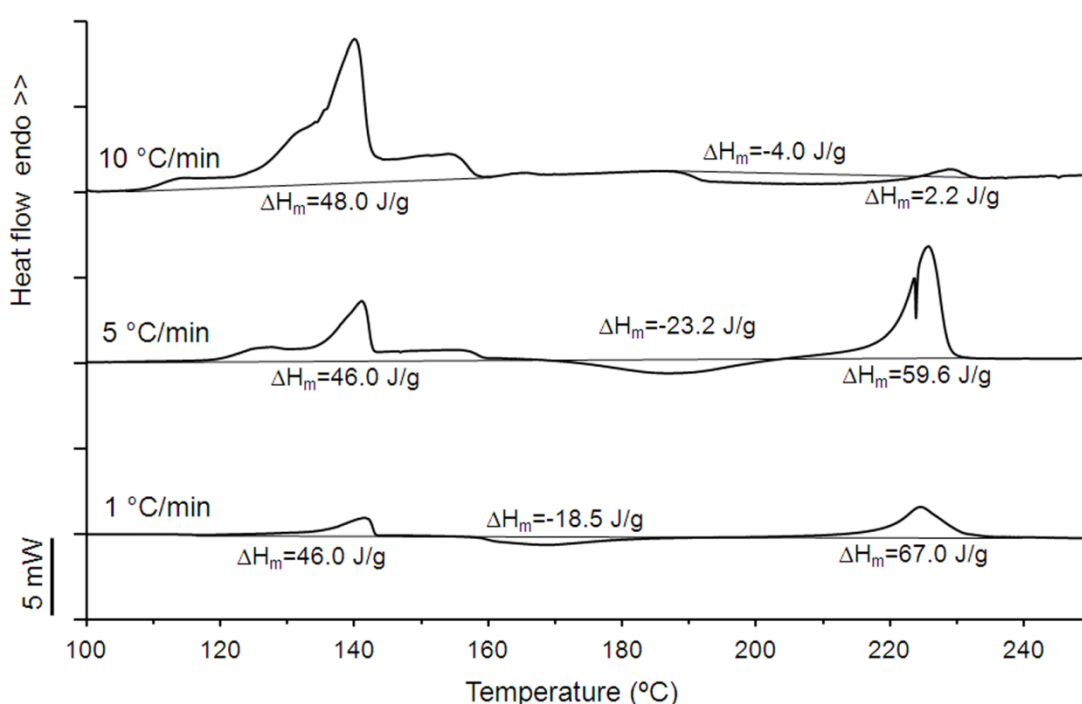


Fig. 6.5: DSC first heating scans of one-component CBT, heating rate: 1, 5 and 10 °C/min.

Regarding cold crystallization, a decrease in enthalpy with increasing heating rate can be seen but enthalpies were difficult to measure due to the broad and not well resolved peak. This tendency is better reflected in the polymer melting enthalpy which decreased from 67 to 2 J/g when the heating rate increased from 1 to 10 °C/min. The observed tendency may be explained by the fact that at low heating rates the molten CBT is given more time to polymerize and crystallize before reaching the polymer melting temperature, *i.e.* simultaneous polymerization and crystallization. However, at high heating rates the polymer melting temperature is reached before ROP and cold crystallization is completed.

At a sufficiently high heating rate, no crystallization and hence no polymer melting is observed. In this case the polymerization and crystallization are consecutive and the ROP mainly takes place above $T_m$. This holds true for heating rates higher than 10 °C/min; at this rate the melting enthalpy is only 2.2 J/g.

Polymer melting temperatures are not markedly affected by the heating rate. At the low heating rate a single pCBT melting peak is observed at 224 °C which increased to 226 and 229 °C when the heating rate was raised to 5 and 10 °C/min, respectively. This increase is ascribed on one hand to another known kinetic effect in DSC analysis: Peak temperatures are shifted towards higher temperatures when heating rates are increased due to the increasing thermal inertia of the polymer [11].

On the other hand, this increase in $T_m$ may be misinterpreted and actually explained by the observation of the aforementioned double melting phenomenon which is apparent at 5 °C/min heating rate. Karger-Kocsis *et al.* performed a modulated DSC (MDSC) study on CBT at a heating rate of 5 °C/min and also observed double melting. More specifically, during the second heating scan they found a prominent exothermic peak with an enthalpy of 37.8 J/g in the non-reversing MDSC trace and ascribed this to massive recrystallization [9].

According to the recrystallization model [12-16], the low-temperature endothermic peak represents the melting of only a part of original crystals. The high-temperature peak represents the melting of reorganized crystals during the DSC heating scan. In other words, the pCBT melting process is the result of melting of small and/or imperfect original crystals, crystal reorganization into more stable crystals through melt recrystallization and finally the melting of recrystallized crystals. The exothermic dip between the double melting endothermic peaks is attributed to the recrystallization.

Double melting is only seen in the intermediate heating rate, whereas at low and high heating rate only a single melting peak is observed. It is not clear if the two single peaks observed at low and high heating rate correspond to each other. It is possible that the peak at low rate corresponds to the lower melting peak, that is the melting of original crystals. The peak observed at high rate may be ascribed to the higher melting peak which is due to partial fusion, crystal perfection and recrystallization which occur simultaneously. Therefore, the apparent increase in $T_m$ with increasing heating rate is possibly due to the observation of the fusion of *recrystallized* crystals (contrary to the

melting of *original* crystals as observed at low heating rate). To clarify this issue a kinetic DSC study was performed.

## Kinetic study: nonisothermal melt crystallization

To further study the double melting phenomenon and degree of crystallinity in pCBT, another kinetic DSC study was conducted. In this study, CBT was *in situ* polymerized in the DSC pan at a heating rate of 10 °C/min up to 250 °C, isothermally held at that temperature for 3 min to assure complete polymerization and then crystallized from the melt at various nominal cooling rates, namely -0.5, -1, -2.5, -5, -10, -25, -50, -75 and -100 °C/min; crystallization exotherms are shown in figure 6.6.

A fresh sample was used for each experiment and the sample weight was 8–10 mg. After the nonisothermal crystallization the samples were subjected to a second heating scan at 10 °C/min heating rate to determine the thermal properties (*c.f.* figure 6.7). The equal heating rate in the first and second heating run assures equal thermal history and thus comparability of the data. Moreover, the aforementioned kinetic effect of peak temperature shift due to high heating rates is equal for all samples and therefore does not need to be considered here.
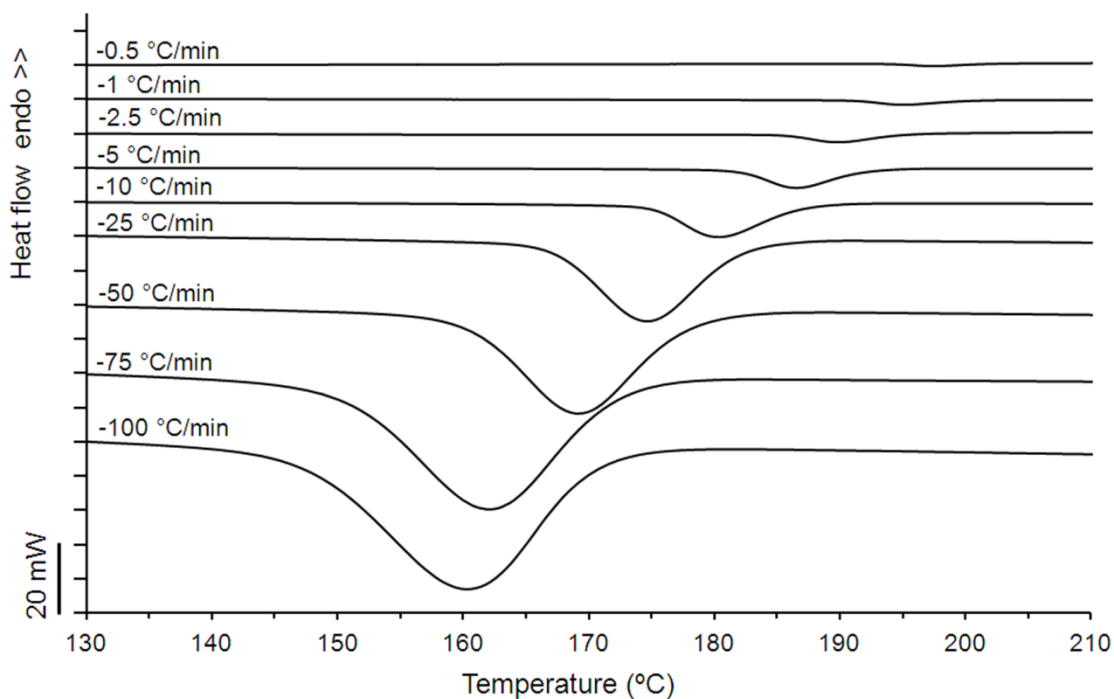
Fig. 6.6: DSC first cooling scans of one-component CBT *in-situ* polymerized in the DSC crucible at 10 °C/min and crystallized at various nominal cooling rates.

As expected, crystallization temperature and crystallization enthalpy decreased with increasing cooling rate. From figure 6.6 it appears that the crystallization enthalpy increases with increasing cooling rate but the opposite is the case; accurate data is compiled in table 6.3. Again, this apparent increase in peak intensity is ascribed to the aforementioned kinetic effect inherent in DSC analysis and is due to the increasing heating or cooling rate.
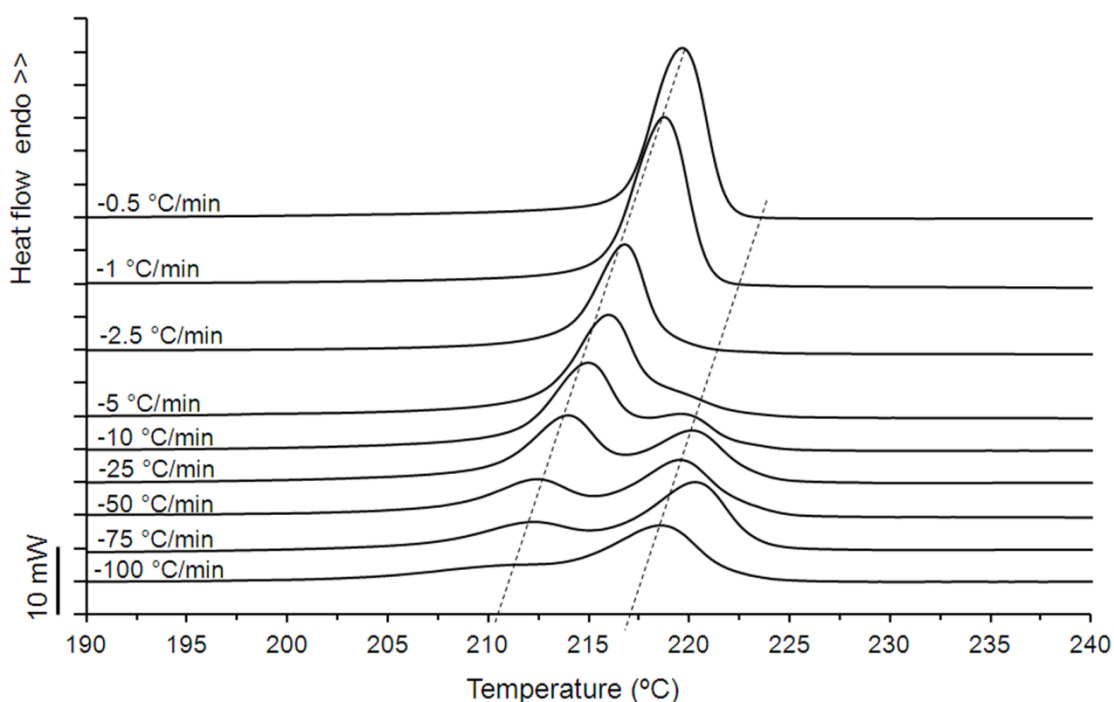
Fig. 6.7: DSC second heating scans of one-component CBT *in-situ* polymerized in the DSC crucible at 10 °C/min and crystallized at various cooling rates. Heating rate: 10 °C/min.

In the second heating scan not only peak melting temperature and degree of crystallinity of pCBT is governed by the preceding cooling rate, also the double melting phenomenon is affected by the thermal history. Both melting peak temperatures decreased to a similar extend with cooling rate, as indicated by the dashed lines in figure 6.7. Low cooling rates up to -2.5 °C/min resulted in a single melting peak which did not undergo recrystallization; the peak height decreased with increasing cooling rate. At -5 °C/min a high-temperature shoulder appeared and further increased in peak height when the cooling rate was increased. While this high-temperature peak increased in peak height, the low-temperature peak broadened and its height decreased and eventually diminished with cooling rate.

Yasuniwa *et al.* found similar results for PBT and poly(hexamethylene terephthalate) (PHT) [14]. This shows that the cooling rate during crystallization from the melt has a significant effect on the double melting phenomenon of pCBT. When crystallization from the melt is conducted at a slow rate, a crystal structure with a high degree of perfection and a large lamellar thickness develops. Since crystal perfection is high, recrystallization and lamellar thickening does not occur. Crystal perfection and

lamellar thickness decrease with increasing cooling rate, giving rise to recrystallization. Since melting and recrystallization in the heating scan are competitive processes, the high-temperature endothermic peak appears when the rate of melting overwhelms the rate of recrystallization [14]. At high cooling rates, small and/or imperfect crystals develop which readily reorganize into more stable crystals. Consequently, the low-temperature endothermic peak height decreases and the high-temperature endothermic peak height increases with increasing cooling rate.

Table 6.3:  DSC data of CBT160 polymerized in the DSC pan and melt crystallized at various cooling rates. DSC first and second heating rate of 10 °C/min.

| Cooling rate | first heating | | first cooling | | second heating | | | Crystallinity * |
|---|---|---|---|---|---|---|---|---|
| | $T_m$ | $\Delta H_{m1+2}$ | $T_c$ | $\Delta H_c$ | $T_{m1}$ | $T_{m2}$ | $\Delta H_{m1+2}$ | $X_C$ |
| (°C/min) | [°C] | [J/g] | [°C] | [J/g] | [°C] | [°C] | [J/g] | [%] |
| -0.5 | 228.4 | 2.4 | 197.4 | -52.6 | 219.8 | – | 57.4 | 40.4 |
| -1 | 228.6 | 0.2 | 194.9 | -47.4 | 218.8 | – | 53.3 | 37.5 |
| -2.5 | – | – | 189.9 | -46.5 | 216.8 | – | 49.2 | 34.6 |
| -5 | 228.2 | 0.2 | 186.6 | -45.8 | 216.0 | – | 48.1 | 33.9 |
| -10 | 228.6 | 2.2 | 180.3 | -45.3 | 215.0 | 224.1 | 46.6 | 32.8 |
| -25 | 228.4 | 1.1 | 174.0 | -39.8 | 214.0 | 220.1 | 45.6 | 32.1 |
| -50 | 227.4 | 0.6 | 169.0 | -38.1 | 212.3 | 219.5 | 42.3 | 29.8 |
| -75 | – | – | 162.4 | -35.2 | 212.3 | 220.3 | 40.5 | 28.5 |
| -100 | – | – | 160.2 | -32.3 | – | 218.6 | 36.5 | 25.7 |

* calculated from second heating melting enthalpy

As expected, the degree of crystallinity also decreased with increasing cooling rate, as can be seen in table 6.3 and figure 6.8. Generally, the degree of crystallinity derived from the second heating scan was higher than the one derived from the first cooling scan. This was ascribed to the recrystallization phenomenon. The degree of crystallinity reached 40% when the preceding cooling rate was -0.5 °C/min and decreased to 26% for a high cooling rate of -100 °C/min (*c.f.* table 6.3). A pronounced decrease in crystallinity (-6%) was found for a range of cooling rates from -0.5 °C/min to -2.5 °C/min; increasing cooling rates

resulted in a less pronounced decrease in crystallinity. This is due to the high nucleation density of PBT (and hence also expected for pCBT) which results in a fast crystallization [17].
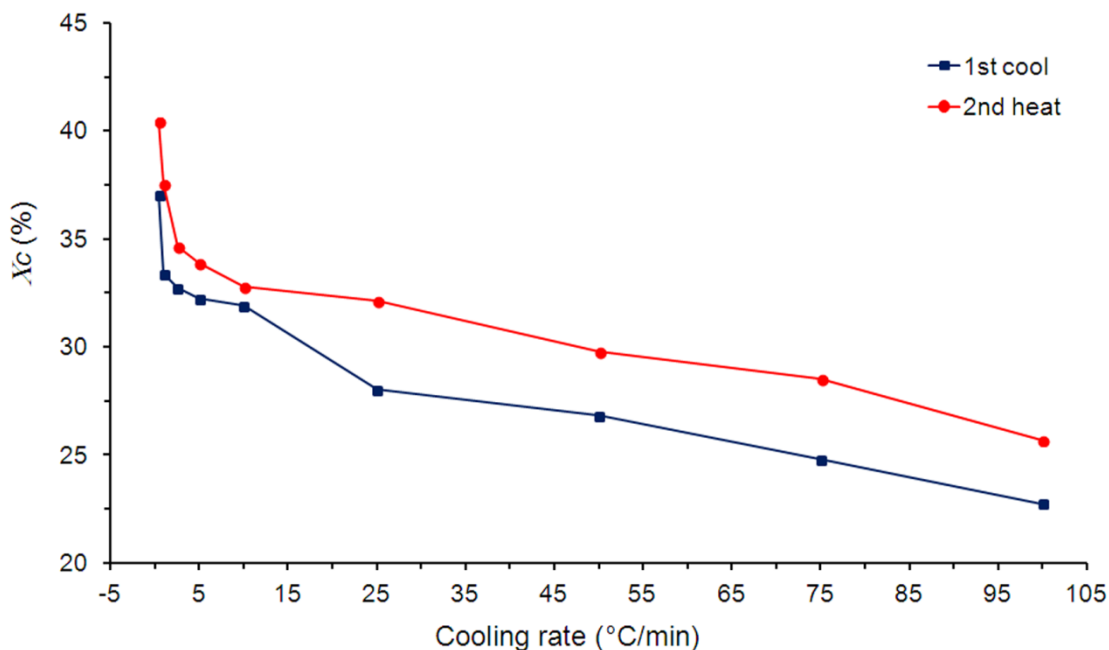


Fig. 6.8: Degree of crystallinity *versus* cooling rate of one-component CBT *in-situ* polymerized in the DSC crucible at 10 °C/min and crystallized at various cooling rates. Data calculated from crystallization enthalpies (1st cool) and melting enthalpies (2nd heat)

From these DSC experiments the following conclusions can be drawn:

- Cold crystallization and hence polymer melting of CBT polymerized during the first heating scan are suppressed when high DSC heating rates (>10 °C/min) are employed.
- The degree of crystallinity formed during cold crystallization is 1.5 times higher than the one formed during melt crystallization.
- pCBT melt crystallized at low cooling rates up to -2.5 °C/min results in a single melting peak which does not undergo recrystallization whereas higher cooling rates lead to double melting phenomenon.

- Degrees of crystallinity ranging from 40 to 26% can be obtained when pCBT is melt crystallized at cooling rates from -0.5 °C/min to -100 °C/min, respectively.

### 6.4.4  DSC analysis of pCBT prepared by CM, MB and SB

**"As-moulded" properties**

The role of the different processing routes, namely compression moulding, melt blending and solvent blending of one-component CBT on the thermal properties such as the melting temperature, crystallization temperature and degree of crystallinity was analysed by DSC and compared to conventional PBT. The "as-moulded" properties were determined from DSC first heating scans (shown in figure 6.9) at a heating rate of 10 °C/min and are listed in table 6.4.
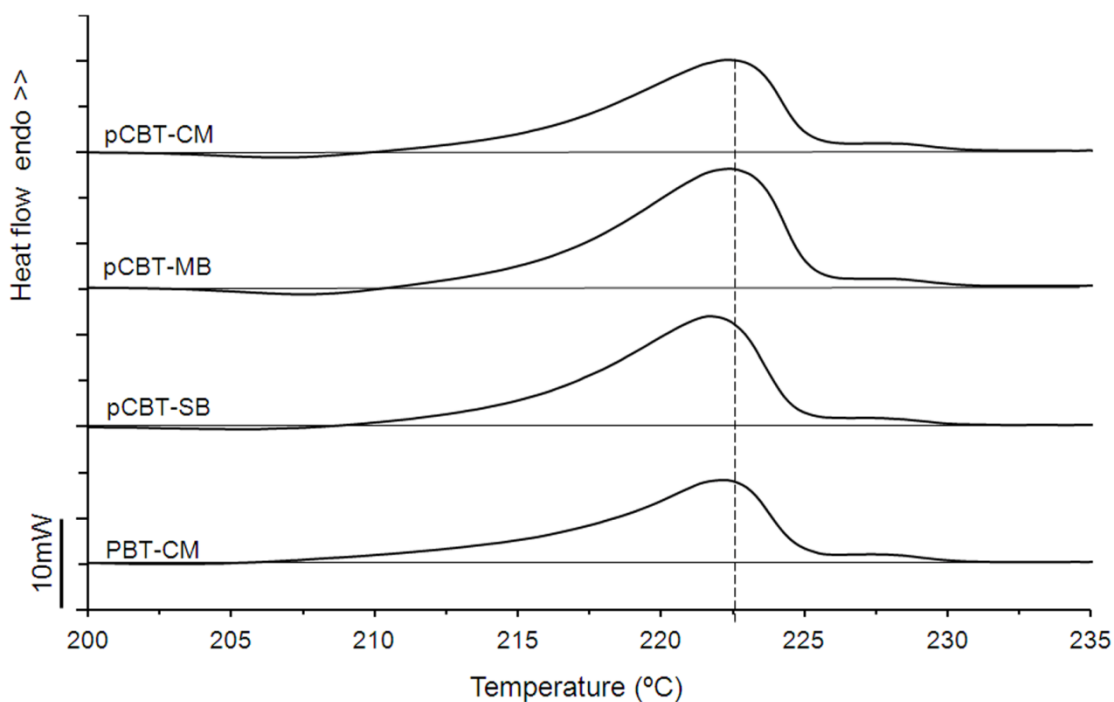


Fig. 6.9: DSC first heating scans of pCBT-CM, pCBT-MB, pCBT-SB and PBT-CM. Heating rate: 10 °C/min.

As expected, no significant difference between pCBT-CM, pCBT-MB, pCBT-SB and PBT-CM was found due to equal thermal histories (melt crystallized at ca. -50 °C/min in the cold stage of the hot plate press). These samples exhibited a small amount of cold crystallization in the range of 200–210 °C with a crystallization enthalpy of -1 to -2 J/g. Moreover, all samples showed a pronounced low-temperature melting peak in the temperature range of 222–224 °C and a high-temperature shoulder around 228 °C. The latter was ascribed to the aforementioned recrystallization phenomenon. The polymer melting enthalpy was also similar, resulting in a range of crystallinity of 32–36%. Interestingly, the overall minimum degree of crystallinity was observed in the solvent blended sample and not as expected in PBT. Parton *et al.* showed that pCBT polymerized below as well as above $T_m$ develops a higher degree of crystallinity with bigger crystallite size and a more perfect crystalline structure compared to conventional PBT [18]. Nevertheless, this difference in crystallinity of these samples is considered to be marginal. This demonstrates that the employed processing routes, namely CM, MB and SB yield a pCBT with similar thermal properties and comparable melting temperature and degree of crystallinity.

**Effect of thermal history**

Samples with different thermal histories, namely pCBT quenched in liquid nitrogen from the melt at 250 °C, pCBT isothermally polymerized and crystallized at 190 °C for 30 min, and pCBT polymerized at 250 °C and crystallized at 205 °C were compared to the above described sample pCBT-CM. The "as-moulded" properties were determined from the first heating scans (shown in figure 6.10) at a heating rate of 10 °C/min and are collected in table 6.4.
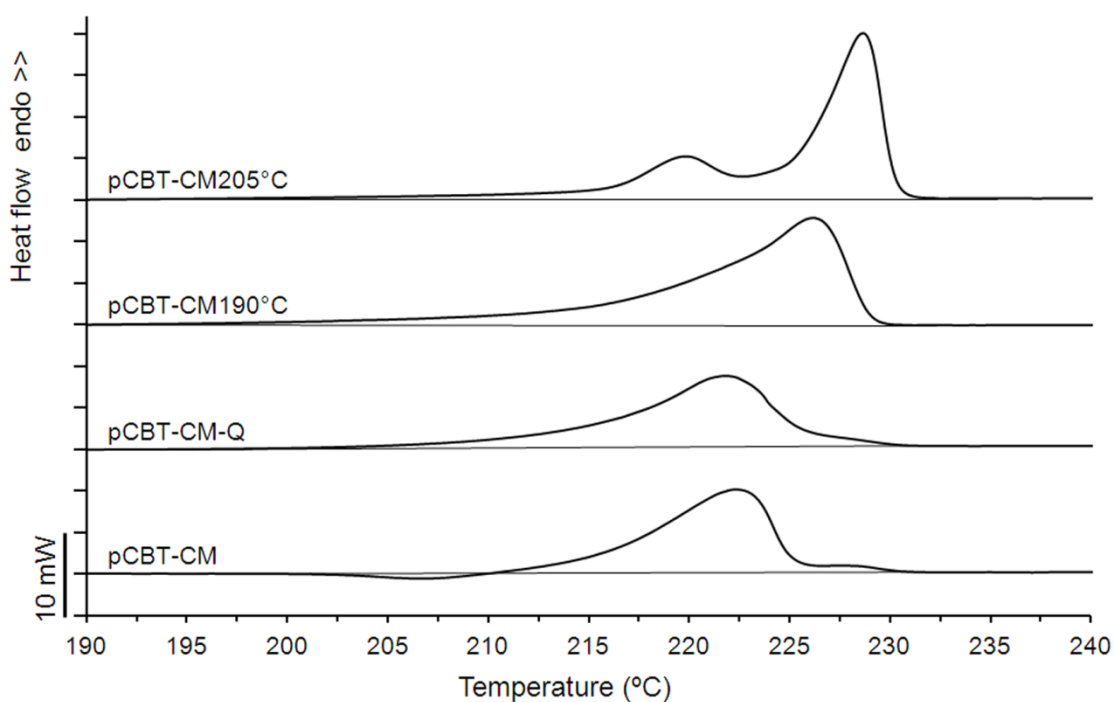
Fig. 6.10: DSC first heating scans of pCBT-CM, pCBT-CM-Q, pCBT-CM190°C and pCBT-CM205°C. Heating rate: 10 °C/min.

Table 6.4: DSC first heating scan data of pCBT produced by compression moulding (CM), melt blending (MB) and solvent blending (SB) with quenching in liquid nitrogen (Q); DSC heating rate of 10 °C/min.

| Sample | first heating | | | Crystallinity |
|---|---|---|---|---|
| | $T_{m1}$ | $T_{m2}$ | $\Delta H_{m1+2}$ | $X_C$ |
| | [°C] | [°C] | [J/g] | [%] |
| pCBT-CM | 224.2 | – | 51.3 | 36.1 |
| pCBT-MB | 222.4 | – | 50.9 | 35.8 |
| pCBT-SB | 221.6 | – | 45.3 | 31.9 |
| PBT-CM | 221.8 | – | 48.0 | 33.8 |
| pCBT-CM190°C | 226.1 | – | 64.4 | 45.4 |
| pCBT-CM205°C | 219.6 | 228.6 | 57.1 | 40.2 |
| pCBT-CM-Q | 222.4 | – | 47.1 | 33.2 |

* calculated from first heating melting enthalpy

Quenching in liquid nitrogen resulted in a decrease in melting temperature and degree of crystallinity of 2 °C and 3%, respectively. Since these decreases were small, it can be assumed that the quenching procedure in liquid $N_2$ was not effective. It was stated in the literature that it is impossible to obtain fully amorphous PBT by quenching molten PBT in liquid nitrogen [17]. This may be due to the fact that when the molten sample was immersed in liquid nitrogen, immediately an insulating gas cushion of evaporating $N_2$ was formed, preventing an effective heat transfer. As a consequence, the resulting thermal properties of pCBT-CM-Q were similar to the ones of conventional pCBT-CM.

The isothermally polymerized and crystallized sample pCBT-CM190°C was different compared to the above described samples; this sample did not undergo cold crystallization and did not show a high-temperature shoulder. A single peak with a peak temperature of 226 °C was found instead which is an intermediate temperature compared to the low- and high-temperature peaks observed in the other samples. This is due to the different thermal history; all other samples were processed above $T_m$ and quickly crystallized from the molten state which can be considered as a truly random melt. In contrast, pCBT-CM190°C was polymerized and crystallized below $T_m$, which resulted in thicker crystals with a higher lamellar thickness and thus a higher melting temperature. This isothermally processed sample showed the highest degree of crystallinity of all studied samples, namely 45%. (*c.f.* table 6.4). This value is concordant with the measured amount of crystal fraction available in literature and obtained by isothermal polymerization and crystallization below $T_m$ [6, 10, 19]. Additionally, the absence of cold crystallization and recrystallization in the first heating scan indicates a high degree of crystal perfection.

Hakmé *et al.* concluded from dielectric sensing experiments that the polymerization and crystallization of pCBT are simultaneous for temperatures below 200 °C [6]. According to Wunderlich [20], simultaneous crystallization and polymerization yields crystals with more extended chain conformation whereas a folded chain conformation is produced by separate polymerization and crystallization, as is the case for quenched polymer melts or solutions. A crystal structure with an extended chain conformation is characterized by a higher degree of crystallinity and crystal perfection as well as a lower tie molecule density [18, 20] which in turn lead to brittleness. Hence, the isothermal processing below $T_m$ yields an intrinsically more brittle pCBT.

The last sample under study was the one polymerized at 250 °C and crystallized at 205 °C. This sample showed double melting with a predominant high-temperature peak at

229 °C which was the highest melting temperature of all studied samples. This increase in melting temperature was ascribed to crystal thickening during the annealing step [13]. The degree of crystallinity was 5% lower compared to pCBT-CM190°C which is consistent with the assumption that a separate polymerization and crystallization leads to a folded chain conformation with a lower degree of crystallinity, as mentioned above.

**Thermal properties**

The intrinsic thermal properties of the pCBT samples were assessed from the second heating and first cooling runs as shown in figure 6.11 and figure 6.12; data is compiled in table 6.5.

Table 6.5: DSC first cooling and second heating scan data of pCBT produced by compression moulding (CM), melt blending (MB) and solvent blending (SB) with quenching in liquid nitrogen (Q); DSC heating and cooling rate of 10 °C/min.

| Sample | first cooling | | second heating | | | Crystallinity * |
|---|---|---|---|---|---|---|
| | $T_c$ | $\Delta H_c$ | $T_{m1}$ | $T_{m2}$ | $\Delta H_{m1+2}$ | $X_C$ |
| | [°C] | [J/g] | [°C] | [°C] | [J/g] | [%] |
| pCBT-CM | 183.9 | -48.8 | 213.4 | 224.8 | 45.2 | 31.8 |
| pCBT-MB | 193.1 | -50.6 | 215.4 | 223.5 | 50.7 | 35.7 |
| pCBT-SB | 187.2 | -44.5 | 214.0 | 222.9 | 44.6 | 31.4 |
| PBT-CM | 185.2 | -46.3 | 216.1 | 222.9 | 46.4 | 32.7 |
| pCBT-CM190°C | 184.9 | -46.7 | 215.8 | 222.3 | 49.5 | 34.9 |
| pCBT-CM205°C | 187.5 | -43.0 | 214.5 | 223.3 | 42.8 | 30.1 |
| pCBT-CM-Q | 185.2 | -43.3 | 215.8 | 223.1 | 46.0 | 32.4 |

* calculated from second heating melting enthalpy

**pCBT-CM, pCBT-MB, pCBT-SB and PBT-CM**

When comparing the conventionally processed samples, namely pCBT-CM, pCBT-MB, pCBT-SB and PBT-CM, it can be seen that all samples exhibited double melting with a predominant high-temperature peak at 223–224 °C. It is noteworthy that pCBT-MB showed higher crystallization and melting enthalpies as compared to the other samples in this comparison. This may be ascribed to a lower molecular weight due to thermo-mechanical degradation during the melt blending step with subsequent compression moulding.
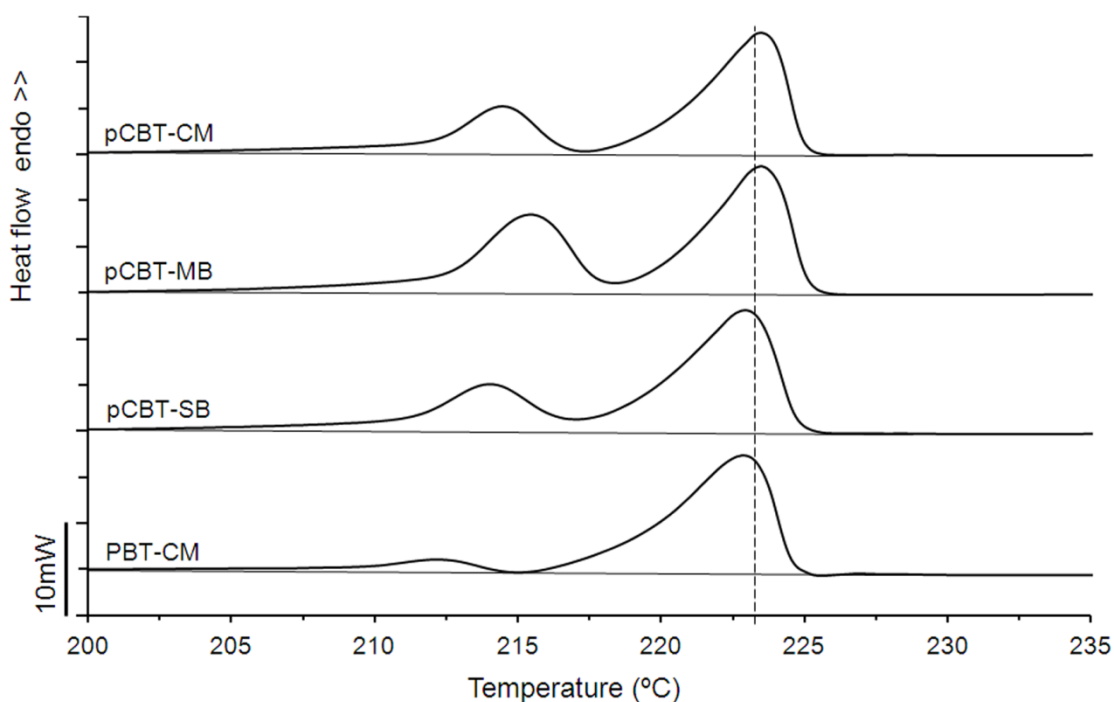


Fig. 6.11: DSC second heating scans of pCBT-CM, pCBT-MB, pCBT-SB and PBT-CM. Heating rate: 10 °C/min.

It is well known that the attainable degree of crystallinity for a given polymer decreases with increasing molecular weight due to increasing topological defects such as entangled chains, loops and knots [21]. Consequently, a low molecular weight leads to a higher amount of crystal fraction as well as to a higher degree of perfection below a certain threshold value of molecular weight. Nevertheless, the assumption of molecular weight

reduction during melt blending is speculative and would require a molecular weight determination in order to be verified. However, this was not the subject of the present study. Except pCBT-MB, the other pCBT samples show a somewhat lower degree of crystallinity compared to the PBT sample. This means, that thermal properties of these samples are essentially the same.

**pCBT-CM, pCBT-CM-Q, pCBT-CM190°C and pCBT-CM205°C**

Regarding the set of samples with different thermal history, it can be seen that upon a controlled crystallization from the melt during the first cooling scan, these samples exhibited also similar thermal properties in the second heating scan. The only exception is pCBT-CM190°C; again this sample revealed a somewhat higher crystal fraction as observed during the first heating scan, similar to the one of pCBT-MB.
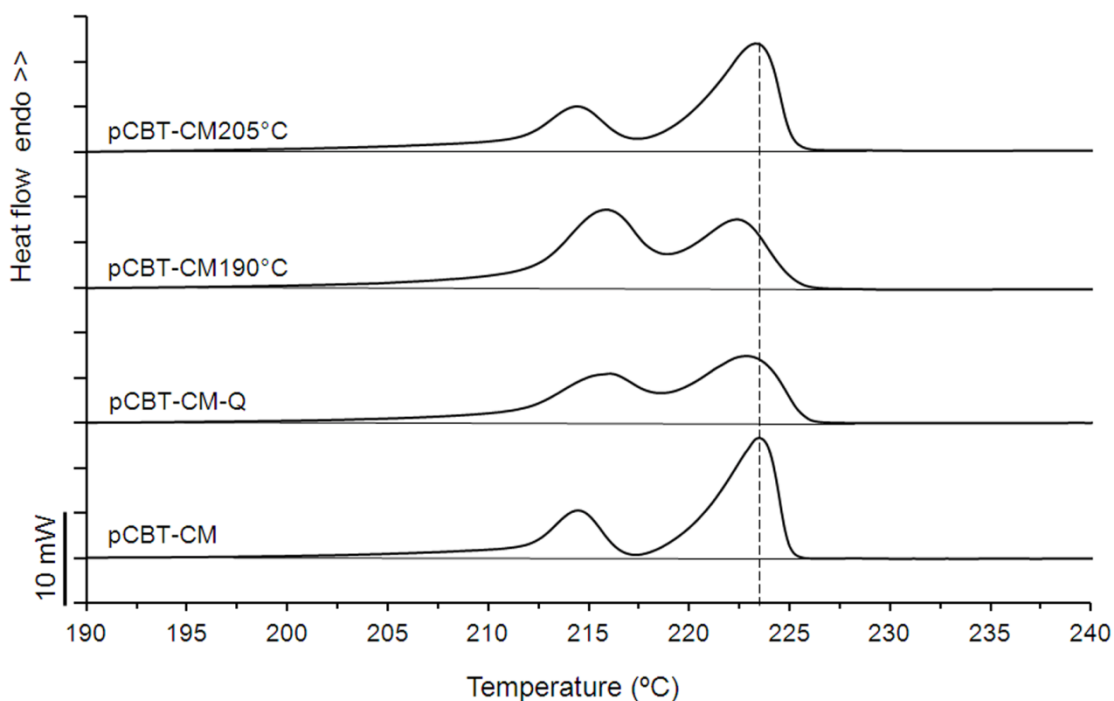


Fig. 6.12: DSC second heating scans of pCBT-CM, pCBT-CM-Q, pCBT-CM190°C and pCBT-CM205°C. Heating rate: 10 °C/min.

Since an extended chain conformation cannot be present in this particular sample after crystallization from a randomly distributed melt during the first cooling scan, the higher crystal fraction cannot be explained by different chain conformations. Instead, this may be ascribed to a lower molecular weight as described above. A low molecular weight may derive from the simultaneous polymerization and crystallization during compression moulding at 190 °C. It was shown that polymerization of CBT at 190 °C led to a lower molecular weight compared to polymerization at 230 °C, which in turn resulted in a more brittle pCBT [2, 18].

To conclude, the processing routes CM and SB yield a pCBT with essentially equal thermal properties whereas a higher degree of crystallinity was found for the melt blended sample, probably due to a lower molecular weight. Moreover, the samples with different thermal histories also showed a higher amount of crystal fraction which is known to cause brittleness. Quenching in liquid nitrogen however did not markedly decrease the degree of crystallinity and anyways would not be a feasible method for industrial processing.

Since crystal fractions of the pCBT samples with equal thermal history are substantially the same as for PBT, a difference in crystal size and perfection is expected. X-ray diffraction was used to analyse these morphological aspects.


### 6.4.5  WAXS analysis of pCBT

X-ray diffraction was used to study the influence of the different processing routes on the crystal structure and crystallite size of pCBT-CM, pCBT-MB and pCBT-SB, respectively. The WAXS diffraction patterns with corresponding Miller indices are shown in figure 6.13 and the experimental and theoretical d-spacings for $\alpha$-form PBT triclinic unit cell  (a = 4.83 Å, $\alpha$ = 99.7°; b = 5.94 Å, $\beta$ = 115.2°; c = 11.59 Å, $\gamma$ = 110.8° [22]) and pCBT were calculated using Bragg´s law [23] and are compiled in table 6.6. The apparent crystallite size $D_{hkl}$ was calculated for directions perpendicular to the planes (001), (0$\bar{1}$ 1) and (010) from the corresponding diffraction peaks using the Scherrer equation [24], results are shown in table 6.7.
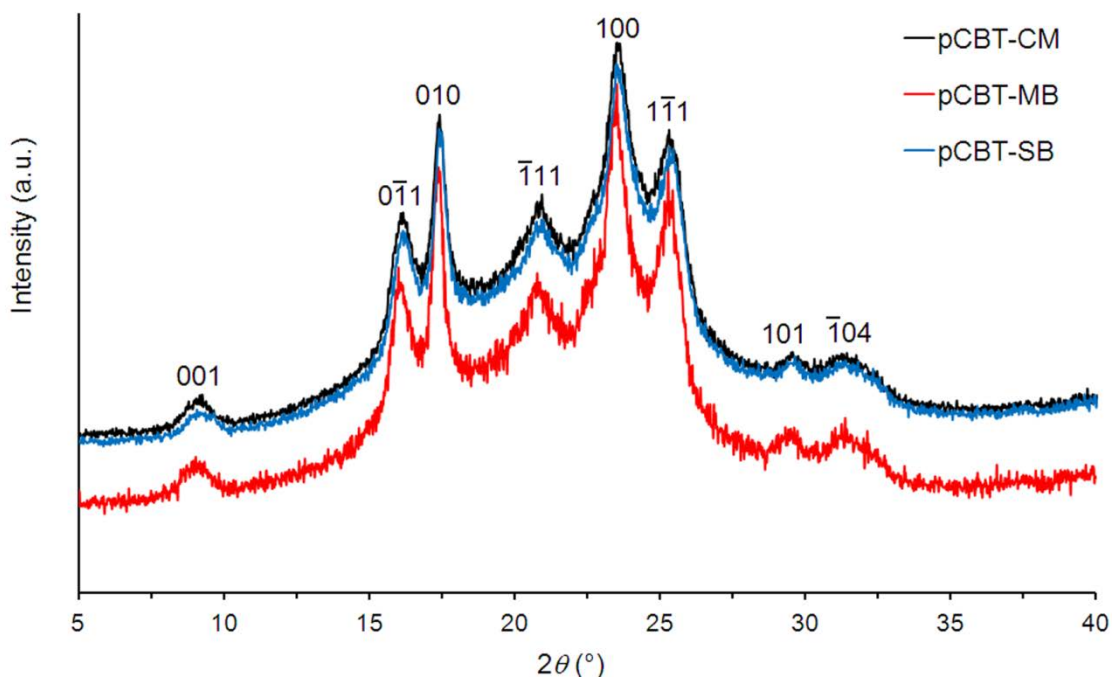
Fig. 6.13: WAXS diffraction patterns of pCBT-CM, pCBT-MB and pCBT-SB with Miller indices.

As expected, the diffractograms in figure 6.13 show at the first sight that there is no significant difference between the different pCBT samples obtained by CM, MB and SB, respectively. All crystallographic reflections characteristic for PBT are also observed in the three pCBT samples; only the peak at $2\theta = 39.3°$ is absent. This peak is solely observed when the crystallization temperature is above 180°C, and it becomes stronger as the crystallization temperature is increased [25]. Its absence in the diffraction patterns is explained by the relatively fast cooling rate in the cold stage of the hot plate press.

**Crystal structure**

As discussed in section 2.4.1, two triclinic polymorphs are known to exist in PBT. The $\alpha$-crystal is the stable form under standard conditions whereas the $\beta$ form develops only under stretching of unoriented crystals [15, 22, 26-28] or during crystallization at pressures above 2000 bar [29]. This $\alpha$ to $\beta$ crystal transition is completely reversible when the stress is removed [22, 26, 28, 30].

Table 6.6: Experimental and theoretical d-spacings for PBT and pCBT triclinic unit cell

| hkl | PBT$_{theoretical}$* | | pCBT-CM | | pCBT-MB | | pCBT-SB | |
|---|---|---|---|---|---|---|---|---|
| | $2\theta$ [°] | d-spacing [Å] | $2\theta$ [°] | d-spacing [Å] | $2\theta$ [°] | d-spacing [Å] | $2\theta$ [°] | d-spacing [Å] |
| 001 | 9.12 | 9.70 | 9.15 | 9.66 | 9.23 | 9.58 | 9.17 | 9.63 |
| $0\bar{1}1$ | 16.10 | 5.50 | 16.14 | 5.49 | 16.26 | 5.45 | 16.18 | 5.48 |
| 010 | 17.22 | 5.15 | 17.41 | 5.09 | 17.52 | 5.06 | 17.44 | 5.08 |
| $\bar{1}11$ | 20.51 | 4.33 | 20.88 | 4.25 | 20.91 | 4.24 | 20.88 | 4.25 |
| 100 | 23.19 | 3.83 | 23.55 | 3.77 | 23.63 | 3.76 | 23.57 | 3.77 |
| $1\bar{1}1$ | 25.37 | 3.51 | 25.32 | 3.51 | 25.43 | 3.50 | 25.38 | 3.51 |
| 101 | 27.44 | 3.25 | 29.52 | 3.02 | 29.51 | 3.02 | 29.57 | 3.02 |
| $\bar{1}04$ | 30.72 | 2.91 | 31.15 | 2.87 | 31.52 | 2.84 | 31.32 | 2.85 |
| 105 | 39.34 | 2.29 | – | – | – | – | – | – |

* theoretical d-spacings for PBT $\alpha$-form triclinic unit cell; data adapted from [25, 31].

The unit cell parameter *c* of PBT crystals is sensitive to the $\alpha$–$\beta$ transition and *c* changes from 11.59 to 12.95 Å in going from $\alpha$ to $\beta$ form. The crystallographic plane ($\bar{1}$ 04) is almost perpendicular to the *c*-axis [26, 32]. Thus the characteristic crystallographic reflection from the ($\bar{1}$ 04) plane is generally used to determine the crystal phase of PBT. This reflection is theoretically situated at $2\theta = 30.7°$ [25] and commonly observed at $2\theta = 31.2$–$31.4°$ for the $\alpha$ polymorph and at $2\theta = 28.2°$ for the $\beta$ polymorph [26, 28, 30, 32-33].

All pCBT samples exhibit $\alpha$ crystal structure as can be seen from the ($\bar{1}$ 04) reflection in table 6.7. The scattering angle of this particular plane is observed at $2\theta = 31.2°$, 31.5° and 31.3° for the samples pCBT-CM, pCBT-MB and pCBT-SB, respectively. The measured scattering angles of this particular plane fairly agree to the theoretical scattering angle. This is reasonable because all samples were crystallized free from any strain as it is known that the $\beta$ polymorph is only observed when PBT is subjected to a tensile deformation greater than 12% during crystallization [22].

**Crystallite size**

The apparent crystallite sizes $D_{hkl}$ were calculated for directions perpendicular to the planes (001), (0$\bar{1}$ 1) and (010) from the corresponding diffraction peaks; results are shown in table 6.7. As can be seen from the diffractograms of the different pCBT samples in figure 6.13, all diffraction patterns exhibited sharp, well-defined peaks which indicate large crystals with a high degree of perfection.

Table 6.7: Apparent crystallite sizes perpendicular to the planes (0 0 1), (0 $\bar{1}$ 1) and (0 1 0) for the samples pCBT-CM, pCBT-MB and pCBT-SB.

| Sample | $D_{001}$ [Å] | $D_{0\bar{1}1}$ [Å] | $D_{010}$ [Å] |
|---|---|---|---|
| pCBT-CM | 102 | 156 | 229 |
| pCBT-MB | 120 | 154 | 235 |
| pCBT-SB | 101 | 154 | 229 |

Apparent crystallite sizes for directions perpendicular to the planes (0$\bar{1}$ 1) and (010) were essentially equal, whereas $D_{001}$ of pCBT-MB was considerably higher. The crystallite size in the (001)-direction corresponds to the lamellar thickness [2]. Recall that during DSC analysis higher crystallization and melting enthalpies were found for pCBT-MB which was possibly due to a molecular weight reduction during processing. The higher lamellar thickness of pCBT-MB compared to pCBT-CM and pCBT-SB fits well to these observations during WAXS analysis.

The apparent crystal sizes of the analysed pCBT samples fairly agree with the ones as reported by other researchers [18, 34], but were substantially larger compared to the ones of PBT [18, 35]. The lamellar thicknesses of these samples were in the range of the one of conventional PBT, which was found to be 8–15 nm, depending on the crystallization conditions [27]. This confirms a well-developed crystal structure of pCBT, giving rise to a more brittle behaviour of pCBT with respect to PBT.

### 6.4.6  SEM analysis of pCBT

SEM analysis was used to see a possible influence of the different processing routes on the morphology of pCBT. Figure 6.14 illustrates the fracture surfaces of pCBT-CM190°C (a and b), pCBT-CM (c and d), pCBT-MB (e and f) and pCBT-SB (g and h).

Regarding the isothermally polymerized sample pCBT-CM190°C, many prism-shaped crystals with an apparently poor interfacial adhesion can be seen in figure 6.14 b. These crystals have been identified previously as oligomer crystals of unpolymerized CBT [36-37], indicating a low degree of conversion for the isothermal processing route below $T_m$. Moreover, these oligomer crystals act as stress concentrators, promoting an unstable crack propagation and brittle fracture under load.

When the samples were processed above $T_m$ (as was the case for pCBT-CM, pCBT-MB and pCBT-SB), conversion to pCBT apparently was more complete. This was deducted from the fact that much less oligomer crystals were present in these samples compared to pCBT-CM190°C, as can be seen in figures 6.14 c–h.

The SEM micrographs indicate a brittle fracture mechanism for all samples except pCBT-SB. This is surprising because all samples have been cryofractured and no macroscopic plastic deformation was detected during fracture. In figures 6.14 g–h a comparably rougher fracture surface with microfibrillation can be seen which indicates a tough fracture mechanism on the microscopic scale. Nevertheless, the sample broke macroscopically in a brittle fashion when cryofractured. A possible toughening effect of the solvent blending route will be further investigated in the subsequent sections.
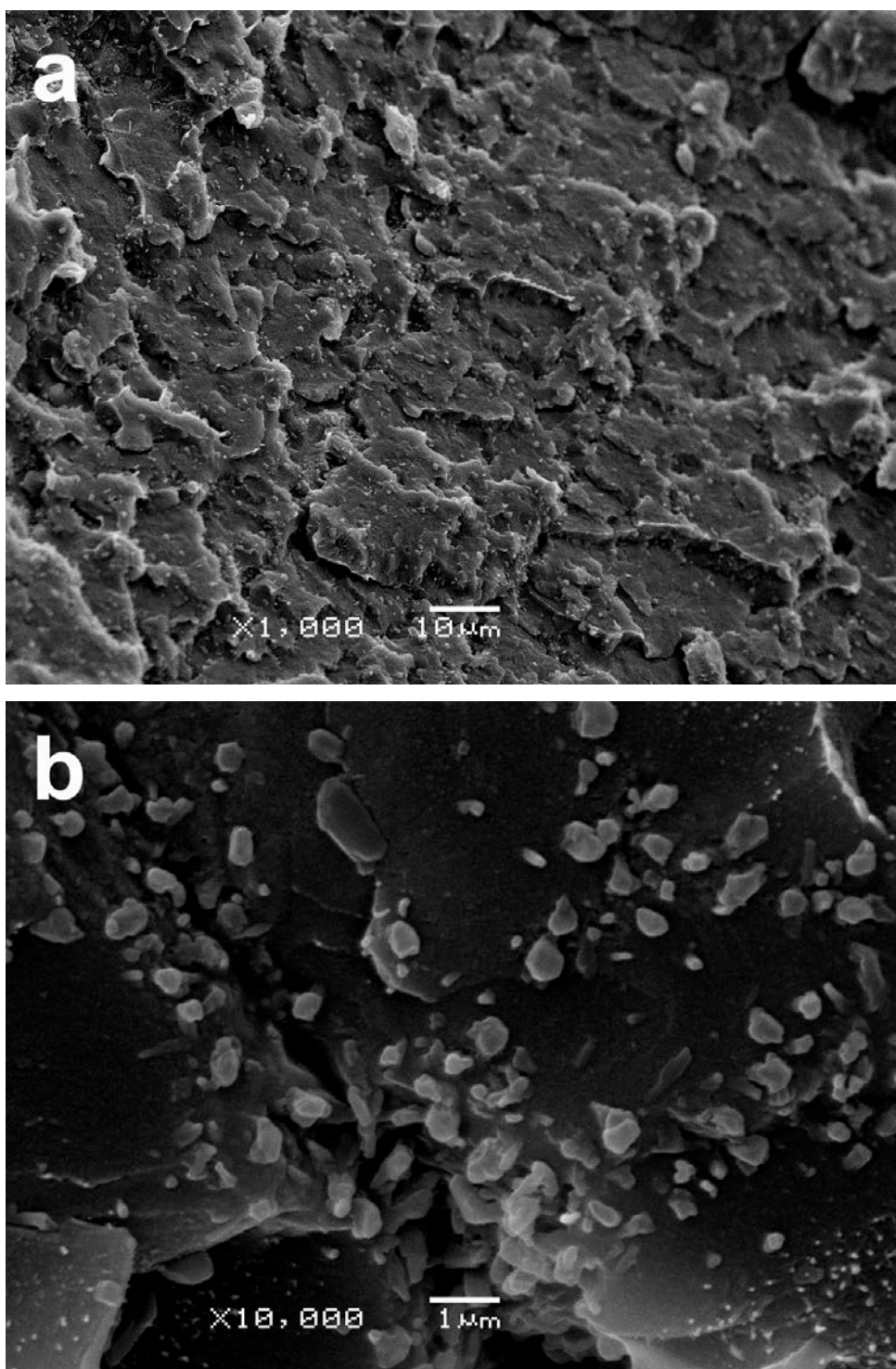
Fig. 6.14: SEM morphologies of pCBT-CM190°C (a and b), pCBT-CM (c and d), pCBT-MB (e and f) and pCBT-SB (g and h).
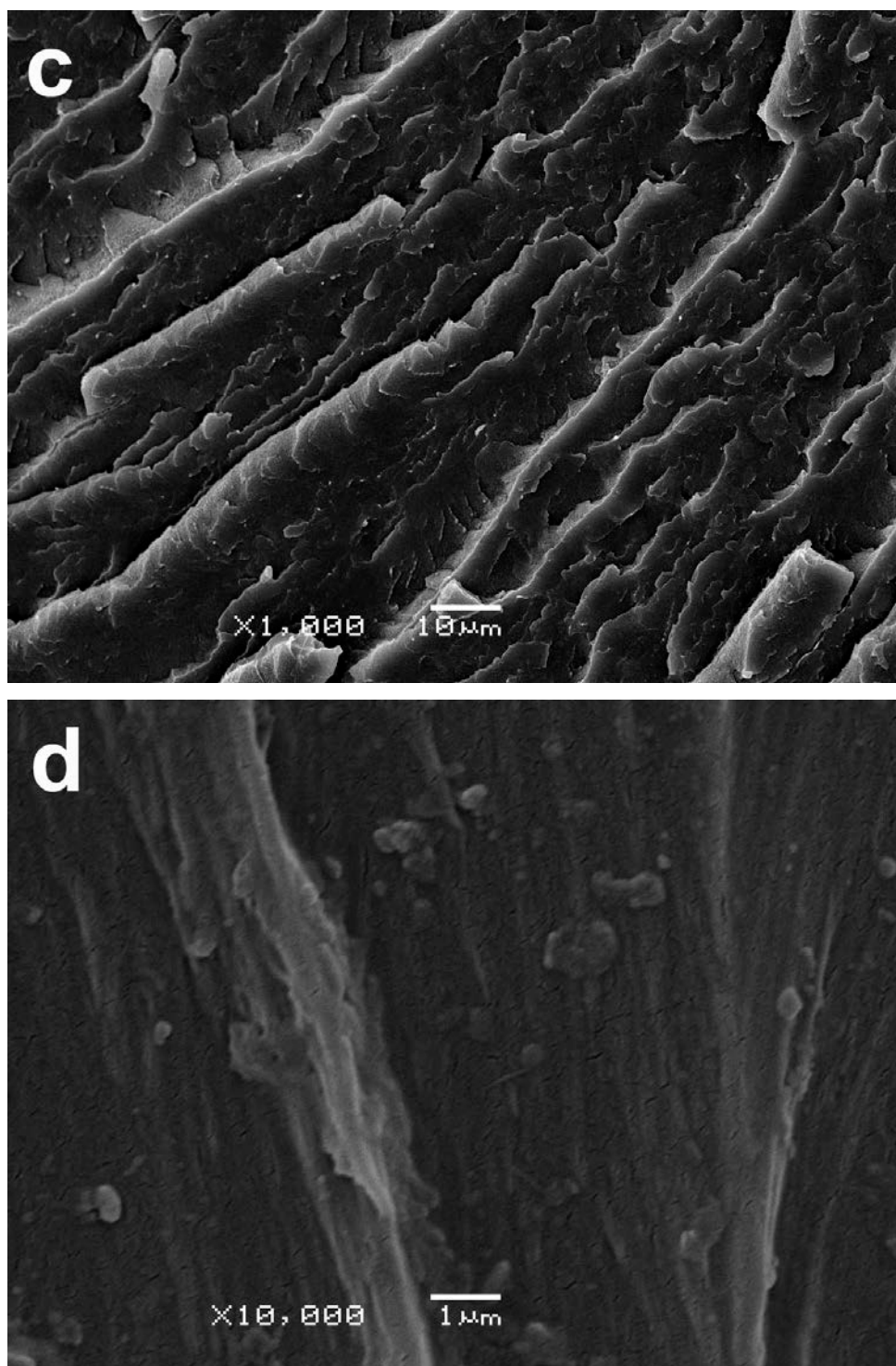
Fig. 6.14: SEM morphologies of pCBT-CM190°C (a and b), pCBT-CM (c and d), pCBT-MB (e and f) and pCBT-SB (g and h). (*continued*)
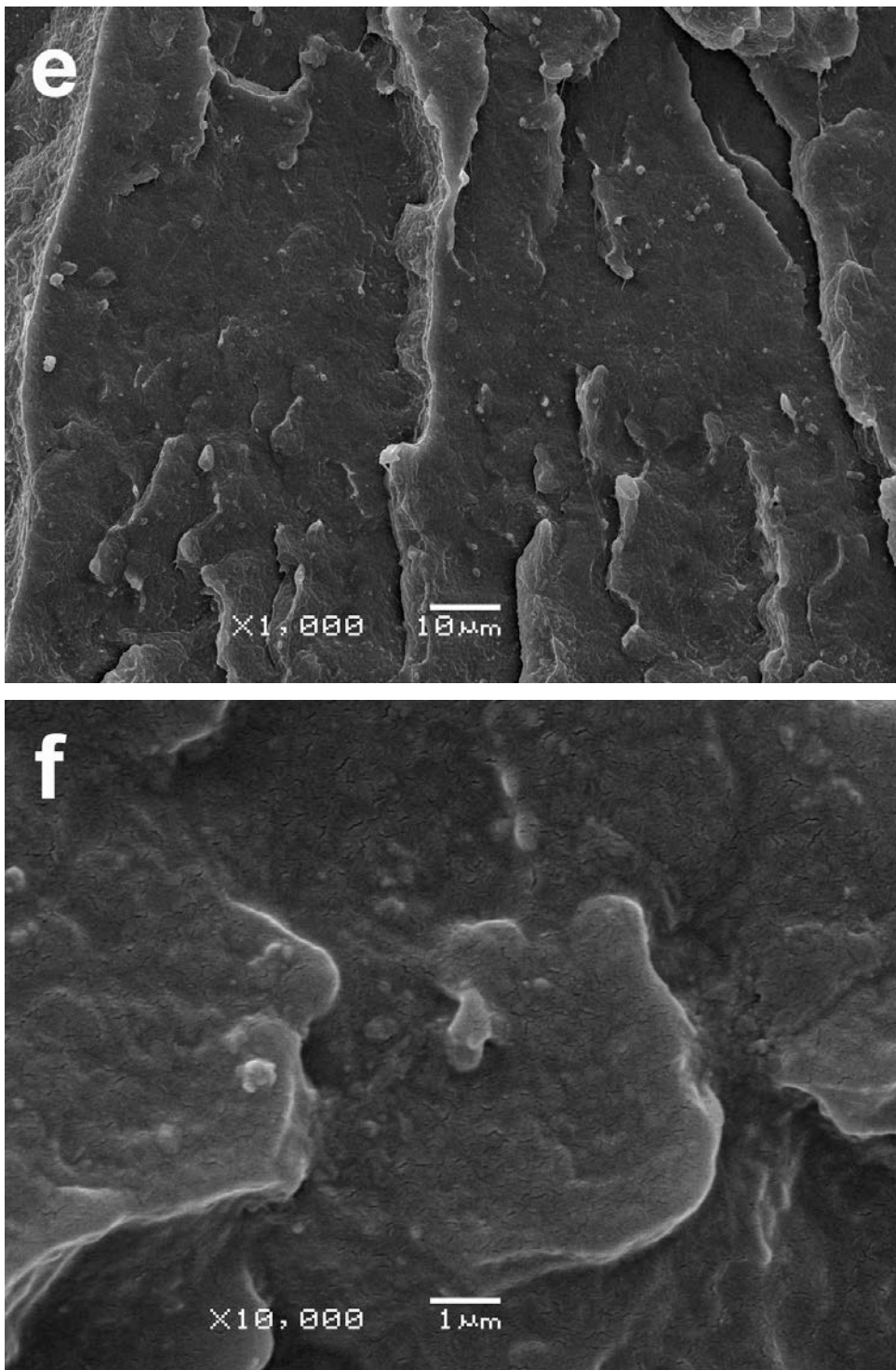
Fig. 6.14: SEM morphologies of pCBT-CM190°C (a and b), pCBT-CM (c and d), pCBT-MB (e and f) and pCBT-SB (g and h). (*continued*)
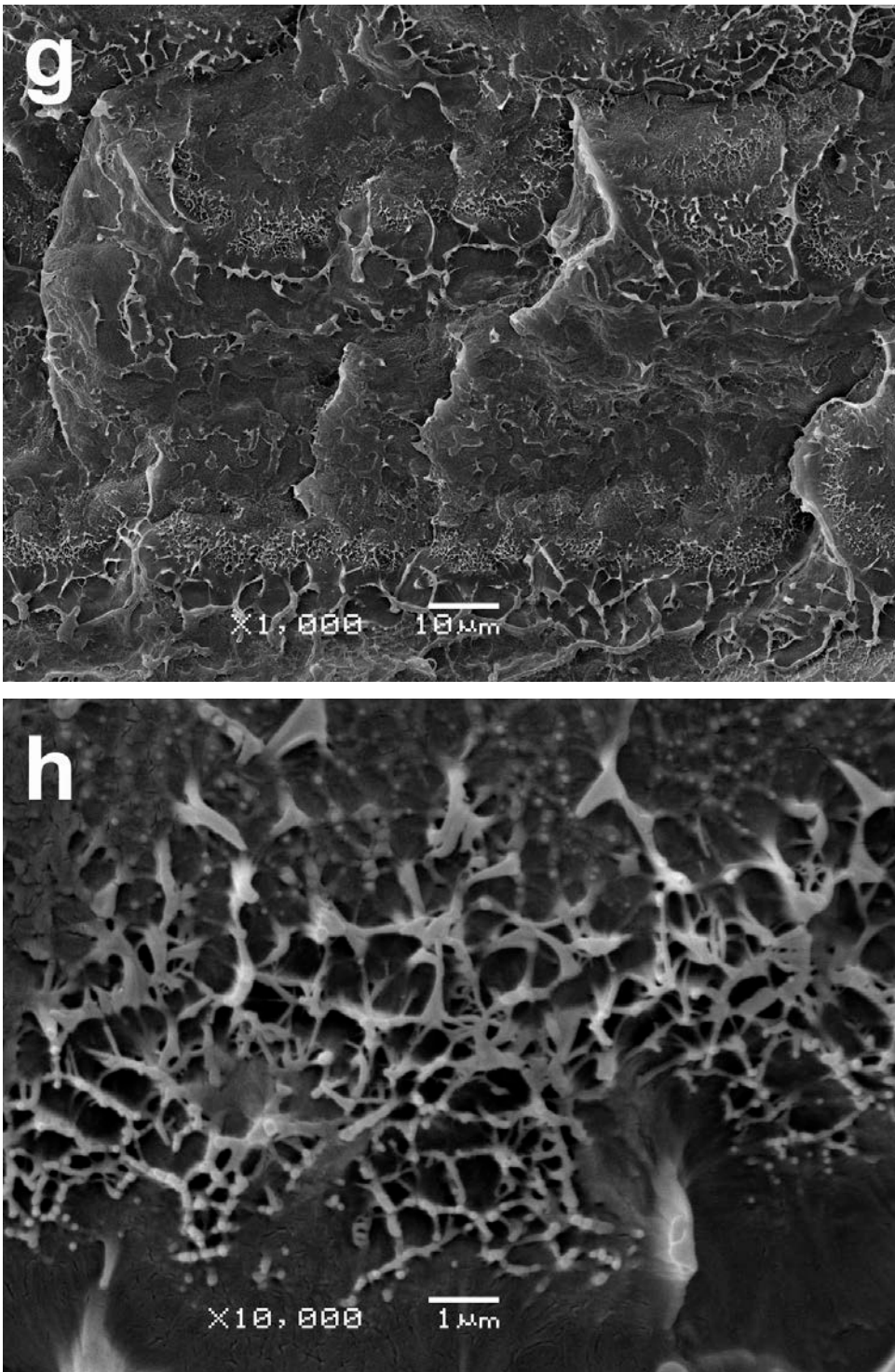
Fig. 6.14: SEM morphologies of pCBT-CM190°C (a and b), pCBT-CM (c and d), pCBT-MB (e and f) and pCBT-SB (g and h). (*continued*)

### 6.4.7  DMTA analysis of pCBT

Dynamic mechanical properties of pCBT obtained by CM, MB and SB, respectively, were assessed by DMTA analysis and compared to the ones of conventional PBT-CM; the results are displayed in figure 6.15. Additionally, in a further study pCBT samples with different thermal history were compared to pCBT-CM (*c.f.* figure 6.16). DMTA data of all analysed samples is compiled in table 6.8 and the influence of the amount of crystal fraction on the glass transition temperature is displayed in figure 6.17.

**Dynamic mechanical properties of PBT and pCBT prepared by CM, MB and SB**

Regarding the influence of the different processing routes on the properties of pCBT, again no significant difference can be found between the pCBT samples as expected but minor differences were detected and are discussed below. All samples experience a drastic stiffness decrease in the glass transition region and finally reach a *ca.* five times lower storage modulus in the rubbery plateau above $T_g$ compared to the one in the glassy region. All curves converge at temperatures above $T_g$.

The storage modulus of PBT is known to increase with degree of crystallinity [25, 27, 38-40] because the crystallites act as physical crosslinks by tying amorphous segments together. Moreover, crystallites also act as rigid fillers, reinforcing the amorphous phase and thus increasing the storage modulus below as well as above the glass transition [39]. An increasing degree of crystallinity is also reflected in a decreasing height of the tan $\delta$ peak due to reduced chain mobility in the amorphous regions [25, 27, 40].
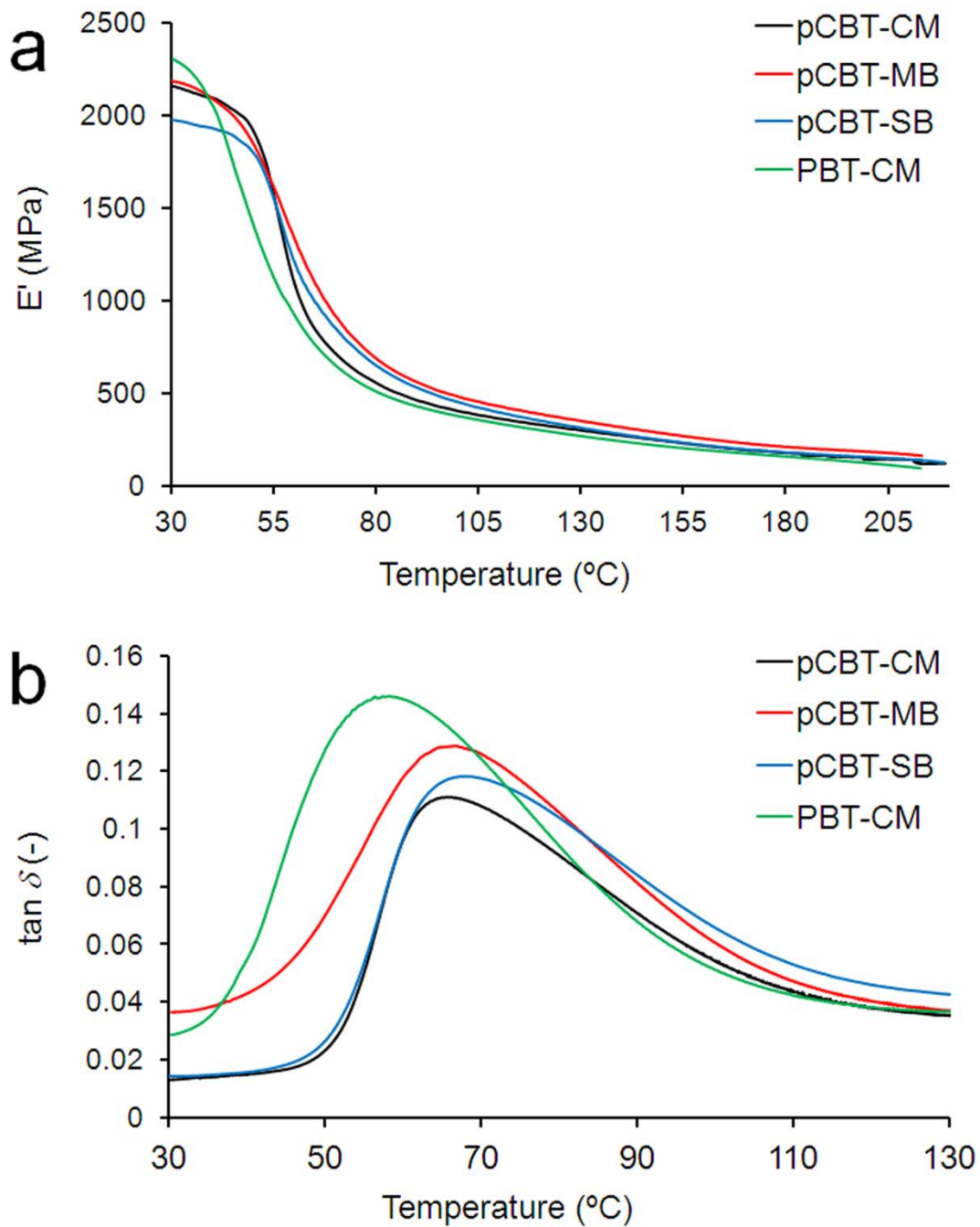
Fig. 6.15: DMTA storage moduli *vs.* temperature (a) and tan $\delta$ *vs.* temperature (b) of pCBT-CM, pCBT-MB, pCBT-SB and PBT-CM.

The storage moduli in figure 6.15 a slightly improved with increasing amount of crystal fraction according to the literature. The best mechanical performance in this comparison was found for pCBT-MB due to its relatively high degree of crystallinity of 36% (*c.f.* section 6.4.4). In comparison, PBT and the solvent blended sample pCBT-SB had a comparably

low degree of crystallinity (*i.e.* 34% and 32% respectively, *c.f.* section 6.4.4) and consequently showed a lower storage modulus throughout the studied temperature range. Most likely due to a higher molecular weight, PBT exhibited the highest storage modulus in the glassy state (*i.e.* below the glass transition) but immediately fell below the other curves. The samples pCBT-CM and pCBT-MB exhibited a similar, intermediate value of $E'$ and finally pCBT-SB showed the lowest storage modulus below $T_g$. A similar tendency is also reflected in the tan $\delta$ curves in figure 6.15 b; the peak height of the solvent blended sample is in between the ones of pCBT-CM and pCBT-MB, whereas PBT showed the highest tan $\delta$ peak height which suggests higher molecular mobility. The glass transition temperature was similar for the three pCBT samples and was found to be in the range 66–68 °C which is in good agreement with the literature [41-42].

Table 6.8:  DMTA data of pCBT samples

| Sample | Storage modulus at 35 °C [MPa] | Storage modulus at 100 °C [MPa] | $T_g$ [°C] |
|---|---|---|---|
| pCBT-CM | 2553 | 471 | 65.7 |
| pCBT-MB | 2156 | 482 | 66.4 |
| pCBT-SB | 1955 | 456 | 67.6 |
| PBT-CM | 2233 | 375 | 58.2 |
| pCBT-CM190°C | 2951 | 885 | 58.5 |
| pCBT-CM205°C | 2048 | 697 | 64.3 |

**Dynamic mechanical properties of pCBT with different thermal histories**

The samples pCBT-CM190°C and pCBT-CM205°C were compared to conventional pCBT-CM in order to study the influence of different thermal histories on the dynamic mechanical properties of pCBT (shown in figure 6.16 and table 6.8).
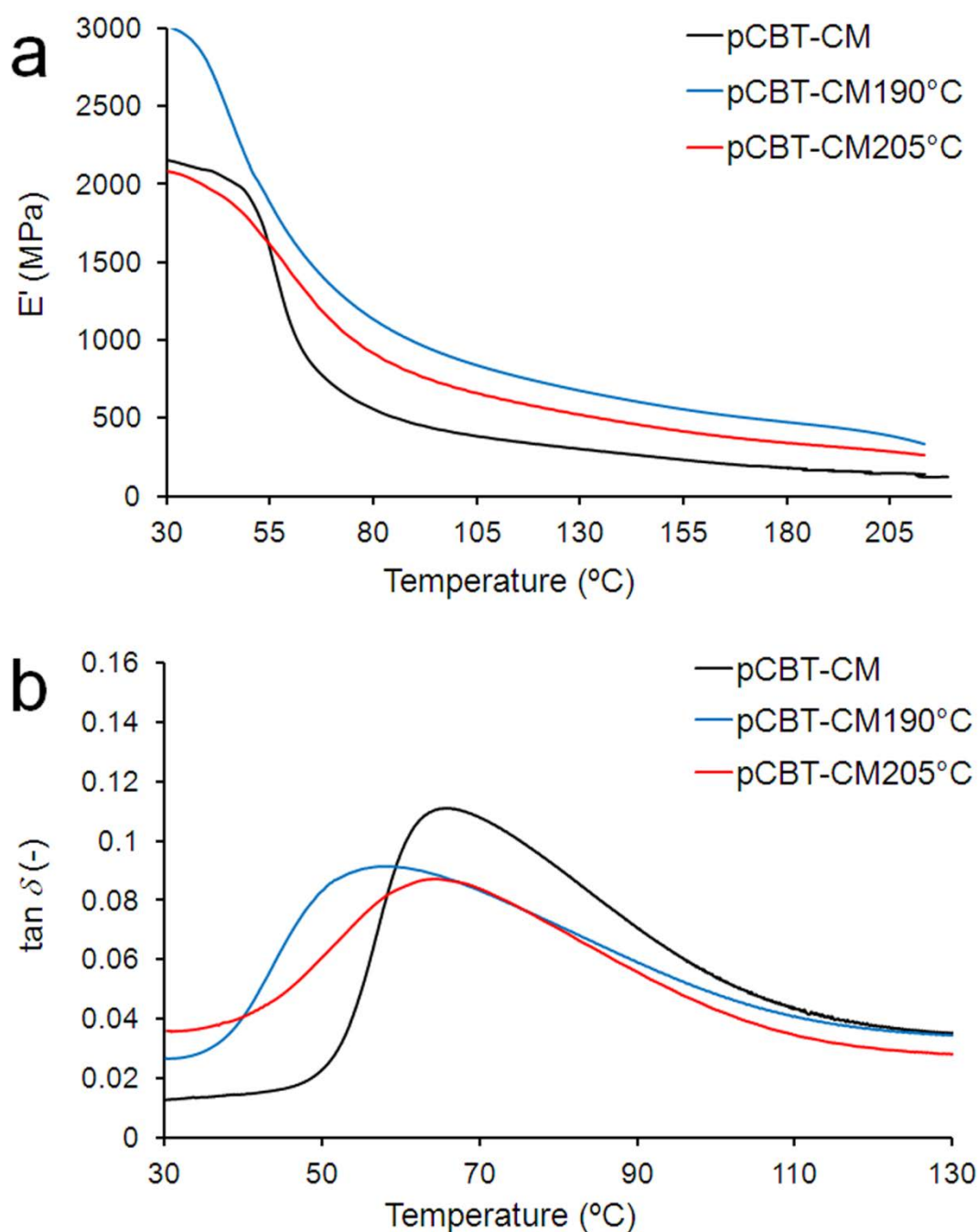
Fig. 6.16: DMTA storage moduli *vs.* temperature (a) and tan $\delta$ *vs.* temperature (b) of pCBT-CM, pCBT-CM190°C and pCBT-CM205°C.

The isothermally polymerized sample pCBT-CM190°C exhibited the highest stiffness throughout the temperature range (*c.f.* figure 6.16 a). This is consistent with the fact that this sample also showed the highest degree of crystallinity ($X_C$ = 45%); the latter

effectively increased the stiffness. A higher crystal fraction of this sample is also evident from the decreased height of the tan $\delta$ peak in figure 6.16 b.

Surprisingly, the storage modulus in the glassy region of pCBT-CM205°C was below that of pCBT-CM which is contradictory to the literature. Nevertheless, the reinforcing effect of the higher crystal fraction came more into play in the rubbery state.

**Influence of degree of crystallinity on the glass transition temperature of pCBT**

A discrepancy exists in the literature regarding the glass transition temperature of PBT. On one hand, it was reported that the $T_g$ of PBT [38] and pCBT [39] increased with increasing degree of crystallinity. The argument therefore is that the crystallites act as physical crosslinks by tying amorphous segments together and thus restricting molecular chain mobility, as mentioned earlier.

On the other hand, it was also stated that the glass transition temperature of PBT was independent of the amount of crystal fraction [27, 43].

Contrary to that, Park *et al.* [25] found a decreasing glass transition temperature of PBT with increasing degree of crystallinity. The glass transition temperature of semicrystalline polymers may decrease or increase with crystallinity depending on the nature and the role of the crystalline phase in the glass transition process [25, 40].

In the present work, the prepared pCBT samples showed a decreasing glass transition temperature with increasing amount of crystal fraction, as can be seen in figure 6.17. Similar results were obtained by Mohd Ishak *et al.* [40] who studied the mechanical properties of woven glass fabric reinforced pCBT composites and found a *ca.* 4 °C lower $T_g$ for the considerably more crystalline pCBT sample as compared to conventional PBT ($X_C$ = 49% *vs.* 36%).
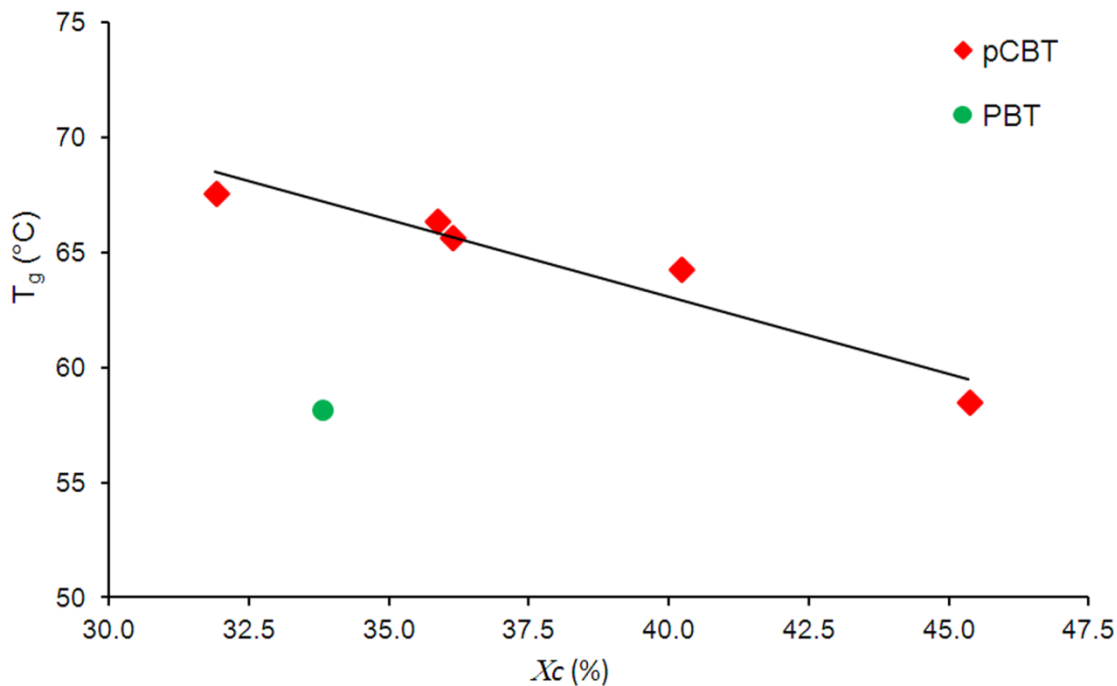
Fig. 6.17: Glass transition temperature vs. degree of crystallinity of pCBT PBT.

When considering figure 6.17, it is clear that pCBT differs from conventional PBT. The latter showed a considerably lower glass transition temperature at a given crystal fraction, indicating higher chain mobility of PBT compared to pCBT. This is also evidenced from the aforementioned higher tan $\delta$ peak height of PBT which is in-line with the above described effect of the crystallinity on stiffness, glass transition and chain mobility.

To sum up, the three studied processing routes CM, MB and SB, respectively, yield a pCBT with similar dynamic mechanical properties and a glass transition temperature around 66 °C. $T_g$ was found to decrease with increasing degree of crystallinity. Conventional PBT showed higher molecular chain mobility as evident by an increased tan $\delta$ peak height and a lower storage modulus throughout the studied temperature range. The stiffness of pCBT, especially above $T_g$, can be effectively increased by different thermal treatments such as s*imultaneous* polymerization and crystallization of CBT but also by *simultaneous* polymerization and crystallization at high temperatures due to a reinforcing effect of the increased crystal fraction. However, a higher degree of crystallinity is known to embrittle the polymer.

### 6.4.8 Tensile properties of pCBT

The mechanical properties of pCBT and the influence of the different processing routes on the former were determined by tensile tests and the results were compared to conventional PBT. Representative stress-strain curves are displayed in figure 6.18 and tensile data is collected in table 6.9.

Attempts were made to also analyze the pCBT samples with different thermal history but the specimens broke during the die cutting operation, clearly demonstrating great brittleness for *simultaneously* polymerized and crystallized samples, *i.e.* pCBT-CM190°C as well as highly crystalline samples such as pCBT-CM205°C. Therefore these two samples will not be considered for further analysis.
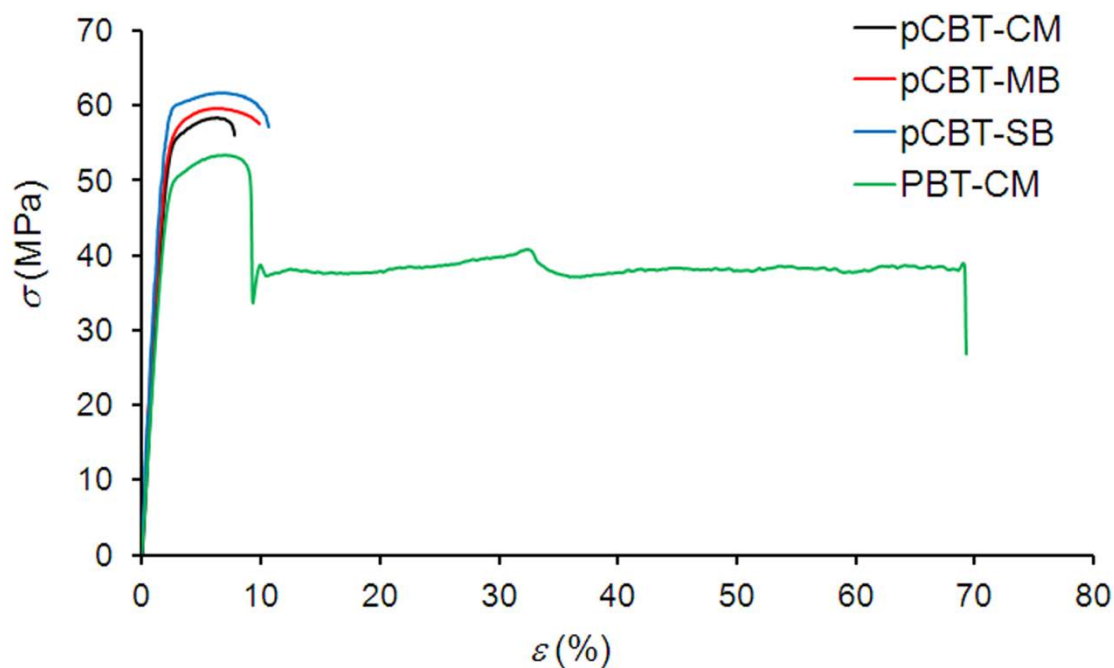


Fig. 6.18: Representative stress-strain curves of pCBT-CM, pCBT-MB, pCBT-SB and PBT-CM. Crosshead speed: 10 mm·min$^{-1}$.

No significant influence of the different processing routes on the mechanical properties of pCBT was found, the corresponding tensile curves in figure 6.18 clearly show a brittle behaviour of unmodified pCBT as stated in the literature [18, 42, 44-45]. All three pCBT

samples exhibited higher tensile modulus, higher tensile strength and much lower failure strain as compared to PBT-CM. The pCBT samples broke at around 8% elongation without yielding. The crack propagation was unstable, resulting in catastrophic failure.

It is noteworthy to mention that a few solvent blended samples showed the beginning of neck formation prior to fracture during tensile tests, indicating a somewhat tougher behaviour. This is in-line with the tough fracture mechanism on the microscopic scale as revealed by SEM observations (*c.f.* section 6.4.6).

Table 6.9:  Tensile data of PBT and pCBT samples

| Sample | Tensile modulus [GPa] | Tensile strength [MPa] | Elongation at break [%] | Strain energy [MJ/m$^3$] |
|---|---|---|---|---|
| pCBT-CM | 2.8 ± 0.4 | 57 ± 5 | 7 ± 3 | 1.3 ± 0.4 |
| pCBT-MB | 2.9 ± 0.3 | 60 ± 2 | 8 ± 1 | 4.2 ± 0.5 |
| pCBT-SB | 3.0 ± 0.2 | 63 ± 4 | 9 ± 2 | 3.8 ± 0.7 |
| PBT-CM | 2.7 ± 0.3 | 54 ± 1 | 72 ± 39 | 27.7 ± 14.6 |

In contrast to the pCBT samples, PBT-CM was less stiff and strong but significantly tougher, as can be seen from the failure strain which was around ten times higher than the one of pCBT. However, the toughness is better described in terms of strain energy which is determined by integrating the area under the stress-strain curve. As can be seen from table 6.9, strain energy data fits well to the observed tendency in failure strain. Strain energy of the pCBT samples was in the range of 1–4 MJ/m$^3$ whereas the one of PBT was around 28 MJ/m$^3$.

### 6.4.9  Tensile impact properties of pCBT

Tensile impact tests were performed on pCBT-CM, pCBT-MB, pCBT-SB and PBT-CM, respectively, to further elucidate this apparent toughening effect which is probably induced by the solvent blending route. Representative tensile-impact stress *versus* time curves are shown in figure 6.19 and impact data is collected in table 6.10.
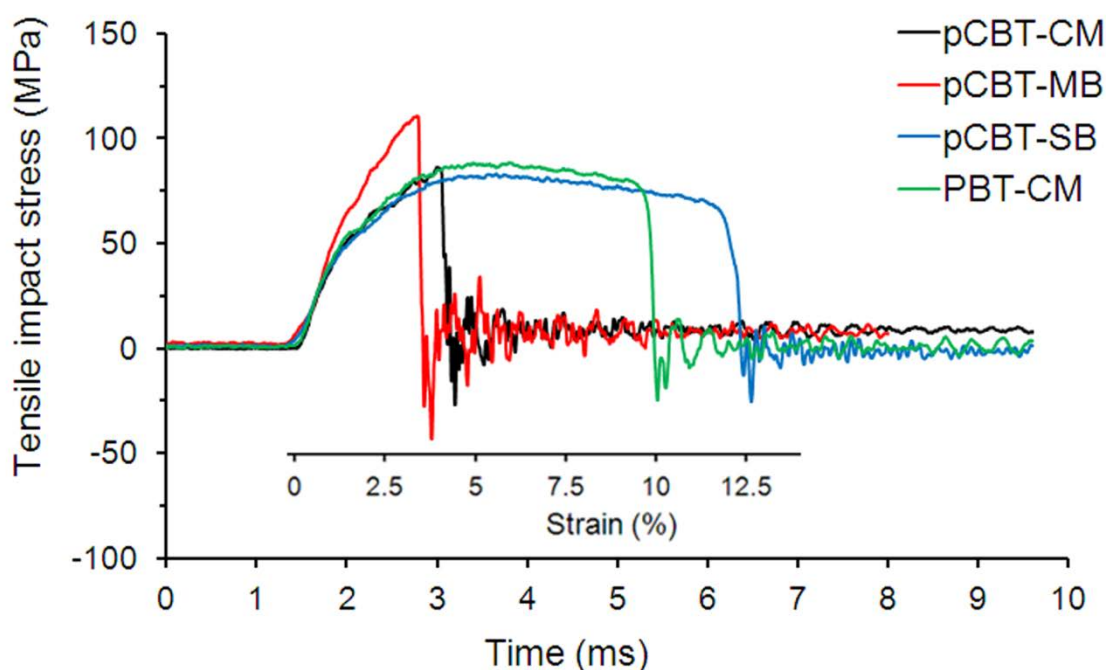


Fig. 6.19: Representative tensile impact stress *versus* time/strain curves of pCBT-CM, pCBT-MB, pCBT-SB and PBT-CM at $v = 1.5$ m/s.

From the stress-time curves it can be seen that the samples pCBT-CM and pCBT-MB broke in a brittle fashion whereas the solvent blended sample and conventional PBT went through a stress maximum with a subsequent stress reduction which is associated with yielding. The melt blended sample showed the highest maximum stress which may be explained by its somewhat higher degree of crystallinity as discussed in section 6.4.3. Nevertheless, this sample broke at relatively shorter impact time which translates to a lower failure strain as compared to pCBT-CM, also indicated by the inset strain axis in figure 6.19.

Table 6.10:  Tensile-impact data of PBT and pCBT samples

| Sample | Tensile impact strength [kJ/m$^2$] | Tensile impact stress max. [MPa] |
|---|---|---|
| pCBT-CM | 149 ± 71 | 86 ± 4 |
| pCBT-MB | 155 ± 39 | 112 ± 11 |
| pCBT-SB | 306 ± 86 | 88 ± 8 |
| PBT-CM | 232 ± 107 | 91 ± 3 |

The tensile-impact strength is related to the absorbed impact energy during fracture (*i.e.* the area under the force-displacement curve, not depicted here). It is apparent from figure 6.19 that pCBT-SB absorbed the highest amount of impact energy and even outperformed PBT, as can be also seen by the tensile-impact strength values in table 6.10. This is, on one hand, quite surprising because no such effect was expected. On the other hand, SEM analysis revealed plastic deformation on a microscopic scale and some neck formation was observed during tensile tests, indicating differences in the mechanical performance of the solvent blended sample pCBT-SB.

## 6.5    Conclusions

Three different processing routes for CBT were introduced in this section, namely compression moulding, melt blending and solvent blending. It was shown that the *in-situ* polymerization of CBT in a batch mixer is a useful process not only to study the ring-opening polymerization of CBT, but also to obtain a batch of polymerized CBT which can be used for subsequent testing. Melt blending at a temperature of 230 °C under nitrogen atmosphere was established as optimum processing condition.

DSC analysis of unpolymerized CBT confirmed that cold crystallization and hence polymer melting of CBT polymerized during the first heating scan is suppressed when high DSC heating rates (>10 °C/min) are employed. The degree of crystallinity formed during cold crystallization was found to be 1.5 times higher than the one formed during melt

crystallization and degrees of crystallinity ranging from 40 to 26% can be obtained when pCBT is melt crystallized at cooling rates from -0.5 °C/min to -100 °C/min, respectively.

The influence of the three processing routes on the properties of polymerized cyclic butylene terephthalate was analysed. The resulting properties of the different pCBT samples were compared to the literature as well as to conventional PBT. No significant differences between pCBT produced by the above described processing routes could be found for the thermal properties. Nevertheless, some differences were observed by SEM and mechanical analysis. It was found that the solvent blended sample pCBT-SB exhibited some microfibrillation and thus plastic deformation on a microscopic scale during cryofractured prior to SEM analysis. Moreover, pCBT-SB showed some unstable neck formation during tensile tests and, most importantly, presented the highest tensile-impact strength of all studied samples and even outperformed conventional PBT. This observed toughening effect is most probably induced by the THF during solvent blending. Toughening of pCBT with solvents has not been reported in the literature yet and therefore deserves a thorough analysis.

To conclude, it was shown that the studied processing routes CM, MB and SB all yield a pCBT with similar properties. The properties of the different pCBT samples were thoroughly studied using various techniques. The obtained properties of unmodified pCBT will serve as a comparative basis in the course of the present thesis. In the subsequent chapters CBT will be modified with the aim to improve the properties, namely to reduce the inherent brittleness of pCBT.

As shown above, the solvent blending route appears to be an interesting way to toughen pCBT and therefore will be studied more in detail in the subsequent chapter.

## 6.6    References for CBT & pCBT

1.    Mandelkern, L. The Relation between Structure and Properties of Crystalline Polymers. Polymer Journal **17**(1), 337-350 (1985).

2.  Parton, H. Characterization of the in-situ polymerization production process for continuous fibre reinforced thermoplastics. PhD thesis. Department of Metallurgy and Materials Engineering. Katholieke Universiteit Leuven: Leuven, Belgium, 2006

3.  Tang, X, Guo, W, Yin, G, Li, B, and Wu, C. Reactive extrusion of recycled poly(ethylene terephthalate) with polycarbonate by addition of chain extender. Journal of Applied Polymer Science **104**(4), 2602-2607 (2007).

4.  Torres, N, Robin, JJ, and Boutevin, B. Chemical modification of virgin and recycled poly(ethylene terephthalate) by adding of chain extenders during processing. Journal of Applied Polymer Science **79**(10), 1816-1824 (2001).

5.  Tuominen, J, Kylmä, J, and Seppälä, J. Chain extending of lactic acid oligomers. 2. Increase of molecular weight with 1,6-hexamethylene diisocyanate and 2,2′-bis(2-oxazoline). Polymer **43**(1), 3-10 (2002).

6.  Hakmé, C, Stevenson, I, Maazouz, A, Cassagnau, P, Boiteux, G, and Seytre, G. In situ monitoring of cyclic butylene terephtalate polymerization by dielectric sensing. Journal of Non-Crystalline Solids **353**(47–51), 4362-4365 (2007).

7.  van Bennekom, ACM, Willemsen, PAAT, and Gaymans, RJ. Amide-modified poly(butylene terephtalate): thermal stability. Polymer **37**(24), 5447-5459 (1996).

8.  Brunelle, DJ, Bradt, JE, Serth-Guzzo, J, Takekoshi, T, Evans, TL, Pearce, EJ, and Wilson, PR. Semicrystalline Polymers via Ring-Opening Polymerization: Preparation and Polymerization of Alkylene Phthalate Cyclic Oligomers. Macromolecules **31**(15), 4782-4790 (1998).

9.  Karger-Kocsis, J, Shang, PP, Mohd Ishak, ZA, and Rösch, M. Melting and crystallization of in-situ polymerized cyclic butylene terephthalates with and without organoclay: A modulated DSC study. eXPRESS Polymer Letters **1**(2), 60-68 (2007).

10. Lanciano, G, Greco, A, Maffezzoli, A, and Mascia, L. Effects of thermal history in the ring opening polymerization of CBT and its mixtures with montmorillonite on the crystallization of the resulting poly(butylene terephthalate). Thermochimica Acta **493**(1-2), 61-67 (2009).

11. Ehrenstein, GW, Riedel, G, and Trawiel, P. Praxis der Thermischen Analyse von Kunststoffen, 2 ed.: Hanser, 2003.

12. Di Lorenzo, ML and Righetti, MC. Morphological analysis of poly(butylene terephthalate) spherulites during fusion. Polymer Bulletin **53**(1), 53-62 (2004).

13. Yasuniwa, M, Murakami, T, and Ushio, M. Stepwise annealing of poly(butylene terephthalate). Journal of Polymer Science Part B: Polymer Physics **37**(17), 2420-2429 (1999).

14. Yasuniwa, M, Tsubakihara, S, and Murakami, T. High-pressure DTA of poly(butylene terephthalate), poly(hexamethylene terephthalate), and poly(ethylene terephthalate). Journal of Polymer Science Part B: Polymer Physics **38**(1), 262-272 (2000).

15. Yasuniwa, M, Tsubakihara, S, Ohoshita, K, and Tokudome, SI. X-ray studies on the double melting behavior of poly(butylene terephthalate). Journal of Polymer Science Part B: Polymer Physics **39**(17), 2005-2015 (2001).

16. Yeh, JT and Runt, J. Multiple melting in annealed poly(butlene terephthalate). Journal of Polymer Science Part B: Polymer Physics **27**(7), 1543-1550 (1989).

17. Cheng, SZD, Pan, R, and Wunderlich, B. Thermal analysis of poly(butylene terephthalate) for heat capacity, rigid-amorphous content, and transition behavior. Die Makromolekulare Chemie **189**(10), 2443-2458 (1988).

18. Parton, H, Baets, J, Lipnik, P, Goderis, B, Devaux, J, and Verpoest, I. Properties of poly(butylene terephthatlate) polymerized from cyclic oligomers and its composites. Polymer **46**(23), 9871-9880 (2005).

19. Brunelle, DJ. Cyclic oligomer chemistry. Journal of Polymer Science Part A: Polymer Chemistry **46**(4), 1151-1164 (2008).

20. Wunderlich, B. Crystallization during Polymerization. Angewandte Chemie International Edition in English **7**(12), 912-919 (1968).

21. Mandelkern, L. Crystallization kinetics of homopolymers: overall crystallization: a review. Biophysical Chemistry **112**(2–3), 109-116 (2004).

22. Yokouchi, M, Sakakibara, Y, Chatani, Y, Tadokoro, H, Tanaka, T, and Yoda, K. Structures of Two Crystalline Forms of Poly(butylene terephthalate) and Reversible Transition between Them by Mechanical Deformation. Macromolecules **9**(2), 266-273 (1976).

23. Bragg, WL. The diffraction of short electromagnetic waves by a crystal. Proceedings of the Cambridge Philosophical Society **17**, 43-57 (1913).

24. Scherrer, P. Bestimmung der Größe und der inneren Struktur von Kolloidteilchen mittels Röntgenstrahlen. Nachrichten von der Gesellschaft der Wissenschaften zu Göttingen, Mathematisch-Physikalische Klasse **26**, 98-100 (1918).

25. Park, C-S, Lee, K-J, Kim, SW, Lee, YK, and Nam, J-D. Crystallinity morphology and dynamic mechanical characteristics of PBT polymer and glass fiber-reinforced composites. Journal of Applied Polymer Science **86**(2), 478-488 (2002).

26. Chen, X, Xu, J, Lu, H, and Yang, Y. Isothermal crystallization kinetics of poly(butylene terephthalate)/attapulgite nanocomposites. Journal of Polymer Science Part B: Polymer Physics **44**(15), 2112-2121 (2006).

27. Radusch, HJ. Poly(Butylene Terephthalate). Handbook of Thermoplastic Polyesters: Wiley-VCH Verlag GmbH & Co. KGaA, 2005. pp. 389-419.

28. Shi, XQ, Aimi, K, Ito, H, Ando, S, and Kikutani, T. Characterization on mixed-crystal structure of poly(butylene terephthalate/succinate/adipate) biodegradable copolymer fibers. Polymer **46**(3), 751-760 (2005).

29. Moneke, M. Die Kristallisation von verstärkten Thermoplasten während der schnellen Abkühlung und unter Druck. PhD thesis. TU Darmstadt: Darmstadt, 2001

30. Geil, PH. Crystal Structure, Morphology, and Orientation of Polyesters: Section 2.2. Handbook of Thermoplastic Polyesters: Wiley-VCH Verlag GmbH & Co. KGaA, 2005. pp. 154-167.

31. Alter, U and Bonart, R. Röntgenuntersuchungen zur Kristallstruktur von Polybutylenterephthalat (PBT). Colloid and Polymer Science **254**(3), 348-357 (1976).

32. Apostolov, AA, Fakirov, S, Stamm, M, Patil, RD, and Mark, JE. Alpha−Beta Transition in Poly(butylene terephthalate) As Revealed by Small-Angle X-ray Scattering. Macromolecules **33**(18), 6856-6860 (2000).

33. Huang, J-W. Poly(butylene terephthalate)/clay nanocomposite compatibilized with poly(ethylene-co-glycidyl methacrylate). II. Nonisothermal crystallization. Journal of Polymer Science Part B: Polymer Physics **46**(6), 564-576 (2008).

34. Harsch, M, Karger-Kocsis, J, and Apostolov, AA. Crystallization-induced shrinkage, crystalline, and thermomechanical properties of in situ polymerized cyclic butylene terephthalate. Journal of Applied Polymer Science **108**(3), 1455-1461 (2008).

35. Song, K. Formation of polymorphic structure and its influences on properties in uniaxially stretched polybutylene terephthalate films. Journal of Applied Polymer Science **78**(2), 412-423 (2000).

36.  Karger-Kocsis, J, Felhos, D, Bárány, T, and Czigány, T. Hybrids of HNBR and in situ polymerizable cyclic butylene terephthalate (CBT) oligomers: Properties and dry sliding behavior. eXPRESS Polymer Letters **2**(7), 520-527 (2008).

37.  Xu, D, Karger-Kocsis, J, and Apostolov, AA. Hybrids from HNBR and in situ polymerizable cyclic butylene terephthalate (CBT): Structure and rolling wear properties. European Polymer Journal **45**(4), 1270-1281 (2009).

38.  Fried, J. Sub-T g Transitions. In: Mark J, editor. Physical Properties of Polymers Handbook: Springer New York, 2007. pp. 217-232.

39.  Liu, Y, Wang, Y-F, Gerasimov, TG, Heffner, KH, and Harmon, JP. Thermal analysis of novel underfill materials with optimum processing characteristics. Journal of Applied Polymer Science **98**(3), 1300-1307 (2005).

40.  Mohd Ishak, ZA, Leong, YW, Steeg, M, and Karger-Kocsis, J. Mechanical properties of woven glass fabric reinforced in situ polymerized poly(butylene terephthalate) composites. Composites Science and Technology **67**(3–4), 390-398 (2007).

41.  Baets, J. Toughening of in-situ polymerized cyclic butyleneterephthalate for use in continuous fiber reinforced thermoplastic composites. PhD thesis. Department of Metallurgy and Materials Engineering. Katholieke Universiteit Leuven: Leuven, Belgium, 2008

42.  Tripathy, AR, MacKnight, WJ, and Kukureka, SN. In-Situ Copolymerization of Cyclic Poly(butylene terephthalate) Oligomers and ε-Caprolactone. Macromolecules **37**(18), 6793-6800 (2004).

43.  Leung, WP and Choy, CL. Physical properties of oriented poly(butylene terephthalate). Journal of Applied Polymer Science **27**(7), 2693-2709 (1982).

44.  Baets, J, Dutoit, M, Devaux, J, and Verpoest, I. Toughening of glass fiber reinforced composites with a cyclic butylene terephthalate matrix by addition of polycaprolactone. Composites Part A: Applied Science and Manufacturing **39**(1), 13-18 (2008).

45.  van Rijswijk, K and Bersee, HEN. Reactive processing of textile fiber-reinforced thermoplastic composites – An overview. Composites Part A: Applied Science and Manufacturing **38**(3), 666-681 (2007).

# Chapter 7: Toughening of pCBT by addition of THF
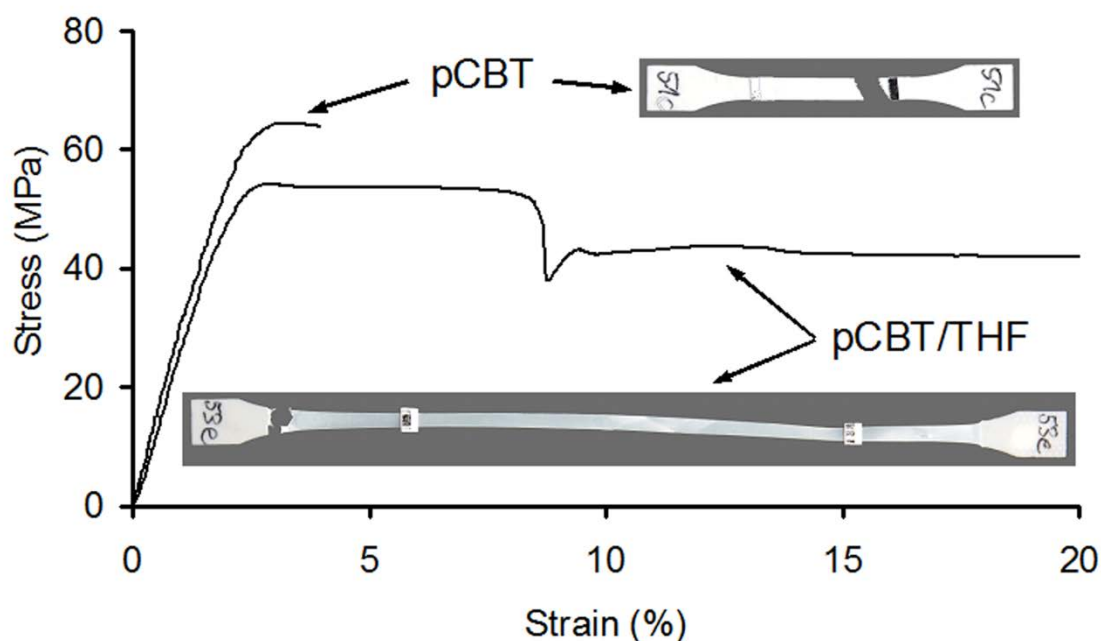


Polymerized CBT was prepared by *in-situ* polymerization of CBT in the presence of tetrahydrofuran, resulting in a toughened, plasticized oligomer-free pCBT with an increased molecular weight.

**Publication derived from this work [1]:**

## Toughening of *in situ* polymerized cyclic butylene terephthalate by addition of tetrahydrofuran

Tobias Abt,[a] Miguel Sánchez-Soto,[a]* Silvia Illescas,[a] Jon Aurrekoetxea[b] and Mariasun Sarrionandia[b]

## 7.1    Introduction

An interesting toughening effect, apparently induced by the solvent blending route, was observed in the sample pCBT-SB as described in the previous chapter. In this chapter, THF was used in small amounts (~1.5 wt.%) to impregnate CBT oligomers prior to *in situ* polymerization and the observed toughening effect was studied more in detail.

A variety of solvent blended pCBT samples with three different solvents and different remaining solvent contents were prepared in a preliminary study. Ethanol was used as a polar protic solvent whereas acetone and tetrahydrofuran were used as polar aprotic solvents. Ethanol and acetone did not show any improvement in mechanical properties, whereas tetrahydrofuran clearly showed a toughening effect. The toughening effect was evaluated in terms of tensile tests.

Furthermore, the possibility of copolymerization of pCBT and polyTHF was also analysed since it may explain the observed toughness increase, as discussed in detail in section 2.4.6.

The long-term toughening effect was studied by thermal ageing at 80 °C, *i.e.* THF-toughened samples were stored at elevated temperature above the glass transition temperature for a predetermined time and were subsequently subjected to tensile tests. The underlying effect of THF on the properties of the resultant material was analysed using various techniques. To the best of the knowledge of the author, there has been no publication on this subject.

## 7.2    Experimental section

### 7.2.1    Materials

One-component cyclic butylene terephthalate oligomers (CBT160®) were used throughout this chapter, for details see section 3.1.2. The used tetrahydrofuran is described in section 3.3.1.

### 7.2.2  Sample preparation

A glass vial equipped with a mechanical stirrer was charged with 100 g of THF. Then 50 g of previously dried CBT powder was slowly added. The CBT/THF suspension was stirred for 5 min and subsequently dried at 80 °C *in vacuo* for 8 h, removing the excess of THF. The resultant material was ground in a mortar into a fine powder and again dried until a THF content of about 1.5 wt.% was reached. THF content was determined as follows. The weight of a small sample (*e.g.* 1 g) of the CBT/THF suspension was carefully determined. Then this sample was dried at 80 °C under vacuum until constant weight. The THF content of the starting material before drying was calculated using the expression

$$X_{THF} = \frac{m_{wet} - m_{dry}}{m_{dry}} \cdot 100\%$$

$(8.1)$

where $X_{THF}$ is the THF content of CBT/THF, $m_{wet}$ is the weight of the initial CBT/THF suspension and $m_{dry}$ is the weight of CBT/THF dried until constant weight.

The CBT/THF suspension containing 1.5 wt.% THF obtained as described above was *in situ* polymerized in a hot plate press at 250 °C for 20 min between two polytetrafluoroethylene (PTFE) sheets in ambient atmosphere, leading to pCBT/THF films having dimensions of 120 × 120 mm$^2$ and a thickness of 0.4 mm. The polymerized samples were then cooled between two water chilled steel plates. A neat pCBT sample was similarly produced for comparison. In fact, the unmodified pCBT sample is pCBT-CM as described in section 6 but will be referred to as pCBT in this section for simplicity reasons. Some pCBT/THF films were manually cut into small pieces and subsequently reprocessed in the hot press at 250 °C for 5 min, referred to as pCBT/THF-RP.

### 7.3  Characterization

Gas chromatography-mass spectrometry was employed to detect volatile THF in the toughened samples. Moreover, the samples were characterized using gel permeation

chromatography, thermogravimetric analysis and dynamic mechanical thermal analysis. X-ray diffraction was used to study a possible effect on the crystal structure of pCBT/THF. The structure of pCBT/THF was characterized using ^{1}H NMR spectroscopy. Polytetrahydrofuran (polyTHF; Aldrich, molecular weight of 1000 g·mol$^{-1}$) was also analysed and compared to pCBT/THF in order to clarify whether a copolymer was formed. To further visualize a possible chemical reaction between CBT and polytetrahydrofuran, both components were melt blended and characterized using torque *versus* time measurements. The mechanical properties of the samples were determined by tensile tests and by instrumented tensile-impact tests. Differential scanning calorimetry was performed as follows:

Polymerized pCBT/THF samples prepared by compression moulding as well as those reprocessed in the hot press were analysed using DSC and compared to neat pCBT. Neat CBT and samples with THF were also *in situ* polymerized during the first heating run of a DSC scan. The first DSC sample was the CBT/THF suspension before drying, containing 2 parts THF and 1 part CBT (referred to as CBT/THF 67%). The second DSC sample corresponded to the dried material with 1.5 wt.% THF content (referred to as CBT/THF 1.5%), similar to the one used for compression moulding. Samples were heated from 30 to 270 °C at a heating rate of 10 °C/min, followed by an isothermal step of 3 min and then cooled from 270 to 30 °C at a cooling rate of 30 °C/min. The second heating scan was performed equally and allowed the examination of the conversion from cyclic oligomers into linear polymer. The presence of a melting peak in the range 120–160 °C during the second heating scan can be ascribed to a not fully completed polymerization reaction. High heating rates in a DSC scan can hinder the cold crystallization of pCBT polymerized during the first heating run [2-3]. To account for this kinetic effect, a heating rate of 1 °C/min was used for CBT as well as for CBT/THF 1.5%. The first stage of the heating rate was done at 10 °C/min between 30 and 60 °C to prevent premature evaporation of the THF and then changed to 1 °C/min between 60 and 250 °C. The resulting DSC traces were then compared to those obtained for a scan performed entirely at 10 °C/min.

## 7.4    Preliminary study on the toughening action of THF

Previous trials showed that an optimum in the toughening effect was achieved with a THF content of 1.5 wt.%. The toughening effect was evaluated in terms of tensile tests. The presence of a yield point with neck formation and post-yield deformation was taken as a criterion for toughness. When the CBT contained less than 1% of THF, then the pCBT/THF was equally brittle as neat pCBT. On the other hand, when the CBT contained more than 2% THF, then the pCBT/THF was toughened, but the used conventional compression moulding system did not allow the production of samples without gas inclusions. This is due to the evaporation of the excess THF during processing, which would need a vacuum extraction in order to be removed from the sample.

## 7.5    Results and Discussion

### 7.5.1  GC-MS analysis

Gas chromatography-mass spectrometry was used to clarify if THF was still present in the pCBT after compression moulding. THF exhibits a low boiling temperature and hence is supposed to completely evaporate during processing at 250 °C. Surprisingly, a large amount of THF was found in pCBT/THF. This result indicates the presence of Van-der-Waals forces between the pCBT matrix and the THF molecules, preventing their complete evaporation. In respect to the peak areas of the analysed samples, pCBT/THF was found to have an 45-fold THF concentration compared to that of neat pCBT (see table 7.1). A small signal corresponding to THF was also detected in pCBT, as it is known that THF is formed during the degradation of PBT [4-6]. As a consequence, the detected THF in neat pCBT could come from a possible initiation of degradation during processing.

Table 7.1: GC-MS results of pCBT and pCBT/THF

| Sample | Retention time [min] | Area [-] | Area % [%] | Compound |
|---|---|---|---|---|
| pCBT | 9.366 | 1.250.637 | 12,4 | THF |
| pCBT/THF | 9.330 | 56.280.805 | 86,2 | THF |

### 7.5.2 DSC analysis

The influence of THF on the in situ polymerization of CBT was studied by DSC. The resulting thermograms are illustrated in figures 7.1 and 7.2 whereas the thermal properties are summarised in tables 7.2 and 7.3.
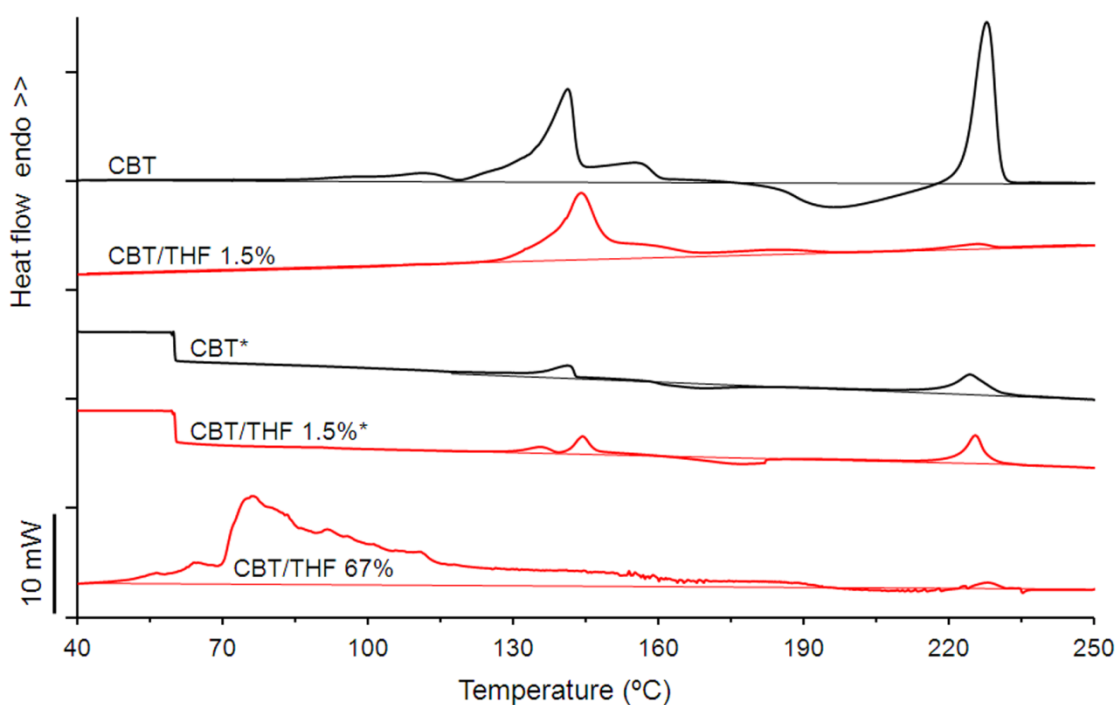


Fig. 7.1: DSC thermograms of CBT, CBT/THF 1.5%, CBT*, CBT/THF 1.5%* and CBT/THF 67%. Heating rate: 10 °C/min. The asterisk indicates a heating rate of 1 °C/min.

189

**Oligomer melting**

Neat CBT non-isothermally polymerized in the DSC pan typically shows a broad melting peak of the cyclic oligomers in the range 120–160 °C with a maximum at 141 °C. A subsequent cold crystallization in the range 170–220 °C with a peak at 197 °C is detected as a broad, exothermic signal. The final polymer melting peak is located at ca 228 °C, as shown in fig. 7.1. This is in agreement with the reported values of other researchers [3, 7-9].

Table 7.2:  DSC first heating run; heating rate: 10 °C/min. The asterisk indicates a heating rate of 1 °C/min.

| Sample | oligomer melting | | cold crystallization | | polymer melting | |
|---|---|---|---|---|---|---|
| | $T_{m, CBT}$ | $\Delta H_{m, CBT}$ | $T_{c, pCBT}$ | $\Delta H_{c, pCBT}$ | $T_{m, pCBT}$ | $\Delta H_{m, pCBT}$ |
| | [°C] | [J/g] | [°C] | [J/g] | [°C] | [J/g] |
| CBT | 141,2 | 46,5 | 196,5 | -36,5 | 227,8 | 35,1 |
| CBT/THF 1,5% | 141,1 | 46,5 | 202,5 | -10,5 | 228,9 | 15,7 |
| CBT/THF 67% | 144,8 | 6,5 | 200,4 | -3,9 | 227,9 | 4,2 |
| CBT* | 141,1 | 46 | 168,7 | -18,5 | 224,4 | 67,0 |
| CBT/THF 1.5%* | 144,2 | 45,5 | 176,2 | -33,6 | 225,5 | 55,0 |
| pCBT | – | – | – | – | 224,2 | 52,8 |
| pCBT/THF | – | – | – | – | 223,1 | 44,0 |
| pCBT/THF-RP | – | – | – | – | 224,7 | 51,6 |

However, some differences were detected in the case of CBT/THF suspensions. THF has a boiling point of 66 °C [10] and therefore evaporated when this temperature was reached during the first heating scan. This phase transition can be observed as a broad endothermic signal with an onset temperature of 53 °C and a peak temperature of 76 °C for the CBT/THF 67% sample. The sample with 1.5 wt.% THF content did not show this phase transition, most likely due to a too small amount of THF to be detected with the DSC technique. CBT/THF 67% showed a markedly reduced oligomer melting enthalpy ($\Delta H_m$ =

6.5 J/g), clearly indicating the effect of THF on CBT oligomers. Since the oligomer melting enthalpy was low, it can be hardly observed in fig. 7.1 but data is provided in table 7.2. This reduction in melting enthalpy of the oligomers may be due to the solubility of CBT in THF. Brunelle *et al.* reported a solubility of CBT up to the heptamer in THF [11]. When CBT was dispersed in 67% THF, part of the crystalline CBT was dissolved and thus the crystallinity was lost. This reduction in oligomer melting enthalpy is not observed for the CBT/THF 1.5% sample which has a melting enthalpy of 46.5 J/g, equal to that of neat CBT. Although this sample was also prepared from an initial THF content of 67%, during the drying procedure up to 1.5% of the dissolved CBT may recrystallize and therefore contribute to the melting enthalpy of the oligomers.

**Ring-opening polymerization**

The ring-opening polymerization cannot be observed using DSC analysis, because it is athermal. The presence of THF does not seem to affect the ring-opening polymerization of CBT to pCBT, because no oligomer melting signal is detected in any second heating scan (not shown here) in the range of 120–160 °C. As mentioned earlier, the absence of oligomer melting signals in the second heating scan suggests a complete conversion from CBT to pCBT.

**Cold crystallization**

The presence of THF affects the cold crystallization and, as a consequence, the subsequent crystalline melting of the formed polymer. Regarding cold crystallization, CBT/THF 1.5% showed only about one-third of the cold crystallization enthalpy of neat CBT, whereas CBT/THF 67% showed only around one-tenth of the original enthalpy (*c.f.* table 7.2). Cold crystallization signals can barely be seen in the DSC traces of fig. 7.1 due to the scale of the thermograms. Peaks can be resolved by focusing on the zone of cold crystallization and calculating crystallization enthalpies by peak integration of the DSC traces using the software included with the equipment. Since the signals of cold crystallization were broad and not very pronounced, for the purpose of analysis more

attention was paid to the polymer melting signals, because they were sharp and well defined. The incorporated THF may increase the intermolecular distance and thus the free volume, and as a result the polymeric chains would have a better mobility. But on the other hand, the molecules cannot crystallize easily because the THF separates adjacent chains. Since ring-opening polymerization, cold crystallization and final polymer melting took place under non-isothermal conditions at relatively high heating rates, the pCBT chains did not have enough time to reach an equilibrium state to cold-crystallize. This explains the lower enthalpy of cold crystallization and melting of samples containing THF compared to neat CBT.

**Polymer melting**

The aforementioned decrease in cold crystallization enthalpies is reflected in a reduction of the polymer melting enthalpies of THF-modified CBT (table 7.2).

Regarding neat CBT, the subsequently formed pCBT had a polymer melting enthalpy of 35.1 J/g, whereas the corresponding pCBT/THF 1.5% showed, under the same conditions, an enthalpy of 15.7 J/g. When THF was in great excess, the corresponding enthalpy was reduced to 4.2 J/g. This decrease in polymer melting enthalpies of polymerized CBT/THF 1.5% and CBT/THF 67% is directly dependent on the amount of crystalline fraction formed during cold crystallization.

**DSC analysis: kinetic effects**

Effects due to both the incorporated THF and the imposed heating rates were investigated by performing DSC scans with heating rates of 1 and 10 °C/min on CBT as well as on CBT/THF 1.5%. For the low heating rate, the first stage was performed from 30 to 60 °C at a heating rate of 10 °C/min and then decreased to 1 °C/min in order to prevent premature evaporation of the THF from the DSC pan. This sudden change in heating rate can be seen as a sharp decrease in heat flow of around 3 mW at 60 °C (*c.f.* fig. 7.1). A known kinetic effect inherent in DSC analysis when working with high heating rates is a shift of the characteristic peak temperatures of a given polymer towards higher values due to the

increasing thermal inertia of the polymer [12]. This kinetic effect becomes noticeable when the peak melting temperatures of CBT *versus* CBT* and CBT/THF 1.5% *versus* CBT/THF 1.5%* are compared. For neat CBT and CBT/THF 1.5% both peak melting temperatures decrease by about 3.4 °C (see table 7.2). Since both samples show the same decrease, it can be fully ascribed to the DSC kinetic effects and not to THF. Another known kinetic effect in DSC analysis is that when high heating rates are used, a better visibility of small signals but less resolution is obtained [12]. This explains the observation that the peak heights in the thermograms of both CBT* and CBT/THF* are lower than those of CBT and CBT/THF, respectively.

In comparison to the 10 °C/min heating rate, the 1 °C/min rate leads to cold crystallization occurring at lower temperatures with a decrease of 28 °C for neat CBT and 26 °C for CBT/THF 1.5%. The enthalpy of CBT at low heating rate is −18.5 J/g in contrast to an enthalpy of −36.5 J/g measured at 10 °C/min. On the other hand, the melting enthalpy of the pCBT formed increases from 35.1 to 67 J/g when using the low heating rate, although apparently less crystalline fraction is formed than during the previous cold crystallization. In regard to the cold crystallization enthalpy of CBT/THF 1.5% and CBT/THF 1.5%*, one can find a similar behaviour. However, in contrast, the increase in cold crystallization enthalpy using the low heating rate is greater for CBT/THF 1.5% as compared to neat CBT, namely an increase from −10.5 to −33.6 J/g. Also the melting enthalpy of pCBT/THF 1.5% increased from 15.7 to 55 J/g when using the low heating rate. The effect of THF on the melting enthalpy of the formed pCBT is clearly evident from table 7.2. When the THF content is increased to 67 wt%, the melting enthalpy shows a continuous decrease from 35.1 to 4.2 J/g. This fact matches well with the observed decrease in the corresponding cold crystallization enthalpy. The hindering effect of THF on both cold crystallization and melting enthalpy can be observed in the sample containing 67 wt.% THF and tested at 10 °C/min. In this case, the degree of crystallinity decreased to an almost amorphous state, as shown in fig. 7.1 and table 7.2.

High heating rates hinder the cold crystallization of CBT, which is in accordance with the literature and was also shown in section 6.4.3. When the ring-opening polymerization is conducted at low heating rates, there is more time for the pCBT to crystallize, whereas at high heating rates the growing crystals do not have time to fully develop before reaching the polymer melting temperature. As a consequence, the enthalpies of both cold crystallization and melting decrease when a high heating rate is used. However, the THF

also hinders the cold crystallization to a great extent, depending on the amount of THF present during cold crystallization. When using a large excess of THF and a high heating rate as in the case of CBT/THF 67%, the degree of crystallinity of the pCBT formed can be decreased to an almost amorphous state.

## DCS analysis: crystallinity

The degree of crystallinity is taken as the melting enthalpy of the second heating run. Neat CBT polymerizes during the first heating scan and crystallizes during the first cooling scan, showing a crystallization temperature $T_C$ of 176.6 °C and a crystallization enthalpy $\Delta H_C$ of −41.7 J/g. Both $T_C$ and crystallization enthalpy increased with increasing THF content up to Tc of 181.1 °C and $\Delta H_C$ of −63.2 J/g for CBT/THF 67% (*c.f.* table 7.3). The THF apparently acts like a nucleating agent, providing heterogeneous nucleation sites for the crystallization of the pCBT as well as increased chain mobility. Moreover, polyesters are known to undergo chemical induced crystallization [13-18]. Therefore, this increase in crystallinity is likely to be due to a solvent-induced crystallization phenomenon. The degree of crystallinity of neat CBT polymerized during DSC analysis was taken from the subsequent second heating run and was found to be 29.6%, which increases to 40.3% when 67 wt.%THF was added.

Table 7.3:  DSC cooling and second heating run; cooling rate: -30 °C/min; heating rate: 10 °C/min. The asterisk indicates a heating rate of 1 °C/min.

| Sample | first cooling | | second heating | | Crystallinity |
|---|---|---|---|---|---|
| | $T_{c,\,pCBT}$ | $\Delta H_{c,\,pCBT}$ | $T_{m,\,pCBT}$ | $\Delta H_{m,\,pCBT}$ | $X_c$ |
| | [°C] | [J/g] | [°C] | [J/g] | [%] |
| CBT | 176,6 | -41,7 | 223,6 | 42,1 | 29,6 |
| CBT/THF 1,5% | 179,4 | -42,7 | 222,9 | 42,7 | 30,1 |
| CBT/THF 67% | 181,1 | -63,2 | 223,6 | 57,2 | 40,3 |
| CBT* | 172,1 | -36,1 | 225,1 | 37,4 | 26,3 |
| CBT/THF 1.5%* | 175,1 | -40,2 | - | - | - |
| pCBT | 183,4 | -48,8 | 224,8 | 40,7 | 28,7 |
| pCBT/THF | 184,4 | -44,1 | 223,7 | 38,2 | 26,9 |
| pCBT/THF-RP | 183,4 | -48,0 | 223,4 | 47,9 | 33,7 |

**DSC analysis: pCBT/THF**

DSC was also performed on samples produced by compression moulding, particularly on pCBT, pCBT/THF and pCBT/THF-RP. In contrast to the *in situ* polymerization of CBT/THF during DSC analysis, thermograms of pCBT/THF prepared in the hot press did not show marked differences (see fig. 7.2).
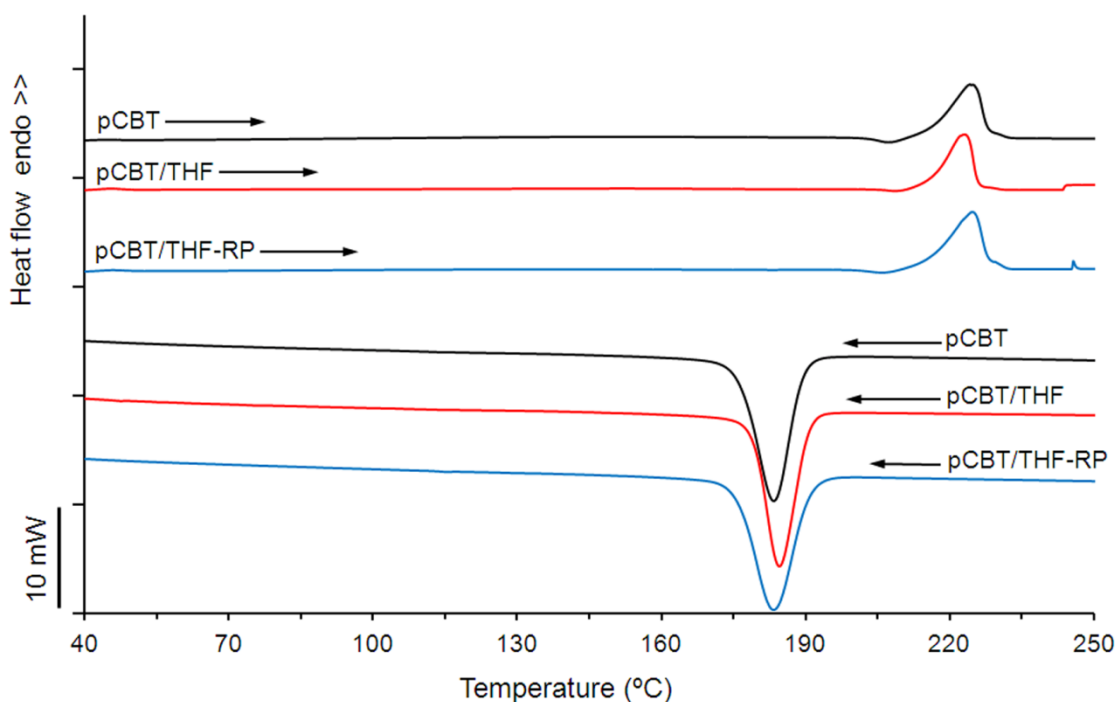
Fig. 7.2: DSC thermograms of pCBT, pCBT/THF and CBT/THF-RP. Heating rate: 10 °C/min; cooling rate: -30 °C/min.

All samples prepared by compression moulding are found to be fully polymerized since none of them show any melting peak of CBT oligomers in the range 120–160 °C. These three samples also show a single polymer melting peak of similar shape at *ca.* 224 °C, but small differences are found in the melting enthalpy, namely 44 J/g for pCBT/THF *versus* 52.8 J/g for neat pCBT (*c.f.* tables 7.2 and 7.3). This decrease in melting enthalpy for pCBT/THF can be ascribed to the same hindrance effects of the THF on the cold crystallization as discussed before for CBT/THF systems. As a consequence, the degree of crystallinity is slightly lower, namely 2% less than that of neat pCBT. The reprocessed sample (pCBT/THF-RP) gives almost similar results to neat pCBT, namely $\Delta H_m$ of 51.6 J/g for CBT/THF-RP. This may be explained by a loss of the remaining THF in terms of evaporation when the reprocessing of pCBT/THF is carried out. Therefore the degree of crystallinity of pCBT/THF-RP is virtually equal to that of neat pCBT.

### 7.5.3 WAXS analysis

X-ray diffraction was employed to discern whether the presence of THF in pCBT has an influence on the crystal structure of pCBT/THF. The diffraction patterns are shown in figure 7.3.
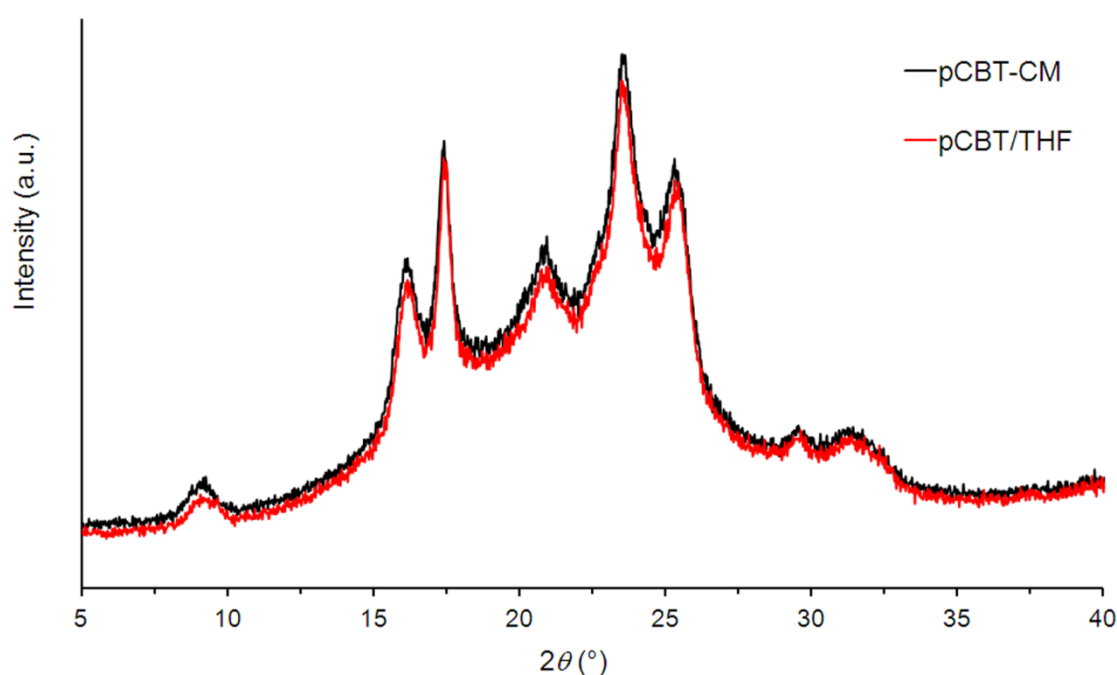


Fig. 7.3: WAXS diffraction patterns of pCBT and pCBT/THF.

As expected, the diffraction patterns do not show any significant difference between unmodified and THF-modified pCBT samples. It was pointed out in section 6.4.5 that two triclinic polymorphs are known for PBT, the $\alpha$ form being the stable polymorph under standard conditions whereas the $\beta$ form is only observed under stretching of unoriented crystals. Again, the crystallographic reflection from the ($\bar{1}$ 04) plane was used to determine the crystal phase of pCBT. This reflection is observed at $2\theta = 31.4°$ for both unmodified and THF-modified pCBT samples, hence both samples exhibit $\alpha$ crystal structure. When comparing pCBT and pCBT/THF, it can be seen from figure 7.3 that the width of the diffraction peaks is similar and therefore suggests a similar crystallite size.

### 7.5.4  GPC analysis

GPC was used to determine the number-average molecular weight ($M_n$), weight-average molecular weight ($M_w$) and dispersity ($M_w/M_n$) of pCBT and pCBT/THF. The results are summarised in table 7.4. Neat pCBT exhibits a GPC trace with a main peak at a retention time of 6.3 min and a shoulder peak at 5.6 min (see figure 7.4). This shoulder indicates the presence of two fractions of different molecular weight. The peak belonging to the remaining oligomers is seen at a retention time of 7.7 min. The degree of conversion from CBT oligomers to pCBT according to equation (6.3.3) was 97.9% for pCBT, which is in accordance with other published results [11, 19-20]. A 100% complete conversion cannot be achieved because polyesters are known to undergo ring–chain equilibrium reactions either in the melt or in solution and oligomers are present in concentrations of about 1 – 3 wt.% [8-9, 11, 16-17, 21-22].

The GCP trace of THF-modified pCBT consists of a single peak at a retention time of 6.0 min which was attributed to the pCBT polymer. The results show that the presence of THF during the ring-opening polymerization led to a higher molecular weight as compared to pCBT without THF modification.

Table 7.4:  GPC results of pCBT and pCBT/THF

| Sample | $M_w$ [g/mol] | $M_n$ [g/mol] | $\alpha$ [%] |
|---|---|---|---|
| pCBT | 22600 | 10000 | 97,9 |
| pCBT/THF | 37000 | 14000 | 100 |
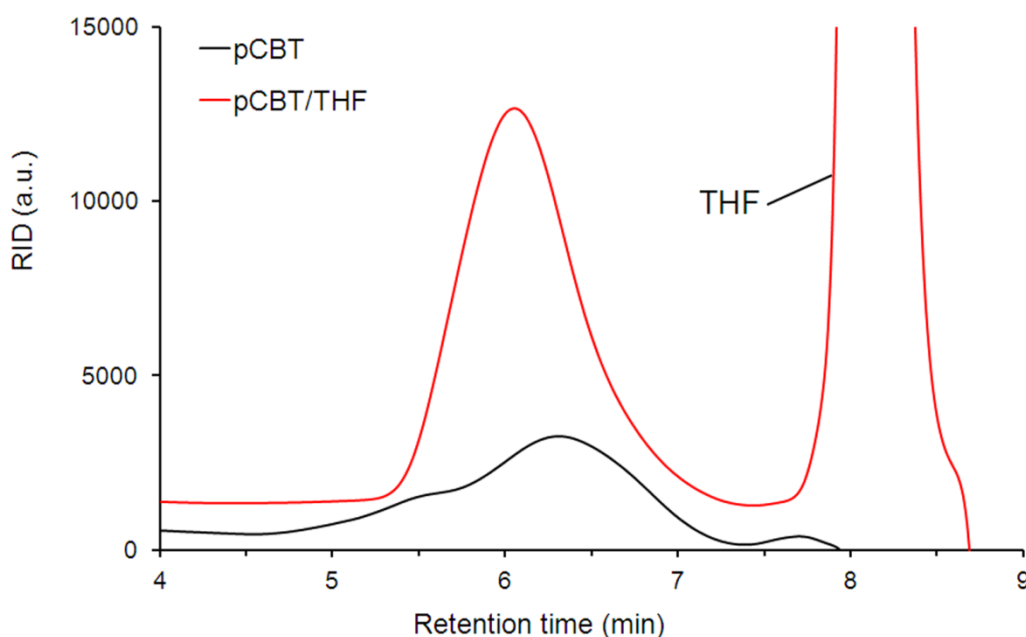
Fig. 7.4: GPC traces of pCBT and pCBT/THF

Interestingly, pCBT/THF did not exhibit any peak in the GPC trace attributed to oligomers. The remaining CBT oligomers after polymerization may be dissolved in THF and thus may be removed from the bulk material by solvent extraction. Cyclic oligomers in polyesters affect processing as well as material properties [16-17, 21-22], and therefore efforts are made to remove them from the bulk polymer by various methods. Vermylen *et al.* [17] prepared a cyclic-oligomer-free poly(ethylene terephthalate) by solvent extraction in a Kumagawa extractor using 1,4-dioxane as the boiling solvent. Also Shukla and Kulkarni [22] extracted cyclic oligomers from PET using extraction and dissolution methods. Although the oligomer peak in the GPC trace is not present, a prominent peak with a corresponding molecular weight of 73.4 g/mol is detected, obviously belonging to THF ($MW_{THF}$ = 72.11 g/mol) and thus proving its presence in the pCBT after compression moulding. This peak is one order of magnitude greater in intensity than the one corresponding to the polymer and therefore is only partially shown in figure 7.4. It should be pointed out that the molecular weight of all analysed samples is still below the theoretical critical molecular weight for entanglements $M_{w,c}$ of 50 000 g/mol [8-9]. Higher molecular weight pCBT has been reported by other researchers [8-9, 11, 19, 23-26]. A possible reason might be the influence of the environment, where in those other works the

ring-opening polymerization was conducted in awell-controlled reaction vessel under nitrogen atmosphere. In the present case, the pCBT was prepared in ambient atmosphere in a more industrial-like process. It is known that humidity inherent in ambient atmosphere partially inhibits catalytic action, leading to an incomplete ring-opening polymerization and hence to pCBT of lower molecular weight [27].

### 7.5.5  Thermogravimetric analysis

The effect of THF on the thermal stability and onset temperature of degradation was investigated using TGA. Mass losses of neat pCBT and pCBT/THF normalized over the initial masses are shown in figure 7.5.

The degradation pathway of pCBT is thought to be equal to the one of conventional PBT, *i.e.* initial polymer scission occurrs *via* a six-membered cyclic transition state with butadiene formation as a result of intramolecular exchange (ionic) reactions [28]. The cyclic oligomers further decompose by a $\beta$-CH hydrogen transfer reaction which generates open chain oligomers with olefin and carboxylic end-groups [29]. Apart from butadiene, a considerable amount of THF is also obtained in the degradation products of PBT. When the well-known acyl-oxygen cleavage of the ester linkages proceeds in the PBT chains, intra- or intermolecular *H* shifts can occur, leading to the formation of hydroxyl-terminated units, which in turn undergo further degradation to yield THF and the carboxylic acid-terminated chain [28].

TGA plots of both pCBT and pCBT/THF consist of one major decomposition step with maximum decomposition temperatures $T_{max}$ at 406 and 403 °C, respectively. The onset of degradation is evaluated from the temperature corresponding to a weight loss of 5% and is found to be 372 and 369 °C for pCBT and pCBT/THF, respectively. These results suggest that there is no significant influence of THF on the thermal stability of pCBT. The amount of residue at 600 °C is found to be 2.2 and 0.9% for pCBT and pCBT/THF, respectively. The onset temperatures of degradation and amounts of residue are consistent with published values for PBT [30] and pCBT [31]. The difference of both residual amounts is very small and is attributed to the inherent experimental error. THF is

an organic volatile solvent with a comparably low boiling point and therefore does not contribute to the amount of residues.
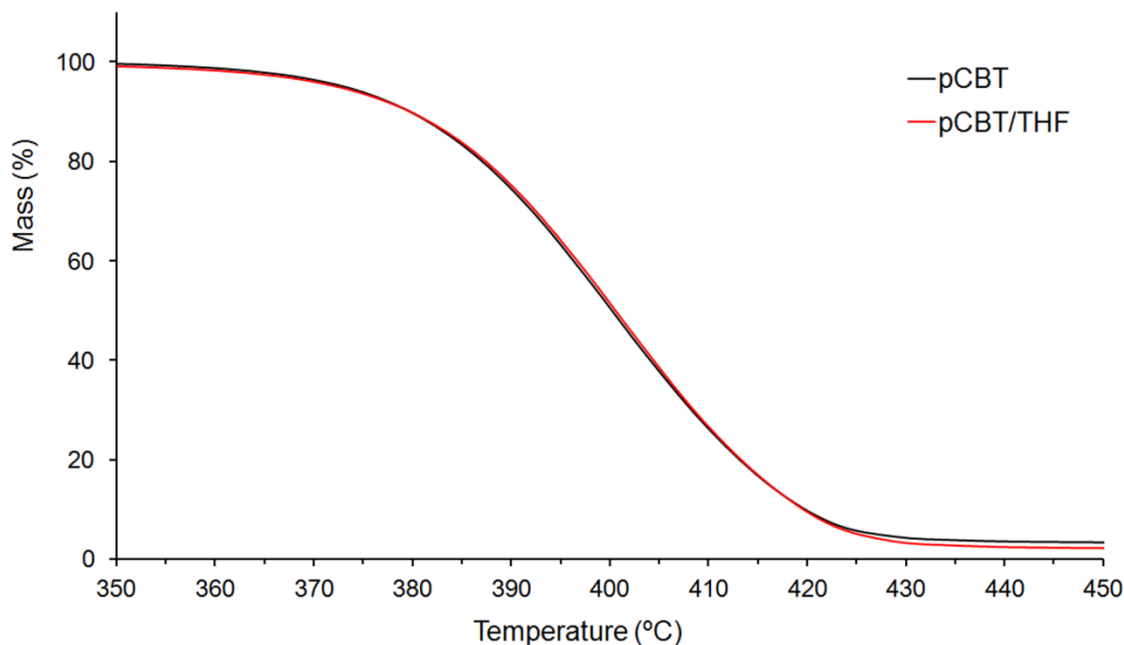


Fig. 7.5: TGA normalized mass of pCBT and pCBT/THF, recorded from 20 °C to 600 °C at a heating rate of 10 °C/min. For the sake of clarity only the interval between 350 °C and 450 °C is shown.

### 7.5.6 Dynamic mechanical thermal analysis

DMTA was employed to study the viscoelastic properties of pCBT and pCBT/THF. THF is found to be present in pCBT/THF after processing, as confirmed by GC-MS and GPC analysis and no evidence for copolymer formation was found, as suggested by DSC. These results lead to the assumption that the THF may separate adjacent chains and thus increase the free volume of the polymer. This increase in free volume leads to a greater mobility of the amorphous polymer chain segments. The gain in mobility of the amorphous phase is responsible for a greater ductility of the polymer. The dynamic mechanical properties are illustrated in fig. 7.6.
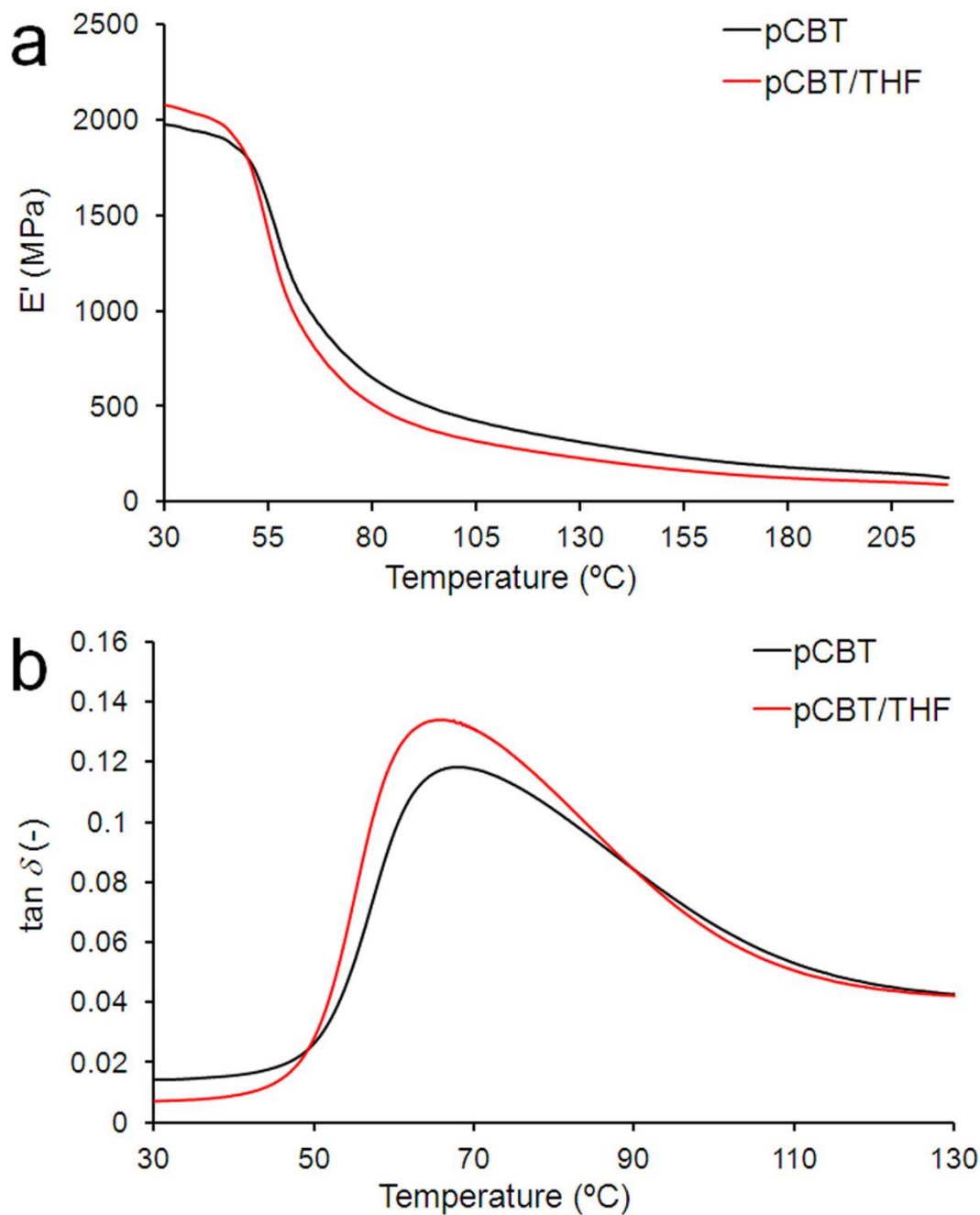
Fig. 7.6: DMTA plots of (a) E' and (b) tan $\delta$ versus temperature for pCBT and pCBT/THF

The THF-toughened sample showed a 5% higher initial storage modulus than neat pCBT, but stiffness decreased more markedly than in pCBT throughout the temperature range. At 50 °C both samples reached an equal value of 1.8 GPa (*c.f.* fig. 7.6(a)). The $T_g$ was considered to be the temperature corresponding to the peak maximum of the dynamical loss factor curve. $T_g$ of neat pCBT was found to be 68 °C, whereas that of pCBT/THF was

determined to be 66 °C (fig. 7.6(b)). This decrease in $T_g$ for the THF-modified sample can hardly be attributed to a conventional plasticizing effect induced by the THF, because the decrease in $T_g$ is only 2 °C. Moreover, the small amount of 1.5 wt.% THF added to the matrix was much less compared to conventional plasticizing agent contents. However, the *tan δ* peak height as well as the area under the tan *δ* curve is larger for pCBT/THF than for neat pCBT, indicating greater chain mobility in the THF-toughened sample.

### 7.5.7   Proton NMR spectroscopy

The ^{1}H NMR spectrum of pCBT/THF is depicted in fig. 7.7(b). Additionally, the ^{1}H NMR spectrum of polyTHF (molecular weight of 1000 g/mol) is shown in fig. 7.7(a) in order to ascertain if copolymerization between pCBT and THF took place during processing. Protons in pCBT are labelled 1 to 5 whereas protons of polyTHF are labelled α and β.

For the pCBT/THF system, the peak at 8.14 ppm is assigned to the aromatic protons (C3). The peak at 4.52 ppm is assigned to oxymethylene protons attached to the ester group. The peak at 2.04 ppm is assigned to the shielded methylene protons (C5) [25-26, 32].

In addition to the pCBT/THF peaks mentioned above, the spectrum of the blend of pCBT/THF and polyTHF shows also the characteristic peaks of polyTHF. The peak located at 3.66 ppm is assigned to the (Cα) methylene protons attached to oxygen, and the peak located at 1.70 ppm belongs to the shielded methylene protons (Cβ) [33]. When comparing figs. 7.7 (a) and (b), it is evident that no peaks belonging to polyTHF can be detected in the spectrum of pCBT/THF, indicating the absence of copolymers between pCBT and THF.
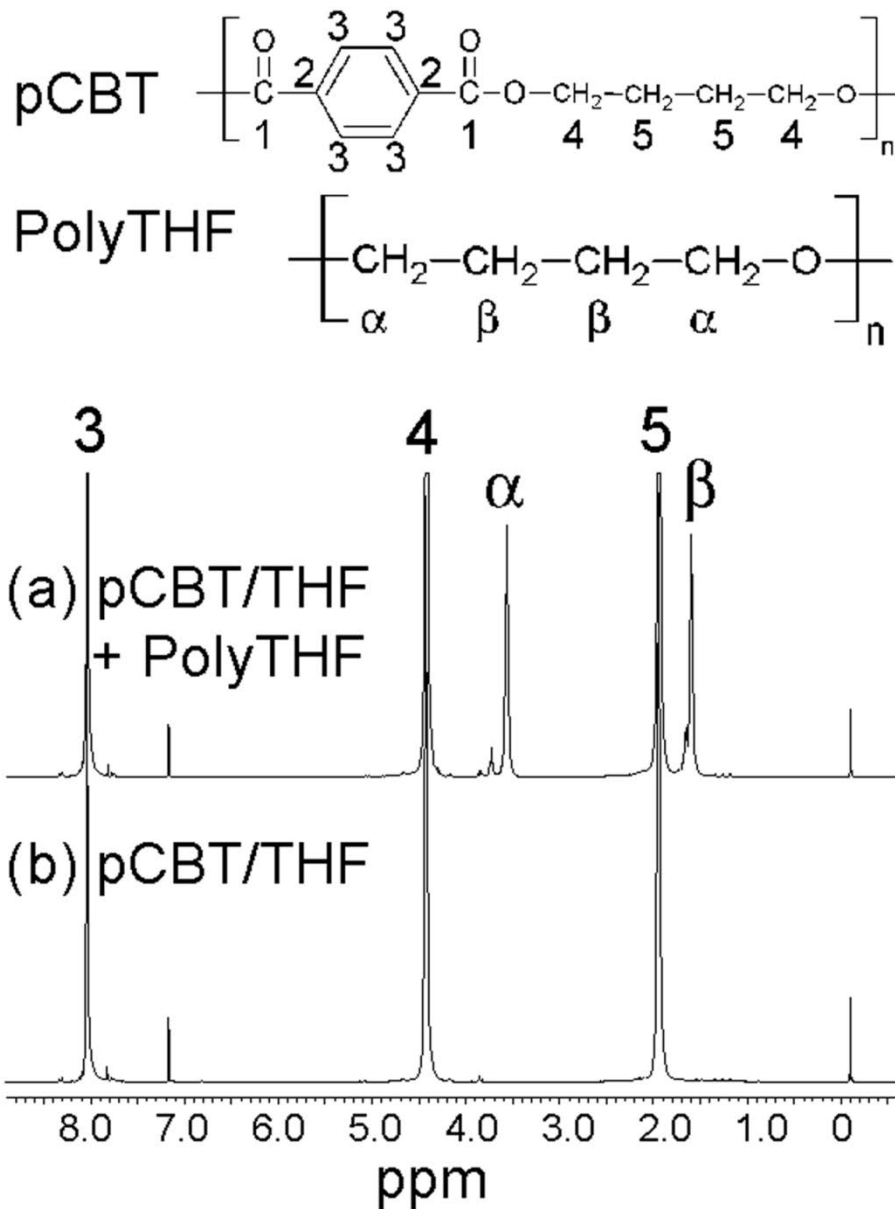
Fig. 7.7: $^1$H NMR spectra of (a) a mix of equal amounts of pCBT/THF and polyTHF and (b) of pCBT/THF

### 7.5.8 Melt blending of CBT and PolyTHF

CBT was *in situ* polymerized in the presence of polyTHF using the melt blending route with the aim to further ascertain whether copolymer formation between pCBT and polyTHF is a feasible way to toughen pCBT. Torque versus time measurements were performed at 240

°C mixing chamber temperature and 60 min$^{-1}$ screw speed in nitrogen atmosphere; the torque signals are illustrated in figure 7.8.
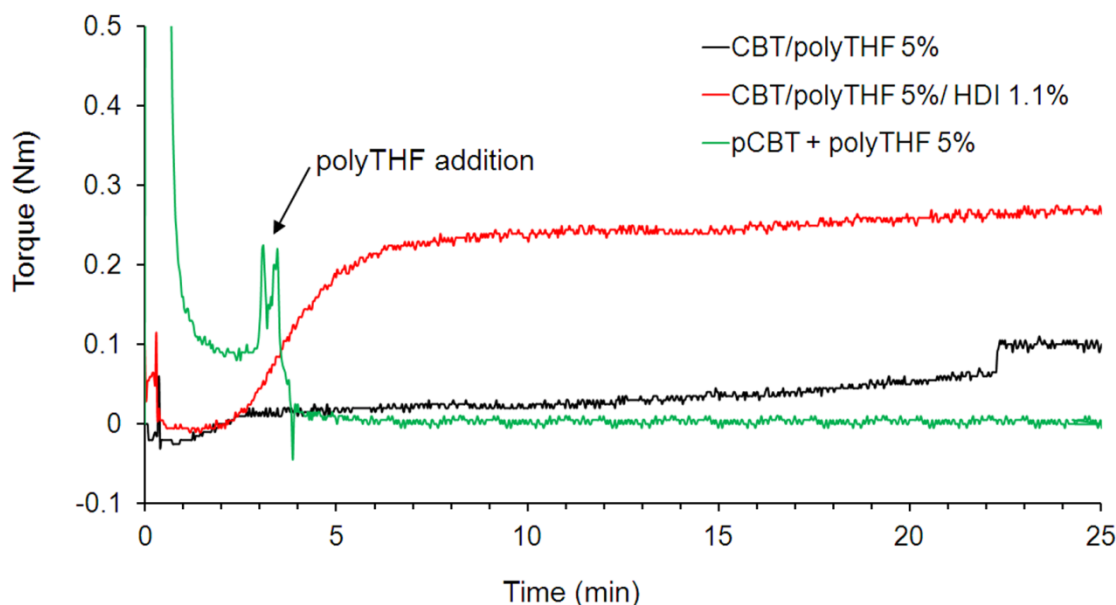


Fig. 7.8: Torque signals of CBT/poly THF 5% binary blend, CBT/PolyTHF 5%/HDI 1.1% ternary blend and pCBT + polyTHF added after 3 min

CBT melt blended with 5 wt.% of polyTHF exhibited an exceptionally low torque signal with a maximum torque value of 0.05 Nm after 20 min. At the end of the experiment the molten material apparently had a very low viscosity and readily flew out of the mixing chamber, indicating a low molecular weight. Nevertheless, it was not clear whether low molecular weight pCBT-polyTHF oligomers were formed or the ring-opening polymerization of CBT was inhibited by the presence of polyTHF, probably by interfering with the polymerization catalyst.

A similar result was reported by Baets *et al.* [24, 34]. They copolymerized CBT with 10 wt.% of polyTHF and found an embrittling effect together with a low molecular weight and attributed this to a "bad chemical interaction".

To clarify this issue, two additional experiments were conducted. First, a pre-dried blend of CBT, 5 wt.% of polyTHF and 1.3 mol equivalents of hexamethylene diisocyanate with respect to the diol polyTHF (*i.e.* 1.1 wt.% with respect to CBT) was melt blended

under the same conditions. Hexamethylene diisocyanate is a bifunctional chain extender which readily reacts with hydroxyl groups. On one hand, if copolymerization between pCBT and polyTHF takes place, then the diisocyanate will chain extend the formed OH-terminated pCBT/polyTHF oligomers and consequently torque increases. On the other hand, diisocyanates cannot react with cyclic CBT oligomers due to the absence of a reactive chain end in the CBT cyclic structure and hence no torque increase is observed. Having said that, a higher torque observed in this particular blend may not necessarily prove copolymer formation; the former may also be the consequence of a possible chain extension exclusively with pCBT chains, as will be discussed in detail in chapter 9.

It is clear from figure 7.8 that the addition of a bifunctional chain extender to the CBT/polyTHF blend resulted in a considerably higher torque of 0.26 Nm after 20 min. This result excludes the aforementioned possibility of a complete ROP inhibition due to the presence of polyTHF but a ROP retardation still may be possible.

In another experiment, already polymerized pCBT granules were melt blended under the same conditions. After complete melting of the pCBT, 5 wt.% of polyTHF was added after 3 min and a sudden torque drop to 0 Nm was observed (c.f. figure 7.8), suggesting the formation of low molecular weight difunctional OH-terminated pCBT-polyTHF oligomers [35].

All three materials obtained from this melt blending study exhibited low torque levels and a great brittleness after cooling. It was not subject of this study to produce and optimize block copolymers of pCBT and polyTHF. Instead, a simple and effective method to toughen pCBT without affecting stiffness and strength is searched. Obviously, imparting elastomeric properties to pCBT is a counterproductive strategy to achieve high stiffness or strength. In anticipation of chapters 8 and 9 of this work, were pCBT is effectively toughened by chain extension with small amounts (< 5 wt.%) of bi- or polyfunctional chain extenders, copolymerization with relatively large amounts of soft segments such as polyTHF was not considered as a feasible toughening method for pCBT and therefore will not be further analysed. On the basis of these torque curves and without any additional analysis it is impossible to definitely prove copolymer formation between pCBT and polyTHF. Nevertheless, DSC, DMTA and proton NMR clearly showed the absence of pCBT/polyTHF copolymers in THF-modified pCBT samples.

### 7.5.9  Tensile properties

The mechanical properties obtained from tensile tests are summarised in table 7.5. The tensile behaviour (shown in fig. 7.9) of neat pCBT is of a brittle nature with very low strain at break (*ca.* 7%), as confirmed by other researchers [3, 8-9, 19, 24, 26, 32, 34] and also demonstrated in chapter 6.

Table 7.5:  Tensile properties of pCBT and pCBT/THF

| Sample | Tensile modulus [GPa] | Tensile strength [MPa] | Elongation at break [%] | Strain energy [MJ/m$^3$] |
|---|---|---|---|---|
| pCBT | 2.7 ± 0.3 | 56 ± 8 | 6.7 ± 2.9 | 1.9 ± 0.4 |
| pCBT/THF | 2.4 ± 0.2 | 52 ± 5 | 227 ± 80 | 98 ± 37 |

In contrast, when a small amount of THF is incorporated in the pCBT matrix, a dramatic change from brittle to ductile behaviour can be observed. The mechanical properties of pCBT/THF are typical for a ductile material, having a yield point, neck formation and cold drawing over a large strain range with subsequent strain hardening until fracture. The strain at break is found to increase markedly from 7 to well above 100% with an average value of 227%.

It should be pointed out that all tested pCBT/THF samples showed the beginning of necking, but in some cases the neck collapsed prematurely due to neck instabilities. Tensile properties of pCBT/THF, namely Young's modulus and tensile strength, were somewhat lower compared to those of neat pCBT.
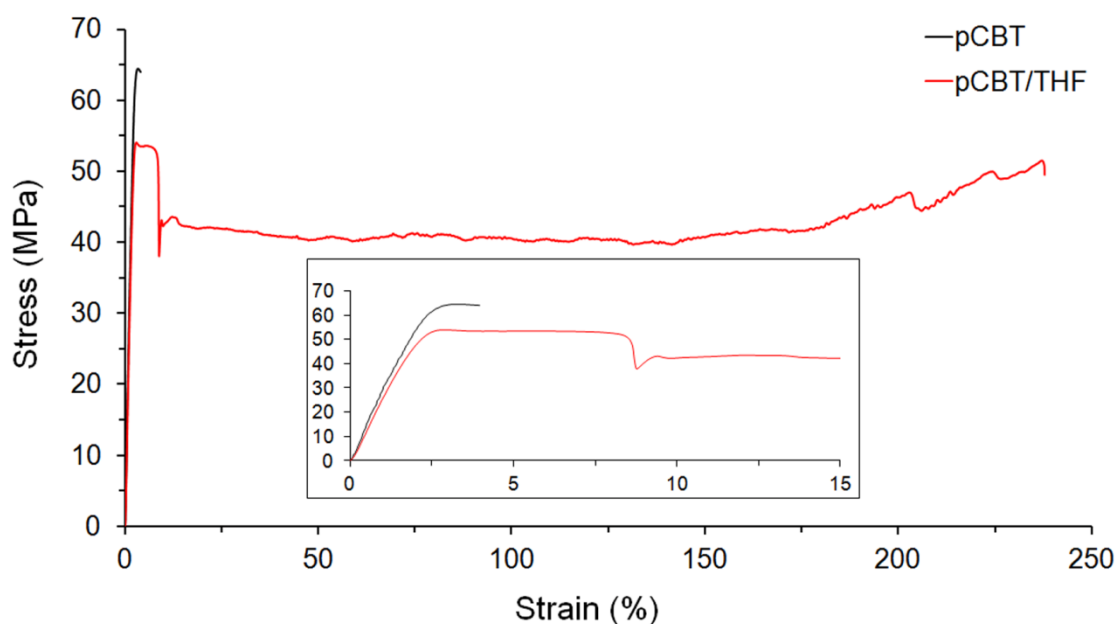
Fig. 7.9: Representative stress-strain curves for pCBT and pCBT/THF

This increase in toughness is believed to be caused by several factors. On the one hand, the increased molecular weight accounts for better mechanical properties. On the other hand, the absence of oligomers in pCBT/THF after polymerization may also contribute to the improved ductility, since cyclic oligomers in polyesters can affect mechanical properties [16-17, 21-22]. Moreover, it is believed that the THF absorbed by the CBT improved the dispersion and the reactivity of the catalyst during ring-opening polymerization. In addition, as THF was still present in the matrix after polymerization, it may have provided greater ease of chain mobility.

### 7.5.10 Tensile impact properties

Tensile impact tests were performed on pCBT and PBT/THF samples; representative tensile-impact stress versus time curves are illustrated in figure 7.10 and impact data is presented in table 7.6.
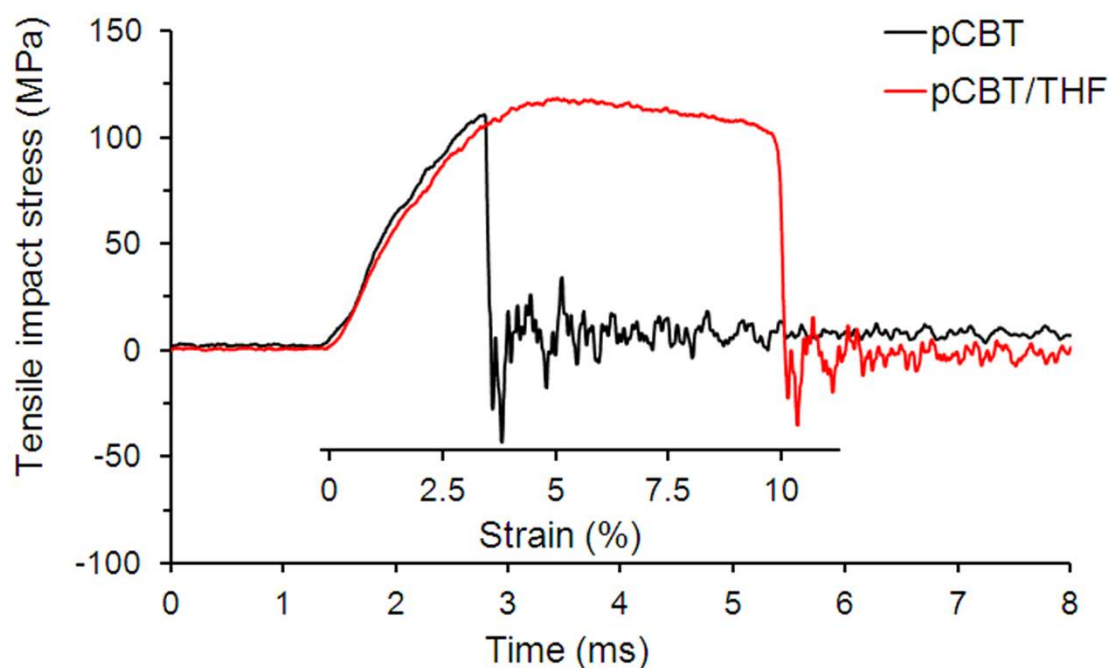
Fig. 7.10: Representative tensile impact stress *versus* time/strain curves of pCBT and pCBT/THF at $v = 1.5$ m/s.

Similar to what was discussed in section 6.4.9, pCBT behaved in a brittle manner whereas the THF-modified sample went through a stress maximum with a subsequent stress reduction which is associated with yielding. As indicated by the inset strain axis in figure 7.10, pCBT/THF exhibited a three-fold failure strain as compared to unmodified pCBT. Tensile-impact strength was 149 kJ/m$^2$ for neat pCBT and increased to 367 kJ/m$^2$ (increase: +146%) with the THF modification.

Table 7.6: Tensile impact properties of pCBT and pCBT/THF

| Sample | Tensile-impact strength [kJ/m$^2$] | Tensile-impact stress max. [MPa] |
|---|---|---|
| pCBT | 149 ± 71 | 86 ± 4 |
| pCBT/THF | 367 ± 17 | 113 ± 7 |

Recall that the solvent blended sample pCBT-SB (described in the initial pCBT characterization in section 6.4.9) showed somewhat lower tensile-impact strength of 306 MJ/m$^2$. Assumingly, the pCBT-SB sample contained less THF as compared to the pCBT/THF sample, which would explain a relatively lower toughness of the solvent blended sample as described in section 6.4.9. To sum up, the THF-toughened pCBT sample exhibited an outstanding toughness in both tensile and tensile impact tests.

### 7.5.11 Ageing

A set of tensile test specimens were subjected to thermal ageing at 80 °C in a desiccator in order to study the migration of THF out of the pCBT. The tensile behaviour of the specimens was then analysed as a function of time. The mechanical properties versus annealing time are shown in figure 7.11.

Due to the volatile nature and low boiling point of THF (66 °C), a rapid migration was expected when subjected to annealing at 80 °C. Therefore most of the samples were tested during the first few days. The last sample was finally tested after 130 days. Tensile modulus and tensile strength remain relatively unaltered, whereas the strain at break was maintained well above 50% during the first 30 days and finally decreased to *ca.* 10% after 130 days. The lack of data between 30 and 130 days does not allow a determination of the exact time at which the behaviour changes from ductile to brittle. Nevertheless, the final sample showed a 1.5-fold ultimate strain as compared to neat pCBT, even though the pCBT/THF sample fractured in a brittle manner when tested after 130 days. It is clear that the THF is attached to the pCBT molecules, because otherwise the brittle behaviour would happen already in an early stage of the ageing procedure. As mentioned earlier, the THF may be attached to the polymer by van der Waals forces, preventing an early migration of the THF.
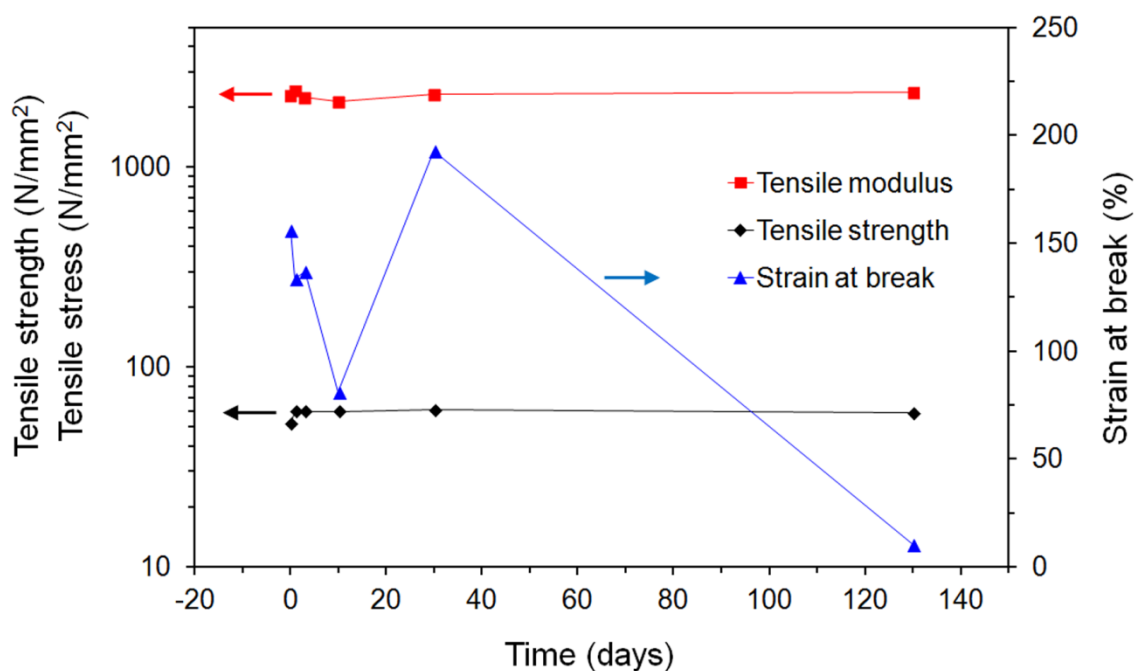
Fig. 7.11: Mechanical properties of pCBT/THF after thermal aging at 80 °C as a function of annealing time

## 7.6 Conclusions

THF was used to toughen *in situ* polymerized CBT. It was shown from GPC and GC-MS that the THF was incorporated in the pCBT after processing. The addition of ca 1.5 wt.% THF to neat CBT prior to its ring-opening polymerization led to an increase in molecular weight. Moreover, no remaining oligomers after polymerization were found. It was assumed that the THF absorbed by the CBT improved the action as well as the dispersion of the catalyst during ring opening polymerization. Additionally, as THF was still present in the matrix after polymerization, it may have provided greater chain mobility. DSC analysis revealed a hindered cold crystallization when the CBT/THF systems were polymerized *in situ* during a DSC scan. Most importantly, the incorporated THF led to a complete elimination of the brittleness inherent in pCBT and to a strain at break well above 100% in a tensile test. Other important properties such as tensile strength, tensile modulus and glass transition temperature were not significantly affected, in contrast to the case where other common methods are used to toughen polymers. The THF was found to migrate out of the polymer matrix, but pCBT/THF remains ductile at 80 °C for at least 30 days.

## 7.7    References for pCBT/THF

1.    Abt, T, Sánchez-Soto, M, Illescas, S, Aurrekoetxea, J, and Sarrionandia, M. Toughening of in situ polymerized cyclic butylene terephthalate by addition of tetrahydrofuran. Polymer International **60**(4), 549-556 (2011).

2.    Mohd Ishak, ZA, Gatos, KG, and Karger-Kocsis, J. On the in-situ polymerization of cyclic butylene terephthalate oligomers: DSC and rheological studies. Polymer Engineering & Science **46**(6), 743-750 (2006).

3.    Mohd Ishak, ZA, Leong, YW, Steeg, M, and Karger-Kocsis, J. Mechanical properties of woven glass fabric reinforced in situ polymerized poly(butylene terephthalate) composites. Composites Science and Technology **67**(3–4), 390-398 (2007).

4.    Gallo, E, Braun, U, Schartel, B, Russo, P, and Acierno, D. Halogen-free flame retarded poly(butylene terephthalate) (PBT) using metal oxides/PBT nanocomposites in combination with aluminium phosphinate. Polymer Degradation and Stability **94**(8), 1245-1253 (2009).

5.    Pellow-Jarman, M and Hetem, M. Comparison of the thermal degradation products of poly(butylene terephthalate) and flame-retardant poly(butylene terephthalate) formulations using a pyrolysis FTIR cell. Polymer Degradation and Stability **47**(3), 413-421 (1995).

6.    Xiao, JF, Hu, Y, Yang, L, Cai, YB, Song, L, Chen, ZY, and Fan, WC. Fire retardant synergism between melamine and triphenyl phosphate in poly(butylene terephthalate). Polymer Degradation and Stability **91**(9), 2093-2100 (2006).

7.    Lanciano, G, Greco, A, Maffezzoli, A, and Mascia, L. Effects of thermal history in the ring opening polymerization of CBT and its mixtures with montmorillonite on the crystallization of the resulting poly(butylene terephthalate). Thermochimica Acta **493**(1-2), 61-67 (2009).

8.    Miller, S. Macrocyclic polymers from cyclic oligomers of poly(butylene terephthalate). PhD thesis. University of Massachusetts Amherst: Amherst, USA, 1998

9.    Parton, H. Characterization of the in-situ polymerization production process for continuous fibre reinforced thermoplastics. PhD thesis. Department of Metallurgy and Materials Engineering. Katholieke Universiteit Leuven: Leuven, Belgium, 2006

10.  Dreyfuss, P. Poly(tetrahydrofuran). New York: Gordon and Breach, 1982.

11.  Brunelle, DJ, Bradt, JE, Serth-Guzzo, J, Takekoshi, T, Evans, TL, Pearce, EJ, and Wilson, PR. Semicrystalline Polymers via Ring-Opening Polymerization: Preparation and Polymerization of Alkylene Phthalate Cyclic Oligomers. Macromolecules **31**(15), 4782-4790 (1998).

12.  Ehrenstein, GW, Riedel, G, and Trawiel, P. Praxis der Thermischen Analyse von Kunststoffen, 2 ed.: Hanser, 2003.

13.  Conix, A and Vankerpel, R. Crystallization behavior and melting properties of meta-phenylene group containing polyesters. Journal of Polymer Science **40**(137), 521-532 (1959).

14.  Lee, WH, Ouyang, H, Shih, MC, and Wu, MH. Kinetics of solvent-induced crystallization of poly(ethylene terephthalate) at the final stage. Journal of Polymer Research-Taiwan **10**(2), 133-137 (2003).

15.  Mago, G, Kalyon, DM, and Fisher, FT. Polymer Crystallization and Precipitation-Induced Wrapping of Carbon Nanofibers with PBT. Journal of Applied Polymer Science **114**(2), 1312-1319 (2009).

16.  Perovic, A and Sundararajan, PR. Crystallization of cyclic olicomers in commercial poly(ethyleneterephthalate) films. Polymer Bulletin **6**(5-6), 277-283 (1982).

17.  Vermylen, V, Lodefier, P, DeVaux, J, Legras, R, Mac Donald, WA, Rozenberg, R, and De Hoffmann, E. Study of the thermal evolution of the cyclic-oligomer formation in a cyclic-oligomer-free PET. Journal of Polymer Science Part a-Polymer Chemistry **38**(3), 416-422 (2000).

18.  Zhang, JL. Alkaline-solution-induced crystallization in poly(butylene terephthalate). Journal of Polymer Science Part B-Polymer Physics **42**(10), 1938-1948 (2004).

19.  Parton, H, Baets, J, Lipnik, P, Goderis, B, Devaux, J, and Verpoest, I. Properties of poly(butylene terephthatlate) polymerized from cyclic oligomers and its composites. Polymer **46**(23), 9871-9880 (2005).

20.  Tripathy, AR, Elmoumni, A, Winter, HH, and MacKnight, WJ. Effects of catalyst and polymerization temperature on the in-situ polymerization of cyclic poly(butylene terephthalate) oligomers for composite applications. Macromolecules **38**(3), 709-715 (2005).

21. Kamau, SD, Hodge, P, and Helliwell, M. Cyclo-depolymerization of poly(propylene terephthalate): Some ring-opening polymerizations of the cyclic oligomers produced. Polymers for Advanced Technologies **14**(7), 492-501 (2003).

22. Shukla, SR and Kulkarni, KS. Estimation and characterization of polyester oligomers. Journal of Applied Polymer Science **74**(8), 1987-1991 (1999).

23. Baets, J, Dutoit, M, Devaux, J, and Verpoest, I. Toughening of glass fiber reinforced composites with a cyclic butylene terephthalate matrix by addition of polycaprolactone. Composites Part A: Applied Science and Manufacturing **39**(1), 13-18 (2008).

24. Baets, J, Godara, A, Devaux, J, and Verpoest, I. Toughening of isothermally polymerized cyclic butylene terephthalate for use in composites. Polymer Degradation and Stability **95**(3), 346-352 (2010).

25. Tripathy, AR, Chen, WJ, Kukureka, SN, and MacKnight, WJ. Novel poly(butylene terephthalate)/poly(vinyl butyral) blends prepared by in situ polymerization of cyclic poly(butylene terephthalate) oligomers. Polymer **44**(6), 1835-1842 (2003).

26. Tripathy, AR, MacKnight, WJ, and Kukureka, SN. In-Situ Copolymerization of Cyclic Poly(butylene terephthalate) Oligomers and ε-Caprolactone. Macromolecules **37**(18), 6793-6800 (2004).

27. Hakmé, C, Stevenson, I, Maazouz, A, Cassagnau, P, Boiteux, G, and Seytre, G. In situ monitoring of cyclic butylene terephtalate polymerization by dielectric sensing. Journal of Non-Crystalline Solids **353**(47–51), 4362-4365 (2007).

28. Levchik, SV and Weil, ED. A review on thermal decomposition and combustion of thermoplastic polyesters. Polymers for Advanced Technologies **15**(12), 691-700 (2004).

29. Montaudo, G, Puglisi, C, and Samperi, F. Primary thermal degradation mechanisms of PET and PBT. Polymer Degradation and Stability **42**(1), 13-28 (1993).

30. Bakirtzis, D, Ramani, A, Delichatsios, MA, and Zhang, J. Structure of the condensed phase and char of fire-retarded PBT nanocomposites by TGA/ATR in N-2. Fire Safety Journal **44**(8), 1023-1029 (2009).

31. Wu, FM and Yang, GS. Poly(butylene terephthalate)/organoclay nanocomposites prepared by in-situ bulk polymerization with cyclic poly(butylene terephthalate). Materials Letters **63**(20), 1686-1688 (2009).

32.    Bahloul, W, Bounor-Legare, V, Fenouillot, F, and Cassagnau, P. EVA/PBT nanostructured blends synthesized by in situ polymerization of cyclic cBT (cyclic butylene terephthalate) in molten EVA. Polymer **50**(12), 2527-2534 (2009).

33.    Dubreuil, MF and Goethals, EJ. Endgroup-functionalized polytetrahydrofurans by polymerization with functional triflate esters .1. PolyTHF-macromonomers. Macromolecular Chemistry and Physics **198**(10), 3077-3087 (1997).

34.    Baets, J. Toughening of in-situ polymerized cyclic butyleneterephthalate for use in continuous fiber reinforced thermoplastic composites. PhD thesis. Department of Metallurgy and Materials Engineering. Katholieke Universiteit Leuven: Leuven, Belgium, 2008

35.    Maier, S. Carbonylbiscaprolactam (CBC): Isocyanat-freier Zugang zu blockierten Isocyanaten, Blockcopolymeren und reaktiven Dispersionen. PhD thesis. Institut für Makromolekulare Chemie Albert-Ludwigs-Universität Freiburg im Breisgau: Freiburg im Breisgau, Germany, 2003

# Chapter 8: Toughening of pCBT with epoxy resin
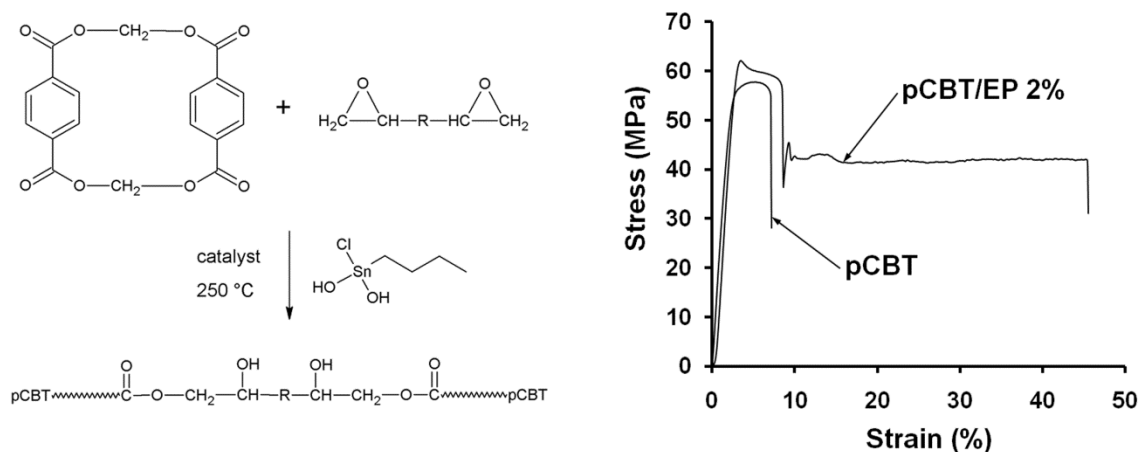


CBT was polymerized in the presence of a low molecular weight bifunctional epoxy resin. The resultant chain extended pCBT showed an increased ductility compared to that of conventional pCBT for all analysed epoxy concentrations (1–4 wt.%). The best toughness was obtained with 2 wt.% of epoxy resin. Other mechanical properties remained relatively unaffected by the epoxy resin.

**Publication derived from this work [1]:**

Toughening of *in situ* polymerized cyclic butylene terephthalate by chain extension with a bifunctional epoxy resin

Tobias Abt [a], Miguel Sánchez-Soto [a,*], Antxon Martínez de Ilarduya [b]

## 8.1    Introduction

It was shown in the preceding chapter that the addition of small amounts of tetrahydrofuran prior to the ring-opening polymerization of CBT leads to a toughened pCBT. Nevertheless, this toughening effect is not permanent due to a slow migration of the THF out of the pCBT matrix, as was demonstrated by thermal ageing and subsequent tensile tests. Moreover, the use of solvents is not environmentally friendly. Due to these reasons a simple, permanent and by-product-free toughening method is sought for pCBT.

Reactive chain extension with low molecular weight bi- or polyfunctional compounds is a common method utilized to improve the properties of polyesters such as toughness, melt viscosity, and hydrolytic stability. These polyfunctional compounds readily react with the carboxyl and/or hydroxyl terminal groups of polyesters. These so-called chain extenders are preferably bifunctional and should react easily through an addition reaction without the generation of any by-products.

For instance, reactive chain extension is widely used in the recycling of PET to compensate for molecular weight loss during melt processing. Chain extended, recycled PET has a higher molecular weight which improves the rheological properties for processes requiring a high viscosity such as low density extrusion foaming or extrusion blow moulding [2-5]. Similarly, chain extenders are employed to improve toughness, impact strength and hydrolytic stability of PBT [2, 6]. They can also be used as coupling agents or compatibilizers for immiscible polymer blends, such as PET-polystyrene [7], PBT-acrylonitrile-butadiene-styrene [8] or PBT-poly(ethylene octene) copolymer blends [9]. Among the various chain extenders, an efffective group proved to be diepoxides. The chain-extension reaction between polyesters such as PET or PBT and epoxides was extensively studied and is well established [2-3, 5, 7-8]. Tripathy *et al.* [10] synthesized a series of copolyesters of CBT and bisphenol A diglycidyl ether (BPADGE) with ratios of CBT/BPADGE from 75/25 to 40/60. Their aim was to improve the flame retardant properties; mechanical properties of the obtained copolyesters were not reported.
In this work a commercial epoxy resin was used in small amounts (1 to 4 wt.%) as a chain extender during in-situ polymerization of CBT in order to increase the toughness of the resulting pCBT. Although epoxy as a potential toughening agent for pCBT was mentioned in the open patent literature [11-12], to the best of the knowledge of the author, there has been no publication on this subject.

## 8.2    Experimental Section

### 8.2.1   Materials

One-component cyclic butylene terephthalate oligomers (CBT160[®]) were used throughout this chapter, for details see section 3.1.2.

Four types of epoxy resins were initially used in a preliminary study, namely Eporai[®] 450/A, Araldite[®] GT 7071, Araldite[®] GT 7004 and Araldite[®] GT 6097. The epoxy resins are described in detail in section 3.4.1.

### 8.2.2   Sample preparation

A mortar and pestle were used to create "homogenous" dry blends of previously dried CBT powder and the corresponding amount of epoxy resin. The resultant CBT/epoxy blends (referred to as CBT/EP) and neat CBT powder were vacuum dried for 8 hours at 80 °C. Approximately 12 g of the CBT/EP blends were *in situ* polymerized during compression moulding in the hot plate press at 250 °C for 20 min in ambient atmosphere. The polymer sheets were then rapidly cooled to room temperature in the cold stage of the press. The resulting pCBT/epoxy films (referred to as pCBT/EP) were used to extract samples for further characterization. A neat pCBT sample was similarly produced for comparison. Again, this unmodified pCBT sample is similar to pCBT-CM as described in section 6 but will be referred to as pCBT in this section for simplicity reasons.

Almost the entire analysis is devoted to these compression moulded pCBT/EP samples, but additional samples were also prepared by melt blending in a later stage of this study in order to see the influence of the processing route on the mechanical properties of epoxy-modified pCBT. *In situ* polymerization during melt blending was carried out with *ca.* 40 g of neat CBT and CBT/EP blends, respectively, in a batch mixer at 230 °C, 60 min$^{-1}$ and under N$_2$ atmosphere for 20 min. At the end of the melt blending the batch mixer was stopped, the polymer was collected, cooled to room temperature, ground into granules using a cutting mill, vacuum dried for 8 h at 80 °C and subsequently compression moulded in the hot plate press at a temperature of 250 °C and a pressure of 4 MPa for 5

min. Melt blended samples were referred to as pCBT/EP-MB in order to distinguish between compression moulded samples. These samples were subjected to DSC analysis and to tensile tests.

## 8.3    Preliminary study on the toughening action of epoxy resins

A preliminary study was conducted in order to analyse the role of the epoxy equivalent weight, *i.e.* the molecular weight of the different epoxy resins on the toughness of pCBT. CBT/epoxy blends with epoxy contents of 2.5, 5 and 10 wt.% were prepared using mortar and pestle, *in situ* polymerized during compression moulding and then tensile tested. As mentioned earlier, the presence of a yield point with neck formation and post-yield deformation was taken as a criterion for toughness.

The result of the tensile tests was that no toughening action was observed in pCBT/EP samples containing high molecular weight Araldite resins, as evidenced by a failure strain of around 8% and a brittle fracture mode without neck formation. Stiffness and strength of all epoxy-modified samples were comparable to the ones of unmodified pCBT. It was assumed that the reactivity of these high molecular weight epoxy resins decreases with increasing molecular weight. In contrast, some pCBT samples containing 2.5 and 5 wt.% of low molecular weight Eporai 450/A showed necking during tensile tests.

On basis of these tensile properties, particularly on basis of the failure strain, the liquid, low molecular weight epoxy resin Eporai 450/A was chosen as a suitable toughening agent for pCBT. Eporai 450/A will henceforth be referred to as EP solely, the other three solid, high molecular weight epoxy resins were not further used in this study. EP contents of 1–4 wt.% were chosen for further studies; CBT/EP blends were *in situ* polymerized during compression moulding in the hot plate press and used for further analysis.

## 8.4    Characterization

The reaction between CBT and epoxy resin was visualized by torque *versus* time measurements in the batch mixer at 250 °C and 60 min$^{-1}$ rotor speed in ambient

atmosphere. This was done to study the chain extension reaction under the same thermal conditions used for compression moulding. Neat CBT was equally processed for comparison.

Unmodified pCBT and epoxy-modified pCBT samples (*in situ* polymerized during compression moulding) were characterized using gel permeation chromatography, gel content determination, $^1$H NMR spectroscopy, differential scanning calorimetry, X-ray diffraction, dynamic mechanical thermal analysis and scanning electron microscopy. The mechanical properties of the samples were determined by tensile tests and by instrumented tensile-impact tests. All characterization methods are described in detail in chapter 5.

## 8.5    Results and Discussion

The chain extension reaction between (growing) pCBT chains and epoxy resin is carried out in two ways in the melt: esterification of the carboxyl end groups and etherification of the hydroxyl end groups and glycidyl functional groups of the polyester and epoxy resin, respectively (*c.f.* figure 8.1).
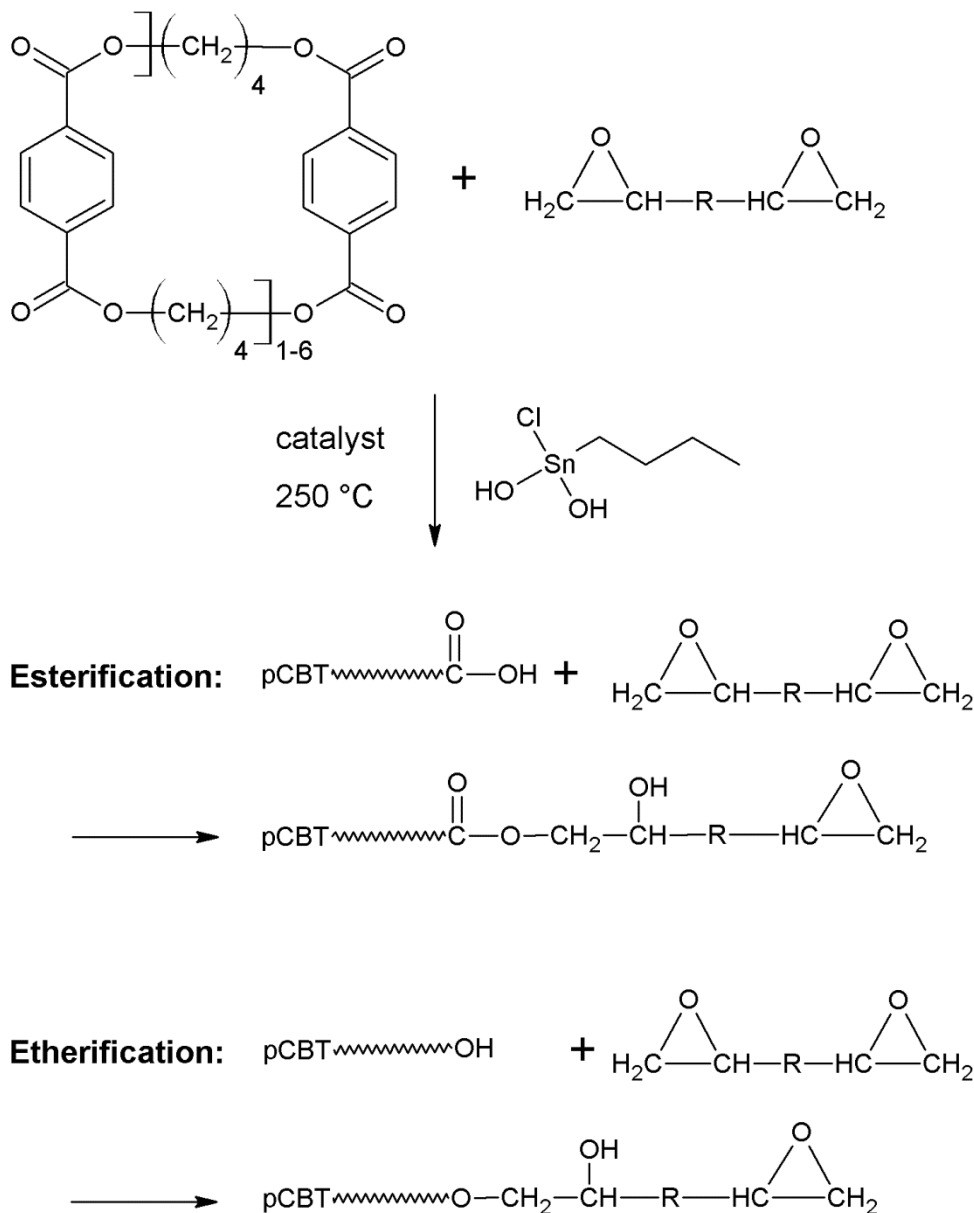
Fig. 8.1: Esterification and etherification reactions of pCBT and diepoxide

The epoxy groups react predominantly with the carboxyl groups due to the strong polarization of the hydroxyl bond of carboxylic acids, but are also known to react with the less nucleophilic hydroxyl groups. Secondary hydroxyl groups arise from these chain extending reactions. These hydroxyl groups can further react with the epoxy functional groups, which leads to branching and eventually to crosslinking, as depicted in figure 8.2 [2-3, 5-8].

**Chain extension:**
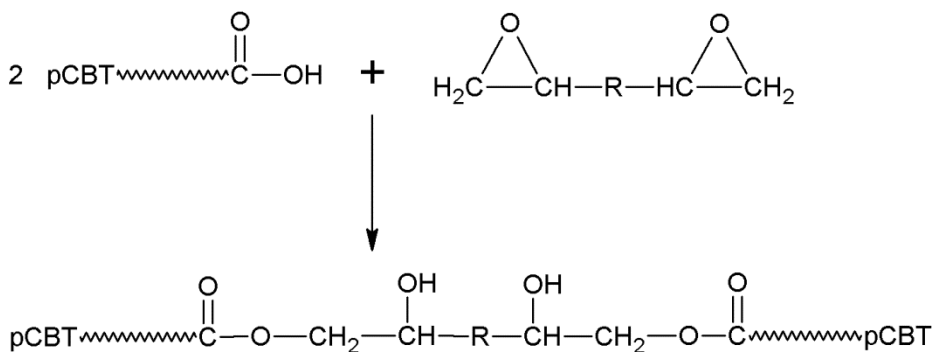


**Branching:**
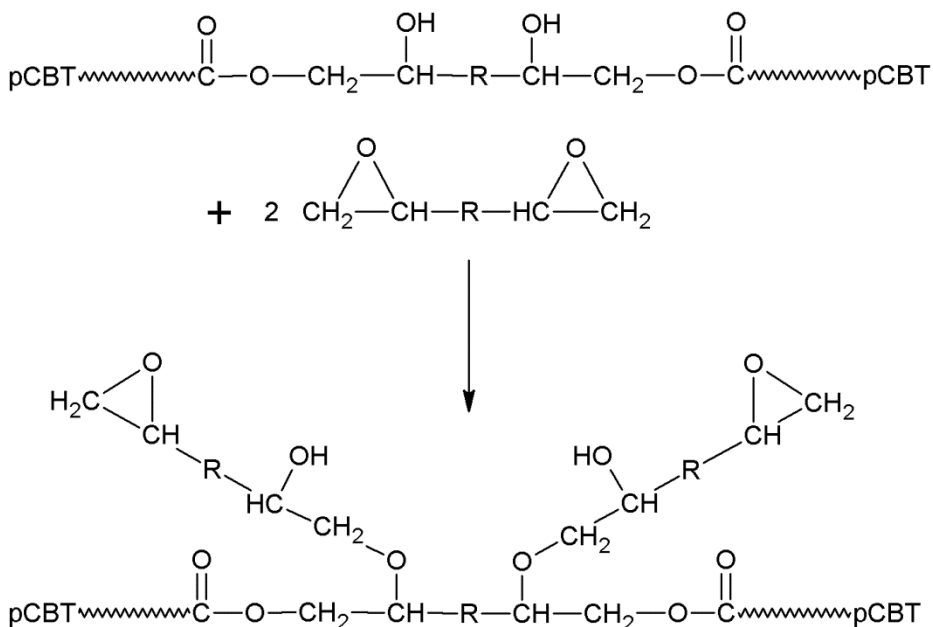


Fig. 8.2: Chain extension and branching mechanism of pCBT and diepoxide

High molecular weights can be obtained with quite small amounts of diepoxide because two or more pCBT chains of relatively high molecular weight are linked together with bifunctional, low molecular weight epoxy molecules. One mole of the chain extender reacts with two moles of polymer in order to obtain linear extended chains and prevent excessive branching and crosslinking. Therefore the theoretical amount of chain extender for the reaction can be calculated from [2-3, 5]:

$$wt.\%_{EP} = \frac{(MW \cdot CC_0)}{2 \cdot 10^4}$$

(8.1)

where wt.%$_{EP}$ is the theoretical amount of chain extender to obtain linear chain extension, MW is the molecular weight of the chain extender and CC$_o$ is the carboxyl content of the initial pCBT in equiv./$10^6$ g.

Unlike conventional polyesters with a given carboxyl content, CBT does not exhibit a constant carboxyl content during the ring-opening polymerization until the conversion into pCBT is complete. Since the ROP of CBT starts in the presence of the chain extender, the epoxy may already react during the ring-opening polymerization with the growing pCBT chains.

### 8.5.1 Torque *versus* time measurements

A chain extension reaction of (growing) pCBT chains and a bifunctional epoxy resin results in an increase in molecular weight. This can be visualized by a viscosity increase with reaction time. Therefore, initial studies in the batch mixer were carried out in order to determine the optimum reaction time of CBT/EP blends for *in situ* polymerization during compression moulding. Torque and melt temperature were monitored over reaction time for neat CBT as well as for the CBT/EP blends (*c.f.* figure 8.3). The maximum torque values with the corresponding times and temperatures are reported in table 8.1.

The torque response of neat CBT was first detected after 3.5 min, before the melt viscosity was too low to be measured. The maximum torque of 2 Nm was detected after ca. 15 min. It slowly but steadily decreased to less than 1 Nm after 60 min due to hydrolysis and thermo-mechanical degradation. The ring-opening polymerization of CBT is athermal, therefore the melt temperature remained constant at 250 °C.
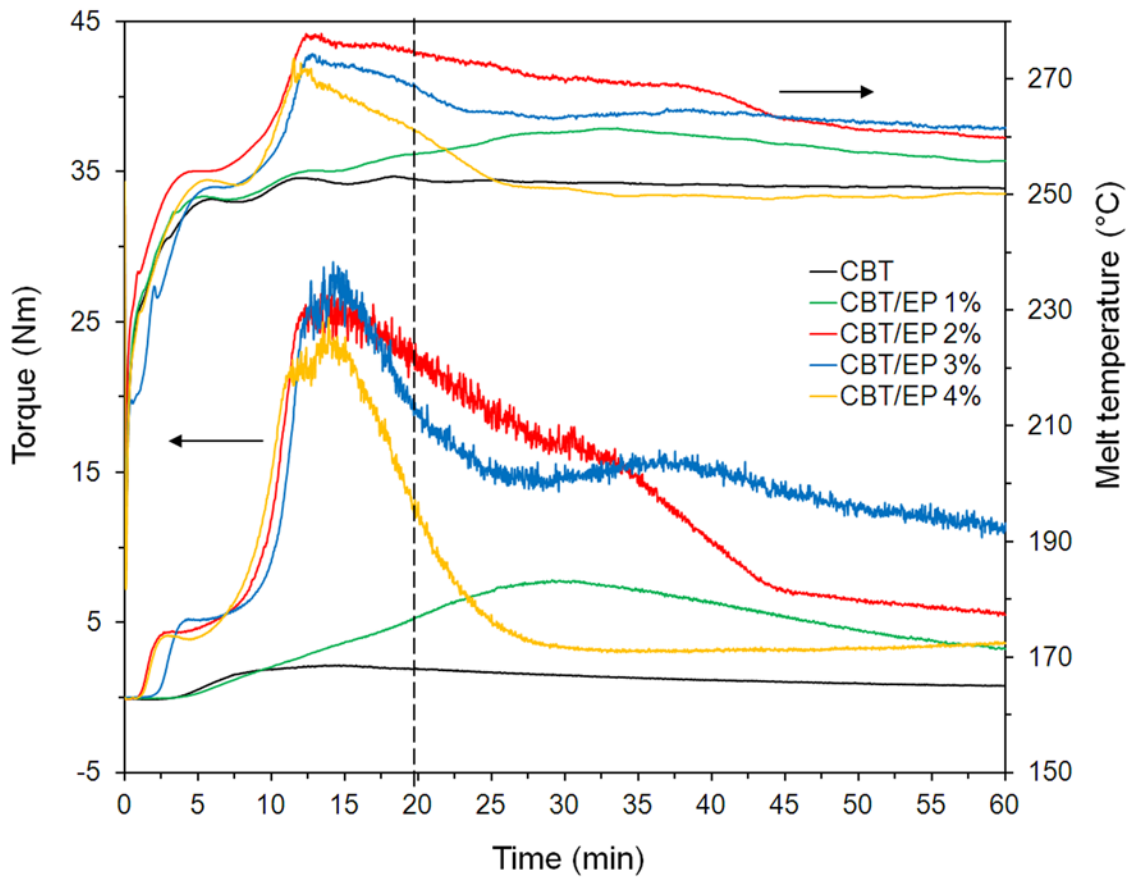
Fig. 8.3: Torque and temperature *versus* time plots at 250 °C and 60 min$^{-1}$ of CBT containing 0, 1, 2, 3 and 4 wt.% diepoxide

Table 8.1: Maximum torque values, reaction time and max. temperature during melt blending. Mixing chamber temperature: 250 °C; Screw speed: 60 min$^{-1}$

| Sample | Torque max. [Nm] | Time* [min] | Temperature max. [°C] |
|---|---|---|---|
| CBT | 2.2 | 14.6 | 252 |
| CBT/EP 1% | 7.8 | 29.1 | 261 |
| CBT/EP 2% | 26.9 | 14.7 | 276 |
| CBT/EP 3% | 29.0 | 14.2 | 273 |
| CBT/EP 4% | 25.2 | 13.9 | 269 |

*Time to reach maximum torque

CBT/EP 1% showed the same onset of torque increase after 3.5 min as neat CBT, but torque steadily increased for ca. 30 min and reached a maximum of ca. 8 Nm. Then the torque slowly decreased to a value of 3 Nm after 60 min. This slow reaction may be due to a too small amount of epoxy resin, which made it difficult for the carboxyl end groups to find a reaction partner.

The torque response of samples containing 2 wt.% or more EP changed significantly. The signal for CBT/EP 2% already appeared after 1 min and exhibited a shoulder at 4 Nm after 3 min. This shoulder may be attributed to the ring-opening polymerization of CBT, suggesting that the ROP was highly advanced before the chain extension reaction began. Therefore one can conclude that the epoxy resin acts as a promoter for the ROP. A strong torque increase with a maximum of ca. 27 Nm after 15 min followed, which was attributed to the chain extension reaction. After reaching this maximum, the torque signal decreased to 7 Nm after 45 min. The signal showed considerable noise after reaching the maximum torque and the noise magnitude steadily decreased. After 45 min the signal was smooth and decreased to a final value of 5 Nm after 60 min. These fluctuations in the torque signal are attributed to rapid changes in melt viscosity and hence changes in molecular weight, indicating an ongoing reaction after reaching the maximum torque. The absence of this noise in the torque signal of CBT/EP 1% suggests a weak reaction because the epoxy resin was the limiting reagent. When the carboxyl end groups are the limiting reagent, the reaction can proceed until all carboxyl end groups are consumed. The remaining diepoxide can also react with hydroxyl end groups as well as with secondary hydroxyl groups previously formed during esterification reaction. Thus an excess of epoxy resin can lead to branching and eventually to crosslinking.

CBT/EP 3% exhibited a very similar shape of the torque curve compared to CBT/EP 2% until the maximum of 29 Nm after 14 min. This was the highest torque value of all analysed CBT/EP blends. The signal also showed considerable torque fluctuations. After reaching the maximum, the torque decreased to 14 Nm after 28 min.

The CBT/EP blend containing 4 wt.% of epoxy resin showed a similar progression of the torque signal. The maximum torque of 25 Nm was slightly lower compared to the blends with 2 and 3 wt.% EP, but it was reached at the same time (14 min). Afterwards the torque response strongly decreased to ca. 4 Nm and remained low, suggesting a considerable decrease in molecular weight. Moreover, it has been reported that high

amounts of unreacted epoxy monomers in PBT/EP blends act as a solvent and thus reduce melt viscosity, melting and crystallization temperature [13]. It will be shown later in NMR analysis that pCBT/EP 2% and pCBT/EP 4% contained a considerable amount of unreacted EP. Therefore, this steep torque decrease was partially attributed to a plasticizing effect of the unreacted epoxy monomers.

The exothermic nature of the chain extension reaction is well reflected in the temperature curves of the CBT/EP blends. The temperature curves followed a similar pattern to that of the corresponding torque responses. Interestingly, the sample CBT/EP 2% generated the highest amount of heat (*c.f.* table 8.1) which indicates a high degree of chain extension reaction. The main increase in melt temperature was attributed to the exothermic chain extension reaction as well as frictional heat generation, since the viscosity of the pCBT melt increased during the chain extension reaction.

According to the torque evolutions in figure 8.3 and the observed torque maxima in table 8.1, a high molecular weight pCBT can be expected from blends containing 2 and 3 wt.% EP. As the torque responses of these samples considerably decreased after reaching the maximum, it appears important to determine the optimum processing time in order to obtain a high molecular weight pCBT. Since temperature and shear rate apparently influence the time to reach the maximum torque, the role of these two parameters were further investigated.

**Effect of temperature and shear on the rate of chain extension reaction**

A high temperature and shear rate increase the rate of the chain extension reaction due to more collisions of pCBT and EP molecules compared to a static reaction, such as the *in situ* polymerization during compression moulding. In order to study the effect of temperature and shear on the rate of chain extension reaction, CBT/EP blends containing 2 wt.% EP were processed at different temperatures (210, 230 and 250 °C) and different rotor speeds (10, 60 and 100 min$^{-1}$); results are shown in figures 8.4 and 8.5 as well as in table 8.2.

Table 8.2:  Effect of temperature and rotor speed on the rate of chain extension reaction of CBT/EP 2%

| Set temperature [°C] | Rotor speed [min⁻¹] | Torque max. [Nm] | Time* [min] |
|---|---|---|---|
| 210 | 60 | 29.8 | 33,9 |
| 230 | 60 | 29.7 | 25,1 |
| 250 | 60 | 26.9 | 14,7 |
| 250 | 10 | 23.4 | 17,2 |
| 250 | 100 | 21.3 | 10,4 |

*Time to reach maximum torque

As expected, the rate of chain extension reaction increased with increasing temperature and shear rate. Increasing polymerization temperatures had little influence on the maximum torque values, but considerably shortened the time to reach these torque maxima. An increase from 210 °C to 250 °C resulted in less than half of the time to reach maximum torque.  Similarly, increasing rotor speeds resulted in decreasing times to reach maximum torque, though less pronounced than the influence of the polymerization temperature.
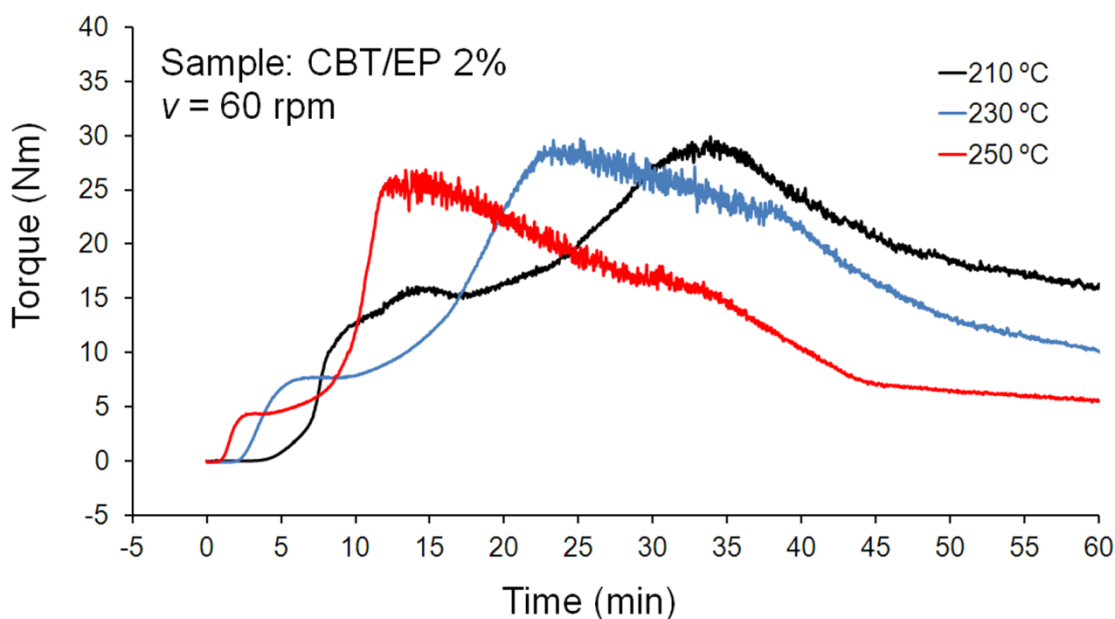


Fig. 8.4: Influence of processing temperature on the polymerization kinetics

At low rotor speed the time to reach the maximum torque was 17.2 min which is 2.5 min longer compared to the one at 60 min$^{-1}$ (*c.f.* table 8.2). Therefore it is reasonable to assume that the chain extension reaction conducted in the hot plate press will need more time than 17.2 min in order to complete the chain extension reaction.

Except CBT/EP 1%, which apparently contained an insufficient amount of chain extender and therefore exhibited a slower reaction, all other CBT/EP blends reached their maximum torque after 14 to 15 min when 60 min$^{-1}$ rotor speed was used (*c.f.* table 8.1).
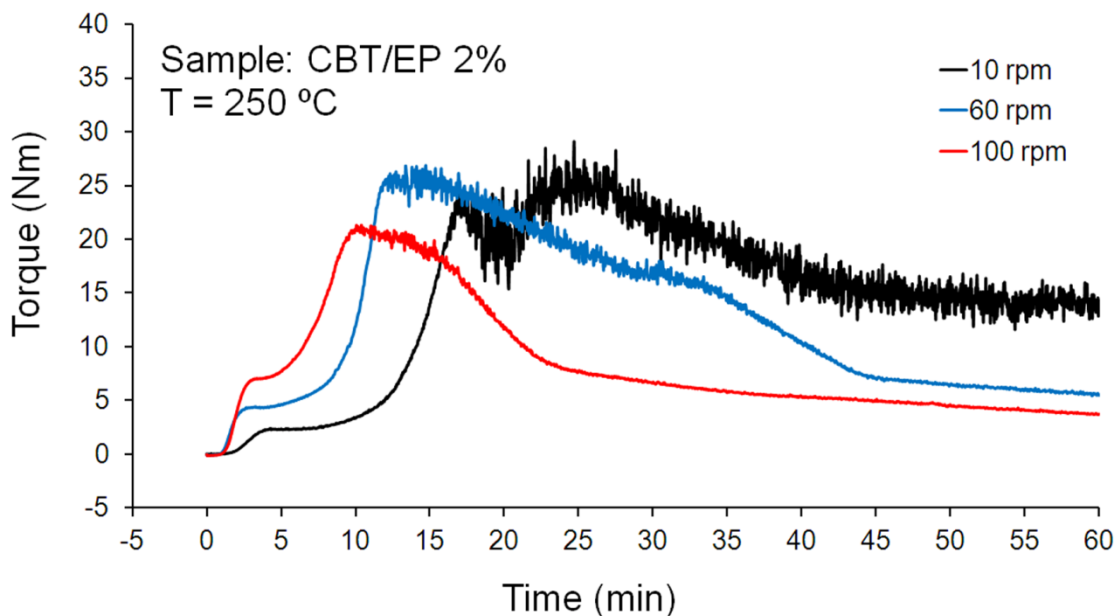


Fig. 8.5: Influence of screw speed on the polymerization kinetics

Considering the above, a polymerization time of 20 min (dashed line, fig. 8.3) was chosen for the compression moulding process in order to assure a complete chain extension reaction. Samples polymerized in the hot plate press were used for analysis, because the aim was to produce sheets using a one-step process. For this reason, no further effort was made to analyze the samples prepared in the batch mixer. Samples polymerized in the hot plate press were analysed instead.

### 8.5.2 GPC analysis

Neat pCBT as well as chain-extended pCBT/EP samples produced by *in situ* polymerization during compression moulding were analysed by GPC and gel content determination; results are shown in table 8.3. The chain-extended pCBT/EP samples may be partly crosslinked, especially at higher EP contents.

No insoluble fraction was detected for samples with 0%, 1% and 2% epoxy content. However, samples pCBT/EP 3% and pCBT/EP 4% contained 37% and 63% of insoluble fraction, respectively.

The molecular weight determined by GPC provides an acceptable estimation of the molecular weight increase of pCBT/EP samples. Nevertheless, analysis of branched polymers using a calibration based on linear polymer standards may result in errors. This is due to the fact that the separation is based on the hydrodynamic volume of a polymer. Since linear and branched polymers of equal molecular weight occupy different hydrodynamic volumes, their measured molecular weight will be different and thus the obtained molecular weights of the chain-extended samples may be lower than the true values [4].

Unmodified pCBT exhibited a remarkably low molecular weight, as also evidenced by its low torque response (*c.f.* figure 8.3). The reason therefore may be a reduced polymerization due to humidity in ambient atmosphere. The polydispersity index (PDI) of pCBT was close to the theoretical PDI of 2.0, typical for ring-opening polymerizations [14-15]. The molecular weight of pCBT/EP 1% was found to be only slightly higher compared to that of neat pCBT. However, the molecular weight distribution broadened considerably. This confirms the low degree of chain extension reaction, as also shown by the torque *versus* time measurements.

A dramatic increase in both molecular weight and distribution was found for pCBT/EP 2%. The weight-average molecular weight and the PDI were three times higher compared to that of neat pCBT (see table 8.3). This high molecular weight is reflected in the high melt viscosity of CBT/EP 2% after the chain extension reaction (figure 8.3). Regarding pCBT/EP 3%, both PDI and molecular weight further increased to values which were *ca.* 5 times higher compared to neat pCBT. When the epoxy content was 4 wt%, the MW decreased to a value much lower than the samples containing 2 and 3 wt.% EP, but still higher than neat pCBT. Also, the PDI slightly decreased with respect to pCBT/EP 3%.

This drop in molecular weight is also well reflected in the steep decrease of the torque response of CBT/EP 4% after reaching the maximum torque, as discussed above. These results confirm the above stated assumption made from the torque curves that the highest molecular weight pCBT was found for blends containing 2 and 3 wt.% EP.

The degree of conversion ($\alpha$) from oligomers to polymer was calculated from the peak areas of the GPC traces as described in section 5.3.3. Neat pCBT showed a conversion of 96.6% which is in agreement with reported values and also with the equilibrium oligomer content of PBT, 1–3% [14, 16]. No oligomers were detected in the GPC trace of pCBT/EP 1%, which suggests a full conversion to pCBT. Higher EP contents slightly decreased the degree of conversion (*c.f.* table 8.3). Though the diepoxide apparently acted as a promoter for the ring-opening polymerization, it did not significantly change the degree of conversion. These results clearly demonstrate that the diepoxide is an effective chain extender for CBT with an apparent maximum molecular weight up to 100 kg/mol when 3 wt.% diepoxide is used.

Table 8.3: GPC results and gel contents of compression moulded pCBT and pCBT/EP samples

| Sample | $M_w$ [kg/mol] | $M_n$ [kg/mol] | PDI [-] | Gel content [%] | Conversion $\alpha$ [%] |
|---|---|---|---|---|---|
| pCBT | 22.6 | 10.0 | 2.26 | 0 | 96.6 |
| pCBT/EP 1% | 23.7 | 6.5 | 3.65 | 0 | 100 |
| pCBT/EP 2% | 65.0 | 9.4 | 6.96 | 0 | 92.0 |
| pCBT/EP 3% | 104.0 | 8.5 | 12.15 | 37 | 95.5 |
| pCBT/EP 4% | 32.0 | 3.3 | 9.78 | 63 | 95.4 |

### 8.5.3 Proton NMR analysis

^{1}H NMR analysis was conducted to analyse the structure of the diepoxide, pCBT as well as chain extended pCBT/EP prepared by compression moulding. The chemical structures and the corresponding spectra are depicted in figure 8.6. Protons in the pCBT sequence

are labelled with numbers. Protons belonging to the diepoxide sequence are labelled with letters.

Regarding pCBT, the signal at 1.9 ppm is assigned to shielded methylene protons (2), the one at 4.4 ppm is assigned to oxymethylene protons (1) and the peak at 8.0 ppm is assigned to the aromatic protons (3) [10]. Peaks belonging to the diepoxide are assigned as follows: Aromatic protons of the Bisphenol A moieties (c, d) show peaks at 6.8 ppm and 7.1 ppm, respectively. Peaks at 3.9 ppm and 4.2 ppm are assigned to methylene protons attached to oxygen (e) whereas the peak at 3.3 ppm and the doublet at 2.9 ppm and 2.7 ppm are assigned to the glydidyl functional group (f, g).

The peaks around 4.7–4.8 ppm came from an esterification of the glydidyl functional groups with the carboxyl end groups of pCBT (a), resulting in ester groups ($R_1$-CO-O-$R_2$). Unfortunately, the corresponding signal of the formed ester group partially overlaps with the peak of $-OCH_2$ of pCBT. Nevertheless, one may conclude that the esterification is the predominant reaction mechanism. Peaks at 5.7 ppm suggest a connectivity of CH with an ester group (b). This leads to the assumption that some of the carboxyl end groups of pCBT are linked (*via* direct esterification) to the secondary hydroxyl groups previously formed during chain extension. The proposed connectivity can be seen as a branch point in the backbone of a chain extended pCBT molecule. Recall that some gel formation was detected in pCBT/EP samples containing more than 2 wt.% of EP, supporting this branching hypothesis.

The presence of glycidyl functional groups in both pCBT/EP 2% and pCBT/EP 4% indicate that not all the epoxy groups have reacted with the pCBT and unreacted diepoxide was dissolved in the pCBT matrix. Note that the corresponding signals of unreacted epoxy resin in the sample containing 2 wt.% EP are weak. The amount of unreacted epoxy groups was calculated to be 17.5 mol% and 32.5 mol% for pCBT/EP 2% and pCBT/EP 4%, respectively. The calculation of the theoretical amount of chain extender according to equation 9.1 is not applicable due to the varying carboxyl content during ROP, as mentioned above. A chain extension mechanism utilizing 2 moles pCBT of $M_n = 10,000$ g/mol (as polymerized in the hot plate press, measured by GPC) and 1 mol epoxy resin of 361 g/mol (as determined by NMR) results in a theoretical amount of 1.8 wt.% epoxy resin, assuming that only carboxyl and glycidyl groups are involved in the reaction.
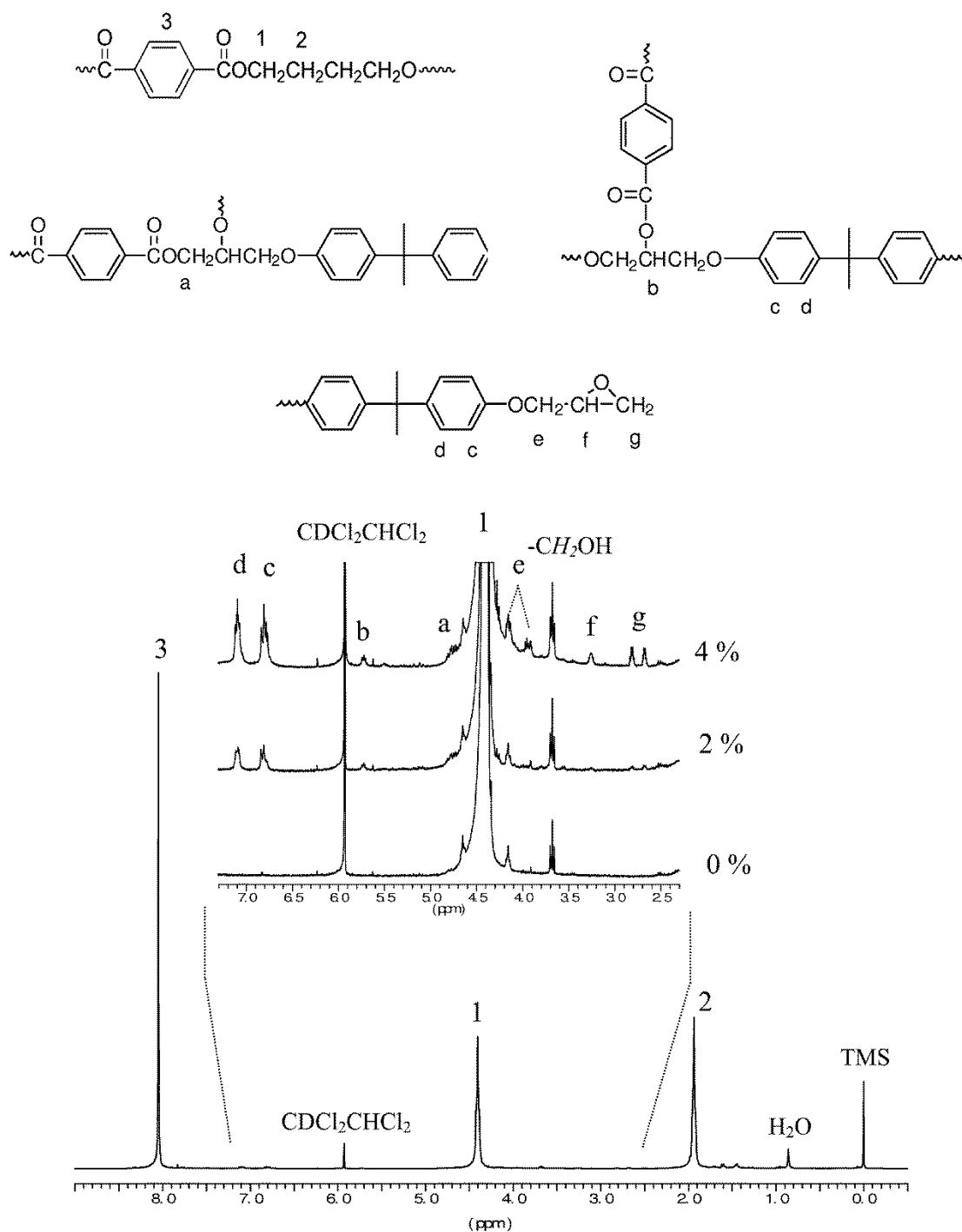
Fig. 8.6: ^{1}H NMR spectrum of pCBT/EP 2%. Inset ^{1}H NMR spectra of pCBT and pCBT/EP samples in the 2.3–7.3 ppm region with peak assignments

### 8.5.4 DSC analysis

The compression moulded samples were analysed in a DSC scan using heating and cooling rates of 10 and -30 °C/min, respectively. The second heating and cooling runs are illustrated in figures 8.7 and 8.8 and the thermal properties are collected in table 8.4.

Neat pCBT exhibits a double melting peak which consists of a small peak at 213 °C and a major peak at 225 °C. Multiple melting peaks are typical for polyesters, including pCBT. They are attributed to melting and recrystallization processes of less perfect crystallites into thicker crystalline structures with a subsequent melting at the polymer´s melting temperature [17-19]. The neat pCBT crystallises during cooling at 184 °C and the crystallinity obtained from the second cooling scan was found to be 32%, as discussed earlier.
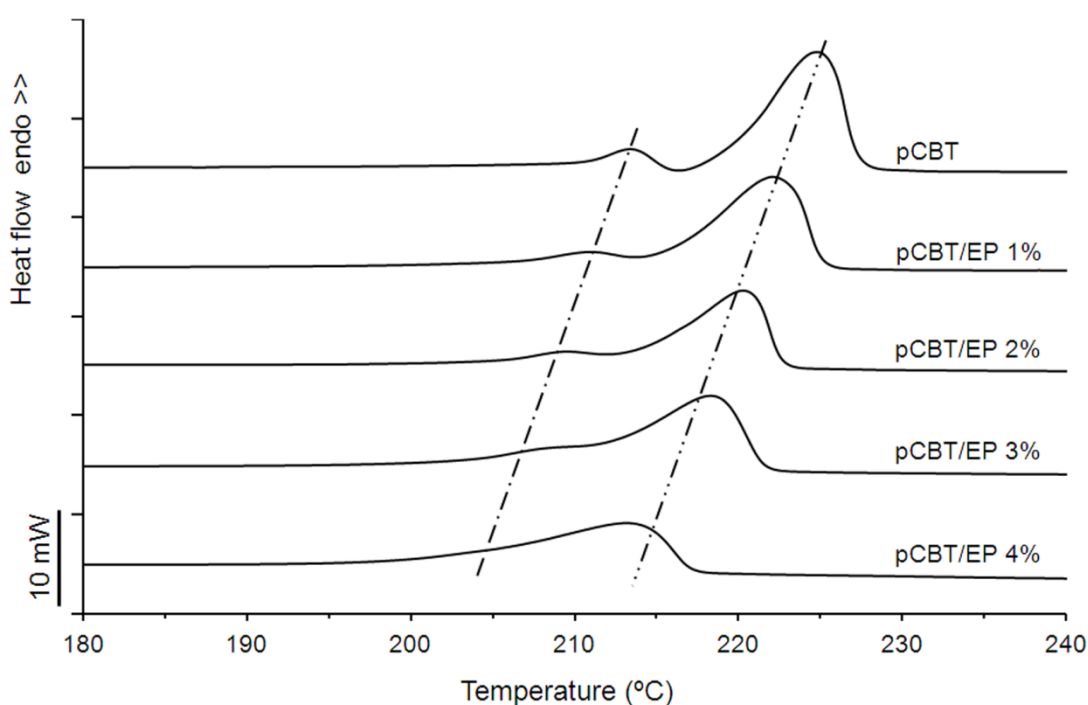


Fig. 8.7: DSC second heating scan of pCBT and pCBT/EP samples polymerized during compression moulding; DSC heating rate of 10 °C/min and cooling rate of -30 °C/min.
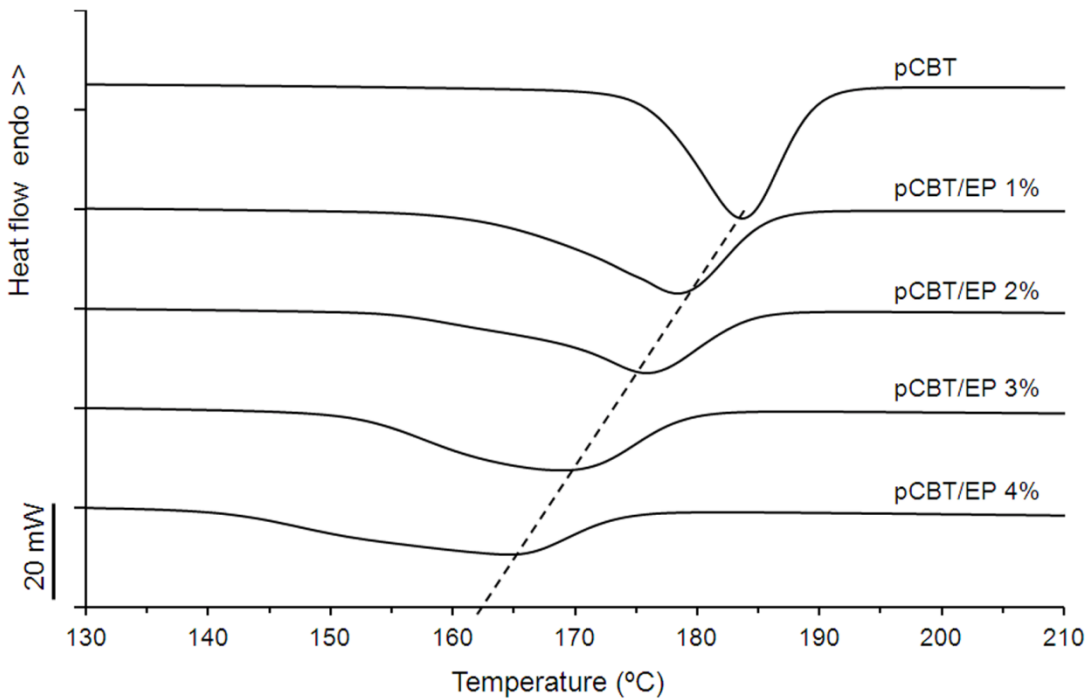
Fig. 8.8: DSC second cooling scan of pCBT and pCBT/EP samples polymerized during compression moulding; DSC heating rate of 10 °C/min and cooling rate of -30 °C/min.

Table 8.4: Thermal properties of compression moulded pCBT and pCBT/EP samples, DSC heating rate of 10 °C/min and cooling rate of 30 °C/min.

| Sample | Second heating | | | Second cooling | | Crystallinity |
|---|---|---|---|---|---|---|
| | $T_{m1}$ | $T_{m2}$ | $\Delta H_{m1+2}$ | $T_c$ | $\Delta H_c$ | $X_c$ |
| | [°C] | [°C] | [J/g] | [°C] | [J/g] | [%] |
| pCBT | 213.4 | 224.8 | 45.2 | 183.9 | -48.8 | 31.8 |
| pCBT/EP 1% | 210.8 | 222.1 | 36.7 | 178.6 | -40.8 | 25.8 |
| pCBT/EP 2% | 209.3 | 220.2 | 34.3 | 176.0 | -38.0 | 24.2 |
| pCBT/EP 3% | 207.9 | 218.4 | 35.5 | 168.6 | -37.4 | 25.0 |
| pCBT/EP 4% | – | 213.2 | 29.8 | 164.5 | -36.4 | 21.0 |
| pCBT/EP 0.5%-MB | 213.9 | 222.9 | 41.6 | 178.2 | -43.7 | 29.3 |
| pCBT/EP 1.0%-MB | 213.5 | 222.0 | 40.4 | 178.1 | -45.5 | 28.5 |
| pCBT/EP 1.5%-MB | 212.6 | 223.7 | 37.5 | 175.7 | -42.8 | 26.4 |

As far as chain extended pCBT is concerned, it can be observed that the melting endotherms as well as the crystallization exotherms progressively shifted towards lower temperatures and increasingly broaden with increasing epoxy content (*c.f.* figures 8.7 and 8.8). The broadening of the melting peaks suggests a broadening of the crystallite size distribution. The depression of the melting temperature is due to the chain extension reaction. With increasing epoxy content, branching and crosslinking takes place. Side branches are thought to be defects which disrupt the local chain symmetry. As a consequence, crystallization rates are decreased which results in a decreased degree of crystallinity [20]. Moreover, the lamellar thickness is reduced, which in turn causes a decrease in melting and crystallization temperatures [4, 6, 19, 21]. At a high epoxy content of 4 wt.%, the two melting endotherms merge together and only one broad melting peak can be observed. This is explained by the hindered recrystallization process of less perfect crystallites below the final polymer melting temperature. The crystal fraction decreased by 10% when pCBT contained 4 wt.% EP.

Regarding the samples prepared by melt blending, a similar tendency can be observed in table 8.4. Melting temperatures and enthalpies as well as crystallization temperatures and enthalpies decreased with increasing epoxy content, though to a less pronounced extent as compared to compression moulded samples with higher amount of epoxy resin.

### 8.5.5  WAXS analysis

A possible influence of the chain extension reaction on the crystal structure of pCBT/EP was studied by means of X-ray diffraction; the diffraction patterns of neat pCBT, pCBT/EP 2% and pCBT/EP 4% are illustrated in figure 8.9.

No significant difference between unmodified and EP-modified pCBT samples was found. The decreasing crystal fraction with increasing EP content is well reflected in the decreasing peak height of the diffraction patterns. As already discussed in section 6.4.5, PBT and hence pCBT exhibit two triclinic polymorphs, the $\alpha$ form being the stable polymorph under standard conditions whereas the $\beta$ form is only observed under stretching of unoriented crystals. Once again, the crystallographic reflection from the ($\bar{1}$ 04)

plane was used to determine the crystal phase of pCBT. This reflection is observed around $2\theta$ = 31.3–31.4° for both unmodified and EP-modified pCBT samples. Therefore it can be concluded that epoxy-modified samples exhibit $\alpha$ crystal structure.
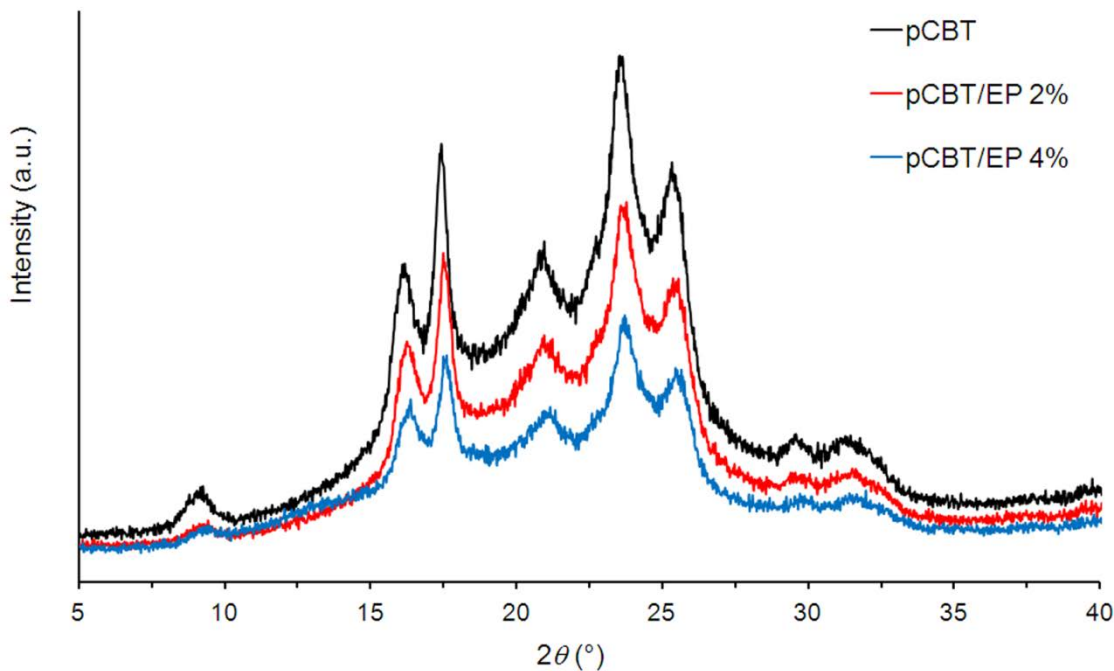


Fig. 8.9: WAXS diffraction patterns of pCBT and pCBT/THF.

### 8.5.6  DMTA analysis

The dynamic mechanical properties of the pCBT/EP samples obtained from compression moulding were determined with DMTA. For clarity only neat pCBT and chain extended pCBT containing 2 and 3 wt.% are shown in figures 8.10a and b. The $\beta$- and $\gamma$-transition temperatures and the storage moduli at 0 °C are collected in table 8.5.

Three different relaxations can be seen in neat pCBT. The melting transition of pCBT homopolymer is ~225 °C, commonly referred to as the $\alpha$ transition. The glass transition of the amorphous phase is termed $\beta$ relaxation and the sub-$T_g$ relaxation is denoted as $\gamma$ [22]. It was suggested that the $\gamma$ relaxation of pCBT may be a secondary relaxation due to the motion of the $-O-(CH_2)_4-O-$ group, the glycol (OH) residue in the amorphous phase or the

carbonyl (COO) residue [17]. The $T_g$ of neat pCBT was found to be 66 °C which is an intermediate value between the glass transitions reported in [23] and [17]. The sub-$T_g$ relaxation was found to be -83 °C, considerably higher than the one reported by Liu et al. [17].

Regarding the chain extended pCBT, a single glass transition can be observed, indicating miscibility of pCBT and EP, which corresponds to the miscibility of PBT and epoxy resin [13, 24]. It can be seen that the $\beta$-relaxation temperature ($T_g$) decreased with increasing epoxy content (*c.f.* table 8.5). It is known that the glass transition temperature of pCBT and PBT increases with increasing crystallinity [22-23]. Since the degree of crystallinity of pCBT/EP decreased with increasing EP content, the $\beta$-relaxation temperature decreased as well. Kulshreshtha and co-workers [13] and Zhang *et al.* [24] found in PBT/epoxy blends with high epoxy contents that the epoxy did not react completely with PBT; the excess EP acted as a solvent. Therefore, the decrease in the $\beta$-relaxation temperature of the pCBT/EP samples was partly attributed to a plasticizing effect of the dissolved excess of epoxy resin which had not reacted with pCBT, as confirmed by ^{1}H NMR analysis. Nevertheless, the amount of unreacted epoxy resin was low, so the expected plasticizing effect was believed to be negligible. Finally, the influence of branching on the $\beta$- and $\gamma$-relaxation of the pCBT/EP systems should be taken into account since gel content determination of the pCBT/EP samples indicated an increasing gel formation at high EP content. The influence of both long-chain branching (LCB) and short-chain branching (SCB) on the $T_g$ is complex. LCB typically increases the degree of crystallinity due to co-crystallization of the side branches. Since a decreasing crystallinity with increasing EP content was observed, only SCB can be considered. Short-chain branching increases the free volume and thus decreases the glass transition temperature, as reported for poly(butylene succinate), poly(ethylene adipate) and other aliphatic polyesters [4].

Therefore the decrease in the $\beta$-relaxation temperature with increasing epoxy content may be due to the sum of all three effects: A decrease in crystallinity, a plasticizing effect of the unreacted epoxy resin, and branching.
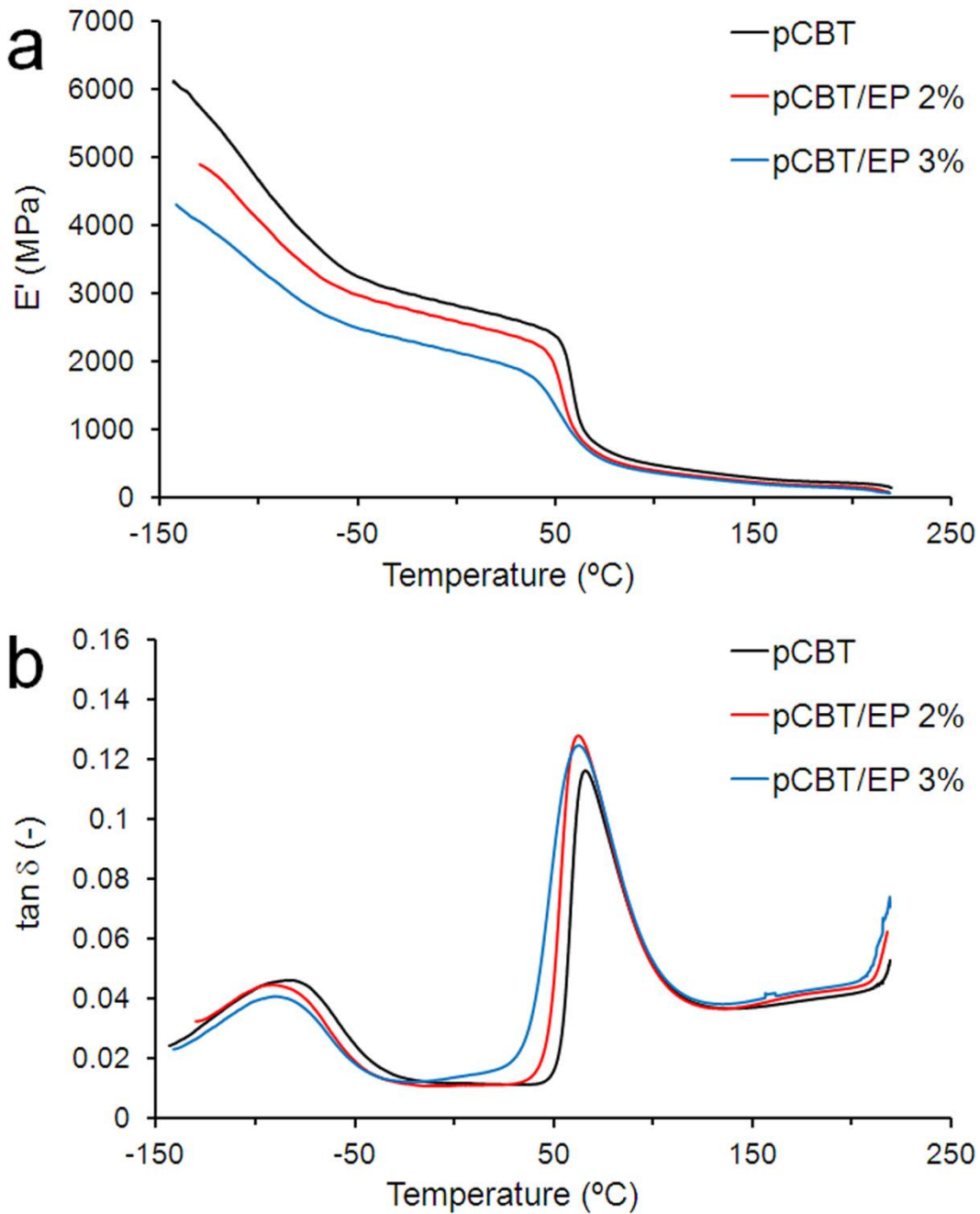
Fig. 8.10: DMTA plot of (a) E' and (b) tan $\delta$ *versus* temperature of compression-moulded pCBT and pCBT/EP samples

As far as the $\gamma$-relaxation of the chain extended samples is concerned, no clear influence of epoxy content can be observed. The $\gamma$-relaxation temperature decreased ~11 °C when 2 wt.% of epoxy resin was added. Further addition of EP led to an increase in the $\gamma$-relaxation temperature.

Table 8.5:  DMTA storage moduli at 0 °C, $\gamma$- and $\beta$-transition temperatures of compression moulded pCBT and pCBT/EP samples, heating rate of 2 °C/min

| Sample | Storage modulus at 0 °C [MPa] | $\gamma$-transition [°C] | $\beta$-transition [°C] |
|---|---|---|---|
| pCBT | 2810 | -82.9 | 65.7 |
| pCBT/EP 1% | 2072 | -88.4 | 67.9 |
| pCBT/EP 2% | 2591 | -94.2 | 62.3 |
| pCBT/EP 3% | 2142 | -92.9 | 62.6 |
| pCBT/EP 4% | 2209 | -86.6 | 60.3 |

Literature suggests that the $\gamma$ transition remains relatively unaffected by the degree of crystallinity [22]. The storage modulus (E') curves of the pCBT/EP samples were lower than the pCBT reference curve. Interestingly, the storage moduli *versus* temperature of the samples containing 1, 3 and 4 wt.% EP were similar to each other (not shown here). The lower stiffness of the chain extended samples was more pronounced at low temperature and diminished above $T_g$. This decrease in stiffness may be attributed to the lower degree of crystallinity of the pCBT/EP samples, as crystallites act as rigid fillers and crosslinks for amorphous segments [17].

### 8.5.7  Tensile properties

Tensile tests were performed on compression moulded and melt blended pCBT/EP samples, the obtained tensile properties are presented in table 8.6. Neat pCBT failed in a brittle manner without yielding and neck formation with an average elongation at break of 7%. In comparison, all tested EP concentrations were found to have increased elongation at break. More than half of all tested pCBT/EP specimens showed neck formation in tensile tests. Brittle failure without necking of compression moulded pCBT/EP specimens may be explained by inhomogeneities in the CBT/EP blends prior to polymerization due to the low mixing efficiency of the blend preparation. As the diepoxide content in the CBT/EP blends increased, more CBT got in contact with epoxy resin and could react in the

subsequent compression moulding process. This is reflected in the increasing percentage of yielded specimens with increasing EP content (see table 8.6). It was also observed that many of the toughened pCBT/EP specimens showed the onset of necking. However, necking did not proceed due to premature failure. For compression moulded samples, the maximum elongation at break of 49% was observed for samples containing 2 wt.% of diepoxide.

Regarding the melt blended samples, it can be seen that relatively smaller amounts of EP resin resulted in a considerably higher toughness. The sample pCBT/EP 1.0%-MB exhibited the highest toughness in terms of failure strain and strain energy of all tested epoxy-modified samples. This may be explained by the fact that the melt blending processing route accounts for higher molecular weight pCBT and better mixing capability with EP resin as compared to the compression moulding processing route. A higher molecular weight pCBT requires less amount of EP resin for the chain extension reaction, thus a good toughness is already achieved with 1 wt.% of EP resin.

Table 8.6: Tensile properties of neat pCBT and pCBT/EP obtained by compression moulding

| Sample | Tensile modulus [GPa] | Tensile strength [MPa] | Elongation at break [%] | Strain energy [MJ/m$^3$] | Percentage yielded samples* [%] |
|---|---|---|---|---|---|
| pCBT | 2.8 ± 0.4 | 57 ± 5 | 7 ± 3 | 1.3 ± 0.4 | 0 |
| pCBT/EP 1% | 2.9 ± 0.1 | 57 ± 1 | 12 ± 9 | 5.9 ± 3.8 | 60 |
| pCBT/EP 2% | 2.8 ± 0.1 | 62 ± 1 | 49 ± 25 | 21.5 ± 10.5 | 80 |
| pCBT/EP 3% | 2.9 ± 0.2 | 60 ± 1 | 11 ± 6 | 5.4 ± 2.8 | 94 |
| pCBT/EP 4% | 2.7 ± 0.2 | 56 ± 2 | 11 ± 7 | 5.2 ± 3.1 | 94 |
| pCBT/EP 0.5%-MB | 2.9 ± 0.4 | 61 ± 3 | 58 ± 33 | 22.8 ± 10.6 | 88 |
| pCBT/EP 1.0%-MB | 3.3 ± 0.5 | 63 ± 1 | 118 ± 75 | 51.9 ± 34.1 | 100 |
| pCBT/EP 1.5%-MB | 2.7 ± 0.4 | 61 ± 1 | 89 ± 40 | 45.7 ± 20.8 | 100 |

*A specimen was defined to have yielded if a yield point with subsequent necking was detected

### 8.5.8  Tensile impact properties

Tensile impact tests were performed on pCBT and epoxy-modified pCBT samples; representative tensile-impact stress versus time curves are displayed in figure 8.11 and impact data is shown in table 8.7.
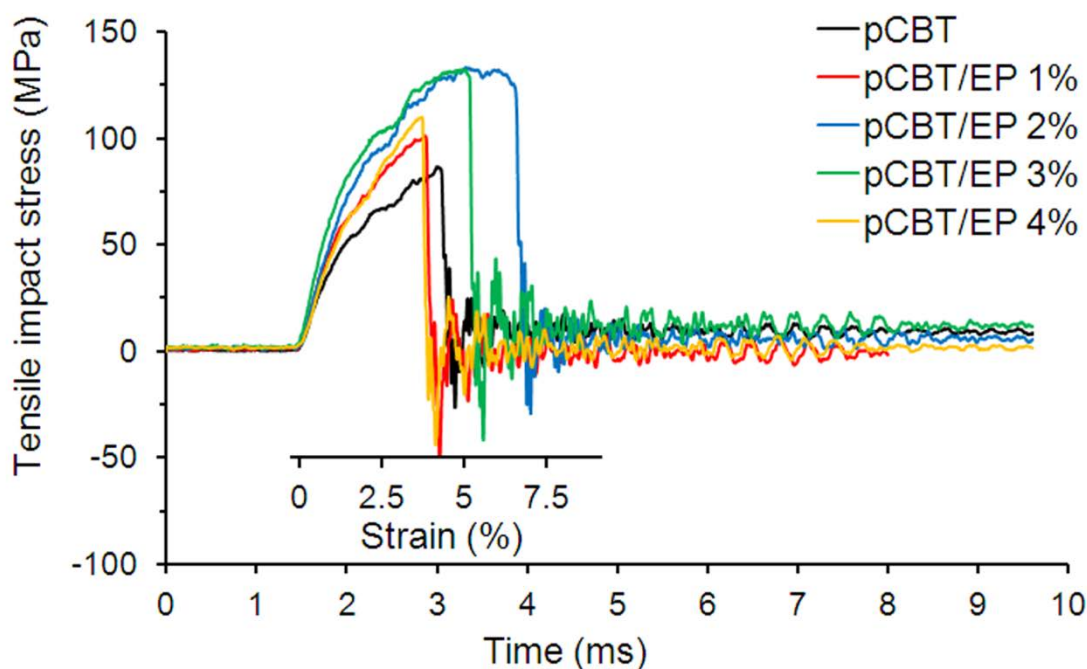


Fig. 8.11: Representative tensile impact stress *versus* time/strain curves of pCBT and epoxy-modified pCBT at $v = 1.5$ m/s.

Similar to what was discussed in sections 6.4.9 and 7.5.10, pCBT fractured in a brittle fashion whereas the epoxy-modified samples containing 2 and 3 wt.% EP resin, respectively, exhibited yielding. Tensile-impact strength was 149 kJ/m$^2$ for unmodified pCBT and increased to 273 and 267 kJ/m$^2$ when samples were modified with 2 and 3 wt.% EP (*c.f.* table 8.7).

It is noteworthy to mention that the epoxy-modified samples were tested one year after their preparation. This clearly demonstrates the long-term toughening action of the epoxy modification as compared to the diminishing toughness with time of the THF-modified samples.

Table 8.7: Tensile impact properties of pCBT and compression moulded pCBT/EP

| Sample | Tensile-impact strength [kJ/m$^2$] | Tensile impact stress max. [MPa] |
|---|---|---|
| pCBT | 149 ± 71 | 86 ± 4 |
| pCBT/EP 1% | 117 ± 21 | 98 ± 3 |
| pCBT/EP 2% | 273 ± 28 | 130 ± 10 |
| pCBT/EP 3% | 267 ± 18 | 126 ± 6 |
| pCBT/EP 4% | 112 ± 65 | 99 ± 8 |

### 8.5.9  SEM analysis

SEM analysis was conducted to study the morphology of the compression moulded pCBT/EP samples. Micrographs of neat pCBT are provided in figure 8.12 (a) and (b) whereas the ones of pCBT/EP 2% are shown in figure 8.12 (c) and (d).

No significant difference in morphology between neat pCBT and the chain extended samples could be detected. As epoxy resin is miscible with pCBT, a single phase (corresponding to pCBT matrix) was observed in all samples. When CBT is polymerized into pCBT, it does not reach a 100% conversion. This is due to the fact that molten polyesters undergo ring-chain equilibrium reactions and therefore contain an equilibrium content of cyclic oligomers of about 1–3% [14-15, 25-26]. These remaining CBT oligomers form platelet-like or prismatic crystals with sizes up to a few microns upon cooling from the melt [15, 27]. SEM analysis revealed the presence of few CBT oligomer crystals in neat pCBT as well as in the chain extended samples. The amount of these oligomer crystals appeared similar in all analysed samples, as the degree of conversion was found to be relatively unaffected by the diepoxide (as determined by GPC).

The oligomer crystals act as a rigid filler and may therefore contribute to the inherent brittleness of unmodified pCBT. Furthermore, the micrographs of neat pCBT (*c.f.* figure 8.12 b) suggest a poor interfacial adhesion between pCBT matrix and CBT oligomer crystals. On the other side, the oligomer crystals present in pCBT/EP 2% (see figure 8.12 d) appear to be covered with polymer matrix, indicating an improved interfacial adhesion

between pCBT/EP matrix and the oligomer crystals. This finding also may contribute to the toughening mechanism observed in pCBT/EP samples.
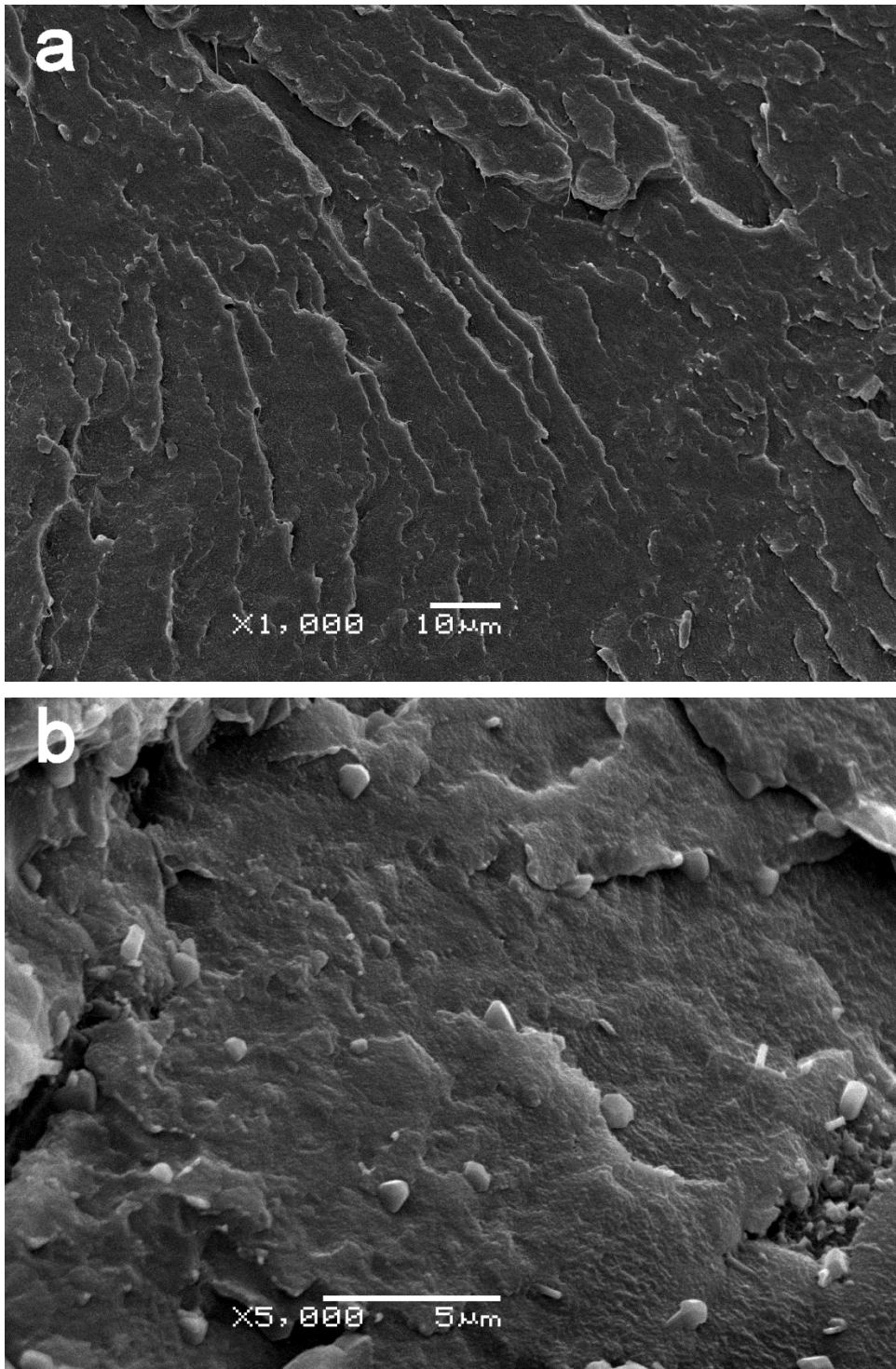


Fig. 8.12: SEM micrographs of compression moulded neat pCBT ((a) and (b)) and pCBT/EP 2% ((c) and (d)).
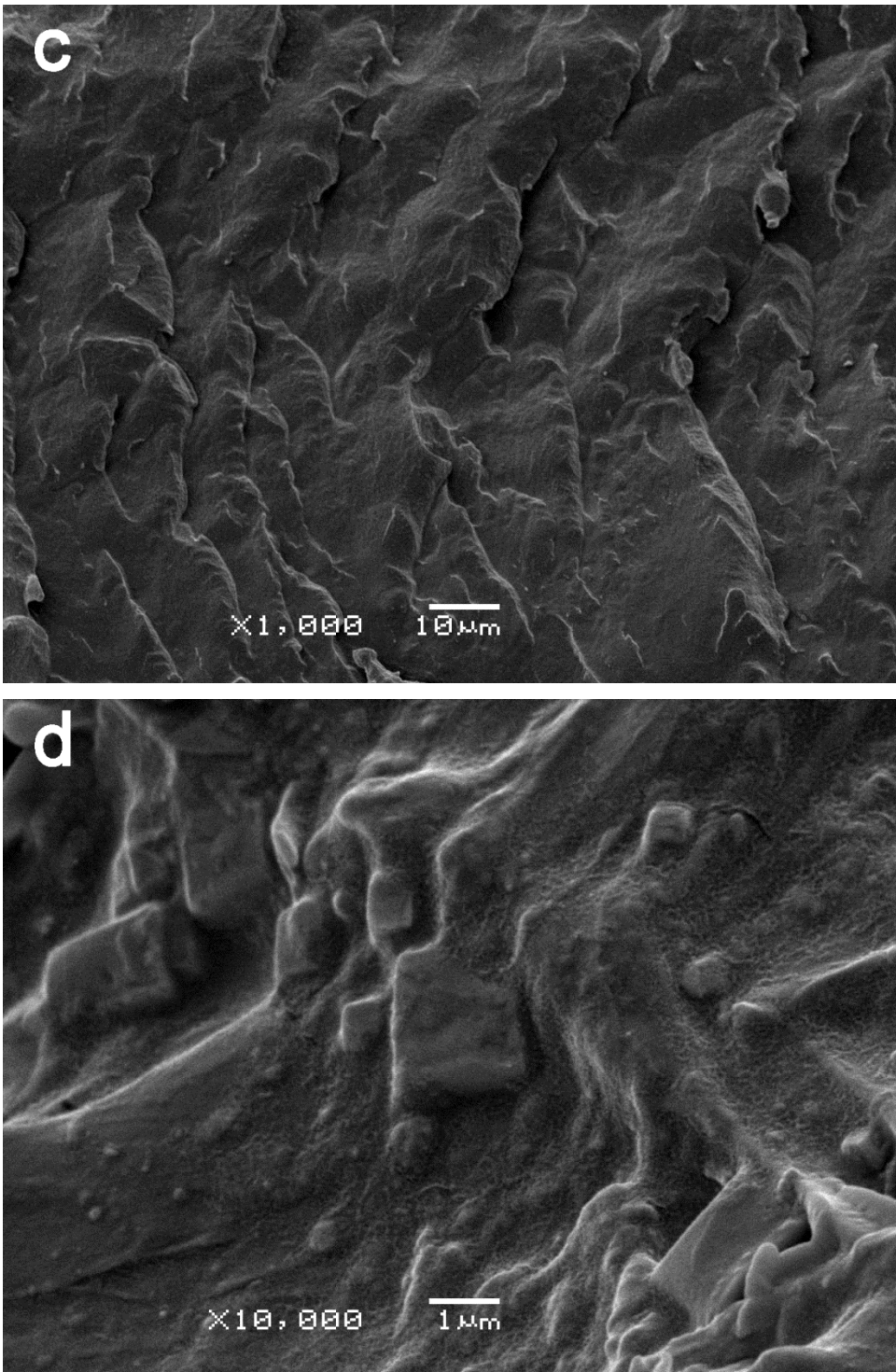
Fig. 8.12: SEM micrographs of compression moulded neat pCBT ((a) and (b)) and pCBT/EP 2% ((c) and (d)). (*continued*)

**Solvent-induced crystallization of CBT**

The fracture surfaces of epoxy-modified samples were etched in THF at room temperature for 15 min and then subjected to SEM analysis with the aim to study a possible migration of unreacted EP resin out of the pCBT matrix; micrographs of the etched samples are provided in figures 8.13 (a)–(f).

No signs of EP migration such as holes or additional phases can be found, but a very interesting and aesthetic phenomenon was observed instead, namely the solvent-induced crystallization (SINC) of CBT. During the solvent exposure, precipitation of CBT oligomers occurred on the fracture surface of pCBT. The precipitated CBT formed oligomer crystals due to the SINC phenomenon. These SINC-induced CBT oligomer crystals were flower-like, with needle-like protrusions growing out of the centre, as shown for instance in figures 8.13 (a),(d) and (f). The here observed solvent-grown oligomer crystals resemble the PET oligomer crystals reported by Burch *et al.* [28], as shown in section 2.3.1.

Unmodified pCBT and pCBT/EP 1% did not show these SINC-induced CBT oligomer crystals but the latter appeared at an EP content of 2 wt.% and apparently increased in number with increasing EP content. Recall from GPC analysis that the samples containing 2–4 wt.% EP exhibited a rather low degree of conversion, namely $\alpha$ = 92–96%. The relatively high amount of unpolymerized CBT in these samples gives rise to oligomer precipitation and solvent-induced crystallization on the fracture surface.
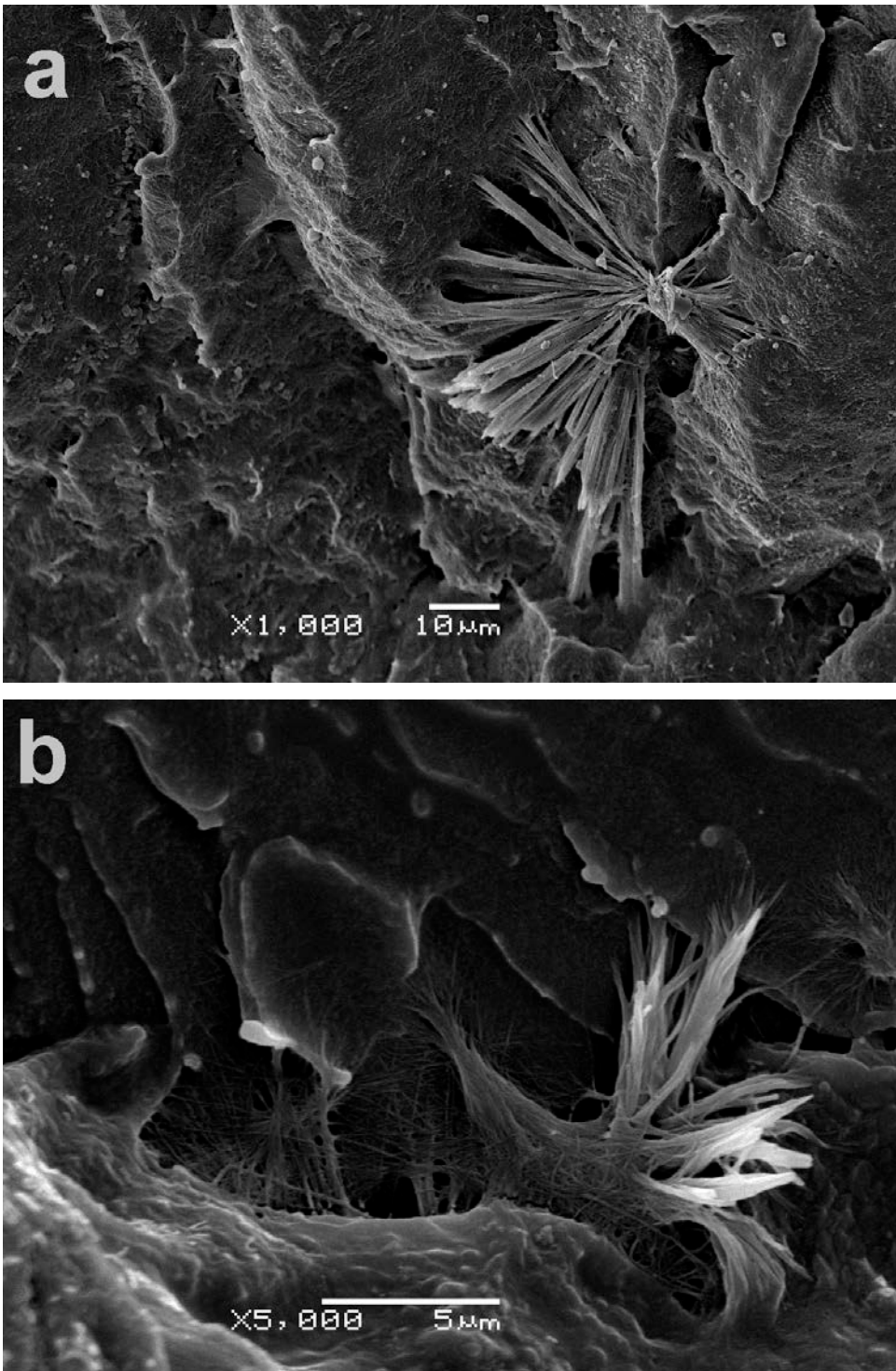
Fig. 8.13: SEM micrographs of compression moulded pCBT/EP 2% (a and b), pCBT/EP 3% (c and d) and pCBT/EP 4% (e and (f) after etching in THF at room temperature for 15 min.
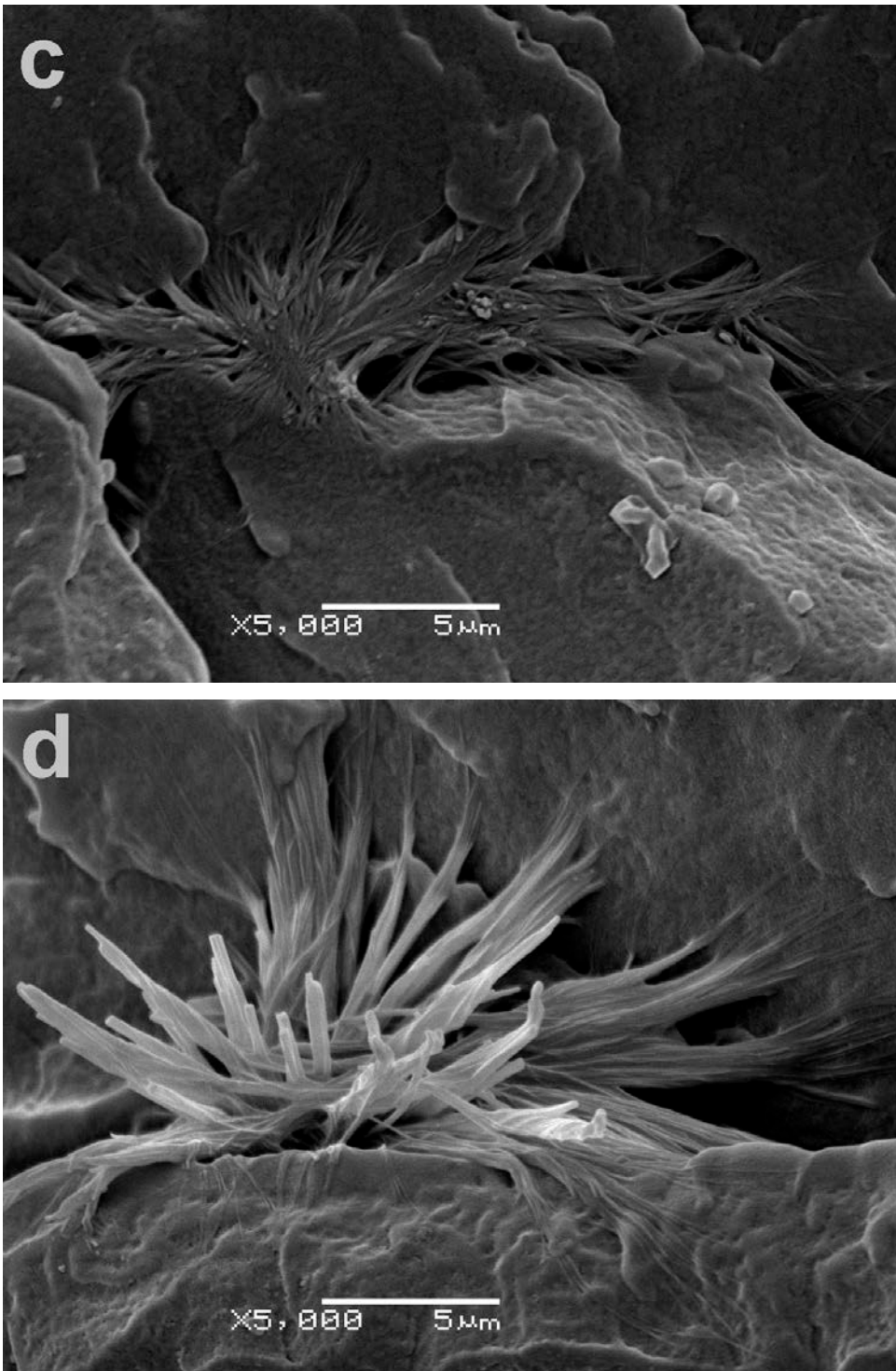
Fig. 8.13: SEM micrographs of compression moulded pCBT/EP 2% (a and b), pCBT/EP 3% (c and d) and pCBT/EP 4% (e and (f) after etching in THF at room temperature for 15 min. (*continued*)
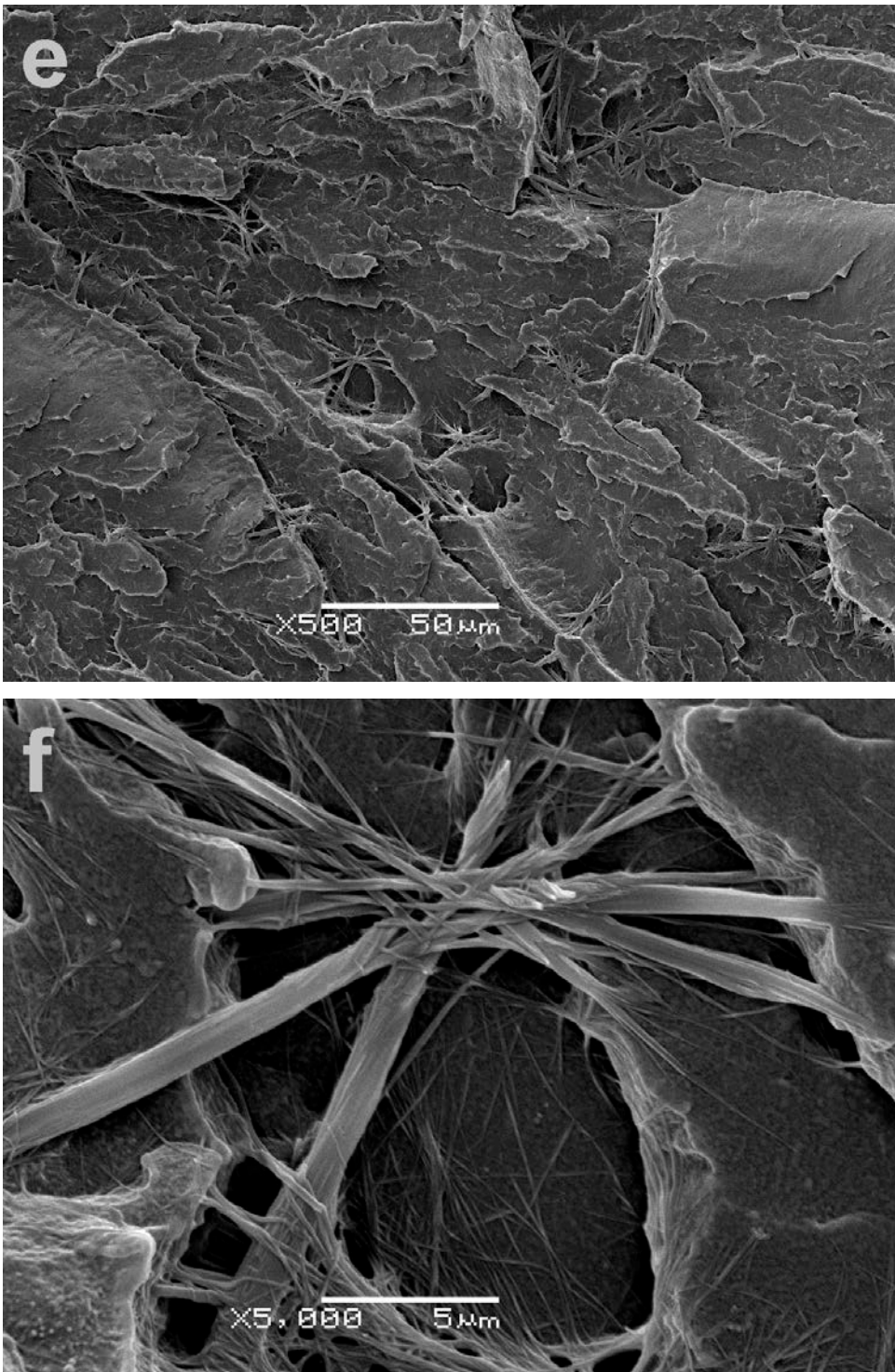
Fig. 8.13: SEM micrographs of compression moulded pCBT/EP 2% (a and b), pCBT/EP 3% (c and d) and pCBT/EP 4% (e and (f) after etching in THF at room temperature for 15 min. (*continued*)

## 8.6 Conclusions

Toughening of polymerized cyclic butylene terephthalate has been achieved by reactive chain extension with a bifunctional epoxy resin. The chain extension reaction was conducted in a Brabender batch mixer in order to determine the polymerization time for the compression moulding process. An optimum polymerization time of 20 min at 250 °C was deducted from these torque *vs.* time measurements and CBT/EP blends with small amounts (1 to 4 wt.%) of diepoxide were compression moulded under the obtained processing conditions. Tensile and tensile impact tests were performed on the compression moulded pCBT/EP samples and an increase in toughness was observed for all chain extended samples. A seven-fold strain at break was found for a diepoxide content of 2 wt.%, compared to that of neat pCBT. Stiffness and strength was not significantly affected by the epoxy resin and the tensile-impact strength also improved substantially.

Moreover, CBT was chain extended with EP during melt blending. Apparently, a higher molecular weight PCBT was achieved with the melt blending processing route and consequently the amount of EP could be reduced to 1 wt.% in order to effectively toughen the pCBT; failure strain increased to well above 100%.

GPC analysis confirmed the low molecular weight of unmodified pCBT, a possible explanation for brittleness. GPC also showed the remarkable increase in molecular weight when 2 or 3 wt.% epoxy resin was used. Moreover, the degree of conversion from CBT oligomers to pCBT polymer was not significantly affected by the epoxy resin. The diepoxide substantially reacts with the carboxyl end groups of pCBT in an esterification reaction and yields a predominantly linear polymer, as suggested by ^{1}H NMR. Gel content determination of the pCBT/EP samples on the other hand showed some gel formation for higher EP contents, indicating a partially branched and crosslinked structure of the chain extended pCBT. Thermal analysis of the chain extended pCBT revealed a decrease in glass transition, melting and crystallization temperature, and degree of crystallinity with increasing epoxy content. This was mainly attributed to decreased crystallinity, branching, and a minimal plasticizing effect of unreacted epoxy resin. SEM micrographs suggested a more favourable adhesion of remaining oligomer crystals to the pCBT matrix when epoxy resin was used. The improved adhesion may have contributed to the increase in toughness of chain extended pCBT.

Flower-like CBT oligomer crystals were found in some THF-etched pCBT/EP samples with relatively low degree of conversion and it was assumed that this was due to the solvent-induced crystallization phenomenon.

To conclude, it was demonstrated that low molecular weight, bifunctional epoxy resin is useful to chain extend pCBT and thus to effectively and permanently toughen the inherently brittle pCBT. Moreover, the proposed chain extension mechanism does not produce any by-products. Recall from section 2.2 that this is a requirement for liquid composite moulding of CBT using closed moulds. Therefore, this toughening method is suitable for closed mould applications.

## 8.7    References for pCBT/EP

1.    Abt, T, Sánchez-Soto, M, and Martínez de Ilarduya, A. Toughening of in-situ polymerized cyclic butylene terephthalate by chain extension with a bifunctional epoxy resin. European Polymer Journal **48**, 163-171 (2012).

2.    Bikiaris, DN and Karayannidis, GP. Chain extension of polyesters PET and PBT with two new diimidodiepoxides. II. Journal of Polymer Science Part A: Polymer Chemistry **34**(7), 1337-1342 (1996).

3.    Fenouillot, F, Hedreul, C, Forsythe, J, and Pascault, J-P. Reaction and miscibility of two diepoxides with poly(ethylene terephthalate). Journal of Applied Polymer Science **87**(12), 1995-2003 (2003).

4.    McKee, MG, Unal, S, Wilkes, GL, and Long, TE. Branched polyesters: recent advances in synthesis and performance. Progress in Polymer Science **30**(5), 507-539 (2005).

5.    Xanthos, M, Young, MW, Karayanndis, GP, and Bikiaris, DN. Reactive modification of polyethylene terephthalate with polyepoxides. Polymer Engineering & Science **41**(4), 643-655 (2001).

6.    Guo, B and Chan, C-M. Chain extension of poly(butylene terephthalate) by reactive extrusion. Journal of Applied Polymer Science **71**(11), 1827-1834 (1999).

7.    Ju, M-Y and Chang, F-C. Polymer blends of PET–PS compatibilized by SMA and epoxy dual compatibilizers. Journal of Applied Polymer Science **73**(10), 2029-2040 (1999).

8.    Sun, SL, Xu, XY, Yang, HD, and Zhang, HX. Toughening of poly(butylene terephthalate) with epoxy-functionalized acrylonitrile–butadiene–styrene. Polymer **46**(18), 7632-7643 (2005).

9.    Aróstegui, A and Nazábal, J. Compatibilization of a poly(butylene terephthalate)/poly(ethylene octene) copolymer blends with different amounts of an epoxy resin. Journal of Applied Polymer Science **91**(1), 260-269 (2004).

10.   Tripathy, AR, Farris, RJ, and MacKnight, WJ. Novel fire resistant matrixes for composites from cyclic poly(butylene terephthalate) oligomers. Polymer Engineering & Science **47**(10), 1536-1543 (2007).

11.   Brunelle, DJ. Method for polymerizing macrocyclic polyester oligomers. U.S. Patent 5,498,651, 1996. 1996.

12.   Takekoshi T., Phelps P.D., Wang Y., and S.J., W. Methods for polymerizing macrocyclic polyester oligomers using catalyst promoters. U.S. Patent Application Publication US 2006/0115666 A1,. 2006.

13.   Kulshreshtha, B, Ghosh, AK, and Misra, A. Crystallization and Equilibrium Melting Behavior of Poly(Butylene Terephthalate)/Epoxy Blends. Journal of Macromolecular Science, Part B **42**(2), 307-323 (2003).

14.   Brunelle, DJ, Bradt, JE, Serth-Guzzo, J, Takekoshi, T, Evans, TL, Pearce, EJ, and Wilson, PR. Semicrystalline Polymers via Ring-Opening Polymerization: Preparation and Polymerization of Alkylene Phthalate Cyclic Oligomers. Macromolecules **31**(15), 4782-4790 (1998).

15.   Hall, AJ and Hodge, P. Recent research on the synthesis and applications of cyclic oligomers. Reactive and Functional Polymers **41**(1-3), 133-139 (1999).

16.   Parton, H, Baets, J, Lipnik, P, Goderis, B, Devaux, J, and Verpoest, I. Properties of poly(butylene terephthatlate) polymerized from cyclic oligomers and its composites. Polymer **46**(23), 9871-9880 (2005).

17.   Liu, Y, Wang, Y-F, Gerasimov, TG, Heffner, KH, and Harmon, JP. Thermal analysis of novel underfill materials with optimum processing characteristics. Journal of Applied Polymer Science **98**(3), 1300-1307 (2005).

18.   Mohd Ishak, ZA, Gatos, KG, and Karger-Kocsis, J. On the in-situ polymerization of cyclic butylene terephthalate oligomers: DSC and rheological studies. Polymer Engineering & Science **46**(6), 743-750 (2006).

19.  Righetti, MC and Munari, A. Influence of branching on melting behavior and isothermal crystallization of poly(butylene terephthalate). Macromolecular Chemistry and Physics **198**(2), 363-378 (1997).

20.  Papageorgiou, GZ, Achilias, DS, Bikiaris, DN, and Karayannidis, GP. Isothermal and non-isothermal crystallization kinetics of branched and partially crosslinked PET. Journal of Thermal Analysis and Calorimetry **84**(1), 85-89 (2006).

21.  Bikiaris, DN and Karayannidis, GP. Thermomechanical analysis of chain-extended PET and PBT. Journal of Applied Polymer Science **60**(1), 55-61 (1996).

22.  Mark, JE. Physical properties of polymers handbook. Woodbury, New Cork: AIP press, 1996.

23.  Tripathy, AR, MacKnight, WJ, and Kukureka, SN. In-Situ Copolymerization of Cyclic Poly(butylene terephthalate) Oligomers and ε-Caprolactone. Macromolecules **37**(18), 6793-6800 (2004).

24.  Zhang, H, Sun, S, Ren, M, Chen, Q, Song, J, Zhang, H, and Mo, Z. Thermal and mechanical properties of poly(butylene terephthalate)/epoxy blends. Journal of Applied Polymer Science **109**(6), 4082-4088 (2008).

25.  Baets, J, Devaux, J, and Verpoest, I. Toughening of basalt fiber-reinforced composites with a cyclic butylene terephthalate matrix by a nonisothermal production method. Advances in Polymer Technology **29**(2), 70-79 (2010).

26.  van Rijswijk, K and Bersee, HEN. Reactive processing of textile fiber-reinforced thermoplastic composites – An overview. Composites Part A: Applied Science and Manufacturing **38**(3), 666-681 (2007).

27.  Xu, D, Karger-Kocsis, J, and Apostolov, AA. Hybrids from HNBR and in situ polymerizable cyclic butylene terephthalate (CBT): Structure and rolling wear properties. European Polymer Journal **45**(4), 1270-1281 (2009).

28.  Burch, RR, Lustig, SR, and Spinu, M. Synthesis of Cyclic Oligoesters and Their Rapid Polymerization to High Molecular Weight†. Macromolecules **33**(14), 5053-5064 (2000).

# Chapter 9: Toughening of pCBT with isocyanates
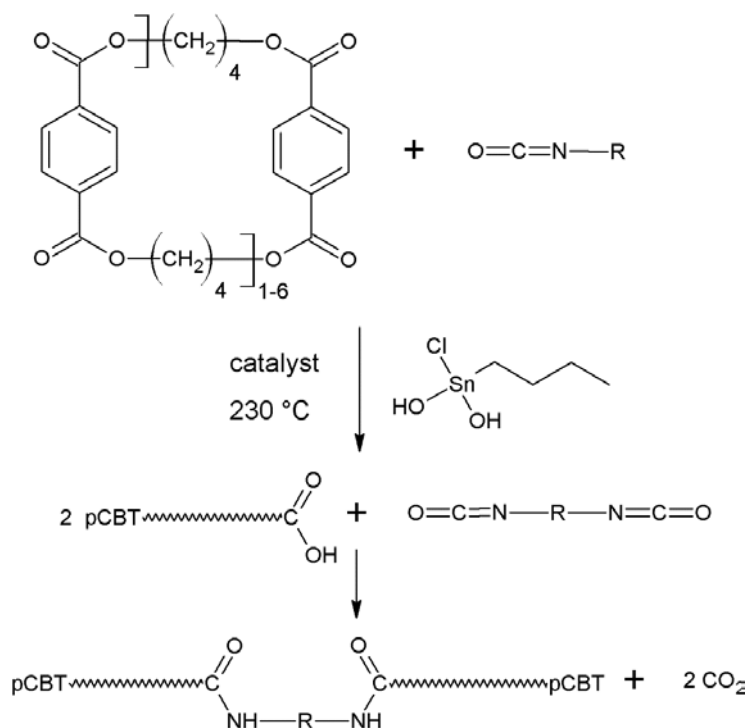


CBT oligomers were reacted in a batch mixer with three types of isocyanates: A bifunctional aromatic type, a bifunctional aliphatic type and a polymeric aromatic isocyanate. The use of 0.5 to 2 wt.% isocyanate led to a dramatic increase in elongation at break of pCBT, from 8% to well above 100%. The stiffness and strength of the modified pCBT, however, were found to slightly decrease.

**Publication derived from this work [1]:**

## Isocyanate toughened pCBT: Reactive blending and tensile properties

T. Abt[1], A. Martínez de Ilarduya[2], J. J. Bou[2], M. Sánchez-Soto[1*]

## 9.1    Introduction

It was demonstrated in the preceding chapter that reactive chain extension of pCBT with a bifunctional epoxy resin is a useful way to increase the molecular weight and to toughen pCBT without considerably affecting other properties. The bifunctional epoxy resin can react with the terminal carboxyl groups of two or more pCBT chains, increasing molecular weight and causing an improvement in toughness. However, the chain extension reaction of pCBT and epoxy resin is rather slow. Moreover, it can result in considerable gel formation if an excess of epoxy resin is used. Therefore, an addition-type chain extender with no by-products, higher reactivity and capable of yielding a linear macromolecular structure is desirable.

Of the available groups of chain extenders for polyesters, isocyanates (referred to as NCO) are promising. They show higher reactivity than epoxides and readily react at moderate temperatures with active hydrogen containing compounds [2-4]. The reaction can be promoted by metals in the form of organometallics and/or salts of organic acids. Tin compounds such as dibutyl tin dilaurate and tin (II) octoate are particularly effective, so the reaction can even be conducted at room temperature [5-6]. This high reactivity and versatility make isocyanates an important group of chemicals and they are used as building blocks, *e.g.* as hard segments in polyurethane chemistry. Linear, branched and crosslinked structures can be obtained with isocyanates, depending on functionality and stoichiometry. Isocyanates can be used as compatibilizers for partially miscible polymer blends [7] as well as chain extenders or toughening agents to improve the properties; particularly the toughness of recycled poly(ethylene terephthalate) [4, 7], polylactide [8], and poly(butylene terephthalate) [9]. These properties render isocyanates a useful group of chain extender and toughening agents for pCBT. Moreover, since isocyanates readily react with water, they may enhance the ring-opening polymerization of CBT by eliminating moisture which would otherwise negatively influence the ROP.

Although isocyanates were mentioned as potential toughening agents for pCBT in the open patent literature [10], to the best of the knowledge of the author, there has been no publication on this subject. In the present chapter, the role of different isocyanates on the ring-opening polymerization and the properties of pCBT were studied. The resultant structures and properties were analysed and discussed.

## 9.2    Experimental section

### 9.2.1  Materials

One-component cyclic butylene terephthalate oligomers (CBT160$^{®}$) were used throughout this chapter.

Three different types of isocyanates were used, namely hexamethylene diisocyanate (referred to as HDI), 4,4'-methylenebis(phenyl isocyanate) (referred to as MDI) and a polymeric methylene diphenyl diisocyanate (referred to as PMDI). The used isocyanates are described in detail in section 3.4.2.

### 9.2.2  Sample preparation

CBT and the corresponding amount of isocyanate (0.25, 0.5, 0.75, 1 and 2 wt.%) were dry blended using mortar and pestle and then vacuum dried at 80 °C for 8 h. The blends were stored in a desiccator over silica gel prior to *in situ* polymerization and simultaneous reactive blending of 40 g of these blends in a batch mixer at 230 °C, 60 min$^{-1}$ and under a blanket of nitrogen for 4 and 7 min, respectively, as will be explained later in section 9.4.1. After polymerization the polymer was collected, ground into granules using a cutting mill, vacuum dried for 8 h at 80 °C and then compression moulded in the hot plate press at a temperature of 250 °C and a pressure of 4 MPa for 5 min. Neat CBT was equally processed for comparison. This unmodified sample corresponds to pCBT-MB, but again for simplicity reasons will be referred to as pCBT in this chapter.

   Samples containing 2 wt.% of isocyanate were subjected to solid-state post-polymerization in the hot plate press at a temperature of 120 °C for 4 h without applying pressure. These samples were marked with an asterisk in order to distinguish the different processing route from the other samples.

## 9.3    Characterization

All characterization methods are described in detail in chapter 5. The reaction between CBT and isocyanates was visualized by torque *versus* time measurements in the batch mixer at 230 °C and 60 $min^{-1}$ rotor speed in $N_2$ atmosphere. Unmodified pCBT and NCO-modified pCBT were characterized using gel permeation chromatography, gel content determination, $^1H$ NMR spectroscopy, differential scanning calorimetry, X-ray diffraction, thermogravimetric analysis, dynamic mechanical thermal analysis and scanning electron microscopy. The mechanical properties of the samples were determined by tensile tests and by instrumented tensile-impact tests.

## 9.4    Results and Discussion

Isocyanates are well known to readily react with compounds that bear active hydrogen. The classical reaction in polyurethane chemistry is the reaction of an isocyanate group with an alcohol group where a urethane group is formed. The reactivity depends mainly on the chemical structure of the employed isocyanate and it was found that aromatic isocyanates are more reactive than aliphatic ones [4, 11]. Urethane bonds are thermally unstable and can dissociate at high temperatures. The decomposition temperature depends on the structures of the isocyanate and alcohol used. Generally, the higher the reactivity of the isocyanate-alcohol system, the lower the thermal stability of the formed urethane. The thermal stabilities of urethanes as reaction products of different isocyanate-alcohol systems  are as follows: alkyl isocyanate-alkyl alcohol (250 °C) > aryl isocyanate-alkyl alcohol (200 °C) > alkyl isocyanate aryl alcohol (180 °C) > aryl isocyanate-aryl alcohol (120 °C) [12]. According to this sequence, the thermal stabilities of pCBT-isocyanate systems are expected to be in the range of 200–250 °C.  Due to their high reactivity, the isocyanate groups can also react with carboxyl end groups leading to amide groups and carbon dioxide as by-product. Amide bonds are thermally more stable than urethane or ester bonds due to their partial double bond character [13].

Secondary reactions with excess isocyanate and the previously formed urethane and amide groups can occur, resulting in allophanates (*c.f.* figure 9.1) and ureas (*c.f.* figure 9.2), respectively. Additionally, isocyanurates can arise from trimerization of isocyanate as

well as from the reaction of allophanate and excess isocyanate. These secondary reactions lead to branching and eventually to crosslinking of the polymer [2, 4, 7, 11-12, 14]. The kinetic rate constants of allophanate, urea and isocyanurate formation are much smaller than the ones of urethane and amide formation [11], and it is well known that these reactions are only favoured at high concentrations of isocyanate groups.
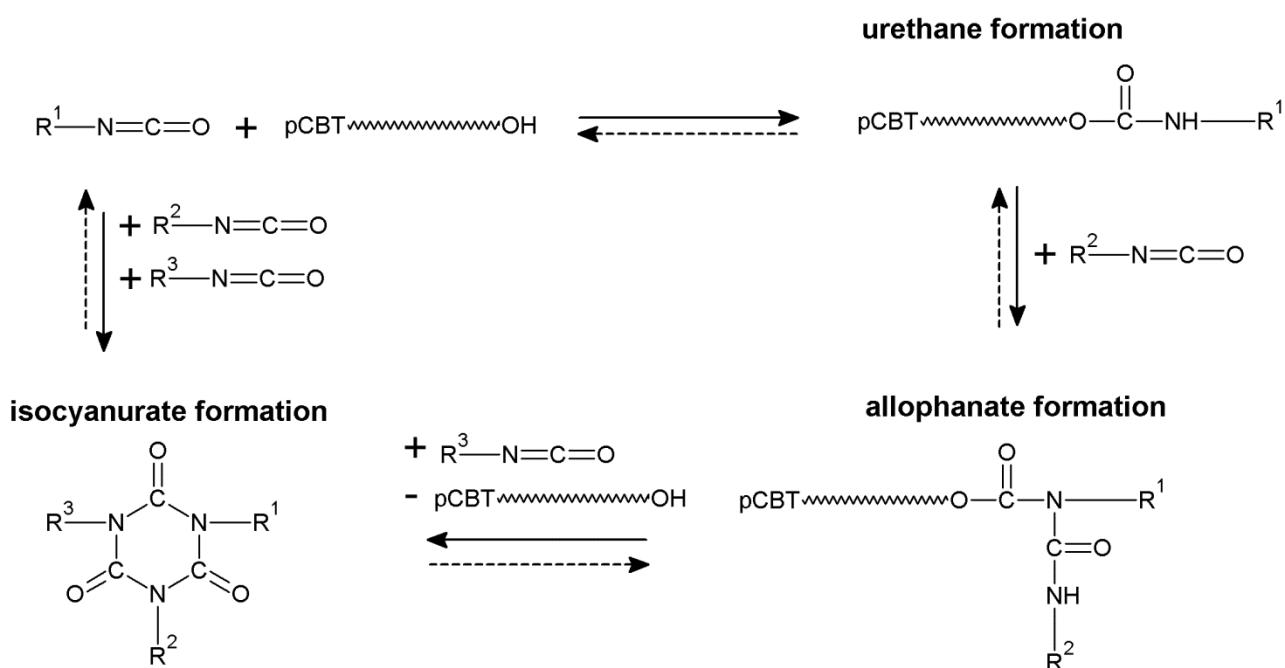


Fig. 9.1: Possible reaction mechanisms of pCBT hydroxyl end groups and isocyanate functional groups

$$R^1-N=C=O \quad + \quad pCBT\text{wwwww}\overset{\overset{\displaystyle O}{\|}}{C}-OH \quad \longrightarrow \quad pCBT\text{wwwww}\overset{\overset{\displaystyle O}{\|}}{C}-O-\overset{\overset{\displaystyle O}{\|}}{C}-NH-R^1$$

$\downarrow\ -\ CO_2$

**amide formation**

**urea formation**

$$pCBT\text{wwwww}\overset{\overset{\displaystyle O}{\|}}{C}-\underset{\underset{\displaystyle R^2}{\underset{|}{NH}}\underset{|}{}}{\underset{\underset{\displaystyle}{\underset{\|}{C=O}}}{N}}-R^1 \qquad \overset{+\ R^2-N=C=O}{\underset{\text{-------}\rightarrow}{\longleftarrow}} \qquad pCBT\text{wwwww}\overset{\overset{\displaystyle O}{\|}}{C}-NH-R^1$$
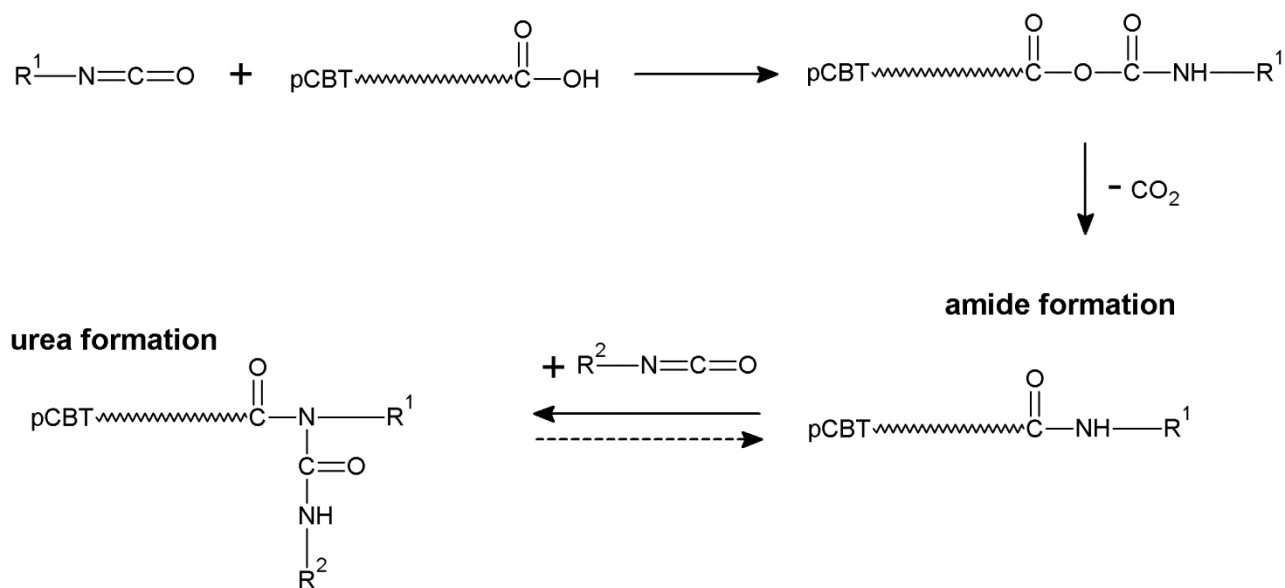
Fig. 9.2: Possible reaction mechanisms of pCBT carboxyl end groups and isocyanate functional groups

### 9.4.1 Torque *versus* time measurements

A chain extension reaction of (growing) pCBT chains and a bi- or polyfunctional chain extender causes an increase in molecular weight due to the coupling of multiple pCBT chains onto a chain extender molecule. This results in an increase in viscosity with reaction time. The ring-opening polymerization and the chain extension reaction were initially carried out in a Brabender batch mixer for a prolonged time (60 min) in order to visualize the torque/time signal, which is taken as an indicator for the viscosity evolution. The torque evolution did not change much after 15 min and therefore torque curves are only shown for the first 15 min of processing. The optimum polymerization times were chosen from these graphs, as will be explained below. The torque curves are depicted in figure 9.3; the maximum torque values and the corresponding times to reach the maximum torque are given in table 9.1.

The torque signal of neat CBT was first detected after 2 min which was considered to be the onset of the ROP. Before this time the melt viscosity of the molten CBT was below the detection limit of the measuring system. The torque curve reached a plateau after 9 min at ca. 6 Nm. Then it slowly increased and reached a maximum of 8 Nm after

~41 min. After reaching the maximum, the torque decreased to 7 Nm after 60 min probably due to thermo-mechanical degradation, as discussed earlier.

Regarding the CBT/NCO blends, apparently all three types of isocyanates act as promoters for the ring-opening polymerization when they are used in small concentrations (until 0.5 wt.%,) because the onset of the torque signal appeared earlier (*c.f.* figure 9.3). The aliphatic HDI was the most effective promoter when 0.5 wt.% was used, showing an onset of only 30 s (*c.f.* figure 9.3b). However, higher isocyanate contents (> 0.5 wt.%) result in an increase of the onset time as well as of the time to reach the maximum torque value (*c.f.* table 9.1).

A remarkable increase in torque can be seen for all blend compositions, confirming the chain extension reaction. The highest torque value was observed with aromatic MDI at a concentration of 0.75 wt.%, likely due to the higher reactivity of aromatic isocyanates compared to aliphatic ones.

When only 0.25 wt.% chain extender was used, a single torque maximum was observed. At higher isocyanate concentrations a second maximum appeared. This may be due to intermediate reactions, *i.e.* an initial urethane formation corresponding to the first maximum, subsequently followed by urethane dissociation into isocyanates and hydroxyl groups, leading to a torque decrease and finally amide formation, resulting in the second torque maximum. This urethane dissociation during processing will be discussed in detail in the NMR section.

After prolonged processing times (>10 min), all curves decreased to an average value of ~17 Nm after 15 min. This suggests that an equilibrium was reached and all blends, regardless of their isocyanate content, exhibited a similar molecular weight. Raffa *et al.* [3] came to a similar conclusion working with recycled PET and its chain extension with di- and multifunctional isocyanates. They found a plateau value of both molecular weight and melt viscosity above a threshold amount of isocyanate and ascribed this stationary condition to a mutual compensation of chain extension and degradation processes.
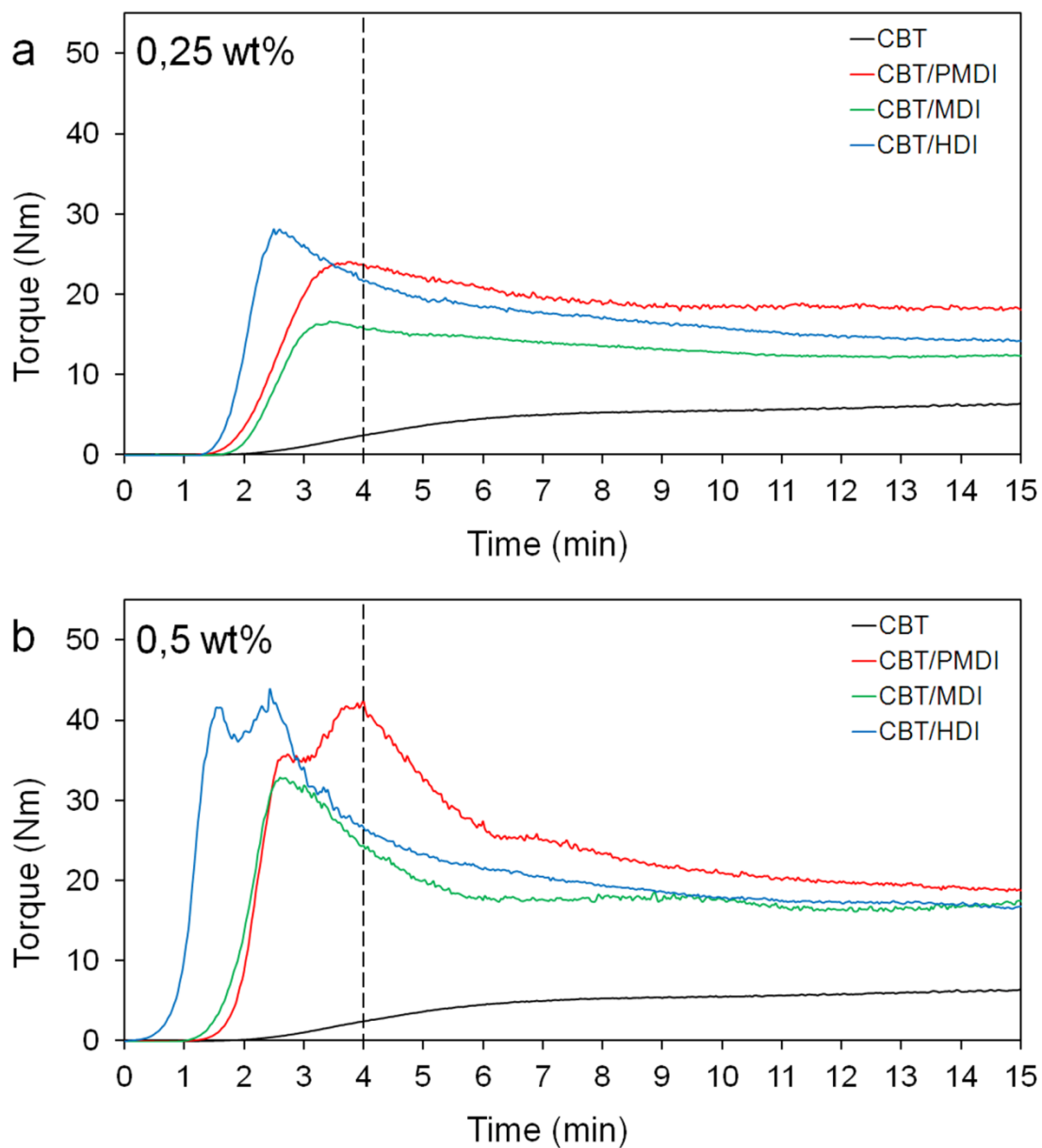
Fig. 9.3: Torque *versus* time plots of CBT/NCO blends with an isocyanate content of (a) 0.25 wt.%, (b) 0.5 wt.%, (c) 0.75 wt.%, (d) 1 wt.% and (e) 2 wt.% polymerized at 230°C and 60 min$^{-1}$ under nitrogen atmosphere.
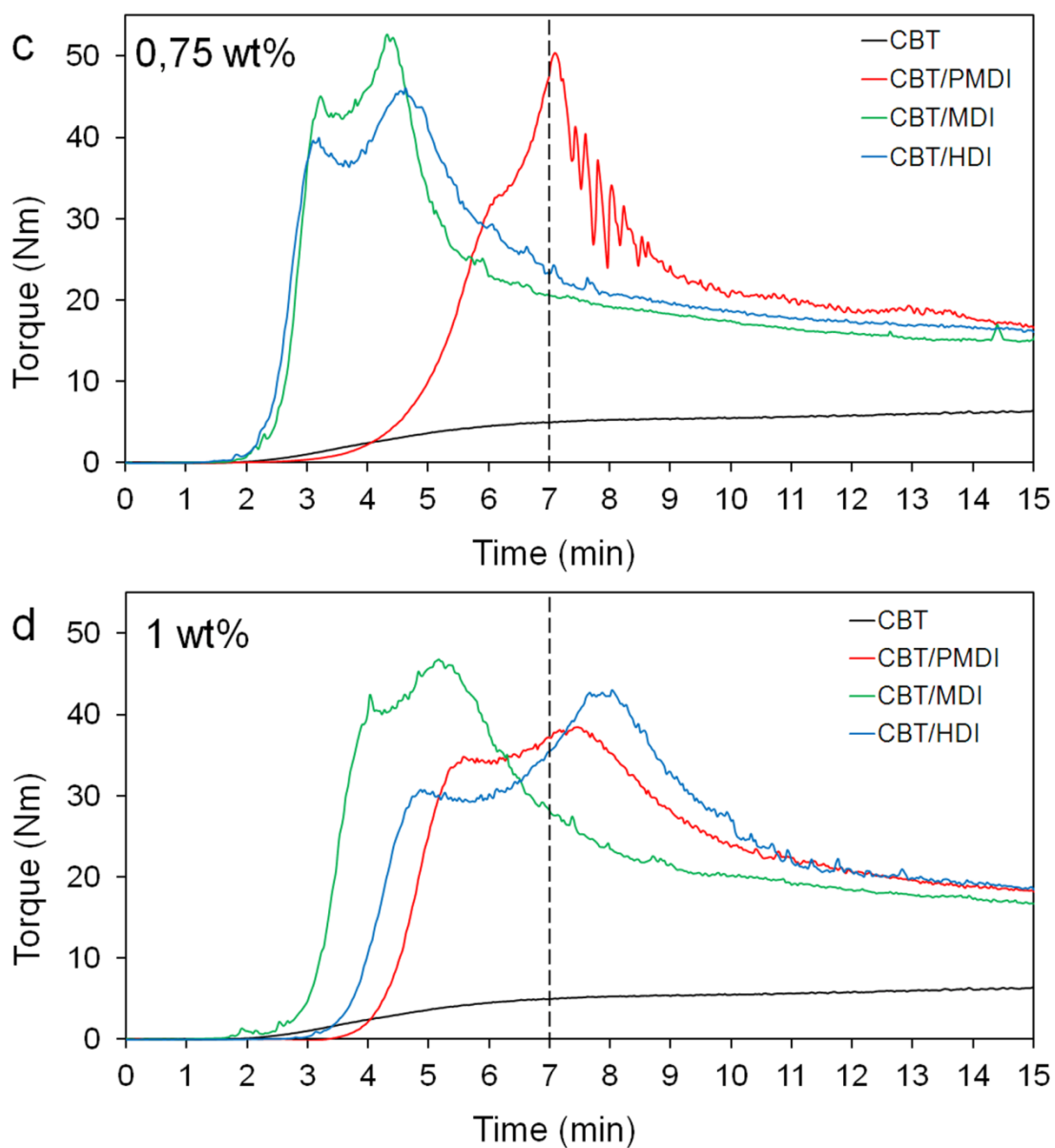
Fig. 9.3: Torque vs. time plots of CBT/NCO blends with an isocyanate content of (a) 0.25 wt.%, (b) 0.5 wt.%, (c) 0.75 wt.%, (d) 1 wt.% and (e) 2 wt.% polymerized at 230°C and 60 min$^{-1}$ under nitrogen atmosphere. (*continued*)
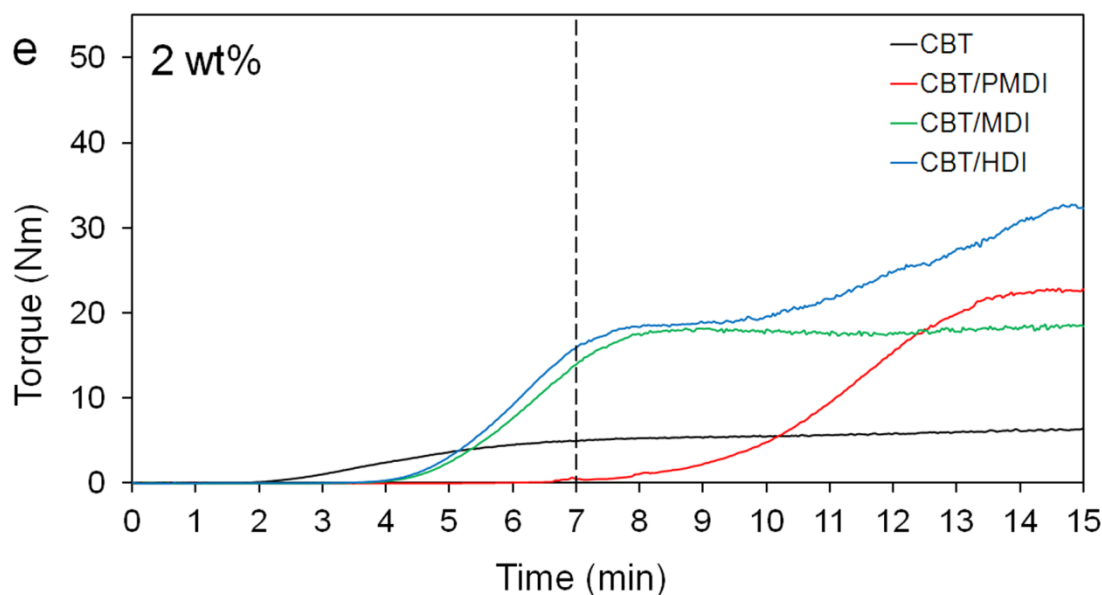
Fig. 9.3: Torque vs. time plots of CBT/NCO blends with an isocyanate content of (a) 0.25 wt.%, (b) 0.5 wt.%, (c) 0.75 wt.%, (d) 1 wt.% and (e) 2 wt.% polymerized at 230°C and 60 min$^{-1}$ under nitrogen atmosphere. (*continued*)

It is apparent from figure 9.3 that higher isocyanate concentrations require a longer time to fully react. The peak of the torque curve was considered as the highest molecular weight of the formed pCBT/NCO. Therefore a polymerization time of 4 min was chosen for blends containing 0.25 and 0.5 wt.% of isocyanate, whereas neat CBT and blends with isocyanate concentrations of 0.75, 1 and 2 wt.% were polymerized for 7 min. The two dashed vertical lines in figures 9.3 c–e represent these selected polymerization times 4 and 7 min. Regarding the blends with 2 wt.% NCO content, the comparably longer times to reach maximum torque and lower maximum torque values indicate an incomplete chain extension reaction with remaining unreacted NCO.

Table 9.1:  Maximum torque values during ring-opening polymerization in the batch mixer, times to reach the maximum torque and gel contents prior to compression moulding

| Chain extender | Content [wt%] | Polymerization[a] | | Gel content |
| | | Torque max. [Nm] | Time[b] [min] | [%] |
| --- | --- | --- | --- | --- |
| - | 0 | 7.7 | 40.7 | - |
| PMDI | 0.25 | 24.0 | 3.7 | - |
| | 0.5 | 42.4 | 4.0 | 2.2 |
| | 0.75 | 50.4 | 7.1 | 1.2 |
| | 1 | 38.5 | 7.5 | 31.5 |
| | 2* | 22.8 | 14.6 | n/d |
| MDI | 0.25 | 16.6 | 3.4 | - |
| | 0.5 | 32.9 | 2.6 | - |
| | 0.75 | 52.7 | 4.3 | - |
| | 1 | 46.8 | 5.2 | - |
| | 2* | 18.9 | 16.1 | n/d |
| HDI | 0.25 | 28.1 | 2.5 | - |
| | 0.5 | 43.9 | 2.4 | - |
| | 0.75 | 46.1 | 4.6 | - |
| | 1 | 43.0 | 8.0 | - |
| | 2* | 32.7 | 14.8 | n/d |

[a] Polymerization conditions: 230 °C, 60 $min^{-1}$, $N_2$ atmosphere

[b] Time to reach maximum torque

* Post-polymerized at 120°C for 4h

n/d: not determined

Fresh CBT/NCO blends were polymerized in the batch mixer under the cited conditions of 4 and 7 min, respectively. A gel-like texture was noticed in pCBT/PMDI samples with higher isocyanate concentrations when the materials were collected from the mixing chamber, therefore the gel content was determined.

The materials were collected from the mixing chamber, cooled to room temperature, ground into granules using a cutting mill, vacuum dried for 8 h at 80 °C and subsequently

compression moulded in the hot plate press at a temperature of 250 °C and a pressure of 4 MPa for 5 min.

Solid-state post-polymerization at 120 °C for 4 h in the hot plate press was applied to samples containing 2 wt.% of NCO due to the remaining unreacted isocyanate. This was done to incorporate the unreacted NCO monomers in the polymeric structure and to further increase the molecular weight.

### 9.4.2 Gel content

The insoluble part of the NCO-modified pCBT samples was determined by dissolution, centrifugation, washing and filtration; the results are compiled in table 9.1. Samples modified with bifunctional MDI or HDI were completely soluble, suggesting a linear chain structure. Only samples containing polyfunctional PMDI showed gel formation, namely 2.2 and 1.2% insoluble content for 0.5 and 0.75 wt.% PMDI concentration. The highest insoluble content of 31.5 % was observed for 1 wt.% PMDI content. Note that gelling was only observed in samples after *in situ* polymerization in the batch mixer. All compression moulded samples were completely soluble for NMR analysis. This leads to the assumption that these crosslinked structures in pCBT/PMDI samples changed to linear or branched structures during compression moulding.

### 9.4.3 GPC analysis

The molecular weight of the chain-extended pCBT/NCO samples as well as neat pCBT-MB was determined by GPC, the results are compiled in table 9.2 and GPC traces are illustrated in figure 9.4 a–c. It must be pointed out that some problems occurred during GPC analysis, namely the column did not separate properly the low molecular weight compounds. For this reason only $M_w$ and $M_z$ are reported and the results have to be interpreted with care.

Neat CBT polymerized during melt blending had a weight-average molecular weight of 45 kg/mol. This is a molecular weight twice as high as compared to compression moulded pCBT (*c.f.* section 8.5.2), which suggests that polymerization during melt

blending in inert atmosphere provides higher molecular weight pCBT as compared to pCBT obtained from compression moulding.

Table 9.2: GPC results of compression moulded pCBT and pCBT/NCO samples

| Chain extender | Content [wt%] | $M_w$ [kg/mol] | $M_z$ [kg/mol] |
|---|---|---|---|
| - | 0 | 44.6 | 136.6 |
| PMDI | 0.25 | 33.5 | 170.4 |
| | 0.5 | 40.4 | 224.5 |
| | 0.75 | 48.6 | 292.1 |
| | 1 | 70.5 | 370.2 |
| | 2* | n/d | n/d |
| MDI | 0.25 | 24.5 | 113.3 |
| | 0.5 | 34.6 | 178.2 |
| | 0.75 | 28.5 | 136.7 |
| | 1 | 39.3 | 209.3 |
| | 2* | n/d | n/d |
| HDI | 0.25 | 32.7 | 167.6 |
| | 0.5 | 40.6 | 205.4 |
| | 0.75 | 37.1 | 169.2 |
| | 1 | 35.5 | 166.3 |
| | 2* | n/d | n/d |

* Post-polymerized at 120°C for 4h

n/d: not determined

Regarding NCO-modified pCBT, it can be seen from figure 9.4 that the GPC traces show various peaks at higher retention times for all NCO types and concentrations, which suggest the presence of low molecular weight tails and thus broader molecular weight distributions as compared to neat pCBT. Moreover, apparently only the polyfunctional PMDI at concentrations higher than 0.5 wt.% increased the molecular weight of pCBT; the other two bifunctional types decreased $M_w$, regardless of the NCO content (c.f. table 9.2).

This result is in disagreement with the torque *versus* time measurements of these materials, which suggested molecular weights similar to neat pCBT due to similar torque levels after 15 min polymerization time. A possible explanation therefore is a relatively stronger molecular weight reduction of the NCO-modified samples during compression moulding, though this is speculative since compression moulded sheets were analysed and not the materials after melt blending.
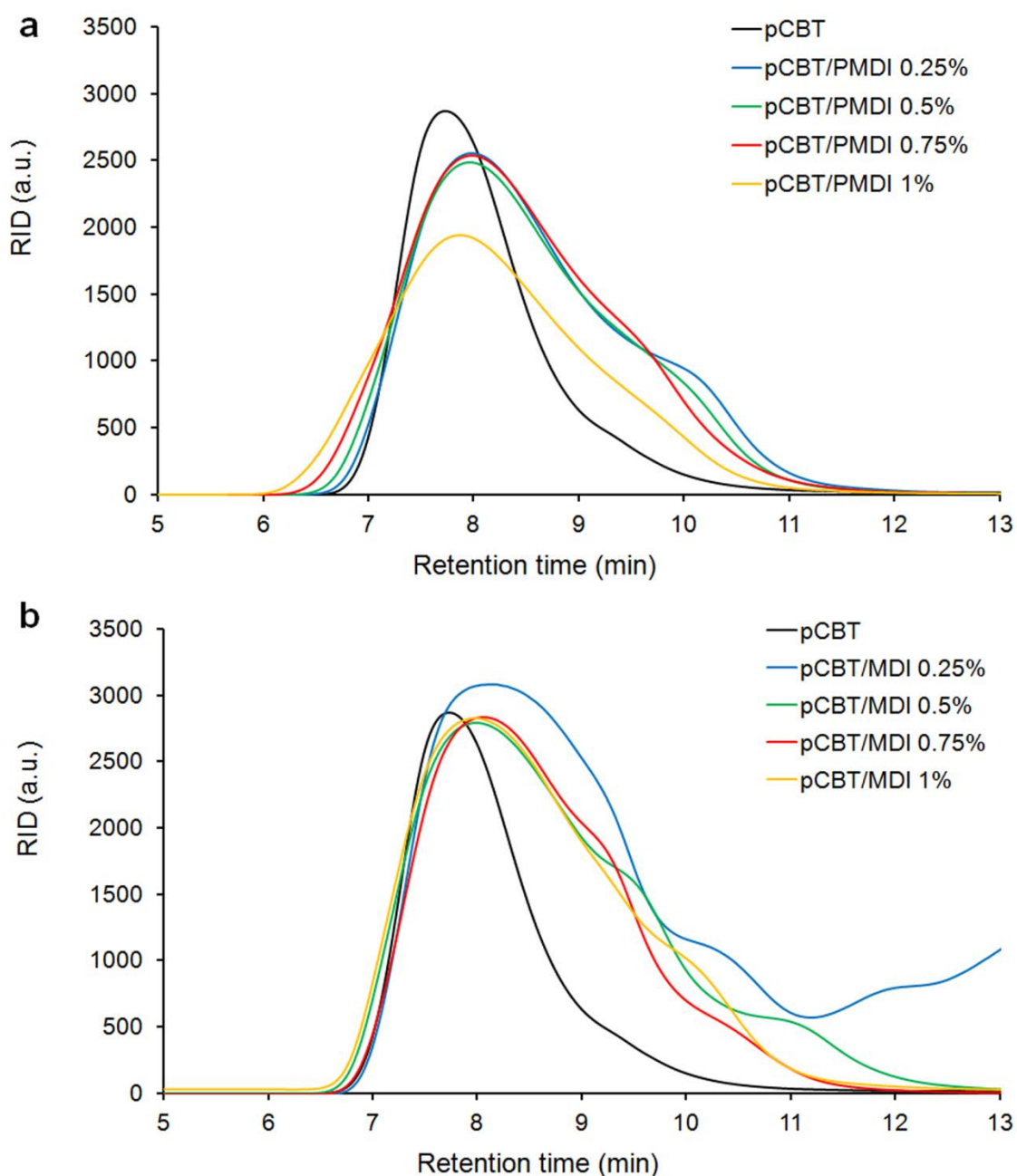


Fig. 9.4: GPC traces of unmodified and (a) PMDI-modified, (b) MDI-modified and (c) HDI-modified pCBT samples.
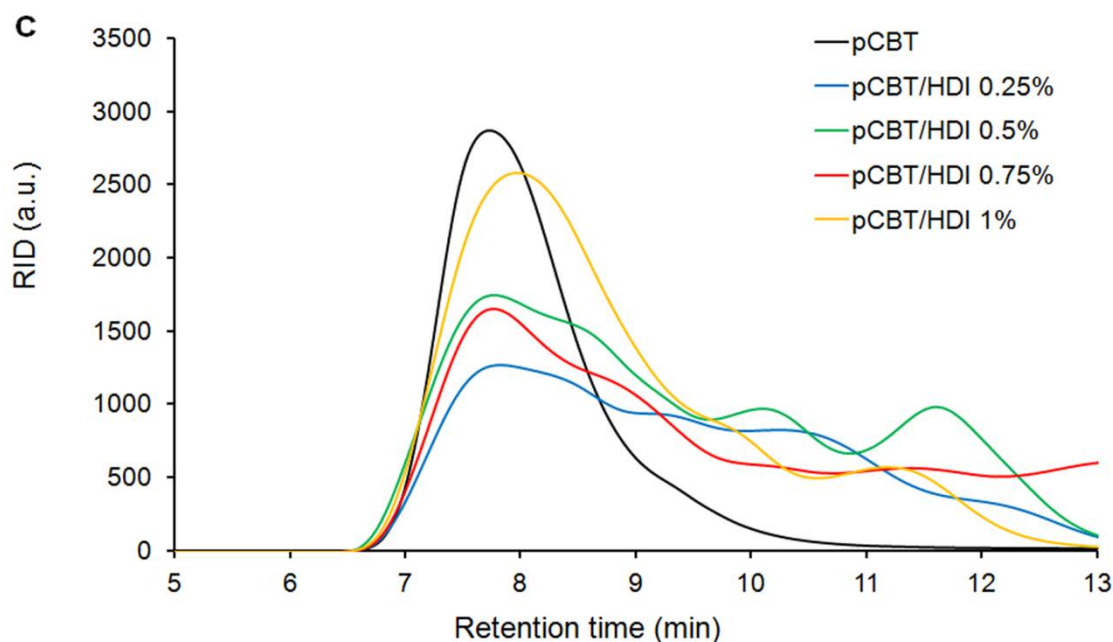
Fig. 9.4: GPC traces of unmodified and (a) PMDI-modified, (b) MDI-modified and (c) HDI-modified pCBT samples. (*continued*)

### 9.4.4 Proton NMR analysis

Proton NMR analysis was used to determine the chemical structures of pCBT and chain extended pCBT obtained from compression moulding. The structures and corresponding spectra are shown in figure 9.5.

In the spectrum of neat pCBT, the signal at 1.9 ppm is assigned to shielded methylene protons, the triplet at 3.7 ppm corresponds to methylenes attached to terminal hydroxyl groups ($-CH_2OH$), the peak at 4.4 ppm is assigned to oxymethylene protons and the one at 8.0 ppm is assigned to the aromatic protons.

The spectra of the pCBT/NCO samples revealed several additional peaks. Samples chain extended with aromatic isocyanate (*i.e.* MDI and PMDI) exhibited new peaks at 4.0, 7.2, 7.5 and 7.8 ppm. The peaks at 4.0 ppm are due to methylene protons of the reacted MDI, the doublets at 7.2 and 7.5 ppm are assigned to aromatic protons of the reacted MDI whereas the doublet at 7.9 ppm is assigned to aromatic protons of the terephthalic moiety which are linked to one ester group and one amide group in *para* position.

In the case of samples containing aliphatic isocyanates (*i.e.* HDI), new peaks at 3.1, 3.4, 4.1, 6.2 and 7.8 ppm arose. The weak peaks at 3.1 and 4.1 ppm are assigned to urethane formation of pCBT hydroxyl end groups and HDI [14]. More pronounced peaks at 3.4, 6.2 and 7.8 ppm are due to amide formation.

Furthermore, no signal of remaining unreacted isocyanates could be detected for samples containing up to 1 wt.% NCO content, suggesting a complete reaction of the isocyanates. Nevertheless, samples with a NCO content of 2 wt.% exhibited a considerable amount of unreacted isocyanate.
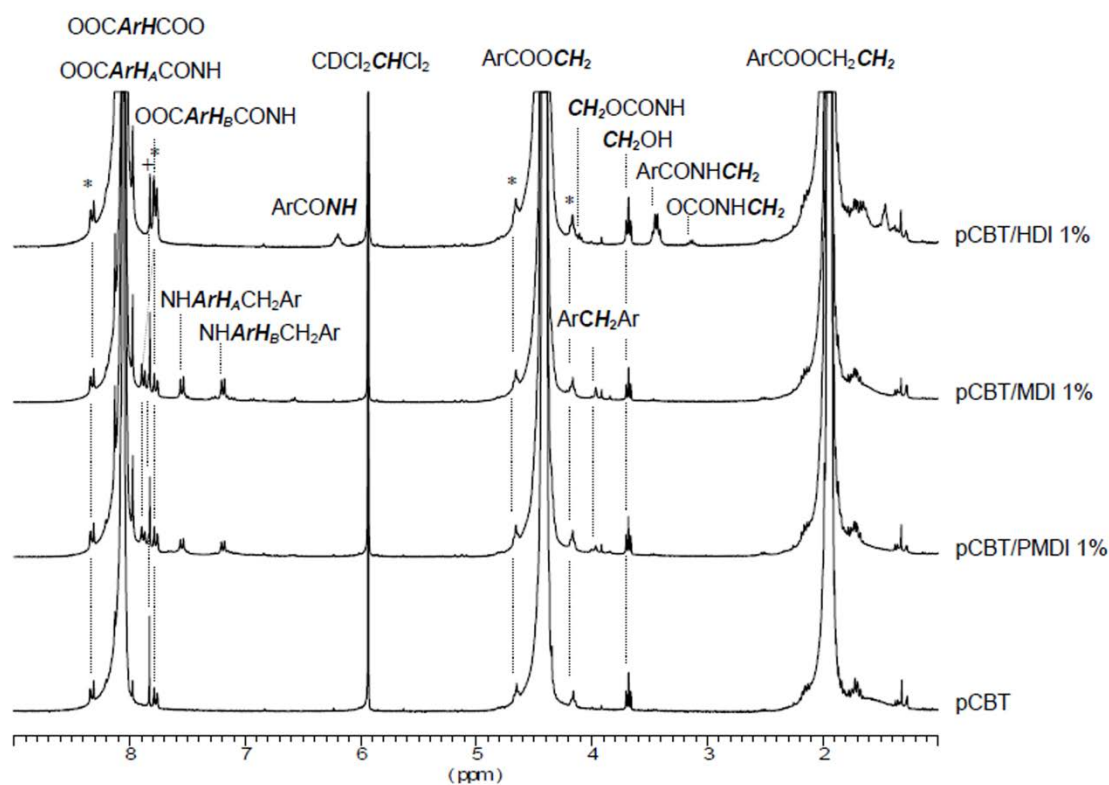


Fig. 9.5: $^1$H NMR spectra of pCBT and chain extended pCBT samples with peak assignments. (*) Satellite signals; (+) Unreacted pCBT; (Ar) Aromatic ring.

No crosslinked structures such as allophanates, ureas or biurets have been detected in compression moulded samples by NMR which is also concordant with gel content measurements. It can be also seen that the number of terminal hydroxyl groups (*c.f.* triplet at 3.7 ppm) is similar for all samples. A possible explanation is that the isocyanate reacted

with terminal hydroxyl groups in the first stage but due to the low thermal stability of urethane at the processing temperature the formed urethane groups dissociated back into –NCO and –OH groups. The liberated isocyanate reacted then with the pCBT terminal –COOH groups, forming thermally stable amide groups and liberating $CO_2$.

Further proton NMR experiments were performed to clarify this assumption and to see the influence of the compression moulding step on the chain extension reaction. Two chain extended samples which contained 1 wt.% HDI were analysed, before and after compression moulding. The corresponding spectra with peak assignments are depicted in figure 9.6. It can be seen that the sample before compression moulding showed higher intensity for the peaks at 3.1 and 4.1 ppm assigned to urethane, as compared to the sample after compression moulding. Moreover, the triplet at 3.7 ppm assigned to hydroxyl end groups and the peaks assigned to amide groups (3.4, 6.2 and 7.8 ppm) increased after compression moulding. This supports the assumption that during compression moulding the urethane groups dissociated into isocyanate and hydroxyl end groups, the former subsequently reacting with pCBT carboxyl end groups. Apart from the above mentioned effect, the increase in hydroxyl end groups is believed to be also caused by hydrolysis to a certain degree during compression moulding in ambient atmosphere.

Therefore it can be concluded that the predominant reaction mechanism of pCBT and isocyanate is amidation, although some urethane groups were detected in pCBT/HDI samples. The amount of formed urethane is less than 10% for pCBT/HDI but this is difficult to quantify for samples containing aromatic isocyanate due to signal overlapping.
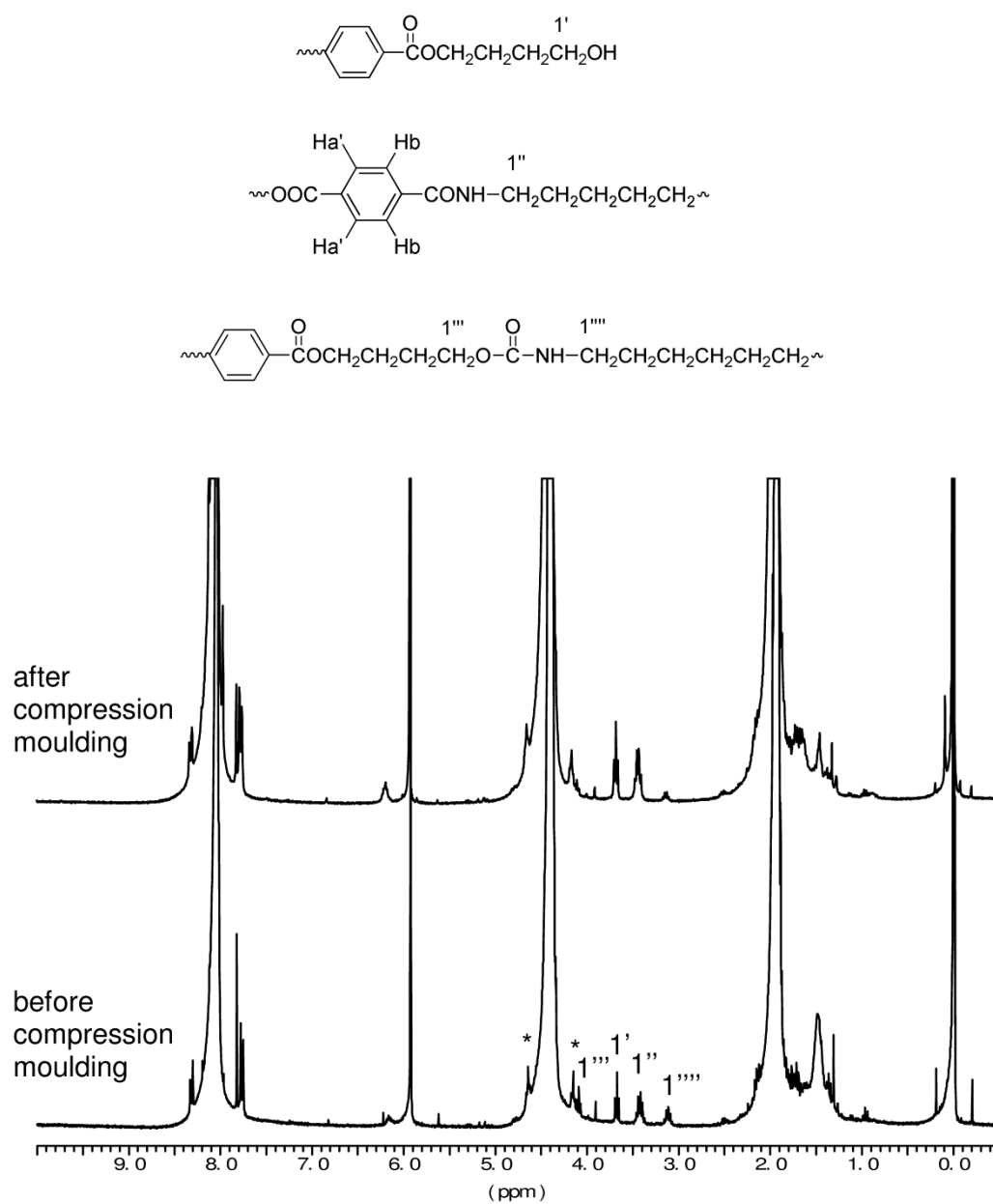
Fig. 9.6: ^{1}H NMR spectra of pCBT/HDI 1% before and after compression moulding with peak assignments. (*) Satellite signals.

## 9.4.5  DSC analysis

The thermal properties of compression moulded pCBT and pCBT/NCO samples were assessed by DSC; the results are depicted in figure 9.7 and table 9.3.

Table 9.3:  DSC data for pCBT and isocyanate-modified pCBT, heating and cooling at 10 °C/min.

| Chain extender | Content | First cooling | | Second heating | | | $X_c$ | $T_g$ [a] |
| | | $T_c$ | $\Delta H_c$ | $T_{m1}$ | $T_{m2}$ | $\Delta H_{m1+2}$ | | |
| | [wt%] | [°C] | [J/g] | [°C] | [°C] | [J/g] | [%] | [°C] |
| - | 0 | 193.1 | -50.6 | 215.4 | 223.5 | 50.7 | 35.7 | 66.4 |
| PMDI | 0.25 | 191 | -49.3 | 214.8 | 222.4 | 47.9 | 33.7 | 66.5 |
| | 0.5 | 190.7 | -47.8 | 215.1 | 222.3 | 46.9 | 33.0 | 67.0 |
| | 0.75 | 189.7 | -47.3 | 212.5 | 221.3 | 40.8 | 28.7 | 63.9 |
| | 1 | 187.0 | -44.4 | 213.5 | 220.8 | 42.5 | 29.9 | 65.3 |
| | 2* | 183.5 | -48.8 | 215.7 | - | 48.7 | 34.3 | 60.3 |
| MDI | 0.25 | 192.1 | -46.7 | 215.5 | 223.6 | 44.1 | 31.1 | 64.0 |
| | 0.5 | 189.8 | -44.9 | 213.5 | 221 | 43.9 | 30.9 | 65.2 |
| | 0.75 | 190.4 | -49.3 | 213.4 | 221.7 | 43.1 | 30.4 | 64.7 |
| | 1 | 188.9 | -48.8 | 213.2 | 221.2 | 45 | 31.7 | 63.4 |
| | 2* | 187.7 | -45.7 | 213.9 | 220.2 | 47.6 | 33.5 | 59.4 |
| HDI | 0.25 | 189.7 | -44.9 | 214 | 221.8 | 45.2 | 31.8 | 65.6 |
| | 0.5 | 188.7 | -42.8 | 213 | 221.1 | 41.3 | 29.1 | 65.6 |
| | 0.75 | 189.6 | -48.2 | 214.4 | 222.5 | 46.3 | 32.6 | 63.0 |
| | 1 | 189.4 | -47.7 | 214 | 222 | 46.2 | 32.5 | 62.7 |
| | 2* | 188.1 | -43.1 | 212.9 | 219.7 | 38.7 | 27.3 | 56.9 |

* Post-polymerized at 120°C for 4h

[a] Determined by DMTA in tensile mode in the temperature range T = 30–220°C, heating rate = 2 °C/min, f = 1Hz, $\varepsilon$ = 0.05%.
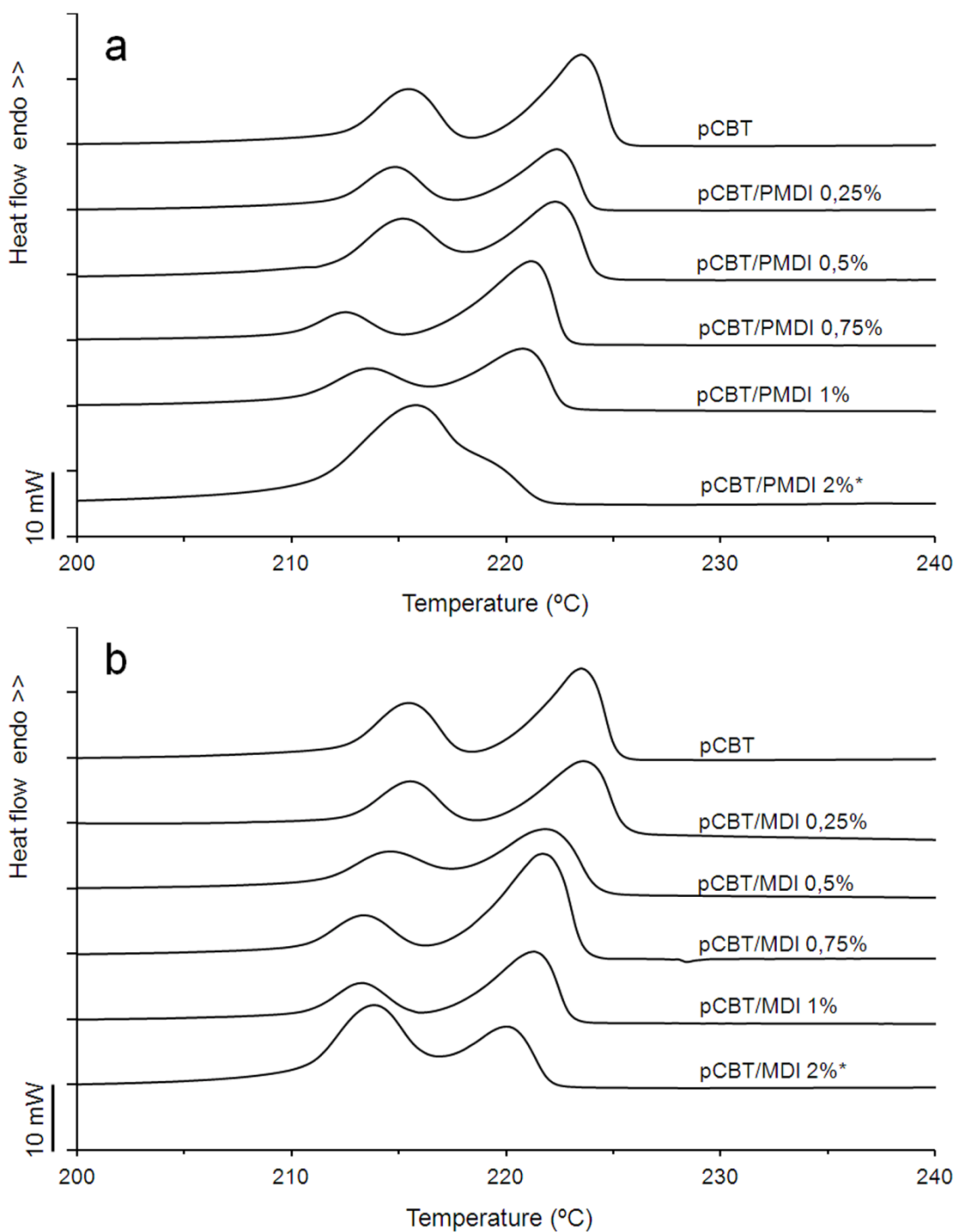
Fig. 9.7: DSC second heating scan of compression moulded pCBT and (a) pCBT/PMDI, (b) pCBT/MDI and (c) pCBT/HDI samples; heating and cooling rate of 10°C/min.
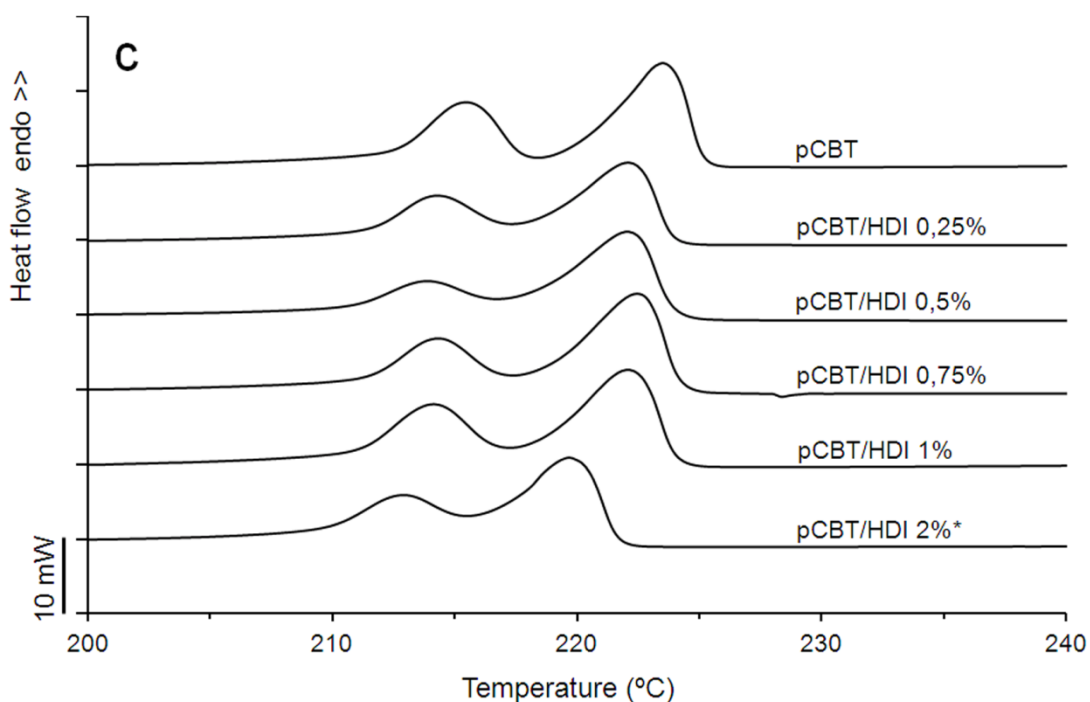
Fig. 9.7: DSC second heating scan of compression moulded pCBT and (a) pCBT/PMDI, (b) pCBT/MDI and (c) pCBT/HDI samples; heating and cooling rate of 10°C/min. (*continued*)

Unmodified pCBT shows a minor melting peak at 215 °C and a major peak at 224 °C, ascribed to the recrystallization and melting of imperfect crystal structures [15], as discussed earlier. The degree of crystallinity was calculated from the sum of both melting enthalpies and was found to be 36%. During the cooling scan the crystallization peak was observed at 193 °C.

Regarding isocyanate modified pCBT samples, a general depression of crystallization and melting temperatures and their corresponding enthalpies can be observed (*c.f.* table 9.3). Both melting temperatures decreased up to 3 °C and crystallization temperatures reduced up to 6 °C. The crystallinity was most effectively decreased by 9% when 2 wt.% HDI was used. Torres *et al.* [4], Zhang and co-workers [16] and Raffa *et al.* [3] modified recycled PET with di- and polyfunctional isocyanates and observed a similar tendency. This depression is due to the amide and urethane groups which form in the isocyanate reaction. These groups along the pCBT backbone disturb the chain symmetry and regularity and hence the crystallization rates are decreased, resulting in a decreased crystallinity and consequently in a higher toughness. Another consequence

of the disturbed chain symmetry is a reduced lamellar thickness which leads to a decrease in melting temperature [4, 16]. No obvious tendency of the isocyanate modification on the glass transition of pCBT can be found, although most samples exhibited a slightly decreased $T_g$ (1–2 °C), indicating an increased chain mobility. This was different in the case of the post-polymerized samples; they exhibited a 6–9 °C lower glass transition temperature.

In view of the samples containing 2 wt.% PMDI and MDI, respectively, and subjected to solid-state post-polymerization, it can be seen that the crystal fraction increased. This is most likely due to the post-polymerization process at 120 °C, which can be also seen as annealing, causing cold crystallization and thus increasing degree of crystallinity and crystal perfection, as discussed earlier. Conversely, the sample pCBT/HDI 2%* exhibited a decrease in $X_C$ (-9%) and $T_g$ (-9 °C) with respect to neat pCBT, suggesting that an increase in crystal fraction did not occur.

### 9.4.6  WAXS analysis

X-ray diffraction was used to determine whether the isocyanate modification has an influence on the crystal structure of pCBT. The diffraction patterns of neat pCBT-MB and pCBT/HDI 0.75% are illustrated in figure 9.8.

As expected, no significant difference between unmodified and NCO-modified pCBT samples can be found, regardless the used NCO type. Therefore, only one NCO-modified sample is exemplarily shown. As already discussed in section 6.4.5, PBT and pCBT exhibit two triclinic polymorphs, the $\alpha$ form being the stable polymorph under standard conditions whereas the $\beta$ form is only observed under stretching of unoriented crystals. Again, the crystallographic reflection from the ($\bar{1}$ 04) plane was used to determine the crystal phase of pCBT. This reflection is observed at $2\theta = 31.5°$ for both unmodified and NCO-modified pCBT samples, thus isocyanate-modified samples exhibit $\alpha$ crystal structure.
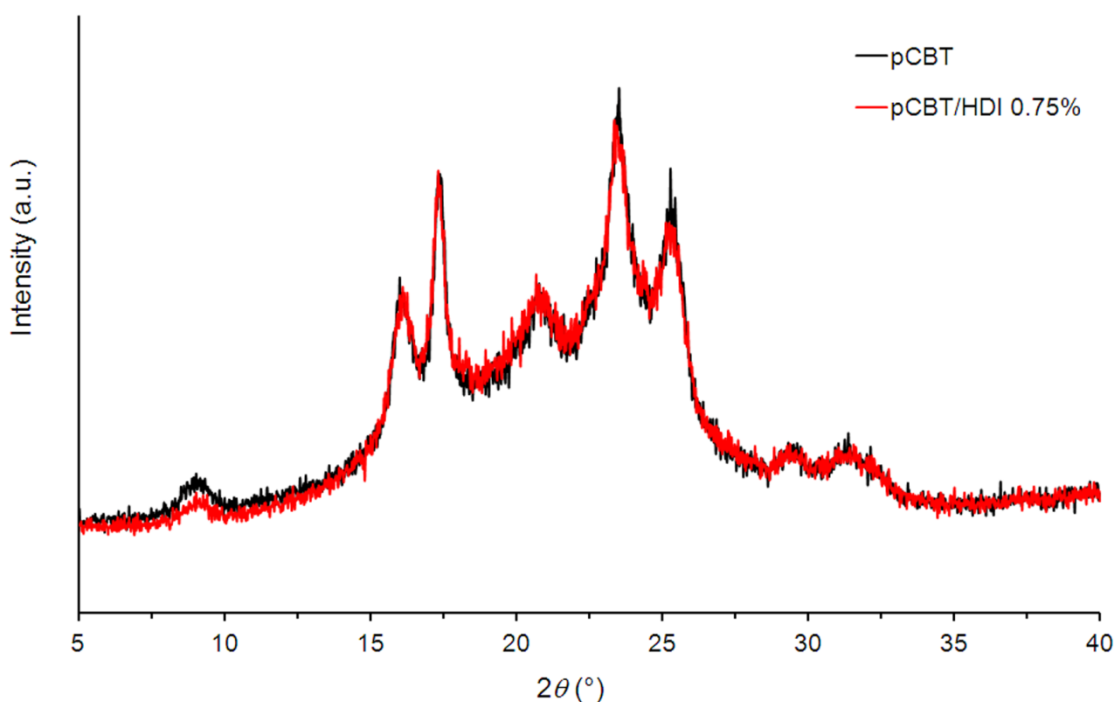
Fig. 9.8: WAXS diffraction patterns of pCBT-MB and pCBT/HDI 0.75%.

### 9.4.7  TGA analysis

The thermal decomposition of pCBT and NCO-modified pCBT was studied using thermogravimetric analysis in nitrogen; results are presented in table 9.4.

A single stage of decomposition ranging from 370 to 430 °C is observed for neat as well as for NCO-modified pCBT samples. Neat pCBT showed a 5% mass loss at 373 °C, the temperature at which the maximum mass-loss rate occurred was found to be 405 °C. After thermal decomposition, an amount of solid residue of 1 wt.% was detected.

NCO-modified pCBT samples generally showed a slightly lower thermal stability as compared to CBT but no clear tendency regarding the NCO content can be seen. The 5% mass loss temperatures and the maximum mass-loss rate temperatures decreased about 1–5 °C. This decrease was ascribed to the presence of some urethane links in the pCBT structure, as confirmed by proton NMR analysis. The thermal stability of these urethane bonds depend on the used isocyanate and were expected to be in the range of 200–250 °C, as mentioned above. This demonstrates that the isocyanate modification of pCBT does not markedly decrease the thermal stability.

Table 9.4: Thermogravimetric data for pCBT and NCO-modified pCBT, heating from 30 °C to 600 °C at 10 °C/min in $N_2$ atmosphere.

| Chain extender | Content [wt%] | $T_{5\ \% \ wt.\ loss}$ [°C] | $T_{max.}$ [°C] | Residue at 600 °C [wt.%] |
|---|---|---|---|---|
| - | 0 | 373.2 | 404.8 | 1.2 |
| PMDI | 0.25 | 371.1 | 400.9 | 2.3 |
|  | 0.5 | 367.9 | 402.5 | 0.8 |
|  | 0.75 | 372.2 | 403.4 | 2.7 |
|  | 1 | 368.9 | 401.6 | 1.2 |
|  | 2* | n/d | n/d | n/d |
| MDI | 0.25 | 372.9 | 401.9 | 1.3 |
|  | 0.5 | 371.4 | 402.1 | 2.7 |
|  | 0.75 | 372.8 | 402.0 | 3 |
|  | 1 | 373.3 | 403.2 | 2.7 |
|  | 2* | n/d | n/d | n/d |
| HDI | 0.25 | 369.7 | 400.3 | 0.5 |
|  | 0.5 | 372.6 | 403.2 | 2.6 |
|  | 0.75 | 374.3 | 404.1 | 2.6 |
|  | 1 | 369.5 | 402.3 | 3.6 |
|  | 2* | n/d | n/d | n/d |

* Post-polymerized at 120 °C for 4h

n/d: not determined

### 9.4.8 Tensile properties

The mechanical properties of compression moulded samples were assessed by tensile tests; the results are shown in table 9.5 and figure 9.9. Unmodified pCBT is inherently brittle and failed at ~8% elongation at break without yielding. By contrast, all isocyanate-modified samples showed a ductile behaviour with an increased elongation at break. It can be seen that only 0.25 wt.% of isocyanate, regardless of type, resulted in a three-fold increase in failure strain although some samples failed in a brittle manner. All samples

showed neck formation when the NCO content was increased to 0.5 wt.%. The maximum failure strain for MDI- (22-fold increase) and HDI- (28-fold increase) modified samples was observed at 0.75 wt.% NCO content. In the case of the polymeric isocyanate, a maximum failure strain (27-fold increase) was found for 1 wt.% PMDI.

Table 9.5:  Tensile properties of compression moulded pCBT/NCO samples

| Chain extender | Content [wt.%] | Tensile modulus [GPa] | Tensile strength [MPa] | Strain at break [%] | Strain energy [MJ/m$^3$] |
|---|---|---|---|---|---|
| - | 0 | 2.9 ± 0.3 | 60 ± 2 | 8 ± 1 | 4.2 ± 0.5 |
| PMDI | 0.25 | 2.8 ± 0.3 | 57 ± 1 | 30 ± 4 | 13.5 ± 1.7 |
| | 0.5 | 2.6 ± 0.3 | 55 ± 3 | 184 ± 94 | 77.9 ± 41.1 |
| | 0.75 | 2.6 ± 0.2 | 55 ± 1 | 167 ± 84 | 70.9 ± 38.3 |
| | 1 | 2.6 ± 0.2 | 51 ± 1 | 215 ± 28 | 87.1 ± 11.7 |
| | 2* | 2.7 ± 0.3 | 61 ± 1 | 133 ± 49 | 57.2 ± 21.8 |
| MDI | 0.25 | 2.6 ± 0.4 | 56 ± 1 | 25 ± 18 | 8.7 ± 4.3 |
| | 0.5 | 2.7 ± 0.4 | 55 ± 1 | 141 ± 71 | 57.0 ± 29.9 |
| | 0.75 | 2.6 ± 0.1 | 55 ± 1 | 174 ± 68 | 71.9 ± 30.0 |
| | 1 | 2.7 ± 0.2 | 55 ± 1 | 79 ± 11 | 30.5 ± 4.6 |
| | 2* | 3.1 ± 0.2 | 61 ± 1 | 101 ± 56 | 43.0 ± 23.4 |
| HDI | 0.25 | 2.4 ± 0.2 | 60 ± 1 | 24 ± 9 | 9.9 ± 4.9 |
| | 0.5 | 2.8 ± 0.3 | 55 ± 1 | 143 ± 85 | 61.2 ± 28.7 |
| | 0.75 | 2.7 ± 0.7 | 54 ± 1 | 227 ± 35 | 95.4 ± 18.4 |
| | 1 | 2.8 ± 0.2 | 54 ± 1 | 109 ± 21 | 44.9 ± 9.0 |
| | 2* | 3.1 ± 0.3 | 58 ± 1 | 206 ± 38 | 89.4 ± 18.0 |

* Post-polymerized at 120 °C for 4h

Toughness is better described by the strain energy calculated from tensile curves than by ultimate strain. Regarding the toughening effect by means of strain energy, the best result was obtained with 0.75 wt.% HDI. But since PMDI was more effective over a wide NCO concentration range (0.5–2 wt.%, see fig. 9.9), it appeared to be the better toughening agent. Stiffness and strength decreased about 10 % when samples contained the optimum

amount of 0.5 to 1 wt.% of isocyanate. This decrease is small compared to other toughening methods like copolymerization and consistent with the marginal amount of isocyanate added.
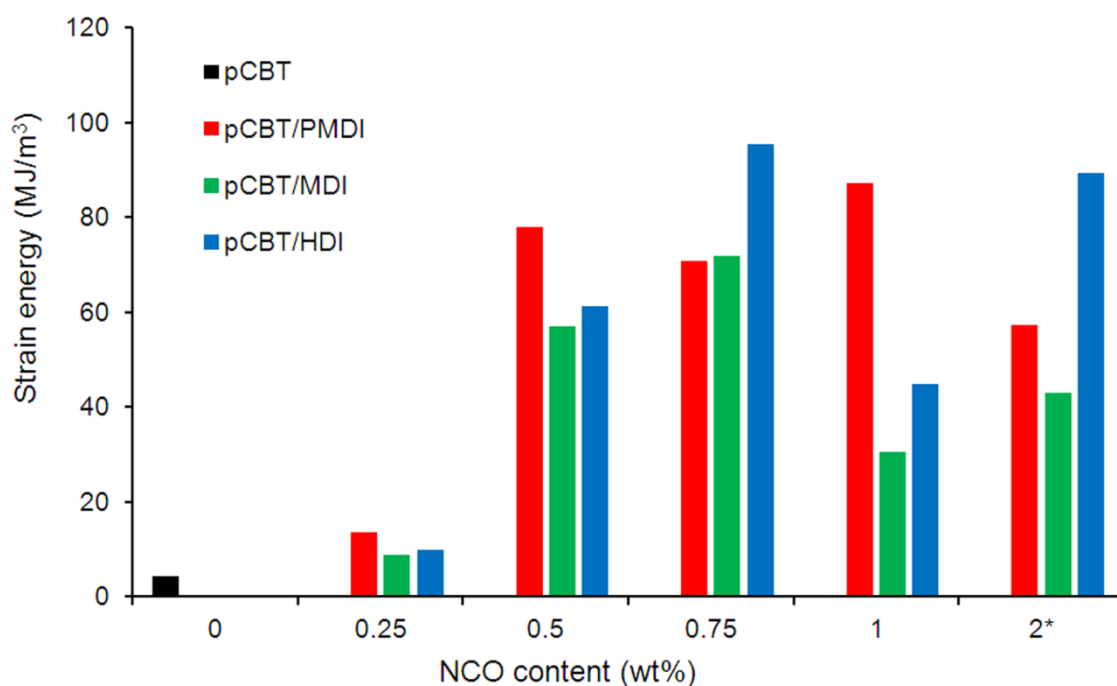


Fig. 9.9: Strain energy *versus* NCO content for NCO-modified pCBT. * Post-polymerized at 120 °C for 4h.

With respect to the post-polymerized samples, it can be seen that stiffness and strength increased as compared to samples containing 1 wt.% of NCO. This was attributed to the relatively higher degree of crystallinity of pCBT/PMDI 2%* and pCBT/MDI 2%* induced by cold crystallization during the post-polymerization, as shown in the DSC section. The higher crystallinity led to a slight toughness reduction relative to the optimum NCO contents of 0.5–1 wt.%. Regarding the sample pCBT/HDI 2%*, a high toughness was observed. This was ascribed to the relatively low degree of crystallinity, as discussed above.

In summary, when these NCO-modified materials are employed, for instance in continuous fibre reinforced composites, the generally observed decrease in matrix stiffness will be compensated by the fibres. Additionally, the excellent toughness of

isocyanate-modified pCBT considerably increases the matrix-governed properties of fibre reinforced pCBT composites, as will be shown later in chapter 15.

### 9.4.9  Tensile impact properties

Tensile impact tests were performed on pCBT and NCO-modified pCBT samples; representative tensile-impact stress versus time/strain curves for neat pCBT and pCBT/PMDI 1% are exemplarily shown in figure 9.10 and impact data is compiled in table 9.6.
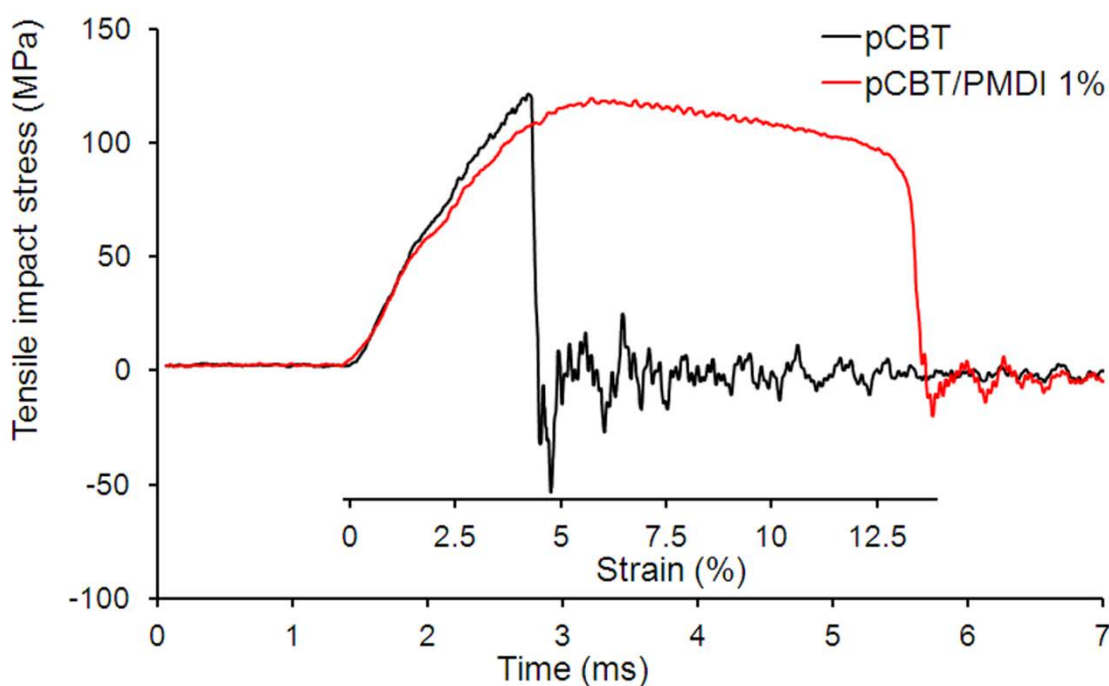


Fig. 9.10: Tensile impact stress *versus* time/strain curves of pCBT and pCBT/PMDI 1 %.

Analogously to what was discussed in preceding chapters, all tested pCBT samples broke in a brittle manner without any neck formation, whereas the majority of the NCO- modified samples failed in a ductile manner and showed yielding. It should be noted that the tensile-impact data correlates well with the one obtained from tensile tests. Tensile-impact strength was 146 kJ/m$^2$ for unmodified pCBT and increased to values ≥300 kJ/m$^2$ for

samples which apparently contained an optimum amount of isocyanate. The highest overall tensile-impact strength was observed for the post-polymerized sample pCBT/MDI 2%*, which outperformed all other produced samples of this whole work.

Table 9.6: Tensile impact data of pCBT and NCO-modified pCBT samples

| Chain extender | Content [wt%] | Tensile impact strength [kJ/m$^2$] | Tensile stress max. [MPa] |
|---|---|---|---|
| - | 0 | 146 ± 48 | 105 ± 15 |
| PMDI | 0.25 | 296 ± 132 | 121 ± 26 |
| | 0.5 | 309 ± 18 | 114 ± 5 |
| | 0.75 | 292 ± 25 | 122 ± 4 |
| | 1 | 301 ± 37 | 110 ± 9 |
| | 2* | 306 ± 35 | 112 ± 1 |
| MDI | 0.25 | 197 ± 25 | 109 ± 20 |
| | 0.5 | 271 ± 40 | 128 ± 8 |
| | 0.75 | 323 ± 21 | 122 ± 5 |
| | 1 | 229 ± 32 | 127 ± 5 |
| | 2* | 378 ± 35 | 121 ± 6 |
| HDI | 0.25 | 228 ± 60 | 103 ± 3 |
| | 0.5 | 275 ± 57 | 104 ± 8 |
| | 0.75 | 300 ± 37 | 113 ± 2 |
| | 1 | 335 ± 34 | 117 ± 3 |
| | 2* | 332 ± 28 | 108 ± 6 |

* Post-polymerized at 120 °C for 4h

It should be pointed out that the post-polymerized samples exhibited a higher degree of crystallinity as compared to NCO-modified samples without post-polymerzation treatment. Nevertheless, the post-polymerized samples showed an outstanding toughness in terms of strain energy and tensile impact strength. This demonstrates on one hand the high capability of isocyanates to toughen pCBT and on the other hand that a tough but highly crystalline pCBT (induced by cold crystallization during post-polymerization) is possible.

Moreover, isothermal processing, preferred from an industrial point of view, in combination with isocyanate toughening and post-polymerization might be a feasible method to obtain tough pCBT.

### 9.4.10 SEM analysis

In comparison to neat pCBT, pCBT/NCO samples were more difficult to break cryogenically. Therefore, small notches of ca. 2 mm depth were inserted with a razor blade on both sides of these specimens prior to cryo-fracture in order to ensure a brittle fracture.

Micrographs of neat pCBT and samples containing 0.75 wt.% of NCO are depicted in figure 9.11. In all samples, including post-polymerized samples with an isocyanate content of 2 wt.%, a single phase was observed and no signs of phase separation or incomplete reaction between pCBT and isocyanate could be found, indicating that the isocyanate had fully reacted with CBT. Moreover, no micron-sized plate- or prism-like crystals of unpolymerized CBT were detected, suggesting a high degree of conversion of CBT to pCBT [17]. Unmodified pCBT showed a smooth and uniform fracture surface. The small crests that are visible in figure 9.11 a were attributed to the rapid propagation of the crack during the fracture at low temperature that caused the crack front to oscillate. The detail at higher magnification (x10000) clearly shows the absence of localized plastic deformation, indicating the brittle nature of unmodified pCBT (see detail of figure 9.11a).

Similarly, all modified samples fractured in a brittle manner (*c.f.* figures 9.11 b–d), as expected due to the presence of notches and the low temperature used. Nevertheless, a somewhat rougher fracture surface compared to neat pCBT can be observed. This granular, rough structure is the result of the fracture of localized stretched matrix [18], as can be well observed at higher magnification. This may indicate a certain amount of plastic deformation at low temperatures on a micrometer scale.
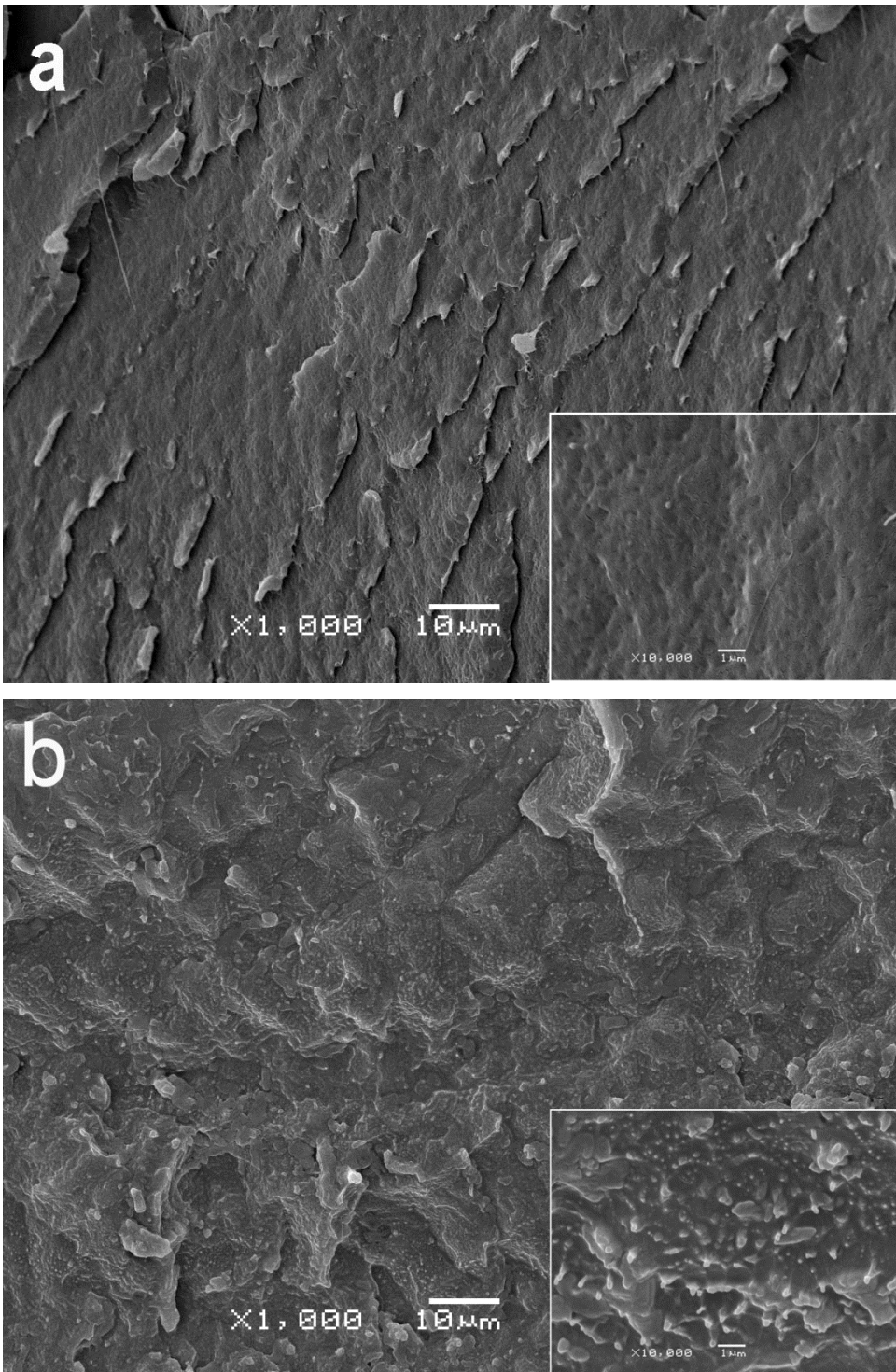
Fig. 9.11: SEM micrographs of (a) compression moulded pCBT, (b) pCBT/PMDI 0.75%, (c) pCBT/MDI 0.75% and (d) pCBT/HDI 0.75%.
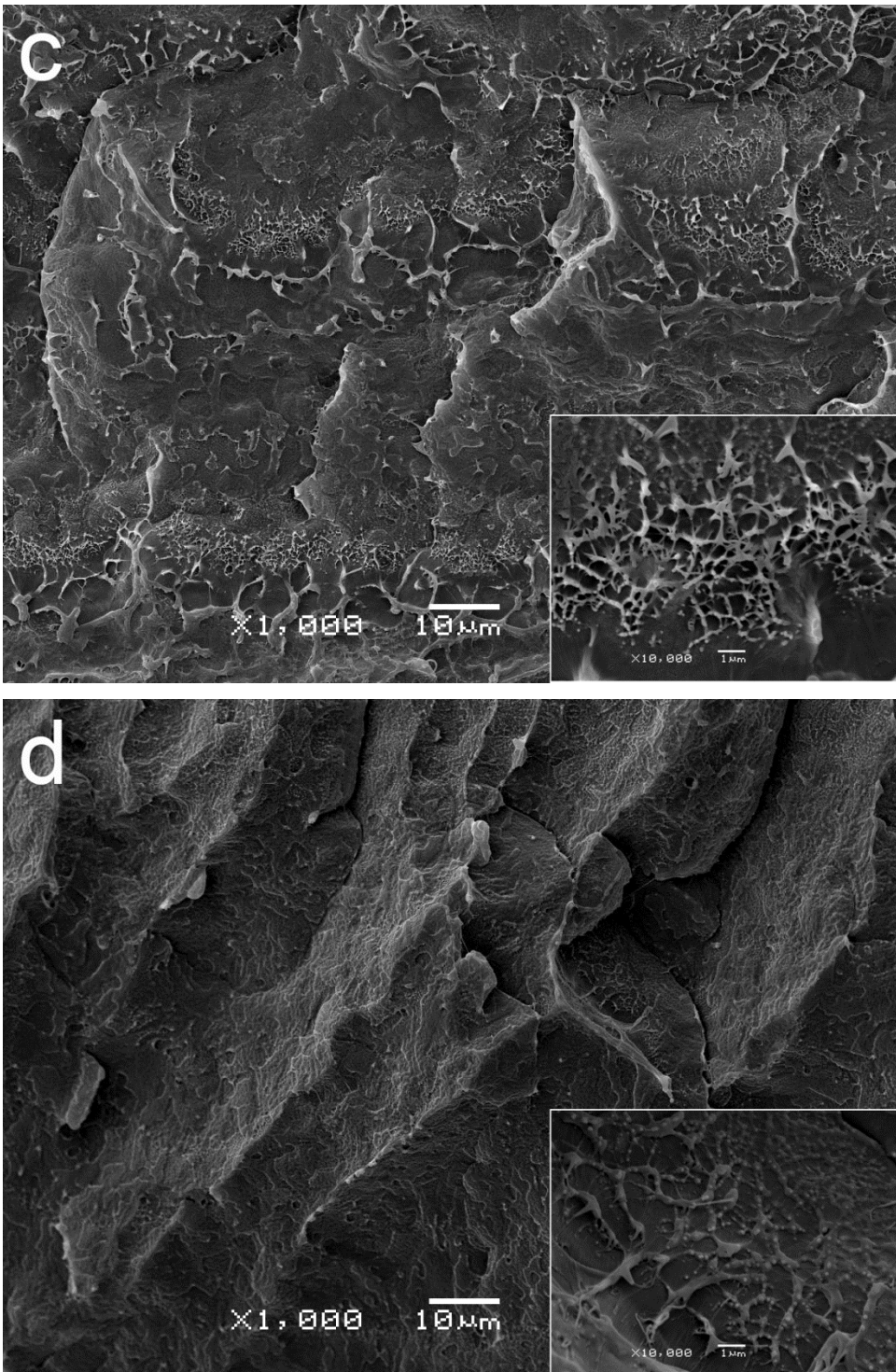
Fig. 9.11: SEM micrographs of (a) compression moulded pCBT, (b) pCBT/PMDI 0.75%, (c) pCBT/MDI 0.75% and (d) pCBT/HDI 0.75%.  (*continued*)

## 9.5    Conclusions

Cyclic butylene terephthalate oligomers were reacted in a ring-opening polymerization with three types of isocyanates: A bifunctional aromatic type, a bifunctional aliphatic type and a polymeric aromatic isocyanate. The studied isocyanate contents were 0.25–2 wt.% and all reactions took place in a batch mixer. The isocyanate-modified samples showed a considerable torque increase compared to unmodified CBT, indicating a higher molecular weight. Nevertheless GPC analysis suggested that apparently only the polyfunctional PMDI at concentrations higher than 0.5 wt.% increased the molecular weight of pCBT; the other two bifunctional types decreased $M_w$, regardless of the NCO content. Gel content measurements prior to compression moulding indicated a linear chain structure for the two bifunctional isocyanate-modified samples, whereas the polyfunctional PMDI-modified pCBT exhibited considerable gel formation at higher NCO contents. All compression moulded samples were completely soluble, indicating that the crosslinked structures in pCBT/PMDI samples had changed to linear or branched structures during this second melting. Proton NMR analysis showed that isocyanate contents up to 1 wt.% did completely react with the pCBT matrix whereas samples containing 2 wt.% of NCO did not fully react during melt blending; these samples were subjected to solid-state post-polymerization at 120 °C for 4 h in order to fully react the isocyanates and to further increase the molecular weight. What is more, NMR showed that the dominant chain extension reaction mechanism is the formation of thermally stable amide groups. It further indicated that pCBT/NCO samples before compression moulding contained more urethane groups, compared to samples after compression moulding. The number of hydroxyl end groups and amide groups slightly increased after the compression moulding step. This supports the assumption that the urethane groups dissociated at the processing temperature into isocyanate and hydroxyl end groups, the former subsequently reacted with pCBT carboxyl end groups. DSC analysis revealed a general depression of melting and crystallization temperatures, glass transition temperature as well as the degree of crystallinity. This decrease in crystallinity partly accounts for the toughening effect of isocyanates. A 22-fold to 28-fold increase in elongation at break was observed in tensile tests when the pCBT contained 0.75 to 1 wt% isocyanate. The highest toughness by means of strain energy was obtained with 0.75 wt% HDI. The most effective toughening agent was PMDI because it showed good toughness from 0.5 to 2 wt% NCO content.

Stiffness and strength generally decreased about 10 %. Tensile impact tests showed a tendency similar to the tensile results. The NCO-modified samples showed necking during impact and had high tensile-impact strengths. The fracture surfaces of isocyanate-modified samples exhibited a network-like fibrillation in a SEM analysis, indicating plastic deformation on a micrometer scale. To conclude, a toughened pCBT can be obtained when 0.5–2 wt%, preferably 0.75–1 wt.% of isocyanate is added to the ring-opening polymerization of CBT.

Since the dominant chain extension reaction mechanism was found to be amidation with the release of $CO_2$, the isocyanate toughening method might not be suitable for closed mould applications due to the requirements for liquid composite moulding as stated in section 2.2.

## 9.6    References for pCBT/NCO

1.    Abt, T, de Ilarduya, AM, Bou, JJ, and Sanchez-Soto, M. Isocyanate toughened pCBT: Reactive blending and tensile properties. eXPRESS Polymer Letters **7**(2), 172-185 (2013).

2.    Guo, B and Chan, C-M. Chain extension of poly(butylene terephthalate) by reactive extrusion. Journal of Applied Polymer Science **71**(11), 1827-1834 (1999).

3.    Raffa, P, Coltelli, M-B, Savi, S, Bianchi, S, and Castelvetro, V. Chain extension and branching of poly(ethylene terephthalate) (PET) with di- and multifunctional epoxy or isocyanate additives: An experimental and modelling study. Reactive and Functional Polymers **72**(1), 50-60 (2012).

4.    Torres, N, Robin, JJ, and Boutevin, B. Chemical modification of virgin and recycled poly(ethylene terephthalate) by adding of chain extenders during processing. Journal of Applied Polymer Science **79**(10), 1816-1824 (2001).

5.    Houghton, RP and Mulvaney, AW. Mechanism of tin(IV)-catalysed urethane formation. Journal of Organometallic Chemistry **518**(1–2), 21-27 (1996).

6.    Segura, DM, Nurse, AD, McCourt, A, Phelps, R, and Segura, A. Chapter 3 Chemistry of polyurethane adhesives and sealants. In: Philippe C, editor. Handbook of Adhesives and Sealants, vol. Volume 1: Elsevier Science Ltd, 2005. pp. 101-162.

7.  Tang, X, Guo, W, Yin, G, Li, B, and Wu, C. Reactive extrusion of recycled poly(ethylene terephthalate) with polycarbonate by addition of chain extender. Journal of Applied Polymer Science **104**(4), 2602-2607 (2007).

8.  Chen, B-K, Shen, C-H, Chen, S-C, and Chen, AF. Ductile PLA modified with methacryloyloxyalkyl isocyanate improves mechanical properties. Polymer **51**(21), 4667-4672 (2010).

9.  Yin, L, Shi, D, Liu, Y, and Yin, J. Toughening effects of poly(butylene terephthalate) with blocked isocyanate-functionalized poly(ethylene octene). Polymer International **58**(8), 919-926 (2009).

10. Dion, RP, Bank, DH, Beebe, MC, Walia, P, LeBaron, C, Oelberg, JD, Barger, MA, Paquette, MS, and Read, MD. Polymerized macrocyclic oligomer nanocomposite compositions. U.S. Patent Application US 2005/0059768 A1. 2005.

11. Lapprand, A, Boisson, F, Delolme, F, Méchin, F, and Pascault, JP. Reactivity of isocyanates with urethanes: Conditions for allophanate formation. Polymer Degradation and Stability **90**(2), 363-373 (2005).

12. Chattopadhyay, DK and Webster, DC. Thermal stability and flame retardancy of polyurethanes. Progress in Polymer Science **34**(10), 1068-1133 (2009).

13. van Bennekom, ACM, Willemsen, PAAT, and Gaymans, RJ. Amide-modified poly(butylene terepthalate): thermal stability. Polymer **37**(24), 5447-5459 (1996).

14. Tuominen, J, Kylmä, J, and Seppälä, J. Chain extending of lactic acid oligomers. 2. Increase of molecular weight with 1,6-hexamethylene diisocyanate and 2,2′-bis(2-oxazoline). Polymer **43**(1), 3-10 (2002).

15. Karger-Kocsis, J, Shang, PP, Mohd Ishak, ZA, and Rösch, M. Melting and crystallization of in-situ polymerized cyclic butylene terephthalates with and without organoclay: A modulated DSC study. eXPRESS Polymer Letters **1**(2), 60-68 (2007).

16. Zhang, Y, Guo, W, Zhang, H, and Wu, C. Influence of chain extension on the compatibilization and properties of recycled poly(ethylene terephthalate)/linear low density polyethylene blends. Polymer Degradation and Stability **94**(7), 1135-1141 (2009).

17. Karger-Kocsis, J, Felhos, D, Bárány, T, and Czigány, T. Hybrids of HNBR and in situ polymerizable cyclic butylene terephthalate (CBT) oligomers: Properties and dry sliding behavior. eXPRESS Polymer Letters **2**(7), 520-527 (2008).

18.    Roulin-Moloney, AC. Fractography and Failure Mechanisms of Polymers and Composites. London and New York: Springer, 1989. pp. 568.

# Chapter 10: Interfacial structure of pristine and modified pCBT

## 10.1   Introduction

There have been controversies for many years about the nature of the interface between lamellar crystallites and the amorphous interlamellar region. The once widely accepted two-phase model of amorphous phase and crystalline phase comprised of regularly folded chains that form well-defined smooth interfaces is a simplified one and it was found to be unable to describe all observations commonly made in semicrystalline polymers. Small-angle neutron scattering experiments and analysis of chain statistics as well as many different polymer properties do not allow to demonstrate the existence of a regularly folded chain structure. Moreover, experimental results of $^1$H NMR and $^{13}$C NMR, small-angle neutron scattering, specific heat measurements, dielectric relaxation, analysis of the Raman internal modes and electron microscopy clearly prove the presence of an appreciable amount of interfacial zone that is characterized by the partial ordering of the chain units [1].

Nowadays, the existence of an interfacial zone or region with distinct properties is widely acknowledged for most semi-rigid polymers, though its formation, nature, location and density is still a matter of controversy. From a theoretical viewpoint, an interfacial zone between amorphous and crystalline regions must exist, because the sequence of ordered chain units cannot be dissipated abruptly at the basal plane of a crystallite. The flux of chains cannot become disordered and isotropic at the sharp boundary. Hence, an interfacial zone, schematically represented in figure 10.1, where the crystalline order is dissipated must exist [1-2].
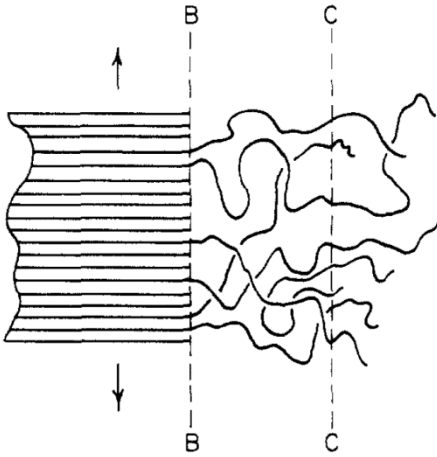
Fig. 10.1: Schematic representation of the interfacial zone (situated between crystalline and amorphous domains in a semi-crystalline polymer) transverse to the chain axis, adapted from [1]

In this diagram, a lamellar crystallite of unlimited lateral dimensions is considered. All polymer chains emerging from the crystallite traverse the plane BB located at the surface and enter the adjoining interfacial zone, situated between the planes BB and CC. Some of these chains will then intersect the plane CC that is situated in the isotropic amorphous phase. The interfacial thickness, $L_b$, (*i.e.* the distance between the planes BB and CC) was found to be in the order of 10 Å for bulk crystallized linear polyethylene with low molecular weights ($10^4$ Da) and increased to about 25 Å for molecular weight ranges of $10^5$–$10^6$ Da [1].

The degree of crystallinity is a quantitative concept and the different methods to measure it show small but significant differences between them. It was demonstrated that the degrees of crystallinity, obtained from density ($X_{C, density}$) as well as from heat of fusion ($X_{C, \Delta H}$), agree well although $X_{C, density}$ is always found to be slightly higher than $X_{C, \Delta H}$. Enthalpy measurements do not account for the interfacial zone, whereas density measurements include the interfacial contribution [1-2]. This has been demonstrated for linear and branched polyethylene, ethylene copolymers as well as for poly(ethylene oxide) and can presumably be applied to other semi-crystalline polymers [2].

### 10.2 Experimental section

The degree of crystallinity obtained from density measurements was calculated using the following expression [3-4]:

$$X_{C,density} = \frac{\rho - \rho_a}{(\rho_c - \rho_a)} \qquad (11.1)$$

where $\rho$, $\rho_a$ and $\rho_c$ are the densities of the sample, the amorphous regions and the crystalline regions, respectively. The density of the fully amorphous and fully crystalline phases of PBT have been reported to be 1.256 g/cm$^3$ and 1.400 g/cm$^3$, respectively [4].

The relative amount of interfacial fraction, $\alpha_b$, was estimated as follows [2]

$$\alpha_b = X_{C,density} - X_{C,\Delta H} \qquad (11.2)$$

where $X_{C, density}$ is the degree of crystallinity obtained from density measurements and $X_{C, \Delta H}$ is the degree of crystallinity obtained from the heat of fusion.

### 10.3 Results and Discussion

Figure 10.2 illustrates the degree of crystallinity, $X_C$, obtained from density *versus* $X_C$ obtained from the heat of fusion. As can be seen, the values of $X_{C, density}$ of the pCBT samples toughened with THF, epoxy and isocyanates, respectively, are all somewhat greater than the values of $X_{C, \Delta H}$ which was related to the interfacial contribution.
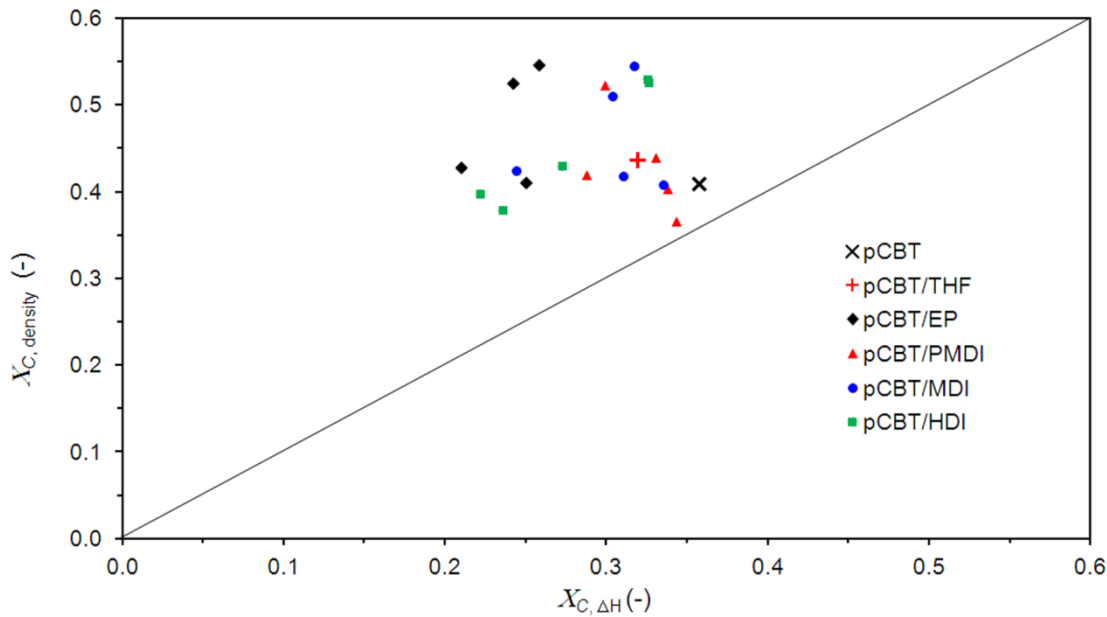
Fig. 10.2: Degree of crystallinity obtained from density, $X_{C, density}$, against the crystal fraction obtained from the heat of fusion, $X_{C, \Delta H}$

The results shown in figure 10.2 and table 10.1 demonstrate that the differences between the two crystallinities exist for both neat and modified pCBT. Interestingly, this difference was small for unmodified pCBT and for the post-polymerized samples containing 2 wt.% of isocyanate. This is explained by a decrease in the relative amount of interfacial region due to crystal perfection, which has already been demonstrated for PBT, PP, PEEK, PPO, PPS, PEN and POM [5]. Parton *et al.* [6-7] showed by TEM analysis that the transition from crystalline to amorphous regions is more pronounced and sharp in the isothermally polymerized pCBT samples. They confirmed a small amount of interfacial region and deduced a lack of tie molecules, leading to material brittleness.

Table 10.1:  Density, degree of crystallinity obtained from density- and heat of fusion measurements, and interfacial fraction for unmodified pCBT-MB as well as THF-, EP- and NCO-modified pCBT.

| Modifier | Content [wt%] | Density (kg/m$^3$) | $X_{C,density}$ (-) | $X_{C,\Delta H}$ (-) | Interfacial zone, $\alpha_b$ (-) |
|---|---|---|---|---|---|
| - | 0 | 1.313 | 0.409 | 0.357 | 0.052 |
| THF | 1.5 | 1.317 | 0.437 | 0.319 | 0.118 |
| EP | 1 | 1.333 | 0.547 | 0.258 | 0.289 |
| | 2 | 1.330 | 0.526 | 0.242 | 0.284 |
| | 3 | 1.314 | 0.411 | 0.250 | 0.161 |
| | 4 | 1.316 | 0.429 | 0.210 | 0.219 |
| PMDI | 0.25 | 1.313 | 0.404 | 0.337 | 0.066 |
| | 0.5 | 1.318 | 0.441 | 0.330 | 0.110 |
| | 0.75 | 1.315 | 0.421 | 0.287 | 0.133 |
| | 1 | 1.329 | 0.524 | 0.299 | 0.225 |
| | 2* | 1.307 | 0.367 | 0.343 | 0.024 |
| MDI | 0.25 | 1.315 | 0.419 | 0.311 | 0.109 |
| | 0.5 | 1.316 | 0.426 | 0.244 | 0.182 |
| | 0.75 | 1.328 | 0.511 | 0.303 | 0.208 |
| | 1 | 1.332 | 0.546 | 0.317 | 0.229 |
| | 2* | 1.313 | 0.409 | 0.335 | 0.074 |
| HDI | 0.25 | 1.309 | 0.379 | 0.236 | 0.143 |
| | 0.5 | 1.312 | 0.398 | 0.222 | 0.177 |
| | 0.75 | 1.330 | 0.526 | 0.326 | 0.200 |
| | 1 | 1.330 | 0.530 | 0.325 | 0.205 |
| | 2* | 1.316 | 0.430 | 0.272 | 0.157 |

* Post-polymerized at 120°C for 4h; for details see section 9.2.2.

Figure 10.3 depicts the estimated interfacial fraction against modifier content for modified pCBT. The pCBT-MB sample was used to represent the unmodified pCBT and exhibited an interfacial fraction of 0.05. All modified samples exhibited a relatively higher amount of interfacial fraction, up to a value of 0.29 for epoxy-modified pCBT. Generally, interfacial

fraction steadily increased with increasing modifier content. An exception were the post-polymerized samples containing 2 wt.% of isocyanate, probably due to crystal perfection as discussed earlier. Also, in case of EP modifier, the interfacial fraction showed a maximum between 1 and 2 wt.%.

Considering the interfacial fractions of these materials and their corresponding toughness, a certain relation is apparent. Recall that toughness increased with isocyanate content whereas maximum toughness was observed for 2 wt.% epoxy content. This tendency is well reflected in the corresponding interfacial fractions.
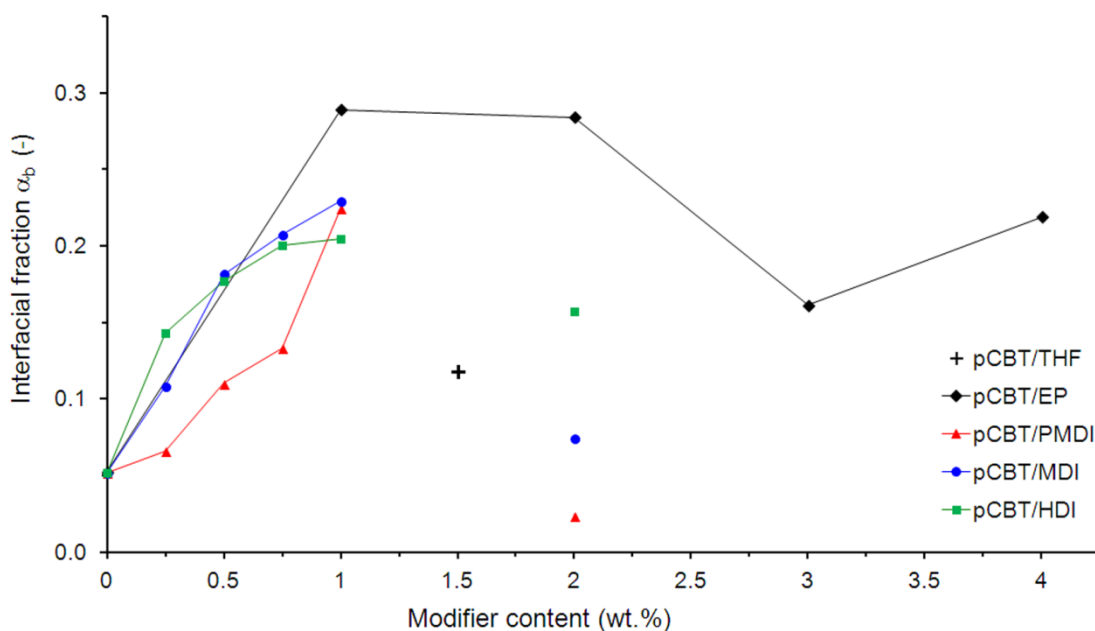


Fig. 10.3: Relative amount of interfacial fraction, $\alpha_b$, *versus* modifier content for neat and THF-, EP- and NCO-modified pCBT.

## 10.4   Conclusions

The degree of crystallinity of neat and modified pCBT, obtained from density, was found to be slightly higher compared to the one obtained from heat of fusion. This difference was found to increase for the modified samples, suggesting an increase in interfacial zone and probably in amount of intercrystalline tie molecules.

It is apparent from the results of this work that a high degree of crystallinity cannot be solely responsible for the pCBT brittleness since some post-polymerized samples had crystal fractions and relative amounts of interfacial zone similar to neat pCBT. The pCBT brittleness may rather ascribed to the sum of different effects, such as high degree of crystallinity together with a low amount of interfacial zone, low molecular weight, high crystal perfection and the lack of tie molecules between adjacent crystallites.

## 10.5    References for pCBT interfacial structure

1.    Mandelkern, L. The structure of crystalline polymers. Accounts of Chemical Research **23**(11), 380-386 (1990).

2.    Mandelkern, L. The Relation between Structure and Properties of Crystalline Polymers. Polymer Journal **17**(1), 337-350 (1985).

3.    Leung, WP and Choy, CL. Physical properties of oriented poly(butylene terephthalate). Journal of Applied Polymer Science **27**(7), 2693-2709 (1982).

4.    Vendramini, J, Bas, C, Merle, G, Boissonnat, P, and Alberola, ND. Commingled poly(butylene terephthalate)/unidirectional glass fiber composites: Influence of the process conditions on the microstructure of poly(butylene terephthalate). Polymer Composites **21**(5), 724-733 (2000).

5.    Cheng, SZD, Pan, R, and Wunderlich, B. Thermal analysis of poly(butylene terephthalate) for heat capacity, rigid-amorphous content, and transition behavior. Die Makromolekulare Chemie **189**(10), 2443-2458 (1988).

6.    Parton, H. Characterization of the in-situ polymerization production process for continuous fibre reinforced thermoplastics. PhD thesis. Department of Metallurgy and Materials Engineering. Katholieke Universiteit Leuven: Leuven, Belgium, 2006

7.    Parton, H, Baets, J, Lipnik, P, Goderis, B, Devaux, J, and Verpoest, I. Properties of poly(butylene terephthatlate) polymerized from cyclic oligomers and its composites. Polymer **46**(23), 9871-9880 (2005).

# Chapter 11: Reactive blending of CBT with benzoxazine[3]
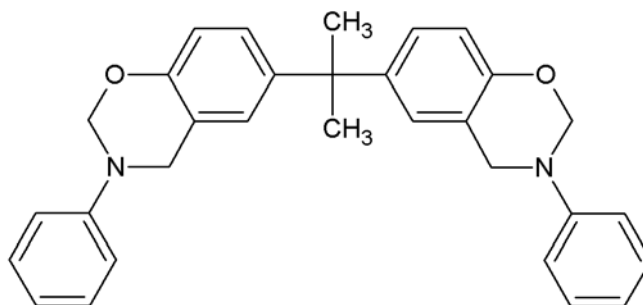
CBT was *in situ* polymerized in the presence of benzoxazine (referred to as BOX) in a batch mixer. It was found that the presence of BOX completely inhibited the ROP of CBT and it was assumed that the transesterification catalyst was consumed during the homopolymerization of BOX. This problem was adressed by first polymerizing CBT for 5 min and then adding the BOX as well as by adding extra catalyst to CBT/BOX systems prior to melt blending.

No sign of reaction was found, suggesting that both CBT and BOX homo-polymerized separately, without forming pCBT-BOX copolymer. The resulting (p)CBT/BOX blends appeared to be of low molecular weight and were exceptionally brittle.

---

[3] Measurements were performed in the Department of Polymer Engineering, Budapest University of Technology and Economics, Hungary.

## 11.1  Introduction

As it was shown in the preceding chapters, reactive chain extension of CBT with bi- and polyfunctional compounds is a feasible method to toughen pCBT. It was demonstrated that epoxy and isocyanate compounds are capable of coupling two or more pCBT chains by reacting with the terminal carboxyl and/or hydroxyl end groups of the polymer and thus the toughness of pCBT increases. Since many different groups of chain extenders exist, it is of interest to explore different types and to study their role on the properties, most importantly on the toughness of pCBT. As discussed earlier, addition-type chain extenders without releasing by-products, with high reactivity and capable of yielding a linear macromolecular structure are of particular interest.

In the 1980s, Inata and Matsumura investigated effective chain extenders for linear polyesters and published their results in a series of articles [1-6]. They studied nitrogen-containing bis-heterocycles, which were reactive with hydroxyl and carboxyl terminals of the polyesters to form addition linkages. Among these bis-heterocycles discussed in these articles, benzoxazine compounds proved to be very effective chain extenders for both PET and PBT [3, 7-8].

Moreover, they are a new class of thermoset materials and are obtained by condensation of primary amines with aldehydes and phenol. The benzoxazine monomers can be thermally cured in a homopolymerization without any catalysts and polybenzoxazines (referred to pBOX) are obtained [9]. These newly developed pBOX resins possess unique features such as near-zero volumetric change upon curing, low water absorption, for some polybenzoxazine-based materials $T_g$ much higher than cure temperature, high char yield, no strong acid catalysts required for curing, and release of no by-products during curing [10].  Although benzoxazines were already synthesized in the 1940s by Holly and Cope [11], the potential of polybenzoxazines has been recognized only recently by Ishida [9, 12]. These properties make benzoxazine potential chain extenders for pCBT. In this chapter, the potential of benzoxazine as a chain extender and toughening agent for CBT is studied.

## 11.2   Experimental section

### 11.2.1 Materials

One-component cyclic butylene terephthalate oligomers (CBT160$^{®}$) were used in this chapter. N-phenyl bisphenol A based 1,3-benzoxazine was used for chemical modification of CBT.

### 11.2.2 Sample preparation

CBT/BOX blends were prepared in a mortar and subsequently dried at 105 °C for 8 h. The prepared blend compositions are listed in table 11.1.

Table 11.1:  CBT/BOX blend compositions

| Sample | Composition CBT/BOX [wt/wt] |
|---|---|
| CBT | 100 / 0 |
| CBT/BOX 2.5 | 97.5 / 2.5 |
| CBT/BOX 5 | 95 / 5 |
| CBT/BOX 25 | 75 / 25 |
| CBT/BOX 50 | 50 / 50 |
| CBT/BOX 75 | 25 / 75 |
| BOX | 0 / 100 |

Previously dried CBT/BOX blends were *in situ* polymerized during compression moulding in a hot press (Collin Teach-Line Platen Press 200E, Dr. Collin GmbH, Ebersberg, Germany) in a metal frame between two PTFE films at 240 °C for 15 min in ambient atmosphere. The polymerized CBT/BOX blends (referred to as pCBT/BOX) were quickly cooled to room temperature in the cold stage of the press. The resulting pCBT/BOX films

had dimensions of ca. 150x150x1 mm$^3$. Nevertheless, the great brittleness of the BOX-modified pCBT samples did not allow specimen extraction for mechanical testing.

## 11.3   Characterization

Torque *versus* time measurements of CBT and BOX were conducted in a lab-scale batch mixer (Brabender Plasti-Corder PL 2000 W50EHT, Brabender GmbH & Co. KG, Duisburg, Germany), equipped with a torque measuring system at 240 °C and 60 min$^{-1}$ rotor speed in ambient atmosphere.

DSC analysis was performed on a Mettler Toledo DSC821 (Greifensee, Switzerland) using a heating and cooling rate of 20 °C/min. Samples of 6–8 mg were heated and cooled in the temperature range of 20–300 °C. The second heating run was performed equally.

## 11.4   Results and Discussion

The chain extension reaction between (growing) pCBT chains and BOX is carried out in the melt; the proposed reaction mechanisms are shown in figure 11.1.

Both reaction pathways are of addition type with no by-products, which is the preferable chain extension mechanism for pCBT.
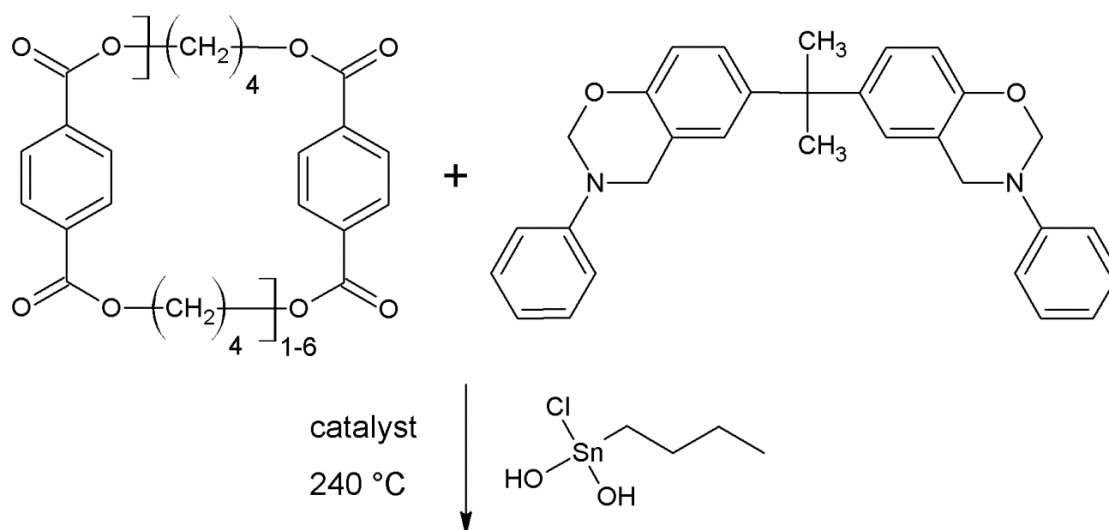
**Carboxyl reaction:**
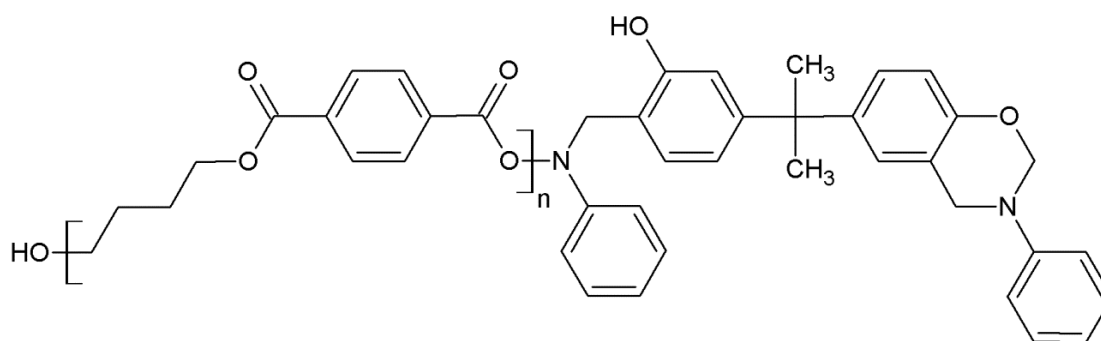
**Hydroxyl reaction:**
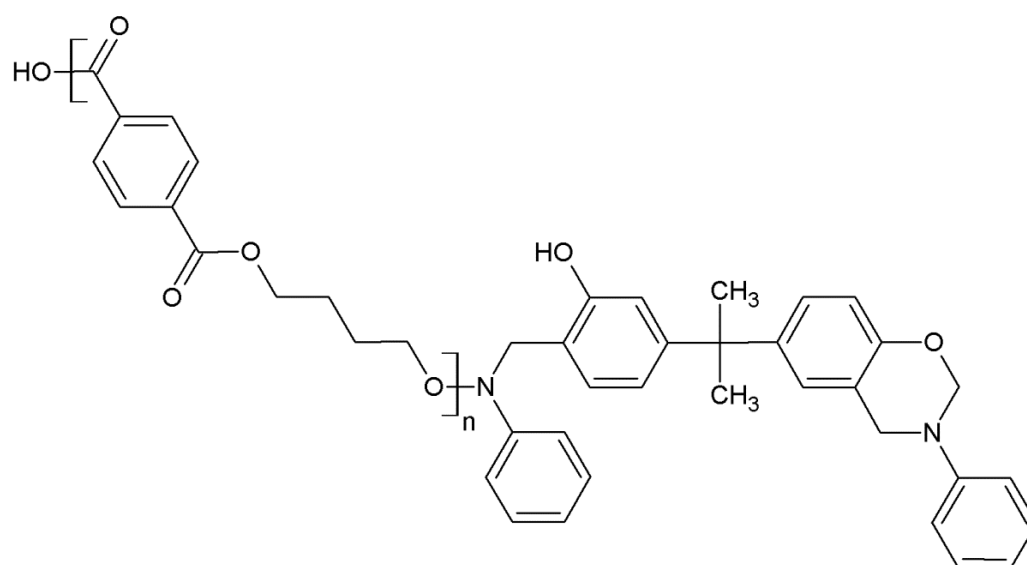
Fig. 11.1: Possible reaction pathways of pCBT carboxyl and hydroxyl end groups and BOX

### 11.4.1 Torque *versus* time measurements

Torque was monitored over reaction time for neat CBT as well as for the CBT/BOX blends (*c.f.* figure 11.2). Unmodified CBT showed a torque onset after 3 min and reached a relatively low torque value of 2 Nm due to the negative influence of the ambient atmosphere on the ROP, as discussed earlier.

A previously dried CBT/BOX blend containing 5 wt.% of BOX was equally processed, but no torque increase could be observed within 15 min (torque curve not shown in figure 11.2). After melt blending, the collected material appeared to be unpolymerized CBT together with apparently phase-separated, molten BOX. This suggests that the ROP of CBT was inhibited due to the presence of BOX. A possible explanation therefore is that the transesterification catalyst may be either deactivated or consumed by the BOX. To address this problem, two different strategies were used.

In a first attempt, neat CBT was melt blended for 5 min and then 5 wt.% of BOX was subsequently added to the polymerizing (p)CBT. The torque decreased slightly, probably due to a plasticising effect of the molten BOX. Nevertheless, the torque value quickly recovered to a similar value prior to BOX addition and remained fairly constant until the end of the experiment. The lower torque of this sample as compared to neat CBT suggests a relatively low molecular weight. The collected material was yellowish and quite brittle.

In another attempt, a ternary blend of CBT/BOX/Fascat 93.5/5/1.5 (*wt/wt/wt*) was melt blended using equal processing conditions. The torque onset was already detected after 1.5 min, but the maximum torque remained much lower as compared to the one of unmodified CBT. Similarly, the collected sample was too brittle to be used for mechanical testing. It is not clear whether BOX reacted with pCBT. Nevertheless, the comparably lower torque values clearly indicate low molecular weight pCBT.
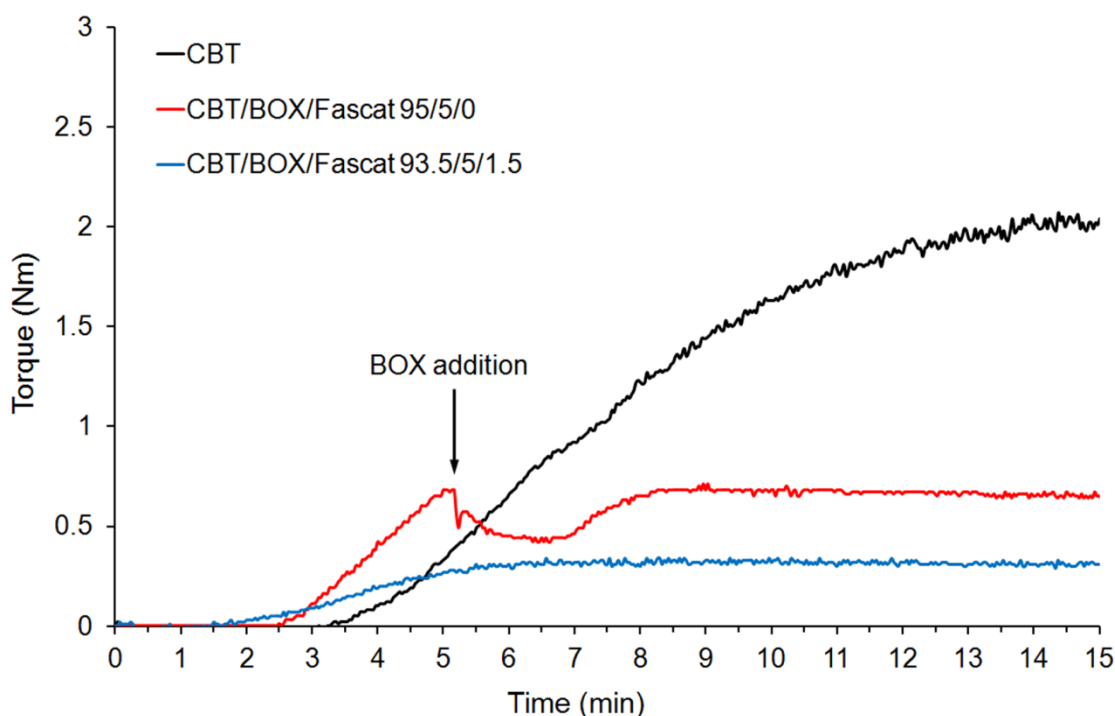
Fig. 11.2: Torque signals of CBT, CBT polymerized for 5 min and subsequently 5 wt.% BOX added, and CBT/BOX 5%/Fascat 1.5% ternary blend.

## 11.4.2 DSC analysis

CBT/BOX dry blends containing various amounts of BOX were analysed by DSC. During the first heating scan (*c.f.* figure 11.3a), it can be seen that the high heating rate of 20 °C/min hindered the cold crystallization of pCBT and subsequent polymer melting. The presence of BOX did not influence this effect.

Neat BOX showed an exothermic peak at 243 °C, which was ascribed to the homopolymerization of BOX, leading to pBOX. CBT/BOX blends containing high amounts of BOX (*i.e.* 25–75 wt.%) exhibited this BOX polymerization peak around 260 °C. This suggests that the (p)CBT reacted with BOX and therefore hindered the homopolymerization of BOX. Consequently, the polymerization of BOX was shifted towards higher temperatures.

Regarding the first cooling scan, it is apparent from figure 11.3b that the pCBT crystallization from the melt was also hindered by the BOX and the crystallization peak

temperature of pCBT was progressively shifted towards lower temperatures with increasing BOX content, namely from 186 °C for neat pCBT to 121 °C for pCBT/BOX 50%; at higher BOX contents the pCBT crystallization peak vanished.

Similarly, melting temperature and degree of crystallinity of pCBT markedly decreased with increasing BOX content during the second heating scan (*c.f.* figure 11.3c). It is clear from these results that a chemical interaction between pCBT and BOX is evident. Nevertheless, torque measurements suggested that the CBT transesterification catalyst is either deactivated or consumed by the BOX, leading to low molecular weight pCBT/BOX materials.
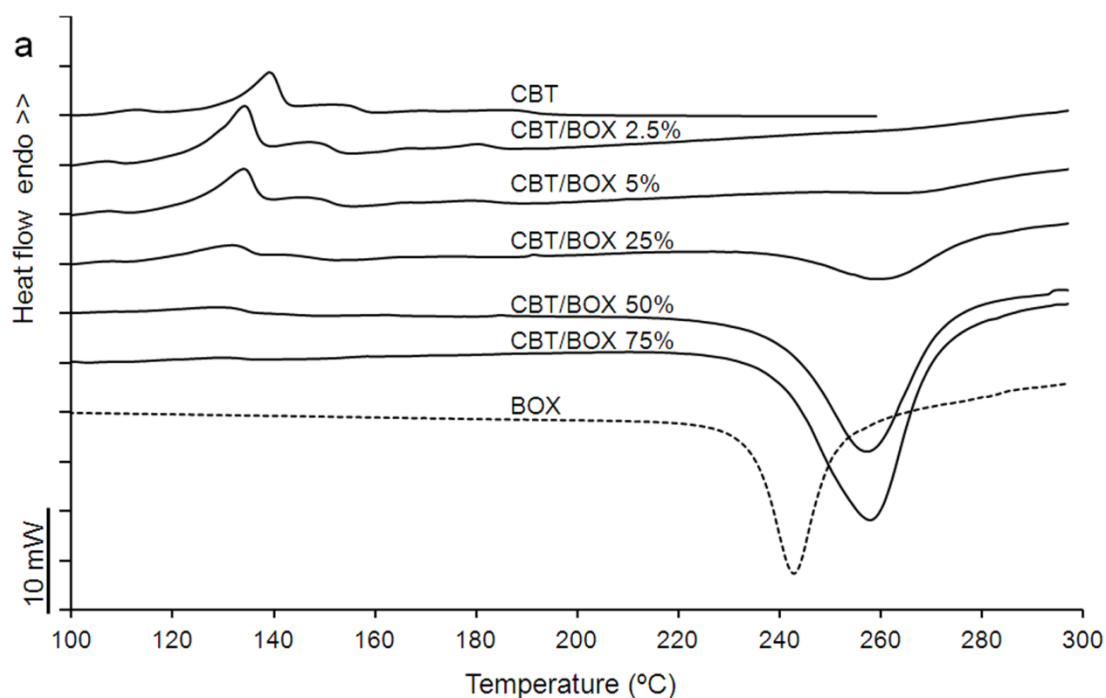


Fig. 11.3: DSC traces of CBT/BOX systems, (a) first heating, (b) first cooling and (c) second heating recorded at 20 °C/min.
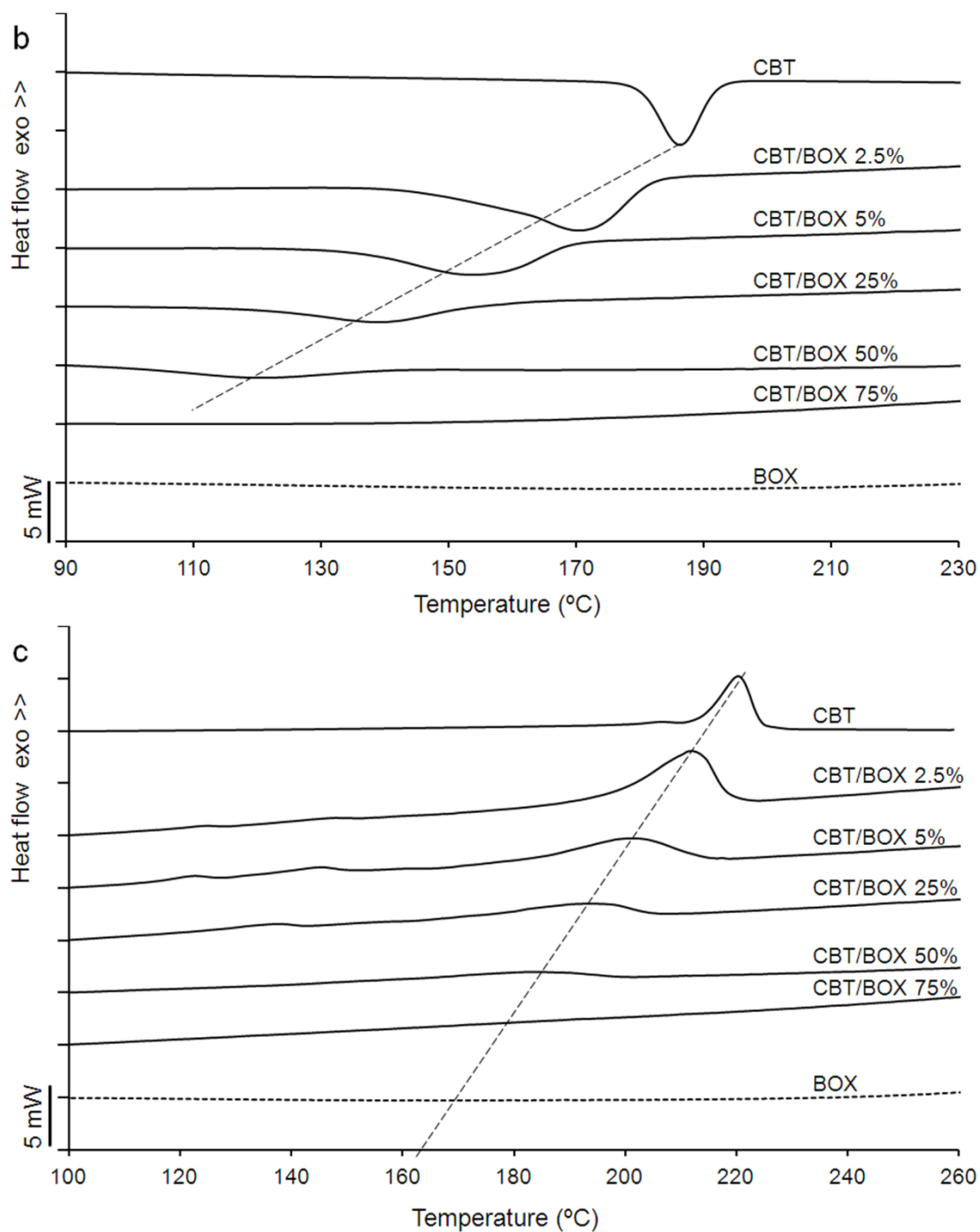
Fig. 11.3: DSC traces of CBT/BOX systems, (a) first heating, (b) first cooling and (c) second heating recorded at 20 °C/min. (*continued*)

## 11.5   Conclusions

Efforts were made to react cyclic butylene terephthalate oligomers with benzoxazine. The studied BOX contents covered the whole composition range. Torque *versus* time measurements revealed that the ROP of CBT was inhibited by the presence of BOX. It was assumed that the transesterification catalyst may be either deactivated or consumed by the BOX. Sequential BOX addition or adding extra catalyst to the CBT did not improve the torque level substantially and the obtained materials were exceptionally brittle. DSC analysis evidenced chemical interaction between pCBT and BOX. The crystallization of pCBT was hindered by the BOX and the peak temperature was progressively shifted towards lower temperatures with increasing BOX content. Similarly, melting temperature and degree of crystallinity of pCBT markedly decreased with increasing BOX concentration. At high BOX contents, the homopolymerization of BOX was shifted towards higher temperatures, suggesting that the pCBT reacted with BOX and therefore hindered the homopolymerization of BOX.

Despite the chemical interaction of pCBT and BOX, low molecular weight pCBT/BOX materials were obtained which were characterized by a great brittleness and sample extraction for mechanical testing was not possible. Therefore it can be concluded that chemical modification of CBT wit bezoxazine is not a useful way to toughen pCBT.

## 11.6 References for pCBT/BOX

1.   Inata, H and Matsumura, S. Chain extenders for polyesters. I. Addition-type chain extenders reactive with carboxyl end groups of polyesters. Journal of Applied Polymer Science **30**(8), 3325-3337 (1985).

2.   Inata, H and Matsumura, S. Chain extenders for polyester. II. Reactivities of carboxyl-addition-type chain extenders; bis cyclic-imino-ethers. Journal of Applied Polymer Science **32**(5), 5193-5202 (1986).

3.   Inata, H and Matsumura, S. Chain extenders for polyesters. III. Addition-type nitrogen-containing chain extenders reactive with hydroxyl end groups of polyesters. Journal of Applied Polymer Science **32**(4), 4581-4594 (1986).

4.   Inata, H and Matsumura, S. Chain extenders for polyesters. IV. Properties of the polyesters chain-extended by 2,2′-bis(2-oxazoline). Journal of Applied Polymer Science **33**(8), 3069-3079 (1987).

5.   Inata, H and Matsumura, S. Chain extenders for polyesters. V. Reactivities of hydroxyl-addition-type chain extender; 2,2′-bis(4h-3,1-benzoxazin-4-one). Journal of Applied Polymer Science **34**(7), 2609-2617 (1987).

6.   Inata, H and Matsumura, S. Chain extenders for polyesters. VI. Properties of the polyesters chain-extended by 2,2′-bis(4H-3,1-benzoxazin-4-one). Journal of Applied Polymer Science **34**(8), 2769-2776 (1987).

7.   Böhme, F, Jakisch, L, Komber, H, and Wursche, R. Multifunctional coupling agents. Part 4: Block copolymers based on amino terminated polyamide-12 and carboxy terminated poly(butylene terephthalate). Polymer Degradation and Stability **92**(12), 2270-2277 (2007).

8.   Wörner, C, Müller, P, and Mülhaupt, R. Toughened poly(butylene terephthalate)s and blends prepared by simultaneous chain extension, interfacial coupling, and dynamic vulcanization using oxazoline intermediates. Journal of Applied Polymer Science **66**(4), 633-642 (1997).

9.   Ishida, H and Rodriguez, Y. Curing kinetics of a new benzoxazine-based phenolic resin by differential scanning calorimetry. Polymer **36**(16), 3151-3158 (1995).

10.  Ghosh, NN, Kiskan, B, and Yagci, Y. Polybenzoxazines—New high performance thermosetting resins: Synthesis and properties. Progress in Polymer Science **32**(11), 1344-1391 (2007).

11. Holly, FW and Cope, AC. Condensation Products of Aldehydes and Ketones with o-Aminobenzyl Alcohol and o-Hydroxybenzylamine. Journal of the American Chemical Society **66**(11), 1875-1879 (1944).

12. Ishida, H. Process for preparation of benzoxazine compounds in solventless systems. U.S. Patent 5,543,516, 1996. 1996.

# Chapter 12: pCBT/POSS nanocomposites

**Publications derived from this work [1-2]:**

## Properties of POSS blends with pCBT, PMMA, PC and POM thermoplastics

### Tobias Abt, Miguel Sánchez-Soto* and Silvia Illescas

Centre Català del Plàstic,
Universitat Politècnica de Catalunya,
Colom 114, 08222 Terrassa, Spain
Fax:+34-93-784-18-27
E-mail: tobias.abt@upc.edu
E-mail: m.sanchez-soto@upc.edu
E-mail: silvia.illescas@upc.edu
*Corresponding author

### Asier Arostegui

Mechanical and Industrial Production Department,
Mondragon Unibertsitatea,
Loramendi 4, 20500 Arrasate-Mondragón, Spain
Fax: +34-94-379-15-36
E-mail: aarostegui@eps.mondragon.edu

## Nanocomposites of *in-situ* polymerized Cyclic Butylene Terephthalate and Polyhedral Oligomeric Silsesquioxanes

T. Abt[1], S. Illescas[1], M. Antunes[1], M.A. Cáceres[1] and M. Sánchez-Soto[1]

1. Centre Català del Plàstic, CCP, Universitat Politècnica de Catalunya, C/ Colom nº 114, 08222 Terrassa, España, tobias.abt@upc.edu

## 12.1  Introduction

Polymer nanocomposites, in which the filler has at least one dimension in the nanometre range, have attracted much interest in the last few years for the development of high-performance materials. In fact, it is well recognised that the behaviour of composites largely depends on interfacial interactions, so that the smaller in size the components, the greater the contribution of interfacial interactions to the material properties. Thus, a major challenge in the development of high performance nanocomposites is the control of nanoparticle dispersion. The mechanical, thermal and physical properties are greatly enhanced by the incorporation of nanoparticles of different sizes and aspect ratios, such as layered silicates [3], carbon nanotubes [4] and polyhedral oligomeric silsesquioxane (POSS) molecules [5-7] into various polymeric matrices. POSS-based materials have received great attention in recent years both as polymer nanocomposites and as organic-inorganic hybrids. POSS molecules have a basic polyhedral silicon-oxygen nanostructured skeleton or cage described by the general chemical structure $R[SiO_{1.5}]_8$. This cage is surrounded by a corona of organic groups linked to silicon atoms by covalent bonds and it may be fully 'condensed' or an 'open' structure. The functionality, solubility, polarity and reactivity of these molecules can be easily changed through modifying the organic groups with a variety of functional groups. The interactions and/or reactions of these organic functional groups with a polymer may result in the nanometric dispersion of POSS into the matrix [5-7].

In order to form stable polymer/nanoparticle systems, different routes have been proposed. POSS molecules can be either physically dispersed in polymer matrices using traditional melt blending processing techniques [8-9], reactive blending [10] or linked to the polymer chains by direct copolymerization or grafting [11-13], *via* suitable reactive side groups of POSS. POSS and its derivatives have been successfully incorporated in various commodity [10, 14], engineering [8, 15] and high-performance [16-17] thermoplastic polymers. The incorporation of POSS or its derivates can lead to dramatic improvements of several properties such as increases in use temperature, oxidation resistance, as well as reductions in flammability and viscosity during processing [5-6, 18].

Many polyester/POSS nanocomposites have already been prepared using PET [19-24], polycarbonate [8-9, 25] or PBT [26-27] as matrix. It is apparent from this large body of articles that synergetic reinforcing effects of POSS were only observed when good

compatibility existed; otherwise POSS aggregation occurred which led to a decrease in mechanical properties. So far, incompletely condensed trisilanol POSS [19-21, 24] as well as mono- and polyepoxy POSS [21, 23, 27] showed a reinforcement effect in PET and PBT nanocomposites. Unreactive octamethyl POSS considerably increased the fire retarding performance of PET [22].

Regarding pCBT/POSS nanocomposites, little information is available. Among the few reports, Wan and co-workers [28] prepared a thermally stable organoclay using aminopropylisooctyl POSS as a surfactant for sodium montmorillonite. In a further step, CBT catalyst was incorporated into the POSS-modified clay. They then used this POSS-clay-catalyst complex to initiate the ROP of CBT and achieved clay exfoliation even at 10 wt.% of clay loading. This nanocomposite was then used as a masterbatch for conventional PBT with a final clay content of 2 wt.%. POSS-modified clay was also directly added to PBT. Both methods resulted in an increase in stiffness and strength which was further enhanced with the masterbatch method.

In a very similar work, McLauchlin *et al.* [29] prepared a masterbatch comprising pCBT and POSS-modified clay, which was subsequently melt blended with PBT to give nanocomposites containing 3 wt.% of clay mineral. An intercalated/exfoliated morphology was obtained and consequently stiffness and strength increased. On the other hand, the CBT ring-opening catalyst caused a depolymerization of the PBT.

Wu *et al.* [30] synthesized a POSS-Sn initiator for the ROP of CBT using trisilanolisooctyl POSS and butyltin trichloride as reactants. This POSS-Sn initiator was used to prepare pCBT/POSS nanocomposites with up to 20 wt.% of POSS content. Glass transition temperature and crystallization temperature slightly increased with POSS loading. On the other hand, molecular weight decreased due to the increasing amounts of catalyst bonded to the POSS. Nevertheless, thermal stability of the nanocomposites improved by up to 11 °C.

This chapter seeks to explore the role of differently substituted POSS types on the ROP of CBT and on the final properties of the pCBT/POSS nanocomposites. The aim is to achieve a nanoreinforcement effect on pCBT by exploiting the low melt viscosity of CBT to obtain good POSS dispersion. Moreover, reactive POSS types may be used as building blocks for pCBT/POSS copolymers or telechelics [6].

## 12.2   Experimental Section

### 12.2.1 Materials

One-component cyclic butylene terephthalate oligomers (CBT160[®]) were used throughout this chapter. Octamethyl POSS[®] (referred to as OM-POSS), Isooctyl POSS[®] (I-POSS), Trisilanolphenyl POSS[®] (T-POSS), Triglycidylisobutyl POSS[®] (TG-POSS) and Glycidyl POSS[®] (G-POSS) were used. The POSS types are shown in figure 12.1 and described in detail in section 3.5.1.
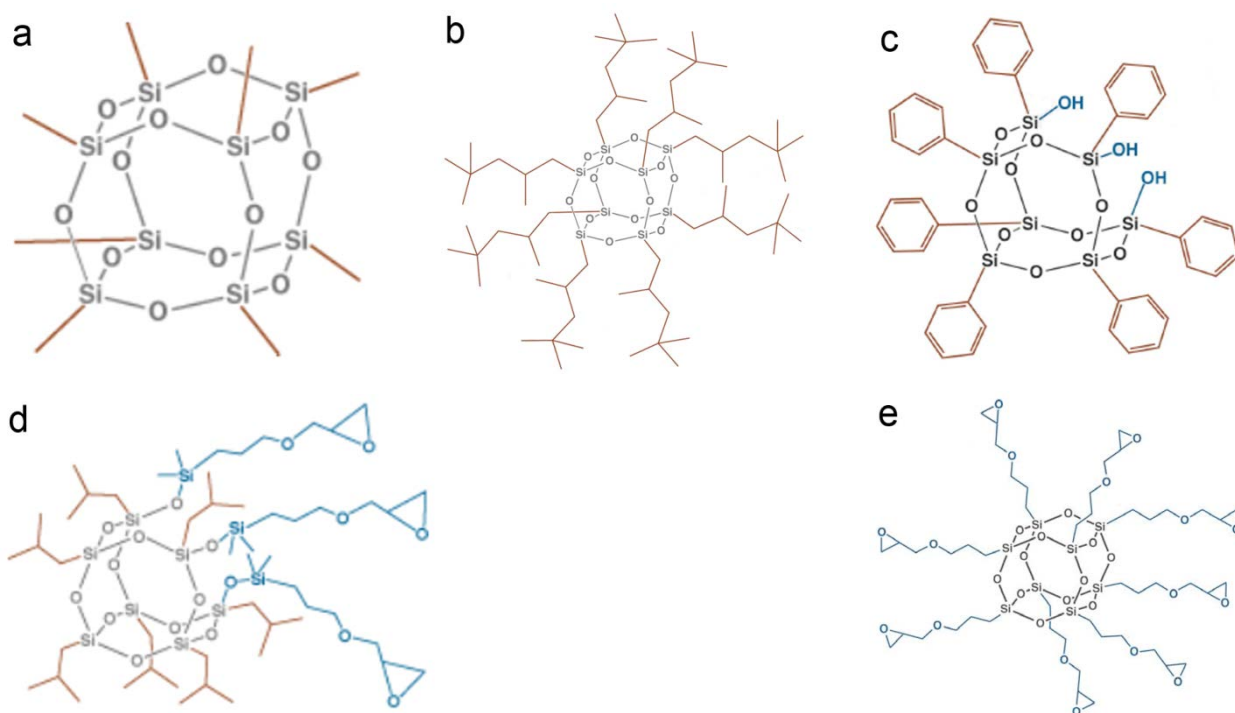


Fig. 12.1: Chemical structures of (a) OM-POSS, (b) I-POSS, (c) T-POSS, (d) TG-POSS and (e) G-POSS.

OM-POSS and I-POSS were chosen as non-reactive POSS types due to their alkyl substitution whereas TG-POSS and G-POSS were considered as reactive POSS types due to their glycidyl functional groups. T-POSS was also considered reactive, because not the pendant phenyl groups but the silanol (–Si-OH) of the incompletely condensed POSS

cage may react with the pCBT chains *via* transesterification. Moreover, this POSS type may interact with the pCBT matrix by the $\pi$–$\pi$ interaction between the phenyl rings of both POSS and pCBT [7, 31].

### 12.2.2 Sample preparation

Only small amounts of POSS were availability for this study, therefore melt blending could not be used for sample production because it would require substancial amounts of POSS. For this reason, only 12 g of "homogenous" CBT/POSS blends containing 2.5, 5 and 10 wt.% of each POSS type were prepared using mortar and pestle. The blends were vacuum dried for 8 hours at 80 °C and then *in situ* polymerized during compression moulding at 230 °C. Since no information about the influence of each POSS grade on the ROP was available, the optimum CBT polymerization time of 20 min as established in chapter 6 was used for all samples.

It is noteworthy that during the preparation of pCBT/I-POSS samples an excess of POSS migrated to the surface was observed for all weight contents of I-POSS, indicating incompatibility of this POSS type with the pCBT matrix. Moreover, most of the prepared pCBT/POSS samples exhibited an exceptional brittleness and broke during demoulding. An exception was pCBT/TG-POSS; these samples appeared somewhat tougher and were subjected to tensile testing. The prepared materials were further characterized despite the apparently poor mechanical properties of most samples.

### 12.3   Characterization

At first, pristine POSS was characterized using DSC and TGA. Then, the influence of POSS on the *in situ* polymerization of CBT was studies using torque *versus* time and DSC measurements. Finally, pCBT/POSS composites prepared by compression moulding were analysed by TGA as well as by SEM and SEM-EDX. The mechanical properties of pCBT/TG-POSS samples were determined by tensile tests.

## 12.4   Results and Discussion

### 12.4.1 POSS characterization

**DSC analysis**

Around 10 mg of pristine POSS was heated under nitrogen atmosphere from room temperature to 250 °C at a heating rate of 10 °C/min; DSC thermograms are shown in figure 12.2.

Both OM-POSS and T-POSS are crystalline solids, whereas I-POSS, TG-POSS and G-POSS are viscous liquids at room temperature. Therefore, only the former two types may exhibit melting signals. In fact, T-POSS showed an endotheric peak at 221 °C which was attributed to the melting of the POSS crystals [9, 21]. Hence, this POSS type was in molten state during compression moulding at 230 °C which is favourable for a good dispersion with resultant small POSS domains, provided that good pCBT-POSS compatibility exists. On the other hand, OM-POSS did not show a signal in the studied temperature range. This POSS type does not exhibit a melting point but sublimes above 200 °C and thermally decomposes above 300 °C [32], as will be also shown later by TGA analysis. Regarding the liquid POSS types, their respective cooling and second heating traces (not shown here) were essentially equal to first heating. This suggests that no POSS–POSS self-reaction occurred upon heating in the studied temperature range.
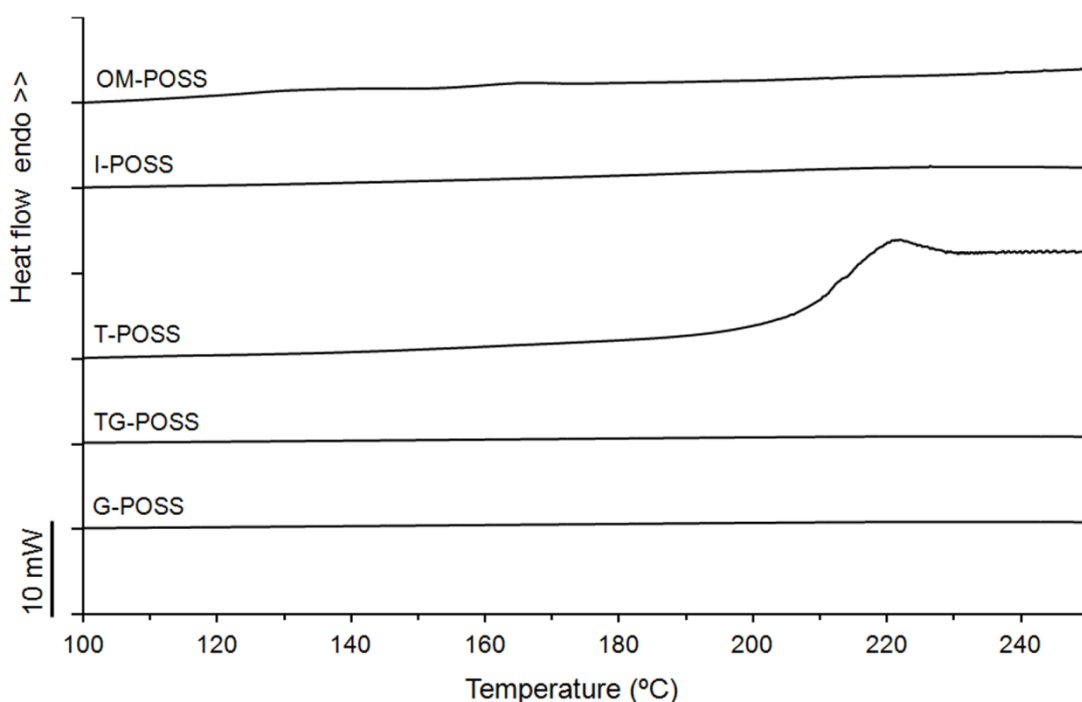
Fig. 12.2: DSC first heating scan of the used POSS types; heating rate of 10°C/min.

**TGA analysis**

The thermal stability of the different POSS types was studied using thermogravimetric analysis in nitrogen atmosphere; results are shown in figure 12.3 and table 12.1.

The thermal degradation pathway of OM-POSS was found to be a two step mass loss; the first one was a major mass loss of 81% at 306 °C and the second one was a minor mass loss of 9% at 469 °C. This was ascribed to an almost complete sublimation of OM-POSS [32] with ca. 10 wt.% of residue at 900 °C.

Regarding I-POSS, thermal stability considerably increased by almost 150 °C with increasing size of the alkyl substituent, *i.e.* the isooctyl groups. The longer alkyl chains lead to almost complete evaporation of POSS instead of its sublimation [32] with a negligible residue at 900 °C.
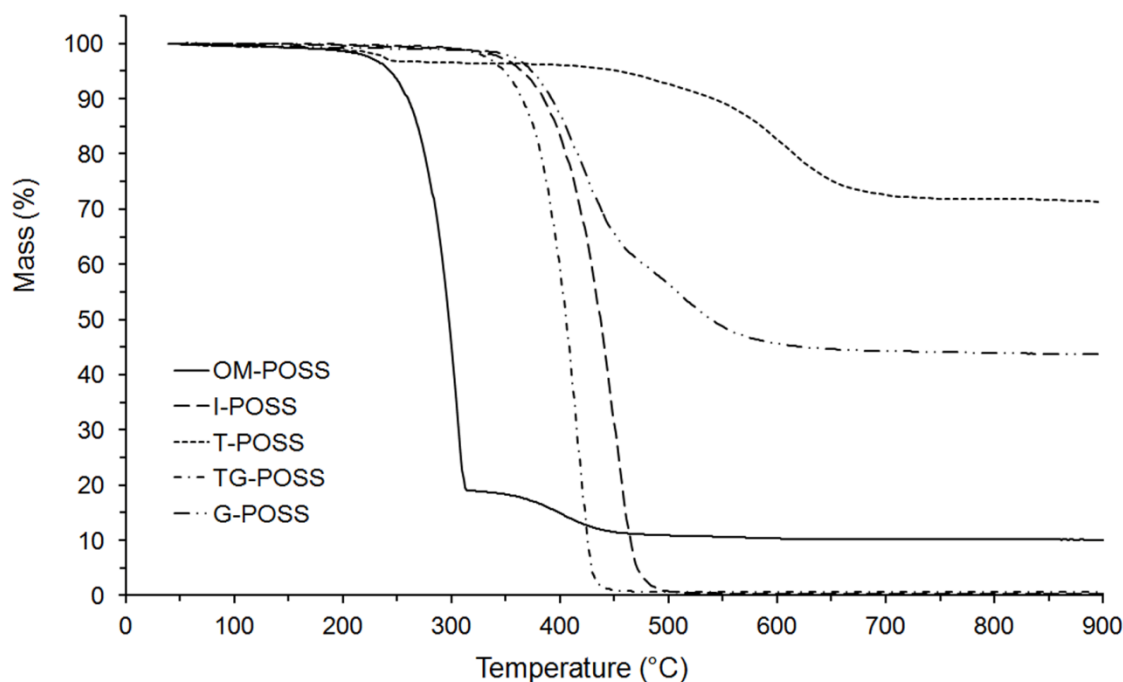
Fig. 12.3: TGA normalized mass *versus* temperature in the range of 30–900 °C of the used POSS types. Heating rate: 10 °C/min; $N_2$ atmosphere.

Two distinct mass losses were detected for T-POSS. The first mass loss occurred in the range of 50 °C and 243 °C. Between 50°C and 225 °C a continuous weight loss of about 1.3% was observed. It was followed by a small step located between 225 °C and 243 °C. The total mass loss of 3.0% was ascribed to the loss of water from the trisilanol, matching well with the theoretical amount of one released water molecule, *i.e.* 1.9%. The second major mass loss occurred at a relatively high temperature above 600 °C, with a final residue of around 75% at 900 °C. This phenyl-substituted POSS was found to thermally decompose by the release of benzene and sublimation of the POSS molecules. The high amount of residue was attributed to the entrapment of carbon in the POSS structure, due to a condensation of phenyl groups [32].

TG-POSS exhibited a single-step mass loss at $T_{max}$ = 415 °C. This POSS type behaved quite similar to I-POSS, *i.e.* a single step degradation with a negligible amount of residue. It was assumed that the degradation mechanism is mainly governed by the 5 isobutyl groups and less by the three glycidyl groups. This is in line with the relatively higher degradation temperatures of I-POSS due to the higher thermal stability of isooctyl as compared to isobutyl.

Table 12.1:  TGA data of of the used POSS types; heating from 30 °C to 900 °C at 10 °C/min in $N_2$ atmosphere.

| Sample | $T_{5\% \, wt. \, loss}$ [°C] | $T_{max,1}$ [°C] | $T_{max,2}$ [°C] | Residue at 900 °C [wt.%] |
|---|---|---|---|---|
| OM-POSS | 243.5 | 305.5 | 399.4 | 10.1 |
| I-POSS | 365.3 | 451.3 | - | 0.3 |
| T-POSS | 454.1 | 241.3 | 581.4 | 71.3 |
| TG-POSS | 348.7 | 414.6 | - | 0.6 |
| G-POSS | 374.3 | 425.3 | 510.6 | 43.7 |

G-POSS showed a comparably high thermal stability with a two step mass loss leading to *ca.* 44% residue at 900 °C. This is a higher amount of residue as compared to the theoretical value based on a total conversion to silica, *i.e.* the inorganic Si–O fraction in G-POSS (*ca.* 31%), suggesting that some of the organic mass was retained in the POSS structure.

In view of the thermal stabilities of the used POSS types, an improvement in pCBT thermal stability might be expected for all POSS types except OM-POSS since the latter possesses a lower thermal stability as compared to pristine pCBT ($T_{max}$ = 405 °C).

### 12.4.2 CBT/POSS characterization

**Torque *versus* time measurements**

The effect of the different substitution groups of POSS on the ROP of CBT was studied by torque versus time measurements. CBT/POSS blends containing 2.5 wt.% of POSS were used for this purpose; torque curves of neat CBT and CBT/ POSS blends are shown in figure 12.4.

As expected, OM-POSS and I-POSS behaved quite similarly due to their unreactive nature. CBT/OM-POSS 2.5% showed maximum torque of 17 Nm after 7 min and the CBT/I-POSS blend showed maximum torque of 21 Nm after 5 min. It is somewhat

surprising though that both types generated a prominent torque peak as well as a considerably higher torque as compared to pristine CBT. This may be explained by physical interactions between POSS and pCBT, leading to a higher viscosity.

The incompletely condensed T-POSS delayed the onset of ROP by 6 min with respect to neat CBT. The trisilanol group of this POSS type apparently affected the ROP. Moreover, as was shown by TGA, loss of water from the trisilanol at the processing temperature should be expected, leading to hydrolysis of pCBT. Although polymerization was slow, a maximum torque of 17 Nm at the end of the experiment was measured.
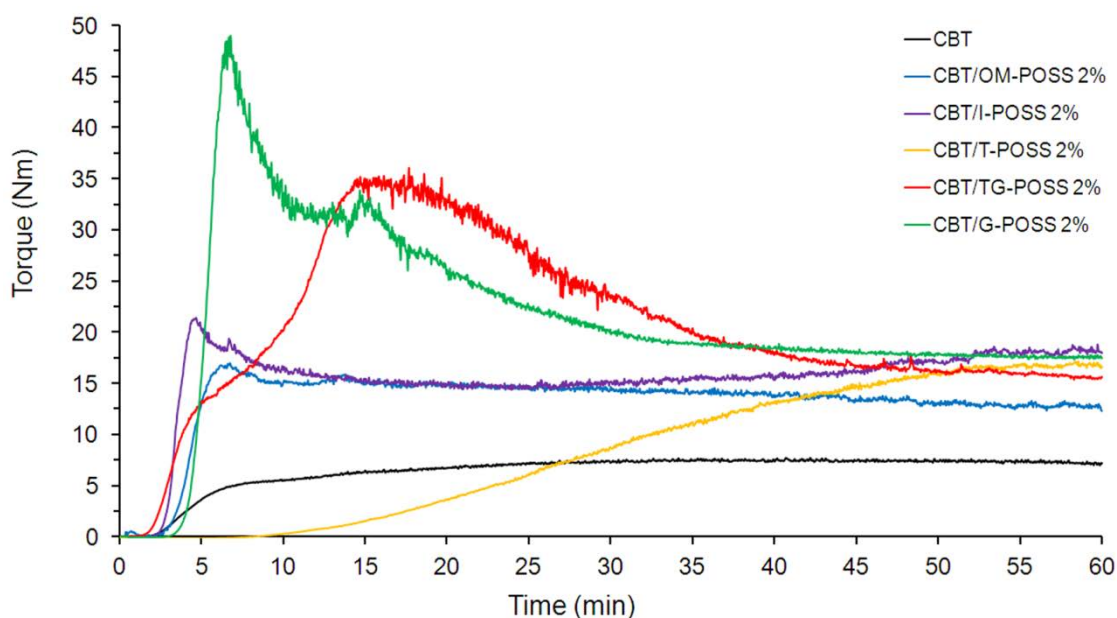


Fig. 12.4: Torque *versus* time plots of CBT and CBT/POSS blends containing 2 wt.% of POSS polymerized at 230°C and 60 min$^{-1}$ under nitrogen atmosphere.

TG-POSS, essentially a trifunctional epoxide, acted quite similarly to bifunctional epoxy resin. Similarly to EP, this POSS type promoted the ROP of CBT, as can be seen by the torque onset which appeared somewhat earlier as compared to neat CBT. The maximum torque of the CBT/TG-POSS blend was 36 Nm after 18 min.

G-POSS, considered as a polyfunctional epoxide, exhibited a torque maximum of 49 Nm after 7 min. As expected, this was the highest torque value of all tested samples.

After the experiment, a brown, foam-like solid was collected. This suggests that the G-POSS had crosslinked the pCBT.

It is interesting to note that all CBT/POSS blends reached a similar torque value around 15 Nm which is twice the one of neat CBT. In viev of the observed time to reach maximum torque, the earlier chosen polymerization time of 20 min appears to be a reasonable compromise, except for blends containing T-POSS.


## DSC analysis

The influence of POSS on the *in situ* polymerization of CBT was analysed using DSC. Figure 12.5 shows the first heating scan of CBT/POSS physical blends with a POSS content of 2.5, 5 and 10 wt.% and DSC data is provided in table 12.2. It was shown in [33] and also in chapter 6 that cold crystallization and hence polymer melting is suppressed when high heating rates are used. In order to avoid this effect, a lower heating rate of 5 °C/min was applied during first heating, whereas cooling and second heating were conducted at -30 and 30 °C/min, respectively.

It can be seen in figure 12.5 that oligomer melting was not affected by the presence of POSS. On one hand, the unreactive OM-POSS and I-POSS reduced the amount of cold crystallization and consequently polymer melting enthalpy. On the other hand, small POSS amounts shifted the melting temperature towards higher temperatures, suggesting the formation of pCBT crystals with higher lamellar thickness. Nevertheless, melting enthalpies decreased with both OM-POSS and I-POSS content, and the sample CBT/I-POSS 10% was apparently amorphous.

Regarding the reactive POSS types, T-POSS completely suppressed cold crystallization and polymer melting, irrespective of POSS content. On the other hand, low amounts of TG-POSS or G-POSS led to some pCBT crystallinity with a somewhat higher $T_m$ whereas composites containing 10 wt.% of the latter POSS types were amorphous. This suggests that POSS, most importantly the reactive types, depress the cold crystallization and consequently pCBT melting enthalpy.
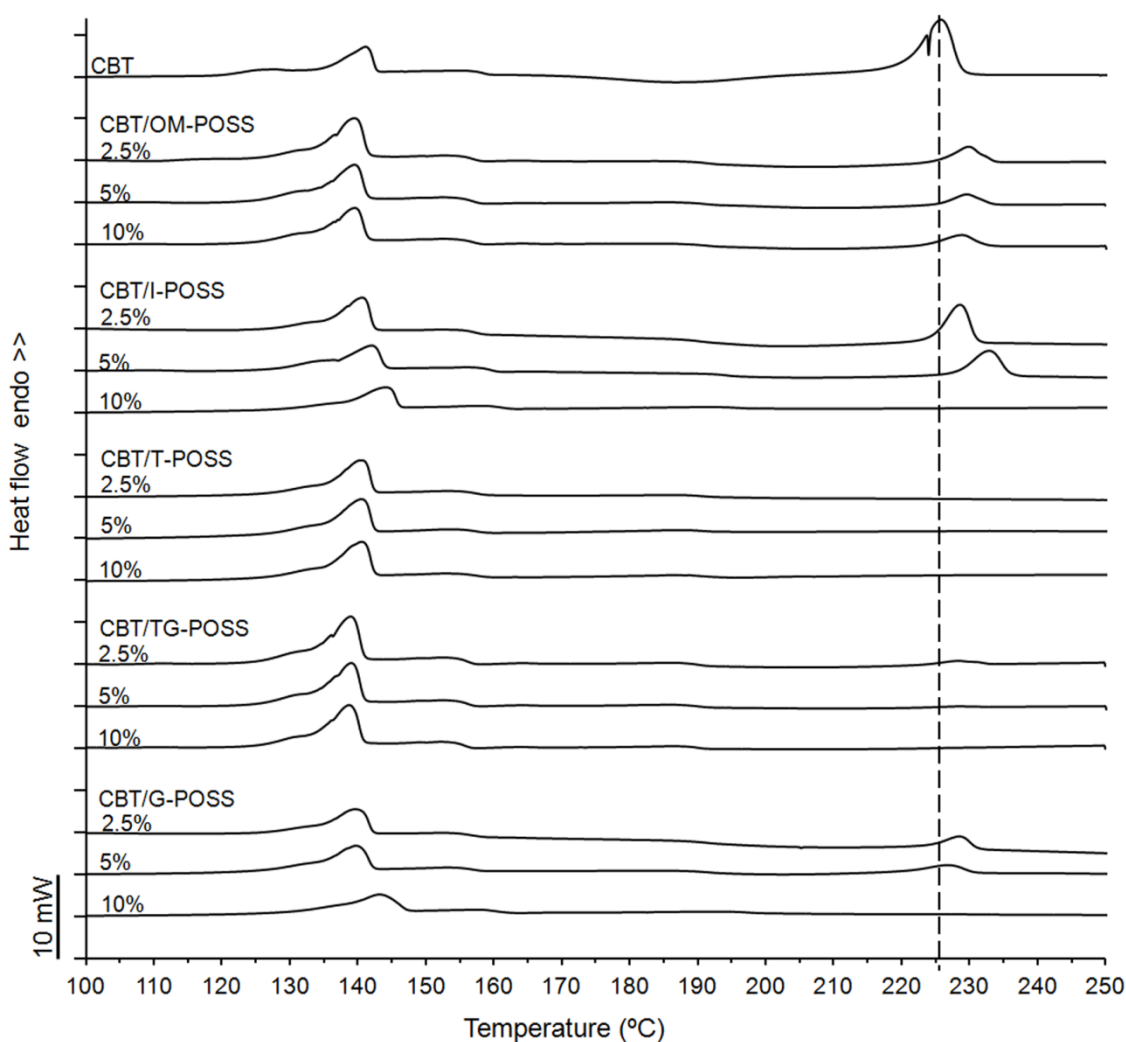
Fig. 12.5: DSC first heating scan of CBT and CBT/POSS blends with 2.5, 5 and 10 wt.% POSS content; heating rate: 10°C/min.

The first cooling scan revealed the effect of POSS on the non-isothermal melt crystallization of pCBT. It is apparent from table 12.2 that the studied POSS types generally slightly decreased pCBT crystallization peak temperature, indicating that POSS also hindered the pCBT crystallization. An exception were the samples containing 10 wt.% of I-POSS and G-POSS which exhibited a 14 and 3 °C higher $T_c$, respectively.

The second heating reflected the same trends as observed in the first heating scan, namely a decreasing pCBT melting enthalpy with increasing POSS content. The sample CBT/T-POSS 10% showed a melting peak at 151 °C which was attributed to the melting of residual CBT oligomers and no polymer melting was detected. This suggests that high amounts of T-POSS completely inhibited the ROP of CBT.

Table 12.2: Thermal properties of CBT and CBT/POSS nanocomposites, heating at 5 °C/min and cooling at -30 °C/min.

| Sample | first heating | | first cooling | | second heating | | |
|---|---|---|---|---|---|---|---|
| | $T_m$ | $\Delta H_m$ | $T_c$ | $\Delta H_c$ | $T_m$ | $\Delta H_m$ | $X_C$* |
| | [°C] | [J/g] | [°C] | [J/g] | [°C] | [J/g] | [%] |
| CBT | 225.7 | 59.6 | 176.6 | -44.3 | 223.6 | 42.7 | 30.1 |
| CBT/OM-POSS 2.5% | 229.9 | 9.1 | 172.7 | -39.6 | 219.6 | 35.0 | 24.6 |
| CBT/OM-POSS 5% | 229.7 | 5.1 | 175.7 | -37.3 | 220.2 | 34.1 | 24.0 |
| CBT/OM-POSS 10% | 228.7 | 7.6 | 175.2 | -36.6 | 220.6 | 34.0 | 23.9 |
| CBT/I-POSS 2.5% | 228.5 | 22.2 | 176.0 | -37.5 | 223.0 | 33.8 | 23.8 |
| CBT/I-POSS 5% | 232.8 | 21.0 | 176.4 | -36.7 | 225.6 | 34.5 | 24.3 |
| CBT/I-POSS 10% | - | - | 190.5 | -35.5 | 228.3 | 27.6 | 19.4 |
| CBT/T-POSS 2.5% | - | - | 175.6 | -40.7 | 218.1 | 40.7 | 28.7 |
| CBT/T-POSS 5% | - | - | 170.6 | -31.6 | 211.9 | 28.0 | 19.7 |
| CBT/T-POSS 10% | - | - | 140.3 | -8.5 | 150.5** | 15.0** | 0 |
| CBT/TG-POSS 2.5% | 228.2 | 2.9 | 173.7 | -37.5 | 218.1 | 36.4 | 25.6 |
| CBT/TG-POSS 5% | 227.8 | 0.7 | 173.2 | -37.6 | 218.6 | 34.9 | 24.6 |
| CBT/TG-POSS 10% | - | - | 173.2 | -37.3 | 218.6 | 33.3 | 23.5 |
| CBT/G-POSS 2.5% | 228.6 | 8.3 | 175.5 | -38.1 | 221.5 | 33.3 | 23.5 |
| CBT/G-POSS 5% | 226.8 | 6.3 | 168.1 | -35.9 | 221.0 | 44.3 | 31.2 |
| CBT/G-POSS 10% | - | - | 180.0 | -28.2 | 227.6 | 27.2 | 19.2 |

DSC data of CBT and CBT/POSS samples polymerized during DSC. DSC first heating at 5 °C/min; cooling at -30 °C/min; second heating at 5 °C/min.

* calculated from second heating melting enthalpy

** oligomer melting, hence no polymer crystallinity

### 12.4.3 pCBT/POSS characterization

**TGA analysis**

The thermal stability of the compression moulded pCBT/POSS composites was measured by TGA in nitrogen atmosphere at a heating rate of 10 °C/min; results are shown in table 12.3.

A single stage of decomposition ranging from 370 to 430 °C was observed for neat pCBT as well as for pCBT/POSS composites. Neat pCBT showed a 5% mass loss at 373 °C, the temperature at which the maximum mass loss rate occurred was found to be 405 °C. After thermal decomposition, an amount of solid residue of 1.2 wt.% was detected. None of the used POSS types significantly altered the degradation pathway or the thermal stability of pCBT but they generally increased the amount of residue, as can be expected from the inorganic POSS structure. OM-POSS which had lower thermal stability as compared to pCBT, showed a drastic decrease in 5% mass loss temperature with increasing POSS content due to the sublimation of OM-POSS *ca.* 100 °C earlier than $T_{max}$ of pristine pCBT. Analogously, $T_{max}$ also slightly decreased due to this effect. I-POSS did not have such an effect on pCBT due to its inherently higher thermal stability as compared to OM-POSS and pCBT.

Regarding the reactive POSS types, pCBT/T-POSS composites showed a somewhat lower thermal stability relative to neat pCBT. This was probably due to the loss of water from the trisilanol of this POSS type, as discussed earlier. The formed water is known to accelerate the degradation of the pCBT matrix by acid-catalysed  hydrolysis of the butylene ester groups of the pCBT backbone [34].

Contrary to that, the epoxide substituted TG-POSS and G-POSS exhibited a slightly higher temperature where maximum mass loss occurred. This was probably due to the presence of some crosslinked structure in the pCBT matrix, somewhat delaying the degradation of the latter.

Table 12.3: TGA data of compression moulded pCBT and pCBT/POSS composites.

| Sample | $T_{5\%\ wt.\ loss}$ [°C] | $T_{max.}$ [°C] | Residue at 600 °C [wt.%] |
|---|---|---|---|
| pCBT | 373.2 | 404.8 | 1.2 |
| pCBT/OM-POSS 2.5% | 375.1 | 403.1 | 3.6 |
| pCBT/OM-POSS 5% | 351.4 | 401.9 | 2.7 |
| pCBT/OM-POSS 10% | 332.0 | 404.5 | 0.7 |
| pCBT/I-POSS 2.5% | 375.1 | 405.5 | 1.9 |
| pCBT/I-POSS 5% | 377.5 | 405.3 | 2.8 |
| pCBT/I-POSS 10% | 369.3 | 404.7 | 3.2 |
| pCBT/T-POSS 2.5% | 376.7 | 401.4 | 4.4 |
| pCBT/T-POSS 5% | 368.9 | 401.3 | 6.9 |
| pCBT/T-POSS 10% | 370.5 | 404.8 | 9.7 |
| pCBT/TG-POSS 2.5% | 375.1 | 406.3 | 3.4 |
| pCBT/TG-POSS 5% | 374.7 | 407.4 | 3.7 |
| pCBT/TG-POSS 10% | 371.5 | 406.2 | 3.9 |
| pCBT/G-POSS 2.5% | 374.1 | 409.7 | 4.4 |
| pCBT/G-POSS 5% | 378.2 | 404.4 | 3.2 |
| pCBT/G-POSS 10% | 371.1 | 406.6 | 8.0 |

**Morphology**

The dispersion of POSS in the pCBT matrix and the morphology of fractured pCBT/POSS composites was studied using SEM and SEM-EDX element mapping; micrographs are shown in figure 12.6 a–f.
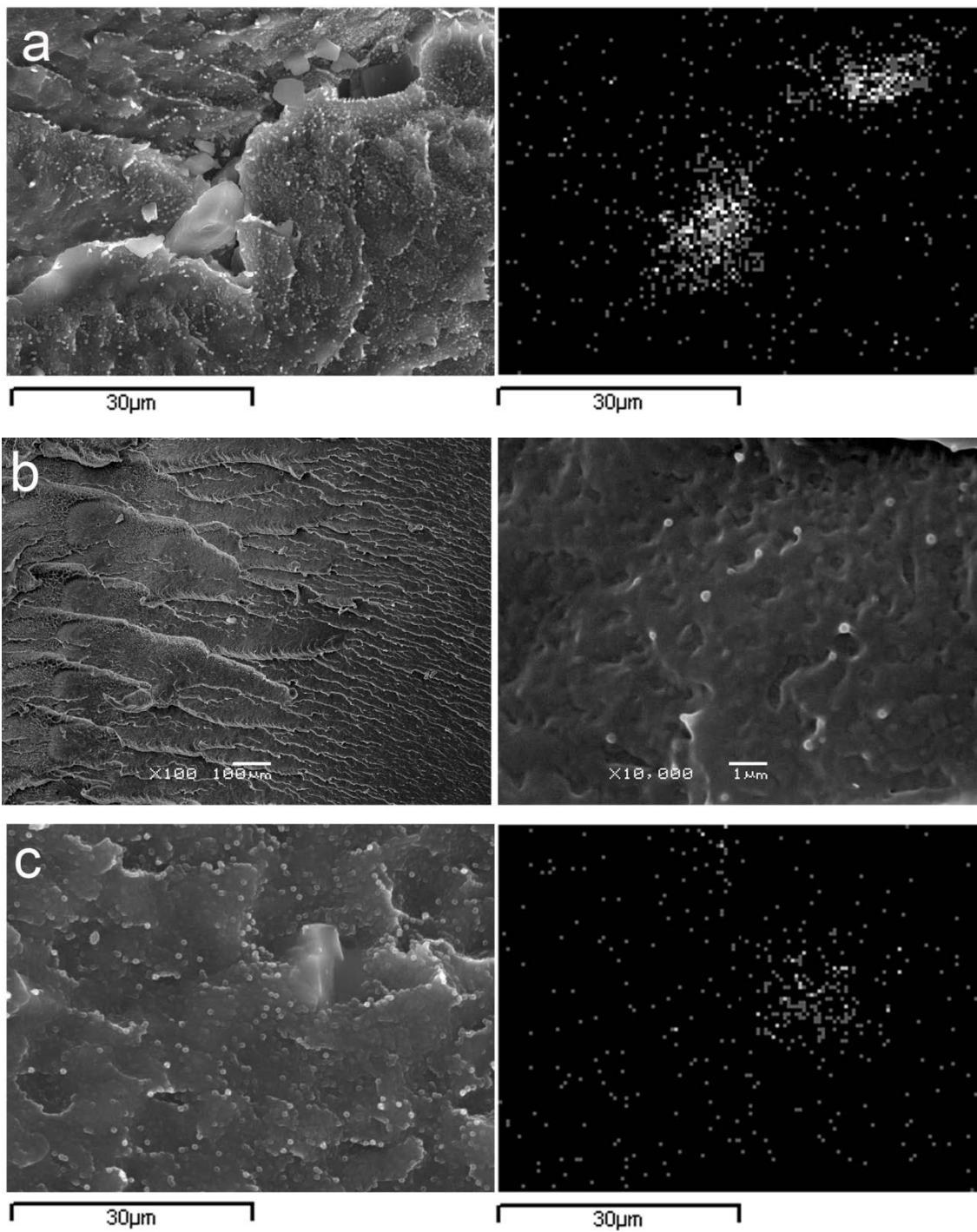
Fig. 12.6: SEM and SEM-EDAX micrographs of compression moulded pCBT/OM-POSS 2.5% (a), pCBT/I-POSS 2.5% (b), pCBT/T-POSS 2.5% (c), pCBT/T-POSS 5% (d), pCBT/TG-POSS 2.5% (e) and pCBT/G-POSS 2.5% (f).
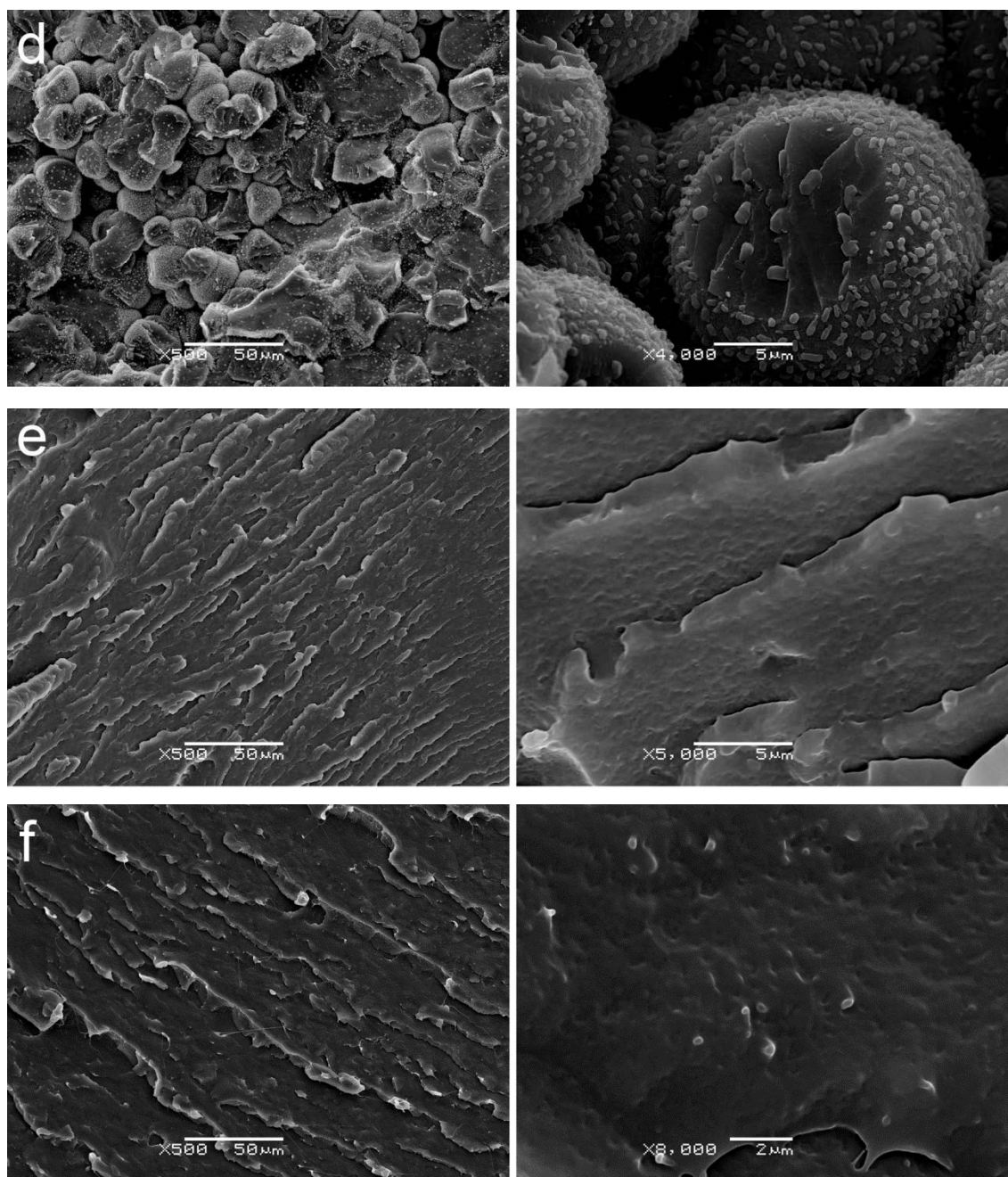
Fig. 12.6: SEM and SEM-EDAX micrographs of compression moulded pCBT/OM-POSS 2.5% (a), pCBT/I-POSS 2.5% (b), pCBT/T-POSS 2.5% (c), pCBT/T-POSS 5% (d), pCBT/TG-POSS 2.5% (e) and pCBT/G-POSS 2.5% (f). (*continued*)

CBT oligomers can form oligomeric crystals in the form of platelets or prismatic crystals with dimensions of a few µm [35-37], as was already shown in chapter 6 for incompletely polymerized pCBT. On the other hand, solid POSS types are capable of self-assembly by aggregation or crystallization, forming POSS crystal domains in the polymer matrix [6-7]. In

order to distinguish POSS crystals from CBT oligomer crystals, EDX element mapping was employed for the crystalline POSS types. In the case of EDX, the study was focused on the determination of Si signal as it is specific and characteristic of the POSS presence. Although POSS cannot be directly imaged by SEM because of the nano-scale of POSS, SEM is a useful technique to study the influence of POSS on the morphology of pCBT.

Figure 12.6 a shows the fractured surface of pCBT/OM-POSS 2.5% with the corresponding element mapping. A mixed morphology can be observed; part of the POSS was well dispersed in form of small agglomerations with a size of about 1 µm but also larger POSS aggregates with a size of about 10 µm can be seen. It is apparent from Si element mapping (figure 12.6a right hand side) that the large particles are POSS agglomerates and not the aforementioned CBT oligomer crystals.

A similar morphology with presumably well dispersed small POSS particles as well as larger POSS agglomerates was observed for the sample containing 2.5 wt.% of I-POSS (figure 12.6b). Nevertheless, both unreactive OM- and I-POSS can be considered only partly compatible since their methyl and isooctyl substituent groups are nonpolar and thus incompatible with the polar pCBT matrix.

Regarding the trisilanol POSS (*c.f.* figure 12.6c), the sample pCBT/T-POSS 2.5% showed a mixed morphology similar to the unreactive POSS types. According to Si element mapping a part of the POSS was well dispersed but also a larger POSS aggregate can be seen. Although this POSS type was considered to be compatible due to its phenyl substituents, no difference in morphology can be observed with respect to the unreactive POSS types (*c.f.* figures 12.6a and b). Nevertheless, higher concentrations of T-POSS led to a different morphology; large amounts of crystalline particles can be observed in the micrograph of pCBT/T-POSS 5% (figure 12.6d). It is obvious that the relatively small amount of 5 wt.% of POSS cannot account for all the observed crystals. Since this POSS type was shown to inhibit the ROP of CBT, the observed crystals most probably are CBT oligomer crystals. The droplet-like surface structure of the pCBT matrix suggests a poor consolidation of the pCBT. Indeed, the produced pCBT/T-POSS samples with higher POSS contents could be easily broken into a fine powder. This was due to the low degree of conversion and the resulting crystallization of the unreacted CBT oligomers.

No particles or agglomerates can be detected in pCBT/TG-POSS 2.5, hence the G-POSS was well dispersed in the pCBT matrix. This POSS type is thought to be covalently bonded to the pCBT matrix *via* esterification and etherification of the pCBT carboxyl and

hydroxyl end groups, respectively, as discussed in detail in chapter 8. In this bottom-up approach, good POSS dispersion is provided by covalent attachment to the pCBT.

The polyfunctional reactive G-POSS exhibited a mixed morphology with few but well dispersed particles. G-POSS acted as a crosslinker but was thought to have little self-reactivity because epoxy groups do not react with each other under normal conditions unless a proton-donating group is present. Since this POSS type is a viscous liquid, the observed particles may be crosslinked pCBT/G-POSS domains.

**Tensile properties**

Only pCBT/TG-POSS samples had the mechanical strength to withstand tensile specimen extraction; all other samples were too brittle and broke during demoulding as mentioned earlier. Samples were tested by tensile tests; results are compiled in table 12.4.

Table 12.4: Tensile properties of melt blended pCBT/TG-POSS samples.

| Sample | Tensile modulus (GPa) | Tensile strength (MPa) | Elongation at break (%) |
|---|---|---|---|
| pCBT-CM | 2.8 ± 0.4 | 57 ± 5 | 7 ± 3 |
| pCBT/TG-POSS 2% | 2.9 ± 0.2 | 62 ± 2 | 3 ± 1 |
| pCBT/TG-POSS 3% | 2.7 ± 0.3 | 53 ± 6 | 3 ± 1 |
| pCBT/TG-POSS 4% | 2.8 ± 0.3 | 50 ± 4 | 3 ± 1 |
| pCBT/TG-POSS 5% | 2.5 ± 0.4 | 45 ± 3 | 4 ± 1 |
| pCBT/TG-POSS 10% | 2.5 ± 0.3 | 44 ± 7 | 4 ± 1 |

A small reinforcing effect can be seen for a POSS content of 2 wt.%; higher amounts resulted in a decrease in tensile properties. At high concentrations, TG-POSS could not fully react with the matrix and in fact these samples exhibited a sticky surface which indicates POSS migration. Thus, one might expect a plasticizing effect of the unreacted POSS since many POSS types are known to plasticise polymers. For instance, T-POSS

and phenethyl-POSS in PC [9, 25], phenethyl-POSS and POSS-styrene in PS [38-39] or methacryl-POSS and hydrogenated methacryl-POSS in PMMA [40]. On the other hand, the increased brittleness indicates incompatibility with this POSS type.

## 12.5 Conclusions

The influence of the functionalisation of fully or partially condensed POSS cages on the properties of pCBT-based nanocomposites was studied. Torque versus time measurements revealed that all studied POSS types increased the melt viscosity. Incompletely condensed T-POSS considerably decreased the polymerization rate whereas the epoxy-POSS types promoted the ROP of CBT. DSC analysis showed that POSS hindered the cold crystallization and hence polymer melting of pCBT. Moreover, it decreased crystallization and melting temperatures and enthalpies, respectively.

Regarding compression moulded pCBT/POSS nanocomposites; good POSS dispersion at the nanoscale level was achieved upon the addition of some reactive POSS types. On the other hand, the dispersion of the POSS, whatever its functionalisation was, led to the presence of micron-sized aggregates. No significant changes in the thermal stability of the nanocomposites was observed. Samples containing small amounts of TG-POSS showed a slightly increased stiffness and strength whereas higher POSS contents led to a decrease in tensile properties, indicating incompatibility.

To conclude, the used POSS types showed rather poor compatibility with pCBT although POSS and its derivates possess good potential for nano-reinforcement. The challenge remains to find a compatible POSS type which does not affect the ROP of CBT. More work is needed on that subject.

## 12.6 References for pCBT/POSS

1.    Abt, T, Illescas, S, Antunes, M, Cáceres, MA, and Sánchez-Soto, M. Nanocomposites of in-situ polymerized cyclic butylene terephthalate and polyhedral

oligomeric silsesquioaxanes. 5º Congreso Nacional de Jóvenes Investigadores en Polímeros. Calella de Palafrugell, Spain, 2010.

2.  Abt, T, Sánchez-Soto, M, Illescas, S, and Arostegui, A. Properties of POSS blends with pCBT, PMMA, PC and POM thermoplastics. International Journal of Materials and Structural Integrity **7**(Nos. 1/2/3), 48-78 (2013).

3.  Sinha Ray, S and Okamoto, M. Polymer/layered silicate nanocomposites: a review from preparation to processing. Progress in Polymer Science **28**(11), 1539-1641 (2003).

4.  Coleman, JN, Khan, U, and Gun'ko, YK. Mechanical Reinforcement of Polymers Using Carbon Nanotubes. Advanced Materials **18**(6), 689-706 (2006).

5.  Joshi, M and Butola, BS. Polymeric Nanocomposites—Polyhedral Oligomeric Silsesquioxanes (POSS) as Hybrid Nanofiller. Journal of Macromolecular Science, Part C **44**(4), 389-410 (2004).

6.  Kuo, S-W and Chang, F-C. POSS related polymer nanocomposites. Progress in Polymer Science **36**(12), 1649-1696 (2011).

7.  Wu, J and Mather, PT. POSS Polymers: Physical Properties and Biomaterials Applications. Polymer Reviews **49**(1), 25-63 (2009).

8.  Sánchez-Soto, M, Schiraldi, DA, and Illescas, S. Study of the morphology and properties of melt-mixed polycarbonate–POSS nanocomposites. European Polymer Journal **45**(2), 341-352 (2009).

9.  Zhao, Y and Schiraldi, DA. Thermal and mechanical properties of polyhedral oligomeric silsesquioxane (POSS)/polycarbonate composites. Polymer **46**(25), 11640-11647 (2005).

10. Fina, A, Tabuani, D, Peijs, T, and Camino, G. POSS grafting on PPgMA by one-step reactive blending. Polymer **50**(1), 218-226 (2009).

11. Misra, R, Alidedeoglu, AH, Jarrett, WL, and Morgan, SE. Molecular miscibility and chain dynamics in POSS/polystyrene blends: Control of POSS preferential dispersion states. Polymer **50**(13), 2906-2918 (2009).

12. Romo–Uribe, A, Mather, PT, Haddad, TS, and Lichtenhan, JD. Viscoelastic and morphological behavior of hybrid styryl-based polyhedral oligomeric silsesquioxane (POSS) copolymers. Journal of Polymer Science Part B: Polymer Physics **36**(11), 1857-1872 (1998).

13. Zhang, W, Fu, BX, Seo, Y, Schrag, E, Hsiao, B, Mather, PT, Yang, N-L, Xu, D, Ade, H, Rafailovich, M, and Sokolov, J. Effect of Methyl Methacrylate/Polyhedral Oligomeric Silsesquioxane Random Copolymers in Compatibilization of Polystyrene and Poly(methyl methacrylate) Blends. Macromolecules **35**(21), 8029-8038 (2002).

14. Chen, J-H, Yao, B-X, Su, W-B, and Yang, Y-B. Isothermal crystallization behavior of isotactic polypropylene blended with small loading of polyhedral oligomeric silsesquioxane. Polymer **48**(6), 1756-1769 (2007).

15. Huang, K-W, Tsai, L-W, and Kuo, S-W. Influence of octakis-functionalized polyhedral oligomeric silsesquioxanes on the physical properties of their polymer nanocomposites. Polymer **50**(20), 4876-4887 (2009).

16. Verker, R, Grossman, E, Gouzman, I, and Eliaz, N. TriSilanolPhenyl POSS–polyimide nanocomposites: Structure–properties relationship. Composites Science and Technology **69**(13), 2178-2184 (2009).

17. Zeng, K, Liu, Y, and Zheng, S. Poly(ethylene imine) hybrids containing polyhedral oligomeric silsesquioxanes: Preparation, structure and properties. European Polymer Journal **44**(12), 3946-3956 (2008).

18. Zheng, L, Farris, RJ, and Coughlin, EB. Novel Polyolefin Nanocomposites: Synthesis and Characterizations of Metallocene-Catalyzed Polyolefin Polyhedral Oligomeric Silsesquioxane Copolymers. Macromolecules **34**(23), 8034-8039 (2001).

19. Ciolacu, FCL, Choudhury, NR, Dutta, N, and Kosior, E. Molecular Level Stabilization of Poly(ethylene terephthalate) with Nanostructured Open Cage Trisilanolisobutyl-POSS. Macromolecules **40**(2), 265-272 (2006).

20. Kim, JK, Yoon, KH, Bang, DS, Park, Y-B, Kim, H-U, and Bang, Y-H. Morphology and rheological behaviors of poly(ethylene terephthalate) nanocomposites containing polyhedral oligomeric silsesquioxanes. Journal of Applied Polymer Science **107**(1), 272-279 (2008).

21. Sirin, H, Turan, D, Ozkoc, G, and Gurdag, S. POSS reinforced PET based composite fibers: "Effect of POSS type and loading level". Composites Part B: Engineering **53**(0), 395-403 (2013).

22. Vannier, A, Duquesne, S, Bourbigot, S, Castrovinci, A, Camino, G, and Delobel, R. The use of POSS as synergist in intumescent recycled poly(ethylene terephthalate). Polymer Degradation and Stability **93**(4), 818-826 (2008).

23. Yoon, KH, Polk, MB, Park, JH, Min, BG, and Schiraldi, DA. Properties of poly(ethylene terephthalate) containing epoxy-functionalized polyhedral oligomeric silsesquioxane. Polymer International **54**(1), 47-53 (2005).

24. Zeng, J, Kumar, S, Iyer, S, Schiraldi, DA, and Gonzalez, RI. Reinforcement of Poly(ethylene terephthalate) Fibers with Polyhedral Oligomeric Silsesquioxanes (POSS). High Performance Polymers **17**(3), 403-424 (2005).

25. Hao, N, Böhning, M, Goering, H, and Schönhals, A. Nanocomposites of Polyhedral Oligomeric Phenethylsilsesquioxanes and Poly(bisphenol A carbonate) as Investigated by Dielectric Spectroscopy. Macromolecules **40**(8), 2955-2964 (2007).

26. Cozza, ES, Ma, Q, Monticelli, O, and Cebe, P. Nanostructured nanofibers based on PBT and POSS: Effect of POSS on the alignment and macromolecular orientation of the nanofibers. European Polymer Journal **49**(1), 33-40 (2013).

27. Zhou, Z, Yin, N, Zhang, Y, and Zhang, Y. Properties of poly(butylene terephthalate) chain-extended by epoxycyclohexyl polyhedral oligomeric silsesquioxane. Journal of Applied Polymer Science **107**(2), 825-830 (2008).

28. Wan, C, Zhao, F, Bao, X, Kandasubramanian, B, and Duggan, M. Surface Characteristics of Polyhedral Oligomeric Silsesquioxane Modified Clay and Its Application in Polymerization of Macrocyclic Polyester Oligomers. The Journal of Physical Chemistry B **112**(38), 11915-11922 (2008).

29. McLauchlin, A, Bao, X, and Zhao, F. Organoclay polybutylene terephthalate nanocomposites using dual surfactant modified montmorillonite prepared by the masterbatch method. Applied Clay Science **53**(4), 749-753 (2011).

30. Wu, F, Xie, T, and Yang, G. Characterization of PBT/POSS nanocomposites prepared by in situ polymerization of cyclic poly(butylene terephthalate) initiated by functionalized POSS. Journal of Polymer Science Part B: Polymer Physics **48**(16), 1853-1859 (2010).

31. Dintcheva, E, Morici, NT, Arrigo, R, La Mantia, FP, Malatesta, V, and Schwab, JJ. Structure-properties relationships of polyhedral oligomeric silsesquioxane (POSS) filled PS nanocomposites. eXPRESS Polymer Letters **6**(7), 561-571 (2012).

32. Fina, A, Tabuani, D, Carniato, F, Frache, A, Boccaleri, E, and Camino, G. Polyhedral oligomeric silsesquioxanes (POSS) thermal degradation. Thermochimica Acta **440**(1), 36-42 (2006).

33.   Karger-Kocsis, J, Shang, PP, Mohd Ishak, ZA, and Rösch, M. Melting and crystallization of in-situ polymerized cyclic butylene terephthalates with and without organoclay: A modulated DSC study. eXPRESS Polymer Letters **1**(2), 60-68 (2007).

34.   Levchik, SV and Weil, ED. A review on thermal decomposition and combustion of thermoplastic polyesters. Polymers for Advanced Technologies **15**(12), 691-700 (2004).

35.   Karger-Kocsis, J, Felhos, D, Bárány, T, and Czigány, T. Hybrids of HNBR and in situ polymerizable cyclic butylene terephthalate (CBT) oligomers: Properties and dry sliding behavior. eXPRESS Polymer Letters **2**(7), 520-527 (2008).

36.   Perovic, A and Sundararajan, PR. Crystallization of cyclic olicomers in commercial poly(ethyleneterephthalate) films. Polymer Bulletin **6**(5-6), 277-283 (1982).

37.   Xu, D, Karger-Kocsis, J, and Apostolov, AA. Hybrids from HNBR and in situ polymerizable cyclic butylene terephthalate (CBT): Structure and rolling wear properties. European Polymer Journal **45**(4), 1270-1281 (2009).

38.   Hao, N, Böhning, M, and Schönhals, A. Dielectric Properties of Nanocomposites Based on Polystyrene and Polyhedral Oligomeric Phenethyl-Silsesquioxanes. Macromolecules **40**(26), 9672-9679 (2007).

39.   Romero-Guzmán, M, Romo-Uribe, A, Zárate-Hernández, BM, and Cruz-Silva, R. Viscoelastic properties of POSS–styrene nanocomposite blended with polystyrene. Rheologica Acta **48**(6), 641-652 (2009).

40.   Kopesky, ET, Haddad, TS, McKinley, GH, and Cohen, RE. Miscibility and viscoelastic properties of acrylic polyhedral oligomeric silsesquioxane–poly(methyl methacrylate) blends. Polymer **46**(13), 4743-4752 (2005).

# Chapter 13: pCBT/organoclay nanocomposites
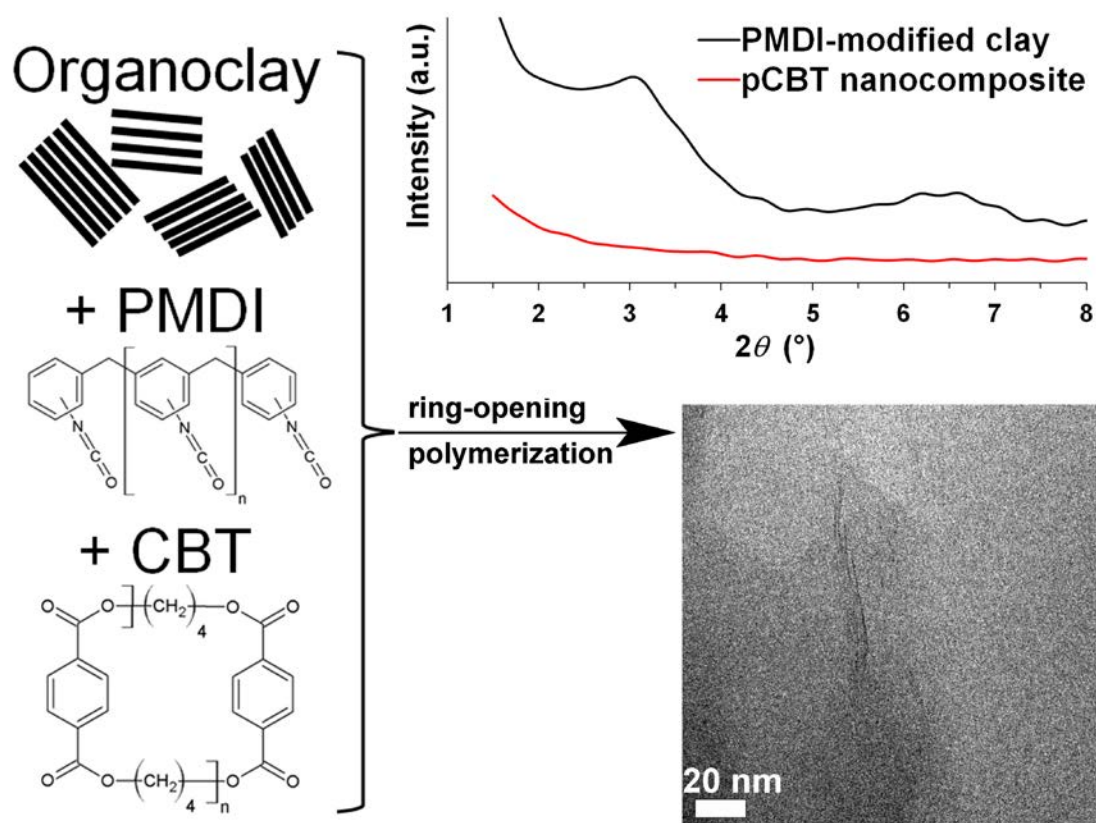


Nanocomposites of CBT and organo-montmorillonite were prepared and the role of the nanoclay on the properties of pCBT was studied using various techniques. The use of 1 to 3 wt.% of organoclay resulted in an increase in stiffness and strength of up to 20%. Nevertheless, the organoclay led to pCBT embrittlement due to poor physical interactions. Adding polymeric isocyanate as a toughening agent to the nanocomposites improved the deformation behaviour and semi-ductile nanocomposites were obtained. However, the isocyanate did not affect the degree of clay dispersion or exfoliation. The compatibility between pCBT matrix and organoclay was further increased by preparing PMDI-tethered organoclay with increased interlayer distance which resulted in exfoliated pCBT/clay nanocomposites. Either increased stiffness/strength or an increased failure strain was observed, depending on the used processing route. The mechanical properties of pCBT/organoclay nanocomposites could be tailored in a fairly wide range from high stiffness and strength to high toughness using PMDI and the proposed clay modification.

## 13.1  Introduction

Nowadays, considerable efforts are made to obtain polymer nanocomposites based on organophilic layered silicates. The driving force of these efforts is the dramatic improvement in material properties such as stiffness and strength (although toughness typically decreases with increasing organoclay content), flame resistance, gas barrier properties and thermal stability. These improvements can already be obtained with very low organoclay contents, usually less than 5 wt.%. Nevertheless, property improvements are only observed when at least intercalation or better complete exfoliation of the clay occurs and individual silicate layers disperse randomly and homogeneously on a nanoscale level in the polymer matrix. Otherwise, a flocculated-intercalated or even immiscible structure due to poor physical interactions between clay and polymer matrix is usually obtained, leading to decreased mechanical and thermal properties. Therefore, exfoliated nanocomposites exhibit unique properties not shared by their micro- and macrocomposite counterparts [1-3].

The key to exfoliation is to match the polarity between the hydrophobic polymer and hydrophilic clay. A common way to increase compatibility is to render layered silicates organophilic by ion-exchange reactions with cationic surfactants including primary, secondary, tertiary, and quaternary alkylammonium or alkylphosphonium cations. These ion-exchanged organic surfactants lead to a larger interlayer spacing and a lower surface energy of the inorganic layered silicates, which improves the wetting characteristics of the polymer matrix and hence intercalation [3]. Moreover, some organic surfactants provide functional groups that can react with the polymer chains or initiate the polymerization of monomers, which in turn enhance the strength of the interface between clay surface and polymer matrix [3-4]. Despite the fact that the intercalation chemistry of polymers has long been known, clay exfoliation still remains a major challenge in the preparation of nanocomposites with improved properties.

PBT/organoclay nanocomposites obtained by traditional melt intercalation or *in situ* polymerization of PBT monomers have been extensively studied and many researchers reported intercalated structures as well as complete clay exfoliation and the related improvements in properties (see for instance [5-9]).

An increasing amount of publications dealing with pCBT/organoclay nanocomposites can also be found in the literature [10-19]. Despite this considerable body

of papers, little is known about the mechanical properties of these materials [12, 16, 18] and information about the deformation behaviour is rare. Most researchers employ the low viscosity of molten or dissolved oligomers in order to obtain a CBT-intercalated organoclay. Subsequent ring-opening polymerization causes then an increase in interlayer distance along with the disintegration of the layered clay structure. Nevertheless, only few reports on complete clay exfoliation are available [10, 19], whereas intercalated or flocculated-intercalated structures are more commonly observed [12, 14, 16-18]. Although several researchers showed that the organoclay was successfully intercalated with CBT oligomers or even completely exfoliated prior to ring-opening polymerization, the silicate layers tended to reorganize due to the low viscosity of the molten CBT during ROP. Consequently, the exfoliated structure was lost and a flocculated-intercalated structure was obtained after polymerization [14, 17-18].

Tethering of clay platelets to pCBT chains might hinder the reorganisation of the former. Furthermore, clay-pCBT coupling might enhance the exfoliation process and interfacial adhesion between pCBT matrix and clay surface which would lead to improved properties. This was already effectively demonstrated for polyurethanes; coupling reactions of organoclay surfactants with polyurethane precursors were employed in the synthesis of thermoplastic polyurethane nanocomposites which resulted in exfoliation and increased mechanical properties [4, 20-22].

The method described herein involves a coupling reaction of the hydroxyl groups of the organic surfactants with –N=C=O functional groups of a polyfunctional isocyanate, intercalating the organoclay. Since the tethered isocyanate is also highly reactive towards pCBT functional groups (mainly towards carboxyl end groups, as shown in chapter 9), pCBT is expected to be grafted onto the NCO-modified organoclay. So far, this has not yet been reported to the best of the knowledge of the author.

## 13.2   Experimental Section

### 13.2.1 Materials

If not otherwise stated, one-component cyclic butylene terephthalate oligomers (CBT160[®]) were used in this chapter. In one case, two-component cyclic butylene terephthalate oligomers (CBT100[®], *c.f.* section 3.1.1) were used for melt blending. For initiation of the ROP, 0.45 wt.% of Fascat[®] 4105 (with respect to CBT) was added to the molten oligomers.

Two types of isocyanates, namely PMDI and HDI, were used for chemical modification of the organoclay as well as to toughen the pCBT nanocomposites. Although it was demonstrated in chapter 8 that epoxy resin effectively toughens pCBT, EP was not considered suitable for organoclay modification because of its relatively low reactivity towards hydroxyl groups, requiring long reaction times at high temperatures. The latter however is known to cause degradation of the clay surfactant, resulting in a collapse of the clay galleries [2-3, 9, 23]. In contrast, isocyanates readily react at relatively lower temperatures in a shorter time, thus probably avoiding surfactant degradation.

A commercial montmorillonite (*viz.* Cloisite[®] 30B) modified with a quaternary ammonium salt (*i.e.* methyl, tallow, bis-2-hydroxyethyl, quaternary ammonium) was chosen as reinforcement; see section 3.5.2. The reason therefore was that the organic surfactant bears two hydroxyl groups which is a requirement for isocyanate coupling. Moreover, it was shown that this type of organoclay is compatible with PBT and capable of intercalation due to polar interactions between the PBT carboxyl groups and the surfactant hydroxyl groups [6, 8] and this type was the preferred one in patent literature [11]. The interlaminar distance $d_{001}$ was 18.5 Å which was confirmed by other researchers [6, 8].

Analytical grade tetrahydrofuran was used as received.

### 13.2.2 Organoclay modification

Cl30B was modified with HDI and PMDI, respectively. The experimental procedure is described in detail in section 4.4. PMDI-grafted organoclay was referred to as PMDI-*g*-Cl30B.

### 13.2.3 Sample preparation

Two processing routes were employed to prepare pCBT/Cl30B nanocomposites, namely melt blending and solvent blending. The studied Cl30B content was 1, 2 and 3 wt.%. Three different groups of samples were prepared:

i)      CBT/Cl30B binary blends

ii)     CBT/PMDI/Cl30B ternary blends; all containing 1 wt.% of PMDI

iii)    CBT/PMDI-*g*-Cl30B binary blends

Melt blending was conducted in the batch mixer. Around 40 g of previously dried CBT and the corresponding amount of chain extender and/or organoclay were *in situ* polymerized at a temperature of 230 °C and a rotor speed of 60 $min^{-1}$ using a protective $N_2$ blanket. Then the materials were collected from the mixing chamber, ground into granules, vacuum dried 8 h at 80 °C and subsequently compression moulded at a temperature of 250 °C and a pressure of 4 MPa for 5 min in the hot plate press. Solvent blending was used to homogeneously disperse the toughening agent and/or the organoclay in CBT prior to ROP and is described in detail in section 4.3. The prepared composites were compared to pristine pCBT specimens obtained by both processing routes.

Additionally to the aforementioned three groups of samples, one sample was prepared as follows. A ternary blend of two-component CBT100 (*i.e.* oligomers without catalyst), 1 wt.% of PMDI and 3 wt.% of Cl30B was melt blended at 200 °C, 180 $min^{-1}$ and $N_2$ atmosphere for 2 h. Then the temperature was raised to 230 °C, the rotor speed was reduced to 60 $min^{-1}$ and transesterification catalyst was added in order to initiate the ROP. The blend was allowed to polymerize for 15 min and then compression moulded at 250 °C for 5 min. This sample was referred to as pCBT100/PMDI/Cl30B 96/1/3. The aim was to take advantage of the low viscosity of the molten CBT oligomers in such way that they

would swell the organoclay by diffusing into the clay galleries and then exfoliate the clay particles upon polymerization, as has been demonstrated by other researchers [10, 14].

All prepared samples are compiled in table 13.1. For instance, a temperature of 230+250 °C and a time of 15+5 min indicate that the sample was melt blended at 230 °C for 15 min and then compression moulded at 250 °C for 5 min.

Table 13.1: Overview over produced pCBT/organoclay nanocomposites.

| Sample designation | Processing | Temperature [°C] | Time [min] |
|---|---|---|---|
| pCBT/Cl30B 1%-MB | MB | 230+250 | 30+5 |
| pCBT/Cl30B 2%-MB | MB | 230+250 | 30+5 |
| pCBT/Cl30B 3%-MB | MB | 230+250 | 30+5 |
| pCBT/Cl30B 1%-SB | SB | 230 | 30 |
| pCBT/Cl30B 2%-SB | SB | 230 | 30 |
| pCBT/Cl30B 3%-SB | SB | 230 | 30 |
| pCBT/PMDI/Cl30B 98/1/1-MB | MB | 230+250 | 15+5 |
| pCBT/PMDI/Cl30B 98/1/1-SB | SB | 230 | 15 |
| pCBT/PMDI-*g*-Cl30B 1%-MB | MB | 230+250 | 15+5 |
| pCBT/PMDI-*g*-Cl30B 2%-MB | MB | 230+250 | 15+5 |
| pCBT/PMDI-*g*-Cl30B 3%-MB | MB | 230+250 | 15+5 |
| pCBT/PMDI-*g*-Cl30B 1%-SB | SB | 230 | 15 |
| pCBT/PMDI-*g*-Cl30B 2%-SB | SB | 230 | 15 |
| pCBT/PMDI-g-Cl30B 3%-SB | SB | 230 | 15 |
| pCBT100/PMDI/Cl30B 96/1/3-MB | MB | 200+230+250 | 120+15+5 |

MB: melt blending; SB: solvent blending

## 13.3   Characterization

Isocyanate grafting onto the clay platelets was verified using FT-IR and SAXS analysis. The optimum processing parameters for nanocomposite preparation were determined using torque *versus* time measurements in the batch mixer. The degree of clay exfoliation in the prepared pCBT nanocomposites was determined using SAXS and TEM and the samples were further characterized using DSC, DMTA and TGA. The mechanical properties were determined by tensile tests according to ISO 527. All characterization methods are described in detail in chapter 5.

## 13.4   Results and Discussion

### 13.4.1 PMDI/organclay grafting

A grafting reaction between PMDI and the hydroxyl groups of the quaternary ammonium salt of the organoclay is proposed in figure 13.1.
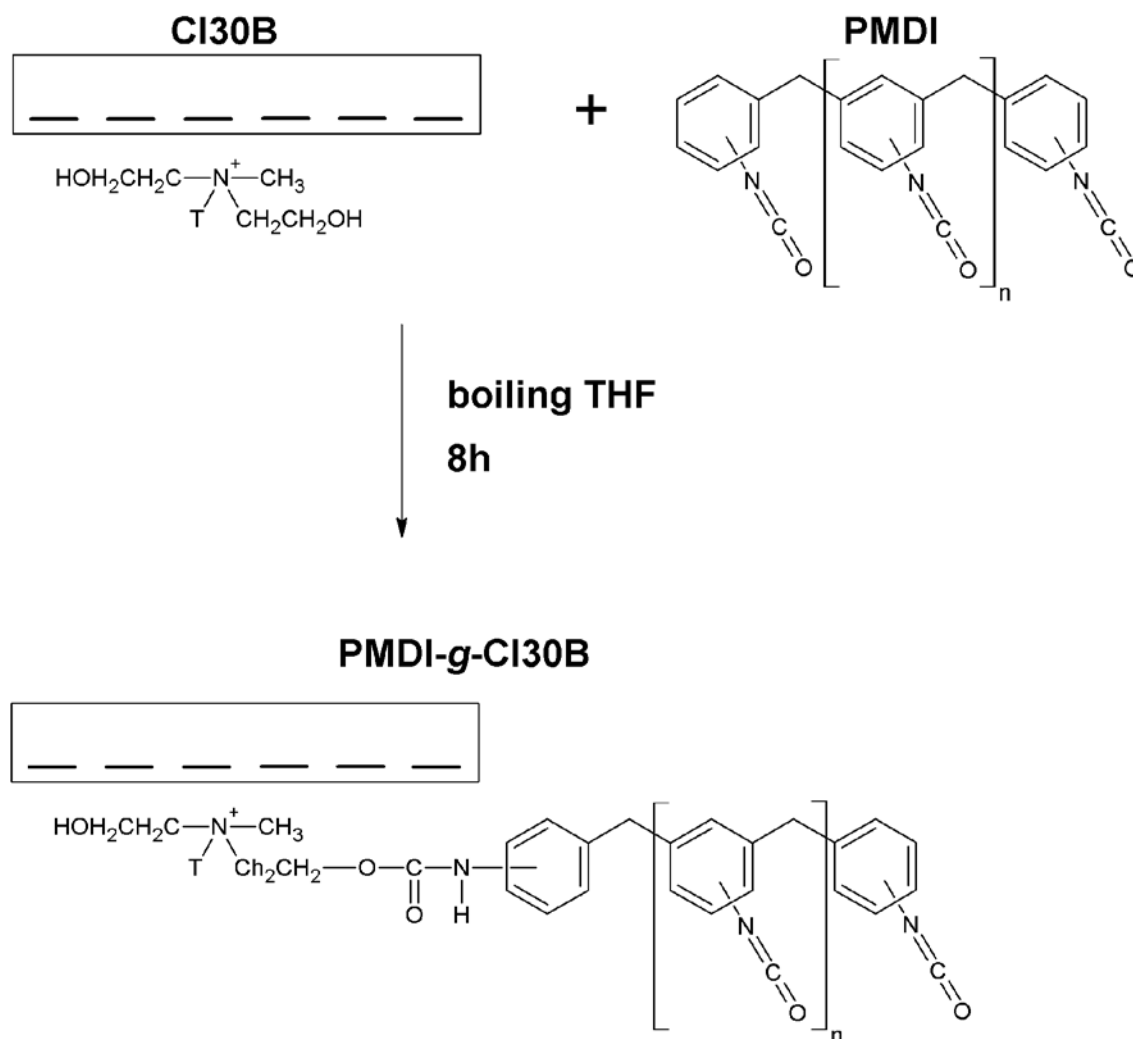
Fig. 13.1: Chemical modification of Cl30B with PMDI. T is tallow (~65% C18; ~30% C16; ~5% C14)

**FT-IR analysis**

The isocyanate/organoclay grafting was studied by FT-IR analysis; spectra are illustrated in figures 13.2 and 13.3. HDI did not show a sign of reaction according to FT-IR analysis while PMDI reacted with the organoclay. Spectra of pristine and PMDI-grafted Cl30B exhibit the characteristic bands of montmorillonite due to Al–O stretching at 3630, 919, 850 and 624 $cm^{-1}$, Si–O stretching at 1048 $cm^{-1}$, and asymmetric and symmetric stretching of methylene groups in hydrocarbon chains of the quaternary ammonium salt at 2852 and

2925 cm$^{-1}$, respectively [4-5, 9]. It can be seen that PMDI-modified organoclay exhibited new absorption bands at wavenumbers of 1716 and 1536 cm$^{-1}$ (*c.f.* figure 13.3) which were attributed to the stretching and deformation vibration of hydrogen bonded C=O and N–H, respectively [4, 24]. These absorption bands are characteristic of a urethane group, suggesting that PMDI had reacted with the quaternary ammonium salt of the organoclay.
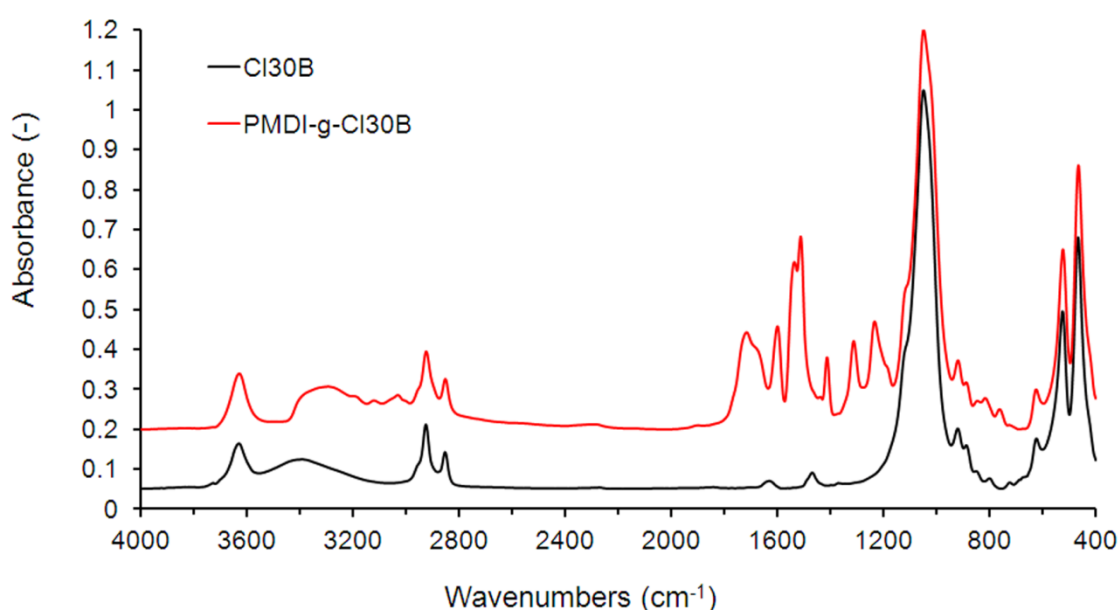


Fig. 13.2: FT-IR spectra of unmodified Cl30B and PMDI-*g*-Cl30B in the wavenumber range 4000–400 cm$^{-1}$.
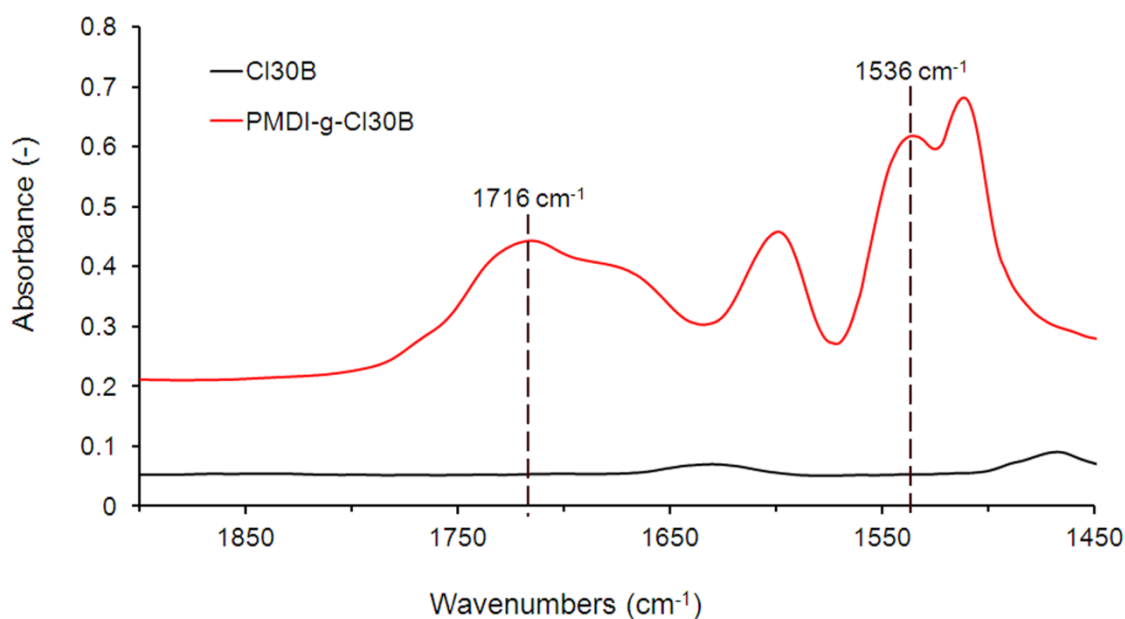
Fig. 13.3: FT-IR spectra of unmodified Cl30B and PMDI-*g*-Cl30B in the wavenumber range 1900–1450 cm$^{-1}$.

**SAXS analysis**

Further evidence of a successful isocyanate grafting onto the clay surface is provided by SAXS analysis; the diffraction patterns of pristine Cl30B and PMDI-*g*-Cl30B are illustrated in figure 13.4. As mentioned earlier, pristine Cl30B has a basal spacing of 18.5 Å according to the literature. The used Cl30B in this work exhibited a reflection at $2\theta = 5.2°$ which corresponds to a slightly lower basal spacing of 17.0 Å, probably due to some agglomeration [3]. In contrast, the diffraction pattern of PMDI-g-Cl30B shows two reflections at $2\theta = 3.0$ and 6.4° which correspond to basal spacings of 29.2 and 13.8 Å. This suggests that the PMDI intercalated into the clay galleries and was grafted onto the platelet surface. Consequently, the interlayer distance between clay galleries markedly increased and a weakening of the interlayer interactions with facilitated exfoliation during processing can be expected. Nevertheless, the reflection at $2\theta = 6.4°$ indicates that a small portion of the clay showed a collapsed interlayer structure with a decreased basal spacing. Again, this might be attributed to some agglomeration as well as to a possible degradation of the organic modifier of the clay (*i.e.* quaternary ammonium salt) [3, 23].
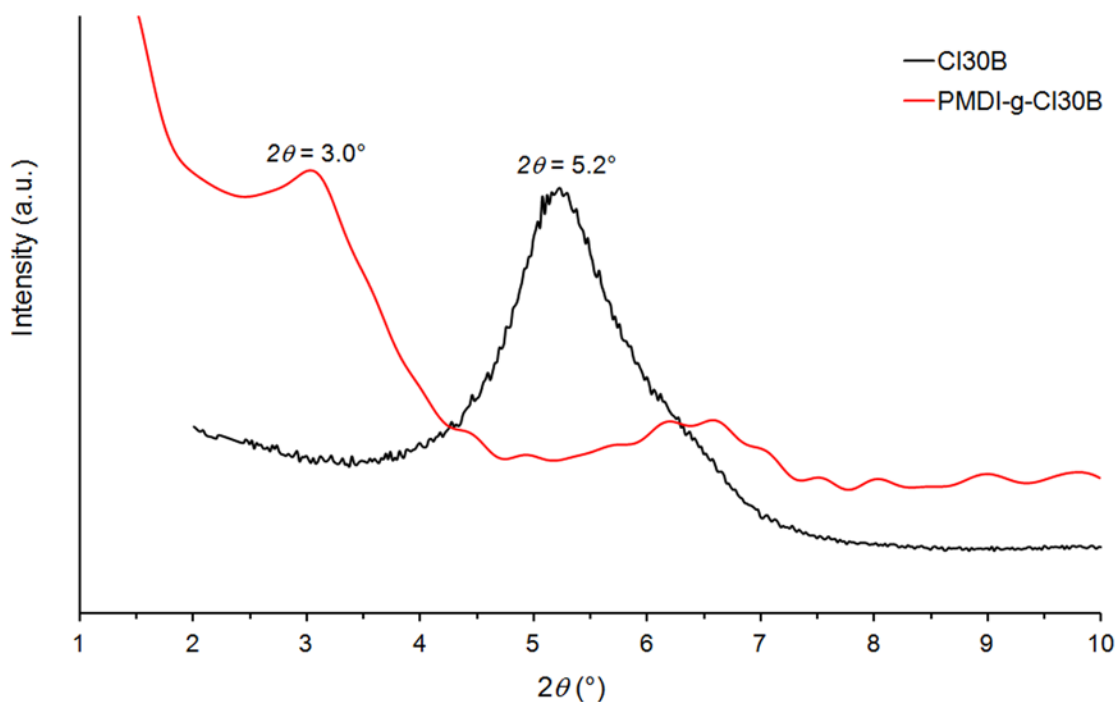
Fig. 13.4: SAXS diffraction patterns of pristine Cl30B and PMDI-*g*-Cl30B

### 13.4.2 Optimization of processing parameters

Prior to sample preparation it was necessary to determine the optimum processing parameters in order to achieve a fully converted high-molecular weight pCBT. The reason therefore was that it has been reported that the presence of organoclay can delay the ROP of CBT, shifting the polymerization towards higher temperatures and affecting the conversion and molecular weight of the resulting pCBT [13-14]. Optimization was achieved by preliminary torque *versus* time measurements in the batch mixer. Figure 13.5 depicts the torque curves of pristine CBT and a CBT blend of each sample group with an organoclay content of 1 wt.%.
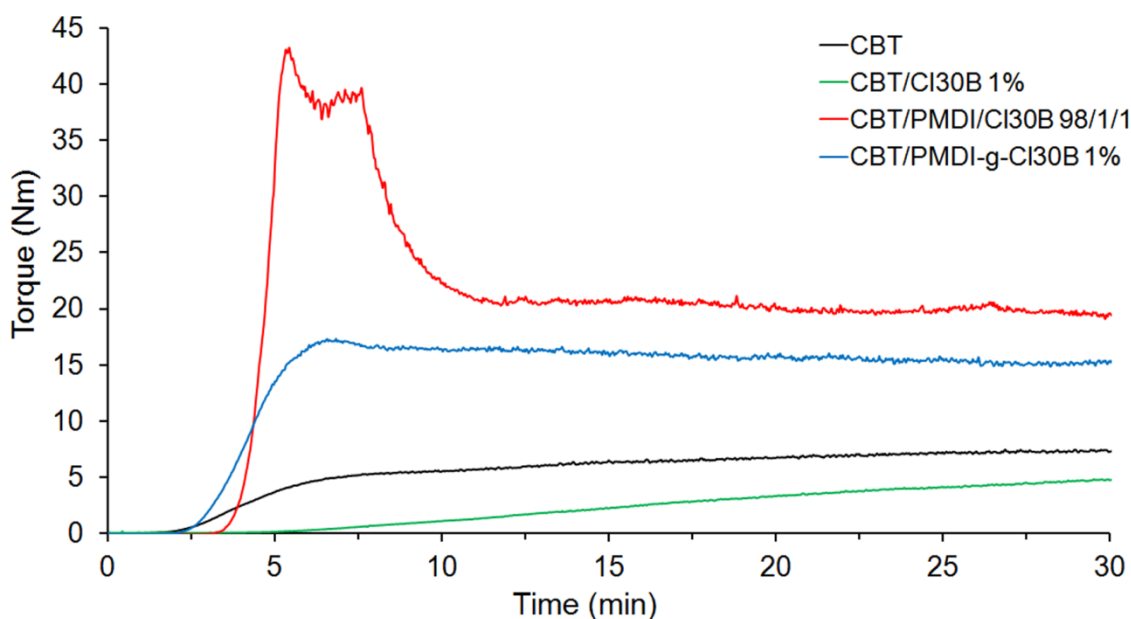
Fig. 13.5: Torque *versus* time plots of CBT, CBT/Cl30B 1%, CBT/PMDI/Cl30B 98/1/1 and CBT/PMDI-*g*-Cl30B 1% blends polymerized at 230°C and 60 min$^{-1}$ under nitrogen atmosphere.

The CBT/Cl30B blend showed a 3 min delayed torque onset and an overall lower torque level relative to pristine CBT. This confirms that the organoclay delays the ROP and affects the final molecular weight as stated by other researchers [13-14]. A possible explanation is that bound crystal water of the clay may have affected the CBT catalyst activity [25] and also have caused pCBT hydrolysis.

In comparison, the ternary blend exhibited a less delayed torque onset and reached its maximum torque of 43 Nm after 5 min due to the fast reaction between PMDI and growing pCBT chains. The torque decreased and reached a stable plateau value of 20 Nm which is considerable higher as the one of neat CBT, suggesting a relatively higher molecular weight.

Similarly, the CBT/PMDI-*g*-Cl30B blend showed a torque onset equal to pristine CBT, a maximum torque of 17 Nm after 7 min and essentially maintained this torque level until the end of the experiment.

This demonstrates on one hand the reactivity of PMDI-*g*-Cl30B since no extra isocyanate was added; thus the organoclay modification was effective. On the other hand it shows that the addition of PMDI to CBT/Cl30B blends as well as the PMDI-grafted Cl30B enhances the polymerization onset time and apparently the final molecular weight.

It is noteworthy that the molten pCBT/PMDI-*g*-Cl30B blend was completely transparent after 30 min mixing time, indicating clay exfoliation, whereas the pCBT/Cl30B blends were somewhat hazy which became more noticeable when PMDI was added to the blends.

In view of the observed torque maxima, a polymerization time of 30 min was chosen for binary CBT/Cl30B blends and 15 min for ternary blends as well as for binary blends containing PMDI-*g*-Cl30B.

### 13.4.3 SAXS analysis

The degree of exfoliation of the various pCBT/organoclay composites was studied using SAXS analysis; the diffraction patterns are illustrated in figures 13.6 and 13.7.
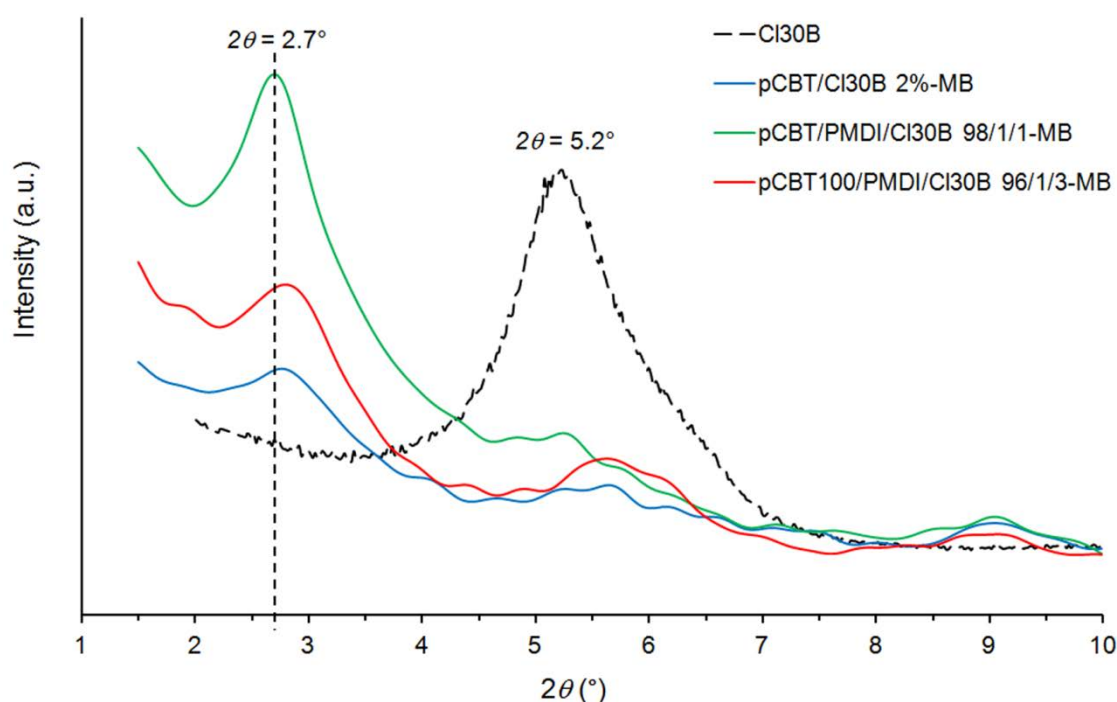


Fig. 13.6: SAXS diffraction patterns of Cl30B and the corresponding melt blended pCBT nanocomposites

The three diffraction patterns of pCBT nanocomposites in figure 13.6 are quite similar but different from the one of pristine Cl30B. They show two reflections at $2\theta$ = 2.7 and 5.2–5.4° which correspond to basal spacings of 32.7 and 17.0–16.4 Å. The weak peak around $2\theta$ = 9° is the (001) reflection of pCBT and can be also seen in the WAXS diffraction pattern. This suggests that most of the organoclay was intercalated by pCBT. On the other hand, the reflection at higher diffraction angles shows that part of the clay was agglomerated. Therefore, an intercalated-flocculated structure can be deduced [3]. These samples represent three groups; melt blended pCBT/Cl30B binary blends, melt blended pCBT/PMDI/Cl30B ternary blends and the sample pCBT100/PMDI/Cl30B 96/1/3 which was melt blended for 2 h in order to swell the organoclay prior to ROP. Moreover, they also represent the studied organoclay content range.

It can be concluded that melt blending produces an intercalated-flocculated nanocomposite structure, regardless of clay content (in the studied range). The presence of PMDI or swelling the organoclay in low-viscous molten CBT oligomers apparently did not affect the basal spacing.

The diffraction patterns of PMDI-modified organoclay and the corresponding melt blended and solvent blended nanocomposites are depicted in figure 13.7. No reflections can be observed in the melt blended sample, suggesting that the organoclay was completely exfoliated and true nanocomposites were formed. The weak reflection around $2\theta$ = 6° in the solvent blended sample suggests that part of the clay was agglomerated. Nevertheless, the peak intensity is very low; indicating that an insignificant amount of agglomeration was present, probably due to clay platelet reorganization during ROP in the absence of shear flow. Again, the weak reflection around $2\theta$ = 9° originates from pCBT as mentioned earlier.

These results suggest that the PMDI-modified organoclay was able to be completely exfoliated and randomly dispersed in the pCBT matrix because the clay was previously intercalated with PMDI. Moreover, since PMDI was grafted onto the organoclay surface, it is likely that pCBT end groups reacted with the PMDI and therefore facilitated clay exfoliation.
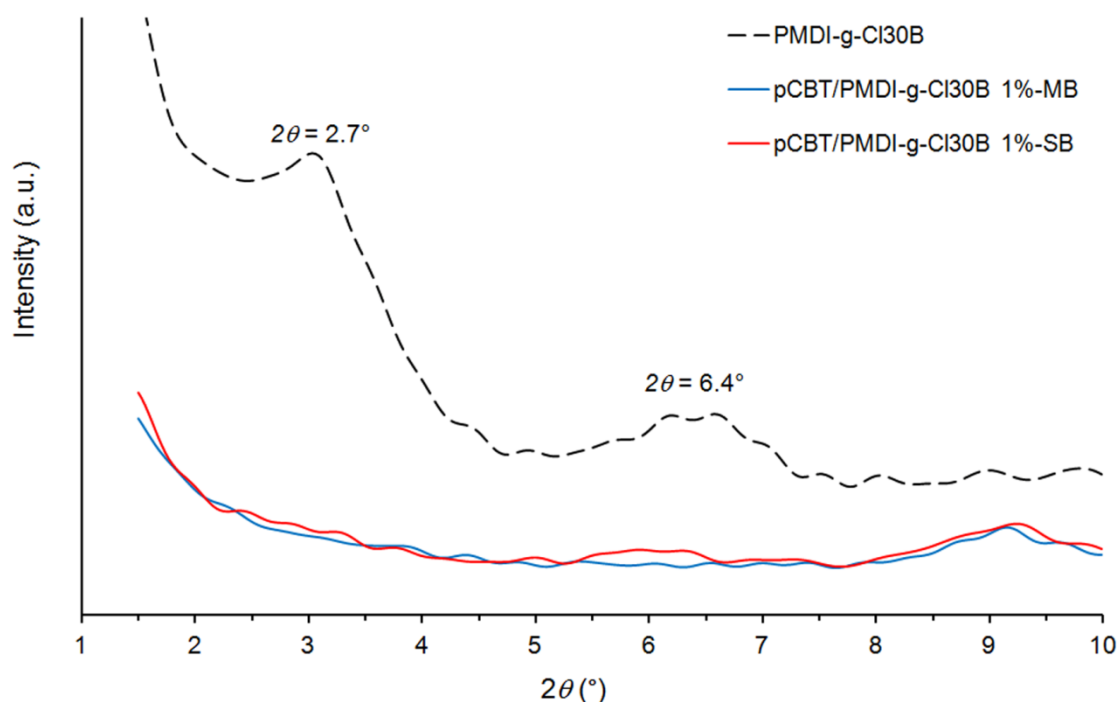
Fig. 13.7: SAXS diffraction patterns of PMDI-*g*-Cl30B and the corresponding melt blended and solvent blended pCBT nanocomposites

### 13.4.4 TEM analysis

The TEM micrographs of binary, ternary and PMDI-modified binary blends are depicted in figure 13.8. It can be noticed that binary pCBT/Cl30B blends (*c.f.* figure 13.8 a) exhibited micron-sized clay tactoids, confirming an intercalated-flocculated structure. Similarly, ternary blends exhibited an essentially equal morphology with large clay tactoids. Nevertheless, a partial clay intercalation with increased *d* spacing is apparent for these samples (*c.f.* right hand sides of figures 13.8a and b).

Figure 13.8 c shows the morphology of pCBT/PMDI-*g*-Cl30B 1%-MB. This sample exhibited a largely exfoliated structure as was also confirmed by SAXS analysis, although some small stacks of a few clay platelets can be seen at high magnification (*c.f.* right hand side of figure 13.8c). This demonstrates that the chemical modification of organoclay is a useful way to achieve clay exfoliation.
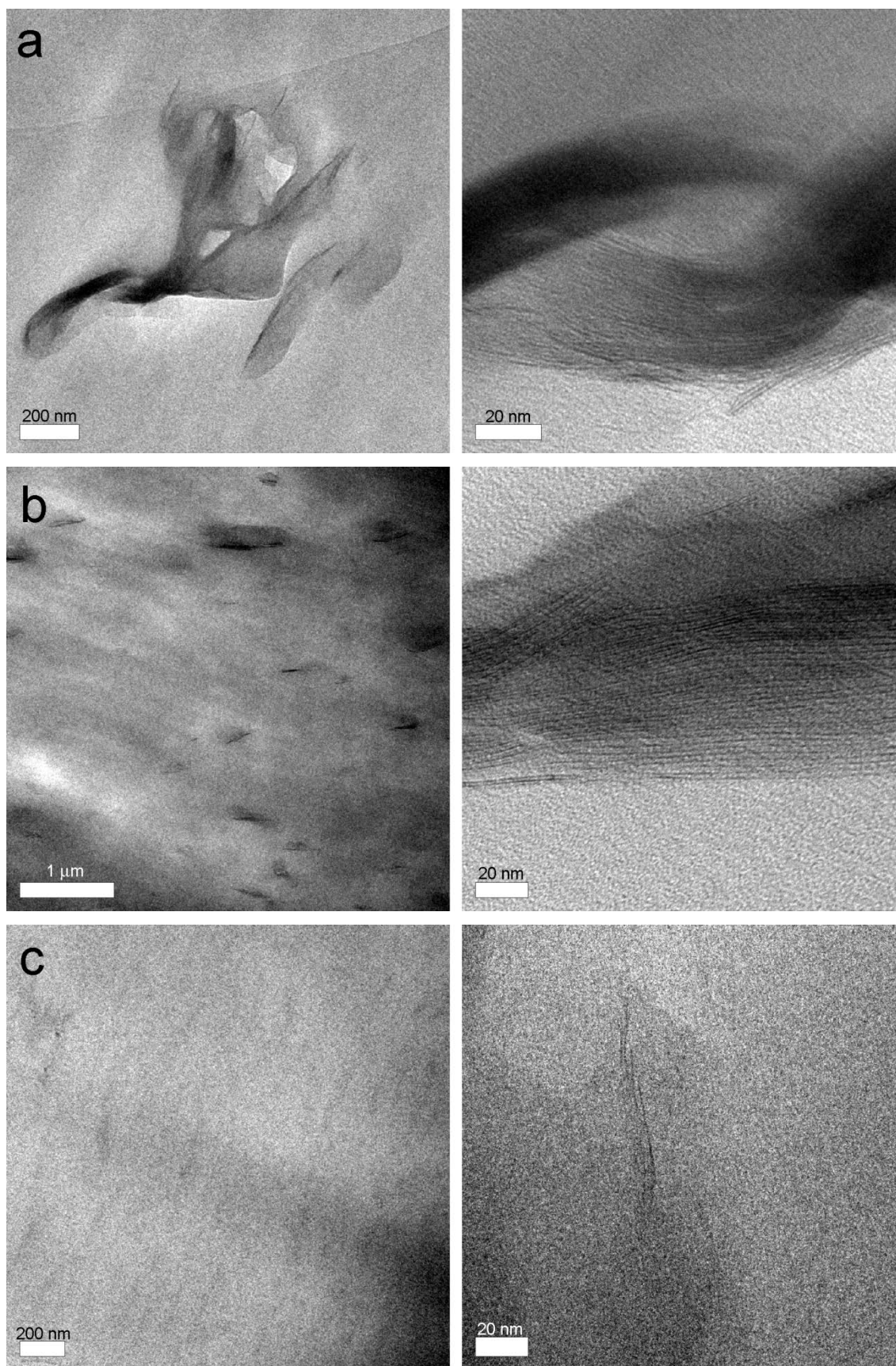
Fig. 13.8: TEM micrographs of (a) pCBT/Cl30B 1%-SB, (b) pCBT/PMDI/Cl30B 98/1/1-MB and (c) pCBT/PMDI-g-Cl30B 1%-MB.

### 13.4.5 DSC analysis

The thermal properties of melt and solvent blended pCBT/organoclay nanocomposites are collected in table 13.2. Since the used processing routes slightly alter the thermal properties, both melt and solvent blended neat pCBT are shown as reference in the table and the nanocomposites were compared to their respective host polymer, depending on the processing route.

Table 13.2: Thermal properties of melt and solvent blended pCBT/PMDI-*g*-Cl30B nanocomposites, heating and cooling at 10 °C/min.

| Sample | first cooling | | second heating | | | |
| --- | --- | --- | --- | --- | --- | --- |
| | $T_c$ | $\Delta H_c$ | $T_{m1}$ | $T_{m2}$ | $\Delta H_{m1+2}$ | $X_c$ |
| | [°C] | [J/g] | [°C] | [°C] | [J/g] | [%] |
| pCBT-MB | 193.1 | -50.6 | 215.4 | 223.5 | 50.7 | 35.7 |
| pCBT-SB | 187.2 | -44.5 | 214.0 | 222.9 | 44.6 | 31.4 |
| pCBT/Cl30B 1%-MB | 194.5 | -48.3 | 216.7 | 224.5 | 45.9 | 32.3 |
| pCBT/Cl30B 2%-MB | 198.7 | -49.8 | 218.0 | 224.6 | 49.4 | 34.8 |
| pCBT/Cl30B 3%-MB | 197.4 | -48.6 | 217.4 | 224.4 | 49.4 | 34.8 |
| pCBT/Cl30B 1%-SB | 191.5 | -48.4 | 215.1 | 223.4 | 44.2 | 31.1 |
| pCBT/Cl30B 2%-SB | 190.1 | -44.4 | 214.0 | 221.8 | 41.7 | 29.4 |
| pCBT/Cl30B 3%-SB | 190.4 | -44.4 | 213.5 | 221.5 | 42.1 | 29.6 |
| pCBT/PMDI/Cl30B 98/1/1-MB | 190.9 | -44.1 | 214.2 | 222.7 | 37.5 | 26.4 |
| pCBT/PMDI/Cl30B 98/1/1-SB | 188.2 | -42.6 | 213.2 | 222.0 | 38.9 | 27.4 |
| pCBT/PMDI-*g*-Cl30B 1%-MB | 193.5 | -49.3 | 215.2 | 223.5 | 44.9 | 31.6 |
| pCBT/PMDI-*g*-Cl30B 2%-MB | 192.4 | -48.1 | 214.0 | 222.4 | 43.0 | 30.3 |
| pCBT/PMDI-*g*-Cl30B 3%-MB | 193.2 | -48.8 | 214.6 | 222.8 | 45.6 | 32.1 |
| pCBT/PMDI-*g*-Cl30B 1%-SB | 190.7 | -48.4 | 214.3 | 222.8 | 45.2 | 31.8 |
| pCBT/PMDI-*g*-Cl30B 2%-SB | 190.4 | -46.9 | 214.1 | 222.3 | 44.3 | 31.2 |
| pCBT/PMDI-g-Cl30B 3%-SB | 189.7 | -45.1 | 213.6 | 221.9 | 42.3 | 29.8 |
| pCBT100/PMDI/Cl30B 96/1/3-MB | 193.4 | -46.0 | 214.3 | 222.8 | 39.2 | 27.6 |

The second heating scans of melt and solvent blended pCBT/PMDI-*g*-Cl30B are shown in figures 13.9 a and b, respectively. As can be seen, melting temperatures as well as melting enthalpies of the nanocomposites slightly decreased with clay content, which is in agreement with published data [13-14]. Although the clay slightly acts as a nucleation agent, it probably also confines the polymer chain segments and thus hinders the segmental rearrangement during crystallization and restricts the formation of perfect crystals in the polymer matrix [26]. The enthalpy decrease is more prominent in ternary blends and thus was partly attributed to the effect of chain extension when PMDI was present in the blend.

It was shown that this type of organoclay suppresses the cold crystallization when the CBT/Cl30B blend was polymerized in a DSC apparatus during the first heating scan. However, pCBT/Cl30B blends [13-14] as well as PBT/Cl30B blends [6] exhibited a nucleation effect during melt crystallization. This was also found for the binary CBT/Cl30B blends ($\Delta T$ = 2–6 °C) and for solvent blended pCBT/PMDI-*g*-Cl30B blends ($\Delta T$ = 3–4 °C). When the latter blends were melt blended, no nucleation effect was observed. Ternary pCBT/PMDI/Cl30B blends did not show a clear tendency due to an antagonistic effect of clay-induced nucleation and PMDI-induced reduction of $T_c$. In view of a difference in pCBT crystallization temperature of 6 °C due to different processing routes or the addition of 1 wt.% of PMDI, the observed nucleation effect ($\Delta T$ = 2–6 °C) is not relevant. This becomes also apparent when considering the fact that Cl30B was reported to increase $T_c$ by 12–18 °C in conventional PBT [6].
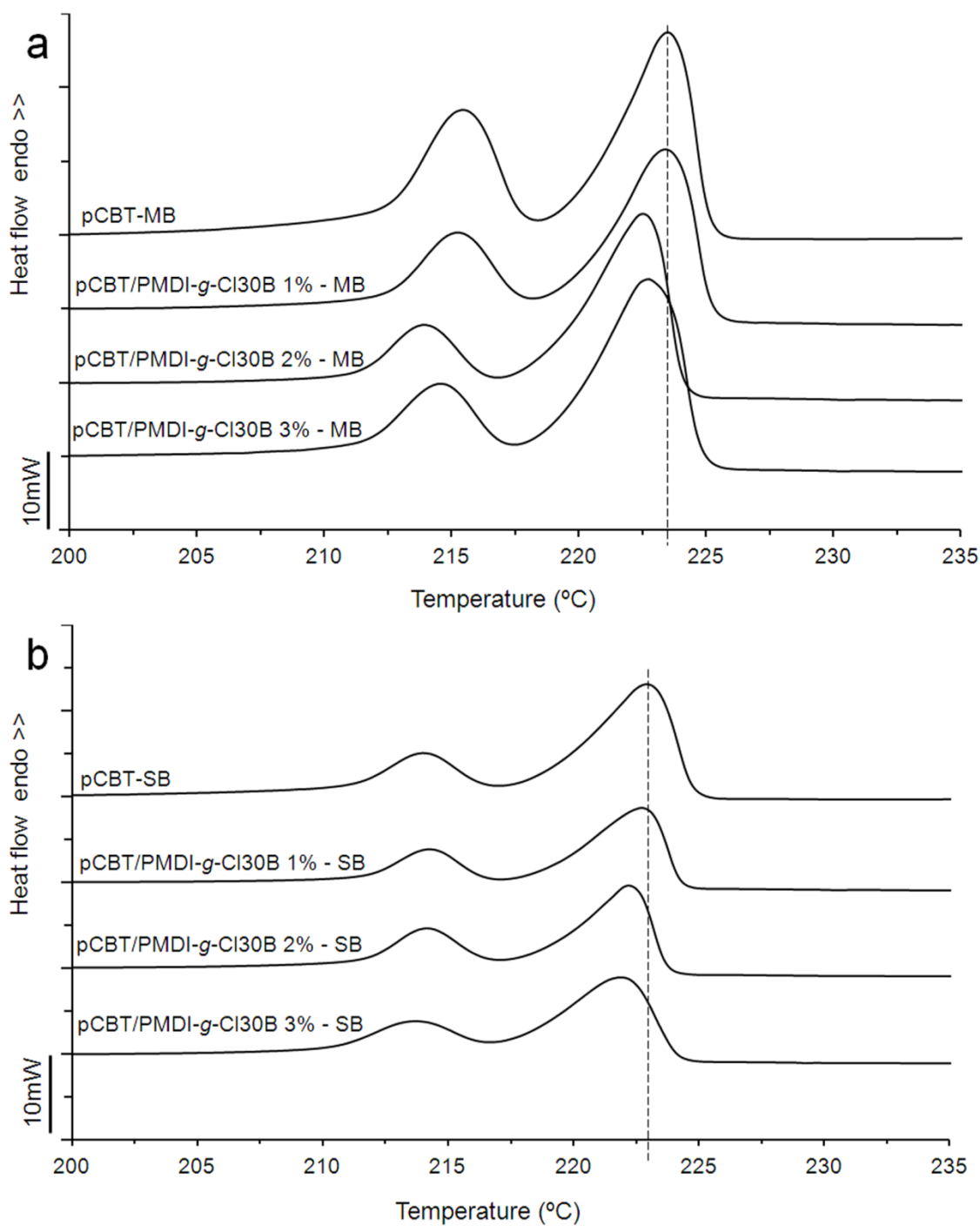
Fig. 13.9: DSC second heating scan of (a) melt blended and (b) solvent blended pCBT/PMDI-g-Cl30B; heating and cooling rate of 10°C/min.

### 13.4.6 DMTA analysis

The dynamic mechanical properties of pCBT/organoclay nanocomposites were determined; dynamic storage modulus curves as a function of temperature are shown in figures 13.10 and 13.11.

The reinforcement effect of pristine Cl30B is illustrated in figure 13.10; storage moduli of pCBT/Cl30B nanocomposites were considerably higher in the glassy state than the one of pristine pCBT and increased further with clay loading. The glass transition was depressed by 6 °C due to the presence of the organoclay which can be seen that storage modulus curves of the nanocomposites ran below the one of neat pCBT in the glass transition range. Nevertheless, the reinforcing effect was again noticeable in the rubbery state. Since these samples had an intercalated-flocculated structure, clay tactoids may have acted as rigid spheres, reinforcing the pCBT matrix [16].
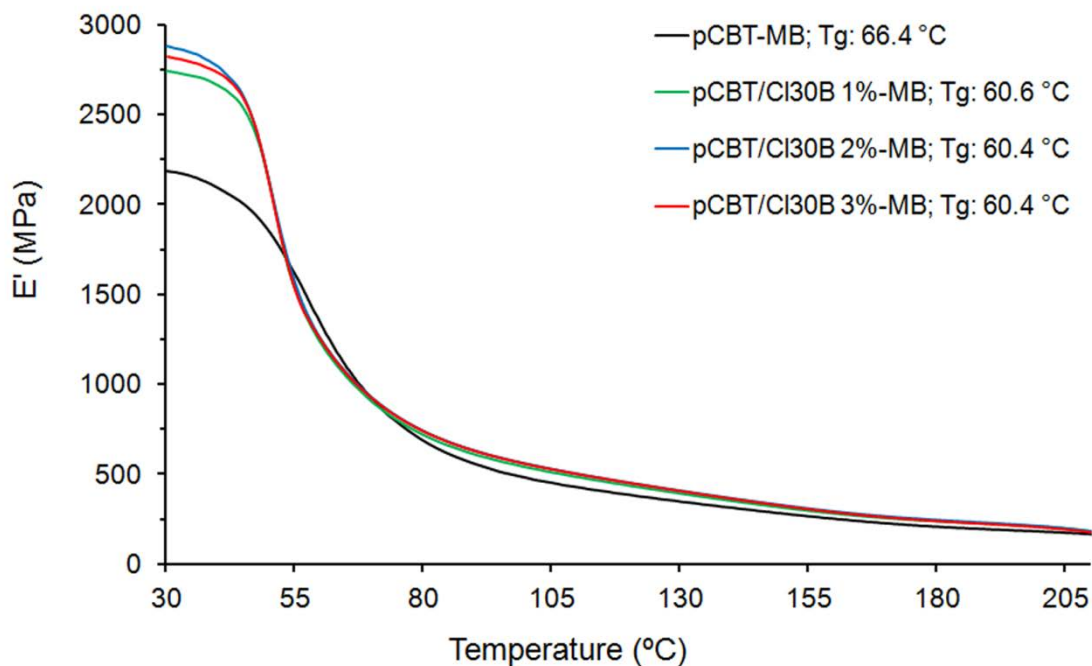


Fig. 13.10: DMTA storage moduli *versus* temperature of pCBT-MB and melt blended pCBT/Cl30B nanocomposites.

The role of PMDI on the reinforcing effect is shown in figure 13.11. It should be noted that PMDI-modified pCBT is more flexible and the decreased stiffness should be taken into account. Therefore, the nanocomposites were compared to melt blended pCBT/PMDI 1%-MB instead of pCBT-MB.

Again, the nanocomposites exhibited an enhanced stiffness throughout the temperature range as compared to the unreinforced sample. As expected, the reinforcing effect in the pCBT/PMDI/Cl30B ternary blend was less pronounced as compared to pCBT/Cl30B due to the opposed effect of PMDI toughening. The clay modification resulted in a relative stiffness decrease in the glassy state as compared to the other nanocomposites but pCBT/PMDI-*g*-Cl30B showed a reinforcing effect quite similar to the one of the ternary blend in the rubbery state.
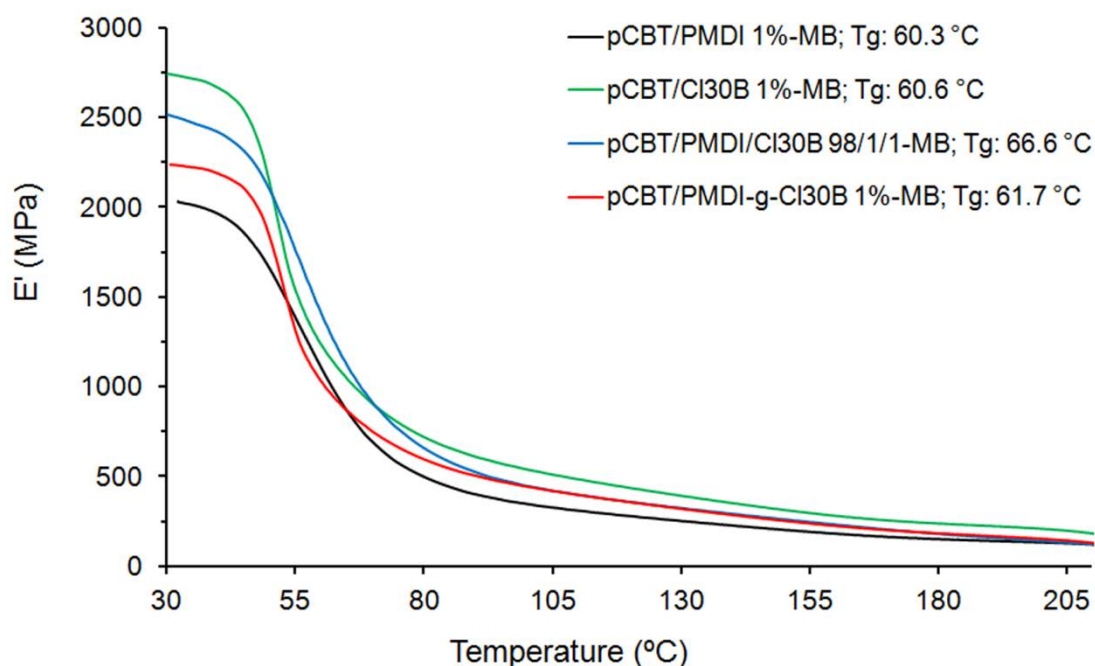


Fig. 13.11: DMTA storage moduli *versus* temperature of melt blended pCBT/PMDI 1%, pCBT/Cl30B, pCBT/PMDI/Cl30B and pCBT/PMDI-*g*-Cl30B nanocomposites.

### 13.4.7 TGA analysis

The thermal stability of the prepared nanocomposites was studied in nitrogen atmosphere; results are shown in table 13.3. Pristine pCBT showed a 5% mass loss temperature of 373 °C, a temperature of maximum mass loss rate of 405 °C and a residual weight of 1%. Ternary blends exhibited no significant difference in thermal stability as compared to pCBT, which is in line with reports of PBT/organoclay nanocomposites having similar structure [9]. In contrast, a slight improvement in thermal stability was noticed for pCBT/PMDI-$g$-Cl30B nanocomposites due to their exfoliated structure. The 5% mass loss temperature and temperature of maximum mass loss rate increased by 3–4 and 2–3 °C, respectively. This increase in thermal stability is quite small. It might be due to an antagonistic effect of mass-transport barrier to the volatile products generated during decomposition and on the other hand an accelerated pCBT decomposition due to bound water of the clay as well as catalytic activity of hydroxyl groups of the organic modifier [9].

Table 13.3: TGA data of melt blended pCBT and pCBT/organoclay nanocomposites.

| Sample | $T_{5 \% wt. loss}$ [°C] | $T_{max.}$ [°C] | Residue at 600 °C [wt.%] |
|---|---|---|---|
| pCBT-MB | 373.2 | 404.8 | 1.2 |
| pCBT/Cl30B 1%-MB | 377.0 | 407.1 | 4.0 |
| pCBT/Cl30B 2%-SB | 372.9 | 403.2 | 4.8 |
| pCBT/PMDI/Cl30B 98/1/1-MB | 376.7 | 407.2 | 3.9 |
| pCBT/PMDI/Cl30B 98/1/1-SB | 376.1 | 403.8 | 4.8 |
| pCBT/PMDI-$g$-Cl30B 1%-MB | 376.9 | 406.9 | 3.7 |
| pCBT/PMDI-$g$-Cl30B 2%-MB | 375.6 | 405.2 | 4.4 |
| pCBT/PMDI-$g$-Cl30B 3%-MB | 376.9 | 407.2 | 5.3 |
| pCBT/PMDI-$g$-Cl30B 1%-SB | 378.6 | 408.2 | 3.9 |
| pCBT/PMDI-$g$-Cl30B 2%-SB | 376.6 | 404.9 | 5.3 |
| pCBT/PMDI-g-Cl30B 3%-SB | 376.5 | 404.3 | 6.6 |
| pCBT100/PMDI/Cl30B 96/1/3-MB | 374.8 | 405.5 | 6.1 |

### 13.4.8 Tensile properties

The tensile properties of the prepared nanocomposites as well as the ones of neat pCBT-MB and pCBT-SB for comparison are compiled in table 13.4; normalized tensile properties are shown in figure 13.12.
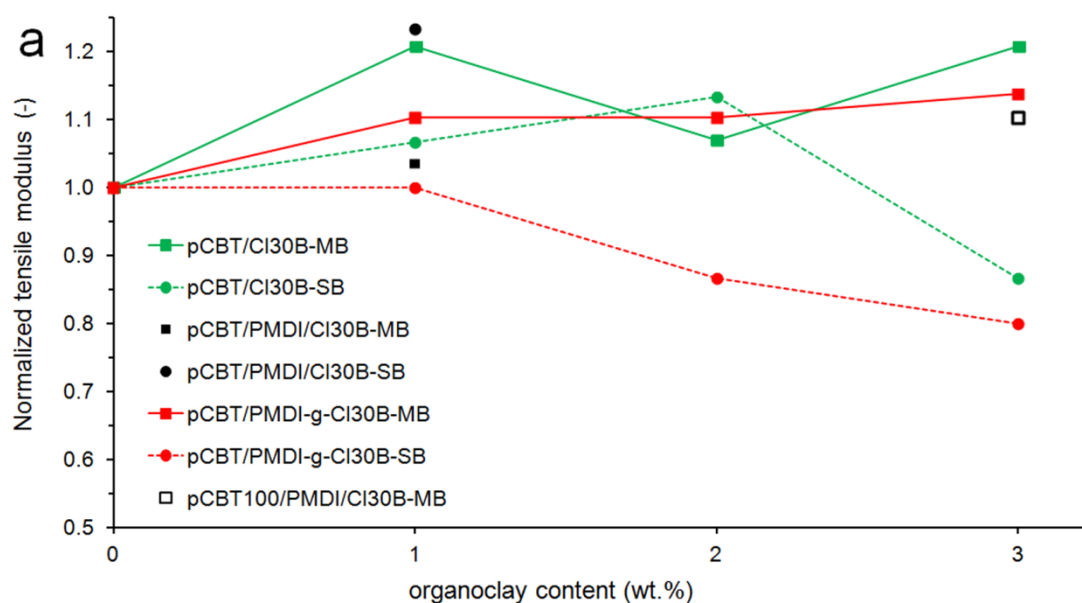


Fig. 13.12: Normalized tensile modulus (a), normalised tensile strength (b) and normalized failure strain (c) of the prepared organoclay nanocomposites. Dashed lines indicate solvent blending; lines are guides for the eyes.
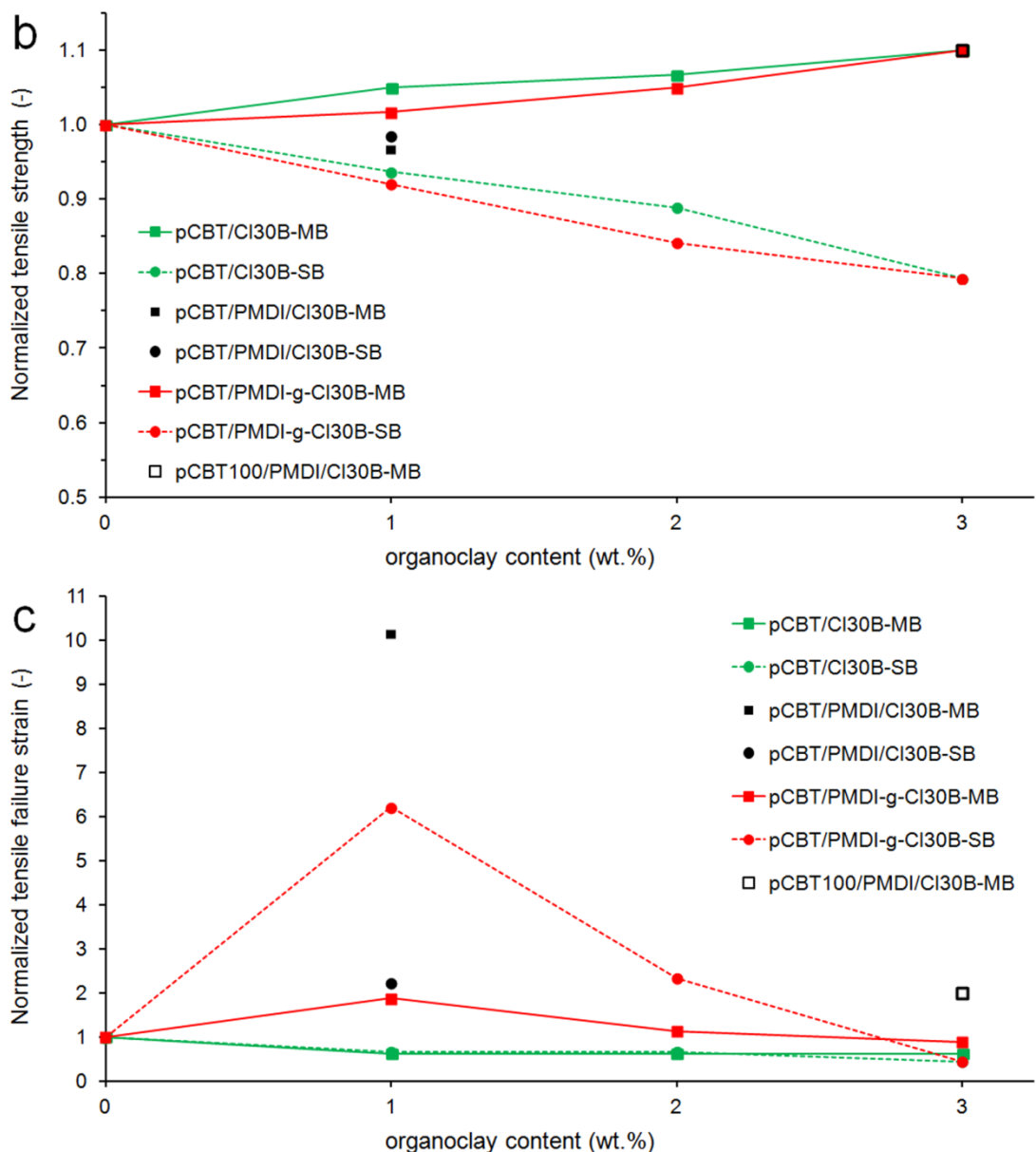
Fig. 13.12: Normalized tensile modulus (a), normalised tensile strength (b) and normalized failure strain (c) of the prepared organoclay nanocomposites. Dashed lines indicate solvent blending; lines are guides for the eyes. (*continued*)

As expected, pCBT/Cl30B nanocomposites showed a higher stiffness but also an exceptional brittleness, regardless of clay loading and processing route. Tensile strength increased with organoclay content for melt blended samples, whereas the opposite was observed for solvent blended nanocomposites due to poor physical interactions between pCBT and pristine Cl30B. Mechanical properties of pCBT/PMDI/Cl30B ternary blends were

different from the ones of binary pCBT/Cl30B blends. A semi-ductile deformation behaviour with yielding and unstable necking (also indicated by the large standard deviation of $\varepsilon_{break}$) along with a stiffness and strength similar to the one of neat pCBT was obtained *via* the melt blending route. The solvent blended sample showed a superior stiffness together with a moderately increased toughness.

Table 13.4:  Tensile properties of pCBT/organoclay nanocomposites.

| Sample | Tensile modulus (GPa) | Tensile strength (MPa) | Elongation at break (%) |
|---|---|---|---|
| pCBT-MB | 2.9 ± 0.3 | 60 ± 2 | 8 ± 1 |
| pCBT-SB | 3.0 ± 0.2 | 63 ± 4 | 9 ± 2 |
| pCBT/Cl30B 1%-MB | 3.5 ± 0.2 | 63 ± 2 | 5 ± 1 |
| pCBT/Cl30B 2%-MB | 3.1 ± 0.2 | 64 ± 1 | 5 ± 1 |
| pCBT/Cl30B 3%-MB | 3.5 ± 0.2 | 66 ± 1 | 5 ± 1 |
| pCBT/Cl30B 1%-SB | 3.2 ± 0.2 | 59 ± 2 | 6 ± 2 |
| pCBT/Cl30B 2%-SB | 3.4 ± 0.3 | 56 ± 1 | 6 ± 1 |
| pCBT/Cl30B 3%-SB | 2.6 ± 0.5 | 50 ± 3 | 4 ± 2 |
| pCBT/PMDI/Cl30B 98/1/1-MB | 3.0 ± 0.4 | 58 ± 1 | 81 ± 77 |
| pCBT/PMDI/Cl30B 98/1/1-SB | 3.7 ± 0.5 | 62 ± 2 | 20 ± 15 |
| pCBT/PMDI-*g*-Cl30B 1%-MB | 3.2 ± 0.4 | 61 ± 3 | 15 ± 13 |
| pCBT/PMDI-*g*-Cl30B 2%-MB | 3.2 ± 0.2 | 63 ± 2 | 9 ± 3 |
| pCBT/PMDI-*g*-Cl30B 3%-MB | 3.3 ± 0.2 | 66 ± 1 | 7 ± 1 |
| pCBT/PMDI-*g*-Cl30B 1%-SB | 3.0 ± 0.2 | 58 ± 1 | 56 ± 21 |
| pCBT/PMDI-*g*-Cl30B 2%-SB | 2.6 ± 0.1 | 53 ± 1 | 21 ± 9 |
| pCBT/PMDI-*g*-Cl30B 3%-SB | 2.4 ± 0.2 | 50 ± 6 | 4 ± 2 |
| pCBT100/PMDI/Cl30B 96/1/3-MB | 3.2 ± 0.2 | 66 ± 1 | 16 ± 10 |

Similarly, melt blended pCBT/PMDI-*g*-Cl30B nanocomposites showed increasing modulus and strength but also a decreasing toughness with PMDI-*g*-Cl30B loading. Stiffness and strength were ca. 10% higher for a clay loading of 3 wt.% as compared to the reference. Contrary to that, solvent blending apparently had a negative effect; mechanical properties markedly decreased with clay loading. At present it is difficult to explain why solvent blending degrades the mechanical properties. A possible explanation therefore might be clay segregation during the compression moulding step due to the low viscosity of molten CBT prior to ROP and the absence of shear during/after polymerization.

The mechanical properties of the herein prepared samples were compared to literature values from pCBT/organoclay composites [12, 18] and also from conventional PBT/Cl30B blends [6, 16]. The found increase in stiffness and strength is in good agreement with the one described in literature for both pCBT and PBT blends. No information on failure strain of pCBT nanocomposites was available but it can be assumed that they were brittle due to the above mentioned pCBT brittleness. Regarding PBT nanocomposites, it is clear that already 1 wt.% of clay loading leads to severe embrittlement with a failure strain below 5% of the otherwise ductile PBT. In contrast, a semi-ductile behaviour was observed in most of the nanocomposites described in this work due to the toughening effect of the isocyanate, either as additive in ternary blends or grafted onto the clay platelets. This demonstrates that the mechanical properties of pCBT/Cl30B nanocomposites can be tailored in a fairly wide range from high stiffness and strength to moderate toughness by adding PMDI or using the proposed clay modification.

## 13.5  Conclusions

Organically modified montmorillonite was used to prepare pCBT nanocomposites. Binary blends of pCBT and pristine organoclay showed an intercalated-flocculated structure which resulted on one hand in high stiffness and strength, but on the other hand led to embrittlement of pCBT. Toughness increased when polyfunctional isocyanate was added to the nanocomposites but the reinforcement effect of the clay was less pronounced due to the opposed effect of isocyanate toughening. The organoclay was further modified by tethering the isocyanate to the clay surfactant which resulted in an intercalated organoclay.

This isocyanate-grafted organoclay reacted then with pCBT and therefore could be fully exfoliated and randomly dispersed in the pCBT matrix during polymerization. Thermal properties and stabilities were not significantly altered by the organoclay, although some nanocomposites showed a decreased degree of crystallinity. It was demonstrated that the mechanical properties of these nanocomposites can be tailored from high stiffness and strength to moderate toughness using PMDI and the proposed clay modification.

## 13.6    References for pCBT/organoclay

1.    Alexandre, M and Dubois, P. Polymer-layered silicate nanocomposites: preparation, properties and uses of a new class of materials. Materials Science and Engineering: R: Reports **28**(1–2), 1-63 (2000).

2.    Kiliaris, P and Papaspyrides, CD. Polymer/layered silicate (clay) nanocomposites: An overview of flame retardancy. Progress in Polymer Science **35**(7), 902-958 (2010).

3.    Sinha Ray, S and Okamoto, M. Polymer/layered silicate nanocomposites: a review from preparation to processing. Progress in Polymer Science **28**(11), 1539-1641 (2003).

4.    Pattanayak, A and Jana, SC. Synthesis of thermoplastic polyurethane nanocomposites of reactive nanoclay by bulk polymerization methods. Polymer **46**(10), 3275-3288 (2005).

5.    Berti, C, Fiorini, M, and Sisti, L. Synthesis of poly(butylene terephtahlate) nanocomposites using anionic clays. European Polymer Journal **45**(1), 70-78 (2009).

6.    Chang, Y-W, Kim, S, and Kyung, Y. Poly(butylene terephthalate)–clay nanocomposites prepared by melt intercalation: morphology and thermomechanical properties. Polymer International **54**(2), 348-353 (2005).

7.    Hwang, S-s, Liu, S-p, Hsu, PP, Yeh, J-m, Chang, K-c, and Lai, Y-z. Effect of organoclay on the mechanical/thermal properties of microcellular injection molded PBT–clay nanocomposites. International Communications in Heat and Mass Transfer **37**(8), 1036-1043 (2010).

8.  Li, X, Kang, T, Cho, W-J, Lee, J-K, and Ha, C-S. Preparation and Characterization of Poly(butyleneterephthalate)/Organoclay Nanocomposites. Macromolecular Rapid Communications **22**(16), 1306-1312 (2001).

9.  Xiao, J, Hu, Y, Wang, Z, Tang, Y, Chen, Z, and Fan, W. Preparation and characterization of poly(butylene terephthalate) nanocomposites from thermally stable organic-modified montmorillonite. European Polymer Journal **41**(5), 1030-1035 (2005).

10. Berti, C, Binassi, E, Colonna, M, Fiorini, M, Zuccheri, T, Karanam, S, and J. Brunelle, D. Improved dispersion of clay platelets in poly(butylene terephthalate) nanocomposite by ring-opening polymerization of cyclic oligomers: Effect of the processing conditions and comparison with nanocomposites obtained by melt intercalation. Journal of Applied Polymer Science **114**(5), 3211-3217 (2009).

11. Dion, RP, Bank, DH, Beebe, MC, Walia, P, LeBaron, C, Oelberg, JD, Barger, MA, Paquette, MS, and Read, MD. Polymerized macrocyclic oligomer nanocomposite compositions. U.S. Patent Application US 2005/0059768 A1. 2005.

12. Hong, Y, Yoon, H, and Lim, S. Preparation of PBT/clay nanocomposites using supercritical process. International Journal of Precision Engineering and Manufacturing **10**(3), 115-118 (2009).

13. Karger-Kocsis, J, Shang, PP, Mohd Ishak, ZA, and Rösch, M. Melting and crystallization of in-situ polymerized cyclic butylene terephthalates with and without organoclay: A modulated DSC study. eXPRESS Polymer Letters **1**(2), 60-68 (2007).

14. Lanciano, G, Greco, A, Maffezzoli, A, and Mascia, L. Effects of thermal history in the ring opening polymerization of CBT and its mixtures with montmorillonite on the crystallization of the resulting poly(butylene terephthalate). Thermochimica Acta **493**(1-2), 61-67 (2009).

15. Lee, S-S, Ma, YT, Rhee, H-W, and Kim, J. Exfoliation of layered silicate facilitated by ring-opening reaction of cyclic oligomers in PET–clay nanocomposites. Polymer **46**(7), 2201-2210 (2005).

16. McLauchlin, A, Bao, X, and Zhao, F. Organoclay polybutylene terephthalate nanocomposites using dual surfactant modified montmorillonite prepared by the masterbatch method. Applied Clay Science **53**(4), 749-753 (2011).

17. Tripathy, AR, Burgaz, E, Kukureka, SN, and MacKnight, WJ. Poly(butylene terephthalate) nanocomposites prepared by in-situ polymerization. Macromolecules **36**(23), 3 (2003).

18. Wan, C, Zhao, F, Bao, X, Kandasubramanian, B, and Duggan, M. Surface Characteristics of Polyhedral Oligomeric Silsesquioxane Modified Clay and Its Application in Polymerization of Macrocyclic Polyester Oligomers. The Journal of Physical Chemistry B **112**(38), 11915-11922 (2008).

19. Wu, FM and Yang, GS. Poly(butylene terephthalate)/organoclay nanocomposites prepared by in-situ bulk polymerization with cyclic poly(butylene terephthalate). Materials Letters **63**(20), 1686-1688 (2009).

20. Cao, X, James Lee, L, Widya, T, and Macosko, C. Polyurethane/clay nanocomposites foams: processing, structure and properties. Polymer **46**(3), 775-783 (2005).

21. Wang, H-H and Chen, K-V. A novel synthesis of reactive nano-clay polyurethane and its physical and dyeing properties. Journal of Applied Polymer Science **105**(3), 1581-1590 (2007).

22. Xu, Z-b, Kong, W-w, Zhou, M-x, and Peng, M. Effect of surface modification of montmorillonite on the properties of rigid polyurethane foam composites. Chinese Journal of Polymer Science **28**(4), 615-624 (2010).

23. Filippi, S, Paci, M, Polacco, G, Dintcheva, NT, and Magagnini, P. On the interlayer spacing collapse of Cloisite® 30B organoclay. Polymer Degradation and Stability **96**(5), 823-832 (2011).

24. Yin, L, Shi, D, Liu, Y, and Yin, J. Toughening effects of poly(butylene terephthalate) with blocked isocyanate-functionalized poly(ethylene octene). Polymer International **58**(8), 919-926 (2009).

25. Brunelle, DJ. Cyclic oligomer chemistry. Journal of Polymer Science Part A: Polymer Chemistry **46**(4), 1151-1164 (2008).

26. Pavlidou, S and Papaspyrides, CD. A review on polymer–layered silicate nanocomposites. Progress in Polymer Science **33**(12), 1119-1198 (2008).

# Chapter 14: pCBT/graphene nanocomposites[4]

Graphene nano-platelets (0.25 to 1 wt.%; referred to as G) were used to prepare pCBT/G nanocomposites by solvent blending and melt blending, respectively, and then characterized using various techniques. Moreover, ternary blends of pCBT, diisocyanate and G as well as binary blends of pCBT and polyisocyanate-modified G were prepared. The isocyanate grafting onto the graphene platelet surface was further verified by dispersion studies, FT-IR and TGA analysis.

Binary blends of pCBT and G exhibited an agglomerated structure due to poor compatibility. Consequently, mechanical properties deteriorated with increasing G content. Compatibility somewhat improved with the addition of diisocyanate and stiffness and toughness were enhanced. Binary blends containing the polyisocyanate-modified G showed a further improved stiffness and strength due to the enhanced compatibility. This was because on one hand the PMDI-grafted graphene was rendered less hydrophilic and on the other hand probably reacted with the pCBT matrix. Nevertheless, TEM, SEM and WAXS analysis revealed the presence of graphene tactoids in all prepared samples. In other words, the strong $\pi$–$\pi$ interactions between the graphene sheets could not be interrupted and thus G exfoliation could not be achieved. The thermal properties, most importantly thermal stability, were not significantly altered by the graphene due to the agglomerated structure, although a pronounced heterogeneous nucleation effect was found.

---

[4] Sample preparation and measurements were partly performed in the Department of Polymer Engineering, Budapest University of Technology and Economics, Hungary.

## 14.1   Introduction

Graphene is a one-atom-thick layer of sp$^2$-bonded carbon atoms densely arranged in a two-dimensional honeycomb crystal lattice and has received enormous attention lately due to its outstanding mechanical, thermal and electrical properties [1-3]. Unfortunately, inexpensive and abundantly available graphite does not readily exfoliate to yield individual graphene sheets [4]. Nevertheless, monolayered graphite-like nano-platelets can be produced by several routes such as micro-mechanical exfoliation of graphite (also known as the 'scotch tape' or 'peel-off' method), growth by chemical vapour deposition and growth on crystalline silicon carbide. These routes yield largely defect-free graphene (hereafter referred to as G) with exceptional physical properties. Nevertheless, they do not yield large enough quantities for use as composite fillers [2-3].

A scalable approach to obtain G from graphite intercalation compounds is the well-known Hummers method [5]. This method involves the oxidation of naturally occurring graphite using a water-free mixture of concentrated sulfuric acid, sodium nitrate and potassium permanganate and yields graphite oxide (GO) with a C:O ratio of approximetly 2:1. GO has an expanded interlayer distance relative to graphite which depends on humidity due to intercalation with water molecules [3]. Moreover, the highly oxygenated GO bears epoxide, diol, ketone, hydroxyl and carboxyl functional groups on the basal plane and additional carbonyl and carboxyl groups located at the edges of the GO sheets. These functional groups render GO platelets highly hydrophilic, allowing them to readily swell and disperse in water [1-3] but direct exfoliation into non-aqueous solvents or hydrophobic polymer matrices is not favoured [6].

Several routes are available to obtain exfoliated and reduced GO, for instance the solution-based chemical reduction of GO [2, 7] or most commonly thermal shocking [3] which yields thermally reduced graphite oxide (TRGO), the latter being suitable for large-scale production. Reduced GO exhibits a C:O ratio of over 10:1 and retains some of the oxygenated functional groups originally present on the GO platelets [3]. The functional groups present on GO and reduced GO, respectively, can be employed for chemical functionalization of graphene to generate stable dispersions of chemically modified graphene in organic solvents as well as to enhance their compatibility with various polymer matrices [1, 3]. Stankovich *et al.* [4, 6] used different types of isocyanate compounds for chemical functionalization of GO. The functionalization reduces the hydrophilic character

of GO by forming amide and carbamate ester bonds to the carboxyl and hydroxyl groups of GO, respectively and effectively prevents restacking of the exfoliated graphene sheets due to reduced $\pi$–$\pi$ interactions. In contrast to the parent GO, these isocyanate-modified GO´s did not disperse at all in water but readily exfoliated and formed stable dispersions in polar aprotic solvents and therefore are suitable for the preparation of polymer-graphene nanocomposites with good exfoliation and dispersion.

Regarding polymer-graphene composites, proper exfoliation and homogeneous dispersion of single graphene sheets in the polymer matrix is crucial for property improvements [2-4]. Similar as for other types of nanofillers such as layered silicates, exfoliation remains a major challenge; in this case this is due to the strong $\pi$–$\pi$ stacking of the $\pi$ orbitals of graphene [1-2]. Since the high melt viscosity of most thermoplastics does not favour exfoliation, G is therefore commonly intercalated/exfoliated by solvents and/or monomers prior to melt blending with thermoplastics [1-4, 6, 8-9]. As CBT exhibits a very low, water-like melt viscosity prior to ROP, it appears to be a convenient matrix material for graphene nanocomposites and some work on this subject has already been reported.

Fabbri and co-workers [9] were the first to report pCBT/G nanocomposites prepared by solvent blending CBT oligomers and 0.5–1 wt.% of graphene nano-platelets, then extracting the solvent and subsequently melt blending the dried compound. Then the catalyst was added to the molten oligomer/G blend and ROP took place. A good dispersion and the absence of macroscopic G stacking were reported. Nevertheless, molecular weight strongly decreased with G content; $M_w$ was below 10 kg/mol when 1 wt.% of G was added. Unfortunately, no information was given about the functionality of the used G although they assumed an unreactive G type but at the same time speculated that the G may have interacted either with the catalyst or with the reactive center of chain propagation. On the other hand, oxygen-containing functional groups were likely present in their graphene type and may have indeed affected the catalyst activity, as it is well known that active hydroxyl groups (such as water) [10-11] but also carboxyl groups inhibit the catalyst activity [12]. Due to the low molecular weight of the pCBT/G materials, the nanocomposites were too brittle for standard specimen preparation. Nevertheless, it was found by nano-indentation that the elastic modulus and indentation hardness increased for G contents lower than 0.75 wt.%. Moreover, thermal stability in oxygen was improved by up to 20 °C and all prepared samples were electrically conductive.

Balogh *et al.* [13] employed the melt blending route to prepare pCBT/G nanocomposites using graphene nano-platelets at concentrations of 1–5 wt.%. They obtained poor dispersion and found that G had a nucleation effect on pCBT. A pronounced reinforcing effect was found; DMTA storage modulus at room temperature increased by 39–89% and the heat conductivity was also markedly enhanced.

Very recently, Chen *et al.* [8] prepared pCBT/TRGO nanocomposites using thermally reduced graphite oxide. CBT and TRGO were solvent blended, vacuum dried and then polymerized at 200 °C. Rheological measurements revealed that the rate and degree of CBT polymerization decreased with TRGO content. This was ascribed to the reaction between carboxyl groups of growing pCBT chains and hydroxyl/epoxy groups situated on the surface of TRGO. The pCBT grafted onto TRGO was confirmed by various characterization techniques and the grafting content was found to be up to 53%.

Literature makes it abundantly clear that chemical functionalization of graphene sheets are of crucial importance in the synthesis of polymer-graphene nanocomposites with good dispersion [1-4, 6]. Moreover, the preceding chapter demonstrated that chemical modification of the nanofiller as well as adding a toughening agent can provide semi-ductile pCBT nanocomposites. Similarly to chapter 13, a method is described herein that involves a coupling reaction of the oxygen-containing functional groups of graphene (situated on the surface and the edges of G nano-platelets) with –N=C=O functional groups of a polyfunctional isocyanate. The isocyanate *grafted-onto* G is also highly reactive towards pCBT end groups; so pCBT is expected to be covalently bonded to the NCO-modified graphene.

## 14.2   Experimental Section

### 14.2.1 Materials

One-component cyclic butylene terephthalate oligomers (CBT160®) and commercial graphene nano-platelets were used throughout this chapter.

### 14.2.2 Graphene modification

Graphene nano-platelets were modified with PMDI as described in detail in section 4.4. PMDI-grafted graphene was referred to as PMDI-*g*-G. A grafting reaction between PMDI and the various oxygen-containing functional groups of the graphene nano-platelets is proposed in figure 14.1. The reaction was studied by FT-IR analysis; spectra are illustrated in figure 14.3 and 14.4. Grafting was further evidenced by TGA analysis (*c.f.* figure 14.5) and dispersion studies on pristine and modified graphene (*c.f.* figure 14.2).
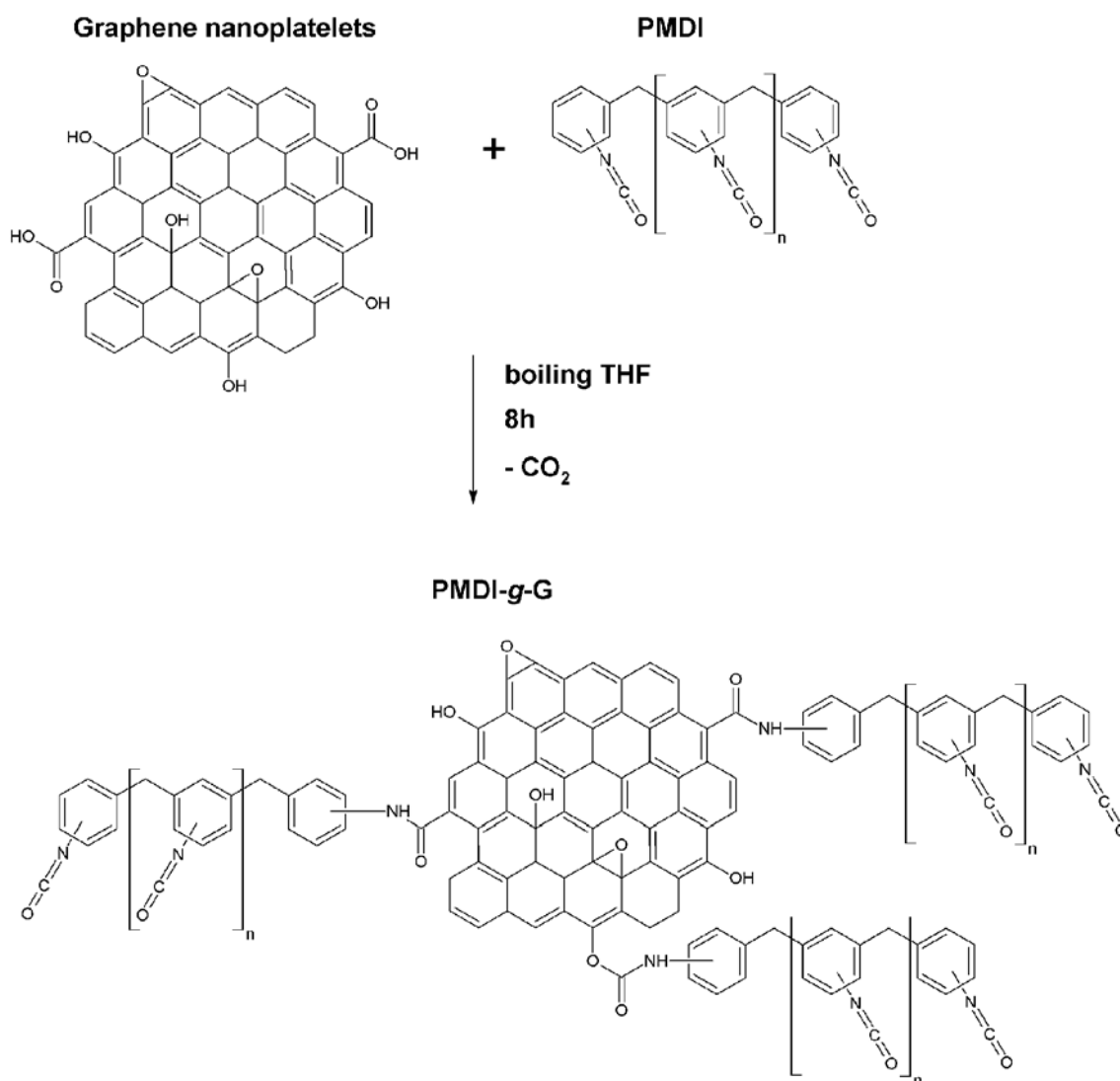


Fig. 14.1: Proposed reaction mechanism for the chemical modification of graphene with PMDI.
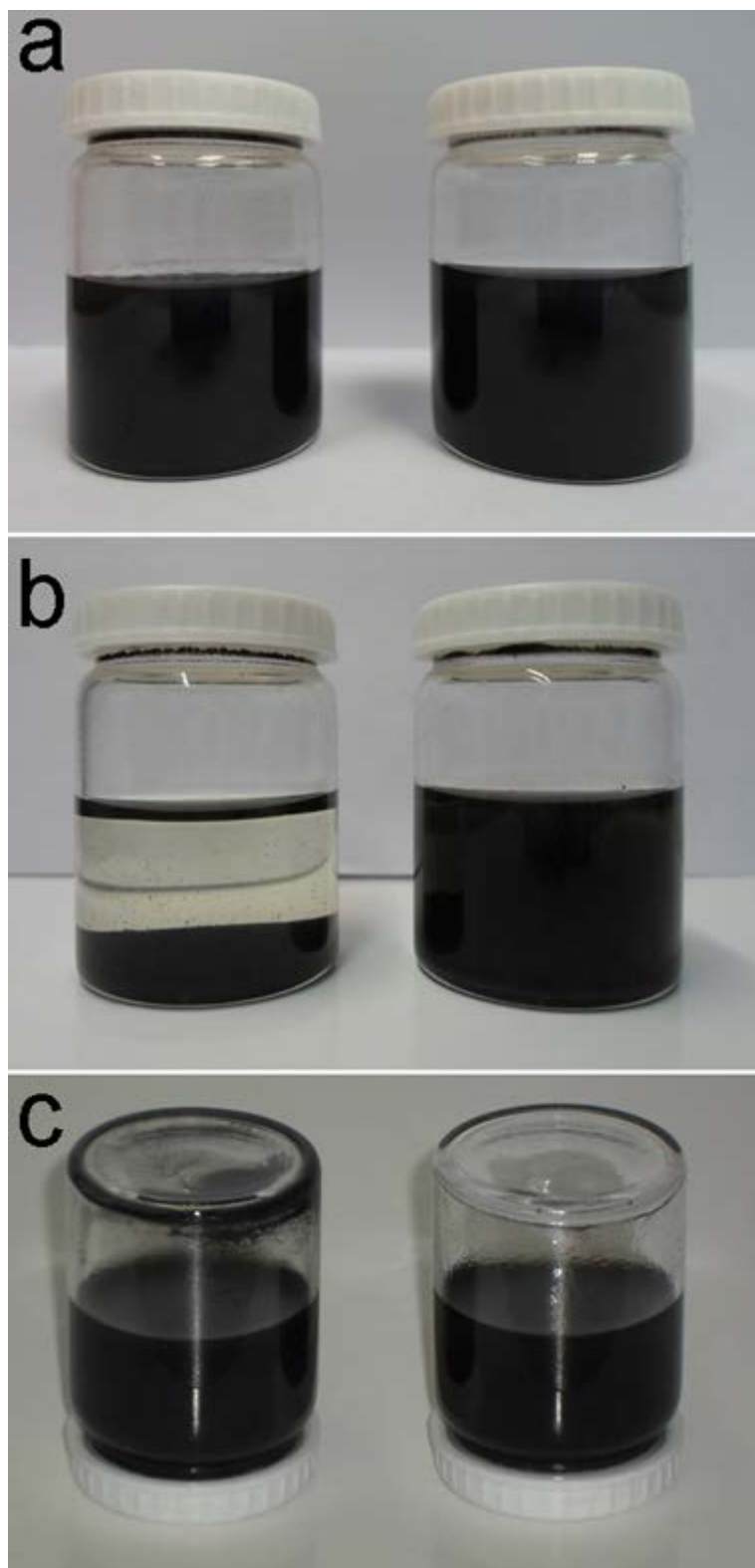
Fig. 14.2: Vials containing dispersions with a concentration of 1 mg/mL of unmodified G (left vial) and PMDI-*g*-G (right vial) in DMF. As-prepared dispersions immediately after bath ultrasonication (a), 24 h after preparation (b) and inverted dispersions (c).

## Dispersions

Figure 14.2 shows dispersions of unmodified G and PMDI-*g*-G in a polar aprotic solvent (DMF, 1 mg/mL). The dispersions were prepared by ultrasonic treatment (Branson 3510E-DHT, 100 W, Branson Ultrasonics, Danbury, CT, USA). Both dispersions were sonicated for 1 h and colloidal dispersions were obtained (*c.f.* figure 14.2 a). The dispersion of unmodified G contained visible precipitates, indicating poor dispersion. After 24 h (figure 14.2 b), this dipersion had completely sedimented, whereas the one containg PMDI-*g*-G was still well dispersed. As can be seen in figure 14.2 c, the unmodified G clearly exhibited precipitates sticking to the bottom of the inverted vial. On the other hand, precipitates were absent in the dispersion containing modified G, suggesting that the graphene was exfoliated. This was attributed to a disruption of the interlayer attractive forces, *i.e.* the $\pi$–$\pi$ interactions of G and hydrogen bonds of GO due to the isocyanate grafting. The isocyanate modification decreased the amount of hydroxyls of G, thus decreasing the strength of interlayer hydrogen bonding and rendering the graphene less hydrophilic [6]. This suggests that isocyanate modification was successful.

## FT-IR analysis

FT-IR spectra (*c.f.* figures 14.3 and 14.4) of both pristine G and PMDI-*g*-G exhibited the characteristic absorption bands of reduced GO at wavenumbers of 3433 cm$^{-1}$ due to O–H stretching mode in carboxylic acid groups and in –OH groups [14]. Moreover, absorption bands at  2926 and 2855 cm$^{-1}$ were ascribed to the stretching vibrations of C–H (*i.e.* –CH$_3$, –CH$_2$– and >C–H groups) [14], whereas signals at 1740 and 1631 cm$^{-1}$ are due to C=O carbonyl/carboxyl stretching vibration [6, 14-16]. The absorption band at 1126 cm$^{-1}$ was attributed to the C–O stretching mode of ether bonds (C–O–C) [14]. This demonstrates that the pristine graphene nano-platelets exhibited some oxygen-containing functional groups and therefore were probably obtained by thermal shocking of GO. Regarding PMDI-modified graphene, various new absorption bands were detected. Among them, one was situated at 1542 cm$^{-1}$ which was attributed to the Amide II vibration, *i.e.* the coupling of the C–N stretching vibration with the CHN deformation vibration. This absorption band suggests the formation of either amides or carbamate

esters [6]. Again, these results suggest that PMDI had reacted with the oxygen-containing functionalities of graphene.
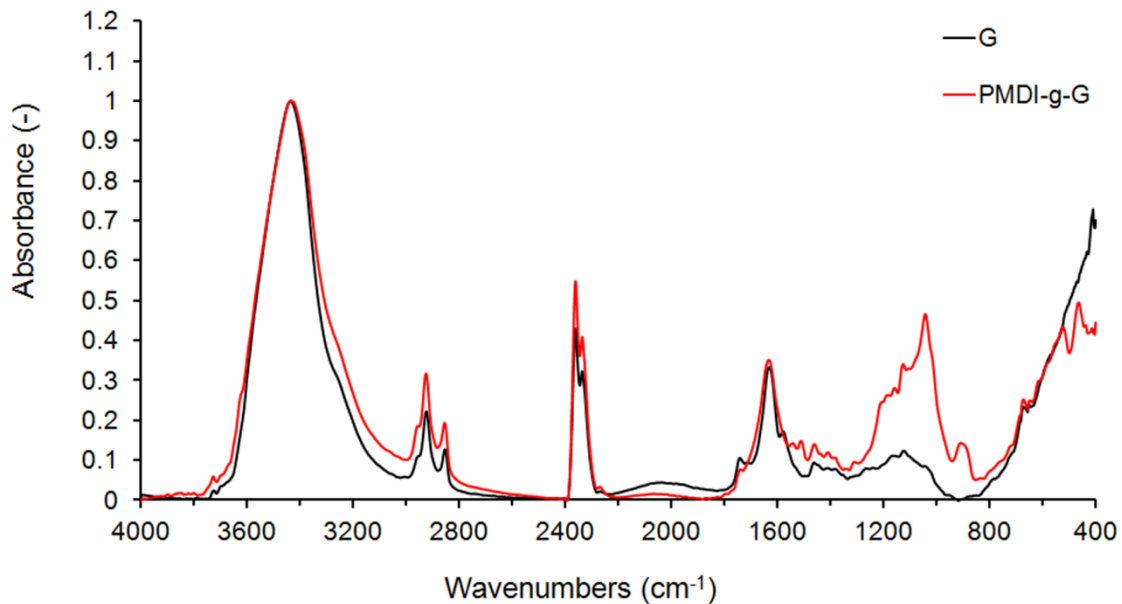


Fig. 14.3: FT-IR spectra of pristine G and PMDI-*g*-G in the wavenumber range 4000–400 cm$^{-1}$.
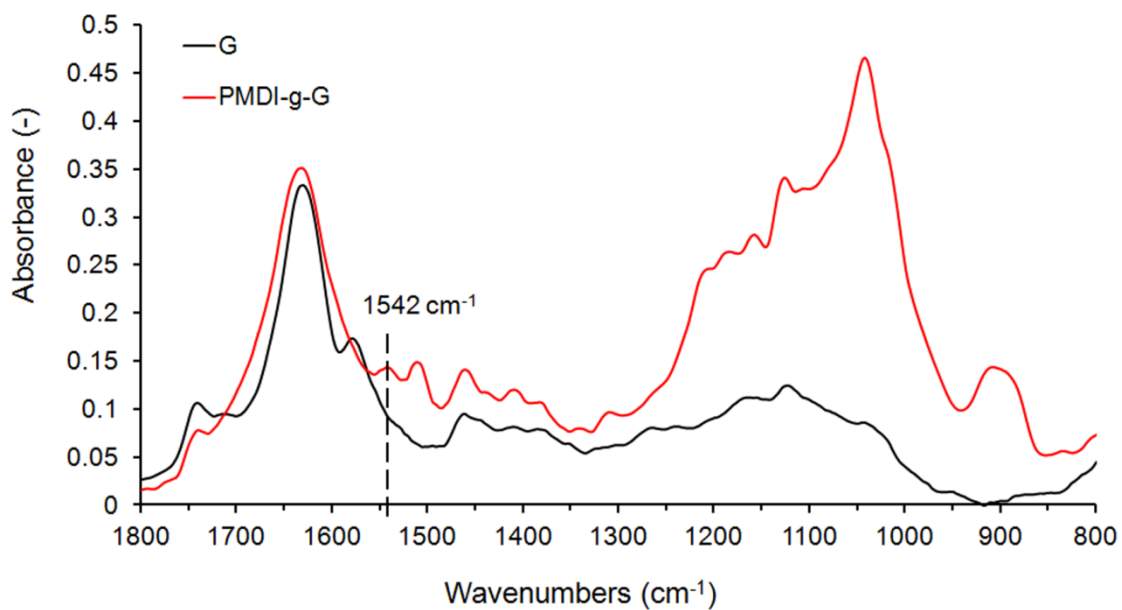


Fig. 14.4: FT-IR spectra of unmodified G and PMDI-*g*-G in the wavenumber range 1800–800 cm$^{-1}$.

**TGA analysis**

Thermogravimetric analysis was carried out in the temperature range of 30–1000 °C, at a heating rate of 10 °C/min and under nitrogen atmosphere; results are shown in figure 14.5.

Unmodified G showed an outstanding thermal stability without major mass loss up to 800 °C. Further heating to 1000 °C led to a slight mass loss, probably due to pyrolysis of the oxygen-containing groups, yielding CO, $CO_2$ and steam [7]. In contrast, PMDI-*g*-G exhibited a significant mass loss in the temperature range of 300–450 °C with a maximum mass loss rate at 332 °C. For comparison, the TGA trace of pristine PMDI is also shown. It is noteworthy that no attempt was made to determine the degradation products and degradation kinetics. PMDI exhibited a two-step degradation with major mass losses at 323 and 523 °C. Hence, the mass loss of PMDI-*g*-G at 332 °C was attributed to the thermal degradation of grafted PMDI. This suggests that isocyanate grafting was successful and a grafting content of approximately 21% was found.
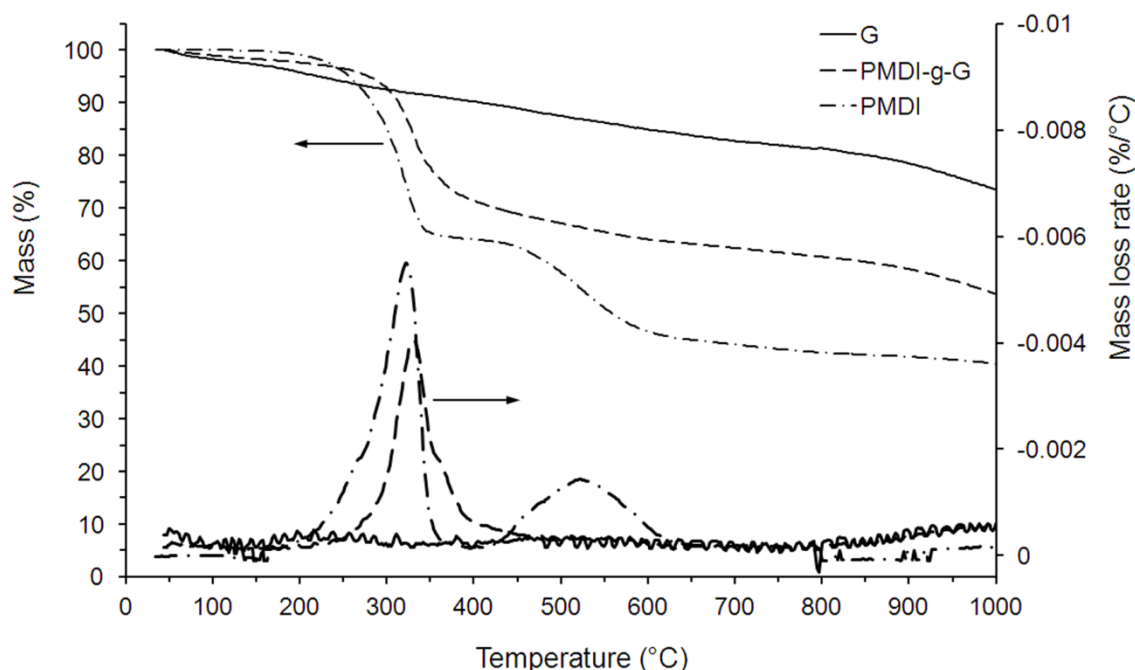


Fig. 14.5: TGA normalized mass *versus* temperature in the range of 30–1000 °C of pristine G, pristine PMDI and PMDI-*g*-G. Heating rate: 10 °C/min; $N_2$ atmosphere.

### 14.2.3 Sample preparation

Similar to the preceding chapter, two processing routes were used to prepare pCBT/G nanocomposites, namely melt blending and solvent blending. The studied graphene content was 0.25, 0.5, 0.75 and 1 wt.%. Three different groups of samples were prepared:

iv)   CBT/G binary blends

v)   CBT/HDI/G ternary blends containing 0.75 wt.% of HDI

vi)   CBT/PMDI-*g*-G binary blends

Melt blending studies were performed in order to determine the optimum processing parameters and to achieve a fully converted high-molecular weight pCBT. This was necessary because it was reported that the rate and degree of CBT polymerization decreased in presence of graphene [8-9]. Figure 14.6 depicts the torque curves of neat CBT and a CBT blend of each sample group with a G content of 0.5–1 wt.%.

The CBT/G binary blend showed a 3 min delayed torque onset with a torque maximum of 16 Nm after *ca.* 30 min. This confirms that the graphene delays the ring-opening polymerization as reported by other researchers [8-9]. The final torque value was around twice the one of neat CBT; therefore a molecular weight reduction caused by the presence of graphene can not be deduced here. Nevertheless, the graphene is thought to increase the melt viscosity of the blend, as is commonly observed in melt blending of thermoplastics and fillers.

Contrary to binary blends, the ternary blend exhibited an essentially equal torque onset as compared to neat CBT and reached its maximum torque of 33 Nm after 4 min. The torque decreased to 18 Nm after 10 min but then increased again to 23 Nm until the end of the experiment. This might be attributed to an initial urethane formation between HDI and pCBT hydroxyl end groups, then dissociation into –N=C=O and –OH groups with subsequent amidation between HDI and pCBT carboxyl groups with $CO_2$ release, as discussed in detail in chapter 9.

Regarding the binary blend containing PMDI-*g*-G, it can be seen that the torque onset was detected somewhat earlier as compared to neat CBT, confirming a promoting effect on the ROP. After torque onset, the maximum torque of 24 Nm was quickly reached after 4 min but decreased to 17 Nm after 30 min. On one hand, this shows the reactivity of

PMDI-*g*-G and therefore confirms that the graphene modification was successful. On the other hand, this demonstrates that the addition of HDI to CBT/G blends as well as the PMDI modification of G enhances the polymerization onset time and probably also the final molecular weight.
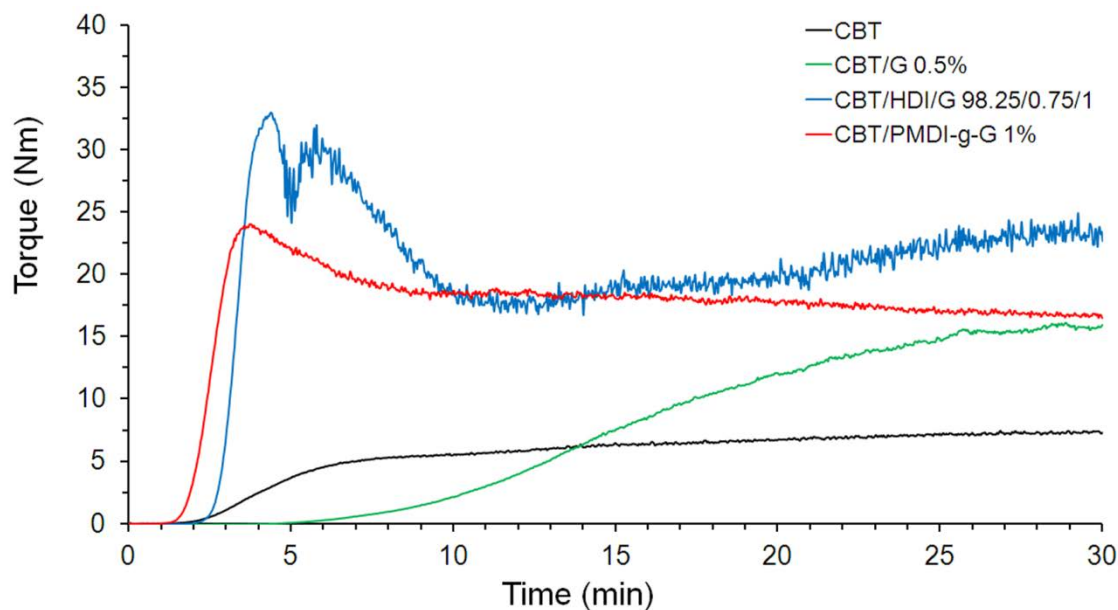


Fig. 14.6: Torque *versus* time plots of CBT, CBT/G 0.5%, CBT/HDI/G 98.25/0.75/1 and CBT/PMDI-*g*-G 1% blends polymerized at 230°C and 60 min$^{-1}$ under nitrogen atmosphere.

In view of figure 14.6, a polymerization time of 30 min was chosen for binary CBT/G blends and 10 min for ternary blends as well as for binary blends containing PMDI-*g*-G. It is noteworthy that the solvent blended samples exhibited some segregation of graphene. This was noticeable by the bright greyish colour on the upper surface of the compression moulded sheets as compared to their relatively darker bottom side. All prepared samples are compiled in table 14.1.

Table 14.1: Overview over produced pCBT/graphene nanocomposites.

| Sample designation | Processing | Temperature [°C] | Time [min] |
|---|---|---|---|
| pCBT/G 0.5%-MB | MB | 230-250 | 30+5 |
| pCBT/G 0.25%-SB | SB | 230 | 30 |
| pCBT/G 0.5%-SB | SB | 230 | 30 |
| pCBT/G 0.75%-SB | SB | 230 | 30 |
| pCBT/G 1%-SB | SB | 230 | 30 |
| pCBT/HDI/G 99/0.75/0.25-MB | MB | 230-250 | 10+5 |
| pCBT/HDI/G 98.75/0.75/0.5-MB | MB | 230-250 | 10+5 |
| pCBT/HDI/G 98.5/0.75/0.75-MB | MB | 230-250 | 10+5 |
| pCBT/HDI/G 98.25/0.75/1-MB | MB | 230-250 | 10+5 |
| pCBT/PMDI-*g*-G 0.25%-MB | MB | 230-250 | 10+5 |
| pCBT/PMDI-*g*-G 0.5%-MB | MB | 230-250 | 10+5 |
| pCBT/PMDI-*g*-G 0.75%-MB | MB | 230-250 | 10+5 |
| pCBT/PMDI-*g*-G 1%-MB | MB | 230-250 | 10+5 |
| pCBT/PMDI-*g*-G 1%-SB | SB | 230 | 15 |

MB: melt blending; SB: solvent blending

## 14.3  Characterization

The pCBT/graphene nanocomposites were characterized using X-ray diffraction, transmission electron microscopy, differential scanning calorimetry, dynamic mechanical thermal analysis and thermogravimetric analysis. The mechanical properties of the samples were determined by tensile tests.

## 14.4 Results and Discussion

### 14.4.1 WAXS analysis

X-ray diffraction was used to study the influence of the used processing routes, the presence of isocyanate and the PMDI modification of graphene, respectively, on the degree of graphene exfoliation in the pCBT matrix; WAXS diffraction patterns are shown in figure 14.7.
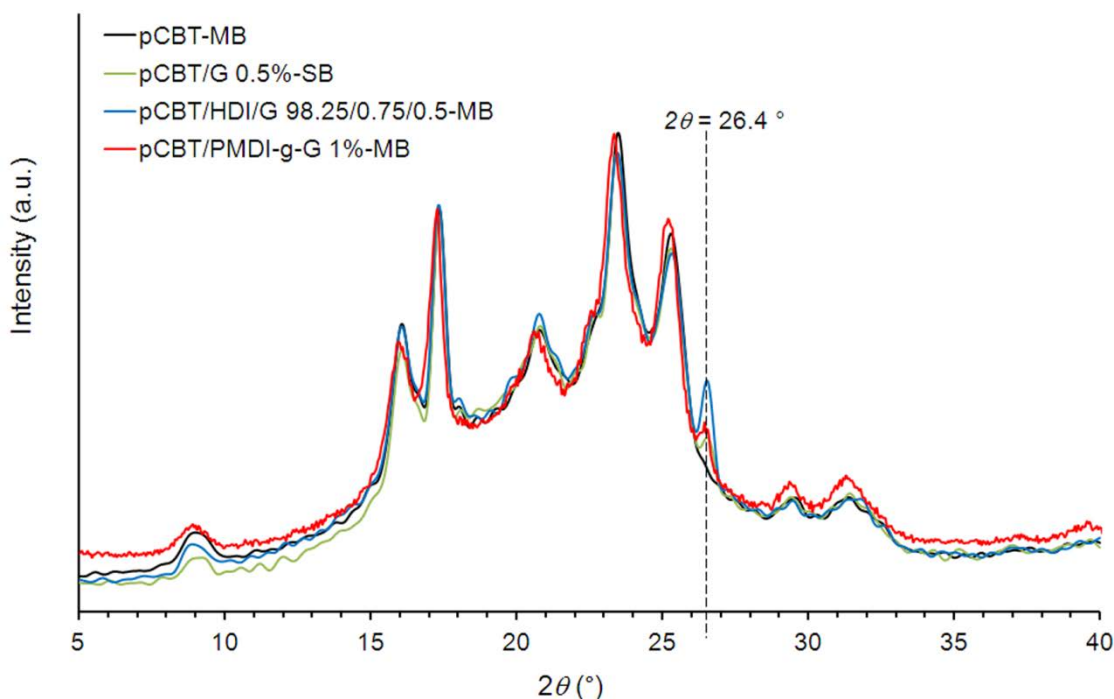


Fig. 14.7: WAXS diffraction patterns of pCBT-MB, pCBT/G 0.5%, pCBT/HDI/G 98.25/0.75/1 and pCBT/PMDI-*g*-G 1% blends polymerized at 230°C and 60 min$^{-1}$ under nitrogen atmosphere.

The diffractograms of samples containing graphene in figure 14.7 exhibited a distinct reflection situated at $2\theta = 26.4°$ which belongs to the the (002) basal reflection of graphite with a corresponding *d* spacing of 0.34 nm [1, 14]. This indicates that the used graphene showed crystalline features typical for graphite, irrespective of the graphene modification

or the presence of isocyanates in ternary blends. Therefore, graphene tactoids can be expected in all prepared samples.

### 14.4.2 TEM analysis

TEM analysis was used to further study the state of dispersion of graphene in pCBT; micrographs are shown in figure 14.8.

It can be seen that all prepared samples, irrespective of the graphene modification or the presence of isocyanates in ternary blends, exhibited micron-sized graphene tactoids. These results are in line with the ones obtained by WAXS analysis, confirming a flocculated structure. Therefore it can be concluded that graphene intercalation and/or exfoliation could not be achieved because apparently neither molten CBT oligomers nor isocyanate molecules in ternary blends were able to penetrate the interlayer spaces of G. On one hand, this is not surprising when considering the fact that the interlayer distance of graphene is around one order of magnitude smaller than the one of organoclay. On the other hand, isocyanate-modified G was expected to exfoliate more easily because it was thought that the tethered pCBT and isocyanate molecules would help pulling the G nano-platelets apart. Nevertheless, the strong $\pi$–$\pi$ interactions could not be interrupted and hence this mechanism was not at work.
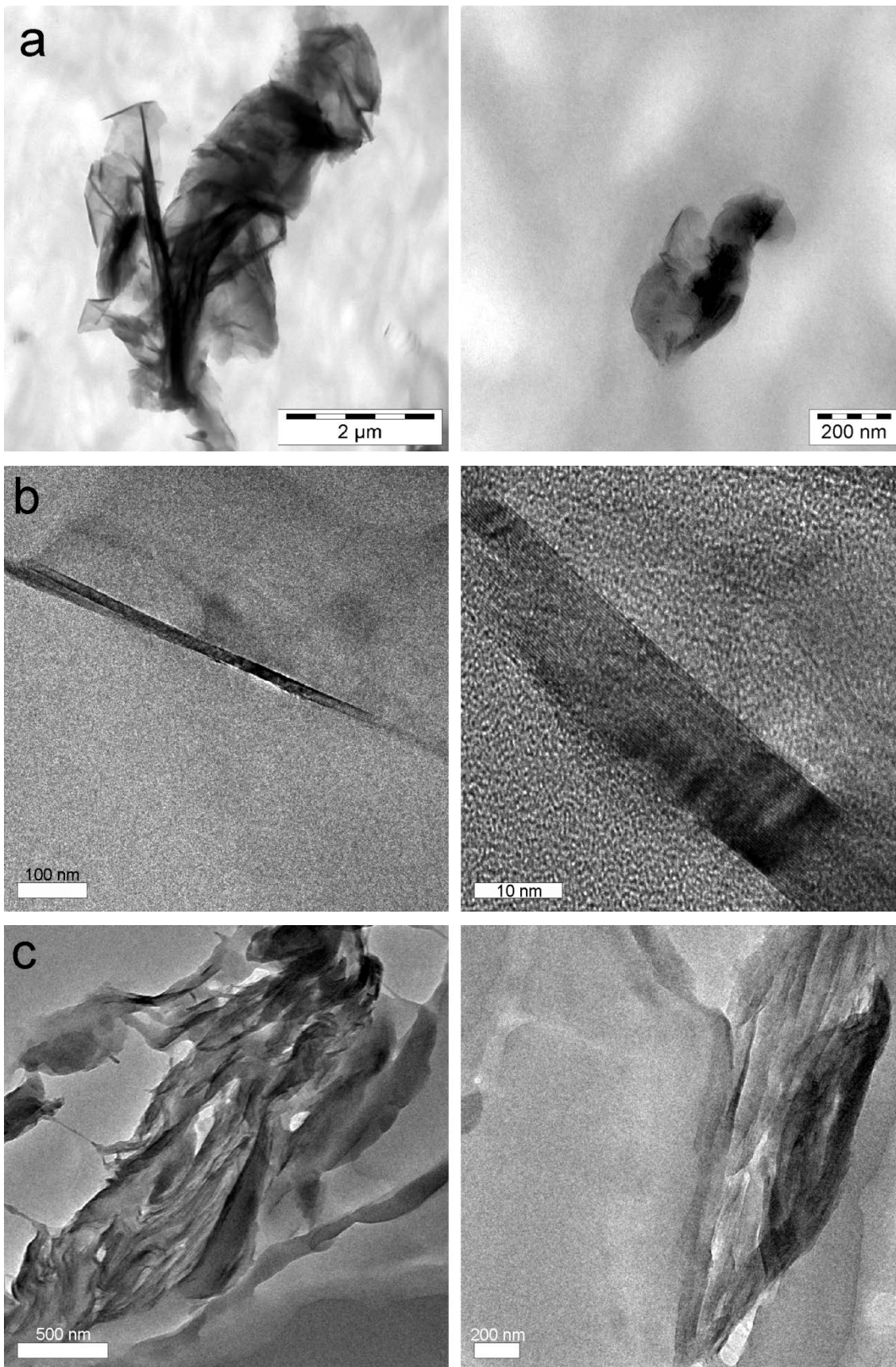
Fig. 14.8: TEM micrographs of (a) pCBT/G 0.5%-MB, (b) pCBT/HDI/G 98.75/0.75/0.5-MB and (c) pCBT/PMDI-*g*-G 0.5%-MB.

### 14.4.3 DSC analysis

The thermal properties were determined using DSC. The prepared samples were compared to their respective pCBT counterparts, depending on the used processing route.

Figure 14.9 depicts the second heating scan of samples containing 1 wt% of graphene and belonging to the different groups of samples. It is interesting to note that the processing routes had an influence on the melting behaviour. Melt blended samples exhibited less "exothermic dip" between the two endothermic melting peaks which is otherwise typically observed. This suggests that recrystallization was disturbed in these samples.
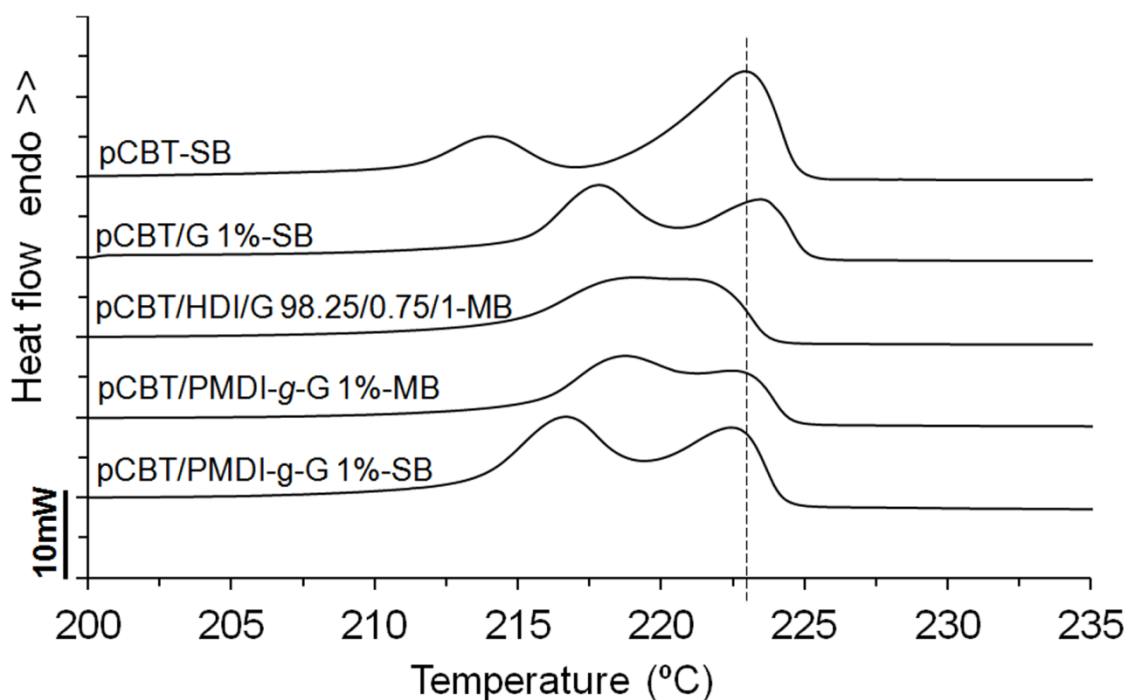


Fig. 14.9: DSC second heating scan of pCBT-SB, pCBT/G 1%-SB, pCBT/HDI/G 98.25/0.75/1-MB, pCBT/PMDI-*g*-G 1%-MB and pCBT/PMDI-*g*-G 1%-SB; heating and cooling rate of 10°C/min.

Table 14.2: Thermal properties of the produced pCBT/graphene nanocomposites.

| Sample | first cooling | | second heating | | | |
|---|---|---|---|---|---|---|
| | $T_c$ | $\Delta H_c$ | $T_{m1}$ | $T_{m2}$ | $\Delta H_{m1+2}$ | $X_C{}^*$ |
| | [°C] | [J/g] | [°C] | [°C] | [J/g] | [%] |
| pCBT-MB | 193.1 | -50.6 | 215.4 | 223.5 | 50.7 | 35.7 |
| pCBT-SB | 187.2 | -44.5 | 214.0 | 222.9 | 44.6 | 31.4 |
| pCBT/G 0.5%-MB | 202.3 | -47.5 | 220.3 | 224.0 | 50.6 | 35.6 |
| pCBT/G 0.25%-SB | 195.9 | -47.9 | 218.2 | 223.0 | 46.3 | 32.6 |
| pCBT/G 0.5%-SB | 196.7 | -45.8 | 218.3 | 223.1 | 46.3 | 32.6 |
| pCBT/G 0.75%-SB | 197.3 | -46.2 | 218.1 | 223.9 | 47.6 | 33.5 |
| pCBT/G 1%-SB | 198.2 | -50.7 | 217.8 | 223.4 | 49.3 | 34.7 |
| pCBT/HDI/G 99/0.75/0.25-MB | 197.9 | -46.9 | 217.5 | 221.3 | 39.7 | 28.0 |
| pCBT/HDI/G 98.75/0.75/0.5-MB | 196.9 | -46.4 | 217.8 | 220.0 | 39.5 | 27.8 |
| pCBT/HDI/G 98.5/0.75/0.75-MB | 198.2 | -46.9 | 218.5 | 221.0 | 42.6 | 30.0 |
| pCBT/HDI/G 98.25/0.75/1-MB | 200.0 | -46.2 | 219.1 | 221.1 | 41.7 | 29.4 |
| pCBT/PMDI-*g*-G-0.25%-MB | 198.4 | -49.9 | 218.3 | 223.5 | 46.1 | 32.5 |
| pCBT/PMDI-*g*-G-0.5%-MB | 198.9 | -49.4 | 218.6 | 223.1 | 43.7 | 30.8 |
| pCBT/PMDI-*g*-G-0.75%-MB | 199.7 | -50.2 | 218.5 | 223.1 | 45.0 | 31.7 |
| pCBT/PMDI-*g*-G-1%-MB | 199.4 | -49.2 | 218.8 | 222.5 | 43.7 | 30.8 |
| pCBT/PMDI-*g*-G-1%-SB | 193.6 | -44.6 | 216.6 | 222.3 | 43.1 | 30.4 |

* calculated from second heating melting enthalpy. DSC heating and cooling rate of 10 °C/min.

Moreover, it can be seen that the presence of graphene had a considerable nucleation effect on pCBT, irrespective of the graphene modification or the presence of isocyanates. Crystallization peak temperatures increased up to 11 °C as compared to neat pCBT (*c.f.* table 14.2). Similar findings were also reported by other researchers [9, 13-14]. Binary pCBT/G blends showed a slight increase in $T_{m1}$, $T_{m2}$ and $X_C$. The increase in melting temperatures and crystal fraction was ascribed to the heterogeneous nucleation effect of graphene on pCBT, resulting in a relatively higher lamellar thickness of the pCBT crystals formed during first cooling. This was different when isocyanate was present, either as a ternary component or grafted onto G. The lower melting peak temperatures increased

slightly but higher melting peak temperatures and crystal fractions decreased due to the presence of isocyanate. The latter acts as defect in the chain architecture of pCBT and is excluded from the crystal fraction, as discussed in detail in chapter 9.

### 14.4.4 DMTA analysis

The dynamic mechanical properties of pCBT/G nanocomposites were studied; dynamic storage modulus curves as a function of temperature are shown in figure 14.10. The tested samples behaved quite similar. The stiffness below $T_g$ considerably increased, irrespective of the used processing route, graphene modification or the presence of isocyanates. As was shown by XRD and TEM analysis, these samples had an agglomerated structure. Therefore the graphene tactoids may have acted as rigid points, reinforcing the pCBT matrix. This demonstrates the reinforcing effect of graphene on the pCBT matrix, as has bee reported in the literature [9, 13-14]. Nevertheless, stiffness decreased more pronounced at the glass transition and reached a level similar to pristine pCBT.
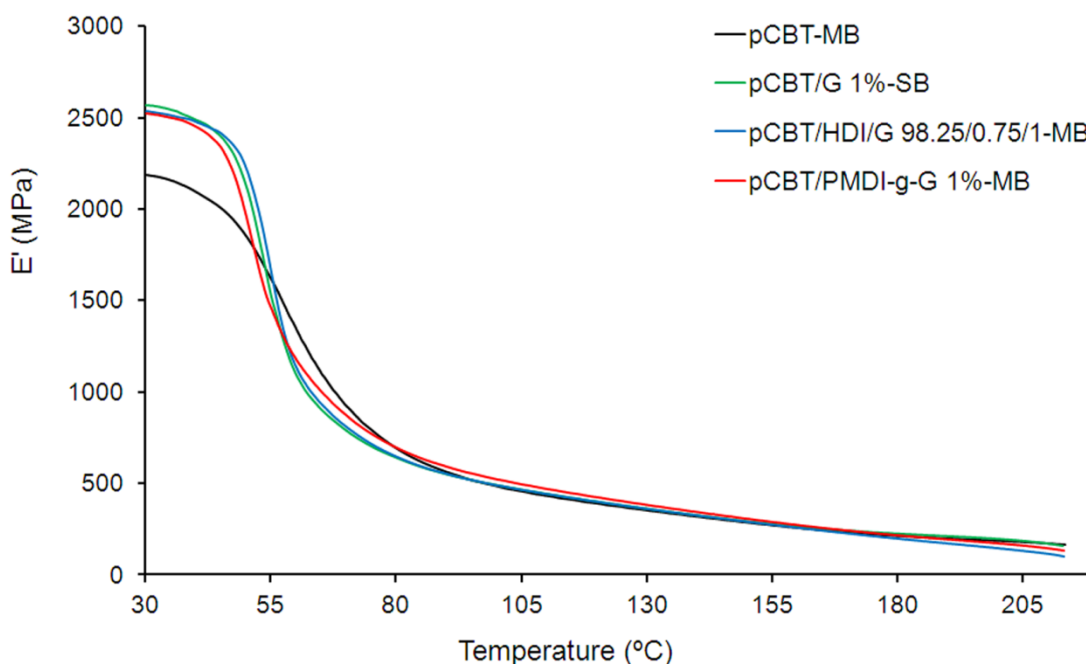


Fig. 14.10: DMTA storage moduli *versus* temperature of pCBT-MB and different pCBT/G nanocomposites

### 14.4.5 TGA analysis

Thermogravimetric analysis was performed in nitrogen atmosphere at a heating rate of 10 °C/min; results are presented in table 14.3.

Table 14.3: Thermogravimetric data of pCBT/graphene nanocomposites.

| Sample | $T_{5\ \% mass\ loss}$ [°C] | $T_{max.}$ [°C] | Residue at 600 °C [wt.%] |
|---|---|---|---|
| pCBT | 373.2 | 404.8 | 1.2 |
| pCBT/G 0.5%-MB | 375.5 | 403.8 | 3.4 |
| pCBT/G 0.25%-SB | 376.3 | 405.1 | 3.1 |
| pCBT/G 0.5%-SB | 375.2 | 404.8 | 3.8 |
| pCBT/G 0.75%-SB | 374.5 | 405.3 | 4.4 |
| pCBT/G 1%-SB | 377.1 | 405.4 | 4.7 |
| pCBT/HDI/G 99/0.75/0.25-MB | 377.2 | 405.9 | 3.6 |
| pCBT/HDI/G 98.75/0.75/0.5-MB | 374.7 | 404.6 | 3.9 |
| pCBT/HDI/G 98.5/0.75/0.75-MB | 373.3 | 403.4 | 4.1 |
| pCBT/HDI/G 98.25/0.75/1-MB | 375.1 | 405.3 | 4.5 |
| pCBT/PMDI-*g*-G-0.25%-MB | 376.2 | 405.3 | 2.1 |
| pCBT/PMDI-*g*-G-0.5%-MB | 377.8 | 405.5 | 3.9 |
| pCBT/PMDI-*g*-G-0.75%-MB | 376.0 | 405.6 | 4.0 |
| pCBT/PMDI-*g*-G-1%-MB | 377.9 | 405.7 | 4.8 |
| pCBT/PMDI-*g*-G-1%-SB | 377.5 | 405.5 | 3.5 |

It is well known that graphene can significantly increase thermal stability of polymers due to the barrier effect of the graphene sheets [2-3]. On one hand, no improvement in thermal stability of pCBT occurred when the graphene was agglomerated [13]. On the other hand, an increase up to 20 °C of the temperature corresponding to the maximum mass loss rate ($T_{max}$) has been reported when the graphene was exfoliated in the pCBT matrix [9]. Since the herein prepared samples exhibited an agglomerated structure, no influence on thermal

stability is expected because the specific surface of the graphene agglomerates is too small to extensively interact with the pCBT matrix. As can be seen in table 14.3, only a slight improvement of around 2 °C was found for both 5% mass loss temperature and maximum mass loss rate temperature. Regarding the experimental error inherent in TGA analysis, this improvement is considered to be insignificant.

### 14.4.6 Tensile properties

The tensile properties of the prepared graphene nanocomposites as well as the ones of neat pCBT-MB and pCBT-SB for comparison are compiled in table 14.4; normalized tensile properties are shown in figure 14.11. The results suggest that binary pCBT/G blends exhibited poor compatibility between the constituting materials, since mechanical properties (namely tensile strength) deteriorated with increasing G content. Similarly to what was observed for pCBT/organoclay nanocomposites, solvent blending of pCBT/G resulted in comparably poorer properties, irrespective of the graphene modification or the presence of isocyanates. As mentioned earlier, solvent blended samples exhibited graphene segregation due to the low viscosity of molten CBT prior to ROP and the absence of shear during/after polymerization. Again, this may have caused graphene segregation and localized agglomeration on the bottom side of the samples, leading to non-uniform mechanical properties throughout the the specimens. Moreover, localized G agglomerates act as crack initiation points which is in line with the decreasing tensile strength with increasing G content. The here observed segregation phenomenon probably might be also at work in solvent blended pCBT/organoclay nanocomposites of the previous chapter. Nevertheless, the pCBT/organoclay samples did not show a visible colour difference due to the natural greyish colour of the clay.

Table 14.4: Tensile properties of pCBT/graphene nanocomposites.

| Sample | Tensile modulus [GPa] | Tensile strength [MPa] | Elongation at break [%] |
|---|---|---|---|
| pCBT-MB | 2.9 ± 0.3 | 60 ± 2 | 8 ± 1 |
| pCBT-SB | 3.0 ± 0.2 | 63 ± 4 | 9 ± 2 |
| pCBT/G 0.5%-MB | 3.4 ± 0.1 | 65 ± 1 | 5 ± 1 |
| pCBT/G 0.25%-SB | 3.1 ± 0.2 | 58 ± 1 | 7 ± 1 |
| pCBT/G 0.5%-SB | 3.2 ± 0.1 | 58 ± 3 | 6 ± 1 |
| pCBT/G 0.75%-SB | 3.0 ± 0.2 | 53 ± 2 | 5 ± 1 |
| pCBT/G 1%-SB | 2.9 ± 0.3 | 54 ± 1 | 4 ± 1 |
| pCBT/HDI/G 99/0.75/0.25-MB | 3.0 ± 0.4 | 62 ± 5 | 52 ± 6 |
| pCBT/HDI/G 98.75/0.75/0.5-MB | 3.2 ± 0.3 | 60 ± 1 | 11 ± 1 |
| pCBT/HDI/G 98.5/0.75/0.75-MB | 3.4 ± 0.3 | 55 ± 7 | 6 ± 3 |
| pCBT/HDI/G 98.25/0.75/1-MB | 3.3 ± 0.2 | 58 ± 1 | 7 ± 2 |
| pCBT/PMDI-*g*-G-0.25%-MB | 3.2 ± 0.3 | 60 ± 1 | 5 ± 1 |
| pCBT/PMDI-*g*-G-0.5%-MB | 3.3 ± 0.2 | 64 ± 1 | 5 ± 1 |
| pCBT/PMDI-*g*-G-0.75%-MB | 3.5 ± 0.3 | 65 ± 1 | 6 ± 1 |
| pCBT/PMDI-*g*-G-1%-MB | 3.5 ± 0.4 | 62 ± 1 | 4 ± 1 |
| pCBT/PMDI-*g*-G-1%-SB | 3.5 ± 0.4 | 55 ± 2 | 4 ± 1 |
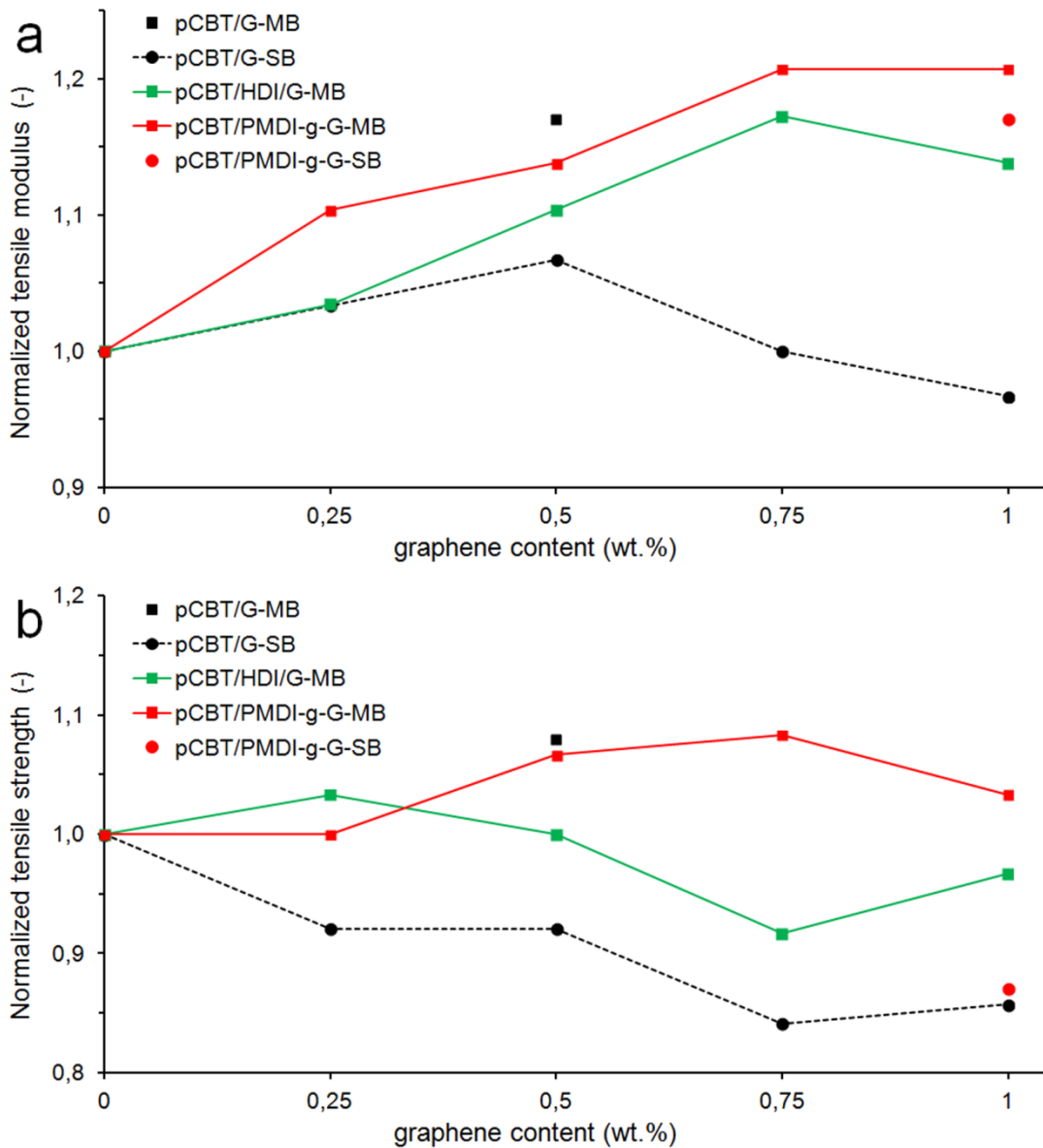
Fig. 14.11: Normalized tensile modulus (a), normalised tensile strength (b) and normalized failure strain (c) of the prepared graphene nanocomposites. Dashed lines indicate solvent blending; lines are guides for the eyes.
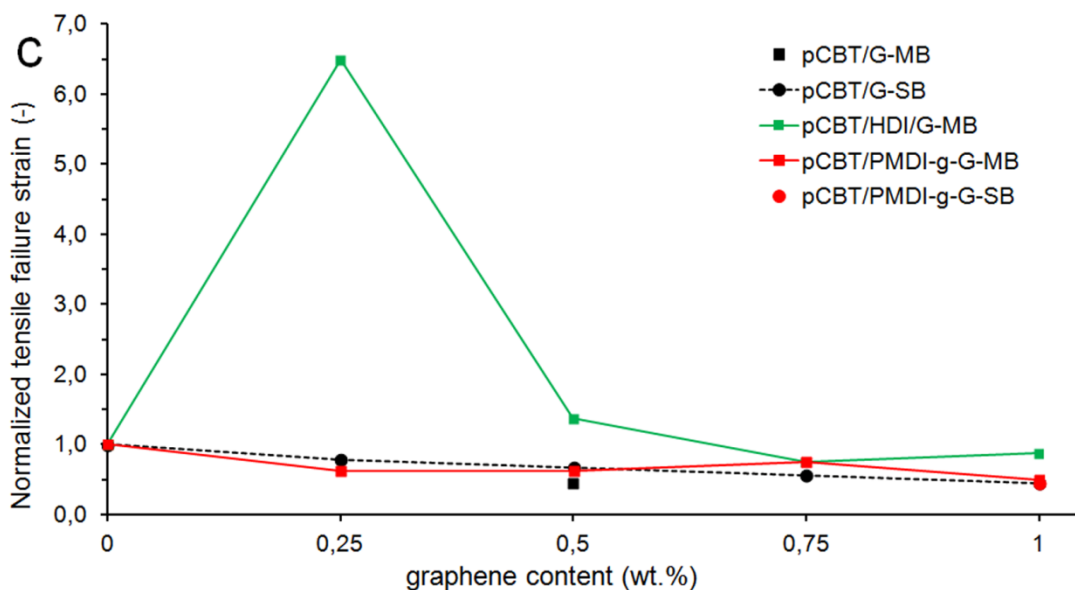
Fig. 14.11: Normalized tensile modulus (a), normalised tensile strength (b) and normalized failure strain (c) of the prepared graphene nanocomposites. Dashed lines indicate solvent blending; lines are guides for the eyes. (*continued*)

Ternary pCBT/HDI/G blends exhibited increasing modulus with G content, while the strength relatively decreased. This indicates that compatibility was somewhat improved by the presence of HDI. Moreover, the added isocyanate renders the material semi-ductile for low G contents, as can be seen in figure 14.11 c.

The isocyanate modification led to stiffness and strength enhancements, although the materials were brittle. This indicates that compatibility between pCBT and graphene was improved due to the grafted PMDI, probably covalently bound to the pCBT chains. Moreover, this also demonstrates that isocyanates enhance the mechanical properties of pCBT/G composites, either as component in ternary blends or grafted onto the graphene.

## 14.5   Conclusions

Graphene nano-platelets were used to prepare pCBT/G composites. Solvent blended binary blends of pCBT and graphene exhibited an agglomerated structure due to poor compatibility. Consequently, mechanical properties deteriorated with increasing G content,

probably also caused by non-uniform G distribution due to a segregation of the graphene during solvent blending. Compatibility somewhat improved with the addition of diisocyanate and stiffness and toughness was enhanced. The graphene was further modified by grafting polymeric isocyanate onto the graphene surface. Dispersion studies of unmodified G and PMDI-*g*-G in a polar aprotic solvent demonstrated that grafting was successful. The related pCBT/ PMDI-*g*-G composites showed an improved stiffness and strength due to the enhanced compatibility. This was because on one hand the PMDI-grafted graphene was rendered less hydrophilic and on the other hand probably reacted with the pCBT matrix. Nevertheless, TEM and WAXS analysis revealed the presence of graphene tactoids in all prepared samples. In other words, the strong $\pi$–$\pi$ interactions between the graphene sheets could not be interrupted; therefore exfoliation could not be achieved. The thermal properties, most importantly thermal stability, were not significantly altered by the graphene due to the agglomerated structure, although a pronounced heterogeneous nucleation effect was found. To conclude, the proposed graphene modification or the addition of diisocyanates did not lead to graphene exfoliation in pCBT. Nevertheless, it did improve mechanical properties of pCBT/graphene composites.

## 14.6   References for pCBT/graphene

1.   Kuila, T, Bose, S, Mishra, AK, Khanra, P, Kim, NH, and Lee, JH. Chemical functionalization of graphene and its applications. Progress in Materials Science **57**(7), 1061-1105 (2012).

2.   Kuilla, T, Bhadra, S, Yao, D, Kim, NH, Bose, S, and Lee, JH. Recent advances in graphene based polymer composites. Progress in Polymer Science **35**(11), 1350-1375 (2010).

3.   Potts, JR, Dreyer, DR, Bielawski, CW, and Ruoff, RS. Graphene-based polymer nanocomposites. Polymer **52**(1), 5-25 (2011).

4.   Stankovich, S, Dikin, DA, Dommett, GHB, Kohlhaas, KM, Zimney, EJ, Stach, EA, Piner, RD, Nguyen, ST, and Ruoff, RS. Graphene-based composite materials. Nature **442**(7100), 282-286 (2006).

5.      Hummers, WS and Offeman, RE. Preparation of Graphitic Oxide. Journal of the American Chemical Society **80**(6), 1339-1339 (1958).

6.      Stankovich, S, Piner, RD, Nguyen, ST, and Ruoff, RS. Synthesis and exfoliation of isocyanate-treated graphene oxide nanoplatelets. Carbon **44**(15), 3342-3347 (2006).

7.      Stankovich, S, Dikin, DA, Piner, RD, Kohlhaas, KA, Kleinhammes, A, Jia, Y, Wu, Y, Nguyen, ST, and Ruoff, RS. Synthesis of graphene-based nanosheets via chemical reduction of exfoliated graphite oxide. Carbon **45**(7), 1558-1565 (2007).

8.      Chen, H, Huang, C, Yu, W, and Zhou, C. Effect of thermally reduced graphite oxide (TrGO) on the polymerization kinetics of poly(butylene terephthalate) (pCBT)/TrGO nanocomposites prepared by in situ ring-opening polymerization of cyclic butylene terephthalate. Polymer **54**(6), 1603-1611 (2013).

9.      Fabbri, P, Bassoli, E, Bon, SB, and Valentini, L. Preparation and characterization of poly (butylene terephthalate)/graphene composites by in-situ polymerization of cyclic butylene terephthalate. Polymer **53**(4), 897-902 (2012).

10.     Brunelle, DJ. Cyclic oligomer chemistry. Journal of Polymer Science Part A: Polymer Chemistry **46**(4), 1151-1164 (2008).

11.     Steeg, M. Prozesstechnologie für Cyclic Butylene Terephthalate im Faser-Kunststoff-Verbund. PhD thesis. Fachbereich Maschinenbau und Verfahrenstechnik. Technische Universität Kaiserslautern: Kaiserslautern, Germany, 2009

12.     Berti, C, Binassi, E, Colonna, M, Fiorini, M, Zuccheri, T, Karanam, S, and J. Brunelle, D. Improved dispersion of clay platelets in poly(butylene terephthalate) nanocomposite by ring-opening polymerization of cyclic oligomers: Effect of the processing conditions and comparison with nanocomposites obtained by melt intercalation. Journal of Applied Polymer Science **114**(5), 3211-3217 (2009).

13.     Balogh, G, Hajba, S, Karger-Kocsis, J, and Czigány, T. Preparation and characterization of in situ polymerized cyclic butylene terephthalate/graphene nanocomposites. Journal of Materials Science **48**(6), 2530-2535 (2013).

14.     Bian, J, Lin, HL, He, FX, Wang, L, Wei, XW, Chang, IT, and Sancaktar, E. Processing and assessment of high-performance poly(butylene terephthalate) nanocomposites reinforced with microwave exfoliated graphite oxide nanosheets. European Polymer Journal **49**(6), 1406-1423 (2013).

15. Rattana, Chaiyakun, S, Witit-anun, N, Nuntawong, N, Chindaudom, P, Oaew, S, Kedkeaw, C, and Limsuwan, P. Preparation and characterization of graphene oxide nanosheets. Procedia Engineering **32**(0), 759-764 (2012).

16. Zhang, D-D, Zu, S-Z, and Han, B-H. Inorganic–organic hybrid porous materials based on graphite oxide sheets. Carbon **47**(13), 2993-3000 (2009).

# Chapter 15: Toughened CF fabric-reinforced pCBT composites[5]

Toughened carbon fibre fabric-reinforced pCBT composites were obtained by chemical modification of CBT with small amounts of bifunctional epoxy resin and bi- or polyfunctional isocyanates as chain extenders. Homogeneous CBT/epoxy and CBT/isocyanate blends were prepared by melt blending the components in a lab-scale batch mixer at low temperatures and high shear rate. Melt blending was stopped before the ROP of CBT could start. The modified CBT was the starting material for carbon fibre fabric-reinforced pCBT composites prepared by a simple powder prepreg method with subsequent *in situ* polymerization during compression moulding.

Interlaminar shear strength, flexural strength and failure strain of the chemically modified composites increased up to 60% with respect to unmodified pCBT composites. Nevertheless, the flexural moduli slightly decreased due to the toughening effect of the chain extender on the pCBT matrix. Low energy impact tests revealed that the energy absorption of the modified composites was relatively higher as compared to unmodified pCBT composites.

---

[5] Sample preparation and measurements were partly performed in the Department of Polymer Engineering, Budapest University of Technology and Economics, Hungary and in the Department of Mechanics and Industrial Production, Mondragon Unibertsitatea, Spain.

## 15.1 Introduction

The aim of this final chapter is to demonstrate that the developed toughening methods not only work for pCBT polymer but also for fibre reinforced pCBT composites. The inherent brittleness of pCBT is a critical problem and hinders a wide application of fibre reinforced pCBT composites as structural materials and at industrial scales. Therefore, considerable efforts have been made to toughen pCBT composites [1-9]. Most publications aim on decreasing the crystallinity and thus increasing the toughness, either by nonisothermal processing using fast cooling [3] or by chemical modification [2, 4-9]. A different approach is to use superelastic shape memory alloy wires in the pCBT composite production [1]. So far, fibre reinforced pCBT composites with toughnesses comparable to the one of PBT-based composites, such as the commercially available PBT-based Twintex[®] have not been achieved yet.

Based on the previous results, epoxy resin and isocyanates were selected for toughening. The difficulty was to obtain homogeneous blends of CBT and toughening agents as starting materials for the pCBT composites in order to achieve uniform material properties. As discussed above, solvent blending is a suitable technique to obtain homogeneity. Nevertheless, long drying times, waste of solvent and the risk of void formation in the pCBT composites due to residual solvent are major drawbacks. To avoid these shortcomings, melt blending was the method of choice. The challenge was to melt blend the components without polymerizing the CBT; this was achieved in a preliminary study by determining adequate processing parameters. Unmodified as well as EP- and NCO-modified pCBT composites were prepared, characterized and the results were compared with the ones published by other researchers.

## 15.2 Experimental Section

### 15.2.1 Materials

One-component cyclic butylene terephthalate oligomers (CBT160®) were used as matrix and Eporai® 450/A was emplyed for toughening. Three types of isocyanates were used to toughen pCBT, namely PMDI, MDI and HDI. The used CF reinforcement is described in detail in section 3.6.

### 15.2.2 Sample preparation

Pristine CBT powder without further processing (except vacuum drying at 80 °C for 8 h) was used to prepare unmodified pCBT-CF as reference sample. The EP- and NCO-modified CBT as starting materials for composite production were prepared by melt blending. CBT and toughening agent were blended in the batch mixer at high shear rate, low temperature and protective $N_2$ atmosphere for a short time. The melt blending route produces more homogeneous blends as compared to manual mixing using mortar and pestle. The difficulty is to operate the batch mixer in such a manner, that good melt homogeneity is achieved *without* prematurely polymerizing the CBT. Preliminary studies were performed to determine the optimum processing parameters. A mixing chamber temperature of 200 °C, rotor speed of 180 min$^{-1}$ and under a blanket of nitrogen for 2 min appeared optimum. These processing parameters were used for all CBT/toughening agent blends.

Proof that the prepared blends did not polymerize prematurely during melt blending is shown in figure 15.1. Here, unmodified CBT, CBT/EP 3% and CBT/PMDI 1% dry blends are exemplarily shown to demonstrate that ROP did not start during the first 2 min of mixing. The dashed vertical line indicates the end of the melt blending process after 2 min. It can be seen that the torque was 0 ± 0.1 Nm during this period; hence the CBT blends were molten and exhibited their typical water-like viscosity prior to ROP. Longer mixing times resulted in a steep torque increase, *i.e.* the onset of polymerization.
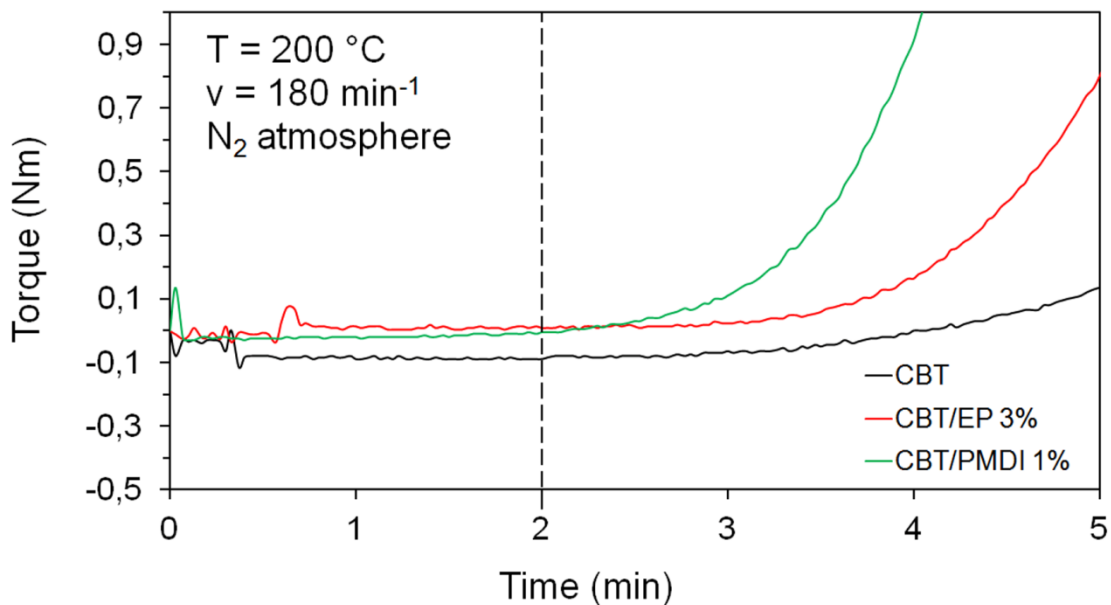
Fig. 15.1: Representative torque curves of pristine and modified CBT pre-mixes

Fresh CBT/modifier blends were prepared in the batch mixer using these conditions for 2 min. Then the liquid materials were quickly collected from the mixing chamber (they readily flowed out of the mixing chamber due to their low viscosity), cooled to room temperature, ground into a fine powder using mortar and pestle, vacuum dried for 8 h at 80 °C and subsequently used to prepare the modified pCBT-CF composites. Pre-mixes containing 2, 3 and 4 wt.% of EP as well as blends containing 1 wt.% of PMDI, MDI and HDI, respectively, were prepared.

A simple powder prepreg method, as described in detail in section 4.5, was used to manufacture unmodified and modified pCBT/CF composites *via* compression moulding. The hot press was operated at a temperature of 230 °C and a pressure of 0–3 MPa. The polymerization time was 20 min for pristine CBT samples as well as for samples containing EP. Isocyanate-modified samples were polymerized for 15 min. Composites with dimensions of *ca*. 110x110x1.5 mm were prepared. The entire analysis is devoted to these composites. Nevertheless, a higher thickness was required for impact tests; therefore composites consisting of 20 layers of CF fabric with a thickness of 3.0 mm were additionally prepared. It is noteworthy that the latter samples with 3.0 mm thickness were not further characterized.

## 15.3   Characterization

Unmodified and modified pCBT-CF composites were characterized using DSC and DMTA. Moreover, the physical properties (namely density, fibre- and void content) as well as the morphology using optical microscopy were determined. The mechanical properties were determined using flexural tests and short beam interlaminar shear strength. Impact properties were determined using puncture impact tests.

## 15.4   Results and Discussion

### 15.4.1 Physical properties

The density, fibre- and void content of the prepared composites are compiled in table 15.1. It can be seen that the chemical modifications did not significantly alter the densities of the polymers and composites, respectively. The void contents of the composites were in the range of 0.7–3.3%, which are in good agreement with the ones published by Mohd Ishak *et al.* [10] for carbon fibre reinforced pCBT prepared by compression moulding under pressure-controlled conditions (<1%) as well as under displacement-controlled conditions (4.7%). Agirregomezkorta *et al.* [11] prepared pCBT-CF composites *via* vacuum infusion and obtained a void content of 3.3%.

Void content was somewhat lower in epoxy-modified samples but increased with EP content and the highest value of 3.3% was found when 4 wt.% of EP was used. This can be ascribed to a hampered fibre impregnation due to the increasing viscosity of the CBT/EP blends with EP caused by the relatively higher viscosity of EP resin as compared to molten CBT. The isocyanate modification led to a void content of 1–3%, depending on the type of isocyanate used. Recall from chapter 9 that under the used processing conditions isocyanates preferably react with pCBT carboxylic end groups (as shown by proton NMR), thereby releasing $CO_2$ during amidation. Therefore, one might expect higher void contents for these samples. On the contrary, relatively smaller values were found as

compared to pCBT-CF. This may be explained by the fact that in the used compression moulding operation a compression step after polymerization was applied, thus the amount of entrapped gas in the composite is thought to be reduced to a similar level in all composites.

Table 15.1: Polymer and composite densities, fibre volume fractions and void contents of unmodified and modified pCBT-CF composites

| Sample | Polymer density [g/cm$^3$] | Composite density [g/cm$^3$] | Fibre volume fraction [vol.%] | Void content [%] |
|---|---|---|---|---|
| pCBT-CF | 1.33 | 1.60 | 70.9 | 2.9 |
| pCBT/EP 2%-CF | 1.33 | 1.62 | 68.1 | 0.7 |
| pCBT/EP 3%-CF | 1.31 | 1.63 | 72.2 | 1.5 |
| pCBT/EP 4%-CF | 1.32 | 1.59 | 70.5 | 3.3 |
| pCBT/PMDI 1%-CF | 1.32 | 1.61 | 67.2 | 0.9 |
| pCBT/MDI 1%-CF | 1.33 | 1.63 | 73.9 | 1.6 |
| pCBT/HDI 1%-CF | 1.32 | 1.59 | 68.0 | 2.9 |

### 15.4.2 Morphology

The morphologies as well as fibre distribution and impregnation of pCBT-CF, pCBT/EP 3%-CF and pCBT/PMDI 1%-CF were assessed by SEM analysis (figure 15.2) and OM analysis (figure 15.3).

Fig. 15.2: SEM morphologies of fracture surfaces of cryo-fractured pCBT-CF (a), pCBT/EP 3%-CF (b) and pCBT/PMDI 1%-CF (c); pictures were taken normal to fibre direction; inset is parallel to fibre direction.
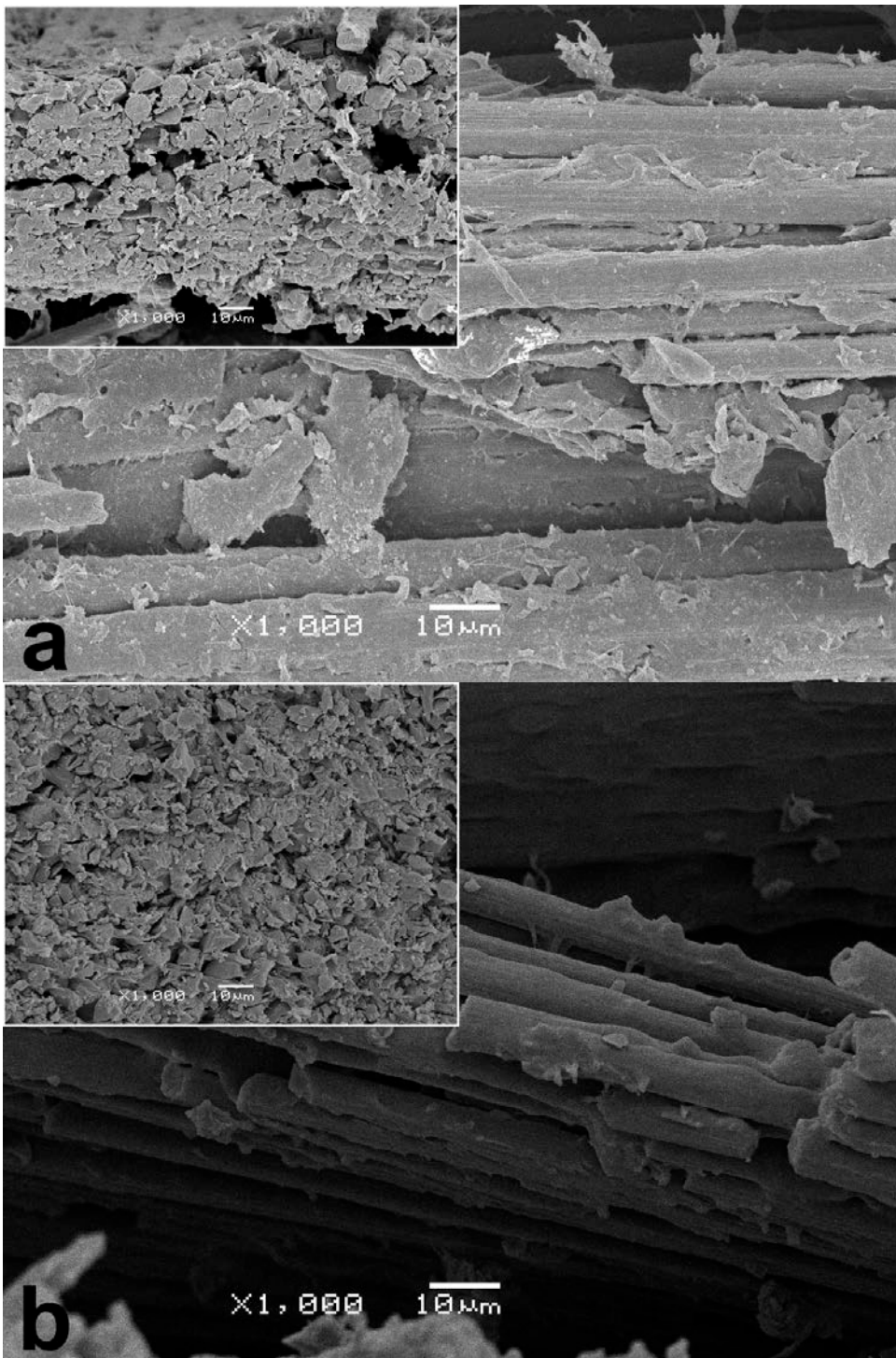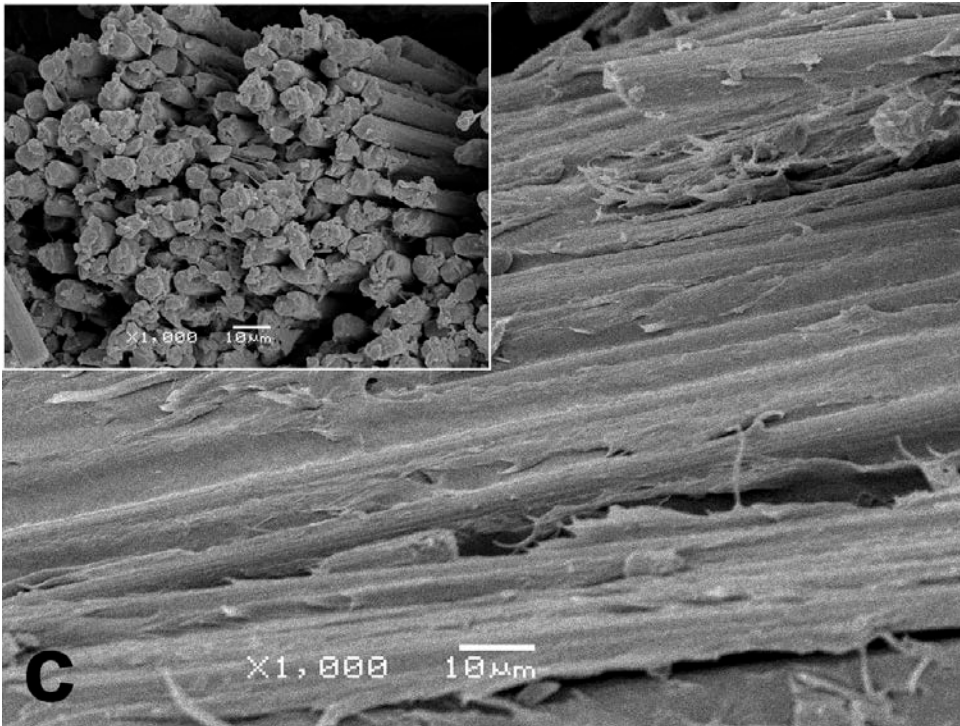
Fig. 15.2: SEM morphologies of fracture surfaces of cryo-fractured pCBT-CF (a), pCBT/EP 3%-CF (b) and pCBT/PMDI 1%-CF (c); pictures were taken normal to fibre direction; inset is parallel to fibre direction.  (*continued*)

Generally, no significant differences between the prepared composites were observed. SEM morphologies show that some matrix material was bonded to the carbon fibres, indicating a good interfacial adhesion between fibre and matrix in all cases. Fibre distribution and impregnation were studied using optical microscopy on polished cross sections of samples mounted in a polyester resin (*c.f.* figure 15.3). On a macroscopic scale, warp and weft rovings and a good macro-impregnation can be seen. Taking a closer look, one can see a uniform inter-fibre distribution and a good micro-impregnation. Good fibre impregnation is commonly observed because the low viscosity of the molten CBT facilitates the penetration of the resin through the fabric and the impregnation of intra-bundle fibres [10-12]. Nevertheless, some intra-bundle voids were detected which are in line with the calculated void contents of 0.7–3.3%.
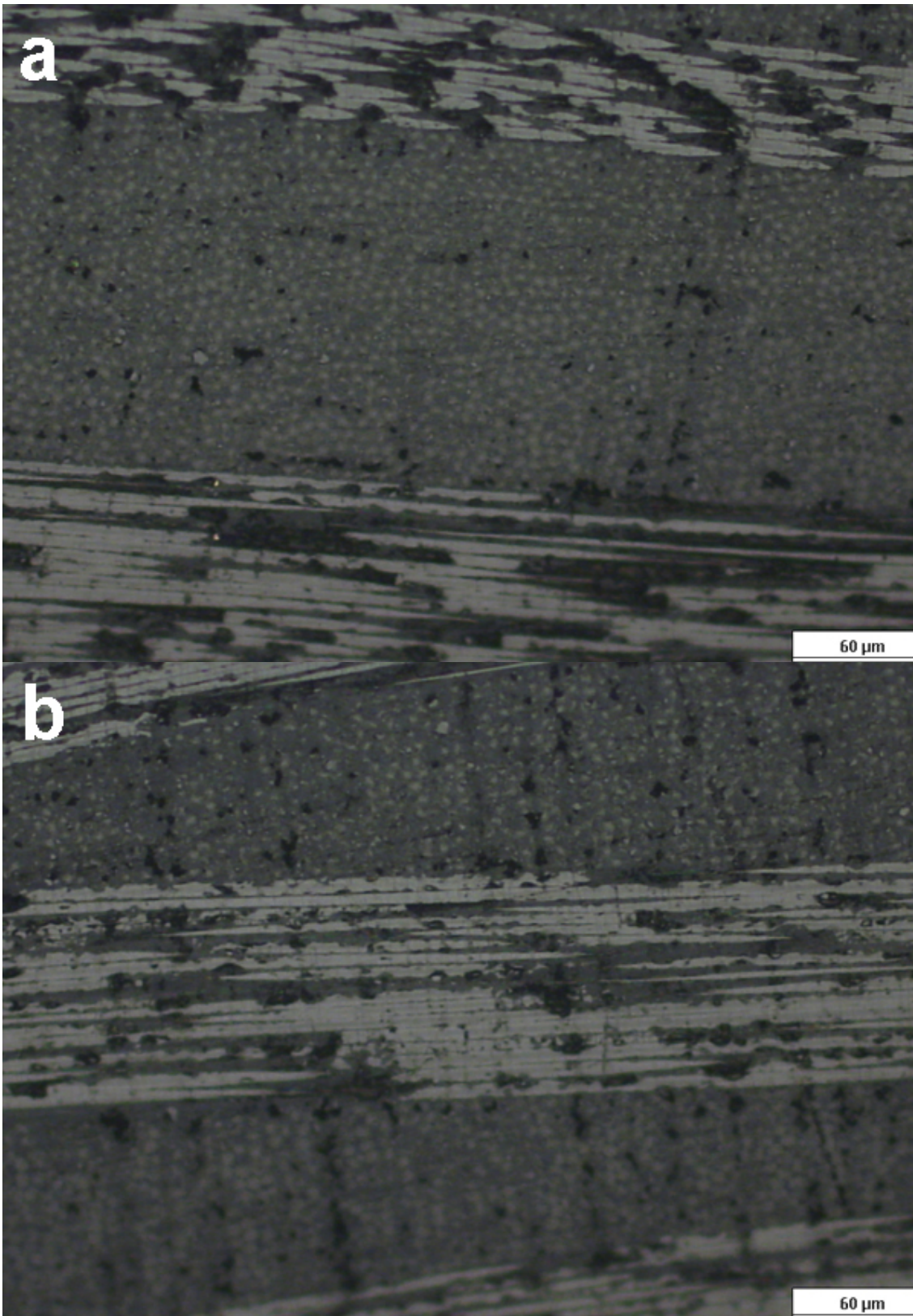
Fig. 15.3: OM micrographs of polished surfaces of pCBT-CF (a), pCBT/EP 3%-CF (b) and pCBT/PMDI 1%-CF (c).
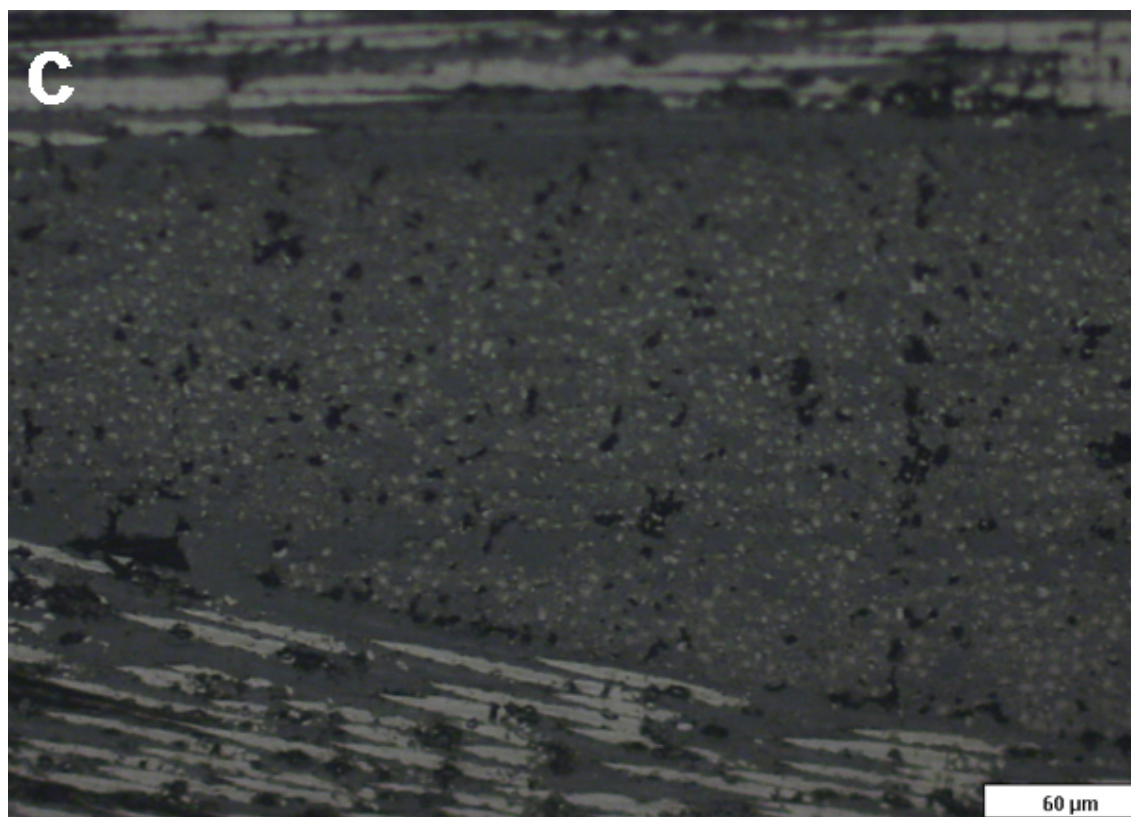
Fig. 15.3: OM micrographs of polished surfaces of pCBT-CF (a), pCBT/EP 3%-CF (b) and pCBT/PMDI 1%-CF (c).  (*continued*)

### 15.4.3 DSC analysis

The as-moulded thermal properties of pristine and modified pCBT composites are presented in table 15.2.

As expected, the fibre reinforcement did not significantly alter the thermal properties; crystal fractions of the composites match well with the ones of their respective host polymer. Nevertheless, melting temperatures of the composites were found to be somewhat lower as compared to the corresponding polymers. Similarly to epoxy- and isocyanate-modified pCBT, the degree of crystallinity slightly decreased in the modified composites as compared to pristine pCBT-CF, which is due to the chain extension reaction of pCBT [13], as was discussed in detail in previous chapters.

Table 15.2: As-moulded thermal properties of pristine, epoxy- and isocyanate-modified carbon fibre reinforced pCBT composites. DSC heating and cooling rate of 10 °C/min; $X_C$ calculated from first heating.

| Sample | first heating | | first cooling | | Crystallinity | |
|---|---|---|---|---|---|---|
| | $T_m$ | $\Delta H_m$ | $T_c$ | $\Delta H_c$ | $X_C$ | $T_g*$ |
| | [°C] | [J/g] | [°C] | [J/g] | [%] | [°C] |
| pCBT-CF | 217.2 | 46.4 | 178.1 | -35.2 | 32.7 | 69.1 |
| pCBT/EP 2%-CF | 218.6 | 44.0 | 183.1 | -40.0 | 31.0 | 68.3 |
| pCBT/EP 3%-CF | 217.0 | 45.1 | 179.6 | -39.3 | 31.8 | 68.3 |
| pCBT/EP 4%-CF | 216.6 | 44.3 | 183.0 | -45.6 | 31.2 | 67.9 |
| pCBT/PMDI 1%-CF | 220.4 | 44.7 | 186.0 | -39.8 | 31.5 | 68.2 |
| pCBT/MDI 1%-CF | 219.3 | 41.6 | 182.4 | -36.5 | 29.3 | 70.0 |
| pCBT/HDI 1%-CF | 217.5 | 46.3 | 188.7 | -45.5 | 32.6 | 66.1 |

* Determined by DMTA in single cantilever mode in the temperature range T = 30–210 °C, heating rate = 2 °C/min, f = 1 Hz, $\varepsilon$ = 0.01%.

### 15.4.4 DMTA analysis

The stiffness as a function of temperature of the prepared composites was studied using DMTA; results for epoxy-modified samples are shown in figure 15.4 whereas the ones for isocyanate-modified samples are depicted in figure 15.5.

The observed DMTA storage moduli at room temperature generally agreed well with the flexural moduli as will be shown later. Regarding the epoxy-modified samples, it can be seen that the highest stiffness at room temperature was found for the sample containing 3 wt.% of EP whereas pCBT/EP 2%-CF showed the lowest stiffness. The stiffness decreased with temperature; this was more pronounced above $T_g$ for EP-modified samples and may be ascribed to the somewhat higher degree of crystallinity of unmodified pCBT as compared to modified samples. Furthermore, this may also be ascribed to a plasticizing effect due to the increasing amount of unreacted EP resin as was shown in chapter 8. The

decreasing glass transition temperatures (*c.f.* table 15.2) as well as the prominent stiffness loss at $T_g$ in the sample containing 4 wt.% of EP support this assumption.
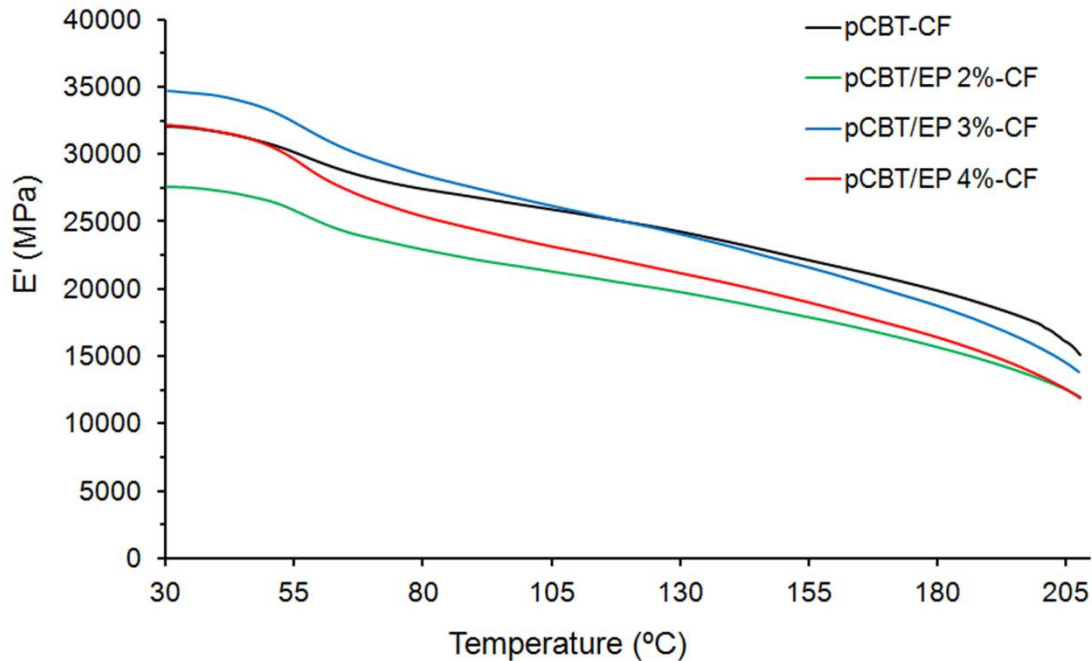


Fig. 15.4: DMTA storage modulus curves of pristine and epoxy-modified pCBT composites.

Storage moduli of isocyanate-modified composites were more similar to the one of pristine pCBT-CF but all curves ran below the one of pristine pCBT-CF. The lower stiffness is indicative that chain extension was successful. This assumption receives further support from the relatively lower glass transition temperatures of the modified samples (*c.f.* table 15.2). An exception was the sample containing MDI which exhibited the lowest stiffness of all tested samples. As will be shown later, this sample also exhibited poor interlaminar shear strength as well as poor flexural properties.
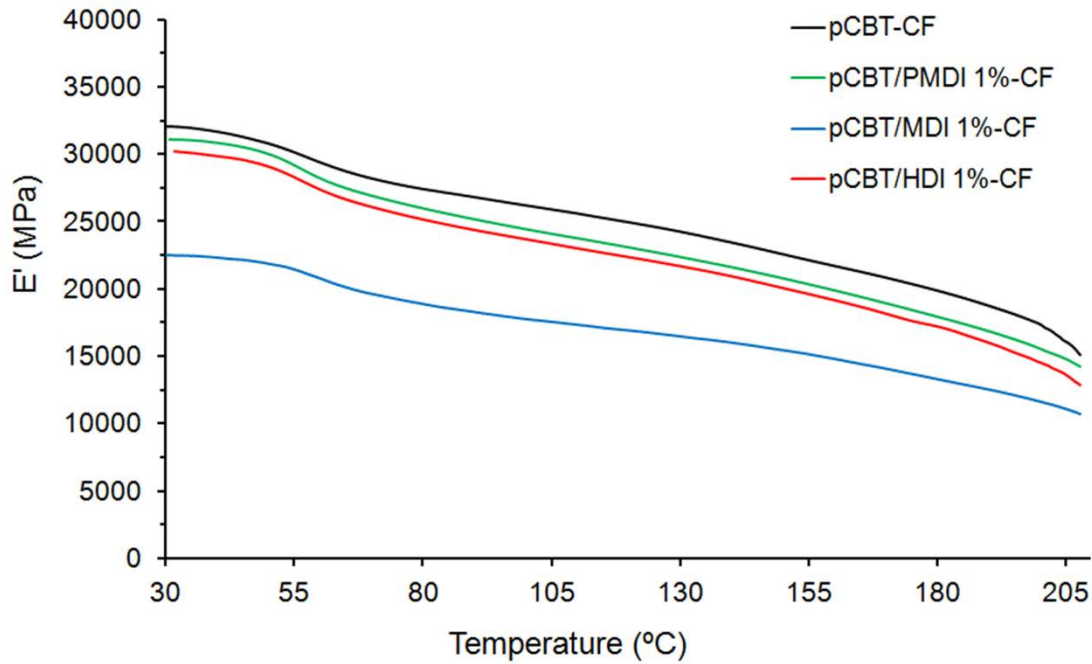
Fig. 15.5: DMTA storage modulus curves of pristine and epoxy-modified pCBT composites.

## 15.4.5 Short beam interlaminar shear strength (ILSS)

The apparent interlaminar shear strengths, *ILSS*, of unmodified and modified pCBT-CF composites were determined; results are listed in table 15.3. All tested samples failed by multiple interlaminar shear failures as exemplarily shown in figure 15.6.

**compressive**



**tensile**
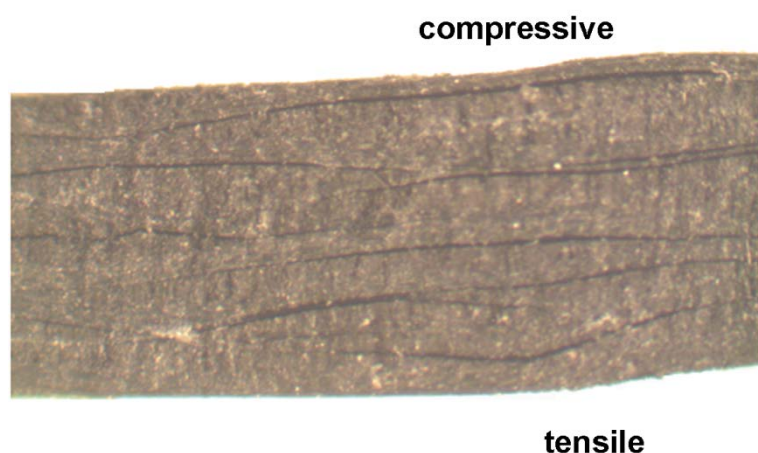
Fig. 15.6: Lateral view of a pCBT-CF composite sample exhibiting multiple interlaminar shear failures after short beam interlaminar shear strength testing.

Table 15.3: Apparent interlaminar shear strength, $\tau$, of unmodified and modified pCBT-CF composites

| Sample | Apparent interlaminar shear strength, *ILSS* [MPa] |
| --- | --- |
| pCBT-CF | 29.6 ± 2.0 |
| pCBT/EP 2%-CF | 45.2 ± 6.0 |
| pCBT/EP 3%-CF | 40.8 ± 3.3 |
| pCBT/EP 4%-CF | 40.1 ± 1.4 |
| pCBT/PMDI 1%-CF | 42.2 ± 3.2 |
| pCBT/MDI 1%-CF | 28.1 ± 3.6 |
| pCBT/HDI 1%-CF | 42.5 ± 2.0 |

It can be seen that the unmodified pCBT composite exhibited a rather low interlaminar shear strength of 30 MPa due to the brittle behaviour of pCBT. The ILSS value of unmodified pCBT-CF is in good agreement with values published in the literature [10-11, 14]. Apparent interlaminar shear strength remarkably increased by 35–53% when the pCBT composites were toughened with EP and NCO; the highest observed ILSS was 45 MPa and was found for the sample containing 2 wt.% of EP. Nevertheless, an exception was the sample containing MDI; its ILSS value decreased by 5% with respect to the

unmodified sample. Recall from chapter 9 that MDI showed only a minor toughening effect on pCBT as compared to PMDI, HDI and EP, respectively.

### 15.4.6 Flexural properties

The failure modes of unmodified and modified pCBT composites were tensile fracture at the outermost layer and compressive fracture including inter-ply fracture, as exemplarily shown in figure 15.7.
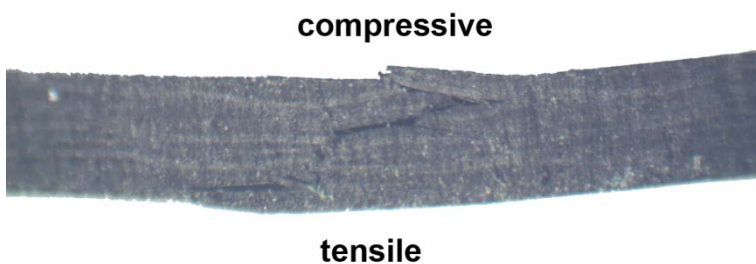


Fig. 15.7: Lateral view of a pCBT-CF composite sample exhibiting tensile and compressive failure including inter-ply fracture.

The inherent brittleness and pronounced notch sensitivity of the unmodified pCBT composite is well reflected in the low flexural strength and failure strain (linked to the maximum stress), whereas the relatively high flexural modulus may be ascribed to the somewhat higher degree of crystallinity (*c.f.* table 15.4). Apparently, the maximum composite strength could not be reached because the matrix failed before the fibre reinforcement reached its maximum strength.

In contrast, all modified samples exhibited a much higher strength and failure strain but a somewhat lower stiffness due to the toughening effect of the chain extenders. Flexural strength generally increased by *ca.* 50% and failure strain increased by up to 63% when the pCBT composites were toughened with EP and NCO. If failure strain is taken as

a criterion for toughness, then the toughest sample was pCBT/EP 2%-CF whereas the stiffest and strongest sample was the one containing 3 wt.% of EP (*c.f.* table 15.4 and fig. 15.8). Again, an exception was the sample containing MDI; this sample showed only minor improvement in strength and toughness (*c.f.* fig. 15.9). These results are in line with the earlier discussed mechanical performances of the EP- and NCO-modified pCBT matrices and demonstrate that EP, PMDI and HDI effectively toughen fibre reinforced pCBT composites.

Table 15.4:  Flexural properties of unmodified and modified pCBT-CF composites

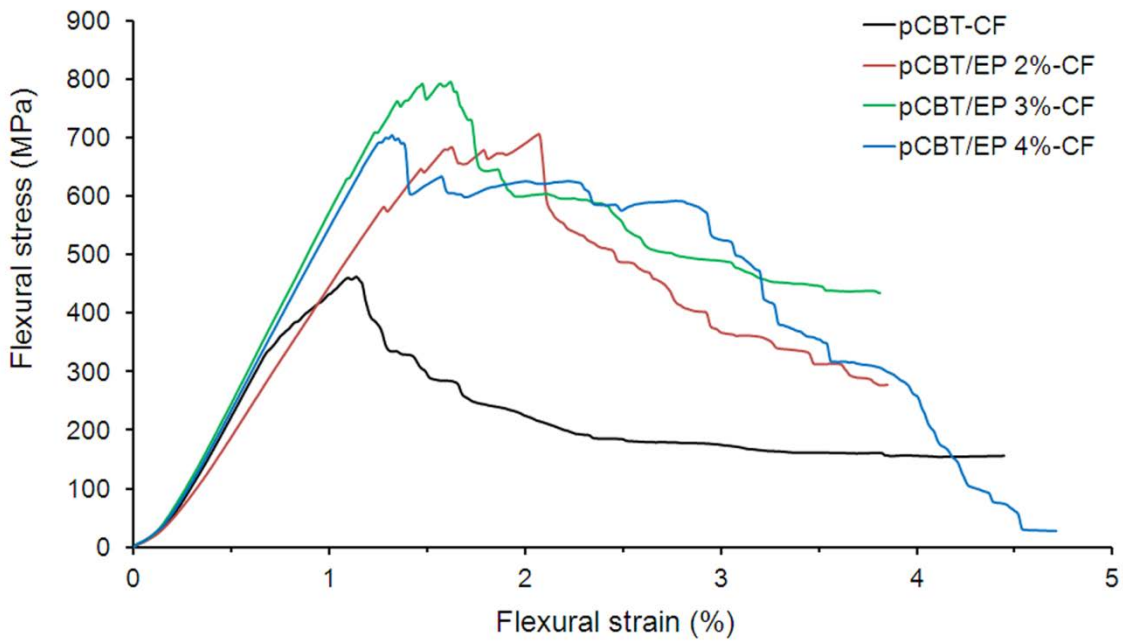| Sample | Flexural modulus [GPa] | Flexural strength [MPa] | Failure strain [%] |
|---|---|---|---|
| pCBT-CF | 35.3 ± 7.0 | 453 ± 31 | 1.1 ± 0.1 |
| pCBT/EP 2%-CF | 27.0 ± 3.8 | 692 ± 53 | 1.8 ± 0.2 |
| pCBT/EP 3%-CF | 37.7 ± 5.5 | 736 ± 86 | 1.5 ± 0.2 |
| pCBT/EP 4%-CF | 33.0 ± 5.5 | 703 ± 66 | 1.4 ± 0.2 |
| pCBT/PMDI 1%-CF | 34.7 ± 6.8 | 668 ± 79 | 1.4 ± 0.2 |
| pCBT/MDI 1%-CF | 34.3 ± 6.5 | 476 ± 29 | 1.2 ± 0.1 |
| pCBT/HDI 1%-CF | 34.1 ± 5.9 | 680 ± 152 | 1.3 ± 0.3 |

Fig. 15.8: Typical 3-point-bending stress-strain curves for neat and epoxy-modified pCBT-CF composites
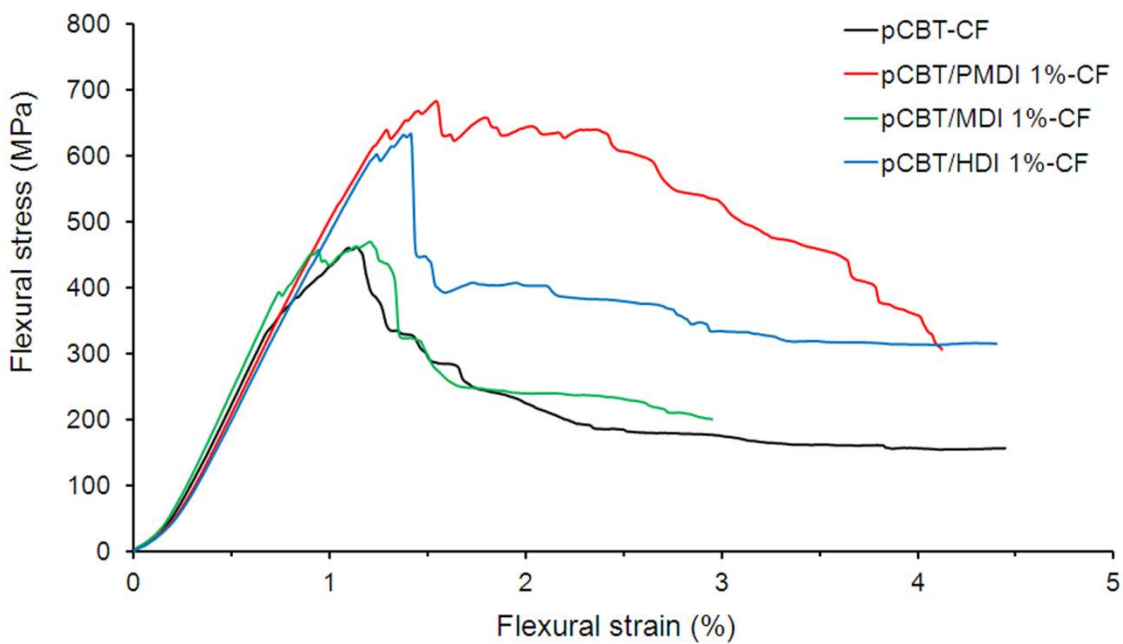


Fig. 15.9: Typical 3-point-bending stress-strain curves for neat and isocyanate-modified pCBT-CF composites

### 15.4.7 Drop weight impact properties

The drop weight impact properties of unmodified and modified pCBT-CF composites were determined; contact force–real time curves with the corresponding impacted surfaces are shown in figure 15.10 and impact data is presented in table 15.5. For the sake of clarity, only one $[0/90]_{20}$ composite for each group of chain extenders with the best mechanical performance was prepared and impact tested as described above, namely pCBT-CF, pCBT/EP 2.5%-CF and pCBT/PMDI 1%-CF.

Impact events can be divided into subcritical impacts with no damage and supercritical impacts with delamination. The impact energy at which the first damage occurs is referred to as the delamination threshold energy or also as the critical energy, $E_{crit}$. The corresponding delamination threshold force, $F_d$, is defined as the point at which a significant drop in contact force occurs (exemplarily marked by an ellipse in figure 15.10 b). It was shown that this delamination threshold force does not depend on the nominal impact energy, $E_0$ [15]. The maximum contact force during impact is referred to as the peak force, $F_M$. The difference between maximum energy, $E_M$, and absorbed energy, $E_{abs}$, is the rebound energy or elastic energy. Total contact time is referred to as $t_c$ and deflection at the peak force is denoted as $l_M$.

As can be seen in figure 15.10, modified composites exhibited higher peak forces together with shorter contact times for all tested energies, suggesting a lower loss of transversal stiffness for these samples [11]. Subcritical impacts occurred at impact energies up to 0.5 J; the force curves in figure 15.10 a are smooth and bell-shaped where no peaks are observed and no visible damage could be seen on the sample surfaces after impact. It is noteworthy that the absorbed energy of pristine pCBT-CF was relatively higher at subcritical impacts. Conversely at supercritical impacts, the absorbed energies of the modified samples were relatively higher, indicating a greater amount of plastic deformation.

At an impact energy of 3 J, the first damages in form of small indentations on the impacted surfaces were found, as is apparent from the load oscillations below the peak maxima of the force curves in figure 15.10 b. Nevertheless, no damages at the back sides of the specimens were found. At this low energy level, the damage mode was local plastic deformation of the matrix. The damage mode at impact energies higher than 3 J was essentially the same for all samples, namely horizontal and vertical cracks oriented parallel

to the (0°/90°) fibre orientations on the impacted surfaces and localized fibre breakage at the impact points on the back surfaces. Crack lengths increased with impact energy, as can be seen from the inserts in figure 15.10. Nevertheless, the modified samples exhibited a more prominent distortion at the back surface which had a hemispherical shape with a diameter similar to the inner diameter of the annular support. This suggests that EP- and PMDI-modified pCBT possessed a greater ability to undergo plastic deformation whereas neat pCBT-CF showed little plastic deformation due to its brittle behaviour, suggesting a greater overall damage.



Fig. 15.10: Force and absorbed energy *versus* time plots of pCBT-CF, pCBT/EP-CF and pCBT/PMDI 1%-CF composites; subcritical impacts (a), damage threshold (b) and supercritical impacts (c–e).

Fig. 15.10: Force and absorbed energy *versus* time plots of pCBT-CF, pCBT/EP-CF and pCBT/PMDI 1%-CF composites; subcritical impacts (a), damage threshold (b) and supercritical impacts (c–f). (*continued*)
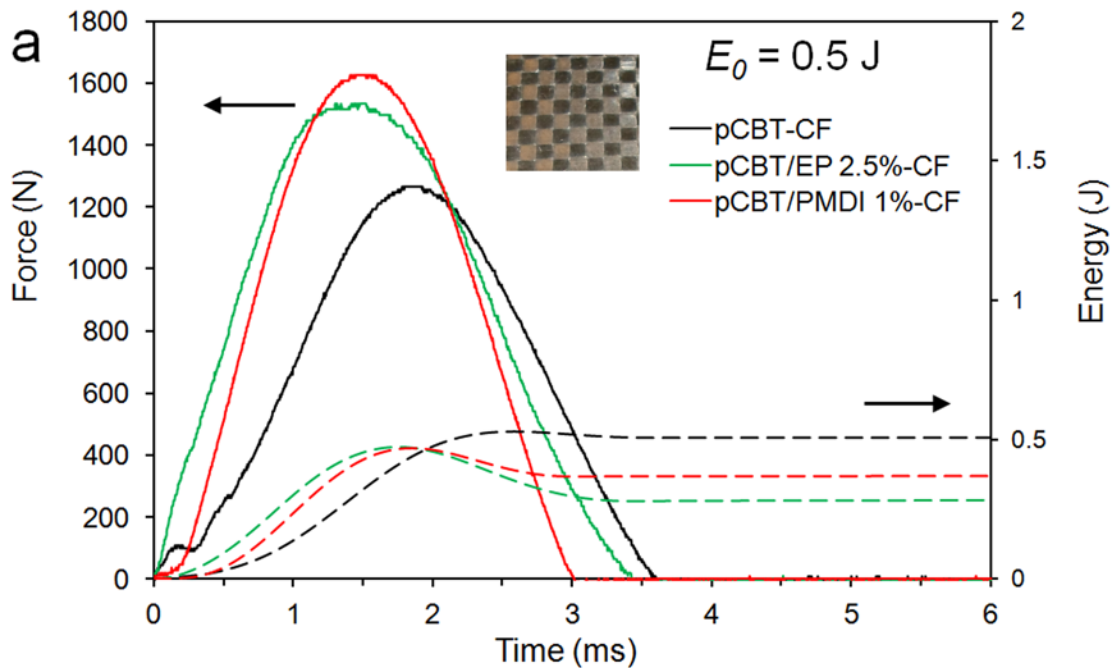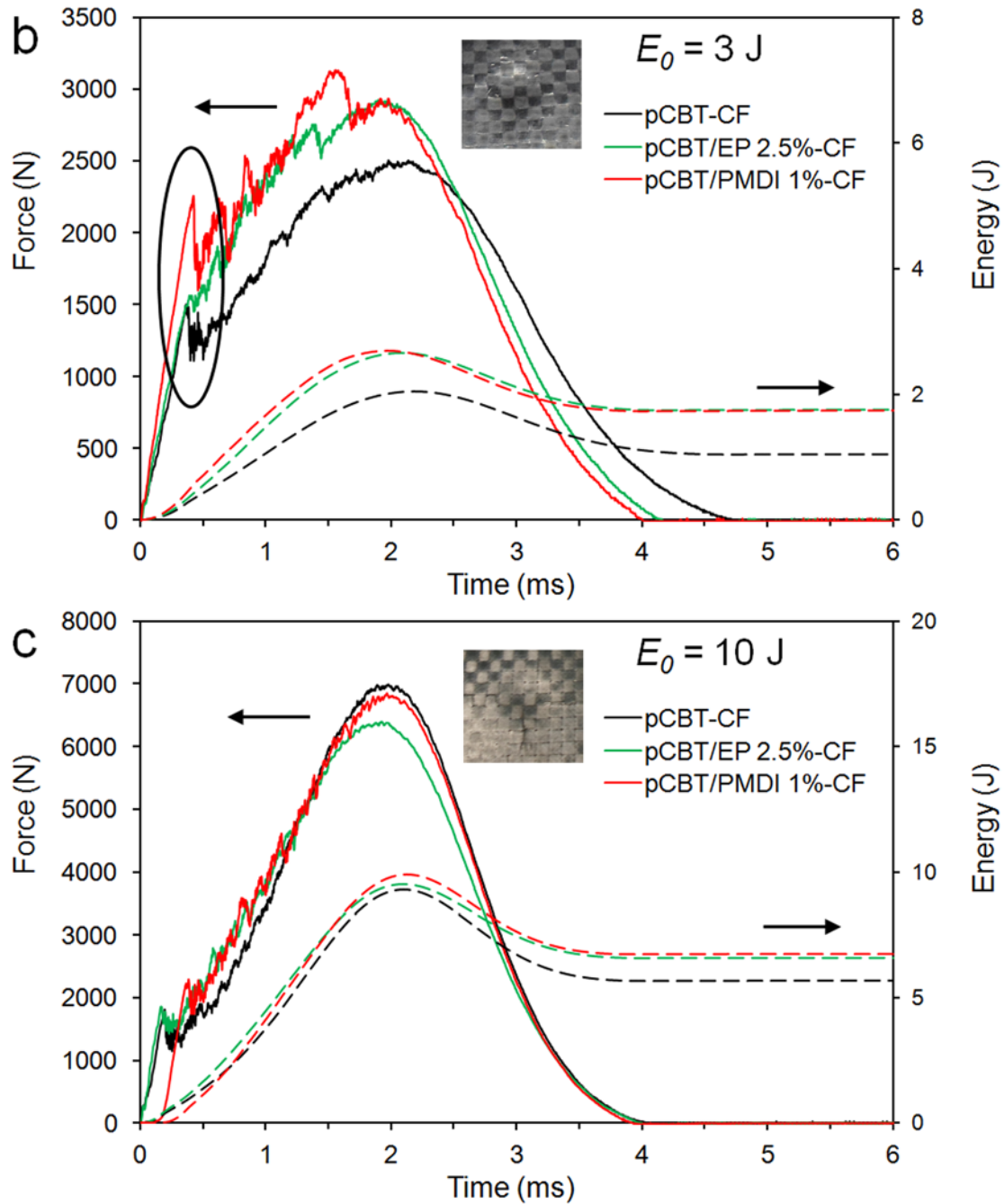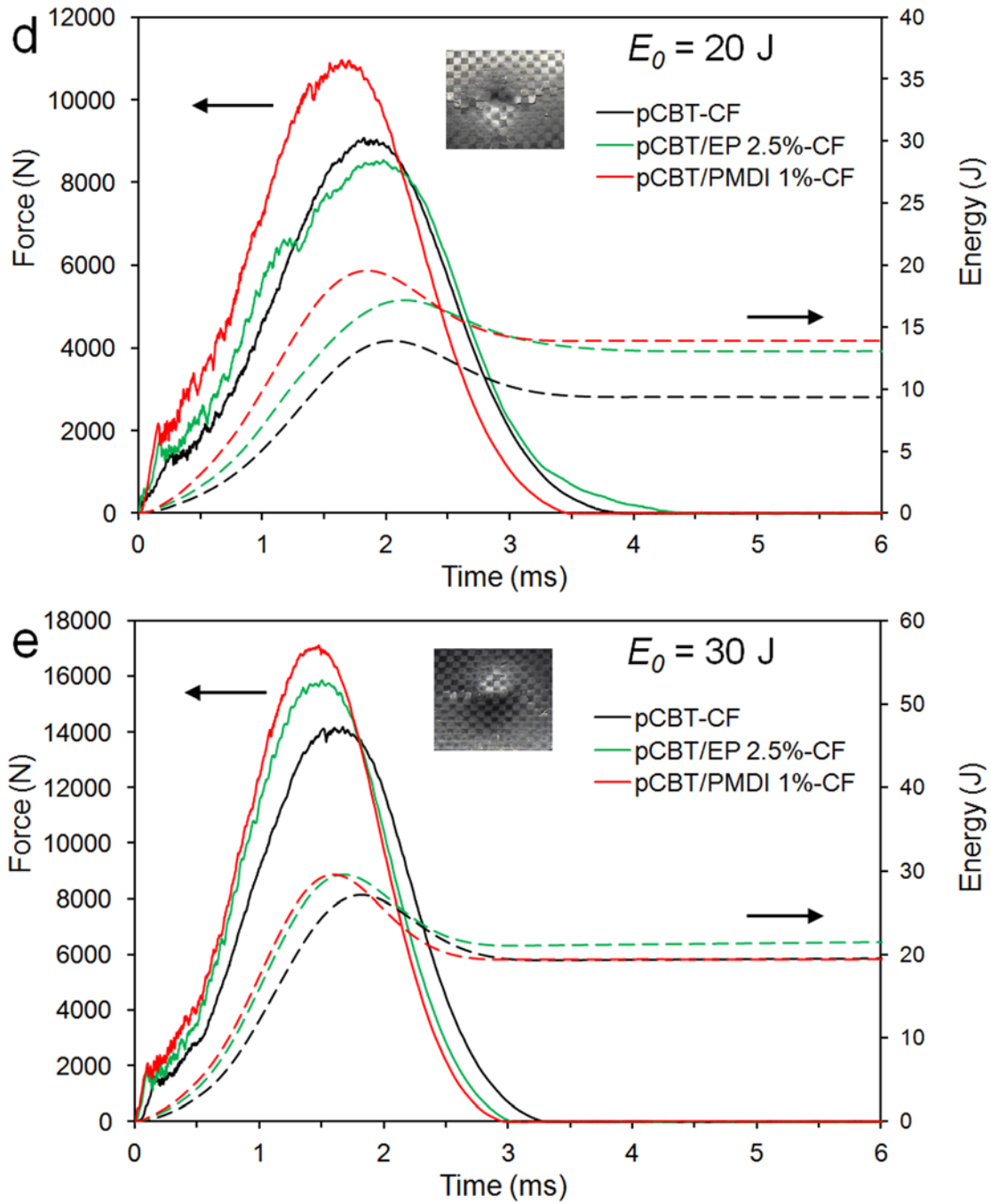
Fig. 15.10: Force and absorbed energy *versus* time plots of pCBT-CF, pCBT/EP-CF and pCBT/PMDI 1%-CF composites; subcritical impacts (a), damage threshold (b) and supercritical impacts (c–e). (*continued*)

Table 15.5: Drop weight impact properties of unmodified and modified pCBT-CF composites.

| $E_0$ [J] | Sample | $E_{crit}$ [J] | $F_d$ [N] | $F_M$ [N] | $t_c$ [ms] | $l_M$ [mm] | $E_{abs}$ [J] |
|---|---|---|---|---|---|---|---|
| | pCBT-CF | - | - | 1264 | 3.6 | 0.8 | 0.4 |
| 0.5 | pCBT/EP 2.5%-CF | - | - | 1535 | 3.4 | 0.5 | 0.5 |
| | pCBT/PMDI 1%-CF | - | - | 1625 | 3.0 | 0.6 | 0.4 |
| | pCBT-CF | 0.3 | 1490 | 2501 | 4.7 | 1.4 | 2.0 |
| 3 | pCBT/EP 2.5%-CF | 0.4 | 1562 | 2926 | 4.1 | 1.5 | 2.6 |
| | pCBT/PMDI 1%-CF | 0.4 | 2256 | 3133 | 4.0 | 1.3 | 2.5 |
| | pCBT-CF | 0.3 | 1643 | 6998 | 4.0 | 3.1 | 9.2 |
| 10 | pCBT/EP 2.5%-CF | 0.3 | 1860 | 6384 | 4.0 | 3.0 | 9.4 |
| | pCBT/PMDI 1%-CF | 0.6 | 2294 | 6854 | 3.9 | 3.2 | 9.7 |
| | pCBT-CF | 0.4 | 1517 | 9066 | 3.9 | 3.8 | 13.3 |
| 20 | pCBT/EP 2.5%-CF | 0.6 | 1806 | 8533 | 4.4 | 4.2 | 16.9 |
| | pCBT/PMDI 1%-CF | 0.5 | 2176 | 10971 | 3.5 | 3.9 | 18.9 |
| | pCBT-CF | 0.3 | 1598 | 14177 | 3.3 | 4.8 | 26.5 |
| 30 | pCBT/EP 2.5%-CF | 0.3 | 1860 | 15839 | 3.0 | 4.6 | 28.6 |
| | pCBT/PMDI 1%-CF | 0.4 | 2068 | 17121 | 3.0 | 4.4 | 29.0 |

$m_{impact}$: 3.62 kg; $h_{impact}$: 13 - 563 mm; $v_{impact}$: 0.5 - 3.3 m/s

Unfortunately, impact energies beyond 30 J could not be studied due to load restrictions of the impact testing machine. Hence, the penetration regime could not be determined and only the delamination threshold is presented here. Critical energy and delamination threshold force were fairly constant in the studied impact energy range (*c.f.* table 15.5) and therefore may be considered as independent of the nominal impact energy [15]. The delamination threshold forces and related critical energies were averaged for all impact energies and results are presented in table 15.6. The found delamination threshold force of pCBT-CF was 1562 ± 71 N, somewhat lower than the one reported by Agirregomezkorta and co-workers [11] (namely 1760 ± 35 N). The results suggest that the modified composites exhibited a relatively higher delamination threshold. $E_{crit}$ increased by

21% and 47% and $F_d$ increased by 13% and 41% for the EP- and PMDI-modified composites, respectively.

The relation between impact energy and absorbed energy can be seen in the energy profile diagrams of the composites in figure 15.11. They show that the three composites behaved similarly for low impact energies up to 10 J. For higher impact energies, EP- and PMDI-modified composites absorbed more energy because they underwent a greater amount of matrix plastic deformation during impact, which was ascribed to the higher toughness of the matrix materials. Due to this greater deformability, a higher penetration threshold was deduced for the modified composites.
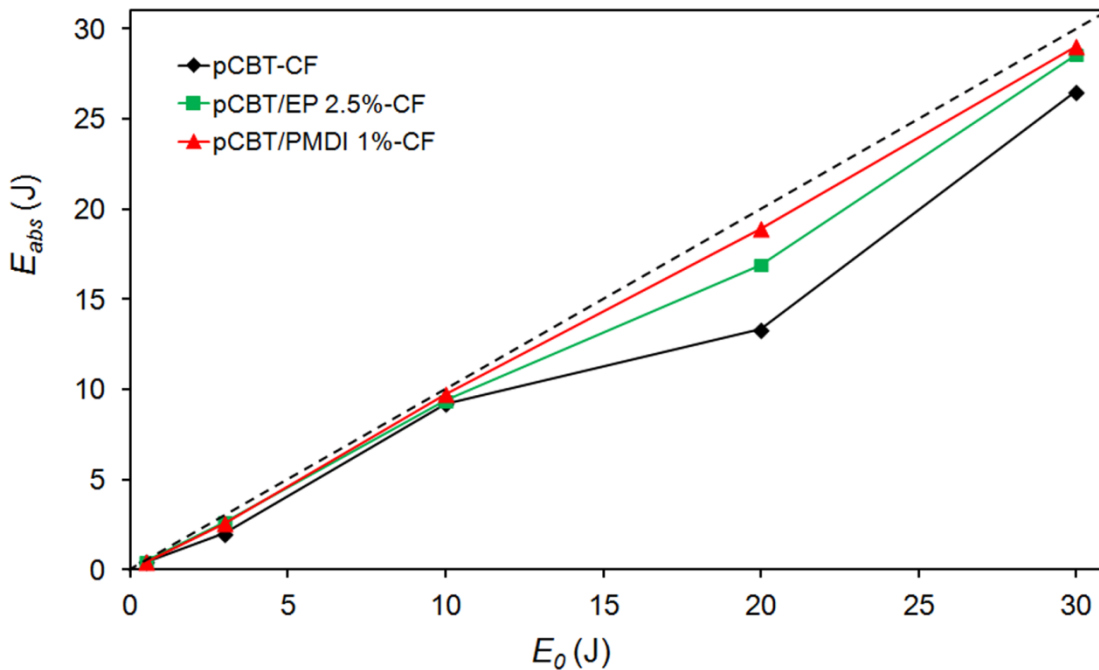


Fig. 15.11: Energy profile diagrams of pCBT-CF, pCBT/EP-CF and pCBT/PMDI 1%-CF composites.

Table 15.6: Delamination threshold forces and critical energies of unmodified and modified pCBT-CF composites.

| Sample | $E_{crit}$ [J] | $F_d$ [N] |
|---|---|---|
| pCBT-CF | 0.33 ± 0.05 | 1562 ± 71 |
| pCBT/EP 2.5%-CF | 0.40 ± 0.14 | 1772 ± 142 |
| pCBT/PMDI 1%-CF | 0.48 ± 0.10 | 2199 ± 100 |

## 15.5 Conclusions

CBT was chemically modified with small amounts of chain extenders, namely bifunctional epoxy resin and bi- or polyfunctional isocyanates. It was found that the chemical modifications did not significantly alter the physical and thermal properties or the morphology of the composites. On the other hand, interlaminar shear strength, flexural strength and failure strain of the chemically modified composites were considerably enhanced. Nevertheless, the flexural moduli slightly decreased due to the toughening effect of the chain extender on the pCBT matrix. Low energy impact tests revealed that the modified composites absorbed relatively more energy as compared to unmodified pCBT composites, especially at high impact energies. Moreover, critical energy and delamination threshold force were higher for modified composites. It can be concluded that toughening of pCBT with epoxy or isocyanates, namely PMDI and HDI, is very effective for improving the mechanical properties, most importantly the toughness of fibre reinforced pCBT composites.

## 15.6 References for pCBT/CF

1. Aurrekoetxea, J, Zurbitu, J, Ortiz de Mendibil, I, Agirregomezkorta, A, Sánchez-Soto, M, and Sarrionandia, M. Effect of superelastic shape memory alloy wires on the impact behavior of carbon fiber reinforced in situ polymerized poly(butylene terephthalate) composites. Materials Letters **65**(5), 863-865 (2011).

2.      Baets, J. Toughening of in-situ polymerized cyclic butyleneterephthalate for use in continuous fiber reinforced thermoplastic composites. PhD thesis. Department of Metallurgy and Materials Engineering. Katholieke Universiteit Leuven: Leuven, Belgium, 2008

3.      Baets, J, Devaux, J, and Verpoest, I. Toughening of basalt fiber-reinforced composites with a cyclic butylene terephthalate matrix by a nonisothermal production method. Advances in Polymer Technology **29**(2), 70-79 (2010).

4.      Baets, J, Dutoit, M, Devaux, J, and Verpoest, I. Toughening of glass fiber reinforced composites with a cyclic butylene terephthalate matrix by addition of polycaprolactone. Composites Part A: Applied Science and Manufacturing **39**(1), 13-18 (2008).

5.      Baets, J, Godara, A, Devaux, J, and Verpoest, I. Toughening of polymerized cyclic butylene terephthalate with carbon nanotubes for use in composites. Composites Part A: Applied Science and Manufacturing **39**(11), 1756-1761 (2008).

6.      Baets, J, Godara, A, Devaux, J, and Verpoest, I. Toughening of isothermally polymerized cyclic butylene terephthalate for use in composites. Polymer Degradation and Stability **95**(3), 346-352 (2010).

7.      Wu, W, Klunker, F, Xie, L, Jiang, B, and Ziegmann, G. Simultaneous binding and ex situ toughening concept for textile reinforced pCBT composites: Influence of preforming binders on interlaminar fracture properties. Composites Part A: Applied Science and Manufacturing **53**(0), 190-203 (2013).

8.      Wu, W, Xie, L, Jiang, B, and Ziegmann, G. Simultaneous binding and toughening concept for textile reinforced pCBT composites: Manufacturing and flexural properties. Composite Structures **105**(0), 279-287 (2013).

9.      Wu, W, Xie, L, Jiang, B, and Ziegmann, G. Influence of textile preforming binder on the thermal and rheological properties of the catalyzed cyclic butylene terephthalate oligomers. Composites Part B: Engineering **55**(0), 453-462 (2013).

10.     Mohd Ishak, ZA, Leong, YW, Steeg, M, and Karger-Kocsis, J. Mechanical properties of woven glass fabric reinforced in situ polymerized poly(butylene terephthalate) composites. Composites Science and Technology **67**(3–4), 390-398 (2007).

11.     Agirregomezkorta, A, Martínez, AB, Sánchez-Soto, M, Aretxaga, G, Sarrionandia, M, and Aurrekoetxea, J. Impact behaviour of carbon fibre reinforced epoxy and non-

isothermal cyclic butylene terephthalate composites manufactured by vacuum infusion. Composites Part B: Engineering **43**(5), 2249-2256 (2012).

12. Parton, H and Verpoest, I. In situ polymerization of thermoplastic composites based on cyclic oligomers. Polymer Composites **26**(1), 60-65 (2005).

13. Torres, N, Robin, JJ, and Boutevin, B. Chemical modification of virgin and recycled poly(ethylene terephthalate) by adding of chain extenders during processing. Journal of Applied Polymer Science **79**(10), 1816-1824 (2001).

14. Balogh, G. Development of cyclic butylene terephthalate matrix composites. PhD thesis. Department of Polymer Engineering. Budapest University of Technology and Economics: Budapest, Hungary, 2012

15. Cartié, DDR and Irving, PE. Effect of resin and fibre properties on impact and compression after impact performance of CFRP. Composites Part A: Applied Science and Manufacturing **33**(4), 483-493 (2002).

# General conclusions

A series of chemical and physical modifications of CBT with toughening agents and nano-reinforcements have been investigated in this thesis in order to increase the toughness of inherently brittle pCBT. Considerable efforts have been made and a large amount of experimental work has been performed in the course of this work. The thesis at hand consists of four parts:

*i.)     Investigation of the processing-structure-properties relationships in pCBT obtained by compression moulding, melt blending and solvent blending:*

The role of the used processing routes on the properties of unmodified pCBT has been studied and in all cases a brittle pCBT has been obtained. However, it was found that a small amount of tetrahydrofuran can toughen pCBT. The THF-modified pCBT was found to be ductile, showing a strain at break of well above 100% in tensile tests. Other mechanical or thermal properties were not significantly altered by the addition of THF. It was found that the presence of THF enhanced the polymerization reaction, resulting in an increased molecular weight and a narrowed molecular weight distribution. Moreover, remaining oligomers after polymerization were extracted by the THF and a toughened oligomer-free pCBT was obtained. The influence of time and temperature on the long-time toughening action of THF was studied. The results indicated that samples became brittle after 3 months when subjected to a temperature of 80 °C, resulting in a reduction of the toughening action.

*ii.)     Improvement of the toughness of pCBT by exploring toughening methods such as reactive chain extension with bi- and polyfunctional compounds:*

A variety of bi- and polyfunctional chain extenders such as epoxy resins, isocyanates, polyTHF and benzoxazine have been evaluated for their effectiveness as toughening agents. Epoxy resins and isocyanates were particularly effective and showed a remarkable toughening effect on pCBT. The chain extended pCBT exhibited an increased failure strain in tensile tests while modulus and strength were not significantly affected; contrary to other

common toughening methods such as blending with other polymers, plasticization or copolymerization with soft segments. The optimum amount of epoxy resin was found to be 2–3 wt.% and the ROP should be conducted above $T_m$ of pCBT, *i.e.* 230 °C for 20 min in order to complete the reaction. Regarding isocyanates, HDI and PMDI effectively toughened pCBT at contents >0.5 wt.% in a shorter time as compared to epoxy due to their higher reactivity. While HDI yields a linear chain extended pCBT, high contents of PMDI can result in a branched or even cross-linked structure. Nevertheless, PMDI was found to be the most effective of all studied toughening agents for pCBT.

iii.)    *Preparation and characterization of pCBT nanocomposites using different types of nano-reinforcements in combination with chain extenders:*

Organo-montmorillonite, graphene as well as polyhedral oligomeric silsesquioxanes have been successfully incorporated into pCBT during *in situ* polymerization. Most of the resulting nanocomposites showed a reinforcing effect but also an increased brittleness. Nanocomposite toughness could be improved in many cases by adding chain extenders. For instance, ternary blends of pCBT, polyisocyanate and organoclay exhibited an intercalated-flocculated structure with high stiffness and strength together with a semi-ductile deformation behaviour. The organoclay was further modified by grafting polyisocyanate to the clay surfactant which resulted in organoclay intercalation. This chain extender-grafted organoclay reacted then with pCBT and therefore could be exfoliated and randomly dispersed in the pCBT matrix during polymerization. A similar strategy was followed in the synthesis of pCBT/graphene nanocomposites but graphene exfoliation could not be achieved due to the strong $\pi$–$\pi$ interactions between the graphene sheets. Binary blends containing the polyisocyanate-grafted graphene showed an improved stiffness and strength due to enhanced compatibility. Moreover, the influence of the functionalisation of fully or partially condensed POSS cages on the properties of pCBT-based nanocomposites was also studied and a good potential for nano-modification was found. However, some POSS types (*viz.* partially caged trisilanol POSS) interfered with the ROP of CBT due to –OH groups present in the POSS structure and the release of water. The challenge was to find a compatible POSS type such as epoxy-POSS which did not affect the ring-opening polymerization of CBT.

iiii.)    *Preparation and characterization of toughened carbon fibre reinforced pCBT composites.*

Toughened carbon fibre fabric-reinforced pCBT composites have been prepared applying the developed toughening method. The chemical modifications did not significantly alter the physical and thermal properties or the morphology of the composites. Most importantly, interlaminar shear strength, flexural strength and failure strain of the epoxy- and isocyanate-toughened composites increased up to 60% with respect to unmodified pCBT composites while the flexural moduli slightly decreased due to the toughening effect of the chain extender on the pCBT matrix. It was found that the modified composites absorbed relatively more energy in low energy impact tests and the critical energy and delamination threshold force were also relatively higher.

In conclusion, this work has demonstrated that reactive chain extension of pCBT is an effective method to improve the toughness of inherently brittle pCBT and can be also employed for the preparation of pCBT nanocomposites and fibre reinforced composites with improved toughness.

# Outlook

The developed toughening methods may serve as a basis for further chemical modification of CBT. The reactive nature of the ring-opening polymerization should be exploited more because grafting reactions can be achieved rather easily. Grafting allows for better polymer-nanoreinforccement interactions which enhance the final properties, as shown in this work. Therefore, these findings could be of interest on both academic and industrial side and may help to establish CBT as matrix in nanocomposites with superior mechanical properties. Based on the results and experience gained in the course of this work, the following is suggested for future investigation:

- Further exploration of new chain extenders for pCBT. Of interest are highly reactive bifunctional types which strictly yield a linear pCBT structure without releasing by-products, such as carbonylbiscaprolactam.
- Further investigation of grafting reactions of pCBT with nano-reinforcements, particularly POSS bearing reactive functional groups.
- Investigation of the possibility of chain extended, nano-reinfoced fibre reinforced pCBT composites.

# Publications

1.  **Abt, T**, Sánchez-Soto, M, Martínez, A, Illescas, S and Arencón, D. Nanocompuestos exfoliados de butilen tereftalato cíclico/arcilla obtenidos por polimerización in-situ. XIII Congreso Nacional de Materiales. Barcelona, Spain, 2014.

2.  **Abt, T**, Maspoch, MLI, Velasco, JI and Sánchez-Soto, M. Toughened carbon fibre reinforced thermoplastic composites. 16th European Conference on Composite Materials. Sevilla, Spain, 2014.

3.  **Abt, T**, Sánchez-Soto, M, Illescas, S, and Arostegui, A. Properties of POSS blends with pCBT, PMMA, PC and POM thermoplastics. International Journal of Materials and Structural Integrity 7(Nos. 1/2/3), 48-78 (2013).

4.  **Abt, T**, de Ilarduya, AM, Bou, JJ, and Sanchez-Soto, M. Isocyanate toughened pCBT: Reactive blending and tensile properties. eXPRESS Polymer Letters 7(2), 172-185 (2013).

5.  **Abt, T**, Sánchez-Soto, M, and Martínez de Ilarduya, A. Toughening of in-situ polymerized cyclic butylene terephthalate by chain extension with a bifunctional epoxy resin. European Polymer Journal 48, 163-171 (2012).

6.  **Abt, T**, Sánchez-Soto, M, Illescas, S, Aurrekoetxea, J, and Sarrionandia, M. Toughening of in situ polymerized cyclic butylene terephthalate by addition of tetrahydrofuran. Polymer International 60(4), 549-556 (2011).

7.  **Abt, T**, Illescas, S, Antunes, M, Cáceres, MA, and Sánchez-Soto, M. Nanocomposites of in-situ polymerized cyclic butylene terephthalate and polyhedral oligomeric silsesquioaxanes. 5º Congreso Nacional de Jóvenes Investigadores en Polímeros. Calella de Palafrugell, Spain, 2010.